

Investigating adaptive laboratory evolution strategies to enhance the growth rate and productivity of cyanobacteria.

Christopher Alexander Martin, MSc, BSc (Hons)

Thesis submitted to the University of Nottingham for the degree of Doctor of Philosophy

21st April 2024



University of Nottingham
UK | CHINA | MALAYSIA



Engineering and Physical Sciences Research Council

Declaration

Except where stated, or otherwise acknowledged, the work presented in this thesis is entirely my own. No part has been submitted for any another degree at an institute of higher learning.

Christopher Martin, 21st April 2024.

COVID-19 Impact Statement

Unfortunately, due to the COVID-19 pandemic our facilities were closed from March until September (2020). The return was then phased and based on a limited shift pattern, which lasted from September until July (2021). This significantly disrupted much of the work I had originally planned for this project. I had intended to profile the metabolomes of multiple species of cyanobacteria and develop targeted engineering strategies to improve their growth based on those results. Attempts were made to mitigate the impact of the closure, by trying to add an in-silico dimension to the project. However, upon return, this no longer aligned with the other project objectives. Shift work also had the unfortunate impact on reducing my daily productivity, as experiments that involved prolonged incubation steps were difficult to perform given the limited hours in the shift. Access to other facilities was also difficult, as many had strict user capacities, something that also made getting access to training more difficult. The use of ALE, therefore, developed from the need to find solutions to these challenges, ultimately developing into the primary strategy of this project. Given that ALE experiments can take many months to be effective, however, COVID-19 reduced the amount of time we had to investigate other ALE selection strategies.

The shift patterns also impacted on my mental wellbeing, the stress that I felt about my project and the progress being made on my project. I had envisaged investigating a few different strategies to push flux towards carbon fixation, however, the significant impact of the pandemic meant I was unable to realise these. While I am very happy with the ALE and the interesting data I have generated, I would have liked more time to characterise the strains and potentially implement some of the other strategies I developed, particularly around alternative carbon fixation pathways and gTME.

Previous Communication of This Work

This work remains unpublished at the time of writing, however, has previously been disseminated in at “A Festival of Algae” (Algae-UK), Edinburgh, United Kingdom, (November 2022), and the “International Conference on Algal Biomass, Biofuels, and Bioproducts” (Elsevier), Waikōloa Beach, Hawai‘i, (June 2023).

Abstract

Increasing global CO_2 emissions, dwindling fossil fuel resources, and environmental damage, collectively present an enormous challenge for our shared future. However, strategies exist to address these challenges. Cyanobacteria are photoautotrophic prokaryotes, capable of fixing carbon and producing a wide range of compounds of commercial interest. These organisms are, however, limited by low growth rates and productivity, when compared to both heterotrophic alternatives, and conventional manufacturing processes.

Adaptive laboratory evolution (ALE) was utilised and shown to be an effective strategy for the selection of both unicellular and filamentous cyanobacteria. Following chemostat selection isolates of *Synechocystis Δhox* showed a 2-fold improvement in biomass accumulation compared to the control and 93.2% of the isolates showed improved biomass formation compared to the control when grown under atmospheric concentrations of CO_2. Furthermore, chemostat selection of *Trichormus variabilis* sp. ATCC 29413 under autotrophic conditions yielded the same increase in biomass. Improvements in biomass accumulation were shown to be as high as 2.7-fold.

The fastest growing *Synechocystis* isolates, Syn.1.11 and Syn.1.19 had an increased μ_{max} following ALE selection. Syn.1.11 showed an increase of 13.5% ±3.6% (standard error) in μ_{max} while Syn.1.19 had an increase of 28% ±17% (standard error) in μ_{max} compared to the control strain Syn.*Δhox*, when grown in BG-11NH_4 and atmospheric CO_2. Both strains showed several phenotypic variations from the progenitor strain, including an average 145% ±60% (standard error) increase in rate of peak oxygen evolution in strain Syn.1.11. This despite cells nominally containing on average 16.1% ±22% (standard error) less chlorophyll per mg·DCW^{-1} than the progenitor strain. Multiple changes were also seen in the genomic DNA including mutations in both the *lexA* gene, a key regulator in the cell and *rppB*, a two-component response regulator, which mediates the stoichiometry between the photosystems. Differences were also seen in the metabolite profile of the cells including, an increase in acetylated amino acids, a key posttranslational modification mechanism in the cell and in the metabolites involved in arginine biosynthesis.

Following chemostat selection of *Trichormus variabilis* with fructose supplementation, 3 heterotrophic organisms were also isolated as part of a consortia with the fastest growing strain. This consortium included at least one organism which is capable of nitrogen fixation independent of

the cyanobacteria and induced up to ~30% higher growth rates in the wild type when co-inoculated and grown with 1.5% CO_2. The fastest growing isolate also showed a decrease in the oxygen evolution rate, despite an improvement in growth, and was more resistant to photoinhibition.

The strains isolated in this work demonstrate the power of ALE coupled with continuous selection for identifying potential targets for rational engineering work, and in generating improved strains for commercial exploitation. Furthermore, this work provides novel insights into the use of ALE for selecting photosynthetic prokaryotes with enhanced carbon fixation and biomass formation and may be the first example of ALE used to enhance the productivity of diazotrophic cyanobacteria.

Acknowledgements

I would firstly like to thank my academic supervisors Dr Samantha Bryan, Dr Dong-Hyun Kim, and my bench supervisor Dr Edward Spence. The undertaking of this project simply would not have been possible without the unwavering support from Dr Samantha Bryan. I will forever be grateful for the opportunity that I have been given to work with you, and to undertake this project. In these 4 years you have made a significant impression on who I have become; you have supported me, challenged me, and I cannot thank you enough for the kindness and patience you have shown me. I'd also like express my appreciation to Dr Edward Spence for his many interesting and creative ideas, impeccably good humour, and insightful advice – to which this project owes a great deal to. To Dr Dong-Hyun Kim for all his kind support with our metabolomics work. I hope the future only brings you all the very best it has to offer.

I thank the University of Nottingham, and EPSRC who have funded this project. I extend my deepest thanks to my colleagues within the Schools of Engineering and Pharmacy, with whom I have had the opportunity to work with over the course of this project. I would especially like to thank Dr Sean Craig for all his assistance over these years. I thank all my friends who have supported me, and endured listening to me talk about my work. I thank my family for all their love and continued support – without which I would not have been able to get to this point. Last, but certainly not least, I thank Joe. Whose support has never faltered, and whom I love with all my heart.

Table of Contents

Declaration 2
COVID-19 Impact Statement 3
Previous Communication of This Work 3
Abstract 4
Acknowledgements 6
List of figures 14
Chapter 1 14
Chapter 2 14
Chapter 3 16
Chapter 4 16
Chapter 5 22
List of tables 27
Chapter 1 27
Chapter 2 27
Chapter 3 27
Chapter 4 28
Chapter 5 29
Abbreviations 30
Introduction 33
1.1 The motivation behind this work 34
1.1.1 *Effects of rising CO_2 emissions* 34
1.2 Strategies to reduce CO_2 emissions 35
1.2.1 *Carbon capture* 35
1.2.2 *Carbon storage* 37
1.2.3 *Catalytic valorisation of captured CO_2* 38
1.2.4 *Carbon fixation in biological systems* 38
1.2.4.1 *Anaerobic Carbon fixation* 39
1.2.4.2 *Aerobic Carbon fixation* 40
1.2.4.3 *RuBisCO* 42
1.2.4.4 *Photoautotrophic organisms* 43
1.2.5 *Carbon assimilation by cyanobacteria* 43
1.2.5.1 *Carbon concentration by cyanobacteria* 44

1.3 Chapter overviews 45
Literature Review 47
2.1 Overview of cyanobacteria 48
2.1.1 *General characteristics of cyanobacteria* 48
2.2 Photosynthesis 49
2.2.1 *Capturing light energy* 51
2.2.2 *Photolysis of water* 52
2.2.3 *Electron transport chain* 53
2.2.4 *ATP synthesis* 53
2.3 Nitrogen fixation by cyanobacteria 54
2.3.1 *Cyanobacteria nitrogenases* 55
2.3.2 *The heterocyst* 57
2.4 Productivity of cyanobacteria 59
2.4.1 *Limitations of using cyanobacteria in large scale production* 59
2.4.2 *Measuring productivity in cyanobacteria* 63
2.5 Strategies to enhance the productivity of cyanobacteria 68
2.5.1 *Genetic tools for cyanobacteria* 68
2.5.2 *Engineering strategies to optimise cyanobacteria productivity* 69
2.5.2.1 *Expression of photosynthetic genes* 71
2.5.2.2 *Strain optimisation* 71
2.5.2.3 *RuBisCO engineering* 72
2.5.2.4 *Limitations of rational engineering strategies* 73
2.6 Adaptive Laboratory Evolution (ALE) 73
2.6.1 *Principles of ALE* 74
2.6.2 *Use of ALE to enhance productivity* 75
2.6.3 *Challenges of using ALE* 86
2.7 Implementing ALE 87
2.7.1 *Selecting an ALE objective* 87
2.7.2 *Cyanobacteria species selection* 88
2.7.2.1 *CO_2 fixation – Synechocystis sp. PCC 6803* 88
2.7.2.2 *N_2 fixation – Trichormus variabilis sp. ATCC 29413* 89
2.7.3 *ALE experimental design* 90
2.7.3.1 *Generating an optimal selective environment for ALE* 90
2.7.3.2 *Selecting a successful culturing strategy to increase cell growth* 90

2.7.3.3 *Determining selective parameters to enhance carbon flux* 93
2.7.3.4 *Adaptation to a controlled environment* 96
2.7.4 *Random Mutagenesis* 97
2.7.4.1 *Mutagens* 99
2.8 Isolation and characterisation of cyanobacteria 105
2.8.1 *Physical characterisation* 106
2.8.1.1 *Growth and biomass formation* 106
2.8.1.2 *Photosynthetic apparatus* 108
2.8.2 *Omic characterisation* 110
2.8.2.1 *Genomic characterisation* 110
2.8.2.2 *Metabolomic characterisation* 113
2.9 Aim and objectives 120
Materials and Methods 121
3.1 Growth and Experimental Media 122
3.1.1 *LB medium* 124
3.1.2 *BG-11 medium and variants* 124
3.1.3 *Antibiotic concentrations* 127
3.1.4 *SOC medium* 127
3.1.5 *General chemicals* 127
3.2 Molecular Biology Manipulations 128
3.2.1 *DNA Quantification* 128
3.2.2 *Plasmid extraction from E. coli* 129
3.2.3 *Genomic DNA extraction from cyanobacteria* 129
3.2.4 *Polymerase Chain Reaction (PCR)* 130
3.2.4.1 *PCR for cloning experiments* 130
3.2.4.2 *PCR for screening transformant colonies* 131
3.2.5 *Visualising DNA using agarose gel electrophoresis* 133
3.2.6 *Extracting DNA from agarose gels* 133
3.2.7 *Post PCR DNA clean-up* 133
3.2.8 *Nuclease restriction digestion of DNA* 134
3.2.9 *HiFi DNA Assembly* 134
3.2.10 *Generation of chemically competent E. coli cells* 136
3.2.11 *Genetic transformation procedures* 136
3.2.11.1 *Transformation of E. coli* 137
3.2.11.2 *Natural transformation of Synechocystis* 138

3.2.11.3 *Electroporation transformation of Synechocystis* 138
3.2.12 *Sanger sequencing analysis* 139
3.3 Cell characterisation 139
3.3.1 *Optical Density (OD)* 139
3.3.2 *Whole cell absorbance spectral analysis* 140
3.3.3 *Pigmentation characterisation* 140
3.3.4 *Clark electrode analysis of oxygen evolution* 141
3.3.5 *ALE isolate 24-well plate screening* 142
3.3.5.1 *Synechocystis Δhox chemostat 24-well plate screening* . 143
3.3.5.2 *Trichormus variabilis mixotrophic 24-well plate screening* 143
3.3.5.3 *Trichormus variabilis autotrophic 24-well plate screening* 143
3.3.6 *Measuring biomass* 143
3.4 Adaptive Laboratory Evolution of cyanobacteria 144
3.4.1 *Chemical mutagenesis of cyanobacteria* 144
3.4.1.1 *Chemical mutagenesis of Synechocystis* 144
3.4.1.2 *Chemical mutagenesis of Trichormus variabilis* 145
3.4.2 *UV mutagenesis of Synechocystis* 146
3.4.3 *Selection of enhanced Synechocystis strains* 146
3.4.3.1 *Multi-cultivator selection* 146
3.4.3.2 *Chemostat selection* 147
3.4.4 *Selection of enhanced Trichormus variabilis strains* 148
3.4.4.1 *Chemostat ALE with mixotrophic selection* 149
3.4.4.2 *Chemostat ALE with autotrophic selection* 149
3.4.5 *Strain consortia analysis* 150
3.4.5.1 *Consortia identification* 150
3.4.5.2 *Isolation of individual microorganisms from the consortia* 150
3.4.5.3 *Assessing Consortia impact on growth* 151
3.5 Genomic characterisation 151
3.5.1 *Genomic sequencing* 151
3.5.2 *Sequence assembly* 152
3.6 Metabolomic characterisation 152
3.6.1 *Growth conditions* 152
3.6.2 *Metabolomic extractions* 153
3.6.3 *Mass spectroscopy* 153

3.6.4 *Untargeted metabolomic data analysis* 154

Adaptive laboratory evolution to enhance carbon fixation 156

4.1 Experimental design 157

4.2 Mutagenesis of *Synechocystis* 157

4.2.1 *EMS mutagenesis in Synechocystis* 158

4.2.2 *UV mutagenesis in Synechocystis* 161

4.3 Multi-cultivator ALE to generate strains with improved carbon fixation in *Synechocystis.* 163

4.3.1 *Serial dilution: Synechocystis strain selection* 163

4.3.2 *Serial dilution: Synechocystis isolate characterisation* 166

4.3.2.1 *Measuring growth and biomass yields from individual MC strains* 166

4.3.2.2 *Determination of growth rate in the four MC strains with the highest biomass* 169

4.3.2.3 *Evaluation of photosynthetic efficiency in the MC strains* 171

4.3.3 *Evaluation of the serial dilution ALE Strategy* 173

4.4 Chemostat ALE of *Synechocystis* Δ*hox* 174

4.4.1 *Strategy overview* 174

4.4.2 *ALE selection based on electron sinks in the Synechocystis cell* 175

4.4.3 *Selection of Synechocystis Δhox strains in a chemostat* 181

4.4.4 *Characterisation of the individual Synechocystis Δhox strains isolated from the Chemostat* 182

4.5 Phenotypic characterisation of *Synechocystis* Δ*hox* strains isolated from the chemostat 182

4.5.1 *Measuring biomass yields from the Synechocystis Δhox strains isolated from the chemostat* 182

4.5.1.1 *Atmospheric CO_2 biomass yields from the Synechocystis Δhox strains isolated from the chemostat* 184

4.5.1.2 *Saturated CO_2 biomass yields from the Synechocystis Δhox strains isolated from the chemostat* 187

4.5.1.3 *Further Synechocystis Δhox strain growth characteristics* 192

4.5.2 *Measuring growth rates of Syn.1.11 and Syn.1.19* 195

4.5.3 *Measuring photosynthetic efficiency in the ALE strains* 203

4.6 Genomic and Metabolomic analysis of the best performing *Synechocystis* (Syn.Δ*hox*) isolates 211

4.6.1 *Genotypic characterisation of strain Syn.1.11* 211

4.6.2 *Metabolomic characterisation of Syn.1.11 and Syn.1.19*..... 215
4.7 Reintegration of *hox* operon into Syn.1.11 and Syn.1.19..... 224
4.7.1 *pGEM-hox reintegration construct*..... 225
4.7.2 *pGEM-T hox construct assembly* 226
4.8 Discussion 227
Adaptive laboratory evolution to enhance nitrogen fixation..... 231
5.1 Experimental design 232
5.1.1 *Identifying strategies to select for enhanced nitrogen fixation*232
5.1.2 *Strategy overview*..... 233
5.2 Mutagenesis of *Trichormus variabilis* 235
5.2.1 *EMS mutagenesis in Trichormus variabilis*..... 236
5.3 Chemostat ALE of *Trichormus variabilis* 237
5.3.1 *Trichormus variabilis strain selection*..... 237
5.3.2 *Isolation of individual Trichormus variabilis strains*..... 238
5.4 *Trichormus variabilis* strain isolation & consortia identification 239
5.4.1 *Measuring biomass yields* 239
5.4.2 *Trichormus variabilis Ava.A.2.20 consortia isolation* 245
5.4.2.1 *Identification of the Ava.A.2.20 microbial consortia*..... 248
5.4.2.2 *Isolation of Trichormus variabilis A.2.20 from consortia*.. 257
5.4.3 *Evaluation of the impact of the microbial consortia upon growth of wildtype Trichormus variabilis* 259
5.4.4 *Measuring the photosynthetic efficiency of Ava.A.2.20 and Ava.A.2.20.P* 268
5.5 Genomic and metabolomic characterisation of the *Trichormus variabilis* isolate Ava.A.2.20.P 273
5.5.1 *Genome analysis of the axenic Trichormus variabilis Ava.A.2.20.P* 273
5.5.2 *Metabolomic characterisation of the isolate Trichormus variabilis* 276
5.6 Evaluating the impact of fructose supplementation on the selection process 278
5.6.1 *Trichormus variabilis autotrophic strain selection* 278
5.6.2 *Trichormus variabilis strain isolation following autotrophic selection* 281
5.6.3 *Measuring biomass yields* 282
5.6.4 *Specific impact of fructose supplementation* 284

5.7 Discussion 285
General discussion and future work 289
6.1 General discussion 290
6.1.1 *ALE to increase carbon fixation* 290
6.1.1.1 *Culturing strategy for increased carbon fixation* 291
6.1.1.2 *Coupling selective environment pressures with engineered strains* 291
6.1.1.3 *Characterising mutant Synechocystis phenotypes* 292
6.1.2 *ALE to increase nitrogen fixation* 294
6.1.2.1 *Potential additive effects of a consortium* 295
6.2 Conclusions 296
6.3 Future work 297
6.3.1 *Continued Characterisation* 297
6.3.2 *Strategy Optimisation* 298
6.3.3 *Optimising Expression* 299
6.4 Plans for Dissemination 299
References 300
Appendices 359

List of figures

Chapter 1

Figure 1.1 | Simplified graphic of strategies for carbon concentration post-combustion.

Figure 1.2 | Schematic view of the CB cycle reactions, taken from BioRender.com.

Figure 1.3 | Simplified schematic showing a cyanobacteria showing inorganic carbon transporters and carboxysome. (Adapted from Price 2011).

Chapter 2

Figure 2.1 | Morphology of the cyanobacteria; (Images taken from Keweenaw Freshwater Algae, 2020). Transmission electron microscopy (TEM) section of *Synechocystis* sp. PCC 6803 showing the internal concentric thylakoid membrane. (Image courtesy of Dr Edward Spence, University of Nottingham).

Figure 2.2 | Simplified routes of light driven electron and proton transport within cyanobacterial thylakoid membrane. Taken from Govindjee and Shevela 2011, (adapted from original of Messinger and Shevela 2011).

Figure 2.3 | Schematic representation of a cyanobacteria PBS light harvesting complex attached to PSII. (Adapted from Shevela *et al*. 2023).

Figure 2.4 | Simplified schematic of an F-type ATP synthase (ATPase). (Adapted from Nishi and Forgac 2002).

Figure 2.5 | Schematic representation of the MoFe nitrogenase and associated metal-cofactors. (taken from Jimenez-Vicente et al. 2018).

Figure 2.6 | Heterocyst metabolism and nitrogen fixation (taken from Böhme 1998).

Figure 2.7 | Simplified overview of engineering targets to enhance growth and productivity in cyanobacteria (taken from Zhou *et al*. 2016).

Figure 2.8 | Overview of ALE strain selection workflow (Taken from Shepelin *et al*. 2018).

Figure 2.9 | Diagram showing the different aims of laboratory evolution experiments, taken from Sandberg *et al*. 2019.

Figure 2.10 | Adaptive Laboratory Evolution studies listed in **Table 2.4** by publication date.

Figure 2.11 | Overview of commonly used ALE strategies (created with BioRender.com).

Figure 2.12 | Overview of potential targets for an ALE to enhance carbon fixation in cyanobacteria. (Created with BioRender.com).

Figure 2.13 | Schematic showing the effects of non-synonymous base pair substitutions, nucleotide insertions and deletions on mRNA transcripts and amino acid sequences (taken from Cotner and Wassenburg, 2020).

Figure 2.14 | Schematic overview of a next-generation genomic analysis workflow, with primary, secondary, and tertiary analysis stages highlighted in respective colours. Taken from Pereira et al. 2020.

Figure 2.15 | Visualisation of an untargeted metabolomics experimental workflow in cyanobacteria, showing key steps (created with BioRender.com).

Chapter 3

Figure 3.1 | Configuration of a culture tube used in ALE within a Multi-Cultivator MC 1000-OD (Photon Systems Instruments™, Czechia). (Created with BioRender.com).

Figure 3.2 | 500 mL MicroCarrier Spinner Flask (Bellco™) configured into a chemostat photobioreactor. (Created with BioRender.com).

Chapter 4

Figure 4.1 | Absolute colony forming units $x10^{5} \cdot mL^{-1}$ of *Synechocystis* prior to chemical mutagenesis sample processing (untreated), and after processing (treated) without mutagenesis.

Figure 4.2 | **A.** Kill curve assessing *Synechocystis* cell viability (%) following ethyl methanesulfonate (EMS) treatment.

Figure 4.3 | Absolute colony forming units $x10^{5} \cdot mL^{-1}$ of *Synechocystis* prior to UV mutagenesis sample processing (untreated), and after processing (treated) without mutagenesis.

Figure 4.4 | **A.** Kill curve demonstrating cell viability (%) following ultra-violet (UV) treatment.

Figure 4.5 | Overview of multi-cultivator ALE experimental design. (Created with BioRender.com).

Figure 4.6 | Selection method for selecting individual colonies isolated from the ALE. (Created with BioRender.com).

Figure 4.7 | Biomass screening workflow of the individual strains. (Created with BioRender.com).

Figure 4.8 | **A.** Biomass (dry cell weight (DCW) $mg \cdot mL^{-1}$) from 10 mL of isolated cultures (Mutants) and Syn.GT grown at 200 µmol photons$\cdot m^{-2} \cdot sec^{-1}$, 30 °C, for 72 hours in BG-11 liquid media. **B.** Frequency distribution of the DCW value from the mutant strains and Syn.GT.

Figure 4.9 | Comparison of the growth of isolates MC.Syn.1, MC.Syn.2, MC.Syn.3, and MC.Syn.6, with Syn.GT. Grown at 200 µmol photons$\cdot m^{-2} \cdot sec^{-1}$, 30 °C, 150 RPM orbital shaking.

Figure 4.10 | Dry cell weights and specific growth rate of multi-cultivator isolates and Syn.GT.

Figure 4.11 | Rates of oxygen evolution in *Synechocystis* GT (Syn.GT), and MC.Syn.6 over increasing light intensities at 30 °C measured using a Clark electrode.

Figure 4.12 | Assembled and functioning chemostat system.

Figure 4.13 | Simplified schematic summarising the transfer of light energy to allow for the fixation of carbon dioxide into glucose in the cell.

Figure 4.14 | Simplified schematic summarising the electron use per reaction of selected electron sinks in *Synechocystis*. (Created with BioRender.com).

Figure 4.15 | Workflow for the combined physical and chemical mutagenesis strategy to generate a diverse population library. (Created with BioRender.com).

Figure 4.16 | Chemostat isolate screening strategy. (Created with BioRender.com).

Figure 4.17 | Dry cell weights from 24-well plate screened isolates at 300 µmol photons·m^{-2}·sec^{-1}, 30 °C, 120 hours, in BG-11NH_4 liquid media.

Figure 4.18 | Proportional frequency of *Synechocystis Δhox* chemostat isolates dry cell weight yields from 24-well plate isolates at 300 µmol photons·m^{-2}·sec^{-1}, 30 °C, 120 hours, in BG-11NH_4 liquid media.

Figure 4.19 | Dry cell weights from 24-well plate screened isolates at 300 µmol photons·m^{-2}·sec^{-1}, 30 °C, 120 hours, 1.5% CO_2, in BG-11NH_4 liquid media.

Figure 4.20 | Proportional frequency of dry cell weight yields from 24-well plate *Synechocystis Δhox* chemostat isolate screening at 300 µmol photons·m^{-2}·sec^{-1}, 30 °C, 120 hours, 1.5% CO_2 supplementation, in BG-11NH_4 liquid media.

Figure 4.21 | Distribution of all individual dry cell weight yields from 24-well plate isolate screening at 300 µmol photons·m^{-2}·sec^{-1}, 30 °C, 120 hours, 1.5% CO_2 supplementation, in BG-11NH_4 liquid media.

Figure 4.22 | Dry cell weights from 24-well plate screened isolates that showed significant ($p < 0.05$) intraspecific differences in growth at 300 µmol photons·m^{-2}·sec^{-1}, 30 °C, 120 hours, in BG-11NH_4 liquid media and screening under ambient CO_2, or with 1.5% CO_2 supplementation.

Figure 4.23 | Culture flasks of *Synechocystis* (Syn.*Δhox*) strains showing settling after 7 days.

Figure 4.24 | Comparison of the growth of isolates Syn.1.11 and Syn.1.19, compared to Syn.*Δhox* in BG-11NH_4 liquid media, grown at 300 µmol photons·m^{-2}·sec^{-1}, 30 °C, 150 RPM orbital shaking. **A.** Growth curve of cultures. **B.** Specific growth rates of cultures.

Figure 4.25 | Comparison of the growth of isolates Syn.1.11 and Syn.1.19, compared to Syn.*Δhox* in nitrate BG-11 liquid media, grown at 300 µmol photons·m^{-2}·sec^{-1}, 30 °C, 150 RPM orbital shaking. **A.** Growth curve of cultures. **B.** Specific growth rates of cultures.

Figure 4.26 | Comparison of the growth of isolates Syn.1.11 and Syn.1.19, compared to Syn.*Δhox* in BG-11NH_4 liquid media supplemented with 10 mM glucose, grown at 300 µmol photons·m^{-2}·sec^{-1}, 30 °C, 150 RPM orbital shaking. **A.** Growth curve of cultures. **B.** Specific growth rates of cultures.

Figure 4.27 | Comparison of the growth of isolates Syn.1.11 and Syn.1.19, compared to Syn.*Δhox* in BG-11NH_4 liquid media supplemented with 10 mM HCO_3^-, grown at 300 µmol photons·m^{-2}·sec^{-1}, 30 °C, 150 RPM orbital shaking. **A.** Growth curve of cultures. **B.** Specific growth rates of cultures.

Figure 4.28 | Comparison of the growth of isolates Syn.1.11 and Syn.1.19, compared to Syn.*Δhox* and Syn.GT in BG-11NH_4 liquid media supplemented with 1.5% CO_2, grown at 300 µmol photons·m^{-2}·sec^{-1}, 30 °C, 150 RPM orbital shaking.

Figure 4.29 | Comparison of μ_{max} of isolates Syn.1.11 and Syn.1.19, compared to Syn.*Δhox* and Syn.GT in BG-11NH_4 liquid media supplemented with 1.5% CO_2, grown at 300 µmol photons·m^{-2}·sec^{-1}, 30 °C, 150 RPM orbital shaking.

Figure 4.30 | *N*,*N*-Dimethylformamide pigment extraction absorbance spectra, normalized to OD_{750nm}, and standardised to dry cell weights of Syn.GT, Syn.*Δhox*, Syn.1.11, and Syn.1.19, grown at 300 µmol photons·m^{-2}·sec^{-1}, 30 °C, 1.5% CO_2.

Figure 4.31 | Comparison of chlorophyll concentrations (μg·mL^{-1}) of Syn.1.11 and Syn.1.19, compared to Syn.*Δhox* and Syn.GT in BG-11NH$_4$ liquid media supplemented with 1.5% CO_2, grown at 300 μmol photons·m^{-2}·sec^{-1}, 30 °C, 150 RPM orbital shaking.

Figure 4.32 | Chlorophyll concentrations in *Synechocystis* strains Syn.GT, Syn.*Δhox*, Syn.1.11, and Syn.1.19 grown at 300 μmol photons·m^{-2}·sec^{-1}, 30 °C, 1.5% CO_2.

Figure 4.33 | Carotenoid concentrations of *Synechocystis* strains Syn.GT, Syn.*Δhox*, Syn.1.11, and Syn.1.19 grown at 300 μmol photons·m^{-2}·sec^{-1}, 30 °C, 1.5% CO_2.

Figure 4.34 | Rates of oxygen evolution in *Synechocystis* sp. PCC 6803 *Δhox* (Syn.*Δhox*), and Syn.1.11 over increasing light intensities at 30 °C measured using a Clark electrode.

Figure 4.35 | Rates of oxygen evolution in *Synechocystis* sp. PCC 6803 *Δhox* (Syn.*Δhox*), and Syn.1.19 over increasing light intensities at 30 °C measured using a Clark electrode.

Figure 4.36 | Putative interactions of identified genes with significant variation, (created using STRING v.12)

Figure 4.37 | PCA scores plot comparing untargeted metabolomic analyses of Syn.*Δhox*, Syn.GT, Syn.1.11, and Syn.1.19 grown at 300 μmol photons·m^{-2}·sec^{-1}, 30 °C, 1.5% CO_2 after 2 days of growth.

Figure 4.38 | OPLS-DA model comparing the untargeted metabolomic analyses of Syn.*Δhox* and Syn.1.11, grown at 300 μmol photons·m^{-2}·sec^{-1}, 30 °C, 1.5% CO_2 after 2 days of growth.

Figure 4.39 | Permutation test of OPLS-DA model Syn.*Δhox* variables comparing the untargeted metabolomic analyses of Syn.*Δhox* and Syn.1.11 grown at 300 µmol photons·m^{-2}·sec^{-1}, 30 °C, 1.5% CO_2 after 2 days of growth.

Figure 4.40 | Permutation test of OPLS-DA model Syn.1.11 variables comparing the untargeted metabolomic analyses of Syn.*Δhox* and Syn.1.11 grown at 300 µmol photons·m^{-2}·sec^{-1}, 30 °C, 1.5% CO_2 after 2 days of growth.

Figure 4.41 | PCA scores comparing untargeted metabolomic analyses of Syn.*Δhox*, Syn.GT, Syn.1.11, and Syn.1.19 grown at 300 µmol photons·m^{-2}·sec^{-1}, 30 °C, 1.5% CO_2 after 4 days of growth.

Figure 4.42 | PCA scores comparing untargeted metabolomic analyses of Syn.*Δhox*, Syn.GT, Syn.1.11, and Syn.1.19 grown at 300 µmol photons·m^{-2}·sec^{-1}, 30 °C, 1.5% CO_2 after 6 days of growth.

Figure 4.43 | PCA scores comparing untargeted metabolomic analyses of Syn.*Δhox*, Syn.GT, Syn.1.11, and Syn.1.19 with outlier Syn.1.19 removed, grown at 300 µmol photons·m^{-2}·sec^{-1}, 30 °C, 1.5% CO_2 after 6 days of growth.

Figure 4.43 | Heatmap showing changes in relative (Log2 Fold) abundance of selected metabolites after 4 days of growth at 300 µmol photons·m^{-2}·sec^{-1}, 30 °C, 1.5% CO_2.

Figure 4.44 | The pGEM-T *hoxEFUYH* integration construct (assembled in SnapGene™).

Figure 4.45 | Assembly of pGEM-T *hox*. DNA marker Gene Ruler 1 kb plus (Fisher Scientific™) **A.** Amplification of upstream and downstream regions. **B.** Amplification of *cmpR*. **C.** Amplification of *hoxEFUYH* operon.

Chapter 5

Figure 5.1 | Simplified schematic of possible electron flow to the nitrogenase within a cyanobacteria heterocyst (taken from Magnuson 2019, originally adapted from Magnuson and Cardona 2016)

Figure 5.2 | Workflow for the combined physical and chemical mutagenesis strategy to generate a diverse population library. (Created with BioRender.com).

Figure 5.3 | **A.** Kill curve assessing *Trichormus variabilis* cell viability (%) following ethyl methanesulphonate (EMS) treatment and proportion of combined viable populations from each EMS treatment.

Figure 5.4 | Single colony plating strategy used to isolate individual *Trichormus variabilis* (Ava.WT) chemostat mutants. (Created with BioRender.com).

Figure 5.5 | Dry cell weights from 24-well plate screened isolates at 300 µmol photons·m^{-2}·sec^{-1}, 30 °C, 120 hours, in BG-11_0 liquid media.

Figure 5.6 | Proportional frequency of dry cell weight yields from 24-well plate isolates at 300 µmol photons·m^{-2}·sec^{-1}, 30 °C, 120 hours, in BG-11_0 liquid media.

Figure 5.7 | Distribution of all individual dry cell weight yields from 24-well plate isolates at 300 µmol photons·m^{-2}·sec^{-1}, 30 °C, 120 hours, in BG-11_0 liquid media.

Figure 5.8 | Dry cell weights from 24-well plate screened isolates at 300 µmol photons·m^{-2}·sec^{-1}, 30 °C, 120 hours, in BG-11_0A liquid media.

Figure 5.9 | Proportional frequency of dry cell weight yields from 24-well plate isolates at 300 µmol photons·m^{-2}·sec^{-1}, 30 °C, 120 hours, in BG-11_0A liquid media.

Figure 5.10 | DCWs from 24-well plate screened Ava.A.Mutant isolates compared to Ava.WT grown at 300 µmol photons·m^{-2}·sec^{-1}, 30 °C, 120 hours, in BG-11_0 liquid media – with, and without 10 mM fructose supplementation.

Figure 5.11 | Diminished structural integrity of chemostat components requiring improvised repairs.

Figure 5.12 | Colony morphology of Ava.A.2.20 streaked for single colonies on LB solid media.

Figure 5.13 | Strategy to elicit distinct consortia phenotypes. (Created with BioRender.com).

Figure 5.14 | Phenotypic variation of the axenic isolates on LB solid media following repeated 4 °C incubation treatment. **A.** Consortia isolate LB3, putative genus *Pseudoxanthnomonas*. **B.** Consortia isolate LB5, putative genus *Achromobacter*. **C.** Consortia isolate LB6, putative genera *Rhizobium* / *Agrobacterium*.

Figure 5.15 | Phylogenetic tree of Ava.A.2.20 LB3 consortia isolate based on the 16S rRNA gene sequence. (Created with iTOL.embl.de)

Figure 5.16 | Phylogenetic tree of the Ava.A.2.20 LB5 consortia isolate based on the 16S rRNA gene sequence. (Created with iTOL.embl.de)

Figure 5.17 | Phylogenetic tree of Ava.A.2.20 LB6 consortia isolate based on the 16S rRNA gene sequence. (Created with iTOL.embl.de)

Figure 5.18 | Growth profiles of Ava.WT, and Ava.WT inoculated with LB3, LB5, and LB6, grown at 300 µmol photons·m^{-2}·sec^{-1}, 30 °C for 18 days. **A.** Optical density measurements (OD_{750nm}). **B.** Chlorophyll concentrations (µg·mL^{-1}).

Figure 5.19 | Growth profiles of Ava.WT, and Ava.WT inoculated with LB3,5, LB3,6, and LB5,6, grown at 300 µmol photons·m^{-2}·sec^{-1}, 30 °C for 18 days. **A.** Optical density measurements (OD_{750nm}). **B.** Chlorophyll concentrations (µg·mL^{-1}).

Figure 5.20 | Growth profiles of Ava.WT, Ava.WT inoculated with LB3, 5, and 6, and Ava.A.2.20, grown at 300 µmol photons·m^{-2}·sec^{-1}, 30 °C for 18 days. **A.** Optical density measurements (OD_{750nm}). **B.** Chlorophyll concentrations (µg·mL^{-1}).

Figure 5.21 | Dry weights of cultures of Ava.WT, Ava.WT inoculated with different combinations of the consortia isolates, and Ava.2.20 grown for 16 days at 300 µmol photons·m^{-2}·sec^{-1}, 30 °C. Dry weight is shown by its source, supernatant or whole cell pellet.

Figure 5.22 | Ratio of recorded estimated chlorophyll concentrations (µg·mL^{-1}) of Ava.WT and Ava.A.2.20 to equivalent recorded OD_{750nm} measurements.

Figure 5.23 | Biofilm formation on triplicates of *Trichormus variabilis* cultures grown in $BG\text{-}11_0$ for 96-hours, at 300 µmol photons·m^{-2}·sec^{-1}, 30 °C. **A.** Ava.WT. **B.** Ava.WT with consortia. **C.** Ava.2.20.

Figure 5.24 | Specific growth rates (h^{-1}) of Ava.WT, Ava.A.2.20.P, Ava.WT with consortia, and Ava.A.2.20 from samples taken between days 1 and 2 of growth at 300 µmol photons·m^{-2}·sec^{-1}, 30 °C, 1.5% CO_2. **A.** Specific growth rates estimated using optical density. **B.** Specific growth rates estimated using chlorophyll concentration.

Figure 5.25 | Growth profiles of Ava.WT, Ava.A.2.20.P, Ava.WT inoculated with LB3,5,6, and Ava.A.2.20 grown at 300 µmol photons·m^{-2}·sec^{-1}, 30 °C, 1.5% CO_2. **A.** Optical density measurements (OD_{750nm}). **B.** Chlorophyll concentrations (µg·mL^{-1}).

Figure 5.26 | *N*,*N*-Dimethylformamide pigment extraction absorbance spectra (normalized to OD_{750nm}) of Ava.WT, Ava.A.2.20.P, Ava.WT with LB3, 5, and 6, and Ava.A.2.20, extracted on days **A.** 2, **B.** 4, **C.** 6 of growth at 300 µmol photons·m^{-2}·sec^{-1}, 30 °C, 1.5% CO_2.

Figure 5.27 | Chlorophyll concentrations of *Trichormus variabilis* strains Ava.WT, Ava.A.2.20.P, and *Trichormus variabilis* strains with consortia Ava.WT LB3,5,6, and Ava.A.2.20, grown at 300 µmol photons·m^{-2}·sec^{-1}, 30 °C, 1.5% CO_2.

Figure 5.28 | Carotenoid concentrations of *Trichormus variabilis* strains Ava.WT, Ava.A.2.20.P, and *Trichormus variabilis* strains with consortia Ava.WT LB3,5,6, and Ava.A.2.20, grown at 300 µmol photons·m^{-2}·sec^{-1}, 30 °C, 1.5% CO_2.

Figure 5.29 | Photoinhibition curve of *Trichormus variabilis* strains Ava.WT and Ava.A.2.20.P.

Figure 5.30 | PCA model comparing untargeted metabolomic analyses of Ava.WT, Ava.A.2.20.P, Ava.WT inoculated with LB3, LB5, LB6, and Ava.A.2.20 grown at 300 µmol photons·m^{-2}·sec^{-1}, 30 °C, 1.5% CO_2 after 2 days of growth.

Figure 5.31 | Dry cell weights (mg·mL^{-1}) from 24-well plate screened Ava.B population libraries, sampled from chemostat spent media every 2-3 days, at 300 µmol photons·m^{-2}·sec^{-1}, 30 °C, 144 hours, in $BG\text{-}11_0$ liquid media.

Figure 5.32 | Distribution of dry cell weight measurements ($mg \cdot mL^{-1}$) across Ava.B chemostat time sampling quartiles, grown at 300 µmol photons$\cdot m^{-2} \cdot sec^{-1}$, 30 °C, 144 hours, in BG-11_0 liquid media.

Figure 5.33 | Dry cell weights ($mg \cdot mL^{-1}$) from *Trichormus variabilis* (Ava.B) mutant isolate screening. Plates grown at 300 µmol photons$\cdot m^{-2} \cdot sec^{-1}$, 30 °C, 120 hours, in BG-11_0 liquid media.

Figure 5.34 | Combined dry cell weights of all Ava. WT and mutant samples screened in BG-11_0 liquid media in 24-well plates, grown at 300 µmol photons$\cdot m^{-2} \cdot sec^{-1}$, 30 °C, 120 hours – in both chemostat experiments.

List of tables

Chapter 1

Table 1.1 | Overview of known natural carbon fixation pathways.

Chapter 2

Table 2.1 | Current challenges and research gaps in optimising cyanobacteria productivity

Table 2.2 | Strategies to assess fixation of CO_2 and / or N_2 in cyanobacteria

Table 2.3 | Overview of selected heterologous overexpression strategies used to improve growth and CO_2 fixation of cyanobacteria.

Table 2.4 | Studies investigating application of ALE to enhance growth and / or substrate utilisation, 1991 - 2023, (adapted from previous work by Sandberg et al. 2019).

Table 2.5 | List of chemical, physical, and biological agents for random mutagenesis strategies.

Chapter 3

Table 3.1 | Bacterial strains used in this study.

Table 3.2 | Composition of BG-11 liquid medium.

Table 3.3 | Composition of BG-11_0 liquid media variants.

Table 3.4 | Woking concentrations of antibiotics by organism studied.

Table 3.5 | Plasmids used in this study.

Table 3.6 | Cloning PCR reaction components.

Table 3.7 | Cloning PCR thermocycler protocol.

Table 3.8 | cPCR reaction components.

Table 3.9 | cPCR thermocycler protocol.

Table 3.10 | Restriction digestion reaction components.

Table 3.11 | HiFi oligo PCR thermocycler protocol.

Table 3.12 | HiFi assembly reaction components.

Table 3.13 | Heat shock transformation thermocycler protocol.

Chapter 4

Table 4.1 | Top non-synonymous genomic variations between Syn.1.11 and Syn.*Δhox* by combined sequences read confidence (P-value). Annotations transferred from RefSeq NC_000911 *Synechocystis* sp. PCC 6803 (NCBI).

Table 4.2 | Significantly different metabolites of Syn.1.11 compared to Syn.*Δhox* from samples grown at 300 µmol photons·m^{-2}·sec^{-1}, 30 °C, 1.5% CO_2, during early exponential, late exponential, and stationary phase.

Table 4.3 | Significantly different metabolites of Syn.1.19 compared to Syn.*Δhox* from samples grown at 300 µmol photons·m^{-2}·sec^{-1}, 30 °C, 1.5% CO_2, during early exponential, late exponential, and stationary phase.

Chapter 5

Table 5.1 | Antibiotic concentrations of BG-11_0 plates used to screen for antimicrobial sensitivity of the Ava.A.20 strain and the consortia.

Table 5.2 | μ_{max} of Ava.WT, Ava.WT with different combinations of consortia inoculated, and Ava.A.2.20 in BG-11_0, at 300 µmol photons·m^{-2}·sec^{-1}, 30 °C.

Table 5.3 | Top non-synonymous genomic variations between Ava.WT and Ava.A.2.20.P by combined sequences read confidence (P-value). Annotations transferred from RefSeq NC_007413 *Trichormus variabilis* ATCC 29413 (NCBI).

Abbreviations

°C	Degrees Celsius
µL	Microlitre(s)
ALE	Adaptive Laboratory Evolution
ANOVA	Analysis of Variance
ATP	Adenosine triphosphate
BG-11	Blue-green medium 11
bp	Base pair(s)
CB	Calvin-Benson
CCS	Carbon Capture and Storage
CFC	Chlorofluorocarbons
CFU	Colony Forming Unit
Chl-*a*	Chlorophyll-*a*
Cit^+	Citrate metabolising
CO_2	Carbon dioxide
cPCR	Colony polymerase chain reaction
cyt b_6f	Cytochrome b_6f
DCW	Dry cell weight
$ddMS^2$	Data dependent tandem mass spectrometry
dH_2O	Deionised water
DMF	*N*-*N*-Dimethlyformamide
DNA	Deoxyribonucleic acid
DOM	Dissolved organic matter
EDTA	Ethylene Diamine Tetra Acetic acid
EMS	Ethyl Methane Sulphonate
EPS	Exopolysaccharides
ETC	Electron Transport Chain
Fd	Ferredoxin
FNR	Ferredoxin-$NADP^+$ reductase
g	Gram(s)
GHG	Greenhouse Gas

gTME	Global transcriptional machinery engineering
H_2	Hydrogen gas
HEPES	4-(2-hydroxyethyl)-1-piperazineethanesulfonic acid
Hox	Bidirectional NiFe-hydrogenase enzyme
HiFi	High fidelity
kb	Kilobase(s)
LB	Lysogeny broth
LC-MS	Liquid Chromatography-Mass Spectrometry
LTEE	Long-term evolution experiment
MC	Multi-cultivator
MNNG	methyl-*N*-nitro-*N*-nitrosoguanidine
mRNA	Messenger ribonucleic acid
MSC	Microbial Safety Cabinet
NADPH	Nicotinamide adenine dinucleotide phosphate (reduced form)
NO_x	Nitrogen oxides
nm	Nanometre(s)
OD	Optical density
OEC	Oxygen Evolving Centre
OPLS-DA	Orthogonal partial least squares-discriminant analysis
PBS	Phycobilisome
PCR	Polymerase chain reaction
PEP	Phosphoenolpyruvate
PHB	Poly hydroxybutyrates
PPP	Pentose Phosphate Pathway
PSI	Photosystem I
PSII	Photosystem II
PTM	Post transcriptional modifications
PQ	Plastoquinone

PQH_2	Plastoquinol
QC	Quality Control
RET	Resonance Energy Tranfer
RNA	Ribonucleic acid
ROS	Reactive Oxygen Species
RPM	Revolutions per minute
RT	Retention time
RuBP	Ribulose-1,5-BisPhosphate
SD	Standard Deviation
SNP	Single Nucleotide Polymorphism
SOC	Super Optimal broth with Catabolite repression
TCA	Tricarboxylic Acid
UHPLC	Ultra-High-Pressure Liquid Chromatography
UV	Ultraviolet
VIP	Variable importance in projection
WLP	Wood-Ljungdahl pathway
WT	Wild-Type

Chapter 1.

Introduction

1.1 The motivation behind this work

In 2020 global temperatures had risen on average by 1.09 °C compared to pre-industrial levels [1], with cumulative emissions of 1.7 trillion tonnes of carbon dioxide (CO_2), 74.73% of total greenhouse gas (GHG) emissions [2]. To achieve the 1.5 °C warming scenario laid out by the Intergovernmental Panel on Climate Change in the 2015 Paris Agreement [3], effective carbon capture and storage (CCS) are essential [4]. Over 120 Gt of carbon must be captured between now and 2050 to realistically achieve these warming targets [5]. Cyanobacteria are photosynthetic prokaryotes, capable of using CO_2 as the sole carbon source, and therefore are an attractive chassis for carbon capture and CO_2 valorisation [6]. However, there are still several challenges which need to be addressed, these include limited biomass productivity, low product titres and scaling from bench to industrial scale. Productivity is often limited by the allocation of resources inside the cell, and the need to drive more metabolic flux towards light harvesting, and carbon fixation [7,8].

Therefore, the development of strategies to engineer strains with enhanced autotrophic substrate utilisation rates (which may lead to increases in sustainable productivity) are essential for cyanobacteria to be a viable carbon capture and valorisation technology.

1.1.1 *Effects of rising CO_2 emissions*

CO_2 is the most abundant GHG produced through human activity [2]. CO_2 and other GHGs trap heat when infrared radiation from the Sun passes through the Earth's atmosphere and is prevented from reflecting into space via absorption [9]. As the concentration of GHGs in the atmosphere increases, a greater proportion of infrared radiation remains trapped, and the Earth's temperature increases relative to that compound's GHG radiative forcing. Radiative forcing is a metric to compare the relative impact of different GHGs on changes to the Earth's temperature [9,10]. The effective radiative forcing of CO_2 is the highest of all GHGs at 3.75 $W \cdot m^{-2}$, 6.7-fold higher than methane (0.54 $W \cdot m^{-2}$), and 8.8-fold higher than chlorofluorocarbons (CFCs) (0.408 $W \cdot m^{-2}$) [11]. The enormous scale of CO_2 emissions is what makes its contribution to rising global temperatures so significant, despite other GHGs such as CFCs having a relatively larger impact per molecule released [12]. However, it is within our power to actively reduce anthropogenic GHG emissions, with CFC emissions having been

significantly reduced following their co-ordinated phase out after the signing of the Montreal Protocol in 1989, with new emissions prohibited since 2010 [13]. This clearly demonstrates what can be achieved to reduce GHG emissions, preventing an ecologically disastrous scenario (see Newman *et al*. 2009) [14]. It is essential that we implement the same co-ordinated approach to decarbonise our global economy.

1.2 Strategies to reduce CO_2 emissions

1.2.1 *Carbon capture*

One solution to reducing CO_2 emissions is the use of Carbon Capture and Storage (CCS) at the point of the emission source. This has the benefit of ensuring that emissions are not released into the atmosphere. While several different technologies have been used to achieve this, on site carbon capture is typically carried out in one of 3 ways: post-combustion, pre-combustion, or by oxy-fuel combustion [15].

A pre-combustion strategy first removes carbon from a combustion gas (thus requiring gasification of solid fuels) – here by the formation of syngas, a mixture of hydrogen and carbon monoxide [16]. First, particulate matter is removed, and the natural gas treated with steam and a nickel catalyst to remove the sulphur [16]. The syngas is then hydrated with steam to create a mixture of CO_2 and H_2, from which the CO_2 is captured and the H_2 used as a 'clean' alternative fuel [16]. For oxy-fuel combustion, oxygen is first separated from nitrogen in air using either cryogenic or membrane separation [17]. The resulting waste stream consists of mostly CO_2 and water, where the water is removed by condensation. Prior to CO_2 separation, NO_x, dust, and sulphur oxides are first removed from the flue gas mixture [15]. These are typically removed using selective catalytic reduction, electrostatic precipitation, and wet flue gas desulphurisation [18]. However, given the additional inefficiencies these strategies place upon industrial processes, it is typically post-combustion strategies which are used to separate CO_2 from the flue gas [19]. This is implemented using several methods (**Figure 1.1**), including absorption with solvents, adsorption onto selective materials, membrane separation, and cryogenic separation [19].

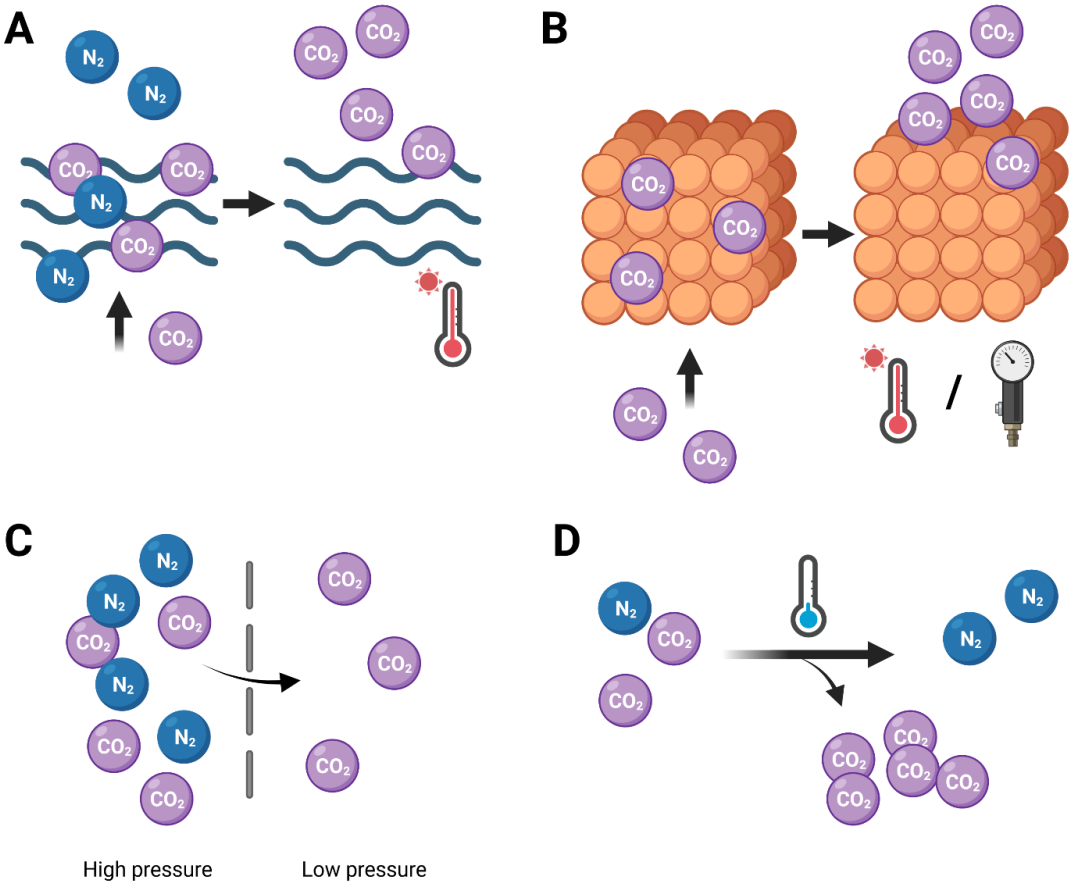


Figure 1.1 | Simplified graphic of strategies for carbon concentration post-combustion. **A.** Absorption. **B.** Adsorption. **C.** Selection via a semipermeable membrane or membranes. **D.** Cryogenic separation. (Created with BioRender.com).

Chemical absorption (**Figure 1.1 A**) involves the reaction of CO_2 with a chemical solvent, typically alkanolamines, however, this strategy can also use compounds such as calcium carbonate and ammonia [20]. In adsorption strategies (**Figure 1.1 B**) CO_2 is removed from flue gas by reacting it with a selective material. Here, CO2 is bound to the surface of a physical material by Van der Waals forces or covalent bonding [21]. These adsorbent materials can include solids such as zeolites (13X) [22], activated charcoal [23], amines (such as polyethylenimine or polyaniline) [24], or metal organic frameworks, where over 100 examples of CO_2 selectively adsorbing structures have been reported (see Li *et al*. 2011) [25]. Alternatively, selective binding materials could be replaced with selectively CO2 permeable membranes (**Figure 1.1 C**). These can include carbonaceous organic membranes [26], inorganic "ceramic" membranes [15], and hybrid membranes comprised of polymeric materials and inorganic fillers [27]. Cryogenic

treatment of flue gas is another possible strategy (**Figure 1.1 D**), in which liquefied natural gas is used to provide cold energy for the sublimation of CO_2. An extremely efficient process [15], generating CO_2 with purities as high as 99.17% [19].

Although promising, these strategies all require some combination of highly energy-intensive heat regeneration cycles, expensive or fragile materials, and a concentrated source of CO_2 to be efficient for CCS (see Madejski et al 2022) [19]. These factors, and the associated financial burdens they add to industrial processes, currently limit the scope of their potential deployment.

1.2.2 *Carbon storage*

Furthermore, as none of the above strategies also utilise the CO_2 emissions captured during these processes, when deploying these capture strategies we must also consider what to do with the carbon that they concentrate. For this, solutions are typically based around long-term storage (geological or biological) [21,28]. The long-term geological storage of CO_2 can be delivered via several strategies, including mineral carbonation, ocean storage, injection into depleted oil and gas fields or saline aquifers, or other suitable geological formations [20]. The injection of CO_2 into geological formations is an established strategy, with projects already at industrial scale [29]. However, burying carbon could potentially risk future leaks [30], and the consequences regarding long-term ocean acidification are difficult to predict (see IPCC, 2005) [31]. Possibly resulting in these strategies posing new, additional long-term risks.

Alternatively, storage strategies that do not rely on CO_2 directly captured from the emission source have also been proposed, in which biological systems are used to sequester carbon (see Wilberforce et al. 2021) [32]. Terrestrial sequestration is when CO_2 from the atmosphere is assimilated into photoautotrophic biomass (usually via afforestation) [28], a strategy which, if implemented effectively, could store an additional 4.9 Gt of CO_2 per year, (cumulatively 410 Gt CO_2 by 2100) [33]. This is achieved both by dedicating available land for this purpose and using land management practices that sequester carbon. However, this would mean dedicating large areas of land indefinitely to carbon storage [34]. Due to the long, slow time scales, the large areas, and types of land needed for this strategy to be effective, bio-sequestration alone will not be sufficient to offset the

scale of current GHG emissions. The strategy often directly competes with agriculture, (increasing the risk of food insecurity) [35].

1.2.3 *Catalytic valorisation of captured CO_2*

Rather than simply storing CO_2, it may also be possible to utilise it as an inexpensive feedstock to produce compounds of interest [36]. Several valuable chemicals can be directly synthesised from CO_2 [37]. Biofuels including methanol and dimethyl ether can be produced from CO_2 with the aid of metal catalysts [21]. Such as $CuO/ZnO/Al_2O_3$ and Cu/ZnO/Zeolite catalysts [38,39]. Despite the relative abundance of the compounds used in such reactions, conversion efficiencies of CO_2 to product are typically < 50% (see Osman *et al*. 2020) [21]. Methane has also successfully been produced from CO_2, using either Cu_2O/TiO_2 hollow nanospheres [40], or a Ni/CeO2/zeolite catalyst [41]. The latter showing a high conversion efficiency, (~85%), however, at 400 °C [41]. In contrast, Mohd *et al*. 2015 showed that by simply sparging 37 °C activated sludge with CO_2 and H_2 under anoxic conditions, methane production increased by 70-fold and with a CO_2 conversion efficiency of 77% [42].

1.2.4 *Carbon fixation in biological systems*

Compared to the abiotic catalytic conversion of CO_2 to compounds of interest, biological systems typically use lower temperatures, do not require mineral extraction and can valorise CO_2 into a diverse array of products [36]. Biomineralization of construction materials could potentially unlock new, less emitting, alternatives. With enhanced properties such as carbon sequestration, circular reuse of the materials, and self-healing properties [43,44]. Advances in molecular tools have also enabled the use of microorganisms to synthesise biofuels, pigments, lipids, nutraceuticals, and other compounds of interest from CO_2 (see Ng *et al*. 2020) [45]. Biological valorisation of CO_2 is, therefore, an attractive potential solution in treating CO_2 waste.

Carbon fixation is a form of autotrophy in which inorganic carbon (typically CO_2) is biologically converted to organic compounds [46]. However, how the CO_2 is used as a source of carbon can vary significantly depending

on the organism [46], (**Table 1.1**). Each pathway has its own advantages and disadvantages for the valorisation of CO_2.

Table 1.1 | Overview of known natural carbon fixation pathways.

C-fixation pathway	Native organisms	Energy source(s)	Reference
A. Anaerobic			
Dicarboxylate/4-hydroxybutyrate	Sulphur bacteria / archaea	H_2 & sulphur	[47]
Reductive TCA	Sulphur bacteria / archaea	Light & sulphur	[48]
Wood–Ljungdahl	Acetogenic & methanogenic bacteria / archaea	H_2	[49]
B. Aerobic			
3-hydroxypropionate	Thermophilic bacteria	Light	[50]
3-hydroxypropionate / 4-hydroxybutyrate	Thermophilic sulphur bacteria	H_2 & sulphur	[50]
Calvin-Benson	Plants, algae, cyanobacteria, (aerobic bacteria)	Light, (H_2)	[51]

1.2.4.1 *Anaerobic Carbon fixation*

Anaerobic CO_2 fixation can be carried out naturally using 3 known pathways, the Wood-Ljungdahl pathway (WLP) [49], the reductive TCA cycle [48], and the dicarboxylate/4-hydroxybutyrate cycle [47] (**Table 1.1 A**). The latter two, however, are present only in green sulphur bacteria and hyperthermophilic archaea [50], and are unsuitable for large scale valorisation due to the extreme temperature requirements (70 - 106°C) [46,50], complex nutrient requirements (including lithic substrates and reduced sulphur species) [46], and slow growth rates of these bacteria (see Berg, 2011) [46]. The use of WLP carbon fixing bacteria, such as *Clostridium autoethanogenum*, has successfully been used to convert CO_2 into useful

products at scale [52]. *Clostridium autoethanogenum*, which fixes CO_2 into acetate via the WLP [53], has already been successfully commercialised by LanzaTech™, producing 30 million gallons of ethanol from 150,000 metric tonnes of CO_2 in 2021 [52].

However, there are several limitations in the utilisation of these organisms. Anaerobic fermentation requires an oxygen free environment. These fermenters are expensive to construct and maintain, and oxygen contamination can significantly reduce the efficiency of these organisms [54]. Furthermore, although organisms using the WLP convert CO_2 into product and biomass with a greater conversion ratio than photoautotrophs, these organisms are often limited by inherently reduced maximum biomass densities, and lower (compared to aerobic microorganisms) product titres [55]. In acetogens, this is because a high biomass density is coupled with high acetate titres which can result in the depletion of intracellular acetyl-CoA, and the subsequent cessation of a cell's metabolism [55]. This is an issue as it can reduce the commercial competitiveness of industrial strategies using these organisms. [55]

1.2.4.2 *Aerobic Carbon fixation*

Two pathways, the 3-hydroxypropionate cycle and 3-hydroxypropionate/4-hydroxybutyrate cycle, are used by thermophilic and sulphur utilising bacteria, (again limited by temperature and complex substrate needs) [50] (**Table 1.1 B**). The Calvin-Benson (CB) cycle, however, is a pathway via which aerobic autotrophs fix CO_2 with high rates, and on a very large scale [55]. The CB cycle, also known as the reductive pentose phosphate cycle, (or 'light independent reactions'), centres around the fixation of atmospheric CO_2 into carbohydrates (see Bassham et al. 1950) (see Bassham et al., 1950). *Cupriavidus necator* H16 is capable of autotrophic growth via the CB cycle [52], however, *Cupriavidus necator* H16 also requires hydrogen gas (H_2) to fix CO_2 [52]. Hydrogen gas is extremely flammable and presents an explosive challenge, given it needs to be coupled with oxygen; therefore, scaling processes with this organism is challenging [56,57]. Alternatively, most autotrophs that use the CB cycle are photoautotrophs, including plants, algae, and cyanobacteria [52].

The CB cycle is characterised by three stages: carbon fixation, reduction, and regeneration (**Figure 1.2**), and is additionally driven primarily by 3 corresponding enzymes: RuBisCO, phosphoribulokinase, and gylceraldehyde-3-phosphate dehydrogenase.

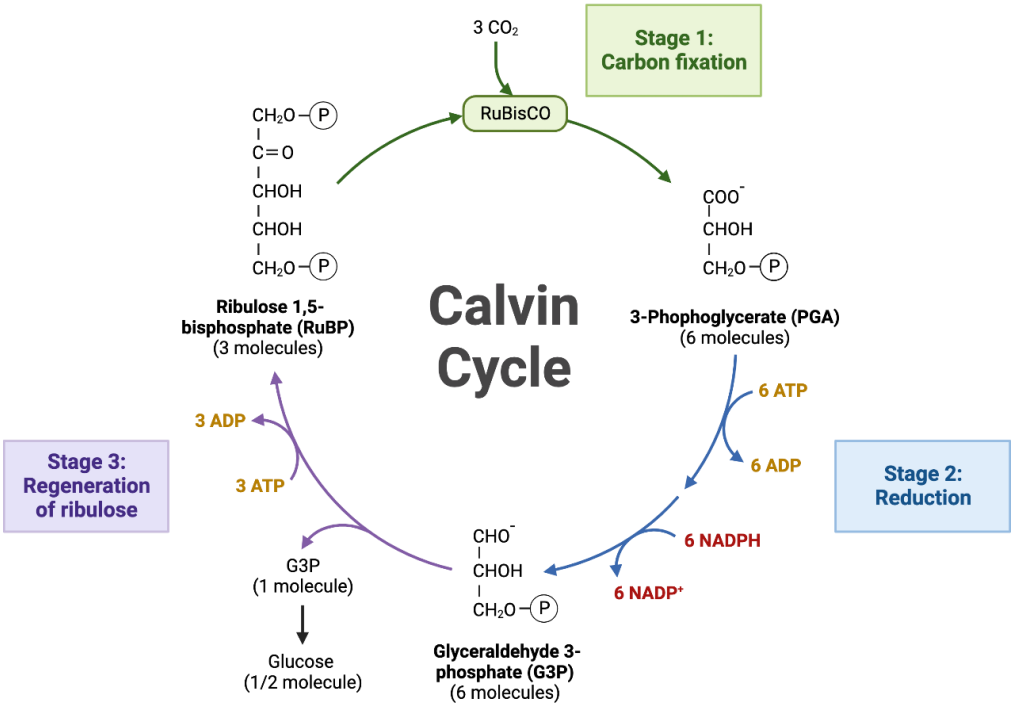


Figure 1.2 | Schematic view of the CB cycle reactions, taken from BioRender.com.

As shown in **Figure 1.2** the 3 stages of the CB cycle can be characterised as follows:

Carbon fixation: During this stage, a single CO_2 molecule is joined to 5-carbon sugar, ribulose-1,5-bisphosphate (RuBP). This process is catalysed by the carboxylase RuBisCO and is the point where carbon-fixation occurs. This results in the generation of a 6-carbon compound that instantaneously dissociates into two 3-carbon molecules of 3-phosphoglyceric acid [50].

Reduction: Here, both ATP and NADPH are used to convert these 3-carbon 3-phosphoglyceric acid molecules into the 3-carbon molecule, glyceraldehyde-3-phosphate [50].

Regeneration: Finally, two glyceraldehyde-3-phosphate molecules are used to regenerate ribulose-1,5-bisphosphate (RuBP). The regeneration

step is complex involving multiple enzymatic steps from the oxidative pentose phosphate pathway (PPP) (see Kruger *et al*. 2003) [58], where glyceraldehyde-3-phosphate is used to synthesise sedoheptulose-7-phosphate, which is then converted back into RuBP.

1.2.4.3 *RuBisCO*

RuBisCO is a key enzyme responsible for the fixation of CO_2 [59]. It is estimated that around 90% of the total percentage of organic carbon is fixed by RuBisCO. It has even been suggested that for every individual person on earth, there are 5 kg of RuBisCO [60]. Therefore, it could be argued that RuBisCO is the single most important enzyme involved in the global carbon cycle, and an essential pillar of life on Earth.

One key limitation, however, is the relative inefficiency of the RuBisCO complex to catalytically integrate CO_2 into RuBP [61]. As this enzyme evolved prior to the presence of atmospheric oxygen, it did not seemingly evolve an exclusive selectivity for CO_2 [62]. Likely due to necessary evolutionary trade-offs, its interactions with chaperone proteins during assembly, and the structure of its active site [62]. As such, it is susceptible to acting upon O_2, resulting in an energy intensive and resource draining corrective action [63]. When RuBisCO combines RuBP with oxygen, this generates the toxic compound 2-phosphoglycolate, and in an average C3-plant RuBisCO can have an error rate of approximately 20% [64]. Under temperatures +3.7°C higher than current averages, this error rate can be more than 40% [64]. When 2-phosphoglycolate is generated, it is eventually recycled in the process of photorespiration, which consumes approximately 30% of the available photosynthetic energy in plants [64]. A previous attempt to enhance the rate of CO_2 conversion to RuBP resulting in even lower affinity for CO_2 [65].

Due to the complex nature of RuBisCO, many possible changes can have highly destabilising effects on the protein's integrity and function, thus have significantly constrained engineering attempts [66]. The enzyme participates in a broad range of molecular interactions within the cell, meaning that any modifications to the enzyme complex often have additional unforeseen, and potentially deleterious, consequences [67]. Analyses of the RuBisCO active site have shown that the binding mechanism of CO_2 to the enzyme inherently inhibits its ability to be properly distinguished from O_2 [68]. Collectively, these issues have even led some to state that, "despite slow catalysis and confused substrate

specificity, all [RuBisCOs] may be nearly perfectly optimized", Tcherkez et al. 2006 [69]. Given further optimisation of RuBisCO is therefore likely to be challenging, strategies to increase CO_2 assimilation by cyanobacteria have often focused on non-RuBisCO dependent approaches (see section **2.5**).[70]

1.2.4.4 *Photoautotrophic organisms*

Plants, algae, and cyanobacteria are all capable of fixing CO_2 directly into biomass via RuBisCO and the CB cycle [52]. Despite this, there are significant drawbacks to the use of plants at a scale necessary to impact overall CO_2 emissions. As discussed in section **1.2.2**, plants, are slow growing, use large areas of land, and therefore directly compete with agriculture. These challenges therefore limit their potential use for CO_2 capture and valorisation.

Through process of elimination, this leaves both microalgae and cyanobacteria. Both show a great deal of potential to fulfil this role. In cyanobacteria and microalgae, most of the components involved in photosynthesis are the same as or similar to higher plants (see Sato 2021) [70]. However, cyanobacteria tend to have faster doubling times than microalgae [71], and convert a greater percentage of available solar energy (per m^2) into chemical energy (including as biomass), 10% compared to 5% in green algae [72]. Many cyanobacteria are also capable of fixing nitrogen as well as carbon [73], which is potentially useful for engineering more sustainable alternatives to the Haber-Bosch process (responsible for > 96% of ammonia production) [74]. An essential component of modern agriculture, but also responsible for 1.2% of global CO_2 emissions because of its energy intensity. Nitrogen fixation also increases both the diversity of potential products that could be made sustainably and potentially reduces nutritional inputs. Furthermore, cyanobacteria have a more advanced genetic toolkit and are easier to manipulate compared to microalgae (see Ng et al., 2020; Vavitsas et al., 2021), and they also possess carboxysomes, which offer additional optimisation targets to improve their carbon fixation efficiencies. As such, these organisms are an attractive prospective chassis for use in industrial processes where CO_2 is utilised as a feedstock.

1.2.5 *Carbon assimilation by cyanobacteria*

Inorganic carbon is assimilated into compounds which are accessible to cyanobacteria through two strategies. The first is the fixation of CO_2 by RuBisCO into 3-phosphoglycerate. The second is via the anaplerotic or other carboxylase reactions, where intermediates of the TriCarboxylic Acid (TCA) cycle or other metabolic pathways which are directly replenished from the assimilation of HCO_3^- [76]. One example of this is the conversion of phosphoenolpyruvate (PEP) and HCO_3^- into the TCA intermediate oxaloacetate by PEP carboxylase. This reaction alone may be responsible for up to ~20% of the carbon fixed by cyanobacteria under certain conditions [77]. Despite the potential of these other reactions to assimilate carbon, however, RuBisCO is by far the most significant enzyme involved in carbon assimilation by cyanobacteria.

1.2.5.1 *Carbon concentration by cyanobacteria*

Cyanobacteria have also evolved a protein microcompartment, known as the carboxysome, which encapsulates RuBisCO and generates a high CO_2 and low O_2 environment. Reducing the impact of photorespiration on the cell and increasing the efficiency of carbon fixation within cyanobacteria [78]. The carboxysome is porous, comprised of a proteinaceous shell [78]. Cyanobacteria cells additionally import bicarbonate (HCO_3^-) via membrane-bound transport proteins located within their cell membranes, such as BicA, SbtA, and BCT1 (**Figure 1.3**) [79,80]. These increase the abundance of HCO_3^- within the cell, which then diffuses into the carboxysome [78]. Whilst the carboxysome enables the influx of HCO_3^- into the compartment, efflux is resisted [81]. HCO_3^- is then converted into CO_2 by the enzyme carbonic anhydrase, further concentrating CO_2 around the RuBisCO complexes [78]. These mechanisms result in efficient carbon assimilation by the cells. Furthermore, this high CO_2 microenvironment enables cyanobacteria to possess a RuBisCO with high catalytic activity, despite a lower specificity for CO_2 [82,83]. Further enhancing the rate of CO_2 fixation by the cells.

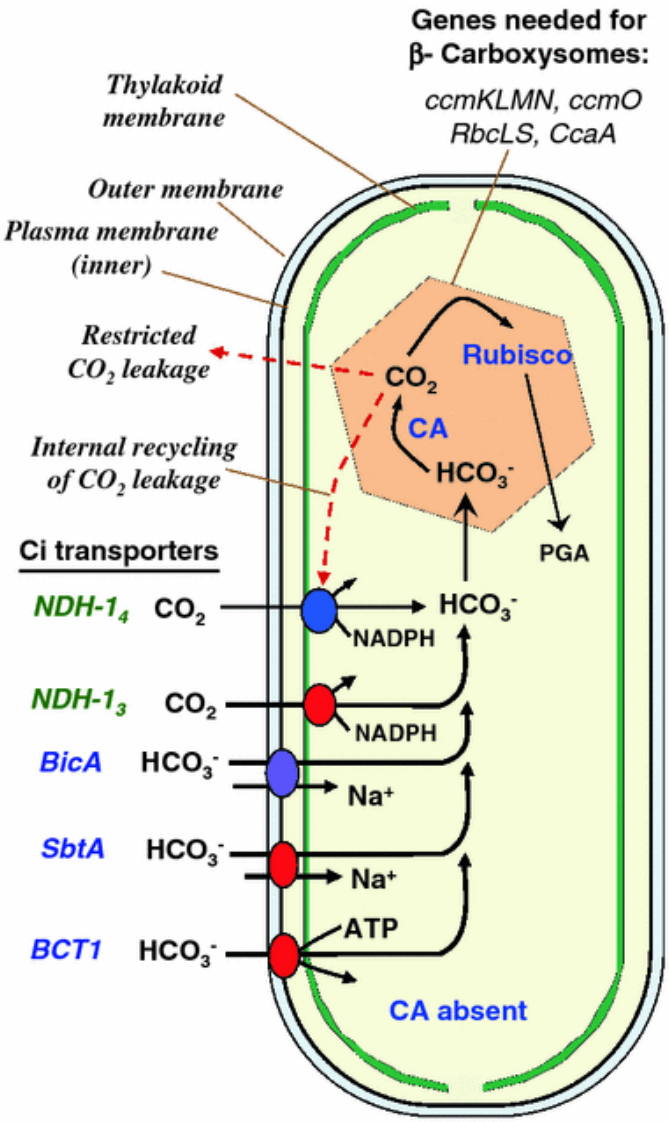


Figure 1.3 | Simplified schematic showing a cyanobacteria showing inorganic carbon transporters and carboxysome. (Adapted from Price 2011) [84].

1.3 Chapter overviews

Due to global GHG emissions, and CO_2 emissions in particular, the Earth is at risk from a changing climate driven by rising temperatures. Extensive research is being carried out to identify new strategies for carbon sequestration. Due to the high energy demand and operational costs of many CCS strategies, biological alternatives offer a promising solution. Strategies such as afforestation could sequester large quantities of carbon, however, they do not address the issues related to why CO_2 is initially released. Cyanobacteria are one group of organisms that show potential

in addressing this. They are a diverse group of photosynthetic microorganisms, and they can be grown without directly competing with other land use. They are genetically tractable and can be engineered to produce compounds of interest directly from CO_2. Potentially allowing us to circularise our carbon economy and produce cleaner alternatives to fossil fuel derived compounds.

However, they are currently limited by their productivity and growth relative to heterotrophic alternatives. Previous work has successfully used cyanobacteria to synthesise CO_2 derived products; however, this has often been limited to niche high value products, and they have been unable to compete with contemporary production methods at scale. Adaptive laboratory Evolution has shown significant promise in tailoring prokaryotic phenotypes, including the improvement of their growth rates. For an ALE strategy to be successful in improving the growth of cyanobacteria, the selective pressure should directly couple the cell's physiology and growth. **Chapter 4** presents the optimisation of selective environments to isolate faster growing cyanobacterial strains with enhanced carbon fixation under standard atmospheric conditions. Selective environments with adjusted CO_2 concentrations, light intensities, and batch / auxostat selections were investigated. The effects of strain engineering to reduce cellular electron sink capacity outside of direct carbon fixation, (in the form of hydrogenase deletion strains) was also investigated.

Agriculture is an industry responsible for a significant proportion of CO_2 emissions. This is due to both land use practices, and the energy intensive Haber-Bosch process. An energy intensive process used to generate ammonia for nitrogenous fertilisers. Filamentous cyanobacteria are known to fix nitrogen from the atmosphere, but like all cyanobacteria, suffer from relatively low growth and productivity. With the ability to fix both inorganic carbon and nitrogen, however, they are particularly attractive as potential industrial chassis, and biofertilizers. **Chapter 5** investigated if auxostat ALE strategies optimised in **Chapter 4** could be adapted to isolate nitrogen fixing cyanobacteria with increased biomass formation, using nitrogen limited media, supplementation of organic carbon (fructose), and light intensity stress.

Chapter 2.

Literature Review

2.1 Overview of cyanobacteria

Cyanobacteria are believed to be some of the oldest known living organisms, estimated to be >2.45 billion years old [85]. Cyanobacteria are a diverse and widespread group of organisms, estimated to be responsible for between 20 – 30% of Earth's primary photosynthetic productivity, fixing ~25 Gt of CO_2 per annum [86].

2.1.1 *General characteristics of cyanobacteria*

Cyanobacteria are a morphologically diverse prokaryotic phylum (**Figure 2.1**). They can be unicellular or filamentous, they are found in both terrestrial and aqueous environments, and in the latter, these can range from freshwater to marine, and even hypersaline [87]. As previously stated, cyanobacteria also have carbon concentration mechanisms, enabling them to fix carbon more efficiently by creating a high CO_2 microenvironment around their RuBisCO complexes [88]. Cells also contain a variety of coloured pigments which enable them to absorb light energy to fix carbon through oxygenic photosynthesis [88].

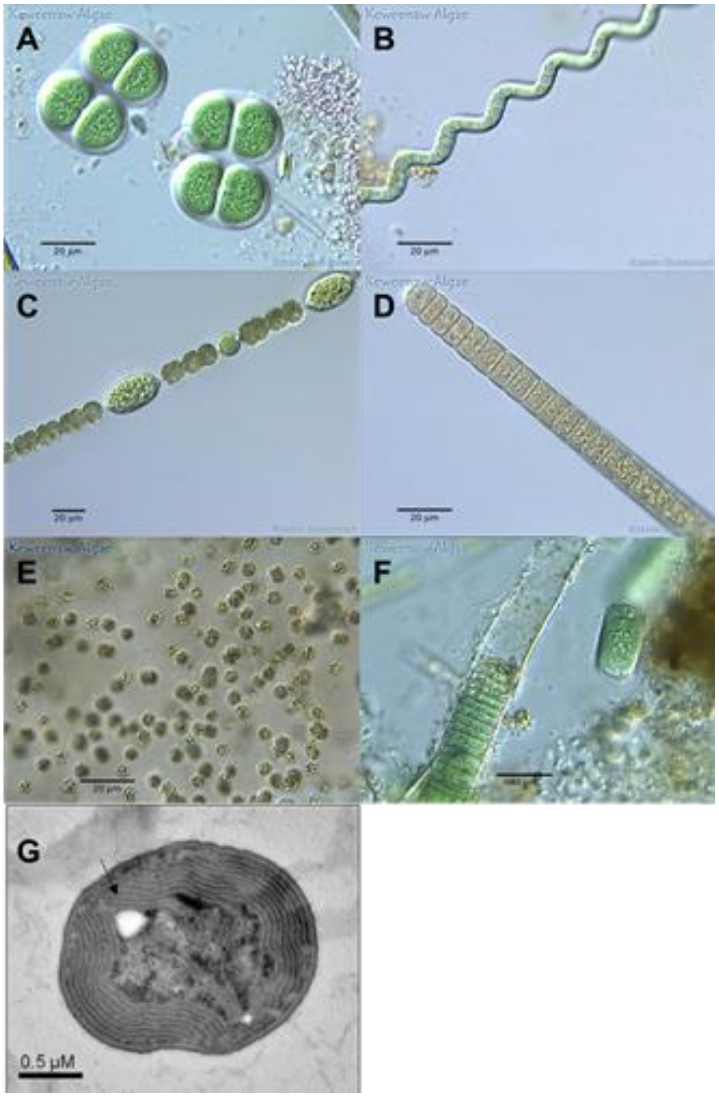


Figure 2.1 | Morphology of the cyanobacteria; **A.** *Chroococcus turgidus*. **B.** *Spirulina*. **C.** *Anabaena*. **D.** *Oscillatoria*. **E.** *Microcystis*. **F.** *Lyngbya*. (Images taken from Keweenaw Freshwater Algae, 2020) **G.** Transmission electron microscopy (TEM) section of *Synechocystis* sp. PCC 6803 showing the internal concentric thylakoid membrane. (Image courtesy of Dr Edward Spence, University of Nottingham).

2.2 Photosynthesis

Photosynthesis is the biological process by which photoautotrophs, including cyanobacteria, fix CO_2 into biomass (see **Figure 2.2**) [59]. This process is driven by the channelling of captured light energy via the electron transport chain (ETC), through the photosystems, and into the CB

cycle [89]. The process of photosynthesis in cyanobacteria can be summarised as follows:

1. The capture of light energy via pigments in the phycobilisomes and photosystem II complexes generate excited electrons by the photolysis of water at the oxygen-evolving centre.

2. Transfer of these electrons via the ETC releases energy and generates NADPH.

3. Protons generated during the photolysis of water and by the ETC are used to synthesise ATP.

4. ATP and NADPH are used in the CB cycle to assimilate inorganic carbon (CO_2) into organic molecules.

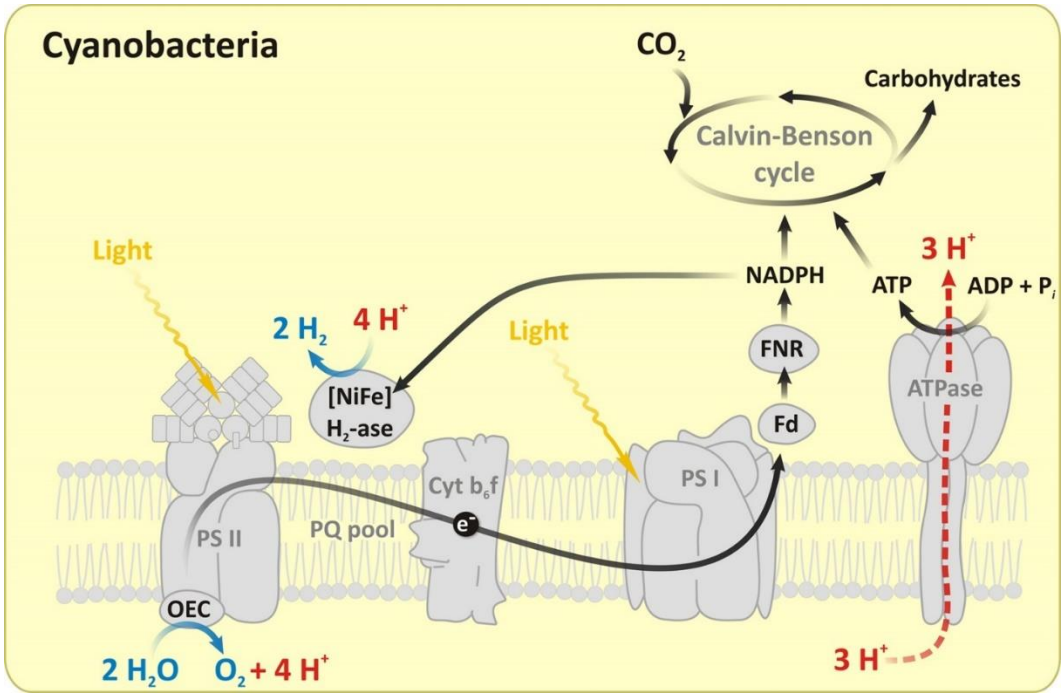


Figure 2.2 | Simplified routes of light driven electron and proton transport within cyanobacterial thylakoid membrane. Taken from Govindjee and Shevela 2011, (adapted from original of Messinger and Shevela 2011) [90,91].

2.2.1 *Capturing light energy*

Capture of light energy is critical to photolysis (splitting of water) and the subsequent transfer of energy towards carbon fixation via the ETC. In cyanobacteria, this begins with the channelling of light energy by multi-subunit antennae, phycobilisomes (PBS), to photosystem II (PSII) (**Figure 2.3**) [89]. PBS are large hemidiscoidal protein-pigment complexes, ranging in sizes of around 3000-7000 kDa [92]. In *Synechocystis* sp. PCC 6803 these are comprised of 6 rods of 3 phycocyanin hexamers, attached to a core comprised of 3 allophycocyanin cylinders [93,94]. However, depending on species and / or light source, these complexes can also contain compounds such as phycoerythrin and phycourobilin [95]. The advantage of diversity in available pigment-protein complexes is that it can allow cyanobacteria to react adaptively to changing conditions in the light. With different pigment-protein complexes exhibiting diversity in which wavelengths of light they can absorb [95].

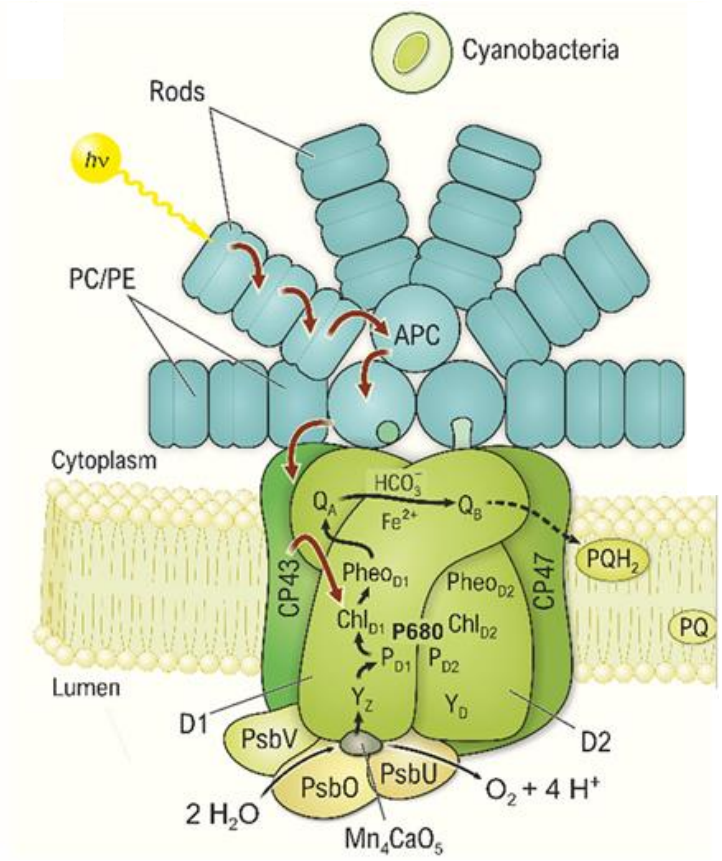


Figure 2.3 | Schematic representation of a cyanobacteria PBS light harvesting complex attached to PSII. (Adapted from Shevela *et al*. 2023) [89].

When located on the surface of the PSII enzyme complex (see **Figure 2.3**), PBS absorb the energy to initiate the cascade of ETC reactions [92]. PSII is a multi-subunit enzyme complex. In cyanobacteria, PSII complexes are comprised of 19 protein subunits, and over 80 co-factors [89]. The PSII reaction centre core contains two large homologous transmembrane proteins, D1 and D2. Together, PSII complexes contain all the necessary co-factors for light induced primary charge separation [89]. Resonance Energy Transfer (RET) is the transfer of excitation energy captured by the PBS antennae down one pigment to the next, until reaching PSII reaction centre [96]. The chlorophyll molecules contain a magnesium ion at the centre of a porphyrin ring, which is excited by this channelled light energy, specifically by raising the excitation state of its electrons [89]. Channelled excitation energy subsequently reaches the primary electron donor of PSII, itself a collection of four chlorophyll molecules, P680 [89]. Following excitation, P680 transfers an excited electron to the flanking primary electron acceptor of pheophytin, which subsequently initiates a further ETC cascade [89]. The transfer and loss of an electron results in the generation of the radical cation $P680^{\cdot+}$ [89], which requires a source of electrons to return it to its original state, these being generated from the photolysis of water.

2.2.2 *Photolysis of water*

The PSII complex includes the oxygen-evolving centre (OEC), located on the lumen side of the thylakoid structure, and containing a manganese catalytic centre [89]. The OEC is buried within the PSII complex, likely to provide shielding from an overabundance of substrate (see Lichtenburg *et al*. 2021) [97]. The $P680^{\cdot+}$ radical cation is reduced by the redox-active tyrosine 161 (Y_z) of the D1 protein [98], returning it to a state ready to accept the next excitation. Y_z donates an electron, and thus forms the neutral radical $Y_z^{\cdot}$, a strongly oxidising residue [98]. This residue is then reduced by the OEC manganese catalytic centre, which in turn acquires electrons by the splitting of water via a mechanism that has not yet been fully elucidated (see Zhang and Sun 2018) [99]. The generation of 1 oxygen molecule and 4 protons occurs following the splitting of 2 water molecules for 8 photons harvested by the PSII complex [100,101]. Captured energy from photons is stored and released from the manganese complex permutating through several states in the Joliot–Kok cycle [102]. The PSII D1 protein is unstable and needs to be replaced via regular turnover [103]. This is carried out via a dedicated repair mechanism, in which the damaged D1 protein is replaced [103].

2.2.3 *Electron transport chain*

The transfer of electrons by the ETC to protein complexes and the CB cycle is shown in **Figure 2.3**. The transfer of an electron from P680 to pheophytin (here $Pheo_{D1}$), results in the generation of a radical anion $Pheo_{D1}^{\cdot -}$ [104]. This electron is then donated to the plastoquinone (PQ) within PSII and then reduced to plastoquinol (PQH_2) [105]. Two electrons and two protons are required for this reaction [106]. The PQ molecules exist in a pool within the thylakoid membrane, and the PQH_2 is substituted for one of these PQ molecules [105]. Following release from PSII, PQH_2 diffuses through the thylakoid membrane, where the molecule is oxidised following a reaction with the cytochrome b_6f (cyt b_6f) complex [106]. During this reaction, protons are released into the lumen side of the thylakoid [107], and one electron is transferred to either plastocyanin or cytochrome c_6, (though typically the former – see Kuchima *et al*. 2012) [106,108]. Transport of the electron is then mediated by these compounds to photosystem I (PSI) [109].

The PSI complex, like PSII, is made up of multiple subunits, including two large transmembrane subunits (PsaA and PsaB) [110]. Together, these form a heterodimer containing many of the PSI redox co-factors. The energy potential of the transferred electron is then increased by a second light reaction in the PSI complex and transferred to ferredoxin (Fd) [111]. Following another transfer to the ferredoxin-$NADP^+$ reductase (FNR), the electron is used to generate 0.5 molecules of NADPH [112]. However, electrons can also be transported to oxidases acting as terminal electron acceptors within the respiratory electron transport chain [113]. These act to protect the organism from both oxidative stresses, and an over reduced PQ pool [114]. These can receive excess electron stress either directly from the PQ pool, as with cytochrome bd-quinol oxidase and plastoquinol terminal oxidase [115,116], or via the cytochrome-c oxidase complex, which receives electrons from cyt b_6f [117]. The latter of these also contributes to the synthesis of ATP by generating a proton gradient [106].

2.2.4 *ATP synthesis*

In addition to electron transport, protons generated during the photolysis of water are also used to generate a proton gradient, subsequently harnessed by F_1F_0-ATP synthases in ATP synthesis (**Figure 2.4**) [118]. This proton motive force results in the synthesis of ATP by driving a rotational mechanism of catalysis [119,120]. This is achieved by the rotation

of the γ-subunit F_1 region of the ATP synthase, as three separate catalytic sites on the β-subunits react with ADP and P^i to synthesise ATP [121]. The synthesised ATP (and NADPH) is subsequently used to fix CO_2 via the CB cycle [51].

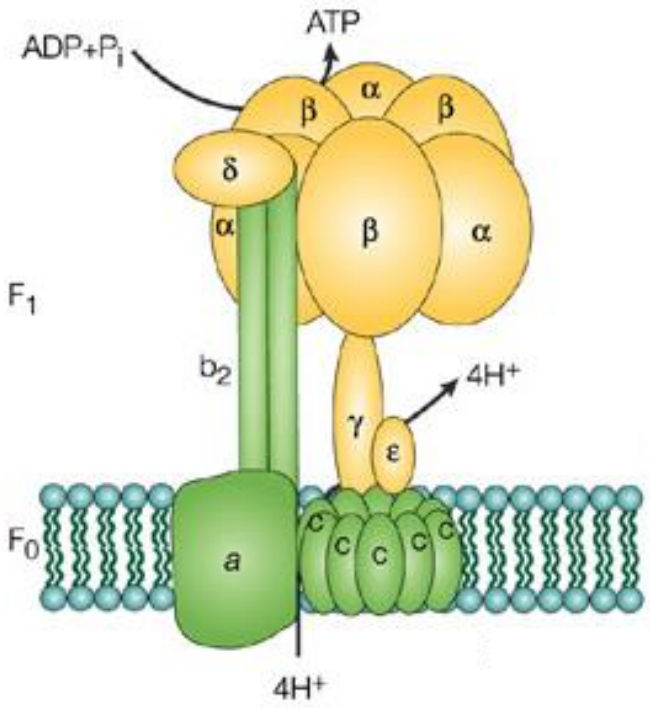


Figure 2.4 | Simplified schematic of an F-type ATP synthase (ATPase). (Adapted from Nishi and Forgac 2002) [122].

2.3 Nitrogen fixation by cyanobacteria

All known living organisms require a source of nitrogen to survive. Nitrogen is an essential component in the synthesis of amino acids, and all organically accessible nitrogen is fixed from atmospheric sources [123], with > 60% of fixed *N* via biological nitrogen fixation [124]. In biological systems, nitrogen gas (N_2) is converted into an organically accessible form by specialised nitrogenase enzymes [123]. This capability to fix atmospheric N_2 is also present within many species of cyanobacteria [123].

Most cyanobacterial nitrogen fixation is carried out by filamentous species, which include *Anabaena*, *Trichormus*, and *Nostoc* [73]. However, nitrogen fixation has also been observed in unicellular cyanobacteria species such as *Gloeocapsa* and *Synechococcus* (*Cyanothece*) spp. [73].

Given that organic nitrogen is essential for the healthy growth of all living organisms, it is not surprising that the production of nitrogen rich fertilisers consumes 2% of the world's energy and is responsible between 1.4% and 5% of global greenhouse gas emissions [125]. The Haber-Bosch process is responsible for > 96% of ammonia production via catalytic nitrogen fixation. It is an essential component of modern agriculture, but it is also highly energy intensive [74]. Therefore, the cultivation of nitrogen fixing bacteria, and their application directly to soil, could offer a potentially more sustainable strategy to reduce humanity's reliance on energy intensive strategies to fix nitrogen [126].

2.3.1 *Cyanobacteria nitrogenases*

Nitrogenase enzymes are responsible for > 95% of all non-industrial nitrogen fixation (see Dashora 2011) [127], and the genus *Trichodesmium* fixes 42% of total global nitrogen, which equates to 240Tg N_2 y^{-1} [128,129]. Nitrogenase enzymes are classified based on the metal co-factor they utilise to catalyse the nitrogen fixation reaction [128]. There are currently 3 known metal co-factor combinations found within nitrogenases, these are iron-iron (FeFe), iron-molybdenum (FeMo), and iron-vanadium (FeV) [73]. The FeMo and FeV nitrogenase enzymes are found in cyanobacteria [73]. The FeFe nitrogenase enzymes are found in other nitrogen fixing bacteria such as *Azotobacter vinelandii* [73].

All nitrogenases are susceptible to oxygen poisoning [73], and this oxygen inactivation is irreversible [130]. Within cyanobacteria, FeMo nitrogenases (**Figure 2.5**) are both the most abundant form of nitrogenase [131], and have a higher catalytic efficiency than FeV nitrogenases [132].

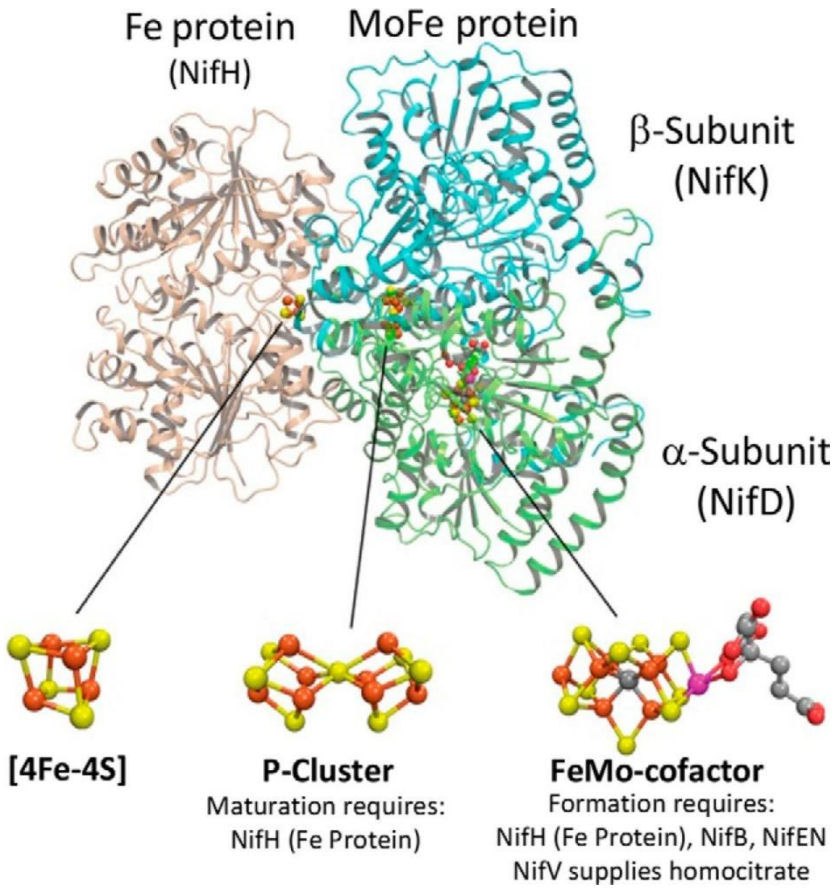


Figure 2.5 | Schematic representation of the MoFe nitrogenase and associated metal-cofactors. Fe protein subunits (*nifH*) are shown in light brown, the MoFe protein α-subunit (*nifD*) is shown in green, and the MoFe protein β-subunit (*nifK*) is shown in blue (taken from Jimenez-Vicente et al. 2018) [133].

All nitrogenase enzyme variants function in a similar manner. They are multi-subunit proteins, that catalyse the conversion of molecular N_2 into ammonia (NH_3) using ATP, with the assistance of their respective metal co-factors [134]. Nitrogen fixation can be summarised by the following equation, (**Equation 2.1**) [135,136].

Equation 2.1 | Stoichiometry of nitrogenase reaction

$$N_2 + 8\ e^- + 8\ H^+ + 16\ ATP \rightarrow 2NH_3 + H_2 + 16\ ADP + 16\ Pi$$

Due to the high energetic costs of nitrogen fixation, it is the limiting biophysical factor in cyanobacterial growth under diazotrophic conditions (see Osburn et al. 2021) [137].

This reaction also acts as an electron sink, given the forward reaction utilises proton-coupled electron transfer to reduce N_2. This makes these reactions particularly sensitive to oxygen, a problem for aerobic micro-organisms. In filamentous cyanobacteria, electrons required for N_2 fixation are primarily generated via the oxidative pentose phosphate pathway, by catabolising carbohydrates imported from neighbouring vegetative cells. The ATP generated drives electron transfer and the conformational change in the nitrogenase, which is essential for N_2 fixation [138]. Ferredoxin proteins are also important electron acceptors via NADPH for N_2 reduction. Cyanobacteria possess ferredoxin-$NADP^+$ oxidoreductase enzymes, which are PSI dependent and generate ATP for nitrogen fixation via cyclic photophosphorylation [73]. This reduces Fd with NADPH produced via carbohydrate oxidation in heterocysts [131]. Under Fe limiting conditions, cyanobacteria can also produce flavodoxins, which transfer electrons from either pyruvate or PSI to the nitrogenase enzyme complex [73].

Nitrogen fixation is therefore an energy expensive process. In nitrogen fixing cyanobacteria, photosynthesis produces energy for both cellular processes and nitrogen fixation. However, photosynthesis produces significant quantities of oxygen, and as stated above, nitrogenase enzymes are oxygen intolerant. Therefore, cyanobacteria have evolved several strategies to minimise the impact of oxygen on the nitrogenase enzyme, including the compartmentalisation of the nitrogenase within specialised cells in filamentous cyanobacteria, called heterocysts [139]. These specialised cells are dedicated to nitrogen fixation and can be supported with energy resources from neighbouring vegetative, photosynthetically active cells [73]. As a result, species which produce these specialised cells often form chains, or ‘filaments’. Creating centralised micro-environments with reduced oxygen which facilitates efficient nitrogen fixation.

2.3.2 *The heterocyst*

Heterocysts are specialised cells, found dispersed amongst the chains of filamentous species of nitrogen fixing cyanobacteria [140]. Their formation is typically triggered in environments where organic nitrogen sources (such as ammonia or nitrate) are not readily available to the cells [141]. Heterocyst formation is therefore triggered by nitrogen limitation. Heterocysts form when vegetative cells along a cyanobacterial filament begin to differentiate. This is due to changes in gene expression, triggered by insufficient organic nitrogen, and cellular differentiation is enabled by

expression of the regulatory protein HetR [142]. Typically, cellular differentiation occurs in semi-regular intervals across the length of the filament, enabling a more even distribution of nitrogen fixing cells across the population. In return for energy provided from neighbouring photosynthetically active cells, heterocysts provide fixed nitrogen in the form of glutamine [143] (see **Figure 2.6**).

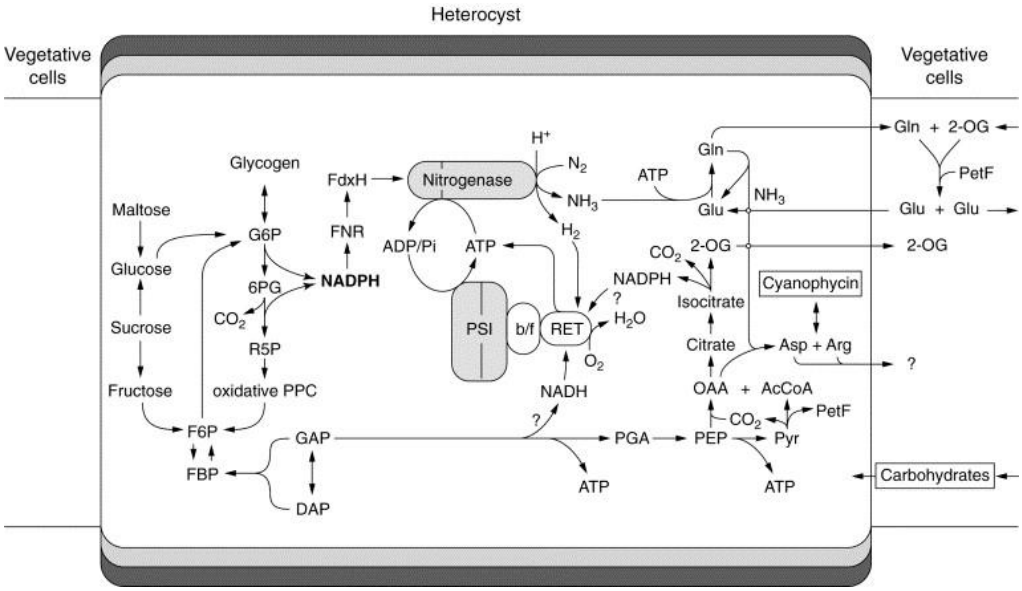


Figure 2.6 | Heterocyst metabolism and nitrogen fixation. Abbreviations: (AcCoA), acetyl coenzyme-A; (Arg), arginine; (Asp), aspartate; (b/f), cytochrome *b6f* complex; (F6P), fructose 6-phosphate; (PetF), vegetative cell type ferredoxin; (Glu), glutamate; (Gln), glutamine; (OAA), oxaloacetate; (2-OG), 2-oxoglutarate; (6PG), 6-phosphogluconate; (PGA), 3-phosphoglycerate; (Pi), inorganic phosphate; (R5P), ribose 5-phosphate (taken from Böhme 1998) [144].

Once a cell begins to differentiate into a heterocyst, the physical and metabolic properties of the cell also begin to change [87]. The cell wall begins to thicken, and some photosynthetic proteins (such as PSII complexes) and pigments are inactivated [145]. This reduces the production of oxygen and enables these resources to be recycled back into new nitrogen fixing enzymes and related proteins [144]. The thickening of a heterocyst's cell wall is also accompanied by the formation of additional glycolipid layers [144], and the destruction of up to 80% of the microplasmodesmata, connecting heterocysts to the rest of the cyanobacteria filament [146]. The latter reducing the ability of oxygen to

diffuse into the cell, while still allowing nutrients such as carbohydrates or glutamate to enter, with carbohydrates acting as an energy source for nitrogen fixation and glutamate reacting with ammonia generated by nitrogen fixation [144,146]. The nitrogenase enzyme is also localised within the cell's cytoplasm, ensuring that it is surrounded by enzymes involved in oxygen consuming reactions (see Hania *et al*. 2023) [147]. The nitrogenase enzyme is further protected from oxygen, therefore, by an abundance of oxygen scavengers including cytochrome c oxidase, and PSI complexes [139].

These adaptations reduce the amount of oxygen present within the cell, and therefore, increase the efficiency of the nitrogenase. Once nitrogen is fixed into glutamine, it is then transported into neighbouring vegetative cells via remaining microplasmodesmata [144]. The 'exchange' of nitrogen for carbon allows the heterocysts and vegetative cells to become highly specialised in their respective roles. This also ensures that the cyanobacteria's capacity to fix nitrogen is intrinsically tied to its ability to fix carbon.

2.4 Productivity of cyanobacteria

If cyanobacteria are to be effective for CO_2 valorisation, a key question is, how effective are these organisms at fixing inorganic CO_2 (and if able, N_2) into useful organic molecules. Currently, however, there are several challenges limiting the potential usefulness of these organisms.

2.4.1 *Limitations of using cyanobacteria in large scale production*

These key challenges are shown in **Table 2.1** and include the substrate (CO_2) to product conversion rate, which is significantly slower than heterotrophic alternatives, and therefore less competitive productivity at scale [148,149]. Cyanobacteria are also vulnerable to abiotic stresses [150], which impacts growth and productivity, they are also prone to contamination issues [151,152], and phenotypic instability [150,153]. Research to enhance the value of cyanobacteria in CO_2 valorisation should therefore seek to address these current knowledge gaps.

Table 2.1 | Current challenges and research gaps in optimising cyanobacteria productivity

Limitation	Description	Opportunities for Further Research	References
Low autotrophic substrate conversion rate	Cyanobacteria show significantly lower productivity compared to heterotrophic organisms	· Strategies to enhance light utilisation efficiency · Strategies to enhance CO_2 utilisation efficiency · Strains not metabolically optimised for growth in controlled commercial environments · Limited understanding of complex metabolic regulatory mechanisms · Removal of redundant pathways	148,149
Vulnerability to abiotic stresses	Cyanobacteria are often sensitive to fluctuations in light intensity, temperature, nutrient availability – resulting in loss of entire cultures to 'crash' events	· Gaps exist in the characterisation of individual stress response mechanisms · Development of strains / engineering strategies to enhance strain resilience to abiotic stresses	150
Contamination of cultures	Cyanobacteria naturally form opportunistic relationships with other microorganisms, resulting in frequent contamination of cultures and / or 'crash' events	· Few effective biocontrol strategies · Limited understanding of inter-microbial interactions	151,152
Phenotypic instability	A challenge in exploiting microorganisms more generally, however, especially acute in large, slower growing cyanobacteria cultures	· Development of strategies to couple production with cellular growth	150,153

While cyanobacteria benefit from lower feedstock input costs, this is offset by their significantly diminished production when compared to heterotrophic alternatives [148]. For example, the Gram-negative bacterium *Klebsiella oxytoca* M5A1 was engineered to express both the pyruvate decarboxylase and alcohol dehydrogenase from the yeast *Zymomonas mobilis* [154]. The strain produced ethanol yields of 40 $g \cdot L^{-1}$ in 24-hours from glucose and xylose substrate, compared to 248 $mg \cdot L^{-1}$ produced by engineered *Synechocystis* sp. PCC 6803 from CO_2 [155]. A significant factor limiting the productivity of cyanobacteria are their relatively slow growth rates [7], constrained by their photosynthetic efficiency and intracellular resource allocation [7]. The fast-growing cyanobacteria isolate, *Picosynechococcus* sp. PCC 11901, has an impressive doubling time of ~2 hours under optimal conditions [156]. However, this is still many times slower than heterotrophic bacteria, with doubling times of just 20 minutes in standard lab *E. coli* strains [157]. This difference is in partly due to the use of sugar as feedstocks for these organisms. As sugar contains a high concentration of both carbon and chemical potential energy, this enables heterotrophic organisms to grow rapidly [7]. Significantly increasing their productivity.

Instead, cyanobacteria currently invest much of their acquired carbon into cellular resources not directly linked to product synthesis. To address these challenges, strategies to streamline the growth, and improve the efficiency of cyanobacteria are necessary. Work to engineer cyanobacteria to improve production must identify strategies to both maximise the use of available metabolic resources, and where possible, identify ways to increase the abundance of those resources (see **Figure 2.7**). Here, the focus should identify ways of improving CO_2 fixation efficiency, and how this fixed carbon can be used to generate biomass, and compounds of interest [158].

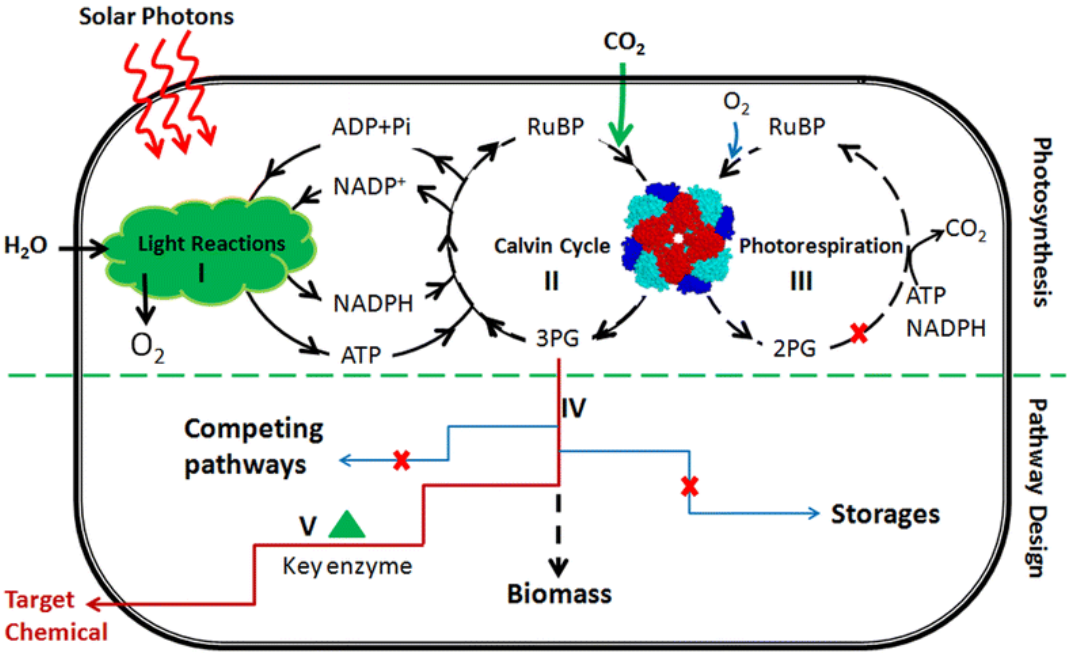


Figure 2.7 | Simplified overview of engineering targets to enhance growth and productivity in cyanobacteria. **I**. Enzymes involved in light capture and photosynthesis. **II**. RuBisCO and the CB cycle. **III**. Disrupting photorespiration. **IV**. Synthesis pathway optimisation. **V**. Engineering molecular bottlenecks. (Taken from Zhou *et al*. 2016) [158].

Further limiting potential productivity of cyanobacteria is the susceptibility of cultures to so called 'crash' events (see Jones, 2014; Zhu et al. 2020) [150], during which most of a culture's population rapidly dies following accumulation of pressure from an external stress (either abiotic or from a contaminant). This can be especially problematic for strains which have adapted to highly controlled laboratory environments; strains which have potentially acquired lower resilience to environmental pressures due to a prolonged lack of exposure to these pressures [150]. However, 're-wilding' of strains is likely undesirable too, given that cyanobacteria aren't 'naturally' cultivated in large industrial processes. Therefore, cyanobacteria strains adapted to the specific pressures of potential commercial environments are necessary. Given the risk of genetic drift within microbial populations away from productivity and towards strain fitness [150,153], successful engineering strategies should seek to couple strain modifications with core characteristics, particularly growth and cell division.

Collectively, these challenges have generally limited the commercial use of cyanobacteria to the production of niche, high value compounds [159].

[160][161][162][163]Where lower production yields are offset by a commodity's high value. However, if cyanobacteria are to be useful in the production of compounds at scale, it will be first necessary to improve their productivity.

2.4.2 *Measuring productivity in cyanobacteria*

To enhance cyanobacterial productivity, strategies will need to address the relative capacity of individual cyanobacteria to fix CO_2 or N_2 are required. As discussed in sections **2.2** and **2.3**, there is already a strong understanding of the underlying cellular mechanisms behind these processes in cyanobacteria, which could allow for more targeted analytical strategies to assess productivity. Furthermore, there is a strong understanding of how photoautotrophic organisms could be applied in the valorisation of waste emissions (see Ray et al. 2022) [160], which emphasises using these organisms at large scale. Given that the key rationale of using cyanobacteria is their ability to use CO_2, when seeking to assess the relative value of individual cyanobacteria here, strategies should seek to assess 'how much' CO_2 is removed. An overview of analytical strategies is shown in **Table 2.2**.

Table 2.2 | Strategies to assess fixation of CO_2 and / or N_2 in cyanobacteria

Strategy	Method	Advantages	Limitations
A. Measuring off-gas composition	Gas analyser	· Whole system approach · Enables calculation of substrate consumption rate	· Assumes all CO_2 removed has been consumed · Highly sensitive to real time changes in cell density and abiotic factors · Practically challenging to implement high-throughput analysis
B. Enzymatic analysis	Activity assay	· Can identify more efficient enzyme structures for future engineering · High-throughput strategies available (enzyme dependent) · Enables calculation of substrate consumption and conversion rates	· Multiple enzymes involved (directly and indirectly) in fixation · Individual enzyme activities cannot predict whole cell metabolisms · Enzymatic assays cannot replicate specific intracellular environments
C. Product quantification	Product dependent	· Practically straightforward · High-throughput strategies available (product dependent) · Enables calculation of substrate conversion rate · Commercially relevant results	· Productivity assessment is product specific · Focus potentially myopic, low yielding strains could still capture significant quantities of CO_2 in biomass

D. Fluxomic analysis	Mass spectrometer	· Allows exact quantification of substrate assimilation · Can show where fixed resources flow within cell metabolic pathways	· Practically challenging to implement high-throughput analysis · Labelled isotope substrates expensive · Flux analysis limited to labelled substrates only · Requires expensive, specialised equipment
E. Elemental composition	Elemental analyser	· Whole system approach · Potential for high-throughput analysis · Exact quantification of element per cell	· Significant intracellular elemental fluctuations (even by time of day) · Requires specialised equipment
F. Biomass	Dry weights	· Whole system approach · Practically very straightforward · Inexpensive · Enables high-throughput analysis	· Non-specific to element of interest

One potential strategy to assess fixation rates by cyanobacteria is to quantify the total CO_2 or N_2 removed from a gas mixture at the point of exhaust (**Table 2.2 A**). This strategy has previously been used to estimate consumption of CO_2 by *Chlorella* microalgae grown using power plant waste emissions [161], and has the advantage of estimating the absolute rate of a substrate's consumption in a contained process (accounting for both cell growth, and any secondary product formation). However, there are limitations to this strategy. As shown by Politaeva et al. 2023 [161], CO_2 consumption can vary significantly over the course of a culture's growth, even over a single growth cycle with fixed abiotic inputs (including constant illumination and temperature). To assess consumption accurately, individual off-gas analysers are required for each culture being investigated, limiting parallel analysis to the total number of individual available instruments. Furthermore, this strategy is an indirect analysis of samples, one that assumes the totality of 'missing' gas has been consumed (rather than lost or dissolved in solution).

Alternatively, rather than assessing the rate of substrate consumption by a whole process, one could characterise individual carboxylase enzyme activities (**Table 2.2 B**). The proteins responsible for fixing CO_2. This would have the advantage of identifying more efficient variants of the specific components which directly act upon the substrate in question. Enzyme variants could be identified with greater substrate specificity / turnover rate, and a lower energy loss to photorespiration (see section **1.2.4.3**). These variants could then be used commercially in engineered cyanobacteria to increase productivity. Enzymatic assays to characterise RuBisCO are well established [162,163], and previous work by Davidi et al. 2020 identified RuBisCO variants with an almost 2-fold increase in turnover rate compared to the fastest known cyanobacteria RuBisCO (from *Synechococcus* sp. PCC 6301) [164]. However, using selected enzyme kinetics to assess productivity has significant limitations. Firstly, multiple enzymes are involved in CO_2 assimilation in cyanobacteria, one more efficient isoform, even one as significant as RuBisCO, does not guarantee greater productivity from a transgenic host. Previous work by Lin et al. 2014 expressing more efficient RuBisCO variants from *Synechococcus elongatus* PCC 7942 in tobacco plants indeed confirmed higher CO_2 fixation rates per unit of enzyme [165]. However, despite an increase in enzymatic activity, the transgenic plants showed a significant overall reduction in biomass formation over the same period compared to the wild-type control [165]. Highlighting the complex interconnected nature of intracellular metabolism, in which more efficient individual enzymes alone are insufficient to enhance overall productivity.

If assessing individual enzymes responsible for fixation cannot accurately predict productivity in the cell, quantifying a metabolite

produced during growth could be an alternative strategy (**Table 2.2 C**). Characterisation methods are well established for a wide variety of commercial products, including alcohols [155], biofuels [166], organic acids [167], and terpenoids [168]. Assessing product formation has several advantages, as the strategy ties productivity assessment with the formation of a commercially useful product. Depending on the product, the strategy could also allow for high-throughput screening of organisms. These advantages, however, can also be a key limiting factor, as measuring the formation of a single product does not inform how productive another industrial strategy for a different product will be. It also does not provide information on how individual cyanobacteria compare to one another more broadly in valorising CO_2, as measuring product formation alone does not include the significant component of fixed CO_2 assimilated into biomass.

Focusing measurements on directly assessing substrate utilisation, including CO_2 uptake via ^{13}C labelling (Adebiyi et al. 2015) [169], and N_2 fixation via ^{15}N labelling (Nieves-Morión et al. 2021) [170], could quantify substrate fixation by individual cyanobacteria cells (**Table 2.2 D**). These isotopic labelling strategies have the additional advantage of identifying where cells distribute these fixed resources. This is therefore a strategy which could also assist in identifying molecular bottlenecks within a cell. However, this strategy is both highly prohibitive with respect to its cost and the practical challenges of its implementation [171]. Significantly limiting its potential usefulness in screening large populations (such as engineered strain libraries), and preventing its use in high-throughput screening.

Alternatively, dedicated instruments to assess overall elemental composition of samples have previously been used to assess elemental composition in cyanobacteria (**Table 2.2 E**), estimating exact quantities of carbon / nitrogen per cell [172]. This strategy could also allow for high-throughput screening of larger population samples (see Lopez et al. 2016) [172]. However, previous work characterising carbon, nitrogen, and phosphorus contents in *Synechococcus* (WH8102) demonstrated significant fluctuations in intracellular elemental abundances, with carbon quotas both doubling and halving in under 24-hours of diurnal growth [172]. Furthermore, relying on productivity measurements focused on an individual element's 'relative' abundance, (even one as central as carbon) doesn't necessarily reflect the productivity of something as complex as a microorganism's biomass, and must be assessed against total biomass generated to be informative.

The primary 'product' of carbon fixation by non-engineered cyanobacteria, is biomass (**Table 2.2 F**). This includes individual cell structures, intra- or extracellular metabolites, and is reflected in a

population's total mass across a defined space (see Zhu et al. 2007; Clark et al. 2019) [173,174]. When this mass per volume is measured per unit of time, this strongly indicates the capacity of a cyanobacteria to fix carbon (see Zavřel et al. 2021) [175]. Of 170 parameters, Zavřel et al. 2021 demonstrated that a cell's rates of photosynthesis and respiration showed the highest correlation with biomass formation in the model cyanobacteria *Synechocystis* sp. PCC 6803 [175]. Although measurement of a cell's individual characteristics offers an insight into how it achieves a specific growth rate or productivity, the measurement of product mass remains the reference against which photoautotrophic productivity is ultimately calculated (see Zavřel et al. 2021) [175]. Therefore, when carbon mass is derived exclusively from photoautotrophic growth, biomass formation is a strong indicator of a cell's photoautotrophic efficiency.

2.5 Strategies to enhance the productivity of cyanobacteria

As previously stated in section **2.4.1**, natural selection has not inherently selected for optimised photosynthetic productivity. Rather, it selects for improved fitness in relation to the environment. Therefore, there exists the potential to enhance the productivity of cyanobacteria through strain engineering [174]. Previous attempts to engineer cyanobacteria for improved productivity have benefitted from an expanding molecular toolkit for these organisms [176]. Many of these genetic toolboxes were originally created for heterotrophic organisms, and they have not always worked effectively when used to engineer cyanobacteria (see Lindblad and Camsund 2014) [177]. Efforts to adapt these tools for use in cyanobacteria have therefore been made in recent years [176].

2.5.1 *Genetic tools for cyanobacteria*

A key limitation in engineering cyanobacteria has been the availability of effective molecular circuitry, or "parts" [176]. Many of the DNA regulatory components, already identified for use with heterotrophic organisms, unfortunately do not always work effectively in cyanobacteria [178]. Promotor sequences such as P_{tet}, P_{lac}, and P_R, (components that work effectively within *E. coli*), have shown very poor efficacy in cyanobacteria [178]. To compensate for this, research has sought to identify and use features specifically found within cyanobacteria to design new components. Native ribosome binding sequences, tuneable promoter regions, and terminator

libraries have been identified in cyanobacteria, and used for effective heterologous gene expression [176]. Furthermore, light inducible promoter sequences allow for expression systems that account for their distinct photoautotrophic physiology [179]. In recent years, the development of effective riboswitches (mRNA secondary structures which affect the level of a gene's expression) [176], has also allowed for more controlled expression of heterologous genes. Allowing engineers to increase productivity by reducing the toxicity of engineering strategies. Both by reducing the formation of inclusion bodies due to overexpression, and through the more targeted expression of different genes [180].

A significant proportion of gene editing within cyanobacteria has been carried out using integration cassettes, as many of these organisms, (including model cyanobacteria such as *Synechococcus elongatus* sp. PCC 7942), have been shown to be naturally competent [176,181]. However, availability of vectors is limited within cyanobacteria, with many constructs being highly strain specific, and with fewer modular designs [176]. Furthermore, the use of integration constructs results in the introduction of antibiotic resistance cassettes to enable the selection of transformants [176]. This can make the process of strain engineering more challenging when organisms begin to accumulate these markers. To resolve this issue, work in recent years has also investigated the potential of using novel markerless systems, such as CRISPR [182], or established strategies such as *sacB* counterselection [183], to engineer cyanobacteria.

2.5.2 *Engineering strategies to optimise cyanobacteria productivity*

Table 2.3 presents an overview of previous work to engineer enhanced carbon utilisation in cyanobacteria.

Table 2.3 | Overview of selected heterologous overexpression strategies used to improve growth and CO_2 fixation of cyanobacteria.

Species	Target(s)	δ Biomass	Reference
Synechocystis sp. PCC 6803	*fbpI*	+ 52%	[184]
Synechocystis sp. PCC 6803	*2 x rubisco*	+ ca. 20%	[185]
Synechocystis sp. PCC 6803	*tktA*	+ 24%	[184]
Picosynechococcus sp. PCC 7002	*bicA*	+ 75%	[186]
Picosynechococcus sp. PCC 7002	*sbtA*	+ 60%	[186]

Species	Target(s)	δ Growth	Reference
Synechocystis sp. PCC 6803	*fbaA*	+ 50%	[184]
Synechocystis sp. PCC 6803	*fbaI*	+ 50%	[184]
Synechocystis sp. PCC 6803	3 x *pepc*	+ 44%	[77]

Species	Target(s)	δ Product	Reference
Synechocystis sp. PCC 6803	3 x *pepc* + *ppsa*	+ 58 - 326%	[187]
Synechocystis sp. PCC 6803	*gpi* + *ΔglgC*	+ ca. 340%	[188]
Synechocystis sp. PCC 6803	*tktA* + *fbaA*	+ ca. 960%	[189]

2.5.2.1 *Expression of photosynthetic genes*

When considering targets to improve growth and productivity within cyanobacteria, genes involved in central metabolism and photosynthesis are natural choices. To date, much of this research has investigated overexpression of genes involved in carbon fixation (see **Table 2.3**).

Here, improvements in growth and productivity have been made through the heterologous introduction of additional copies of native gene sequences [77,184–186,189], overexpression of orthologous proteins [187], and by overexpression strategies coupled with targeted gene deletions [188]. The rationale is straightforward, if a certain protein is involved in carbon fixation, increasing its abundance should increase productivity. As shown in **Table 2.3**, this strategy has been successful in increasing biomass accumulated, cell growth rates, and the productivity of cyanobacteria. Whilst improvements in cyanobacteria productivity have been observed using these methods, these have still been insufficient to outcompete heterotrophic platforms or conventional manufacturing methods. Overexpression in *Synechocystis* of both the native aldolase (*fbaA*) and transketolase (*tktA*) (enzymes responsible for RuBP regeneration within the CB cycle), resulted in an increase of ca. 960% in ethanol synthesis. Whilst impressive relative to what was produced before modification, 1.2 $g \cdot L^{-1} \cdot d^{-1}$ after 20 days of growth is still significantly lower than previously cited example of 40 $g \cdot L^{-1}$ using *Klebsiella oxytoca* M5A1 [154].

2.5.2.2 *Strain optimisation*

The knockout of competing pathways is a common strategy used in strain optimisation within all organisms, and when coupled with product synthesis, can be an efficient strategy for directing metabolic flux down desired pathways [158]. The blocking of glycogen synthesis, for example, has been shown to significantly increase productivity within cyanobacteria [188]. Glycogen is a carbohydrate storage molecule used by cyanobacteria to accumulate carbon, and the deletion of this metabolic sink has been shown to significantly increase the productivity of cyanobacteria on several occasions (see Zhou *et al*. 2016) [158].

Synechococcus elongatus UTEX 2973 is an example of where only limited changes to an organisms' genome, have had significant impacts on its growth. Although an isolate, and not the product of targeted

engineering work, this organism is closely related to *Synechococcus elongatus* sp. PCC 7943 [190]. Containing only 55 polymorphisms, which result in a 2-fold increase in their growth rate. Of these changes, 4 single nucleotide polymorphisms in 3 proteins have been identified by the authors as being significant [190]. Identified as C252Y in *atpA*, E260D in *ppnk*, and Q121R/E134K in *rpaA* [190,191]. These alleles were subsequently transformed into *Synechococcus elongatus* sp. PCC 7943 by Ungerer *et al*. 2018, reducing the doubling time of this strain from 6.8 to 2.3 hours [192]. This is a combination of mutations that would have been extremely challenging to predict from rational engineering. This is further complicated, however, as in a letter published by Zhou and Li (2019) they do not identify many of the SNPs in their own lab strain [191]. Suggesting there are further challenges to fully understanding how this strain has adapted to grow so fast.

2.5.2.3 *RuBisCO engineering*

Given the key role this enzyme plays in carbon fixation, it has been the subject of extensive efforts to engineer both greater CO_2 selectivity, and productivity (see Zhou *et al*. 2016; Whitney *et al*. 2011) [158,193]. However, this has been constrained by several factors, including the conformation of the enzyme's active site. Its interaction with multiple protein chaperones during its maturation and assembly, and its involvement in other molecular processes other than CO_2 fixation [193]. Incremental gains, however, have been made. For example, through use of an *E. coli*-based activity directed selection strategy, Cai *et al*. 2014 identified residue substitutions which increased both the specificity and activity of the carboxylation reactions by the *Picosynechococcus* sp. PCC 7002 enzyme, (by 85% and 45% respectively) [194], highlighting the potential of such directed evolution strategies to enhance CO_2 fixation. Furthermore, work has also been carried out to identify variants of the enzyme complex elsewhere in nature, which may be more productive (see Iñiguez *et al*. 2020) [195]. These could be harnessed by engineering their expression into photoautotrophic platforms, including cyanobacteria.

However, given the significant effort already invested in engineering RuBisCO, cyanobacteria carboxysomes, and carbon concentrating mechanisms have also been evaluated [158]. Here, bicarbonate and inorganic carbon uptake have been increased to help mitigate the RuBisCO oxygenase activity by increasing the relative abundance of CO_2 in its proximity. This can be achieved as the soluble bicarbonate is converted into CO_2 via the carbonic anhydrase enzymes within the carboxysomes [158].

As shown in **Table 2.3**, overexpression of both the *bicA* and *sbtA* bicarbonate transporters in *Picosynechococcus* sp. PCC 7002 significantly increased cyanobacteria biomass formation, by 75% and 60% respectively [186].

2.5.2.4 *Limitations of rational engineering strategies*

Despite these successes, cyanobacteria are complex organisms and directing metabolic flux towards only one pathway will inevitably reduce it from another. This trade-off could result in strains becoming highly specialised to produce a single compound of interest. Engineering strategies, such as the increased transport of bicarbonate to the carboxysome, or efforts to improve RuBisCO, have demonstrated that they can increase the productivity of cyanobacteria. However, they have not resulted in strains capable of competing with heterotrophic alternatives, and the latter is beset with many challenges.

Work by Kanno *et al*. 2017 also showed that through rational design, biomass formation could be increased by redirecting metabolic flux within the *Synechococcus elongatus* PCC 7942 CB towards 2,3-butanediol and biomass formation, by introducing genes to enhance growth under mixotrophic conditions [196]. The productivity of the strain was measured as 1.1 $g \cdot L^{-1} \cdot d^{-1}$, significantly higher than previous work by Oliver *et al*. 2013 which showed peak production of ~200 $mg \cdot L^{-1} \cdot d^{-1}$ [197]. However, given the importance of the addition of glucose to achieve these yields, this production strategy is still reliant sugar (see Lips 2022) [198].

These strategies have shown the potential to enhance both growth and productivity, however, with many potential avenues of investigation having been explored, new strategies are necessary to identify targets to enhance the growth of cyanobacteria. Given both the challenges involved in rationally engineering cyanobacteria to improve their growth, it is perhaps worth considering strategies which exploit the organism's own selective mechanisms.

2.6 Adaptive Laboratory Evolution (ALE)

At its core, ALE is a strategy to achieve the accelerated evolution of an organism, in which the criteria determining fitness during natural selection are predetermined by the investigator [199]. Access to whole

genome sequencing has expanded since the 2010s, coupled with decreasing sequencing costs, which has enabled researchers to use ALE more effectively for strain engineering [200,201]. As changes within selected strains can be more easily identified and replicated in other production strategies. The use of ALE has since become increasingly popular (see Sandberg et a. 2019) [202]. This is perhaps both because of its straightforwardness compared to extensive metabolic engineering, and because the strategy allows rapid screening of an organism's innate genetic potential [201].

2.6.1 *Principles of ALE*

Unlike many heterologous approaches, ALE can create relatively unbiased modifications, where fitness of the selected strain is a determining factor in selection [201–203]. ALE works by exploiting those innate selective mechanisms of evolution and directing selection towards a desired phenotypic outcome (see **Figure 2.8**) [202].

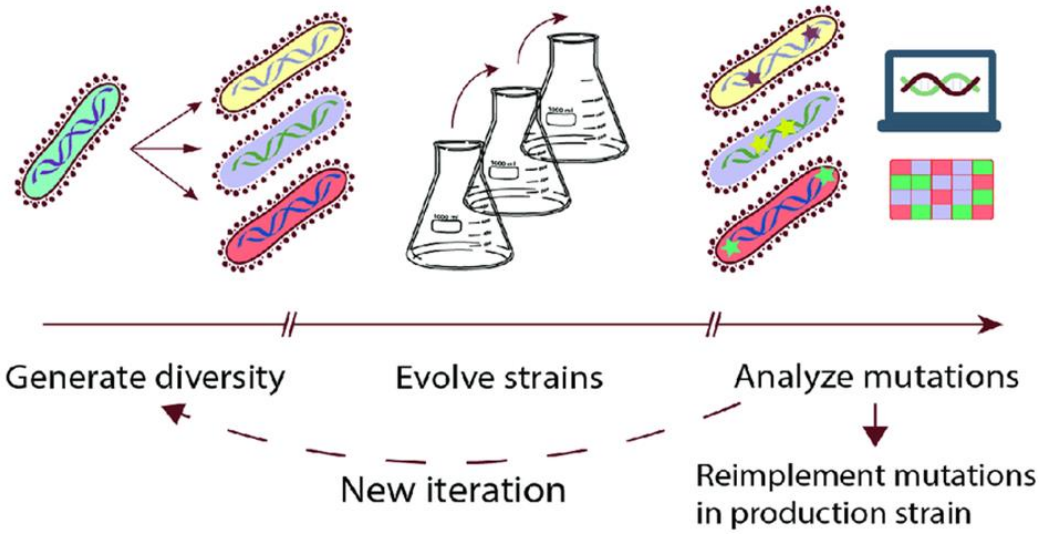


Figure 2.8 | Overview of ALE strain selection workflow (Taken from Shepelin *et al*. 2018) [204].

The aim of an ALE experimental design where specific phenotypes are preferred, and progeny are created through asexual reproduction, is to create a selective environment in which it is statistically more likely for

those selected phenotypes (and therefore relevant alleles) to occur (see Gerrish and Lenski, 1998) [205]. Each progeny in a fixed environment replaces, at random, another potential individual of that population by consuming finite resources, space, and parentage (see Uecker and Hermisson, 2011) [206]. Therefore, the most successful ALE strategies should simultaneously seek to increase the replication rate of organisms with desirable alleles, and reduce the fitness of organisms with less advantageous (or even deleterious) alleles. To assess an ALE strategy's efficacy and specificity in selecting for preferred individual characteristics, it is important to characterise not only individual strains of interest, but to ascertain the frequency of these characteristics within a selected population (see Dragosits and Mattanovich, 2013; Sandberg et al. 2019) [202]. This can be assessed by measuring both the relative abundance and statistical significance of changes in non-discrete characteristics, among randomly selected isolates.

Many ALE investigations begin by first increasing the genetic diversity of the population [204], typically through the use of mutagenesis [201]. An ALE investigation can select for all types of mutations, including SNPs, insertions and deletions, translocation of transposable elements, as well as amplification and loss of large regions of DNA [201]. However, ALE experiments often result in specific types of mutations over others, SNPs account for the majority of identified mutations [207]. When considering how to carry out ALE using cyanobacteria, an additional consideration is the multiple copies of their genome. This enables allelic mutations in genes, otherwise lethal to the cell, and may possibly explain why strains are lost after selection (see Patel *et al*. 2016) [208]. Furthermore, Leon *et al*. 2018 demonstrated that when selective pressure is removed from organisms before full acquisition of a novel phenotype, this can cause the regression of the partially adapted strains [209]. During selection, a strategy must apply sufficient selective pressure to push strains beyond what they are capable of simply 'tolerating'. This is to ensure that isolates are indeed mutants with authentic genotypic variation, and not as the result of phenotypic plasticity, which could obscure selection if the selective pressure is insufficient (see Lalejini *et al*. 2021 [210]).

2.6.2 *Use of ALE to enhance productivity*

Regarding experimental design, ALE therefore generally favours experiments which focus on very specific goals, as these enable researchers to apply specific and directed selection pressure. It is therefore

primarily used to investigate improved efficiencies surrounding single substrate objectives (see **Figure 2.9**). Out of 159 studies reviewed by Sandberg et al. 2019, 69.8% of the ALE experiments focused on the improved tolerance, utilisation, or yield of a single substrate. With only 11.3% employing the strategy to specifically enhance growth rates [202]. This may be in part due to the more abstract nature of using ALE for such a purpose, as selecting for improved growth does so under a chosen set of parameters which are unlikely to be universal in their application.

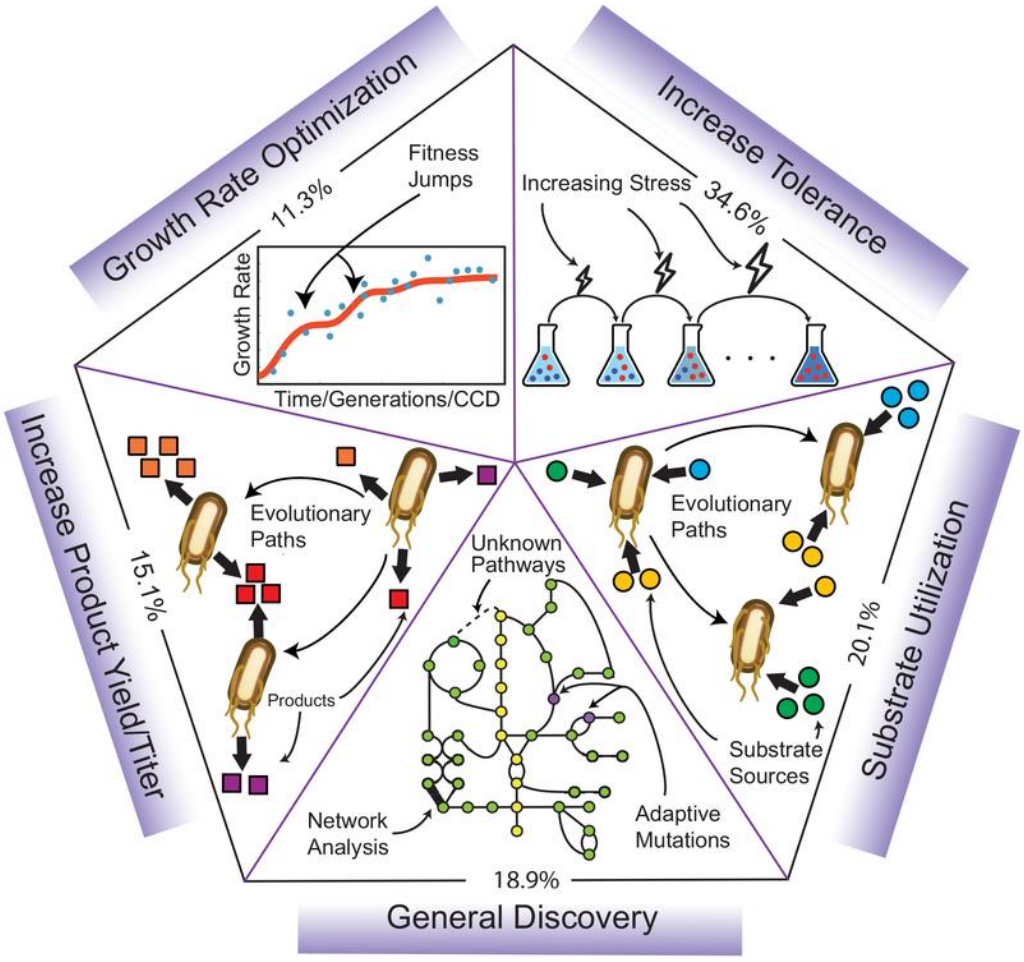


Figure 2.9 | Diagram showing the different aims of laboratory evolution experiments, detailing the percentage of studies which investigated strategies to optimise growth rates, increase tolerance, increase substrate utilisation, increase product titre, or identify novel adaptions, pathways, and mutations (*N* = 159). Taken from Sandberg *et al*. 2019 [202].

ALE has also been shown to be highly effective in improving existing substrate utilisation, which is itself often linked to enhancing an organism's growth and productivity. Based on analysis of previous publications and previous work by Sandberg et al. 2019 [202], an overview of ALE experiments investigating strategies to improve microorganism growth and / or substrate utilisation is shown in **Table 2.4**. This includes how organisms were selected, over how many generations / how long, what (if any) relative improvements were recorded, and which analytical methods were employed to characterise mutant isolates, (omics includes only comprehensive analyses, and excludes analysis of selected individual genes, transcripts, metabolites etc.).

Table 2.4 | Studies investigating application of ALE to enhance growth and / or substrate utilisation, 1991 - 2023, (adapted from previous work by Sandberg et al. 2019) [202]

Studies	Organism	Trophy	Mutagenesis	Selection Method	Generations / Duration	Outcome Measure [a]	Result (+%) [b]	Analytical Methods [c]
Lenski et al. 1991 [211]	*E. coli*	heterotrophic	-	batch [d]	2000 [e]	growth	37%	
Lenski et al. 1994 [212]	*E. coli*	heterotrophic	-	batch [d]	10000 [e]	growth	n/a	
Weikert et al. 1997 [213]	*E. coli*	heterotrophic	-	continuous [d]	217	growth	23%	B, S
Lenski et al. 1998 [205]	*E. coli*	heterotrophic	-	batch [d]	10000 [e]	growth	50%	
Ferea et al. 1999 [214]	*S. cerevisiae* [f]	heterotrophic	-	continuous [d]	250 [e]	growth	200%	T
Sonderegger et al. 2003 [215]	*S. cerevisiae* [g]	heterotrophic	chemical	continuous [d]	170 [e]	growth	150%	B
Kuyper et al. 2004 [216]	*S. cerevisiae* [g]	heterotrophic	-	batch	30	growth	3500%	B, S
Jansen et al. 2004 [217]	*S. cerevisiae* [g]	heterotrophic	-	continuous [d]	<100 [e]	utilisation	150%	B, S, T
Kuyper et al. 2005 [218]	*S. cerevisiae* [g]	heterotrophic	-	continuous	85 [e]	growth	33%	B, S
Guimarães et al. 2008 [219]	*S. cerevisiae* [g]	heterotrophic	-	batch	>120	utilisation	100%	B, S
Lee et al. 2010 [220]	*E. coli* [f]	heterotrophic	-	batch	700 [e]	growth	n/a	B, G, S
Garcia Sanchez et al. 2010 [221]	*S. cerevisiae* [g]	heterotrophic	-	batch	20	growth	1250%	B, S
Hong et al. 2011 [222]	*S. cerevisiae* [g]	heterotrophic	-	batch	400 [e]	growth	24%	B, G, S, T
Zelle et al. 2011 [223]	*S. cerevisiae* [g]	heterotrophic	-	continuous [d]	30 days	growth	n/a	S
Ochoa-Estopier et al. 2011 [224]	*S. cerevisiae*	heterotrophic	-	continuous [d]	90	growth	1900%	B, S

Merico et al. 2011 [225]	*S. cerevisiae* [f]	heterotrophic	-	batch	111 [e]	growth	138%	**B**
Cadiere et al. 2011 [226]	*S. cerevisiae*	heterotrophic	-	batch	200 [e]	utilisation	425%	**B**, **M**, **S**
Utrilla et al. 2012 [227]	*E. coli* [g]	heterotrophic	-	batch	15 transfers [e]	utilisation	100%	**G**, **P**, **S**
Kim et al. 2012 [228]	*S. cerevisiae* [f]	heterotrophic	-	batch	7 cycles	utilisation	247%	**G**, **S**
Zhou et al. 2012 [229]	*S. cerevisiae* [g]	heterotrophic	-	continuous	<100	utilisation	n/a	**B**, **S**, **T**
Scalcinati et al. 2012 [230]	*S. cerevisiae* [g]	heterotrophic	-	batch	10 cycles	utilisation	n/a	**B**, **S**, **T**
de Kok et al. 2012 [231]	*S. cerevisiae* [f]	heterotrophic	-	batch	10 [e]	growth	17900%	**B**, **G**, **S**, **T**
Yu et al. 2013 [232]	*C. reinhardtii* [g]	autotrophic (CO_2)	-	batch	28 cycles	growth	48%	**B**
Carroll et al. 2013 [233]	*M. extorquens* [f]	heterotrophic	-	batch	600 [e]	growth	150%	**T**
Klimacek et al. 2014 [234]	*S. cerevisiae* [g]	heterotrophic	-	batch	61	growth	n/a	**B**
Novy et al. 2014 [235]	*S. cerevisiae* [g]	heterotrophic	-	batch	91 days	utilisation	150%	**B**, **S**
Smith et al. 2014 [236]	*S. cerevisiae* [g]	heterotrophic	chemical	batch	220	growth	867%	**B**, **S**
Zha et al. 2014 [237]	*S. cerevisiae* [g]	heterotrophic	-	batch	7 cycles	growth	700%	**G**, **S**, **T**
Lenski et al. 2015 [238]	*E. coli*	heterotrophic	-	batch [d]	60000 [e]	growth	5.10%	
LaCroix et al. 2015 [239]	*E. coli*	heterotrophic	-	batch [d]	39-81 days	growth	47%	**B**, **G**, **S**, **T**
Latif et al. 2015 [240]	*T. maritima*	heterotrophic	-	batch	240	growth	40%	**G**, **T**
Sandberg et al. 2016 [241]	*E. coli*	heterotrophic	-	batch	1000 generations [e]	growth	40%	**B**, **G**, **M**
Szappanos et al. 2016 [242]	*E. coli* [f]	heterotrophic	-	batch	40 days [e]	growth	n/a	**G**
Rajaraman et al. 2016 [243]	*E. coli*	heterotrophic	-	continuous	450 [e]	growth	24%	**B**, **G**, **T**
van Rossum et al. 2016 [244]	*S. cerevisiae* [g]	heterotrophic	-	batch	70 [e]	growth	n/a	**G**
Cordova et al. 2016 [245]	*T. thermophilus*	heterotrophic	-	continuous	~30 days	growth	100%	**B**, **G**, **M**

Radek et al. 2017 [246]	*C. glutamicum* [g]	heterotrophic	-	batch	35 [e]	growth	260%	**B**, **G**, **S**
Pfeifer et al. 2017 [247]	*C. glutamicum*	heterotrophic	-	batch [d]	630	growth	26%	**B**, **G**
Ho et al. 2017 [248]	*S. cerevisiae* [g]	heterotrophic	-	batch	25 [e]	growth	38%	**G**
Sandberg et al. 2017 [249]	*E. coli*	heterotrophic	-	batch	1000	growth	67%	**G**, **T**
Moser et al. 2017 [250]	*P. pastoris*	heterotrophic	-	batch [d]	250 [e]	growth	140%	**B**, **G**
Marques et al. 2017 [251]	*S. cerevisiae* [g]	heterotrophic	-	batch	100 - 500 [e]	growth	212.50%	**G**, **T**
Thyer et al. 2018 [252]	*E. coli* [f]	heterotrophic	-	batch	2500 [e]	growth	n/a	**G**
Wannier et al. 2018 [253]	*E. coli* [f]	heterotrophic	-	batch	1100 [e]	growth	100%	**G**
Strucko et al. 2018 [254]	*S. cerevisiae* [g]	heterotrophic	-	batch	380	growth	300%	**B**, **G**, **M**, **P**, **S**, **T**
Papapetridis et al. 2018 [255]	*S. cerevisiae* [g]	heterotrophic	-	batch	13 transfers	utilisation	150%	**B**, **G**
Zhang et al. 2018 [256]	*S. cerevisiae*	heterotrophic	-	batch	400 [e]	utilisation	47.90%	**G**, **S**, **T**
Mohamed et al. 2019 [257]	*E. coli* [g]	heterotrophic	-	batch	40 days [e]	utilisation	272%	**G**, **S**
Igeño et al. 2019 [258]	*P. pseudoalcaligenes* [f]	heterotrophic	-	batch	4 transfers	utilisation	700%	**S**
Tsiamis et al. 2019 [259]	*C. glutamicum*	heterotrophic	-	continuous	73 days	growth	35%	**B**
Diao et al. 2019 [260]	*C. cohnii*	heterotrophic	-	batch	210 cycles [e]	growth	30%	**B**
Espinosa et al. 2020 [261]	*S. cerevisiae* [g]	heterotrophic	-	batch	230	growth	37%	**G**, **M**, **P**, **T**
Millán et al. 2020 [262]	*A. vinelandii*	heterotrophic	-	batch	387 [e]	growth	100%	**B**, **S**
Wang et al. 2020 [263]	*C. glutamicum*	heterotrophic	-	batch	7 cycles	growth	568%	**B**, **G**, **S**, **T**
Promdonkoy et al. 2020 [264]	*S. cerevisiae* [g]	heterotrophic	-	batch	12 cycles	growth	42%	**B**, **G**
Liu et al. 2020 [265]	*B. subtilis* [f]	heterotrophic	-	batch [d]	1000 [e]	growth	43.53%	
Lakhssassi et al. 2020 [266]	*C. carboxidivorans*	autotrophic (CO_2)	chemical	batch	1 cycle	utilisation	313%	**S**
Lim et al. 2021 [267]	*P. putida* [g]	heterotrophic	-	batch	203 - 479 [e]	growth	420%	**B**, **G**, **T**

Bennett et al. 2021 [268]	*E. coli* [g]	heterotrophic	chemical	batch	5 cycles	utilisation	16%	**B**, **G**, **S**
Nahel et al. 2021 [269]	*S. obliquus*	autotrophic (CO_2)	UV	continuous	~150 days	growth	24%	**B**
Gassler et al. 2022 [270]	*P. pastoris* [f]	autotrophic (CO_2)	-	batch	62	growth	125%	**B**, **G**
Zhang et al. 2022 [271]	*H. bluephagenesis* [f]	heterotrophic	-	batch	71 cycles	growth	82.32%	**B**, **G**, **S**
Du et al. 2022 [272]	*K. marxianus*	heterotrophic	-	batch	300	utilisation	n/a	**G**, **S**
Gjetø et al. 2022 [273]	*C. vulgaris*	autotrophic (CO_2)	-	continuous [d]	14 days [e]	growth	n.m.	**B**
Arora et al. 2022 [274]	*N. oculata*	autotrophic (CO_2)	chemical	batch	24 cycles [e]	growth	43%	**B**, **M**
Mueller et al. 2022 [275]	*P. putida* [g]	heterotrophic	-	batch	105 days [e]	growth	30%	**G**
Ling et al. 2022 [276]	*P. putida* [g]	heterotrophic	-	batch	14 days	utilisation	n/a	**M**, **S**
Barten et al. 2022 [277]	*Picochlorum sp. BPE23*	autotrophic (CO_2)	-	continuous	322 days	growth	22.30%	**B**, **G**, **T**
Varunraj et al. 2023 [278]	*C. vulgaris*	autotrophic (CO_2)	-	batch	35, 8 cycles [e]	growth	n.s.	**B**
Neto et al. 2023 [279]	*C. reinhardtii*	autotrophic (CO_2)	UV	batch	267 days [e]	growth	31%	**B**
Wickham-Smith et al. 2023 [280]	*C. necator*	autotrophic (CO)	-	batch	18 days [e]	growth	151%	**G**
Antonicelli et al. 2023 [281]	*C. carboxidivorans*	autotrophic (CO_2)	-	batch	10 cycles [e]	growth	14%	**B**, **G**, **S**
Li et al. 2023 [282]	*Chlorella AE1*	autotrophic (CO_2)	-	batch	31 cycles	growth	56%	**B**
Wefelmeier et al. 2023 [283]	*O. polymorpha* [g]	heterotrophic	-	batch	25 cycles	growth	55%	**B**, **G**, **S**

[a] - Strain growth (biomass formation / specific growth rate) or substrate utilisation (uptake / conversion)
[b] - (standardised to % where possible) δ strain biomass, growth rate, or substrate utilisation - average (if stated), highest (otherwise)
[c] - Mutant characterisation - **B** - biomass; **G** - genome; **M** - metabolome; **P** - proteome; **S** - δ substrate / product; **T** – transcriptome
[d] - Selection under nutrient limitation [e] - Multiple, parallel populations under selection [f] - Strain is engineered
[g] - Strain is engineered, to direct substrate metabolic flux
n/a - Not applicable n.m. - Not measured n.s. - Not significant

Although not exhaustive, the examples listed in **Table 2.4** provide an overview of previous ALE work focused on increasing growth and substrate utilisation. This offers insight into the common themes of related ALE experimental designs, and provides references to assess experimental outcomes from ALEs to increase cyanobacteria carbon / nitrogen fixation against. Most of the examples listed show improvements in cell physiology and productivity, with a few exceptions. Sandberg et al. 2014 reported no significant changes in adaption when culturing with isotopically labelled (^{13}C) glucose compared to unlabelled glucose [241], and Gjetø, 2022 investigated the optimisation of their chemostat array designs for microalgal ALE, rather the application of these designs for ALE (see Gjetø, 2022) [273]. This is potentially an issue, as the development of effective selection strategies to enhance growth and substrate utilisation may need to address unforeseen pitfalls previously encountered, but not necessarily reported in the literature.

Despite this, the examples above demonstrate the potential of ALE to enhance strain productivity; of the 74 examples listed in **Table 2.4** increases were reported in growth as a result of ALE (biomass yield / μ_{max}) in 58 publications, and increased substrate utilisation was directly measured in 16 publications. Reported increases in substrate utilisation range from +16% [268] to +700% [258], and increases in growth from +5.1% [238] to +17,900% [231]. Changes in growth and substrate utilisation have been standardised to percentages to allow relative comparison of ALE experiments. However, these do not necessarily reflect the scale of quantitative changes; with the upper and lower range bounds of increased substrate utilisation being +16% and +17,900%, indicating final substrate utilisation rates of 7.4 $mg \cdot h^{-1}$ and 2.9 $mg \cdot h^{-1}$ respectively [258,268]. A relatively modest increase (+150%) of μ_{max} was seen in chemically mutagenised *Saccharomyces cerevisiae* strains, which had been evolved in a chemostat with a limited carbon source, Sonderegger et al. 2003. However, this increase in μ_{max} resulted in +0.4 – 0.5 $g \cdot g^{-1}h^{-1}$ of substrate utilisation (see Sonderegger et al. 2003) [215]. Therefore, when characterising cyanobacteria isolates from ALE strategies to enhance carbon or nitrogen fixation, relative changes in growth should also be considered in context of total productivity.

Regarding characterisation, 93% of the studies in **Table 2.4** assessed mutant isolates with one of the following analytical methods: biomass formation (62%), genome sequencing (51%), substrate consumption (45%), transcriptomic analysis (26%), metabolomic analysis (11%), and proteomic analysis (4%). A majority (62%) of studies employed two or more of these methods, however, only one study characterised mutants using all 6

methods listed above, (see Strucko et al. 2018) [254]. Biomass, the most assessed characteristic in mutant isolates, has also been used as a baseline for assessing relative changes in product formation and substrate consumption. This is perhaps unsurprising, as the strategy is both practically straightforward, and reliable indicator of enhanced substrate utilisation (see section **2.4**).

To select for evolved strains, 82% of studies used batch, semi-batch, or automated batch cultivation, and 18% of studies used continuous cultivation. Given that standardised (%) increases in growth or substrate utilisation are relative, it's challenging to assess which strategy may be more effective, and while batch strategies are more popular, this is possibly a reflection of their more straightforward implementation, rather than relative efficacy. When culturing organisms to enhance substrate utilisation efficiency, nutrient limitation is frequently employed (20% of studies), with the rationale that cultivation under these conditions will select for mutants which assimilate or metabolise these nutrients more efficiently into biomass / product (see Sandberg et al. 2019) [202]. However, this strategy has been more frequently used in earlier studies, utilised in 9 of 17 of studies published between 1991 – 2011, and only 6 of 57 studies between 2012 – 2023. It is unclear why the popularity of this strategy has decreased over time, and it remains a frequently cited example of an effective strategy to select for mutants with more efficient substrate utilisation (see Sandberg et al. 2019) [202].

The duration of an ALE experiment is also a key factor. However, there is a lack of consensus on how best to record an ALE's duration, with 53% of the studies in **Table 2.4** assessing duration by the estimated number of generations, and 23% or 19% listing only the number of cycles or days of selection. A previous review by Dragosits & Mattanovich, 2013 highlighted that in ALE experiments involving either *E. coli* or *Saccharomyces cerevisiae*, most of relative fitness increases occurred within the first 100 – 500 generations of selection [201]. Furthermore, the shortest listed ALE durations of 10 generations [231] and 1 cycle [266], recorded relative improvements of 17,900% and 313% in growth and substrate uptake, respectively. Highlighting that the selective environment employed in an ALE is more important than its duration in determining outcome. Additionally, while the use of biological replicates to assess reproducibility is common in the experimental design process, the use of replicate / parallel selection populations is only reported in 51% of ALE studies here. Of these, some studies even eschew sustained selection of discrete replicate populations by generating new population replicates each selective cycle, derived from the previous cycle's fastest growing

population to enrich for advantageous phenotypes [239,265]. One reason for this may be the phenomenon of "parallelism" (Dragosits & Mattanovich, 2013) across replicate ALE populations [201]. Where parallel populations exhibit evolutionary convergence, and selective environments narrowly constrain phenotypic variation to specific fitness characteristics in the short term.

Although many previous studies have investigated the use of ALE to enhance heterotrophic productivity, fewer have investigated its application in selecting for more productive autotrophic organisms. Of the studies listed above, 84% selected for increased heterotrophic productivity. Of the 16% investigating ALE to increase autotrophic productivity, 11 of these 12 studies were published only recently, between 2020 – 2023 (**Figure 2.10**). Of all organisms investigated, *Saccharomyces cerevisiae* is the most frequently studied, accounting for almost 2 in 5 studies (38%). Cadière et al. 2011, suggested this was down to "poor public acceptance of GMO-based food and beverages", therefore efforts to engineer yeast strains for commercial purposes have necessitated the development of alternative, evolutionary-based strategies [226]. Given the potential for both outdoor cultivation of cyanobacteria, and their use as nutraceuticals, this previous work to develop effective ALE strategies in yeast could benefit similar work here.

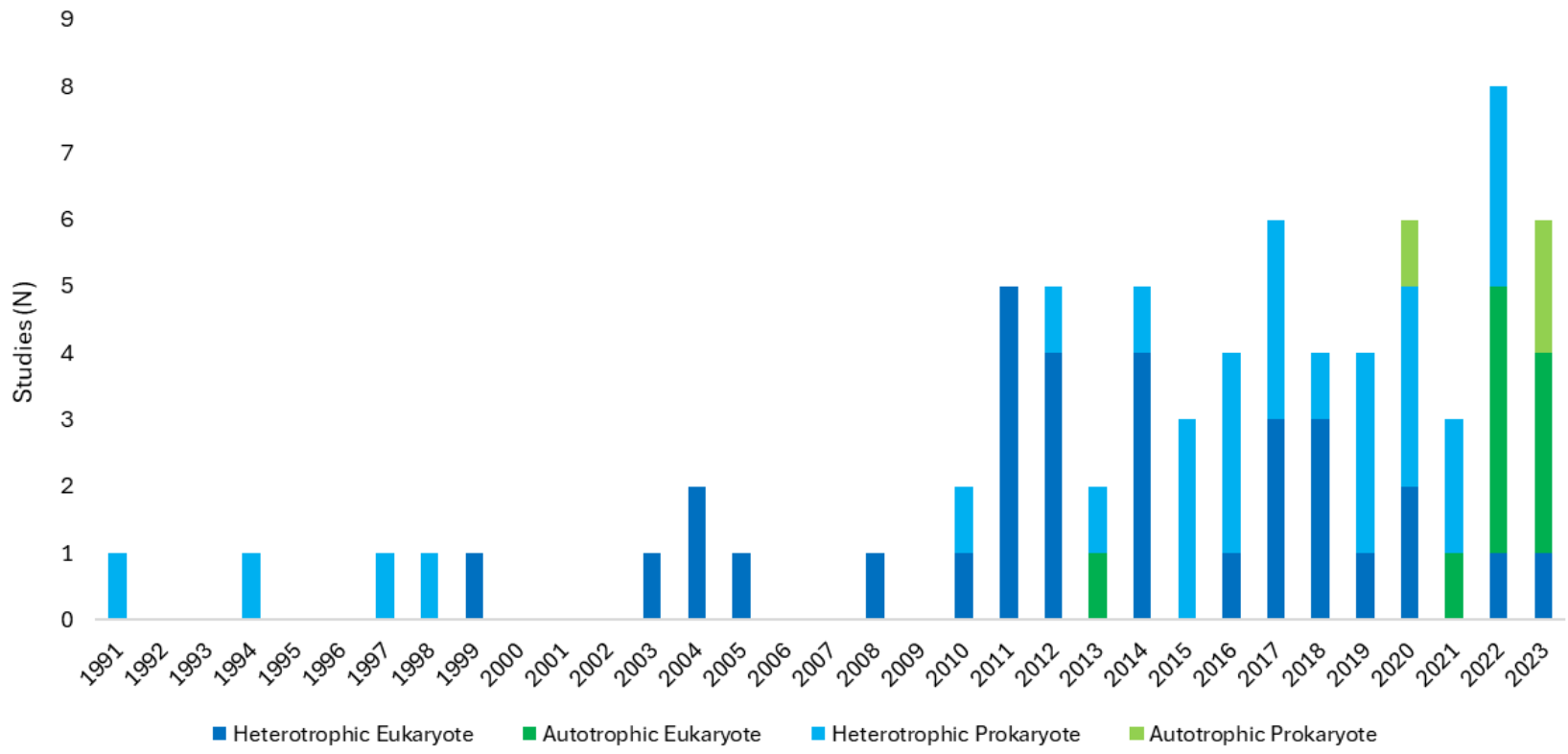


Figure 2.10. | Adaptive Laboratory Evolution studies listed in **Table 2.4** by publication date, highlighted to show organism trophic level and superkingdom.

Most ALE studies investigating autotrophic growth used eukaryotes (75%), and none of these investigations have assessed the use of ALE to select for enhanced substrate utilisation in photosynthetic prokaryotes. Previous work investigating ALE in cyanobacteria for increased light tolerance, including research by Dann et al. 2021, which isolated strains with ~4.3-fold higher maximal light tolerances compared to wild-type strains [284]. However, despite isolates tolerating light intensities of $\geq$ 3000 µmol photons $m^{-2}s^{-1}$, no strains showed significant increases in biomass formation at these light intensities, when compared to wild-type cultures at 100 µmol photons $m^{-2}s^{-1}$. In fact, significant decreases in biomass formation were reported in most isolates. One other factor in strain selection, was the use of previously engineered strains, accounting for 58% of ALE studies in **Table 2.4**. Of these 40 studies, 30 involved the use of strains which had specifically been engineered to direct metabolic flux – towards a product or certain pathways. Use of cyanobacteria strains engineered to direct metabolic flux, could therefore be a useful strategy to further direct selection towards fixation and biomass formation.

2.6.3 *Challenges of using ALE*

ALE also comes with some relatively significant trade-offs, however, when compared to targeted approaches. An immediate practical difference is that the identification of the very mutations responsible for a phenotype is itself a challenge. Using ALE, it is possible to generate the same phenotype observed in *Synechococcus elongatus* UTEX 2973, however understanding how that phenotype occurred is still challenging (see Ungerer *et al*. 2018; Zhou and Li 2019) [191,192]. Traditional strategies of confirming gene to phenotype links in ALE experiments, through the knock-in / knock-out of genes and pathways, can become very challenging, or even impractical. Owing to the prohibitively large number of overall genomic changes. Furthermore, the use of ALE will inevitably generate different results each time it is employed, due to the randomness of mutations generated (see Dragosits and Mattanovich 2013) [201]. Even if phenotypic convergence is observed under chosen conditions, this would require multiple populations under simultaneous selection. A potentially labour-intensive approach depending on the selection strategy.

ALE strategies have also been less useful in enabling strains to synthesise or metabolise novel products of interest. The *E. coli* long-term evolution experiment (LTEE) begun in 1988 by Richard Lenski [285], is an example of where ALE has led to the emergence of a novel metabolic

adaptation [286]. This example showed the emergence of a previously absent phenotype, Cit^+, enabling the adapted *E. coli* to metabolise a previously inaccessible source of carbon within their growth medium. It took an estimated ~31,000 generations, and ~15 years of diligent labour and observation before this phenotype emerged, and it emerged in only 1 of 12 parallel populations [287].

However, previous work in microalgae has successfully shown that ALE can improve growth rates. ALE work by Perrineau *et al*. 2014 using *Chlamydomonas reinhardtii* and serial dilution successfully improved growth rates of strains by > 35% compared to the progenitor population [288]. This work was carried out over 17 months, with a sustained selective dilution pressure. Similar work by Yu *et al*. 2013 also showed how a successful microalgal ALE using serial transfer could be achieved in only 84 days [232]. A key consideration in ensuring the success of ALE in cyanobacteria to improve their growth, will be how to identify a suitable strategy for directing metabolic flux into carbon fixation, and photosynthesis.

At a fundamental level, however, all these above issues facing an ALE experiment are due to one key challenge: the inability to predict how an organism will evolve in each selective environment [202]. This said, as contributions to research in this field continue to grow it is increasingly possible to design ALE experiments which direct organism phenotypes towards broad growth, tolerance, and substrate utilisation characteristics (see Sandberg et al. 2019) [202].

2.7 Implementing ALE

To implement an effective ALE strategy, experimental parameters must be evaluated. With consideration given to how each of these could be optimised to direct a cyanobacteria's evolution towards enhanced growth and productivity.

2.7.1 *Selecting an ALE objective*

As highlighted in **Table 2.1**, a key factor limiting the potential commercial use of cyanobacteria is their low autotrophic productivity in converting substrate into product. Previous use of ALE has shown the potential to enhance both growth and substrate utilisation across a broad

range of heterotrophic organisms and autotrophic eukaryotes (Table 2.4). Furthermore, ALE has previously been used to address another key limitation highlighted in **Table 2.1**, having successfully been used to select for strains of cyanobacteria with increased abiotic stress tolerances, including light [284,289], salt [290], and temperature [291]. As described in section **2.4.1**, the capacity for cyanobacteria to fix CO_2 is the limiting factor in product formation under photoautotrophic growth conditions; as described in section **2.3**, the energetically expensive fixation of N_2 is the limiting factor for growth in cyanobacteria under diazotrophic conditions. As shown in **Figure 2.7**, a cyanobacteria's capacity for product formation is directly linked to its capacity for biomass formation, and therefore, how rapidly a cyanobacteria can accumulate biomass is reflective of its productivity.

Therefore, there is an existing gap in literature for the development and implementation of ALE strategies to enhance carbon and nitrogen fixation within cyanobacteria, which could potentially be achieved by selecting for increased growth and biomass formation.

2.7.2 *Cyanobacteria species selection*

To ensure ALE strategies are effective at directing cyanobacteria towards enhanced growth and biomass formation, suitable strains to investigate selection on carbon and nitrogen fixation must be selected. Strains should be representative of different cyanobacteria phenotypes, including in their morphology (unicellular, and filamentous), and ability to fix nitrogen (diazotrophic and non-diazotrophic).

2.7.2.1 *CO_2 fixation – Synechocystis sp. PCC 6803*

Synechocystis sp. PCC 6803, hereafter *Synechocystis*, has long been established as a model organism for research into cyanobacteria physiology, photosynthesis, and to demonstrate synthetic biotechnology pathways (see Mills et al. 2020) [292]. First isolated in 1968 from freshwater in California [293], the organism has since been deposited in multiple strain culture collections across the world [294]. Uptake and use of the organism is so widespread in fact, that distinct strains have even emerged from the organism's maintenance at different research sites [294], with glucose utilising substrains perhaps even surpassing the original in their

contemporary use (see Koskinen et al. 2023) [295]. Furthermore, in 1996, it was the first photoautotrophic organism to have its genome fully sequenced [296,297]. Something which could greatly aid in future genomic characterisation of any ALE mutant isolates, with ~30 years of previous genomic work to aid analysis. Therefore. the consensus of this organism as a model cyanobacterium, and wealth of established literature, make it an especially useful tool for the characterisation of ALE selection methods for enhanced carbon fixation in cyanobacteria.

2.7.2.2 *N_2 fixation – Trichormus variabilis sp. ATCC 29413*

Like *Synechocystis*, *Trichormus variabilis* sp. ATCC 29413, (formerly *Anabaena variabilis*), hereafter *Trichormus variabilis*, is a model cyanobacteria, which has been utilised primarily in the study of filamentous, and nitrogen fixing cyanobacteria. The genome has been fully sequenced [298], although it exhibits a relatively slow doubling time, approximately ~14 hours under both autotrophic and heterotrophic conditions [299]. However, this is still significantly faster (~2-fold) than other model filamentous cyanobacteria, including *Anabaena* sp. PCC 7120, which has a doubling time of ~24-30 hours under nitrogen fixation conditions [300]. A factor which could significantly impede the latter's use for ALE. Furthermore. there has been extensive previous research into the ability of *Trichormus variabilis* to fix nitrogen [298], and it is therefore a suitable strain for investigating how genetic modifications may impact on cyanobacteria when selected under diazotrophic conditions. The organism natively synthesises 3 different nitrogenase proteins (2 FeMo and 1 FeV) [298]. This offers *Trichormus variabilis* additional possibilities in generating novel enhanced nitrogen fixation phenotypes, especially when compared to filamentous strains which only possess one type of nitrogenase, such as another model filamentous species *Nostoc punctiforme* ATCC 29133 (see Meeks et al. 2001) [301]. *Trichormus variabilis* is also capable of growing mixotrophically, utilising fructose as a source of additional organic carbon supplementation and has also shown a propensity to form symbiotic relationships with other organisms [298]. All characteristics which make it a potentially attractive model for investigation here.

2.7.3 *ALE experimental design*

Directing cyanobacteria evolution towards increased growth and biomass formation will require both an effective culturing methodology, coupled with abiotic parameters, which encourage mutants to rely on these phenotypic characteristics to survive.

2.7.3.1 *Generating an optimal selective environment for ALE*

Any given environment can apply a selective pressure upon a population. Selecting the environment is therefore crucial when trying to select for cells with an improved fitness phenotype, as it should provide an optimal background for the selection of these cells [202]. Although ALE can select for desirable variants within a population, strains will ultimately become specialised to the selective conditions through the 'fittest' adaptations. Therefore, they may adapt without preferred phenotypic characteristics or with evolutionary trade-offs to growth [302]. The appearance of these adaptive trade-offs has previously been seen during microalgal ALE work (see LaPanse *et al*. 2021) [303]. *Chlamydomonas reinhartdii* isolates adapted to 33°C showed lower growth rates when compared to strains adapted to 14°C and subsequently cultured at 33°C [304]. Highlighting how a strain 'fitter' for an environment is not necessarily one that 'grows faster'. It also highlights that selective pressures could be used more creatively to select for phenotypes indirectly.

To generate cells with improved growth phenotypes, the selective environment needs to "push" the strains to grow faster. This can be done through competitive selection in a continuous process, where cells need to adapt to an increasing dilution rate. Those which are unable to sustain a high growth rate are simply washed out, and those which remain are the ones which hopefully grow faster [305].

2.7.3.2 *Selecting a successful culturing strategy to increase cell growth*

Consideration must also be given to what vessel an organism will be cultured in, and how the selective environment will be maintained in that vessel. Choosing a vessel with a smaller volume may enable the running of multiple ALE cultures simultaneously, such as a multi-well

plate-based system. This could allow the parallel screening of many different growth conditions in less than a millilitre of media per experiment [201]. However, although more experiments can be run in parallel using these strategies, the population size being screened under each condition is lower. Furthermore, there are negative impacts, for instance limited passage volumes can prolong ALE experiments. Previous work by LaCroix *et al*. 2017 showed that when lower proportions of an ALE population are transferred, this increases the time necessary for beneficial mutations to emerge [306]. Although transfer of smaller proportions of a population can reduce the workload needed to maintain an ALE by several fold, this is problematic as it also reduces the proportion of emerging genotypes with small populations carried over each time [306]. A more useful strategy, therefore, may be to select strains in a larger vessel, where constant selective pressure can be applied such as a chemostat and other auxostats (see Trovão *et al*. 2022) [307].

Common ALE strategies which are currently utilised to improve cell growth are outlined in **Figure 2.11**. Although the ALE strategy utilised will be specific to the experimental design, and the desired phenotype of the cell, there are 2 primary modes of selective pressure which can be applied, specifically to change the population phenotypes [201]. Strategy one, the cells undergo cyclical growth, and manual transfer is used to move cells or media between different vessels via population transfer / dilution (**Figure 2.11 A**). Strategy two, the cells are maintained at a specific dilution rate, often altered by an automated system (**Figure 2.11 B**). As media flows out, new media is pumped in once the cells reach their maximum growth rate or μ_{max} – then the experiment ends. Both strategies are effective in producing strains with altered phenotypes (see Sandberg *et al*. 2019) [202]. However, without automation the investigator needs to constantly adjust the experimental protocol to maintain pressure on the cells. Failure to do so can result in divergent populations emerging, which may not be adapted with the desired phenotype [308].

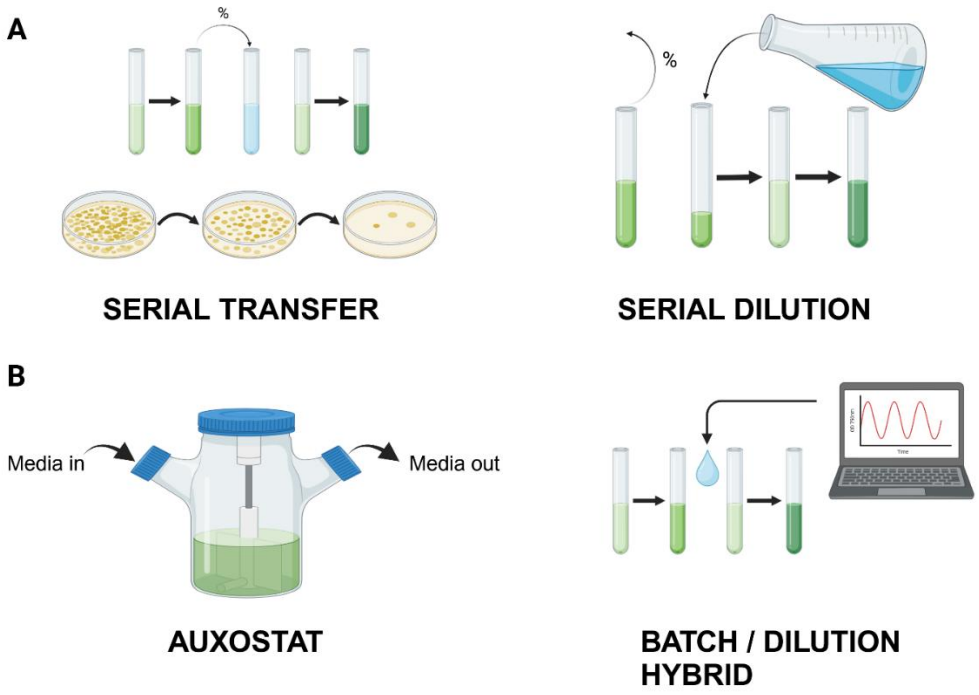


Figure 2.11 | Overview of commonly used ALE strategies. **A.** serial dilution / serial transfer methods. **B.** Auxostat and hybrid batch / dilution methods. (Created with BioRender.com).

The longest running, and perhaps best-known ALE experiment, the LTEE by Richard E. Lenski, has been monitoring the evolution of *E. coli* cells since 1988 [285]. The experiment involves the serial transfer of 1% of 12 independent populations to fresh medium. This experiment has seen the growth rates of all the independent populations under selection increase over time, resulting in the appearance of a new citrate catabolism phenotype [285]. However, the time scales involved in that work are very long and are not always suitable for most ALE experiments. The time scales involved in ALE can vary considerably, Carmona *et al*. 2020 were able to recover a fast-growing strain of *E. coli,* which had a deletion in the phosphoenolpyruvate–carbohydrate phosphotransferase system [309]. They were able to select for this strain after only 80 hours of ALE. Given the relative ease of carrying out the process, serial passage-based approaches, constitute many all the current ALE investigations carried out to date [199,202].

Strategies which apply a constant selective pressure have the advantage of reducing the time necessary to select for enhanced phenotypes, whilst maintaining higher overall selective pressure on the

strains (see Dragosits and Mattanovich, 2013) [201]. A chemostat based strategy was investigated by Basso *et al*. in 2023 to select for strains of *Saccharomyces cerevisiae* engineered to degrade xylose [310]. Incremental increases in the dilution rate, led to the selection of a strain with a 35% increase in specific productivity compared to the parental strain. Similarly in 2023, Bromig and Weuster-Botz successfully used an automated batch dilution system to evolve *E. coli* strains capable of utilising glycerol as a carbon source [311]. Increases in growth rates were seen after ~127 hours of selection, compared to the 40 – 50 days required to enhance growth via serial passage [312]. Cabanelas *et al*. 2016 utilised a hybrid approach with batch growth and dilution, subjecting the marine algae *Chlorococcum littorale* to repeated rounds of nitrogen starvation [313]. Two populations were cyclically grown in nitrogen replete, and nitrogen-limited media, alternating between either 8 or 14 days with nitrate, and 6 or 12 days in nitrogen-limited media. No significant differences were observed in the strains [313]. It is important to note that this strategy neither sustained selective pressure, nor did it include a mutagenesis step prior to the selection process.

Patel *et al*. 2016 demonstrated that simply by plating EMS treated *Synechocystis* sp. PCC 6803 cells, and then selecting phenotypes based on colony size and morphology, they could select strains with altered nutrient profiles [208]. Identifying strains with up to 64% more carbohydrate, and 82% more lipids than the control.

Together, these different strategies highlight the diversity of strategies available to carry out strain improvements utilising ALE and mutagenesis. They also highlight the challenges of effectively implementing an ALE experiment, particularly the need to add a sustained selective pressure.

2.7.3.3 *Determining selective parameters to enhance carbon flux*

To enhance growth and carbon fixation in cyanobacteria utilising an ALE approach, it is important to select suitable parameters which apply directed selective pressure towards the target phenotypes. An overview of the different potential parameters and metabolic pathway targets is shown in **Figure 2.12**. Parameters were initially selected based on strategies that had previously been used to enhance the growth of bacteria, (including cyanobacteria), microalgae, and yeast.

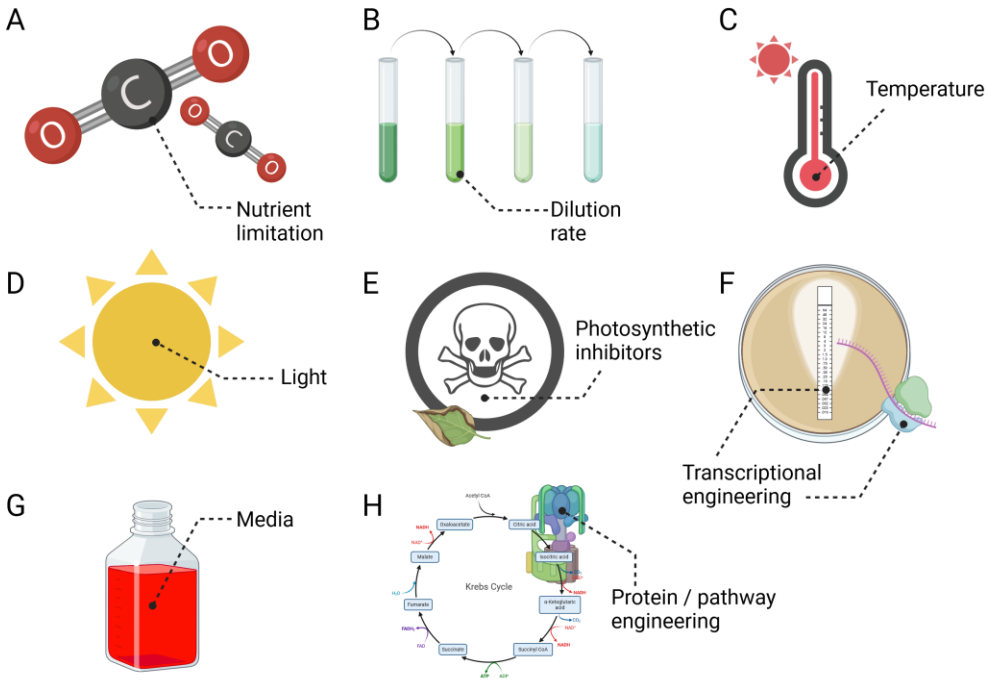


Figure 2.12 | Overview of potential targets for an ALE to enhance carbon fixation in cyanobacteria. (Created with BioRender.com).

In ALE strategies that aim to enhance growth rates, a common parameter is nutrient limitation [202]. This can include the targeted growth of microorganisms on media which have specific pathway intermediates either present or absent to direct metabolic flux towards a preferred pathway [226]. Utilising media with reduced nutrient components can force the cell to find solutions to increase nutrient uptake efficiencies, and thus potentially enhance their growth rate (see LaPanse *et al*. 2021) [303]. Chemostats can be used to increase the selective pressure on the cells by increasing the dilution rate. Only cells which can maintain a rate of growth which matches the maximal dilution rate will be able to remain the vessel. The remaining cells being washed out, thus selecting for the best performing strains [314].

Temperature can be another parameter which can be altered to enhance selection in ALE experiments. Temperature can be either increased or decreased depending on the phenotype required. Selection of *Schizochytrium* cells at higher temperatures not only increased the cells temperature tolerance by ~5 °C, but also increased the growth rate of the cells and fatty acid synthesis [315]. Strains can also be selected at higher light intensities, which in theory could select for organisms with greater

industrial productivities. If this improved tolerance to high light stress can be directed into biomass formation. The risk, however, is that selected strains adapt to tolerate the high stress, rather than exploit it. Dann *et al*. 2021 showed significant increases in the tolerance of *Synechocystis* sp. PCC 6803 to light intensities of > 2000 µmol photons·m^{-2}·sec^{-1}, when strains were selected utilising a passage-based ALE strategy [284]. Despite several of the isolates being more resilient to light stress than the wild-type, these strains also demonstrated diminished growth at lower light intensities and did not accumulate as much biomass at higher light intensities as the wild-type did when it was grown at lower light intensities for the same period [284].

Photosynthetic inhibitors such as atrazine and DCMU could also be utilised to select for beneficial phenotypes. These compounds inhibit photosynthesis in cyanobacteria by acting as competitive inhibitors, targeting the plastoquinone binding sites of the D1 protein of PSII [316,317]. Similarly, the antimicrobial rifampicin, can also be used to select for phenotypic variation. It targets the RNA polymerase subunit *rpoB*, and mutations in this gene have been shown to significantly impact the transcriptional machinery of resistant strains. The strategy could therefore potentially be used for strain development [318].

Media can also be utilised to aid selection, via nutrient limitation but also via the addition of specific components as well. For example, salt can be added to the media to select for strains which are more resistant to salt stress [290]. The requirement for fresh water is a serious challenge for large scale fermentation, salt water and brackish water offer more sustainable solutions.

One of the most crucial parameters in ALE is time. ALE can be performed over several hours, but also over a prolonged period of months or even years. Barrick *et al*. 2009 demonstrated that a significant proportion of the relative fitness acquired by selected *E. coli* strains in the LTEE occurred within the first couple of hundred generations [319]. Assuming a doubling time of ~12 hours for *Synechocystis* sp. PCC 6803 [320], this suggests that between 50 and 100 days of selection should be a sufficient period to isolate mutants with enhanced fitness.

Given the aim should be to select for increased growth and biomass formation, abiotic parameters previously identified for optimal growth and substrate utilisation are a rational basis for initial investigation here. For Synechocystis, this includes light intensities between 250 – 500 µmol photons·m^{-2}·sec^{-1} [321], and a temperature of 30 – 33°C [322,323]. For environments where CO_2 is not limiting, a gas mixture containing 5% CO_2

has previously been used to investigate optimisation of *Synechocystis* CO_2 fixation, as this concentration creates a CO_2 saturated environment (see Martínez et al. 2011) [322]. Given that previous ALE work to enhance substrate utilisation has previously shown nutrient limitation to be a potentially useful strategy (see **Table 2.4**), CO_2 limited selections could use sub-atmospheric concentrations (< 0.04%). Previous work investigating medium optimisation of *Trichormus variabilis* has also used similar abiotic conditions, Shafay et al. 2021 culturing strains at 30 ± 2°C and 300 µmol photons·m^{-2}·sec^{-1} [324].

2.7.3.4 *Adaptation to a controlled environment*

While ALE of cyanobacteria under highly controlled conditions will likely adapt the organisms to the those chosen parameters, (reducing the usefulness of any isolates outside of these conditions), the purpose of this investigation is to identify the feasibility of using ALE to engineer photoautotrophic prokaryotes with enhanced growth and biomass formation. To ensure investigations align with the motivation behind this work (see **Chapter 1**), this investigation should focus on conditions which emulate proposed industrial strategies to valorise CO_2 into useful products. Use of photobioreactors for cultivation would allow greater control over abiotic parameters, reduce issues related to contamination, and enable the use of continuous production strategies in industry (see Khan et al. 2018) [325]. The current limitations in productivity of cyanobacteria have therefore necessitated cultivation in larger, less controlled, outdoor 'ponds' [325]. Given that industrial processes typically aim for consistency and predictability, photobioreactors could also provide more consistent outcomes than outdoor systems (see Khan et al. 2018) [325]. Engineering strains with enhanced productivity in photobioreactor systems would therefore be valuable to addressing this gap in process viability.

Furthermore, the ALE selection of cyanobacteria in highly controlled environments could also select for strains which eliminate now unnecessary metabolic burdens. In their natural environments, cyanobacteria must adapt to fluctuating diurnal light cycles, temperatures, and nutrient availability [326], unnecessary if illumination is continuous and medium replenished. Their environment contains a diverse mix of different organisms, some of which could be symbiotically beneficial, others may even predate on cyanobacteria [327]. In nature, there is also a constant risk of infection by cyanophage viruses, capable of killing large proportions of the cyanobacteria population [328]. Unlike in a

photobioreactor, surfaces in nature are highly varied and uneven, allowing for (or even encouraging) biofilm formation (see Rossi & Philippis, 2015) [329]. If in static water in the environment, where there is no mixing or sparging and access to CO_2 / O_2 is limited to the gas / liquid interface, this potentially requires cell motility, and an accompanying array of abiotic sensory mechanisms to direct the cell [330]. Given that cells must respond to each of these conditions in nature, selection of cyanobacteria cells in a controlled photobioreactor could select for phenotypes optimised for continuous growth and productivity, and reduced metabolic investment in pathways now superfluous for industrial environments.

2.7.4 *Random Mutagenesis*

As part of an ALE strategy, random, untargeted mutagenesis can be an effective initial step to artificially increase the base variation within a population. This is often done to ensure that the pool of genetic diversity is increased prior to selection [331]. During cell division, incorrect replication of the DNA can naturally lead to errors being introduced [332], however, this is a slow process. Random mutagenesis aims to significantly accelerate this process, enabling more rapid strain isolation.

Effective treatment with a mutagenic agent can introduce a wide range of genetic variation, including insertions, deletions, and point mutations, which in turn can lead to amino acid substitutions, transcriptional frame shifts and truncations (**Figure 2.13**) [333]. Work has previously shown the evolutionary model organism *Daphnia magna* has a natural mutation rate of 8.96×10^{-9} bases per generation in its nuclear genome [334]. In comparison, one individual treatment with 25 mM Ethyl MethaneSulfonate (EMS), can lead to a base substitution rate of 1.75×10^{-6} [335]. Therefore, one treatment with EMS could increase the base substitution rate by nearly 195-fold. The choice of mutagen, and the subsequent dosage of that mutagen, is vital to ensuring that a good rate of substitution can be established. However, there is a trade-off between dose and mutation rate, as an increased number of mutations can lead to cell death (see Shibai *et al*. 2017) [336]. A high dosage of mutagen can result in only a small subset of the cell population being viable, whereas an insufficient dosage could result in a large population of cells with relatively few mutations (see Tillich *et al*. 2012) [291].

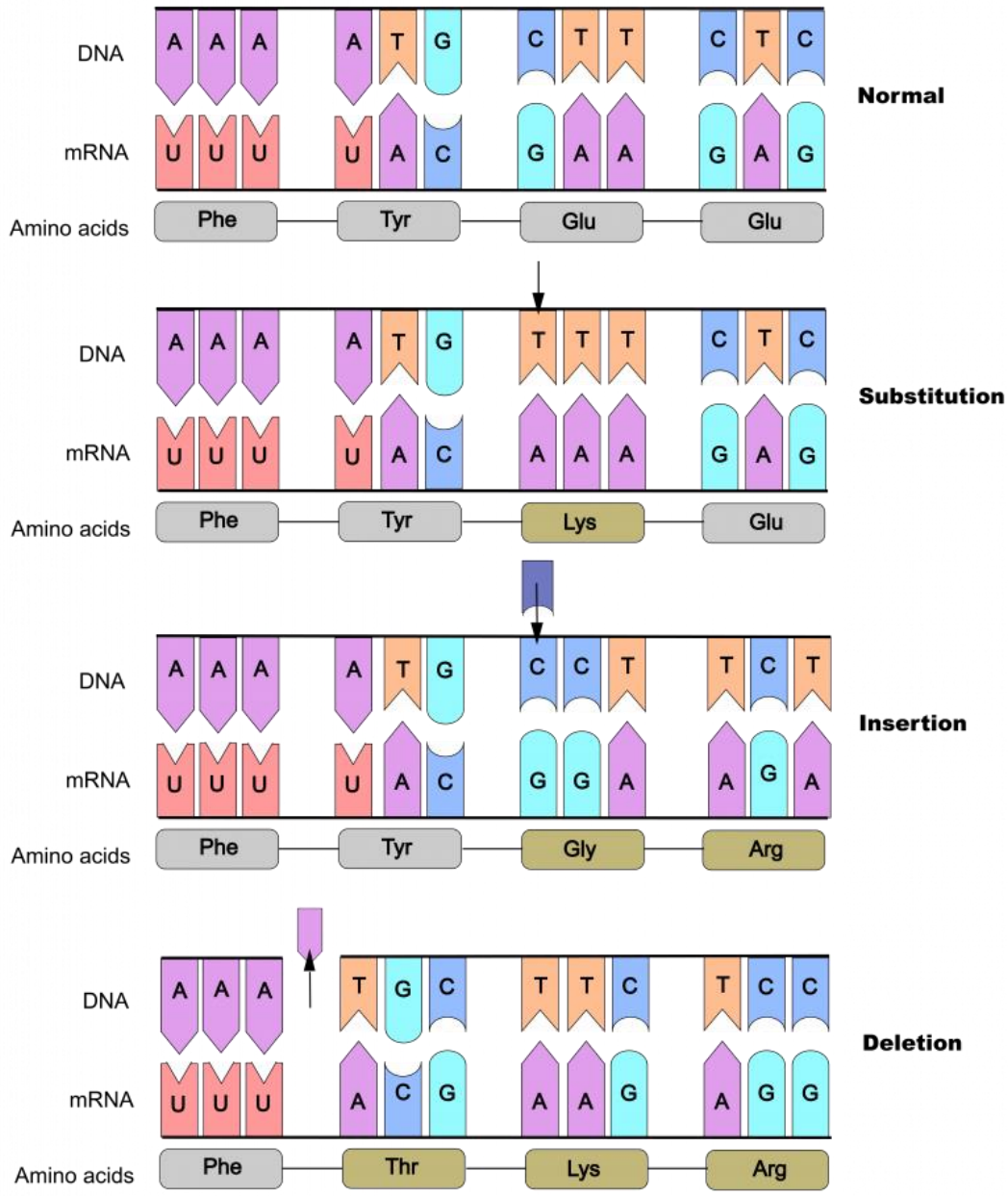


Figure 2.13 | Schematic showing the effects of non-synonymous base pair substitutions, nucleotide insertions and deletions on mRNA transcripts and amino acid sequences (taken from Cotner and Wassenburg, 2020) [333].

However, research into the impact of initial genetic variation upon the outcome of the ALE experiment has shown that the duration of the experiment may offset fitness advantages from the initial genetic variation [337]. Izutsu and Lenski 2022 showed that the initial genetic variation

amongst *E. coli* populations contributed strongly to their ability to adapt to a new selective environment, in this case from utilising glucose to using D-serine as the sole carbon source [337]. However, after 500 generations, there was no significant difference in relative fitness observed between any of the populations [337]. Therefore, to maximise the efficiency of an ALE experiment, genetic diversity should be coupled with effective and sustained selection.

2.7.4.1 *Mutagens*

There are 3 primary strategies to mutagenise cells (**Table 2.5**), these are biological agents, physical agents (radiation), and chemical agents [338].

Table 2.5 | List of chemical, physical, and biological agents for random mutagenesis strategies.

Mutagen	Sequence Targeting Biases	Point Mutations	Base Substitution Bias	Insertions	Deletions	Rearran-gements [g]	Duplication [h]	Specific limitations	Ref.
A. Chemical									
EMS [a]	G, C	☒	C>T, G>A	☒	☒	☐	☐	High bias for substitutions	335
MMS [a]	A, C	☒	A>G/T, C>A/G/T	☒	☒	☐	☐	" "	339
MNNG [a]	G/C	☒	G/C>A/T	☒	☒	☐	☐	Mutations cluster around DNA replication forks; substitution bias very high (96.6% of all mutations)	340
Sodium azide [b]	CC	☒	C>T	☒	☒	☐	☐	Substitution bias high (79.1% of all mutations)	341
5-bromouracil [c]	A/T, G/C	☒	AT>G/C, G/C>A/T	☐	☐	☐	☐	Limited to base substitutions	342
Ethidium bromide [d]	n/a	☐	n/a	☒	☒	☐	☐	High lethality, low mutagenicity; limited to indels	343

B. Physical									
UV-C $_{254\ nm}$ [e]	CC, TT	☒	C>T, CC>TT	☒	☒	☐	☐	Sample density / aggregation	344
Ion beam [f]	G/C	☒	C>T, G>A	☒	☒	☒	☒	Ionising radiation sources require specialist facilities	345
X-ray radiation [f]	n/a	☒	n/a	☒	☒	☒	☐	" "	346
Gamma radiation [f]	TGGC, G/C	☒	C>T, C>A	☒	☒	☒	☒	" "	347
C. Biological									
Homology knockout cassettes	Construct homology	☐	n/a	☒	☐	☐	☐	Typically, one insertion per mutant; limited by strain transformation efficiency	348
Transposon	Transposase dependent	☐	n/a	☒	☐	☐	☐	Mutations unstable (insertion elements mobile)	349

[a] - Alkylating agent [b] - Deaminating agent [c] - Base analogue [d] - Intercalating agent
[e] - non-ionising radiation [f] - ionising radiation [g] - Including inversions and translocations
[h] - Including regions and genomes n/a - Not applicable

2.7.2.1 *Chemical agents*

The range of possible chemical mutagens, (agents capable of causing mutations), is extremely diverse [342]. Owing to the diversity in possible chemical structures, they are perhaps among the most diverse sources of mutation. The most common causes of mutations derived from chemical agents, however, are from compounds that act as DNA alkylating and methylating agents, DNA deaminating agents, and compounds that act as base analogues [307,342], (**Table 2.5 A**).

For DNA alkylating and methylating agent mutagenesis of microalgae, typically sulfonates or nitrosoguanidine are used [307]. These compounds add alkyl groups to nucleotides within a DNA sequence. Nucleotide adducts are then capable of forming mismatch base pairs, (such as ethylated guanine pairing with thymine) [350]. These include ethyl methanesulphonate (EMS), methyl methanesulphonate (MMS), and methyl-*N*-nitro-*N*-nitrosoguanidine (MNNG) [307]. Following treatment, mutations are introduced into the DNA when base mispairing errors are carried through during DNA replication. These chemical agents primarily result in base substitution mutations [307], however, can also generate double strand breaks [351]. This strategy has the advantage of introducing a high frequency of point mutations, and therefore of generating significant diversity across a treated genome [307]. Deaminating agents such as sodium azide, nitrous acid, and sodium bisulfite can lead to the deamination of A, C and G bases, which leads to mutations in the new strand [342]. Base analogues such as 5-bromouracil or 2-aminopurin can lead to faulty pairing and errors in the replication of the DNA, causing AT-GC or GC-AT transition mutations [342]. Intercalating agents such as ethidium bromide, unlike other listed chemical agents, predominately cause insertion and deletion mutations [343]. This is because their mechanism of action is to insert between nucleotide bases, rather than binding to, or in place of them.

Treatment with only one chemical agent, therefore, will only result in specific types of mutations. EMS can only generate half of the theoretical base substitutions, and even within the possible base substitutions it can generate, there is a preference bias for G:C to A:T transitions [335]. This may limit the diversity of the mutations generated.

2.7.2.2 *Radiation*

Radiation induced random mutagenesis utilises electromagnetic radiation such as ultraviolet (UV) light, X-rays, gamma rays, and ion beams to cause genome wide mutations (**Table 2.5 B**). This strategy introduces mutations by causing double or single strand breaks, or by generating nucleotide dimers in the DNA [344,352]. The damage to the DNA sequence is caused either by a direct ionisation of the nucleotides by the radiation, or through indirect Reactive Oxygen Species (ROS) damage [342,352]. Mutations are then introduced into the DNA through the inaccurate repair of these breaks (see Brown 2002) [342]. In extreme cases during a double strand break, repairs may lead to sequence translocation, significantly disrupting gene function [353]. More generally, however, mutations are introduced through either the incomplete or erroneous repair of these breaks, which causes nucleotide insertions, deletions, or even base substitutions (see Brown 2002) [342]. The ability of any fixed UV radiation source to cause mutations can be determined by 3 factors: wavelength, distance from the radiation source, and the time the cells are exposed to the mutagen. Mutagenicity and cytotoxicity both increase as wavelength decreases [354], as do the types of mutations observed. For example, UVC wavelengths (100 - 280 nm) are highly efficient at DNA damage via the formation of cyclobutane pyrimidine dimers and 6-4 photoproducts [355].

Individual base substitutions often have little effect upon the cellular phenotype, as they often occur outside of the coding regions, or alter only a single amino acid (see Brown 2002) [342]. However, if the codon is changed from an amino acid to a premature stop codon, or if a frame shift results from the insertion / deletion of an individual base, then this can have a significant effect on the normal functioning of a specific gene [342]. Random mutagens target the entire genome, which often generates a high-level of genetic diversity in the mutant library pool. Creating many novel phenotypes for investigation [356].

From the current methods available for the irradiation of cells, there are specific challenges when applying these effectively to mutagenize cyanobacteria. Cyanobacteria, being photoautotrophs, have evolved under regular exposure to sunlight, which has resulted in them developing strategies to increase their resilience to UV light exposure [357]. The presence of pigments such as carotenoids mitigates the effects of UV radiation. Carotenoids are capable of absorbing and dissipating UV radiation, thus reducing the formation of ROS or breaks in the DNA sequence [357]. Cyanobacteria can also repair their DNA using a photoreactivation

mechanism, utilising photolyase enzymes, these enzymes reverse the dimerization of nucleotides caused by UV [358].

Photolyase mediated repair of UV damage has been shown to be very effective in cyanobacteria, in studies with both *Trichormus variabilis* and *Anabaena* sp. infected with UV inactivated cyanophage N-1, there was a 1000-fold increase in plaque formation following photoreactivation of the phage by photolyases [359]. These enzymes function by repairing the cyclobutene pyrimidine dimers induced by UV damage [360]. Following UV induced mutagenesis, cells need to be protected from the light to prevent photolyase mediated photoreactivation [291].

2.7.2.3 *Biological agents*

In cyanobacteria the use of biological agents to carry out mutagenesis primarily refers to the use of transposons. Transposons, or transposable elements, are nucleic acid sequences that change their loci within a sequence of DNA, which can result in random gene knockouts [342]. Transposons either produce additional copies themselves across different loci and are reverse transcriptase mediated (class I transposons), or excise and reinsert themselves into another locus and are transposase mediated (class II transposons) [342]. Therefore, class II transposons can cause reversible inactivation of genes, if these mobile elements subsequently move locus within an organism's DNA [342]. Within cyanobacteria, transposon mediated mutagenesis strategies have been developed for a variety of organisms including *Synechocystis* and *Synechococcus elongatus* sp. PCC 7942 [349], and *Anabaena* sp. PCC 7120 [361].

Whilst this mutagenesis strategy has proven useful in elucidating the roles of different genes in cyanobacteria [361–363], this strategy has several limitations that reduce its usefulness for ALE investigations. The most significant of these is the instability of such insertions (see Brown, 2002) [342]. The stability of transposon induced mutations can be increased if class I transposons are utilized, however, as these remain at the locus from which they are initially copied. However, mutants will be limited to only a small number of knockout mutations, and no intragenic variation will be generated.

If antibiotic cassette mediated mutagenesis is used, it will suffer from the same shortcoming in generating variation as above, as one locus of antibiotic resistance is sufficient to confer resistance (see Koksharova et al. 2020) [363]. Hence, construction of a knockout library of plasmids with

resistance cassettes flanked by regions of host DNA randomly amplified by degenerate primers (see Wells et al. 1985) [348], were integrated into the host's genome. To ensure stability of these inserts, it may also be necessary to maintain the selective resistance pressure, and the generation of naturally resistant mutants (without any insertions) is also a risk here [348,363].

These mutagenesis strategies are also only possible where there are already transposon insertion motifs at a gene locus, or a region of DNA has been amplified by degenerate primers. Further limiting the overall variation that can be generated using these strategies. Collectively, these limitations reduce the usefulness of biological agents in generating mutant libraries for ALE experiments.

2.7.2.4 Choice of mutagenic agents

As stated in section 2.7.2.3, there are significant limitations in the use of biological mutagenic agents for an ALE strategy. Therefore, use of chemical and physical mutagenic agents is preferred. Given the need for dedicated facilities to utilise ionising radiation sources, non-ionising (UV) mutagenesis is considered more practical. Furthermore, work by Tillich et al. 2012 has previously investigated the optimisation of both physical and chemical mutagen dosage in the model cyanobacterial strain *Synechocystis* sp. PCC 6803 [291]. This investigation used alkylating agents for chemical mutagenesis and clearly demonstrated the advantage of a mutagenised population in adapting to temperature stress over a non-mutagenised population. In this current investigation, both physical and chemical mutagens were used.

2.8 Isolation and characterisation of cyanobacteria

A strategy is also necessary to obtain individuals of this population for characterisation. A common methodology is the selection of strains from single colonies (see Hirasawa and Maeda, 2023) [200], enabling selection of clonal mutants. However, it is also important that an isolation strategy avoids exaggerating the abundance of undesirable phenotypes [202]. Including those akin to "genetic hitchhikers", alleles surviving without statistically significant reoccurrence within a population (Sandberg et al. 2019) [202]. Isolation strategies should avoid selecting from distinct populations likely to have evolved equivalent (undesirable) fitness-

optimised characteristics [202]. For example, if seeking to isolate cyanobacteria strains with increased growth rates from a serial dilution-based ALE experiment, biofilms are a discrete population from that within the planktonic culture. Which have collectively evolved more resilient persistence mechanisms, rather than desired phenotype of more efficient cell metabolisms. To avoid genetic hitchhikers, isolation from ALE experiments should be performed following sustained selective pressure over many generations, often at least ~100 [202], however, progressive phenotypic adaptation will occur even after tens of thousands of generations [212,337].

2.8.1 *Physical characterisation*

Following isolation of individual cyanobacteria strains, it is necessary to characterise these organisms to identify which (if any) exhibit phenotypes aligned with experimental objectives. If strains with improved growth and biomass formation are successfully isolated, further characterisation of cellular photosynthetic apparatuses could provide insight into how these strains have adapted to increase their growth rates.

2.8.1.1 *Growth and biomass formation*

As shown in **Table 2.3**, both growth rates and biomass formation have previously been used as a proxy to measure the efficacy of targeted engineering strategies to increase the productivity of *Synechocystis* through increased carbon fixation. Biomass formation has also been previously used to assess the effectiveness of ALE to select for strains of *Trichormus variabilis* with increased cell sizes [364], and as a method to assess both carbon assimilation and nitrogen metabolism in isolates of the algae *Nannochloropsis oculate*, adapted to increase temperature tolerance [274]. Given that carbon and nitrogen respectively comprise 51.38% and 11.29% of dry *Synechocystis* biomass [382], and protein and carbohydrates 48.3% and 24.53% of *Trichormus variabilis* biomass [365], measurement of dry weights can be an effective estimate of a strain's carbon and / or nitrogen fixation – when those resources are limiting. Measurement of dry weight can be obtained using pre-dried and pre-weighed tubes, with samples heat desiccated at temperatures between 70 – 80°C [366]. To enable high-throughput screening of ALE isolates, parallel

growth of strains in multi-well dishes have previously been used for both heterotrophic yeast [248] and prokaryotes [213].

Furthermore, given the link between biomass formation and efficient intracellular allocation of photoautotrophic metabolic flux (see Shastri and Morgan, 2008) [367], measurement of growth under conditions which alter a cell's metabolic burden could offer insights into how cells have adapted during selection. *Synechocystis* growth rates have previously been measured using optical density [77,184], using a wavelength of 750 nm. This wavelength is advantageous for estimating a culture's density (turbidity), as it reduces interference from the many light-sensitive pigments within cyanobacteria (see Wojtasiewicz and Stoń-Egiert, 2016) [368]. Any changes in relative growth rate are also an accepted measure to assess the relative "fitness" of two strains for an environment (see Lenski et al. 2015) [238]. Using optical density to measure growth of filamentous cyanobacteria may be less reliable, due to potential interference caused by variation in the filament lengths. However, previous work has shown a strong linear relationship exists between filament densities and 750 nm optical density measurements in *Planktothrix rubescens* [369].

To ensure accuracy of biomass and growth measurements, samples are measured in triplicate using biological replicates (see Beal et al. 2020) [370]. To ensure precision of measurements, statistical analysis of results using standard deviation can be performed (see Beal et al. 2020) [370]. Given the inherent variation among living organisms (especially when a species has been mutagenised to increase this variation), use of replicates increases the reliability of results by more accurately representing variation between samples (see Osborne and Killeen, 2008) [371]. Across sample replicates (typically $\geq$ 3) quantifying this variation is possible by measuring the dispersion of quantitative variables from the mean via standard deviation [372]. Isolates with statistically significant changes in biomass or growth are identified using Student's *t*-test [373]. A measure of probability frequently used to quantify the likelihood that variation between two means is a result of random chance, with the usually accepted threshold for determining significance being when that probability is less than 5% [371].

Therefore, to effectively identify mutants with greater carbon or nitrogen fixation capacities, strains which consistently exhibit significant increases in biomass formation and growth should be selected.

2.8.1.2 *Photosynthetic apparatus*

As previously stated, there is a strong correlation between rates of photosynthesis and respiration with biomass formation (see section 2.4.2 and Zavřel et al. 2021) [175]. Changes in these attributes would likely result in significant changes to a strain's phenotype, and therefore, characterisation of mutant photosynthetic apparatus could provide insights into how strains have adapted to increase growth and biomass formation. Measuring relative pigment contents and oxygen fluxes are two widely used methods to assess this (see Zavřel et al. 2021) [175]. Furthermore, these measurements can also enable for indirect assessment of the abundance and composition of intracellular photosynthetic photosystem complexes [175].

2.8.1.2.1 *Pigmentation*

As previously stated, cyanobacteria use pigmented compounds to capture solar energy for use in carbon fixation [92]. To characterise the abundance of these pigments, cells are usually lysed using solvents in which the target compound is soluble (see Chamovitz et al. 1993; Englund et al. 2015) [374]. Using a spectrophotometer, sample pigment concentrations of sample extracts can be calculated using established formulae and conversion constants, which can be then normalised to culture characteristics (such as per cell or dry weight) to allow for relative comparison [375]. Given the role of chlorophyll in cyanobacteria photosystems for capturing light energy (see section 2.2.1), any changes in its relative abundance would be useful for understanding the necessary investment into photosynthetic apparatus of mutant strains to achieve increased biomass formation. A relatively higher abundance could show mutants have adapted by increasing their light-harvesting capacity, whereas a relatively lower abundance could indicate cells use their resources more efficiently. Additionally, previous work has shown that cyanobacteria adapt to high light and oxidative stress by increasing the abundance of carotenoid molecules (see Dann et al. 2021) [284]. These molecules are less efficient than other pigments (such as chlorophyll) at harvesting light energy for photosynthesis [376], however, they serve an additional photoprotective role in cyanobacteria by dissipating excess excitation stress as heat in a process known as non-photochemical quenching [377]. Changes in the relative abundance of these molecules could indicate

changes in a mutant's abilities to regulate / its need to alleviate damage caused by light stress.

2.8.1.2.2 *Measuring oxygen evolution*

As oxygen is released during photosynthesis and consumed during aerobic respiration, measuring the change of oxygen concentration in growth medium an established method to assess photosynthetic and metabolic activity of cyanobacteria cells (see Zavřel et al. 2021) [175]. To allow for relative comparison between strains, samples are typically standardised to physical characteristics, such as chlorophyll concentration per mL^{-1} or cell density [378,379]. Oxygen flux can be measured using a Clark electrode, a device which determines the partial pressure of oxygen in solution by measuring the current produced when oxygen diffuses across a membrane and is reduced at a platinum cathode [380]. Photosynthetic activity can be assessed by calculating the rate of oxygen evolution within a culture when illuminated, and respiration rates calculated when cultures are incubated without light [378]. Due to the constant interplay between different factors such as shading, metabolic activity, and substrate availability, rates of oxygen evolution and consumption tend to fluctuate in cyanobacteria cultures during measurement, even in steady state conditions (see Brindley et al. 2010) [378]. Therefore, rates of evolution / consumption are measured following the acclimatisation of cultures to steady state conditions over several minutes and measuring the change in dissolved oxygen over time [378]. When linked to chlorophyll content, measurement of oxygen evolution can be useful for estimating photosynthetic efficiency, given that if samples evolve more O_2 per unit of chlorophyll, more photolysis is occurring, and more light energy is being captured per unit of chlorophyll (see sections 2.2.1 and 2.2.2; Li et al. 2014) [379]. Such observations could indicate that isolates have evolved more efficient photosynthetic machinery, or more efficient organisation of photosynthetic apparatus. When assessing O_2 flux using this method, however, consideration should be given for reproducibility across biological (rather than technical) replicates, given the potential for variation caused by changes in pigmentation abundance by a culture's growth state / conditions (see Brindley et al. 2010) [378].

2.8.2 *Omic characterisation*

As shown in **Table 2.4**, to assist determining the basis of any isolated mutant's phenotypes, multi-omic analysis can offer insights here. To identify any mutations linked to more productive phenotypes, and to characterise the metabolic profile of these phenotypes, genomic and metabolomic analyses were selected respectively for use in this study, to assess mutants at the molecular level.

2.8.2.1 *Genomic characterisation*

Given that phenotypes are the protein manifestations of hereditary DNA templates, identifying genetic differences between isolates and the parental strain is useful in understanding the molecular basis of any observed changes within isolated strains. Sequencing of DNA at scale become possible following the development of chain termination sequencing by Sanger et al. 1977 [381], subsequently leading to the development of an entire 'genomics' industry (see Chait et al. 1988) [382]. The first full cyanobacterium genome was published only 19 years later, using a commercial dye-primer cycle sequencing device based on those same principles from 1977 [296]. However, full genome sequencing remained both practically challenging, and extremely costly until the development of "next-generation" sequencing devices in the mid-2000s [383]. A lack of accessible sequencing technologies limited the ability of researchers to use ALE as an engineering strategy, due to the challenges of characterising selected isolates [202]. Something which can be observed in the number of substrate utilisation and growth optimisation ALE publications per year in **Figure 2.10**.

Despite the advantages of lower financial and labour costs, and an increased rate of analysis next-generation sequencing tools have over traditional Sanger tools [383], Sanger sequencing is still considered more reliable per base called [384]. With contemporary Sanger sequencing accuracy as high as 99.999% [385], compared with accuracies of ~92-93% for Oxford Nanopore Technology, and ~86% Pacific Biosciences next-generation tools in calling nucleotide variations (see Hu et al. 2021) [383]. To mitigate these issues, large DNA libraries are prepared (following the relevant manufacturer's instructions), which enable these devices to read the same region of DNA 100s, if not 1000s of times (see Pereira et al. 2020) [386].

Next-generation sequencing devices have enabled high-throughput and accurate analysis of entire genomes in as little as 24 hours, and for a fraction of the cost of earlier sequencing technologies [383]. Many devices are now available commercially, based on either short-read sequencing (2nd generation), or long-read-sequencing (3rd generation) technologies [383]. As implied by their respective names, the key difference between these technologies is the length of sample fragment analysed per read. While each of these technologies has advantages and disadvantages, they are both very able to deliver high-quality bioinformatic data for analysis (see Hu et al. 2021) [383]. From the perspective of ALE experimental design, therefore, (depending on cost and / or availability), which sequencing device is used is significantly less important than how the data from this device is processed (see Hu et al. 2021) [383].

Genomic data analysis pipelines benefit significantly from a wealth of online resources, with many software tools and add-ons having been developed to automate more laborious aspects of data processing (see Pereira et al. 2020) [386]. Pipeline specifics vary depending on which sequencing generation (or even device) was used, however, can be divided into 3 stages: primary, secondary, and tertiary analysis (**Figure 2.14**).

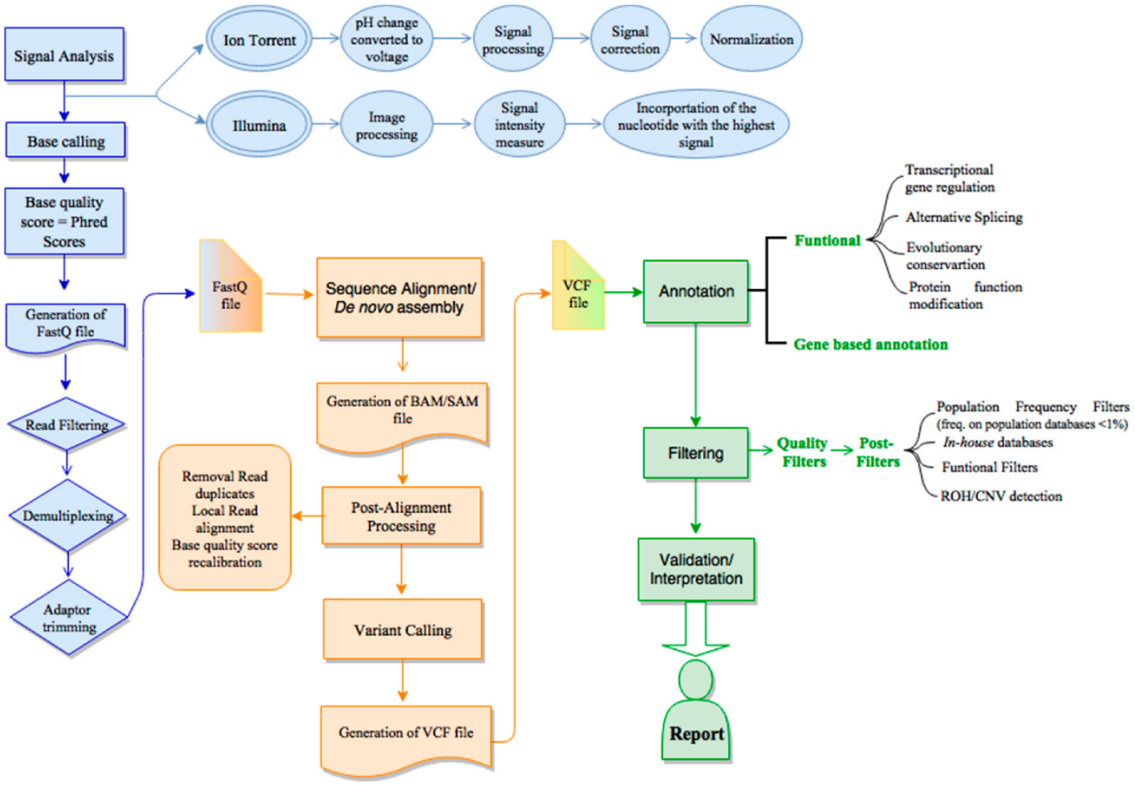


Figure 2.14 | Schematic overview of a next-generation genomic analysis workflow, with primary, secondary, and tertiary analysis stages highlighted in respective colours. Taken from Pereira et al. 2020 [386].

During primary data analysis, the detection and analysis of 'raw' signals is performed, with these signals dependent on a device's detection method, which can include measurement of fluorescence or electrical conductivity [386]. Individual sequencing reads are generated during this "base calling" stage, and weighted scores generated to determine base quality based on signal intensity and / or clarity [386]. Here, the reproducibility of reads acts as a quality control, both for integrity of the sequencing device, and for the quality of the data produced [386]. Post-sequencing "trimming" of data can then be performed to remove low quality reads which deviate significantly from an average or pre-determined signal quality threshold (see Pereira et al. 2020) [386].

Secondary analysis is subsequently performed on these processed individual reads to create an aligned consensus sequence [386]. Crucially for ALE, nucleotide variants can also be identified at this stage, when aligning sequencing contigs against a reference genome scaffold [386]. However, given that cyanobacteria are polyploid, (with *Synechocystis* possessing between 42 – 142 genome copies per cell depending on growth stage [387]) this presents additional analytical challenges for identifying mutant variations, when trying to distinguish 'mutants' from natural variation. To mitigate the potential impacts of polyploidy on results, the use (and sequencing) of a single colony clonal isolate prior to ALE allows the generation of an accurate reference genomic template. This ensures that any mutations present in the mutant genome, but not the template, can confidently be attributed to nucleotide variations. Furthermore, the relative abundance of identified nucleotide variants could offer insights into the abundance of any mutation across a polyploid genome (see Griffin et al. 2023) [388].

Following the generation of a single, aligned consensus sequence, tertiary analysis of this template can be performed. Here, sequences are annotated with biologically relevant information, typically coding sequences [386]. Variations identified during secondary analysis can then be refined based on how these are predicted to affect any annotated protein's predicted structure or expression (see Pereira et al. 2020) [386]. A bottleneck for genomic analysis, therefore, is the quality of available annotation data, typically drawn from large reference databases including Ensembl (http://www.ensembl.org), RefSeq (http://www.ncbi.nlm.nih.gov/RefSeq/)

[386]. Annotation data can therefore vary in both depth and quality, depending on the organism being analysed (see Ejigu & Jung, 2020) [389]. Although mutations in essential gene promoter sequences would likely have highly significant impacts on a strain's phenotype, identification of such mutants from genomic analysis would be challenging without accurate genetic feature databases to annotate from. While tools have been developed to predict promoter sequences within genomic data, these are currently limited to only a few organisms (such as *E. coli*) (see Chevez-Guardado et al. 2021) [390]. This said, the coupling of genomic and transcriptomic datasets can be a useful strategy for identifying mutations relevant to gene expression [389].

2.8.2.2 *Metabolomic characterisation*

Metabolomics is the study of 'metabolites', the small molecules which comprise biological systems, and aims to characterise the identity and abundance of these molecules [391]. Metabolomics experiments are either targeted or untargeted. Where targeted metabolomics is used to analyse predefined sets of known metabolites; untargeted metabolomics aims to profile as many metabolites in a sample as possible [392]. For characterising ALE mutants, where changes in a strain's metabolome are unknown prior to characterisation, untargeted metabolomics can be a useful strategy to identify novel changes in cell metabolic pathways. Therefore, assisting in understanding how novel phenotypes are generated [200].

To obtain reliable metabolomics data, however, experimental protocols should mitigate potential error and biases which could obfuscate relevant metabolic variation [393]. While there is no universally accepted consensus on best practice across all metabolomic analyses, there have been attempts in recent years to standardise methodologies, both in experimental design (see Viant et al. 2019) [393], and analysis (see Schymanski et al. 2014; Viant et al. 2019) [391,393]. Here, use of metabolomics is aimed at identifying significantly altered metabolites within mutant phenotypes, to gain insight into the physiological mechanisms of a mutant's adaptations [202]. An overview of the untargeted metabolomics workflow is shown in **Figure 2.15**.

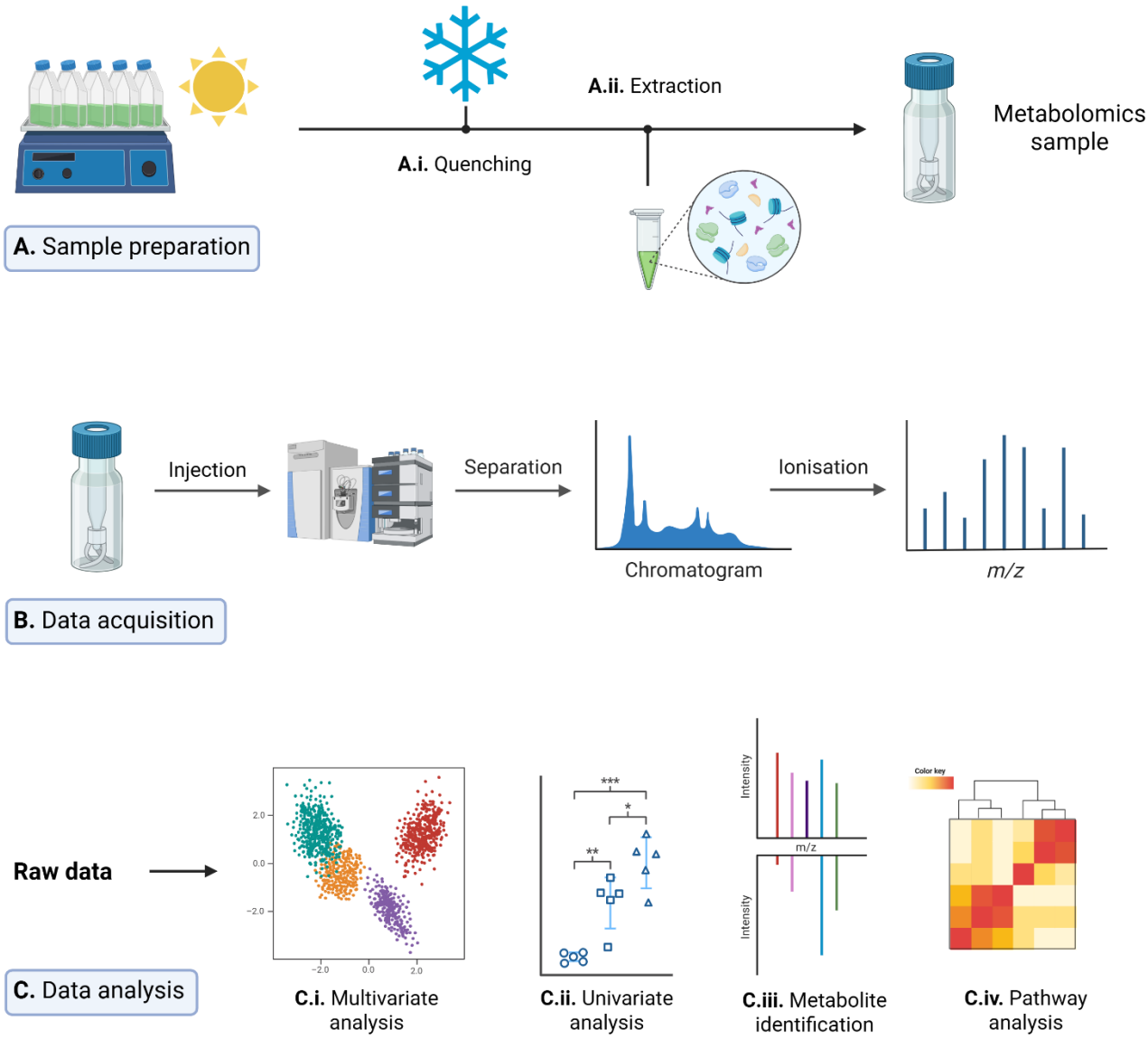


Figure 2.15 | Visualisation of an untargeted metabolomics experimental workflow in cyanobacteria, showing key steps of **A.** Sample preparation, **B.** Data acquisition, and **C.** Data analysis. (Created with BioRender.com).

2.8.2.2.1 *Metabolomic sample preparation*

Prior to analysis, samples must first be generated and collected. The key considerations of metabolomic sample preparation are as follows:

Growth – culturing of the cyanobacteria under conditions where the 'desirable' phenotypic characteristics of mutants are exhibited. For strains with enhanced growth and biomass formation, this should include samples

of exponential growth stages, and parental strain controls to assess mutants with “normal metabolism” references (see Viant et al. 2019) [393]. For metabolomics experiments, to ensure statistical power and reliability, a minimum of 3 biological replicates is necessary [393], with some suggesting it should be ≥ 5 [394].

Metabolite extraction – when harvesting samples for extraction, it is essential to ensure that samples remain reflective of the growth environment. It is therefore necessary to “quench” samples, rapidly, upon harvest [393]. While precise strategies to quench cyanobacteria metabolisms vary (see Sake et al. 2020) [395], the aim of this step is to rapidly cool samples while preserving the separate integrities of the intra- and / or extracellular metabolomes [393]. Once quenched, samples should be maintained at cooler temperatures, and either centrifuged or filtered to separate the intra- and extracellular metabolomes [393]. If investigating intracellular metabolites, cell pellets should be washed in cold buffer to prevent cross-contamination with extracellular metabolites [393]. Once cooled and washed, intracellular metabolites are typically extracted using solvent lysis (see Prasannan et al. 2018) [396]. Previous work in cyanobacteria has typically used ice-cold methanol solutions [396]. Extraction does not have to be performed using the same solvent as analysis, however, if samples are then dried [393].

Sample handling – following extraction, samples should be appropriately handled prior to analysis. For long-term (or even short-term) storage, this is typically at -80°C (see Viant et al. 2019) [393]. However, to avoid damage to sample quality, efforts should be made to minimise sample freeze-thaw cycles [393]. To enhance detection of lower abundance metabolites, samples are often concentrated, done so by either partially or fully drying samples [393], reconstituting in a smaller volume of appropriate solvent if the latter.

Further to the above, experimental procedures should also prepare process blanks, and intrastudy Quality Control (QC) samples for analysis. A process blank is prepared by extracting uncultured medium, and ensures the possible contaminants of the extraction procedure can be controlled for during analysis [393]. An intrastudy QC is a pooled-sample comprised 10 – 50 µL of each study sample (no blanks or standards), which allows the investigator to both prepare instruments prior to data collection, and subsequently to assess instrument stability during data analysis (see section 2.9.3.2.1) [393].

2.8.2.2.2 *Metabolomic data acquisition*

Once samples are prepared, data collection using can begin. Given that the aim of untargeted metabolomics is to reliably detect as many metabolites as possible, a common strategy to reduce sample complexity is separation via complementary liquid chromatography prior to spectral analysis [393], (though non-chromatographic methods to analyse biological samples have emerged in recent years, see Gertsman & Barshop, 2018) [392]. However, not only does chromatographic separation of metabolites reduce the interference among sample components, it also adds an additional parameter, retention time (RT), which can be used to differentiate between metabolites with similar masses and / or fragmentation patterns [392].

To avoid potential biases from the order of analysis (due to sample degradation or otherwise), samples should be randomised prior to data collection [393]. Furthermore, QC samples should be injected prior to analysis to "condition" the analytical system (see Viant et al. 2019) [393]. This is necessary to stabilise the instrument and reduce variability from data acquisition (see Viant et al. 2019) [393]. Additionally, injections of the intrastudy QC throughout the experiment allows for analysis of intrastudy reproducibility, and (depending on data processing methodology) to correct for systematic errors caused by analytical drift [393]. These injections are typically performed every 5 to 10 samples (see Dunn et al. 2011) [397], however, should ideally be performed as often as experimentally practical.

Following chromatographic separation, eluted metabolites are ionised (see Gertsman & Barshop, 2018) [392]. This transforms charge neutral molecules into charged ions, enabling them to be detected and characterised by their mass-to-charge ratio (*m/z*) (see Milman, 2015) [398]. A mass spectrometer's scanning parameters determine which ions can be detected during data acquisition. These parameters include instrument polarity, to detect either positive or negative ions, and *m/z* selectivity, to capture either predetermined masses or all masses within calibrated range [393,398]. To ensure comprehensive metabolomic profiling, acquisition using both polarities and of all masses is typically recommended for untargeted analysis [393]. While use of 'full scan' is effective for capturing *m/z* 'features' and estimating their relative abundances, full scan coupled fragmentation reduces the quality and coverage of the generated fragmentation data [399]. These limitations can be reduced by performing fragmentation analysis during separate sample injections (see Guo & Huan, 2020) [399], however, at the cost of extra acquisition time and sample volume [399]. To enhance fragmentation ion coverage, and therefore to improve the identification of

molecules, stepped collision energy (the fragmentation of ions over a collision energy gradient) can also be used [400]. The coverage of metabolites captured for fragmentation analysis can be further increased using data-dependent acquisition based on an *m/z* selectivity informed by previous acquisitions during an experiment [399]. Typically using the intrastudy QC sample. To further assist identification of metabolites, injection of reference (known) standards in calibrated mixes is also typically performed for untargeted experiments (see Viant et al. 2019) [393].

2.8.2.2.3 *Metabolomic data processing*

Following acquisition, 'raw' data is transformed from an incoherent mess of *m/z* signals and intensities, into discrete signals, with relative intensities. Due to instrument variability, exact quantification of many individual metabolites is not practical during an untargeted experiment [393], and so abundances are considered as 'relative' [393]. As laid out by the supplementary information of Viant et al. 2019, processing of untargeted acquisition data involves four key steps: peak detection, retention time alignment, grouping / matching, and peak integration [393]. The result is the putative identification of distinct, individual metabolites within a sample. To account for the impacts of instrument or sample variation on signals, post-processing and normalisation is typically performed [393]. Normalisation is the scaling of signals by a factor to account for variations in the biological sample's characteristics, for variations in extracted samples' dilutions, or signal variability during acquisition [393]. Batch correction is also often performed to account for intrastudy variability, with signals commonly scaled to intrastudy QC samples (as these should theoretically be consistent) [393]. To ensure data reliability, "noise" signals are reduced [393], often by removing infrequent signals (present in < 50% of QC samples), or signals present in either media or process blanks [393,397].

Following the transformation of raw data into pre-processed data, statistical analysis can then be performed to identify any significant differences in metabolites or metabolomic profiles between sample groups. To identify if data is suitable for further analysis, results are assessed using an unsupervised multivariate analytical method, typically via a Principal Component Analysis (PCA) (see Viant et al. 2019) [393]. This method builds a statistical model in which variables (*m/z*, RT) are transformed into spatial vectors [401]. From correlation of these transformed (now directional) variables, principal components are generated which represent the largest variation of variables across the experiment [401]. To

ensure validity of experimental results, inclusion of intrastudy QC samples within the model can identify if there are issues in stability or reproducibility of the analytical instrument [393]. Tightly clustered and centred QC samples is typically a strong indication of stability and reproducibility within an experiment [393]. Intrastudy QC samples can also be used to assess Relative Standard Deviation (RSD) of data, another measure of instrumental variance [397]. The RSD is a measure of each variable's standard deviation, divided by the variable mean, and multiplied by 100 to express the variance as a percentage [402]. As RSD of less than 20-30% is generally considered acceptable for an experiment [393,397].

To identify if there are direct significant differences between the metabolomes of two biological groups, supervised multivariate models are often used [393]. Unlike PCA analysis where sample groups are only used for visualising the data, Orthogonal / (...) Partial Least Squares Discriminant Analysis (OPLS-DA / PLS-DA) assesses variation directly within and between groups [401]. An OPLS-DA again builds a model by transforming variables into vectors; vectors are here directly scaled along predefined axes however, for either inter- or intrasample variance [401]. Given the risk of exaggerating variance by predefining principal component direction, however, it is necessary to validate OPLS-DA models to ensure that they are not 'over fitted' [401]. A strategy to validate if this is true is to use an OPLS-DA permutation test, in which class labels are randomly shuffled or 'permutated', and the model's permutated predictive strength, here its Q^2 value, compared against the original model's Q^2 [401]. If a model is not over corrected, permutated Q^2 values will therefore be significantly lower than the original model. Once validated, an OPLS-DA model can also be used to identify differences between individual variables of each class, often using Variable Importance in Projection (VIP) scores [393]. Essentially an assessment of a variable's 'weight' in contributing to the previously assessed OPLS-DA components. Generally, VIP scores greater than 1 are considered indicative of influential variables (see Yamamoto et al. 2014) [403]. Univariate analysis between individual variables can also assess significance between specific metabolites [393]. Given the scale of how many variables are in an untargeted metabolomics experiment, and given the inherent 5% risk of false discovery using standard p-value analysis, more stringent adjusted p-values which correct for the total number of variables are used (see Gertsman & Barshop, 2018) [392].

Once data has been acquired and validated, the process of identifying individual metabolites can begin. Similar to other aspects of metabolomic experimental practice, there is no universal consensus on best practice (see Viant et al. 2019) [393]. A commonly used framework however, as described

by Schymanski et al. 2014, is to identify metabolites based on 'level of confidence' [391]. These are as follows:

- **Level 1**: Confirmed identification using two orthogonal properties (e.g. exact mass, retention time, fragmentation pattern) and direct comparison to authentic standards.
- **Level 2**: Putatively annotated compounds based on two orthogonal properties. This includes comparison with external spectral libraries.
- **Level 3**: Identification of compound class, however, not specific metabolite.
- **Level 4**: Isolation of an unambiguous ion formula, however, without identifying features.

While the use of untargeted metabolomics to characterise metabolic variation between ALE adapted mutants and parental strains can offer valuable insights in adapted strain phenotypes; the reliable and accurate implementation of such a strategy is a practically challenging and requires robust analytical methodologies.

2.9 Aim and objectives

Based on the literature reviewed in **Chapter 2**, including current limitations on the use of cyanobacteria commercially (section **2.4**), the previous limitations of rational engineering work (section **2.5**), the potential of ALE to select for strains with enhanced growth and substrate utilisation, (section **2.6**). Given the existing knowledge gap in the application of this strategy with photosynthetic and diazotrophic prokaryotes, this research aims to investigate the use of ALE to enhance the productivity of cyanobacteria by selecting for increased biomass accumulation and growth rates, and subsequently increased carbon and nitrogen flux. The objectives are as follows,

1. Evaluation of ALE as an effective strategy to increase carbon fixation in the unicellular cyanobacterium *Synechocystis* sp. PCC 6803.

2. Evaluation of ALE as an effective strategy to increase nitrogen fixation in the filamentous cyanobacteria *Trichormus variabilis* sp. ATCC 29413.

3. Characterisation of the *Synechocystis* and *Trichormus variabilis* strains from the ALE experiments with the greatest biomass formation to evaluate how the strains have evolved via growth rates, pigmentation, photosynthetic analysis, and omics.

Chapter 3.

Materials and Methods

3.1 Growth and Experimental Media

All strains used in this study are listed in **Table 3.1**. For general laboratory growth, Lysogeny Broth (LB) medium [404] was used to culture all *E. coli* strains used in this study. Cyanobacteria strains were grown using variations of minimal medium Blue-green 11 (BG-11) [405]. *Synechocystis* sp. PCC 6803 strains were grown using the base BG-11 medium composition. *Trichormus variabilis* strains were grown using nitrogen-limited BG-11 medium ($BG\text{-}11_0$). Bacterial growth was assessed using optical density as a proxy for population density (see section **3.3.1**). Bacterial growth was presented in logarithmic format, and variance assessed using standard deviation (see Zwietering et al. 1990; Koch et al. 2007) [406,407]. Unless otherwise stated, all media was autoclave sterilised prior to use.

Table 3.1 | Bacterial strains used in this study.

Organism	Genotype	Source
E. coli		
DH5α	*fhuA2 Δ(argF-lacZ)U169 phoA glnV44 Φ80 Δ(lacZ)M15 gyrA96 recA1 relA1 endA1 thi-1 hsdR17*	NEB™, USA
***Synechocystis* sp. PCC 6803**		
GT	Glucose tolerant strain	Carrie Eckert, University of Colorado Boulder
Δhox	*hox*$^-$ (Hyg^R)	Carrie Eckert, University of Colorado Boulder
Syn.1.11	*hox*$^-$ (Hyg^R) mutagenised	*This study*
Syn.1.19	*hox*$^-$ (Hyg^R) mutagenised	*This study*
***Trichormus variabilis* sp. ATCC 29413**		
WT	Wild type strain	American Type Culture Collection (ATCC)
Ava.A.2.20.P	Wild type mutagenised	*This study*
Consortia isolates		
Achromobacter sp.	Isolate strain	*This study*
Pseudoxanthomonas sp.	Isolate strain	*This study*
Rhizobium sp.	Isolate strain	*This study*

When grown on solid media, *Synechocystis* strains were cultured using BG-11, and *Trichormus variabilis* using BG-11_0 solid media.

3.1.1 *LB medium*

Liquid LB medium was prepared by dissolving 25 $g \cdot L^{-1}$ Miller's LB Base (Sigma-Aldrich™) in deionised water. Media consisted of 10 $g \cdot L^{-1}$ NaCl, 10 $g \cdot L^{-1}$ tryptone, and 5 $g \cdot L^{-1}$ yeast extract. For solid medium, 1 $g \cdot L^{-1}$ agar was added.

3.1.2 *BG-11 medium and variants*

Liquid BG-11 medium chemical components are listed in **Table 3.2**. BG-11 medium was supplemented with 10 mM HEPES buffer (Sigma-Aldrich™) and adjusted to pH 7.8 prior to autoclave using 0.1 – 10 M NaOH. For solid medium, BD Difco™ Bacto™ Agar (Fisher Scientific™) was added to each BG-11 variant. 1 $g \cdot L^{-1}$ for strain isolation and cyanobacteria transformant patching, and 1.5 $g \cdot L^{-1}$ for transformations on solid medium.

Table 3.2 | Composition of BG-11 liquid medium.

Compound	**mass·L^{-1}**
$NaNO_3$	1.5 g
$MgSO_4 \cdot 7H_2O$	75 mg
$K_2HPO_4 \cdot 3H_2O$	40 mg
$CaCl_2 \cdot 2H_2O$	36 mg
Citric Acid	6 mg
Ferric Ammonium Citrate	6 mg
H_3BO_3	2.86 mg
$MnCl_2 \cdot 4H_2O$	1.81 mg
$Na_2EDTA \cdot 2H_2O$	1 mg
$NaMoO_4 \cdot 2H_2O$	0.391 mg
$ZnSO_4 \cdot 7H_2O$	0.222 mg
$CuSO_4 \cdot 5H_2O$	0.079 mg
$Co(NO_3)_2 \cdot 6H_2O$	0.049 mg
Deionised Water	Fill to 1 L^{-1}

For culture of *Trichormus variabilis*, and during the ALE strain generation phases, further modifications were made to growth medium composition. Variants of BG-11 utilised for culture of *Trichormus variabilis* and ALE seed culture preparations are described in **Table 3.3**.

Table 3.3 | Composition of BG-11_0 liquid media variants.

Media	Base Media	Modification(s)
BG-11_{NH4}	BG-11	- $NaNO_3$, + 10 mM NH_4Cl
BG-11_0	BG-11	- $NaNO_3$
BG-11_0.mk2	BG-11_0	- deionised water, + tap water (NG7 5RD)
BG-11_0.mk3	BG-11_0	1.955 mg·L^{-1} $NaMoO_4 \cdot 2H_2O$
BG-11_0.mk4	BG-11_0	+ 1mM $NiO_4S \cdot 6H_2O$
BG-11_0.mk5	BG-11_0	- deionised water, + tap water (NG7 5RD), 1.955 mg·L^{-1} $NaMoO_4 \cdot 2H_2O$, + 1mM $NiO_4S \cdot 6H_2O$
BG-11_0A	BG-11_0	- $NaNO_3$, + 10 mM fructose
BG-11_0A.mk2	BG-11_0A	- deionised water, + tap water (NG7 5RD)
BG-11_0A.mk3	BG-11_0A	1.955 mg·L^{-1} $NaMoO_4 \cdot 2H_2O$
BG-11_0A.mk4	BG-11_0A	+ 1mM $NiO_4S \cdot 6H_2O$
BG-11_0A.mk5	BG-11_0A	- deionised water, + tap water (NG7 5RD), 1.955 mg·L^{-1} $NaMoO_4 \cdot 2H_2O$, + 1mM $NiO_4S \cdot 6H_2O$

3.1.3 *Antibiotic concentrations*

Based on previous work to determine inhibitory concentrations (see Heidorn et al. 2011; Eckert et al. 2012) [408,409], when required, the following concentrations of antibiotics (**Table 3.4**) were used with the corresponding organisms.

Table 3.4 | Woking concentrations of antibiotics by organism studied.

	Concentration ($\mu g \cdot mL^{-1}$)		
Antibiotic	***E. coli***	***Synechocystis***	***Trichormus variabilis***
Hygromycin	-	200	-
Chloramphenicol	35	10 - 35	-
Gentamicin	-	-	10 - 200
Ampicillin	-	-	100

3.1.4 *SOC medium*

Super Optimal broth with Catabolite repression (SOC) medium (NEB™) was used during the transformation of *E. coli* cells.

3.1.5 *General chemicals*

Unless otherwise stated, all chemical compounds used in this study were purchased from Sigma-Aldrich™.

3.2 Molecular Biology Manipulations

All plasmids used in this study are listed in **Table 3.5**.

Table 3.5 | Plasmids used in this study.

Plasmid	Description	Resistance	Source
pGEM®-T	f1 *lacZ*	AmpR	Promega, USA
pGEM®-*hox*	f1 *lacZ hoxEFUYH*	Amp^R, Cmp^R	*This study*

3.2.1 *DNA Quantification*

DNA was quantified using a uLite+ Spectrophotometer (BioDrop™). To prepare the instrument it was first cleaned and then blanked using 1.5 µL of nuclease free deionised water (dH_2O). 1 µL of sample was then loaded onto the spectrophotometer and measured at A_{230nm}, A_{260nm}, and A_{280nm}. A_{260nm} was used to determine the concentration of DNA in the sample by the instrument. A_{230nm} and A_{280nm} were used to determine the quality of the sample, by dividing the A_{260nm} reading by these values to determine the relative 260 / 230 and 260 / 280 ratios. These ratios estimate respectively the relative abundance within samples of carry-over contaminants (especially guanidine), or with proteins. Values of $\geq$ 1.8 for 260 / 230 ratios, or $\geq$ 2.0 for 260 / 280 ratios were considered acceptable for further applications.

3.2.2 *Plasmid extraction from E. coli*

Plasmid DNA was extracted using a Monarch® Plasmid Miniprep Kit (NEB™) following the manufacturer's instructions. For the elution step, dH_2O was used instead of the manufacturer's elution buffer. Elution was consistently carried out using the minimum recommended volume (30 µL). DNA concentration and quality were then determined using the uLite+ Spectrophotometer (Biodrop™), as described above.

3.2.3 *Genomic DNA extraction from cyanobacteria*

Cyanobacteria cultures were grown until exponential phase (OD_{750nm} ~ 1-1.5 for *Synechocystis*, and ~ 20 µg·mL^{-1} Chlorophyll-*a* (Chl-*a*) for *Trichormus variabilis*) was reached. Genomic DNA (gDNA) was extracted from cyanobacteria using either a Quick-DNA Fungal/Bacterial Kit (Zymo™) or Quick-DNA Fecal/Soil Microbe Kit (Zymo™) in each case following the manufacturer's instructions and using the maximum recommended volume of elution buffer (100 µL). Both kits yielded quantities of DNA from cyanobacteria, suitable for sequencing as per the manufacturer's instructions. Following gDNA extraction, DNA quantity and quality were assessed. Quantity was typically sufficient; however, sample quality was consistently below the stated threshold for usefulness in further applications. Therefore, gDNA samples were further purified using a previously established method [410].

Samples were adjusted to 200 µL using dH_2O. 20 µL of 3M sodium acetate and 450 µL ethanol (99.9%) were added. Samples were incubated at -20 °C for 24 hours. Samples were then centrifuged at 15000 g, 4 °C, for 20 minutes, and supernatants carefully discarded using a pipette. 200 µL of 4 °C 70% ethanol was added to the sample, with care taken not to disturb the pellets. Samples were again centrifuged at 15000 g, 4 °C, for 10 minutes, and supernatants carefully discarded. The 70% ethanol washing step was repeated a total of 3 times, and the sample allowed to air dry at room temperature following the final wash for 10 minutes. Samples were resuspended in 50 µL of dH_2O, and quantity and quality were reassessed.

3.2.4 *Polymerase Chain Reaction (PCR)*

All PCR reactions were carried out in 0.2 mL (Greiner Bio-One). Reactions were performed in either a Mastercycler® nexus GX2e (Eppendorf™) or a TurboCycler 2 Thermal Cycler (Blue-Ray Biotech Corporation), depending on instrument availability. All PCR reactions were analysed using gel electrophoresis.

3.2.4.1 *PCR for cloning experiments*

PCR was used to amplify components for cloning experiments to be transformed into *E. coli*. Q5® High-Fidelity DNA Polymerase (NEB™) was used to amplify these reactions, and reaction mixtures were formulated as in **Table 3.6**.

Table 3.6 | Cloning PCR reaction components.

Component	Volume (µL)
Q5® High-Fidelity DNA Polymerase Master Mix (2X)	12.5
Forward Primer (10 µM)	0.5
Reverse Primer (10 µM)	0.5
DNA Template (1-50 ng·µL)	1
Nuclease Free Water	Fill to 25 µL
Total reaction volume	25 µL

The reaction mixtures were then placed into a thermocycler, and the reaction carried out using the protocol in **Table 3.7**.

Table 3.7 | Cloning PCR thermocycler protocol.

Protocol step	Temperature (°C)	Time
Hot start denaturation	98	30 seconds
Denaturation	98	10 seconds
30-35 cycles	40-72	30 seconds
Annealing		
Extension	72	30 seconds·kb^{-1}
Final extension	72	5 minutes
Hold	10	N/A

Completed reactions were then visualised using gel electrophoresis, and successfully amplified cloning components identified. Depending on the quality of amplified components, reactions were prepared for processing via either post-PCR DNA clean-up or gel excision.

3.2.4.2 *PCR for screening transformant colonies*

Following transformation experiments, single colonies were picked from selective solid media plates using a sterile toothpick. First the toothpick was used to inoculate a labelled second plate, (containing the same antibiotics from which the colony was selected from), and then inoculated directly into a PCR reaction tube containing the colony PCR (cPCR) reaction mixture. Reaction mixtures were formulated as in **Table 3.8**. cPCR was used to identify successful *E. coli* and cyanobacteria transformants that contained the DNA of interest. GoTaq® G2 DNA Polymerase (Promega™) was used to amplify these reactions.

Table 3.8 | cPCR reaction components.

Component	Volume (µL)
GoTaq® G2 DNA Polymerase Master Mix (2X)	12.5
Forward Primer (10 µM)	0.5
Reverse Primer (10 µM)	0.5
DNA Template (1-50 ng·µL)	1
Nuclease Free Water	Fill to 25 µL
Total reaction volume	25 µL

The reaction mixtures were then placed into a thermocycler, and the reaction carried out using the protocol in **Table 3.9**.

Table 3.9 | cPCR thermocycler protocol.

Protocol step		Temperature (°C)	Time
Hot start denaturation		95	2 minutes
30-35 cycles	Denaturation	95	30 seconds
	Annealing	40-72	45 seconds
	Extension	72	60 seconds·kb^{-1}
Final extension		72	10 minutes
Hold		10	N/A

Completed reactions were visualised using gel electrophoresis, and successfully transformed colonies identified. Referring to the corresponding patch plate, successful transformants were then inoculated into appropriate selective liquid media.

3.2.5 *Visualising DNA using agarose gel electrophoresis*

1% agarose gels were prepared by dissolving 0.5 g of molecular biology grade agarose in 50 mL of 1X TAE buffer (40 mM Tris-acetate and 1 mM EDTA, pH 8.3). This solution was then microwaved at 900 W for ca. 5 minutes, before being allowed to reach ca. 60 °C. SYBR® Safe DNA gel stain (ThermoFisher Scientific™) was added at a 1:10,000 dilution, and the gel set at room temperature. PCR samples without loading buffer in their reaction mixture were supplemented with either TriTrack® (6X) Green Gel Loading Dye (ThermoFisher Scientific™) or 6X Purple Gel Loading Dye (NEB™). Samples were loaded with an accompanying DNA ladder, GeneRuler 1kb Plus (ThermoFisher Scientific™) or Fast DNA Ladder (NEB™), to determine fragment size. Gels were then electrophoresed in 1X TAE buffer at 110 V (400 mA) for 30 – 60 minutes. Gels were visualised using a UV transilluminator (GelDoc™) for characterisation or using a Blue Light Transilluminator (Cleaver Scientific) for gel extraction.

3.2.6 *Extracting DNA from agarose gels*

If multiple bands were present during initial DNA visualisation, DNA bands of the expected size were excised from a subsequent agarose gel under blue light visualisation using a scalpel. These were placed into a pre-weighed 1.5 mL microcentrifuge tube and purified using a Monarch® DNA Gel Extraction Kit (NEB™) following the manufacturer's instructions. For the elution step, dH_2O was used instead of the manufacturer's elution buffer. Elution was consistently carried out using the minimum recommended volume (6 µL). DNA concentration and quality was then determined.

3.2.7 *Post PCR DNA clean-up*

If only one band of the expected size was present during initial DNA visualization, samples were routinely purified using Monarch® PCR & DNA

Cleanup Kit (5 µg) (NEB™) following the manufacturer's instructions. Again, for the elution step, dH_2O was used instead of the manufacturer's elution buffer, and carried out using the minimum recommended volume (6 µL). DNA concentration and quality was then determined. Samples with useful DNA concentrations, but poor quality, were sometimes cleaned following the same protocol outlined in 2.2.2, and re-measured.

3.2.8 *Nuclease restriction digestion of DNA*

All DNA fragments and plasmids were digested using restriction enzymes supplied by ThermoFisher Scientific™ from the FastDigest® catalogue. All reactions were carried out in 25 µL volumes, using the series' 10X Green Buffer, and all in 0.2 mL PCR_Tubes (Greiner). Reaction compositions can be seen in **Table 3.10**. Reaction mixtures were incubated using a thermocycler at 37 °C for 20 – 30 minutes and then analysed using gel electrophoresis.

Table 3.10 | Restriction digestion reaction components.

Component	Quantity
10X Green Buffer	2 µL
Restriction enzyme(s)	1 µL per enzyme
DNA	1-1.5 µg
Nuclease Free Water	Fill to 20 µL
Total reaction volume	20 µL

3.2.9 *HiFi DNA Assembly*

NEBuilder® HiFi DNA Assembly was used to assemble pGEM-*hox* constructs. Insert fragments were amplified using cPCR reactions (see

2.2.4.1), and a modified thermocycler protocol (**Table 3.11**) This protocol was used as the primers necessary for generating suitable fragments were 29 – 39 bp long, reducing their specificity and increasing their melting temperature. The removal of the annealing step early in the protocol helped reduce the number of off target amplifications.

Table 3.11 | HiFi oligo PCR thermocycler protocol.

Protocol step		Temperature (°C)	Time
Hot start denaturation		98	30 seconds
5 cycles	Denaturation	98	10 seconds
	Annealing	40-72	30 seconds
	Extension	72	30 seconds·kb^{-1}
30 cycles	Denaturation	98	10 seconds
	Annealing	72	30 seconds
	Extension	72	30 seconds·kb^{-1}
Final extension		72	5 min
Hold		10	N/A

Following amplification, insert fragments were purified using either gel extraction (2.2.6) or PCR clean-up (2.2.7), and elutions of sufficient quantity and quality of DNA were obtained. Linearised backbones were obtained by restriction digestion (2.2.8), and then purified using gel extraction. Reactions consisting of 2 fragments (1 insert and 1 backbone) were prepared in 0.2 mL (Greiner) in the quantities and ratios listed in **Table 3.12**. Reactions were incubated at 50 °C for 90 minutes in a thermocycler.

Table 3.12 | HiFi assembly reaction components.

Component	Quantity
HiFi assembly master mix (2X)	3 µL
Fragment DNA	~100 ng each
Nuclease Free Water	Fill to 6 µL
Total reaction volume	6 µL

Following incubation samples were chilled on ice and then transformed via heat shock into chemically competent *E. coli* cells.

3.2.10 *Generation of chemically competent E. coli cells*

Chemically competent *E. coli* cells were prepared following a previously established protocol [411]. 10 mL of LB liquid media in a 50 mL centrifuge tube was inoculated using a single colony picked from a plate of non-selective LB solid media and cultured at 37 °C, 150 RPM orbital shaking, overnight. 0.5 mL of culture was then inoculated into a new centrifuge tube, containing 49.5 mL of fresh LB liquid media the following day. This new centrifuge tube was returned to the shaking incubator. The culture was monitored until it reached OD_{A600nm} = 0.3, at which point the culture was harvested at 5000 g, at 4 °C, for 5 minutes. The supernatant was discarded, and cells carefully resuspended in 1 mL of 4 °C, 0.1 M $CaCl_2$. The cells were incubated on ice for 30 minutes, and centrifuged again at 5000 g, at 4 °C, for 5 minutes. Cells were then carefully resuspended in 1 mL of a 4 °C, 0.22-µm filter sterilised 0.1 M $CaCl_2$, 15% v/v glycerol solution. 200 µL of cells were aliquoted into 5 pre-chilled 1.5 mL microcentrifuge tubes, and samples stored at -80 °C overnight prior to use.

3.2.11 *Genetic transformation procedures*

E. coli was used for propagation of assembled molecular constructs.

3.2.11.1 *Transformation of E. coli*

Chemically competent *E. coli* cells were transformed using heat shock transformation [412]. Competent cells stored at -80 °C were thawed on ice. Reaction tubes were prepared in the interim by aliquoting appropriate concentrations of DNA into 0.2 mL (Greiner), which were also kept on ice until used. Once thawed, 50 µL of chemically competent *E. coli* cell suspension was added aseptically to each reaction tube. These tubes were placed into a pre-chilled thermocycler at 4 °C and transformed using the heat shock protocol outlined in **Table 3.13**.

Table 3.13 | Heat shock transformation thermocycler protocol.

Protocol step	Temperature (°C)	Time
Incubation with DNA	4	30 minutes
Heat shock transformation	42	30 seconds
Post-transformation incubation	4	5 minutes
Hold	10	N/A

Once transformed, reaction mixtures were inoculated into 950 µL of SOC outgrowth medium and incubated at 37 °C, 250 RPM orbital shaking for 1 hour. From the outgrowth culture, 50 µL of cells were plated directly onto a 37 °C selective LB plate containing an appropriate concentration of antibiotics. The remaining 450 µL were concentrated by centrifugation at 5000 g for 5 minutes, removing 400 µL of supernatant, and resuspending the pellet in the remaining 50 µL of medium. This was then also plated onto a pre-warmed selective LB plate. Plates were incubated at 37 °C overnight until colonies appeared. A subset of colonies that appeared were then screened using cPCR to distinguish successful transformants from false positives.

3.2.11.2 *Natural transformation of Synechocystis*

Natural transformation of *Synechocystis* can be performed by adding DNA to concentrated cell cultures, as this species is naturally competent [413].

Natural transformation was performed by growing cultures at 60 µmol photons·m^{-2}·sec^{-1} of white light, 30 °C, 150 RPM orbital shaking, until the culture entered late exponential / early stationary phase (OD_{750nm} = 5 – 6). 5 – 15 mL of culture was then transferred to a sterile 15 mL centrifuge tube and centrifuged at 5000 g for 5 minutes. Supernatants were discarded and pellets resuspended in 10 µL of BG-11 per 1 mL of culture harvested for transformation. Transformations were carried out using 50 µL aliquots per reaction. Aliquots were transferred to individual, sterile 1.5 mL microcentrifuge tubes, and 2.5 – 5 µg of DNA was added to each tube. Tubes were mixed using gentle flicking at the base and incubated at 60 µmol photons·m^{-2}·sec^{-1} of white light, 30 °C for 5 hours. Reactions were mixed using further gentle flicking at the base of the tube every hour and plated onto 50 mL of BG-11 solid medium at the end of the incubation period.

Plates were incubated until confluent green growth was observed (approximately 24 hours) at 60 µmol photons·m^{-2}·sec^{-1} of white light, 30 °C. Following this outgrowth, 1 mL of appropriate antibiotic, dissolved in deionised water, was injected under the solid media to generate the working concentration of antibiotic across the plate through diffusion. Transformants typically appeared and were picked for further selection after 7 – 10 days.

3.2.11.3 *Electroporation transformation of Synechocystis*

Cultures of 10 mL of *Synechocystis* were grown to between OD_{750nm} ~0.8 – 1 at 60 µmol photons·m^{-2}·sec^{-1} of white light, 30 °C, 150 RPM orbital shaking. Cultures were transferred to 50 mL centrifuge tubes and centrifuged at 3000 g for 5 minutes. Supernatants were discarded and samples resuspended in 50 µL 1 mM HEPES, pH 7.2. Between ~3 – 5 µg of DNA were added per reaction, and samples transferred into Flowgen Electroporation Cuvettes 2 mm (Scientific Laboratory Supplies), (pre-chilled on ice). Cuvettes were placed into a GenePulser™ (Bio-Rad™) and pulsed with at 12 $kVcm^{-1}$ 400 Ω for 9 ms. 450 µL BG-11 liquid media was

immediately added to each cuvette, and samples were transferred to 1.5 mL microcentrifuge tubes. Tubes were incubated for 5 hours at 60 µmol photons·m^{-2}·sec^{-1} of white light, 30 °C – mixed every hour with gentle flicking. Transformed cultures were plated on BG-11 solid media and grown for 24 – 48 hours at 60 µmol photons·m^{-2}·sec^{-1} of white light, 30 °C (until plates showed visible growth). 1 mL of deionised water containing an appropriate concentration of antibiotic was added at this stage to the base of the agar plate. Plates were incubated at 60 µmol photons·m^{-2}·sec^{-1} of white light, 30 °C for 7 – 14 days, (until colonies appeared).

3.2.12 *Sanger sequencing analysis*

Sanger sequencing of purified DNA fragments from cPCR reactions was carried out by either Eurofins Genomics (Ebersberg, Germany), or Source BioScience (Nottingham, United Kingdom). Sanger sequencing of whole plasmids was carried out exclusively by Source BioScience (Nottingham, United Kingdom).

3.3 Cell characterisation

Cell cultures were analysed by measuring the relative abundance of their densities, pigmentation, and biomass.

3.3.1 *Optical Density (OD)*

Optical Density (OD) of bacterial cultures was measured using a UV-1280 Spectrophotometer (Shimadzu™). *E. coli* cultures were measured using OD_{600nm}, and cyanobacteria cultures were measured using OD_{750nm}. Readings were taken between 0.1 – 0.8, and cell cultures were diluted appropriately to ensure they were within this range during measurement. Light scattering measurements were used to determine the relative density of cell cultures.

3.3.2 *Whole cell absorbance spectral analysis*

Whole cell spectra of liquid cultures were measured using a UV-2600 Spectrophotometer (Shimadzu™). Measurements were taken between OD_{400nm} and OD_{800nm}, using cultures adjusted (by dilution) to OD_{750nm} 0.01 – 0.9.

3.3.3 *Pigmentation characterisation*

Comprehensive pigment extraction from cyanobacteria was carried by adapting a previously established method [374,414]. A 1 mL sample of media was removed from triplicate cultures during exponential growth of cells and transferred to 1.5 mL microcentrifuge tubes. Samples were centrifuged at 15000 g for 10 minutes, and supernatants discarded. Cell pellets were then resuspended in 1 mL of *N*-*N*-Dimethlyformamide (DMF) (99.8%) and mixed by pipetting repeatedly to ensure thorough and even lysis. Samples were then incubated at 4 °C in the dark for 30 minutes, before being centrifuged at 15000 g for 10 minutes to remove cell debris. 800 µL of supernatant was transferred to a quartz cuvette, and a whole sample spectrum between OD_{400nm} and OD_{800nm} was taken using a UV-2600 Spectrophotometer (Shimadzu™). Sample OD values for 461 nm and 664 nm were extracted from these spectra to quantify sample carotenoid and chlorophyll concentrations respectively.

To quantify carotenoid concentration the following equation was used:

$$[\mu g \cdot mL^{-1}] = (OD_{461nm} - (OD_{664nm} \times 0.046)) \times 4$$

Chlorophyll concentration was determined using the following equation:

$$[\mu g \cdot mL^{-1}] = OD_{664nm} \times 11.92$$

Quantification of chlorophyll for growth curves and standardisation was extracted following an adapted iteration of a different established protocol (Schemlling, 2016) [415]. 1 mL of media was removed from triplicate cultures during sampling and transferred to 1.5 mL microcentrifuge tubes. Samples were centrifuged at 15000 g for 10 minutes, and 900 µL of

supernatant were discarded. After adding 900 µL of methanol (≥ 99.9%) samples pipetted to resuspend pellets and incubated at 4 °C in the dark for 30 minutes, before being centrifuged at 15000 g for 30 minutes to remove cell debris. 800 µL of supernatant were transferred to a cuvette, and the 665nm and 750nm OD values measured. Chlorophyll concentrations were determined using the following previously calibrated conversion formula (see Zavřel et al. 2015; Schmelling, 2016) [375,415]:

$$[\mu g \cdot mL^{-1}] = (OD_{665nm} - OD_{750nm}) \times 13.9$$

3.3.4 *Clark electrode analysis of oxygen evolution*

For analysis of *Synechocystis* strains, cultures were grown in triplicate in 25 mL of BG-11_{NH4} liquid medium, and BG-11_0 for *Trichormus variabilis* strains. *Trichormus variabilis* strains were grown under ambient CO_2 concentration (ca. 0.04%), and *Synechocystis* was cultured with CO_2 supplementation (~1.5%). When grown under ambient CO_2 concentrations, the light used for these experiments was of a Multitron Pro Light Incubator (Infors HT), at an intensity of 60 µmol photons·m^{-2}·sec^{-1}, measured using a Quantitherm PAR/Temp Sensor (Hansatech Instruments™), and 150 RPM orbital shaking. For cultures grown under CO_2 supplementation, these were incubated on an orbital shaker placed within a Reach-in Growth Chamber, Fitotron SGC (Weiss Technik), inside a transparent, sealable acrylic box, custom built by the University of Nottingham, Department of Engineering workshop team. A mixture of air and CO_2 gas was created using calibrated gas flow meters prior to delivery into the sealed container. The conditions used for these experiments were 300 µmol photons·m^{-2}·sec^{-1}, 30 °C, 150 RPM orbital shaking.

Culture growth was monitored using OD_{750nm} to determine when exponential growth phase occurred, ~ 1-1.5 (exact OD_{750nm} was recorded at time of measurement). Prior to analysis using the Clark electrode, samples of cultures in the exponential phase were standardised to 5 µg·mL^{-1} of chlorophyll, by measuring the concentration of chlorophyll within 1 mL of sample culture (as described in 3.3.3). An appropriate volume of culture to generate a final 5 µg·mL^{-1} chlorophyll concentration in 1 mL was removed and transferred to a 1.5 mL microcentrifuge tube. Samples were centrifuged at 2500 g for 5 minutes for *Synechocystis*, and 15 minutes for *Trichormus variabilis*, (due to challenges in obtaining a stable pellet of this

organism). The supernatants were removed, and the pellets resuspended in 1 mL of fresh medium, (the same medium used during their respective cultivations).

Samples were transferred to a DW2/2 Electrode Chamber with an S1 Electrode Disc (Hansatech Instruments™). Respiratory oxygen consumption was measured in the absence of light, and photosynthetic oxygen evolution rates were measured in 5-minute intervals using a LS2 White Light Source (Hansatech Instruments™) across a stepwise gradient of light intensities of 0 – 932 µmol photons·m^{-2}·sec^{-1}.

3.3.5 *ALE isolate 24-well plate screening*

Adaptive Laboratory Evolution (ALE) mutant single colonies were isolated by serial dilution plating of chemostat terminal spent media onto BG-11 solid media (*Synechocystis*) or BG-11_0 solid media (*Trichormus variabilis*). Colonies were selected by no specific characteristic, picking from the centre of the plate outwards. This was to ensure population diversity was represented. Picked colonies were patched onto the same media used for selection and grown under the same light intensities and temperature as respective selections. Once patched colonies possessed sufficient biomass, isolates were screened for enhanced biomass formation using Corning™ Costar™ 24-well Clear TC-treated Multiple Well Plates (Fisher Scientific™). Sterile 24-well plates were opened and handled exclusively within a Microbial Safety Cabinet (MSC). An aliquot of 1.1 mL of appropriate media was added to all wells prior to inoculation. Strain position was decided randomly for each individual 24-well plate, with triplicate samples across 3 separate plates.

For chemostat selection of *Synechocystis Δhox*, and *Trichormus variabilis* single colony isolates, each plate well was then inoculated using a sterile 1 µL loop by removing a small consistent quantity of biomass from the prepared plate of single colony isolates. This same loop was also to check for contamination by patching a corresponding LB solid media plate (incubated at 30 °C for 48 hours). For library samples *Trichormus variabilis*, wells were inoculated directly into wells using 1.1 mL of exponentially growing cultures in BG-11_0 liquid medium, adjusted to OD_{750nm} 0.1.

One well in each plate contained only sterile media as a negative control and all experimental batches contained triplicate inoculated wells of their respective progenitor strain as a positive control. 24-well plates were grown under a range of conditions and biomass accumulation

estimated by harvesting and measuring Dry Cell Weights (DCW) (see below).

3.3.5.1 *Synechocystis Δhox chemostat 24-well plate screening*

Following single colony isolation, 44 isolates were screened in 1.1 mL of BG-11NH_4 liquid media, at 300 µmol photons·m^{-2}·sec^{-1}, 30 °C, 120 hours, and under the same conditions with 1.5% CO_2 supplementation. 1 mL of each well was harvested for analysis following growth (see 2.3.6).

3.3.5.2 *Trichormus variabilis mixotrophic 24-well plate screening*

Following single colony isolation, 44 isolates were screened in 1.1 mL of BG-11_0 liquid media, at 300 µmol photons·m^{-2}·sec^{-1}, 30 °C, 120 hours, and the same conditions with BG-11_0A liquid media. 1 mL of each well was harvested for analysis following growth (see 2.3.6).

3.3.5.3 *Trichormus variabilis autotrophic 24-well plate screening*

Following single colony isolation, and single colonies shown to be non-axenic were recorded. Forty-four isolates were screened in 1.1 mL of BG-11_0 liquid media, at 300 µmol photons·m^{-2}·sec^{-1}, 30 °C, 120 hours. Twenty-four-well plate screened Ava.B population libraries, sampled from chemostat spent media every 2-3 days, were also screened at 300 µmol photons·m^{-2}·sec^{-1}, 30 °C, for 144 hours. A 1 mL sample of each well was harvested for analysis following growth (see 3.3.6).

3.3.6 *Measuring biomass*

Dry Cell Weight (DCW) measurements were used to estimate biomass content. All 1.5 mL microcentrifuge tubes were thoroughly dried at 80 °C for 24 hours prior to use as tubes lost between 0.3 – 0.5 mg of mass following the drying process alone, preventing the DCW of samples from being accurately determined. Dried microcentrifuge tubes were weighed using an HR-250AZ (A&D Company Limited) analytical balance.

When measuring the biomass of liquid cultures from growth curves or 24-well plate screening, 1 mL of media was removed from the culture vessels and transferred to a pre-dried and weighed 1.5 mL microcentrifuge tube. Samples were dried at 80 °C for 48 hours before being re-weighed using the same analytical scale used to weigh the dry, empty microcentrifuge tubes. Final DCWs were determined by subtracting the initial dried weight from the final weight recorded on the scale.

3.4 Adaptive Laboratory Evolution of cyanobacteria

Mutagenesis was performed before ALE selection to increase population genetic variation. Prior to carrying out ALE investigations, progenitor strains were selected for each cyanobacteria species being investigated, (this was to facilitate easier identification of mutagenised genomic elements post the selection process). Cyanobacteria cultures were first each grown at 60 µmol photons·m^{-2}·sec^{-1}, 30 °C, 150 RPM orbital shaking, until exponential growth was reached, (~ 1-1.5 OD_{750nm}). All initial *Synechocystis* cultures were grown using BG-11, and *Trichormus variabilis* using BG-11_0. These cultures were then plated onto their respective equivalent solid media, using serial dilution to generate single colonies. A single colony of *Synechocystis*, *Synechocystis Δhox*, and *Trichormus variabilis* was then selected as the progenitor strains for future ALE investigations and dubbed "Syn.GT", "Syn.*Δhox*", and "Ava.WT" respectively.

3.4.1 *Chemical mutagenesis of cyanobacteria*

Chemical mutagenesis of selected cyanobacteria strains was carried out by adapting a previously established protocol [208], using EMS to chemically mutagenise cells.

3.4.1.1 *Chemical mutagenesis of Synechocystis*

Cultures of Syn.*Δhox* or Syn.GT were grown in BG-$11NH_4$ or BG-11 respectively, at 300 µmol photons·m^{-2}·sec^{-1}, 30 °C, 150 RPM until exponential growth was reached, (OD_{750nm} ~ 1-1.5). To assess the chemical mutagen dosage impact on *Synechocystis* viability, kill curves were carried

out on Syn.*Δhox* cultures. For kill curves, 20 mL of culture per EMS reaction was transferred to 50 mL centrifuge tubes, and cells harvested via centrifugation at 3000 g for 5 minutes. Cell pellets were resuspended in 1 mL of BG-11NH_4 media and transferred to a 1.5 mL microcentrifuge tube. These were washed twice using 1 mL sterile BG-11NH_4 and resuspended in 0.5 mL of sterile 0.1 M Phosphate Buffer (pH 7.0). 100 µL of one sample of cells were then plated in triplicate onto BG-11 solid media using serial dilution to generate single colonies for a pre-treatment live count.

Cells were then exposed to one of 3 different concentrations of EMS (0.25 M, 0.5 M, and 0.75 M), and a control being exposed to only 0.1 M phosphate buffer, for 1 hour. Treatment was carried out in the dark at room temperature. Following treatment, cells were centrifuged at 3000 g for 5 minutes, and supernatants discarded. The EMS was inactivated by resuspending all samples in 1 mL of 10% (*w/v*) sodium thiosulphate solution for 10 minutes. Cells were centrifuged at 3000 g for 5 minutes, inactivation solution was removed, and the cells were washed three times using 1mL of BG-11NH_4 media. Cells were then resuspended in 1 mL of fresh BG-11NH_4 media, transferred to a 15 mL centrifuge tube, and incubated in the dark at room temperature for 24 hours.

Aliquots of 100 µL of treated cultures were plated in triplicate via serial dilution onto BG-11 solid media for single colonies. All plates were incubated at 60 µmol photons·m^{-2}·sec^{-1}, 30 °C, for 1 – 2 weeks, until single colonies appeared. The mortality rate of both the treatment process, and exposure to EMS, was then calculated by comparing the relative Colony Forming Unit (CFU) counts of untreated cells, processed cells not exposed to EMS, and processed cells exposed to different concentrations of EMS.

Following calculation of EMS treatment dosage viability counts, the mutagenesis process was repeated for all 3 measured EMS concentrations. Chemically mutagenised cultures were then combined in a T25 cell Nunc™ Non-treated Flasks (ThermoFisher Scientific™), and the volume was adjusted to 15 mL using BG-11NH_4 media.

3.4.1.2 *Chemical mutagenesis of Trichormus variabilis*

A modified version of the process used to chemically mutagenise Syn.*Δhox* (see 2.4.1.1.1) was used to treat Ava.WT. BG-11NH_4 liquid media was replaced with either BG-11_0A or BG-11_0, and BG-11 solid media by $BG11_0$ solid media. Centrifugation steps were carried out at 3000 g for 10 minutes due to difficulties in obtaining stable pellets with shorter

centrifugation steps. To reduce filamentous culture clumping, cell suspensions were vigorously mixed using pipetting prior to treatment with EMS, or when carrying out serial dilution for plating.

Following generation of treatment viability counts and subsequent mutagenesis of Ava.WT for selection, the final collation of mutagenised Ava.WT libraries was first carried out in a 15 mL centrifuge tube. This combined library was then divided among 6 T25 cell Nunc™ Non-treated Flasks (ThermoFisher Scientific™). Equal volumes of library culture was transferred to each flask, and volumes were then adjusted to 10 mL using one BG-11_0 or BG-11_0A media variant (**Tables 3.2; 3.3**) per flask.

3.4.2 *UV mutagenesis of Synechocystis*

Cultures of Syn.*Δhox* were grown in BG-$11NH_4$ at 300 µmol photons·m^{-2}·sec^{-1}, 30 °C, 150 RPM orbital shaking until exponential growth was reached, (OD_{750nm} ~ 1-1.5). To determine optimum dosages, kill curves were again carried out prior to mutagenesis. 20 mL of culture per condition were harvested by centrifugation at 3000 g for 5 minutes, and each resuspended in 20 mL of fresh BG-$11NH_4$ liquid media. One hundred µL of cell culture was removed to assess the effects of the treatment process on cell viability and plated for single colonies via serial dilution. Using GuardOne® Workstation-Laminar Flow (Starlab™) cultures was transferred to 90 mm diameter petri dishes. One petri dish was not exposed to UV radiation, remaining petri dishes were exposed to 2.5, 5, and 10 minutes of 254 nm UV radiation using a TUV 15W G15T8 (Philips™), ~70 nm from the radiation source. Samples were dosed independently and covered with aluminium foil immediately following each treatment. All samples were incubated in the dark for 24 hours at 30 °C. Cultures were plated on BG-11_0 in triplicate via serial dilution to assess the impact of the mutagenesis treatment on cell viability by counting CFUs. Prior to ALE selection, UV mutagenesis was repeated.

3.4.3 *Selection of enhanced Synechocystis strains*

3.4.3.1 *Multi-cultivator selection*

A culture of 20 mL of ~1 OD_{750nm} GT WT was mutagenised using a 0.5 M EMS treatment (see 2.4.1.1.2). Mutant libraries were outgrown in 3

cell cultureflasks for ~24 hours at 60 µmol photons·m^{-2}·sec^{-1}, 30 °C, 150 RPM orbital shaking. Mutagenised cultures were transferred to individual culture tubes of a Multi-Cultivator MC 1000-OD (Photon Systems Instruments™, Czechia) configured for ALE culture growth (see **Figure 3.1**). Cultures were grown in BG-11 liquid media, at 200 µmol photons·m^{-2}·sec^{-1}, 30 °C, and a 200 ppm CO_2 air mixture. Cultures were adjusted to 0.1 OD_{750nm} every 72 – 96 hours using fresh BG-11 liquid media. Following selection for 84 days (23 passage events), surviving cultures were plated for single colonies to isolate individual mutant strains for characterisation.

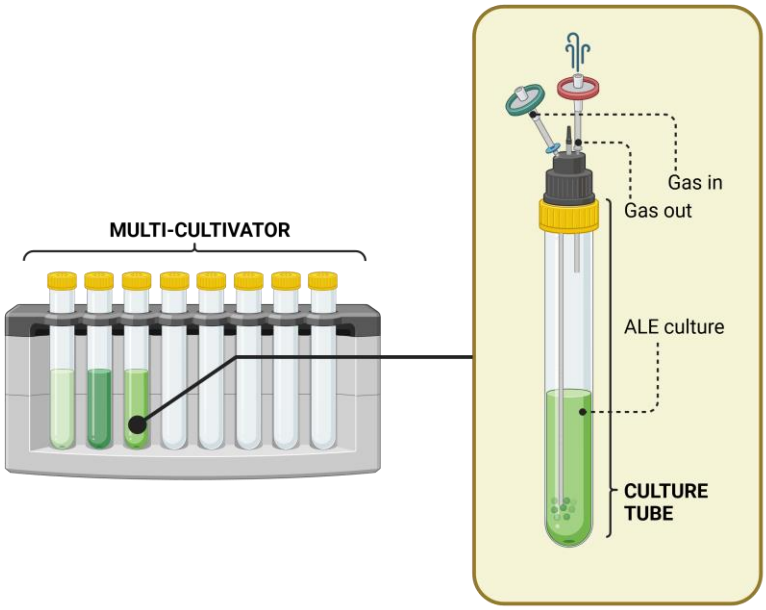


Figure 3.1 | Configuration of a culture tube used in ALE within a Multi-Cultivator MC 1000-OD (Photon Systems Instruments™, Czechia). (Created with BioRender.com).

3.4.3.2 *Chemostat selection*

Following mutagenesis of Syn.*Δhox* in 2.4.1.1.2 and 2.4.1.2.2, mutant libraries were outgrown in cell culture flasks for 16 hours at 60 µmol photons·m^{-2}·sec^{-1}, 30 °C, 150 RPM orbital shaking. Cell cultures were transferred to a 500 mL MicroCarrier Spinner Flask (Bellco™), assembled into a chemostat photobioreactor set-up (**Figure 3.2**). Culture total volume was adjusted to 100 mL using BG-11NH_4 via the media-in inlet and grown for 24 hours at 300 µmol photons·m^{-2}·sec^{-1}, 30 °C, 150 RPM impeller speed,

5% CO_2 supplementation. Mutant libraries were initially grown in batch mode for 24 hours to allow culture populations to recover. Chemostat media volume was then further increased to 200 mL, and batch growth continued for a further 24 hours without dilution. Following these 48 hours of population recovery and acclimatisation of the library culture to the chemostat environment, dilution was initiated.

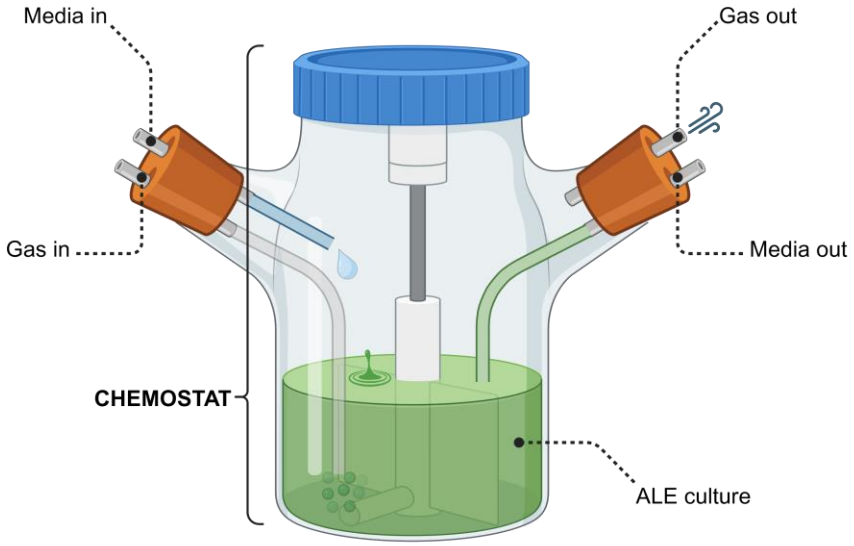


Figure 3.2 | 500 mL MicroCarrier Spinner Flask (Bellco™) configured into a chemostat photobioreactor. (Created with BioRender.com).

Dilution was initiated at 0.04 mL·min^{-1} and the OD_{750nm} measured ca. every 24 hours. Dilution was gradually increased stepwise to 0.56 mL·min^{-1}, until OD_{750nm} values stopped increasing and the maximum growth rate had been reached. Once the OD_{750nm} 0.01 was reached after 84 days, the cells were collected from the spent media via centrifugation was and screened for mutants with enhanced biomass formation using 24-well plates (see 2.3.5).

3.4.4 *Selection of enhanced Trichormus variabilis strains*

Following generation of Ava.WT mutant libraries (see 2.4.1.1.1 and 2.4.1.2.1), these were also outgrown in tissue culture flasks. Here, 6

inoculums were prepared for each *Trichormus variabilis* ALE investigation, (for inoculum media refer to **Tables 3.2; 3.3**, BG-11_0 and BG-11_0A variants). Inoculums were each grown for 16 hours at 60 µmol photons·m^{-2}·sec^{-1}, 30 °C, 150 RPM orbital shaking. Shake flask culture volumes were then increased to 20 mL using their respective BG-11_0 variant, and inoculums grown for a further 48 hours at 300 µmol photons·m^{-2}·sec^{-1}, 30 °C, 150 RPM orbital shaking. Following population recovery in these different selective environments, cultures were transferred to a 500 mL MicroCarrier Spinner Flask (Bellco™), in a chemostat set-up (**Figure 3.2**). Culture total volume was adjusted to 200 mL using either BG-11_0A or BG-11_0 via the media-in inlet, for ALE utilising fructose supplementation and ALE utilising no fixed carbon supplementation, respectively. Dilution was then initiated in each case.

3.4.4.1 *Chemostat ALE with mixotrophic selection*

Dilution with BG-11_0A was initiated at 0.04 mL·min^{-1} and the OD_{750nm} measured ca. every 24 hours. Dilution was gradually increased stepwise to 0.28 mL·min^{-1}, until OD_{750nm} values stopped increasing. Once spend media OD_{750nm} 0.01 was reached, the spent media was centrifuged, and the cell pellet was screened for mutants with enhanced biomass formation using 24-well plates (see 2.3.5).

3.4.4.2 *Chemostat ALE with autotrophic selection*

Dilution with BG-11_0 was initiated at 0.04 mL·min^{-1} and effluent OD_{750nm} measured ca. every 24 hours. The dilution rate was gradually increased stepwise to 0.28 mL·min^{-1}, until OD_{750nm} values stopped increasing and the maximum growth rate had been reached. This dilution rate was maintained, and once OD_{750nm} 0.01 was reached, the spent media was centrifuged and the cell pellet was screened for mutants with enhanced biomass formation using 24-well plates (see 2.3.5).

3.4.5 *Strain consortia analysis*

3.4.5.1 *Consortia identification*

Growth from Ava.A.2.20 on LB solid media was streaked for single colonies onto a new LB solid media plate. To identify species, 10 distinct colonies were selected at random and patched onto an LB plate. As none of these colonies exhibited visible differences from one another, 1 of these colonies was then selected for analysis using 16S rRNA cPCR reactions (2.2.4.2), using oligos pA (5'-AGAGTTTGATCCTGGCTCAG-3'), and pH (5'-AAGGAGGTGATCCAGCCGCA-3') [416]. Following gel visualisation, amplifications were appropriately processed for analysis by sequencing. Sample sequence analyses putatively identified the genus of selected samples as *Rhizobium* and *Achromobacter*. To distinguish colonies of the previous putatively identified *Rhizobium* from other colonies, a temperature strategy based on work carried out by Lamovšek et al., 2014 was devised.

On new LB Plates, Ava.A.2.20 liquid culture was streaked for single colonies using a sterile 1 µL loop. Plates were grown at 30 °C for ~16 hours to generate biomass. Plates were then transferred to 4 °C for 7 days, before being allowed to continue growing at 18 °C for 5 days. Treatment of cultures at low temperatures altered the phenotypic appearance of single colonies present on the LB solid media. A total of 3 distinct phenotypes were identified and selected for analysis using 16S rRNA cPCR reactions. Following putative identification, each consortia isolate was plated to achieve an axenic strain. These isolates were dubbed "LB3", "LB5", and "LB6" – from LB patch plate position.

3.4.5.2 *Isolation of individual microorganisms from the consortia*

Ava.A.2.20 was plated via serial dilution onto BG-11_0 solid media containing 200 µg·mL^{-1} gentamicin and incubated at 300 µmol photons·m^{-2}·sec^{-1}, 30 °C, until small colonies appeared. One colony was selected and inoculated into 2 mL of BG-11_0 liquid media containing 100 µg·mL^{-1} gentamicin. This was grown for ~16 hours at 60 µmol photons·m^{-2}·sec^{-1}, 30 °C, 150 RPM orbital shaking. Gentamicin concentration was then adjusted to 200 µg·mL^{-1} using 2 mL of fresh BG-11_0, and growth resumed for ~16 hours. The culture was plated onto BG-11_0 solid media (without antibiotics) via streaking for single colonies. The plate was incubated at 250 µmol photons·m^{-2}·sec^{-1}, 30 °C for ~2 days, before visible growth appeared. A

small portion of biomass was removed using a sterile 1 µL loop and plated onto BG-11_0 solid media containing 200 µg·mL^{-1} gentamicin and 100 µg·mL^{-1} ampicillin. The same loop was streaked on to non-selective LB solid media, which was incubated at 30 °C for 48 hours. Once visible green biomass appeared on the selective BG-11_0 solid media, the process of patching between non-selective solid media and selective solid media was repeated until no growth was observed on companion LB solid media plating.

Following this, *Trichormus variabilis* biomass was allowed to recover to a bacterial lawn on non-selective BG-11_0 solid media, and this was patched onto LB solid media. No growth was observed on the LB plate, and the strain was determined to be free from the other microorganisms. The new axenic strain was dubbed "Ava.A.2.20.P".

3.4.5.3 *Assessing Consortia impact on growth*

Cultures of Ava.WT set up with and without the heterotroph consortia isolates, and Ava.A.2.20, were grown in BG-11_0 at 300 µmol photons·m^{-2}·sec^{-1}, 30 °C. To assess the impact of each individual consortia isolate on the growth of *Trichormus variabilis*, measurements of OD_{750nm} and estimates of chlorophyll were taken every ~24 hours. Following 16 days, 1 mL samples were taken to assess relative DCW.

3.5 Genomic characterisation

Full genome sequencing was carried out on *Δhox* and the Ava.WT progenitor strains, and strains isolated from the ALE carried out on both *Synechocystis Δhox*, and *Trichormus variabilis*.

3.5.1 *Genomic sequencing*

gDNA was extracted (see 2.2.3 and 2.4.4.1) from Syn.*Δhox* Syn.1.11, Ava WT, Ava.A.2.20.P, and Ava.A.2.20 consortia biomass. Once samples of sufficient quality ($A_{260}/A_{230} \geq 2.0$, A_{260}/A_{280} ~1.9±0.1), and quantity (> 1 µg of DNA) were obtained, gDNA quality was further assessed using gel electrophoresis (see 2.2.5) to determine DNA integrity. Samples were then processed following the ligation sequencing gDNA protocol SQK-LSK109

according to the manufacturer's instructions, and loaded onto a MinION® (Oxford Nanopore Technologies, United Kingdom) sequencing device. Sequencing was carried out using a FLO-MIN114 Flow Cell (R10.4.1).

3.5.2 *Sequence assembly*

Sequence assembly and annotation was performed using Geneious™ Prime (v. 2024.0). *Synechocystis Δhox* contigs were mapped to RefSeq NC_000911 *Synechocystis* sp. PCC 6803 (NCBI), and *Trichormus variabilis* (*Ava.WT*) contigs were mapped to RefSeq NC_007413 *Trichormus variabilis* ATCC 29413 complete sequence (NCBI) via reference mapping. *Syn.1.11* and *Ava.A.2.20.P* contigs were reference mapped to the *Δhox* and *Ava WT* consensus sequences respectively. Assemblies were each iterated 5 times. Sequences were annotated using annotation transfer from NC_000911 and NC_007413. Generated strains were then aligned using Mauve (v. 1.1.3) [418] to respective progenitor strains for variation analysis. Low coverage regions were annotated in protein coding sequences with deviation > 2 standard deviations from the mean and excluded from further variant analysis. Variations and SNPs were called with a minimum variant frequency threshold of 0.5, a maximum variant error P value of 10^{-6}, and minimum strand bias P value of 10^{-5} for greater than 65% stand bias. Predicted interaction maps of coding region regions with variants was done using STRING v.12 (open access software) [419].

3.6 Metabolomic characterisation

Metabolomes of *Δhox* and *Ava WT* progenitor strains, and strains isolated from ALE carried out on *Synechocystis Δhox*, and *Trichormus variabilis* WT were analysed and compared using liquid chromatography-mass spectrometry (LC-MS).

3.6.1 *Growth conditions*

Samples were prepared by culturing strains using T25 Nunc™ Non-treated Flasks (ThermoFisher Scientific™), in 25 mL of respective media, under 300 µmol photons·m^{-2}·sec^{-1}, 30 °C, 1.5% CO_2.

3.6.2 *Metabolomic extractions*

For whole cell analysis, culture OD_{750nm} was determined prior to harvesting, and to allow standardisation of harvested material. Harvesting was performed by removing volume equivalent to 2 OD_{750nm} equivalent per mL^{-1}, and quenching performed using a modified version of a previously established protocol [395]. Samples were rapidly transferred to a 50 mL centrifuge tube containing a phosphate buffer saline at pH 7.4 as a quenching solution, 5 times the sample culture volume, which was pre-chilled to -0.5 – 1 °C. The strategy was validated with phosphate buffer saline and BG-11_0 solutions to ensure that temperatures reached $\leq$ 5 °C upon mixing (data not shown). Care was taken to ensure that samples remained $\leq$ 5 °C from this point onwards. Samples were centrifuged at 5000 g for 5 minutes (*Synechocystis*), 10 minutes (*Trichormus variabilis*) – at 4 °C. Supernatants were removed using a pipette, and cell pellets were resuspended in 100 µL of 100 % LC-MS grade methanol, pre-chilled to -80 °C. Samples were mixed thoroughly by pipetting and transferred to 1.5 mL centrifuge tubes (pre-chilled to -20 °C) and then stored at -80 °C. Process controls were prepared using 5 mL of respective growth medium, treated following the same methodology for biological sample preparation.

To ensure thorough lysis, samples were thawed for further processing. Samples were maintained on ice and vortexed for 10 periods of 30 seconds each. Sample solutions were then adjusted to 50% methanol using deionised 0.22 µm filtered water, (pre-chilled to 4 °C), and centrifuged at 10,000 g for 30 minutes at 4 °C. 100 µL of sample were transferred to clean pre-chilled (-20 °C) microcentrifuge tubes and stored at -80 °C prior to analysis. Twenty-four hours before analysis samples were thawed on ice and centrifuged at 4 °C, 10,000 g for 30 minutes. 20 µL of each sample were transferred to a glass screw top vial containing a glass insert, and henceforth maintained at 4 °C prior to analysis.

3.6.3 *Mass spectroscopy*

Mass spectrometry was performed by adapting a previously established protocol, (see Abdelrazig et al. 2020) [420]. Adaptations made were to increase sample throughput by reducing running time. Previous metabolomic data acquisitions using this reduced running time were shown to still produce representative data (data not shown), however, additional strain on column durability was noted.

Briefly, the metabolite separation was carried out using a Dionex™ UltiMate 3000 Ultra-High-Pressure Liquid Chromatography (UHPLC) (ThermoFisher Scientific™), with a SeQuant™ ZIC™-pHILIC 4.6 x 150mm column (Merck™). Mass quantification and fragmentation were carried out using a linked Q-Exactive™ Plus Hybrid Quadrupole-Orbitrap™ Mass Spectrometer (ThermoFisher Scientific™). Ten µL (adapted from 5 µL) of each sample were injected and eluted using a 15-minute method (adapted from 24 minutes) at 45 °C. Samples were chromatographically separated using a mobile phase gradient consisting of different mixes of aqueous 20 mM ammonium carbonate (**A**) and acetonitrile (**B**). Initial mobile phase (at a flow rate of 300 $\mu L \cdot min^{-1}$) was 80% **B**, decreasing to 5% over 8 minutes, followed by an increase back to 80% **B** over 5 minutes, with the flow rate steadily increasing to 400 $\mu L \cdot min^{-1}$. The flow rate was then decreased to 300 $\mu L \cdot min^{-1}$ over 1 minute, and the column was re-equilibrated for a further 1 minute (adapted from 2 minutes) prior to next sample injection.

Once eluted, samples were ionised using electro spray ionisation in switching positive and negative acquisition, at 4 kV (positive and negative). Capillary and auxiliary gas heater temperatures were 275 °C and 150 °C. The sheath, auxiliary and sweep gas flow rates were 40, 5, and 1, respectively (positive and negative). Full scan data acquisition of *m/z* 70 to 1050 was carried out for all samples. For metabolite fragmentation characterisation, quality control (QC) samples were also processed using a data dependent tandem mass spectrometry protocol ($ddMS^2$) for top 5 most abundant metabolites – in both positive and negative only scans. Full scan was carried out at a resolution of 70,000, and $ddMS^2$ at a resolution of 17,500. $ddMS^2$ was carried out using stepped, normalised collision energies of 15, 30, and 60.

3.6.4 *Untargeted metabolomic data analysis*

Sample files were processed, and metabolites identified using Compound Discoverer 3.3 (CD 3.3) (ThermoFisher Scientific™). Spectra were selected between 0.5 and 14.5 minutes (the period during which injection was from the UHPLC and not wash syringe), in any polarity, and compounds detected with a minimum intensity of 10,000. Features were merged with a mass tolerance of 5 ppm, and a retention time (RT) tolerance of 20 seconds. Peak retention times were aligned within ± 1 minute and selected with a signal to noise threshold of 1.5. Compounds were putatively identified by first aligning with mass lists of standard compounds, subsequently mzCloud, BioCyc, ChemSpider, Metabolika, and

compound discoverer predicted composition were used. Compounds were considered putatively annotated by confidence level (see Schymanski *et al*. 2014) [391]. No metabolites were identified to level 1 confidence. Level 2 confidence was assigned on metabolite peaks with either a ≥ 75% mzCloud score, or by matching accurate masses (±5 ppm) and retention times (±0.5 minutes) of ≥ two independent samples with those of the authentic standards. Level 3 confidence was assigned to compounds with a ≥ 50% mzCloud score, or ≥ 60% FISh score coverage with ±0.5 minutes retention time alignment with a mass list standard, and level 4 confidence was assigned to metabolite peaks with unambiguous molecular formulas, however, insufficient information for possible structures.

Post-processing multivariate analysis of results was performed using Simca™ P (Sartorius™). Principal Component Analysis (PCA) were generated, with Pareto scaling of data (see Abdelrazig et al. 2020) [420]. Instrument stability was assessed by assessing the consistency of PCA QC sample clustering and QC sample RSD (see section **2.8.3.2.3**; Abdelrazig et al. 2020) [420]. Highly clustered QC samples, and an RSD of < 30% in ≥ 70% of all peaks was considered to indicate high intra-study instrument stability. Orthogonal partial least squares-discriminant analysis (OPLS-DA) was used to assess changes in the metabolomes of *Synechocystis* and *Trichormus variabilis* samples. The efficiency and reliability of OPLS-DA models was assessed by comparing variation in R^2X and R^2Y values, (with "R^2" indicating the proportion of data variance), and predictive strength assessed using model Q^2 value (see Hong et al. 2010) [421]. Models were considered robust if R^2 and Q^2 values were > 0.5 (see Abdelrazig et al. 2020) [420]. Model validation was assessed using permutation analysis (100 permutations) and considered valid if Q^2 < 0.05 (see Kim et al. 2011) [422]. Metabolites with the significant variation between the independent classes was determined from variable importance in projection (VIP) values. VIP values ≥ 1 were considered significant. Univariate analysis of these metabolite peaks was also performed using CD 3.3, metabolites with P values ≤ 0.05 were considered significantly altered. CD 3.3 was used to visualise highlighted Log2-fold changes.

Chapter 4.

Adaptive laboratory evolution to enhance carbon fixation

4.1 Experimental design

The use of ALE selection coupled with nutrient limitation has previously been utilised to enhance the growth rates of several prokaryotic organisms, including the *E. coli* chemostat ALE by Weikert *et al*. 1997, and Notley-McRobb and Ferenci 2022 [213,423]. Each used glycerol and glucose limitation respectively, and both generated selected populations with faster growth rates. The former noting that 90% of all chemostat isolates showed improved growth when isolated on plates [213]. To adapt this strategy for cyanobacteria, a gas mixture was selected with a lower than atmospheric concentration of CO_2, 200 ppm of the mixture's molecules, (compared to an atmospheric concentration of 417 ppm). This was selected to assess if substrate limitation could select for greater CO_2 assimilation efficiency, based on the reduced availability of CO_2. It was hypothesised this may subsequently lead to more flux being pushed around the Calvin-Benson cycle under an atmospheric CO_2 concentration. The gas was utilised to sparge the *Synechocystis* cultures during ALE. This gas mixture specifically contained 79.08% ±0.16% nitrogen, 21.09% ±0.04% oxygen, and 200 ±4 ppm CO_2 (Air Products™, United Kingdom). This gas mixture contained a 50% lower concentration of CO_2 than current atmospheric levels, and a >28% lower concentration of CO_2 than pre-industrial concentrations [424].

As a strategy to sustain selective pressure, serial dilution has also been used effectively to select for altered phenotypes in ALE experiments, which have included strategies to enhance prokaryotic growth rates (see LaCroix *et al*. 2015) [239]. Serial dilution (or serial transfer) maintains the selective pressure upon a population by retaining only a fraction of that population during nutrient replacement. This selects for cells which in theory are more adapted to growth under those conditions. Initial experiments were done utilising a multi-cultivator.

4.2 Mutagenesis of *Synechocystis*

As stated in **2.7.2.1**, *Synechocystis* was selected as the strain for this investigation, primarily because of its status as a model cyanobacteria species (see Mills *et al*. 2020) [292]. As stated above, different mutagenesis strategies result in different types of mutations (see **Table 2.5**). This results in cells with different combinations of mutations. Therefore, these different mutagenesis strategies were evaluated prior to the ALE selection

processes. Physical (UV light) and chemical mutagens, (EMS treatment) were selected to evaluate the impact of these mutagens on *Synechocystis*.

4.2.1 *EMS mutagenesis in Synechocystis*

Optimisation of mutagen dosage using both physical and chemical mutagens had previously been carried out in *Synechocystis* [291]. The use of EMS to chemically mutagenise *Synechocystis* has previously been described and has successfully been used to generate mutants with rapid division phenotypes [208]. EMS and other methanesulfonates are reactive with water, with EMS undergoing a hydrolysis reaction as follows:

$$CH_3SO_2OC_2H_5 + H_2O \rightarrow CH_3SO_2OH + C_2H_5OH$$

Both breakdown products, ethanol and methanesulfonic acid, can be toxic to a cell, and tend to increase in abundance over time [425]. The result is that the treatment process with EMS is likely toxic to the cells not only through the mutations it induces. Potentially reducing the size and diversity of the population library recovered. A 1-hour exposure time was selected based on previous work and used as a benchmark to calibrate the mutagen dosage. Cell viability was used to effectively measure dosage; when dosage increased so did the death rate of the cell population.

Following treatment with EMS, the compound is typically inactivated using a 10% sodium thiosulfate solution. This reduces the half-life of EMS from 93 hours at 20 °C in water, to 1.4 hours at 20 °C [425]. This prevents further mutagenesis and reduces the risk of mutagen exposure. No reports in the literature were found indicating the toxicity of sodium thiosulfate to cyanobacteria. However, sodium thiosulfate has previously been shown to reduce the depletion rate of PSII, PSI, and the phycobilisomes in *Synechocystis* cells grown in the presence of glucose. Possibly by scavenging of ROS [426].

To assess the impact of the treatment process without the addition of EMS, cell viability was assessed prior to treatment. Untreated cultures were grown in triplicate and plated onto BG-11 solid media via serial dilution. A sample of the population was also processed, which had not been treated with EMS, and plated in triplicate by serial dilution. Colony

Forming Units (CFU) were counted following incubation of the plates for ~14 days (**Figure 4.1**).

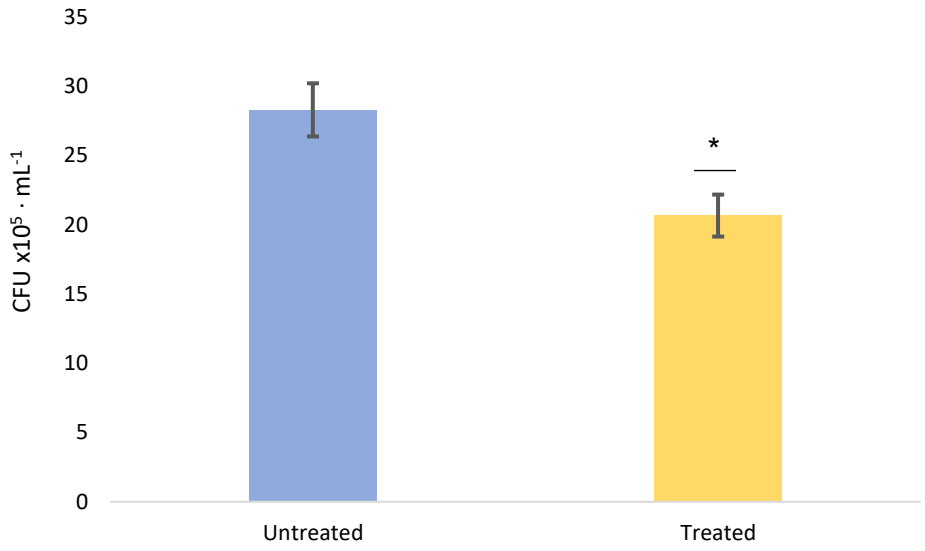


Figure 4.1 | Absolute colony forming units $x10^5 \cdot mL^{-1}$ of *Synechocystis* prior to chemical mutagenesis sample processing (untreated), and after processing (treated) without mutagenesis (*$p < 0.05$, $n = 3$, error bars show standard deviation).

Cell viability was significantly lower ($p < 0.015$) in the treated cells compared to the untreated cells, with a 27.0% ±1.9% (SD) decrease in CFU formation with 1 in 4 cells dying due to the treatment process alone, (without any EMS). However, the cell survival rate was around 2.07 $x10^6$ $CFU \cdot mL^{-1}$ of surviving cells, (~4.14 $x10^7$ CFU per 20 mL treatment sample). This very comparable with the rates seen in other studies using *Synechocystis*, which used 5 $x10^7$ cells per mutagenesis reaction [291].

To determine the specific effect of EMS upon cell viability and generate a kill curve, treated cell CFUs were used a benchmark, and relative cell viability was calculated from CFU counts of cultures treated with different concentrations of EMS (0.25 M, 0.5 M, and 0.75 M) (**Figure 4.2**). As stated in section **3.4.1**, effective dosage of EMS for *Synechocystis* has previous been assessed. Here, the purpose of this experiment was to increase the genetic variation of cells prior to selection. The effects of different concentrations of mutagen on the adaptation of *Synechocystis* to selective environments was not assessed.

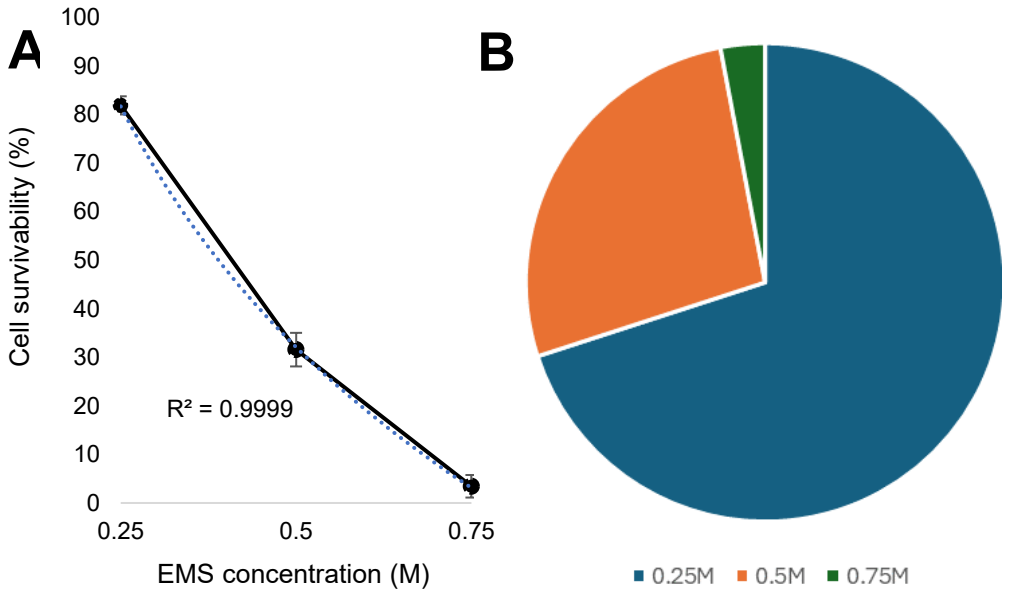


Figure 4.2 | **A.** Kill curve assessing *Synechocystis* cell viability (%) following ethyl methanesulfonate (EMS) treatment. Populations were compared to cells processed without EMS, with exponential regression line y = -71.53ln(x) - 17.47 (R^2 = 0.999). **B.** Proportion of combined viable populations from each EMS treatment. (*n* = 3, error bars show standard deviation).

Compared to the treated non-mutagenised culture, the viable cell count decreased by 18.1 – 96.6% from the lowest concentration of EMS to the highest. This decrease in cell viability showed a strong correlation with an exponential fit (R^2 = 0.9999) within the concentration range investigated (**Figure 4.2 A**). These results are similar to previous work by Patel et al. 2016, in which EMS mutagenesis of *Synechocystis* was shown to reduce viable cell counts by 18.1%, 31.7%, and 79% in treatments with 0.23M, 0.47M, and 0.7M EMS respectively [208]. From the total surviving population of cells following the different EMS treatments, 69.9% ±4.4%, 27.2% ±4.2%, and 3.0% ±0.4% (± SD) of the viable cells were from the 0.25M, 0.5M, and 0.75M treatments respectively (**Figure 4.2 B**). However, if the cells from each of the treatments were combined, the genetic diversity in the overall mutagenised population would predominately consist of cells from the 0.25 M EMS treatment. This may be an issue if the subsequent rounds of chemical mutagenesis were done utilising cells from this population, as *E. coli* cells first adapted with 0.5 μg·mL^{-1} of alkylating agent *N*-Methyl-*N*′-nitro-*N*-nitrosoguanidine have previously shown 6000-fold lower mutation rates than cells mutagenised for the first time [291,427].

4.2.2 *UV mutagenesis in Synechocystis*

UV mutagenesis was evaluated as a tool to introduce mutations into the genome of *Synechocystis*. UVC wavelengths (100-280 nm) have been shown to be effective for this [291]. UV dosage on the culture surface can be summarised as follows: **µW / cm² × t** (see Bolton and Linden 2003) [428]. Therefore, the dosage can be increased by increasing exposure time for any given fixed distance from the radiation source. *Synechocystis* cultures in 20 mL of BG-11NH_4 liquid media were aliquoted into sterile 90 mm petri dishes (total surface area of 63.62 cm^2).

Unlike chemical mutagenesis, cell viability between the process treated and untreated cells did not change (**Figure 4.3**), ("treated" being cells processed using the same methodology as the mutagenized cells, however, without UV mutagenesis).

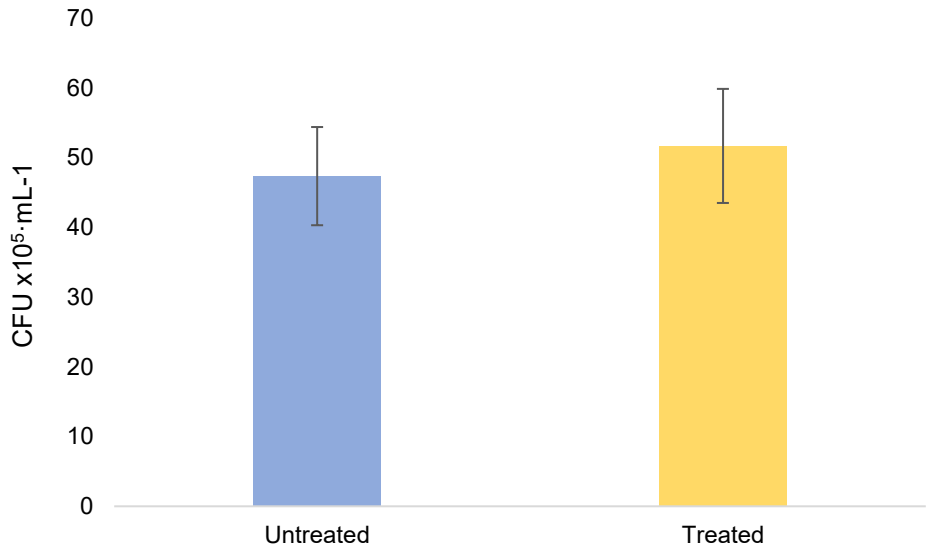


Figure 4.3 | Absolute colony forming units x10^5·mL^{-1} of *Synechocystis* prior to UV mutagenesis sample processing (untreated), and after processing (treated) without mutagenesis ($P \geq 0.55$, $n = 3$, error bars show standard deviation).

This is unsurprising as (excluding the mutagenesis) the treatment process only involved dark incubation, which cyanobacteria experience as part of their natural circadian rhythm. Photosynthesis ceases during the night

phase, and cells change from photoautotrophic to chemotrophic growth on energy storage molecules, (such as glycogen) [326]. The UV mutagenesis treatment protocol seemed to have no significant impact on the viability of the cells available for selection which could be a potential advantage compared to the EMS treatment.

To generate a kill curve, the effect of 3 different UV treatments on cell viability were investigated. Cultures were treated with UV treatments of 2.5, 5, and 10 minutes (**Figure 4.4**). A suitable UV compatible radiometer was not available to measure exact UV dosage, however, for details of materials used see 2.4.1.2.1.

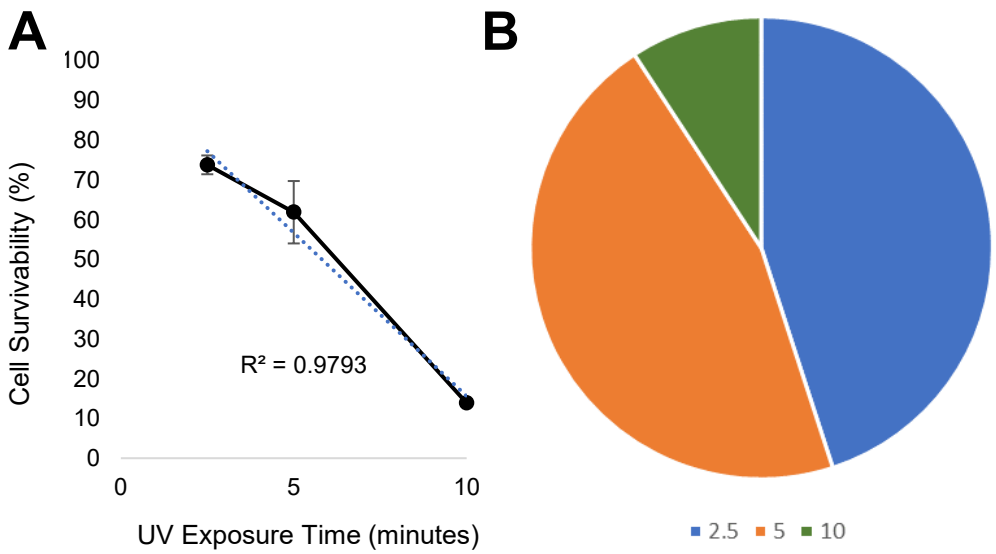


Figure 4.4 | **A.** Kill curve demonstrating cell viability (%) following ultra-violet (UV) treatment. UV treated populations were compared to cells processed without UV, with linear regression line y = -8.217x + 97.785 (R^2 = 0.9793). **B.** Proportion of combined viable populations from each treatment, 2.5, 5, and 10 minutes of UV exposure (*n* = 3, error bars show standard deviation).

Compared to the previous treatment with EMS, the UV treatment showed a decrease in cell viability that correlated with a linear best fit (R^2 = 0.9793) over the range investigated. Comparing the treated cells with the ones which had not been exposed to UV radiation, the cell viability decreased by 26.2 – 86.1%. During the experiment, a UV radiometer was not available to measure UV intensity. Therefore, the exact UV dosage could not be

calculated, however, the equipment and conditions used are described in detail in **3.4.2**. Without dosage data, it is challenging to compare these results to previous work elsewhere. The range of cell survivability generated in this experiment is similar to the survivability range of previous work by Tillich et al. 2012, in which UV dosage for mutagenesis was optimised [291], and survivability ranges of 90% to < 1% were calculated.

Given the efficiency of the photolyase mediated repair mechanism (see Levine and Thiel, 1987) [359], this is a positive indication that the UV mutagenesis protocols were effective in causing DNA damage in the cell and generating genetic diversity within the population. This is despite the absence of a prolonged outgrowth utilising a UV filter, a strategy which has been used in other UV mediated approaches to limit the effectiveness of the DNA repair mechanism [291]. The final combined populations of cells consisted of viable cells with a viability of 49.3 % and 41.3% respectively, derived from the 2.5- and 5-minute treatments. A two tailed t-Test of samples with equal variance showed no significant difference between the two treatments ($P > 0.1$). Given the impact that the environment can have upon strain selection, outgrowth steps without targeted selective pressure could potentially lead to the selection of undesirable phenotypes. Mitigation steps were included by minimising prolonged population recovery.

4.3 Multi-cultivator ALE to generate strains with improved carbon fixation in *Synechocystis.*

The impact of ALE was evaluated to improve the carbon fixation and subsequent growth of *Synechocystis*. Following the kill curves generated above a serial dilution-based approach utilising EMS was selected using the wild type, glucose tolerant progenitor strain of *Synechocystis* sp. PCC 6803, herein “Syn.GT” (see **3.1**).

4.3.1 *Serial dilution: Synechocystis strain selection*

To generate a mutant library, the Syn.GT progenitor strain was chemically mutagenized using 0.5 M of EMS (**Figure 4.5 A**). The subsequent cell library was initially dived into 3 separate populations and outgrown for a period of 16 hours at 60 µmol photons·m^{-2}·sec^{-1}, 30 °C. An outgrowth step was introduced following a previous failed attempt to initiate

selection immediately following mutagenesis. Cyanobacteria rapidly undergo phenotypic changes when cultured under dark conditions, including a decrease in ribosomal activity [429]. However, during exposure to high light stress cyanobacteria actively need to reduce pigmentation to prevent photoinhibition due to excess electron excitation [430]. It was therefore hypothesised that immediate exposure to relatively high light (200 µmol photons·m^{-2}·sec^{-1}), following a period of dark incubation may be too damaging for the cells. The inclusion of this outgrowth step following mutagenesis was therefore included in future experiments as a result.

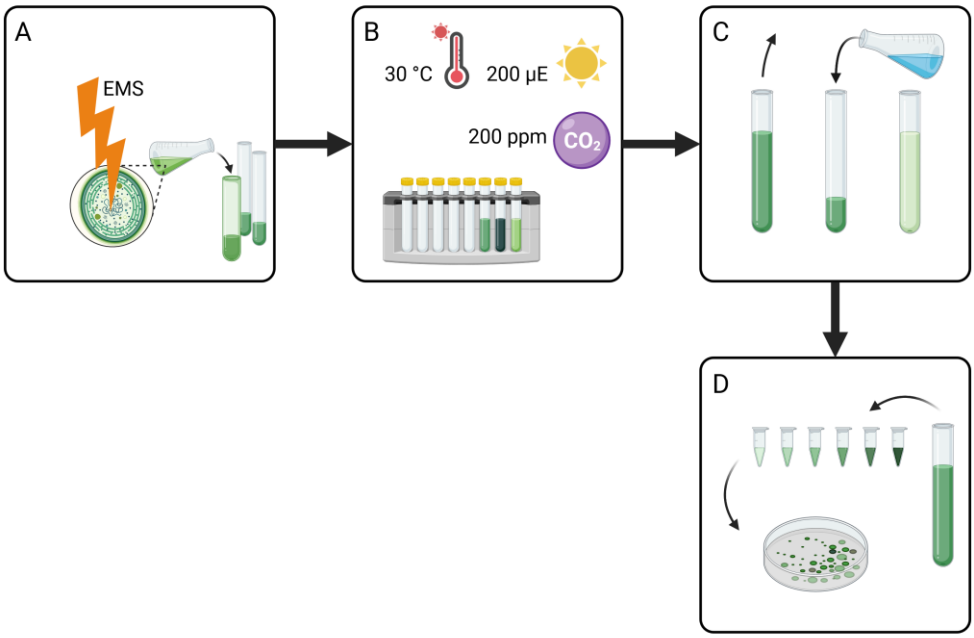


Figure 4.5 | Overview of multi-cultivator ALE experimental design. **A.** *Synechocystis* sp. PCC 6803 GT strain (Syn.GT) was mutagenized using 0.5 M EMS treatment (see 2.4.1.1.2), divided into 3 populations, and outgrown for 16 hours at 60 µmol photons·m^{-2}·sec^{-1}, 30 °C. **B.** mutagenized populations were cultured at 200 µmol photons·m^{-2}·sec^{-1}, 30 °C, 0.02% CO_2 supplementation. **C.** selective pressure was maintained for 84 days (24 passage events), adjusting OD_{750nm} to 0.1 every ~3 – 4 days with fresh media. **D.** surviving culture was plated onto BG-11 solid media using serial dilution to isolate strains. (Created with BioRender.com).

Following the mutagenesis and outgrowth, the cell libraries were grown in a Multi-Cultivator MC 1000-OD (Photon Systems Instruments™,

Czechia) by culturing samples in growth tubes (see **Figure 3.1**). 2 of the 3 cell populations perished shortly after transfer to the multi-cultivator, showing no growth on BG-11 solid media. 1 population was successfully maintained for 84 days, being passaged every ~3 – 4 days, (total 23 passages). This is relatively shorter than previously reported in Dann *et al*. 2021 who, having also utilised a multi-cultivator approach, previously carried out serial transfer mediated ALE of *Synechocystis* to high light intensities of up to 2300 µmol photons·m^{-2}·sec^{-1}. However, in this case the strain selection was maintained for over a year [284]. That investigation also used considerably longer culturing periods of ~15 days and employed both physical as well as chemical mutagenesis strategies.

Following sustained selective pressure, strains were isolated via serial dilution onto BG-11 solid media (**Figure 4.5 D**). Isolation plates were incubated at 200 µmol photons·m^{-2}·sec^{-1}, 30 °C, and colonies selected at random for characterisation. Random selection was performed by placing a mark in the centre of the selection plate and selecting colonies closest to that point (**Figure 4.6**). Selection of colonies was random to reduce bias, however previous studies have shown that selecting the largest colony has been useful in selecting strains with desirable growth phenotypes [208,431]. Furthermore, isolates that grow well on solid media, do not always grow well in liquid media, as these two environments are very different to one another (see Gao *et al*. 2020; Riaz *et al*. 2022) [432,433].

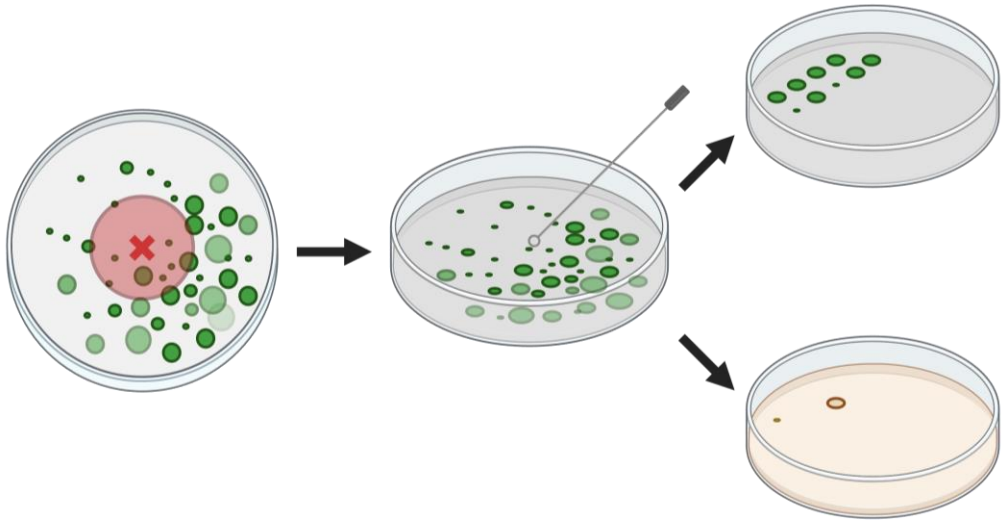


Figure 4.6 | Selection method for selecting individual colonies isolated from the ALE. Individual colonies were picked by proximity to the centre of serial dilution plates. 100 colonies were selected and patched onto BG-11 solid

media, with companion plating onto LB solid media to check for contamination. (Created with BioRender.com).

4.3.2 *Serial dilution: Synechocystis isolate characterisation*

One hundred colonies were originally selected from the serial dilutions and patched onto BG-11 media, 17 of these did not grow. The remaining isolates were each assigned a designation following the format, "MC.Syn.[number]", for "Multi-cultivator *Synechocystis*". Due to the large number of isolates, and limitations on glassware and light incubator space, the first 12 isolates were selected for characterisation in liquid media with the Syn.GT strain as a control.

4.3.2.1 *Measuring growth and biomass yields from individual MC strains*

Carbon comprises a significant proportion of biomass, and within bacterial cells it accounts for around ~50% of dry cell biomass [434–436]. Therefore, to identify isolates with enhanced carbon assimilation efficiencies, dry cell mass was selected as an indicator. The individual ALE isolates were screened following the protocol outlined in **Figure 4.7**.

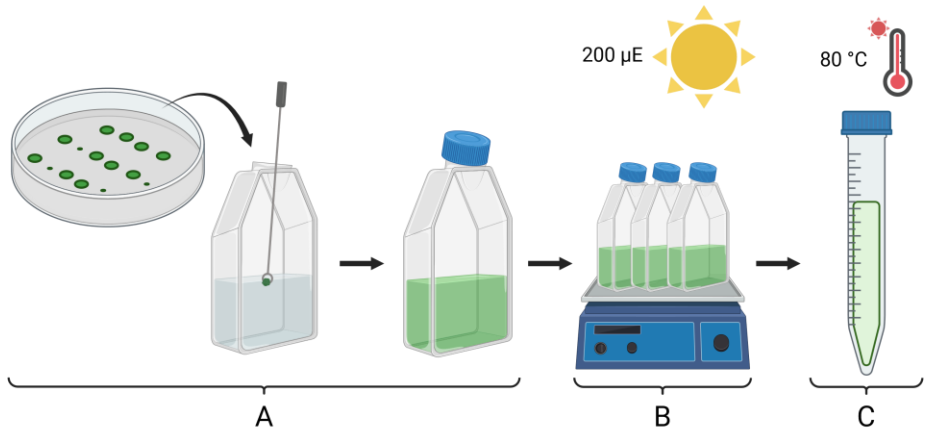


Figure 4.7 | Biomass screening workflow of the individual strains. **A.** Single colonies inoculated from BG-11 solid media into 10 mL BG-11 liquid media to create starter cultures. Cultures were grown at 200 µmol photons·m^{-2}·sec^{-1}, 30 °C for 72 hours until all cultures growing exponentially. **B.** Triplicate cultures of isolates inoculated into 15 mL BG-11 at 0.1 OD_{750nm} from respective starter cultures. Cultures grown at 200 µmol photons·m^{-2}·sec^{-1}, 30 °C, for 72 hours. **C.** 10 mL of each culture transferred to pre-dried, pre-weighed 15 mL centrifuge tubes. Cultures dried at 80 °C for 48 – 72 hours. Dried cultures weighed to determine dry biomass. (Created with BioRender.com).

From the 12 isolates initially characterised, MC.Syn.1, 2, 3, and 6 showed significant increases in biomass (p < 0.007, 0.02, 0.05, and 0.007 respectively) (**Figure 4.8 A)**. Of these, MC.Syn.1 and MC.Syn.6 both showed the greatest increase in biomass of 39.6% ±5.3%. The distribution mean of the overall recorded mass values amongst the mutant isolates also aligns strongly with the mean of the Syn.GT strain (**Figure 4.8 B**). This appears to suggest that the overall distribution of biomass accumulation within the adapted population had not shifted towards increased biomass formation compared to the wildtype average under the same conditions. However, the maximum increase in biomass formation observed here was similar to previous work carried out by Yu et al. 2013, in which batch ALE selection of eukaryotic microalgae *Chlamydomonas reinhardtii* resulted in mutants with increased biomass formation of between 7% - 20% [232].

To determine the effect of the adaptation process on growth rates, the 4 strains with the highest biomass accumulation were selected for further characterisation.

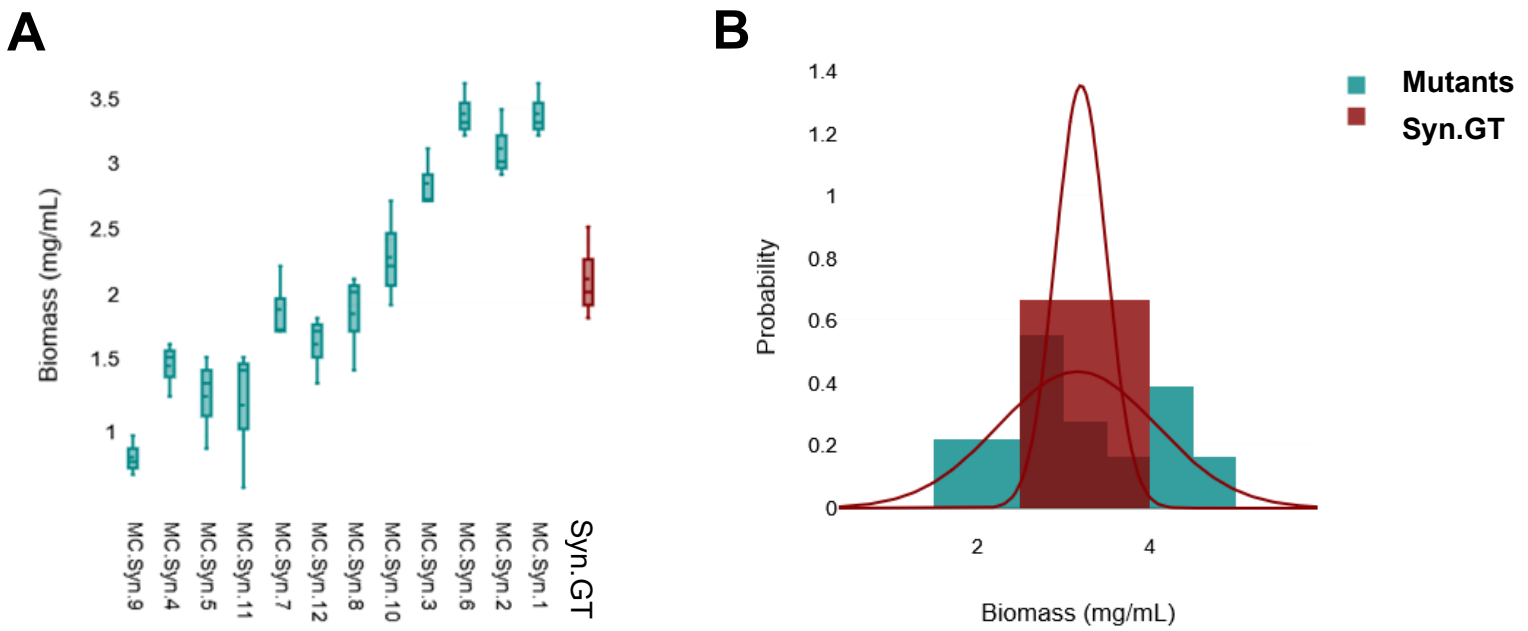


Figure 4.8 | **A.** Biomass (dry cell weight (DCW) mg·mL^{-1}) from 10 mL of isolated cultures (Mutants) and Syn.GT grown at 200 µmol photons·m^{-2}·sec^{-1}, 30 °C, for 72 hours in BG-11 liquid media (n = 3, error bars show standard deviation). **B.** Frequency distribution of the DCW value from the mutant strains (Mutants) (N = 36) and Syn.GT (N = 3) with sample range normal distributions overlayed.

4.3.2.2 *Determination of growth rate in the four MC strains with the highest biomass*

The 4 strains selected (MC.Syn.1, 2, 3 and 6) and Syn.GT were cultured in triplicate at 200 µmol photons·m^{-2}·sec^{-1}, 30 °C, for 13 days in BG-11 liquid media (**Figure 4.9**). 1 mL samples were taken to measure biomass on days 6 and 13, and the specific growth rate was determined from exponential phase between days 6 and 7.

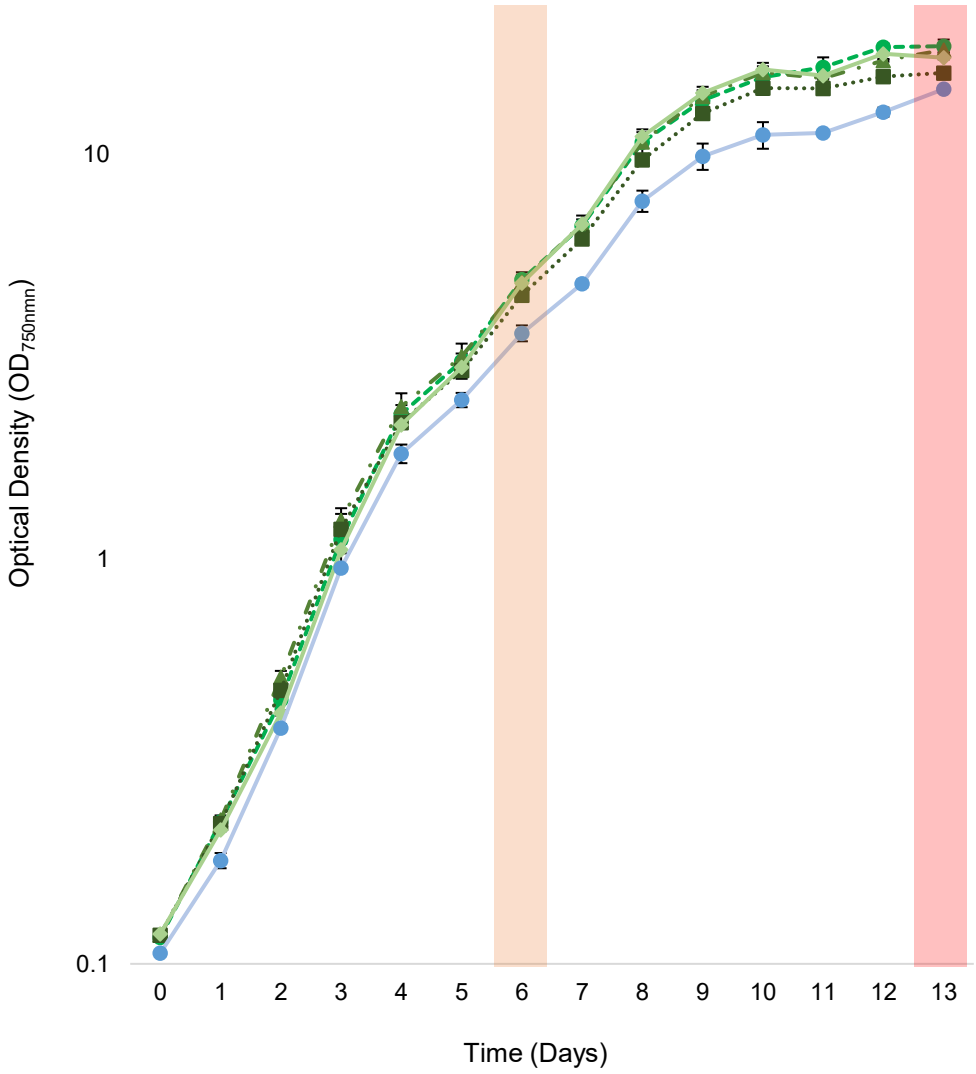


Figure 4.9 | Comparison of the growth of isolates MC.Syn.1 (circle), MC.Syn.2 (triangle), MC.Syn.3 (square), and MC.Syn.6 (diamond), with Syn.GT (square). Grown at 200 µmol photons·m^{-2}·sec^{-1}, 30 °C, 150 RPM orbital shaking. Point at which specific growth rates determined highlighted between days 6 and 7 (peach). 1 mL samples harvested at both

highlighted time points to estimate culture DCWs (peach and rose). (n = 3, error bars show standard deviation).

Despite observing significant increases in the biomass from each of the selected isolates during screening (see **Figure 4.8 A**), this did not translate into significant improvements in the growth rates of each of the *Synechocystis* strains. There was no significant increase in biomass at either of the time points sampled for any isolates (**Figure 4.10**).

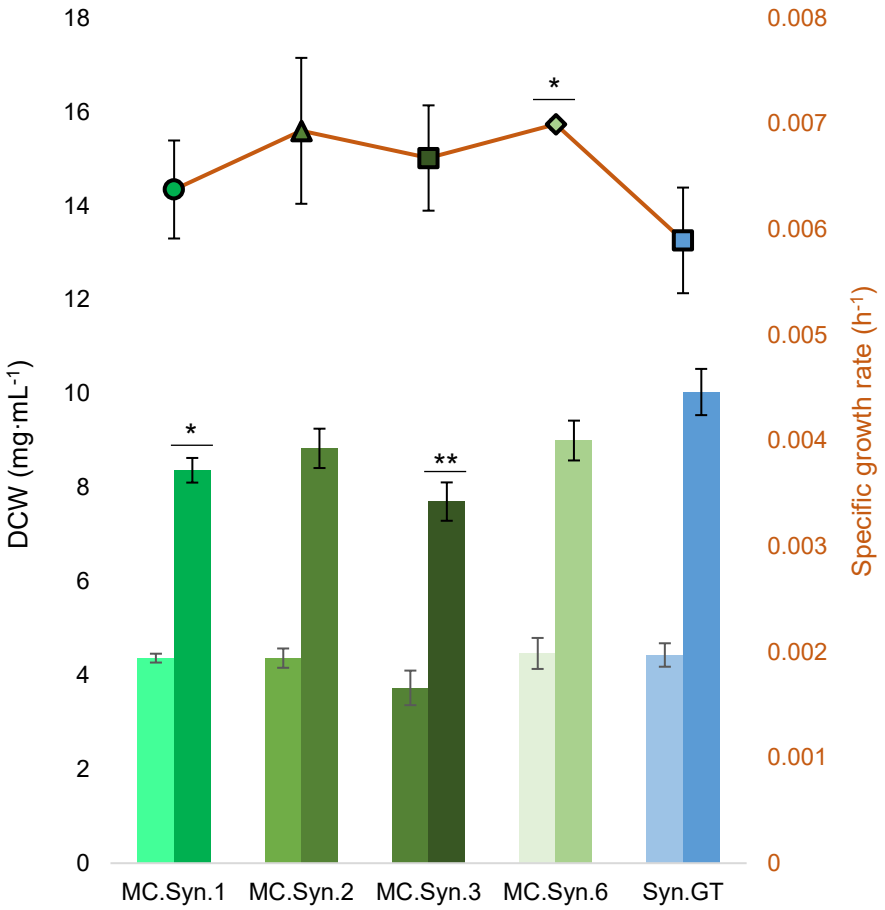


Figure 4.10 | Dry cell weights of multi-cultivator isolates and Syn.GT sampled on days 6 (left bars) and 13 (right bars). Above is the specific growth rate of isolates and Syn.GT between days 6 and 7. (n = 3, *p < 0.05, **p < 0.01, error bars show standard deviation).

In fact, isolates MC.Syn.1 and MC.Syn.3 showed significant decreases in final biomass accumulation on day 13, at -16.6% (p < 0.014)

and -23.3% ($p < 0.007$) respectively. Only MC.Syn.6 showed a nominal average increase in the peak growth rate of 18.6% when compared to the wildtype *Synechocystis* (Syn.GT) ($p < 0.04$).

These results may suggest that the isolates only showed an enhanced rate of biomass formation during lag-phase. Comparisons between T0 and T1, demonstrated that the growth rates of both MC.Syn.2 and Syn.GT significantly favoured the former, with an increase in the growth rate of 24.7% ($p < 0.025$). However, there was no significant increase in the growth rate beyond this time except in MC.Syn.6. This selective improvement in the growth rate also aligns with improved biomass formation, which was observed during the initial isolate screening, in which the biomass was harvested after only 72 hours of growth. Reduction in, (or even elimination of) lag phase has previously been reported across multiple ALE experiments (see Wang et al. 2022) [437], and could have influenced the initial increases in biomass originally recorded.

Interestingly, the decrease in biomass, agrees with observations made by Dann et al. 2021 [284]. A significant decrease in biomass accumulation was observed in *Synechocystis* populations, which had been selected using a serial transfer method and a multi-cultivator unit to select for high light tolerance. Multiple populations in that study showed > 50% decrease in dry mass compared to the original progenitor population, when cultured at 50 µmol photons·m^{-2}·sec^{-1}. This study did demonstrate, however, that selection for tolerance at increased light intensities >2000 µmol photons·m^{-2}·sec^{-1} could still be achieved using this approach.

4.3.2.3 *Evaluation of photosynthetic efficiency in the MC strains*

At lower optical densities, relative light intensity across a batch culture is relatively higher than when compared to the later stages of growth. This is because as cell density increases, relatively more light is absorbed before reaching cells further from the light source due to increased culture self-shading [438]. As a result, this reduces a culture's overall photosynthetic productivity [439]. The observed increases in growth rate and biomass accumulation of the selected isolates within the earlier stages of growth, therefore, may suggest an increase in photosynthetic productivity. To investigate this, oxygen evolution measurements were conducted for 3 independent cultures of both MC.Syn.6 and the wildtype

Syn.GT strain. MC.Syn.6 was selected as the best performing strain (**Figure 4.11**).

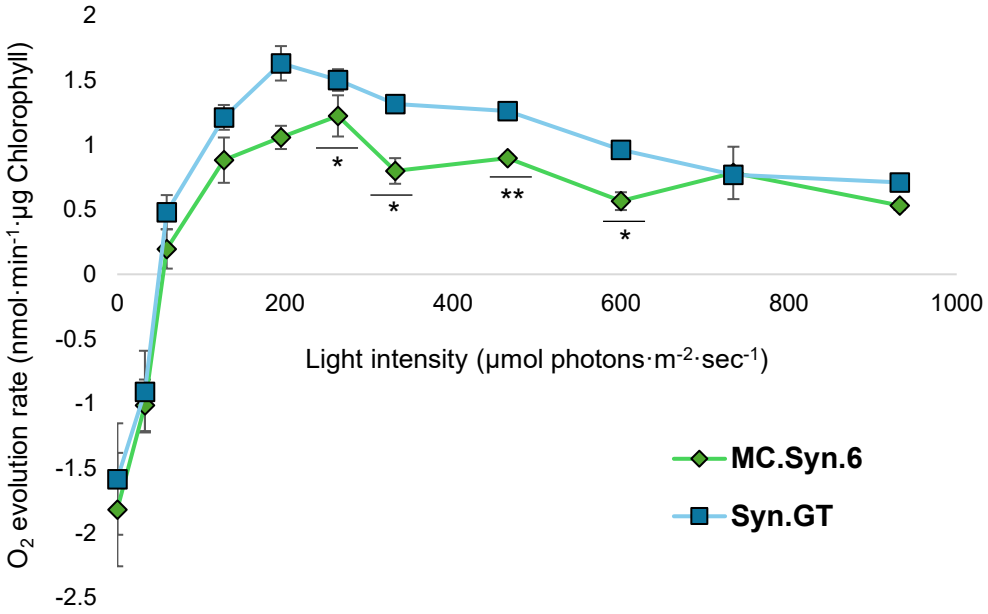


Figure 4.11 | Rates of oxygen evolution in *Synechocystis* GT (Syn.GT), and MC.Syn.6 over increasing light intensities at 30 °C measured using a Clark electrode. Cultures were grown in BG-11 and harvested during exponential growth phase (OD_{750nm} = ~1). Data is shown from the mean ± standard error of triplicate independently grown replicates (n = 3, *p < 0.05, **p < 0.01).

No significant differences were observed in the rate of respiration (P > 0.76). At 195 µmol photons·m^{-2}·sec^{-1}, however, MC.Syn.6 began to exhibit a significantly lower rate of oxygen evolution and photosynthetic activity (p < 0.045), approximately the light intensity under which the strain was selected. Syn.GT showed a 33.2% ±22% higher rate of oxygen evolution than MC.Syn.6 during respective peak evolutions. Although the O_2 evolution seen here is not as diminished as loss of function mutants, such as PSI knockouts in *Synechocystis* (see Wang et al. 2012) [440], the reduced O_2 evolution in MC.Syn.6 suggests that photosynthetic activity has decreased. This could also suggest that adaptation has occurred through more efficient use of cellular resources, rather than greater substrate utilisation. As samples were harvested based on the OD_{750nm} measurement (~1 OD_{750nm}) without a corresponding sample to assess DCW, determination of chlorophyll per cell / mg of biomass was not possible. However, the

decreased O_2 evolution profile of MC.Syn.6 suggests that the isolate did not exhibit an improved rate of photosynthesis compared to the original progenitor strain.

4.3.3 *Evaluation of the serial dilution ALE Strategy*

Although enhanced growth rates and biomass accumulation were observed during lag phase, this was deemed unlikely to result in useful improvements to the selected strains. Lag phase is a time when cells adapt to the environment in which they have been inoculated, accumulating resources whilst they acclimatise. There is significant synthesis of proteins, additional genome copies, and molecules of central metabolism, however, not yet a production of more complex secondary metabolites [441–443].[458,459]Lag phase is only a short and temporary state before the cells grow exponentially. Investigating the effects of diurnal growth on *Synechocystis*, Werner et al. 2019 observed that the lag phase within cells could be as short as 2 – 6 hours, before cell division occurred [444]. Significant variation has also been observed between cells of the same population during the lag phase, despite cells being grown under the same conditions [441]. Reduction in duration of (or even elimination of) the lag period, (potentially seen in the mutant phenotypes) may not be an undesirable characteristic, particularly for industrial process where a short lag phase is desirable. However, this was not the aim of this study, and the ALE methodology was re-evaluated to optimise growth and carbon flux.

To select for strains with enhanced biomass accumulation, it is necessary to use a strategy where the selective pressure can be applied continually. During the serial dilution / transfer process, cyanobacteria populations need to regularly adapt to sudden changes in resource concentration and turbidity. However, the selection pressure is not as intense as being continually perturbed, given the time between serial dilutions, days vs minutes. Therefore, the selection pressure on the population is less intense and less effective at driving selection. As discussed in 3.1.3, continuous chemostats and other steady state culturing strategies function by maintaining population densities at a selected parameter. Therefore, to maintain selective pressure upon mutant libraries during exponential growth, a chemostat strategy was evaluated.

4.4 Chemostat ALE of *Synechocystis* Δ*hox*

4.4.1 *Strategy overview*

As discussed in **2.7.3.2**, chemostats are one possible strategy that can be employed to maintain a constant growth pressure upon selected strains. Here, a strategy was designed to integrate this cultivation method with other targeted approaches to direct electron flux towards carbon fixation. However, no dedicated photobioreactors were available to use in this experiment as a chemostat, therefore, a novel approach was selected to assemble a chemostat from available materials.

To provide light, heat, and sufficient space to house a chemostat, a Reach-in Growth Chamber (Weiss Technik™) was used. Consideration was given to the use of 500 mL – 1 L^{-1} Schott bottles (DURAN™) and other similar glassware items; however, these were deemed to be unsuitable due to effort necessary to convert them into functioning chemostats. A 500 mL MicroCarrier Spinner Flask (Bellco™) was selected and adapted for use as a chemostat in this investigation. Culture agitation was performed using an internal overhead bearing impeller (Bellco™), spun using a magnetic stirring plate. Two 120U Peristaltic Pumps (Watson Marlow™, United Kingdom) were calibrated using 2.3 mm internal diameter Norprene™ tubing (Fisher Scientific™, United Kingdom), and configured to deliver fresh media and remove spent media at the same time from and to 1 L^{-1} bottles. Given the unusual shape of the Spinner Flask, finding suitable fittings to control media and gas exchange, was challenging. This issue was resolved with assistance from Kwon Jun Lee (Cyanetics, United Kingdom). Two bespoke polyurethane acrylate resin fittings were designed, with 316 marine grade stainless steel tubes designed to mirror the curvature of the interior of the Spinner Flask arms, whilst avoiding the impeller. Resin components were 3D printed and assembled into a functional and calibrated chemostat system (**Figure 4.12**). Finally, a gas supply was provided by running gas grade tubing from the source to the assembled chemostat.

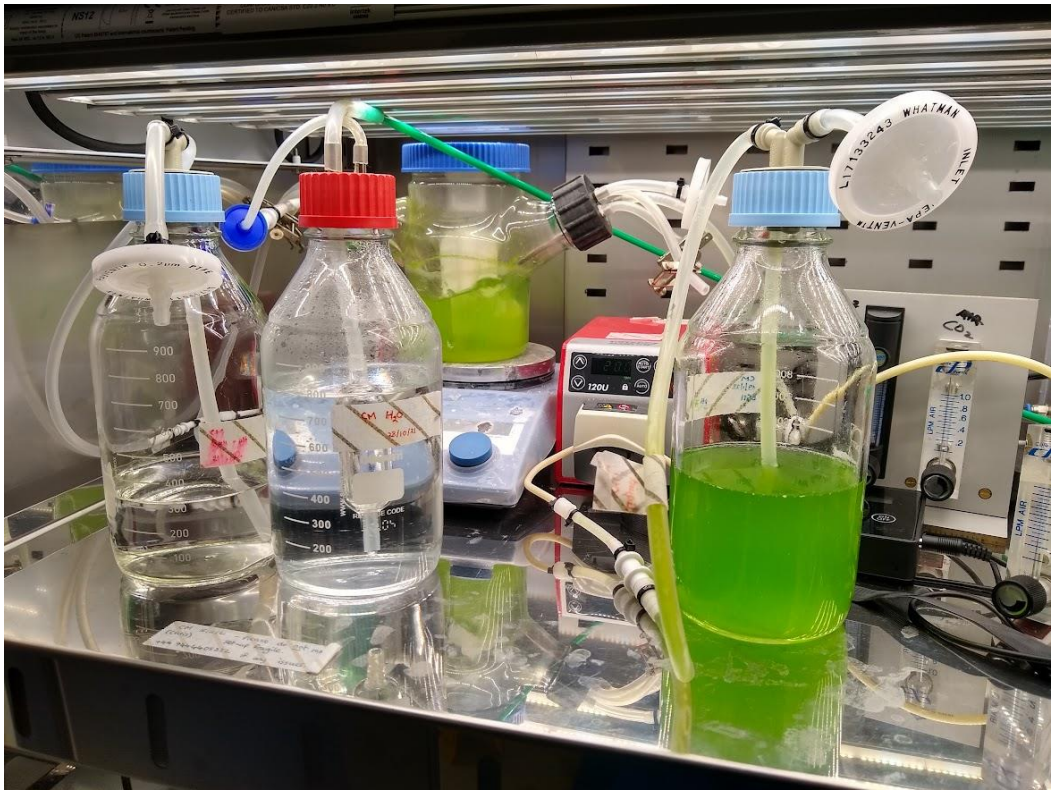


Figure 4.12 | Assembled and functioning chemostat system.

However, no devices were available to automatically moderate the dilution rate. Therefore, the dilution rate was manually adjusted according to feedback from optical density (OD_{750nm}) measurements made using the spent culture. Although a more labour-intensive solution, initial optimisation of the system showed that this could be achieved and sustained. The use of optical density to inform chemostat selection ensured that the selective pressure of the chosen experimental parameters was sustained by preventing both premature wash out of cultures, and overgrowth of cultures (see Rajaraman et al. 2016) [243].

4.4.2 *ALE selection based on electron sinks in the Synechocystis cell*

As stated in **2.7.3.3**, light stress can be utilised to direct excess electrons towards carbon assimilation and enhance cyanobacterial growth. In the CB cycle carbon dioxide is converted into glucose using NADPH and ATP, both being derived from the splitting of water driven by light energy (**Figure 4.13**) [59].

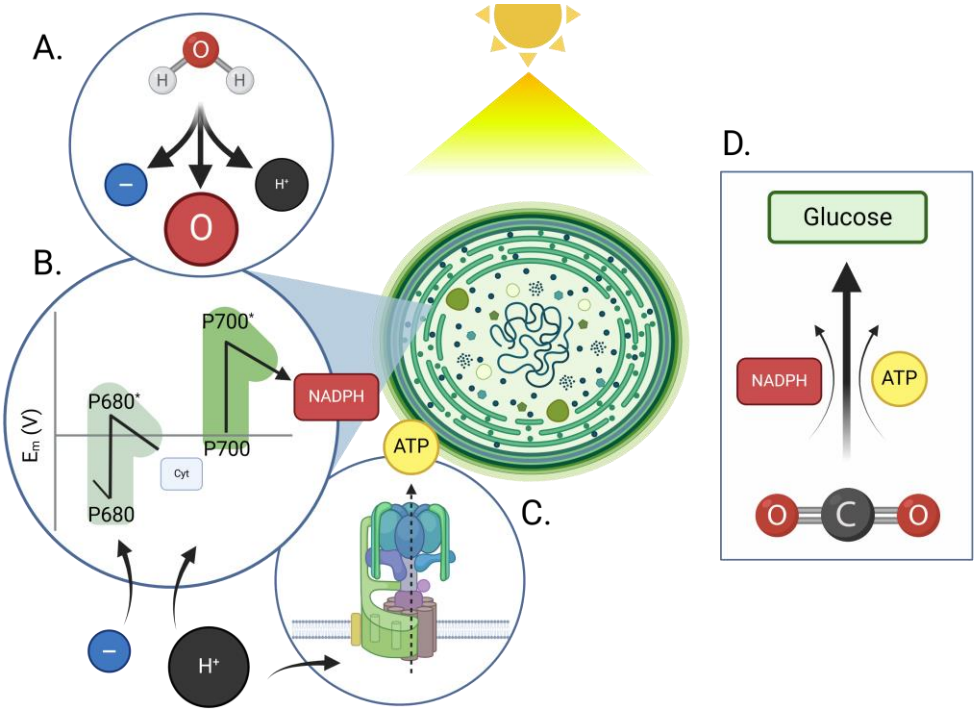


Figure 4.13 | Simplified schematic summarising the transfer of light energy to allow for the fixation of carbon dioxide into glucose in the cell. **A.** splitting of water by redox reaction in oxygen evolving centre (OEC) to release oxygen, protons, and electrons. **B.** electron mediated reduction of $NADP^+$ to NADPH via PSII and PSI. **C.** ATP synthesis by ATP synthase using a proton gradient. **D.** NADPH and ATP used to fix CO_2 into glucose via the Calvin-Benson cycle.

Therefore, if the light energy is increased, there could be more energy available for the cyanobacteria to fix more carbon dioxide. However, this is not always true in practice, because if the light intensities are sustained at very high levels this can result in photoinhibition. The resulting degradation of the PSII D1 proteins by photodamage reduces the ability of the cyanobacteria to harvest light, eventually leading to death [445]. Additionally, excess electrons can be particularly problematic if they exceed electron consumption in the cell, this can result in oxidative stress or even cell death from generated ROS [446]. Furthermore, as demonstrated by Dann et al. 2019, cyanobacteria cells can adapt to light stress by developing more resilient excitation stress tolerance mechanisms, such as increased carotenoid abundance, and decreased biomass formation [284]. However, if these electrons can be effectively diverted into the Calvin-Benson cycle, they could be used to increase biomass and productivity. If a strategy is employed that encourages adaptation to this stress

specifically through enhanced carbon fixation, it could select for phenotypes that reduce electron stress with greater carbon fixation rates. High light was therefore selected as a central component of the experimental design.

Following the unsuccessful multicultivation approach utilised above, a new strategy was devised, to try and push excess electrons into the Calvin-Benson cycle by removing competing electron sinks in the cell. The theory being that in a strain with the competing electron sinks removed the cell, will have no other option than to funnel those excess electrons into the Calvin-Benson cycle. Particularly if the cell is grown continually under selective conditions which favour electron generation. Such a strategy would also align with ALE design principles to increase growth and biomass formation described in **Table 2.4**, in which 30 ALE experiments utilised strains engineered to direct metabolic flux.

The media was also evaluated, to identify if potential electron sinks could be removed without the need for molecular strain engineering. Nitrate and ammonium are both nitrogen sources, which have different degrees of reduction, nitrate requires 8 additional electrons per assimilated nitrogen atom and therefore acts as a significant electron sink [447]. BG-11 liquid media contains large amounts of inorganic nitrogen in the form of nitrate (15 $g \cdot L^{-1}$). Therefore, to eliminate this electron sink the nitrate was replaced with an already reduced source of nitrogen, ammonium chloride. This has the effect of negating both nitrite reductase (NirA) and nitrate reductase (NarB), (enzymes responsible for nitrate assimilation [448]) as electron sinks, without requiring strain engineering (**Figure 4.14**).

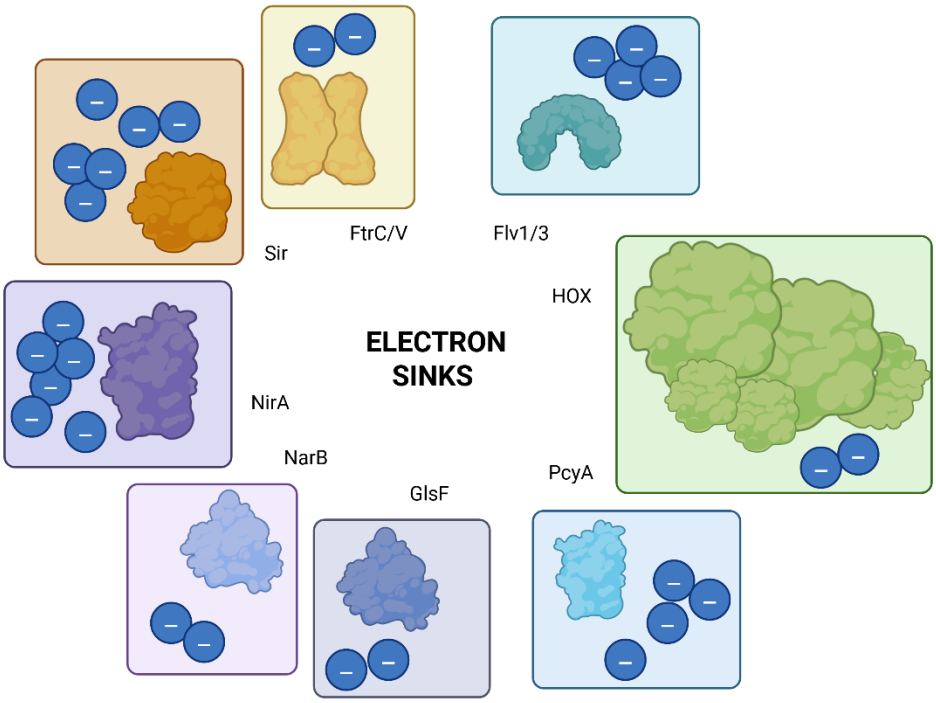


Figure 4.14 | Simplified schematic summarising the electron use per reaction of selected electron sinks in *Synechocystis*.
(Created with BioRender.com).

There are several potential electron sinks in the cell, as shown in **Figure 4.14**. However, not all of them can be easily removed without impacting negatively on the cell. Glutamate synthase (GlsF) for example, catalyses the conversion of glutamine and 2-oxoglutarate into glutamate [449]. As part of the GS/GOGAT, GlsF supports the assimilation of nitrogen into biomass via ammonium assimilation by glutamine synthase [449]. The glutamate is then converted into protein and other nitrogenous compounds via trans-amination [450]. Removal of this electron sink would therefore likely be lethal. The Flavodiiron (Flv) proteins, such as Flv1 and Flv3, are more transient in nature than other electron sinks. They often act as an ad hoc response mechanism to fluctuating light stress [451]. It has previously been shown that around 20-30% of the electrons released from the splitting of water are directed to oxygen via Flv1 and Flv3 under high light conditions [452]. Thus, functioning as powerful electron sinks. Deletion of both Flv1 and Flv3 seemed to have no detrimental effect on the cell under standard conditions, however, a shift from low light and air CO_2 to standard light and 5% CO_2 in combination with a Δ*gcvT* mutation rendered the cell deficient in photorespiratory 2-phosphoglycolate metabolism [452]. Their subsequent deletion in the cell has been shown to decrease both phycobilisome excitation [453,454] and integrity [455].

Other potential electron sinks such as the ferredoxin:thioredoxin reductase (comprised of FtrC and FtrV) have been shown to have an active role in regulating CO_2 fixation by the Calvin-Benson cycle [456]. The bacterial-type ferredoxin, Fed7 has been shown to be induced under low CO_2 and high light treatment, the *Δfed7* mutant was shown to have elevated levels of chlorophyll and PSI and a reduced abundance of PSII [457]. Fed7 is thought to be aligned with photooxidative stress. PcyA, the phycocyanobilin:ferredoxin oxidoreductase enzyme catalyses the synthesis of phycocyanobilin, which is the chromophore of all the antenna phycobiliproteins in *Synechocystis* [458]. The sulfite reductase (Sir) enzyme is a rather 'expensive' enzyme with regards to electron consumption; 6 electrons are consumed per reduction of one sulfite to sulfide molecule [459]. However, given the essential role this enzyme plays in sulphur metabolism, it is once again challenging to see how this electron sink could effectively be eliminated without significantly impacting the growth of the cells.

This leaves the bidirectional NiFe-hydrogenase enzyme (Hox), a multi-subunit enzyme, composed of the diaphorase unit (HoxEFU), which reacts with NADPH, ferrodoxin and flavodoxin and the hydrogenase subcomplex, HoxHY, which catalyses the production and consumption of H_2 [409]. Previous work has demonstrated that Hox could contribute to electron transport regulation specifically under prolonged dark adaptation [460], likely due to inactivation of catalytic activity in the presence of oxygen (abundant when photosynthesis is occurring). Despite this, however, the protein is constitutively expressed in both light and dark conditions, constantly consuming intracellular resources which could be utilised elsewhere [461]. Furthermore, the protein is quickly (< 90s) reactivated following removal of oxygen [461], which could enable the strain to alleviate electron stress at higher culture densities where self-shading occurs, reducing the selective need to enhance carbon fixation. The enzyme complex also appears to regulate both glucose and arginine metabolism under oxic conditions, with *ΔhoxH* strains unable to consume either under constant illumination [462]. Given that both metabolites are necessary for healthy photoautotrophic growth, (with the former the primary product of photosynthetic carbon fixation), use of this strain could select for mutants with reduced regulation of glycolysis, and potentially enhanced growth if the cell adapts by increasing glucose supplies through enhanced carbon fixation.

Given the time scale of generating knockouts in *Synechocystis* and the availability of the *Δhox* strain, which was previously gifted by Dr Carrie Eckert to our laboratory [409], the *Δhox* strain was utilised for the chemostat screening. A single colony of *Synechocystis Δhox* was selected and used as

the progenitor strain for mutagenesis, and as a benchmark for characterising mutants obtained from the ALE, (dubbed "Syn.*Δhox*").

In a change to the previous ALE strategy and to build upon the knowledge gathered from the multi-cultivator approach above, the ALE strategy was expanded. Given the inherent mutation biases of the different mutagens already discussed, multiple mutagenic agents were integrated into the experimental design (see **Figure 4.15**). The chemostat was also supplemented with a 5% CO_2 gas mixture to force more flux through the CB cycle and encourage the population to utilise the substrate as a solution to increased oxidative stress.

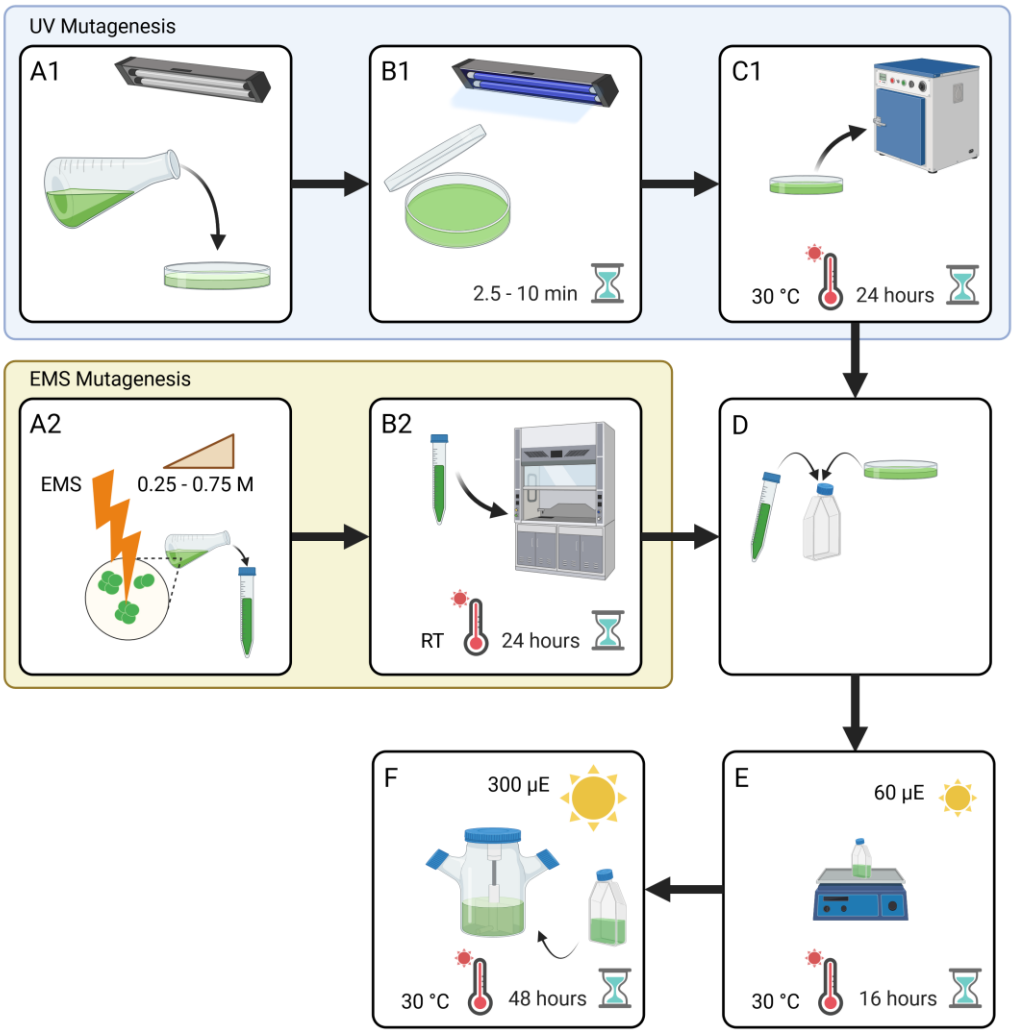


Figure 4.15 | Workflow for the combined physical and chemical mutagenesis strategy to generate a diverse population library. **A1 – C1.** *Synechocystis* sp. PCC 6803 (Syn.*Δhox*) progenitor strain subjected to

physical mutagenesis using UV radiation. **A2 – B2.** Syn.*Δhox* chemically mutagenised. **D.** Mutant libraries combined. **E.** Outgrowth of mutant libraries at 60 μmol photons·m^{-2}·sec^{-1}, 30 °C for ~16 hours. **F.** Inoculation of mutant libraries into chemostat selective environment, with batch growth for ~48 hours. (Created with BioRender.com).

Careful consideration was also given to how the strains would be isolated and characterised. This is necessary to ensure that isolated strains represent the phenotypes of interest, and not transient adaptations due to phenotypic plasticity (see Lalejini et al. 2021) [210]. Therefore, when isolating strains, it is necessary to ensure that the selective pressure is maintained, in this case, light, nitrogen source and CO_2.

4.4.3 *Selection of Synechocystis Δhox strains in a chemostat*

Following EMS and UV mutagenesis as described above in 3.3.1 and 3.3.2, cell libraries were added to the Chemostat, and the dilution rate was originally set to 0.04 mL·min^{-1}. Growth was monitored by measuring OD_{750nm}. This was measured ca. every 24 – 48 hours. Given that this strategy aims to select organisms with the fastest growth rates, the dilution was calibrated to try and constantly maintain a sustained pressure upon the cell population. This means that cells which are unable to maintain a faster growth rate are washed out of the chemostat as the dilution rate increases. This step-up wash-out strategy aligns with previous work for selecting prokaryotic mutants with enhanced growth; growth of engineered *E. coli* on acetate increased by 24% following selection in a chemostat in which the dilution rate was steadily increased to 0.5 h^{-1} [243]. The dilution rate in this experiment was steadily increased until the cells reached a point where the μ_{max} had been achieved, as determined by OD_{750nm} values. Reaching a maximum dilution rate of 0.56 mL·min^{-1} (therefore $\mu < 0.56$ h^{-1}), and a turnover of 633.6 mL of media per day. This dilution rate was maintained, and culture density slowly decreased. Once OD_{750nm} 0.01 was reached, the selection was considered completed, and the final cells were subject to screening to evaluate the individual strains.

4.4.4 *Characterisation of the individual Synechocystis ∆hox strains isolated from the Chemostat*

To mitigate the risk of selection bias, colonies were once again selected at random. Strains were selected from the centre of serial dilatation plate outwards. To maintain the stress on the cell during the isolation process colonies were grown at 300 µmol photons·m^{-2}·sec^{-1}.

4.5 Phenotypic characterisation of *Synechocystis ∆hox* strains isolated from the chemostat

The previous approach to screening individual isolates was determined to be impractical. The method was both resource and space intensive, and it also failed to isolate strains with increased biomass accumulation. Whilst the latter issue could potentially be solved by longer incubation times of the cultures being screened, the former could only be resolved with equipment that was not available in the laboratory. Evaluation of the literature highlighted other ALE strategies utilised to approach the issue of isolate screening. Many of these strategies adopt high-throughput methodologies which enable the rapid screening of many of individual colonies in one go. These include selecting visual phenotypes [208,463], or assessing smaller growth volumes in multi-well plates [464–466]. Furthermore, a then recent ALE of cyanobacteria *Synechococcus elongatus* sp. PCC 11801 to select for increased alcohol tolerance utilised a 24-well plate methodology to screen isolates, successfully identifying mutants with 2-fold increased solvent tolerance [467]. Therefore, to allow the characterisation of a representative sample number, and to avoid subjective bias, isolates were screened using transparent polystyrene 24-well plates.

4.5.1 *Measuring biomass yields from the Synechocystis ∆hox strains isolated from the chemostat*

Prior to evaluating the individual strains, the 24-well plates were evaluated to assess the impact of the position of the individual wells on growth, as the 24-well plates were irregular in shape. Therefore, to identify any inherent bias in well position, Syn.*∆hox* was used to inoculate each of

the individual wells. Cells were inoculated into 1.1 mL of BG-11 media (n = 3). Growth rates were then determined for each cell utilising OD_{750nm}, this was then used to evaluate the potential growth bias depending on the position of the cell (see **Table S1** in **Appendix**). The inter-well variance was assessed using a single-factor Analysis of Variance (ANOVA), as this statistical method allows for the comparison of each well position simultaneously and has previously been used to assess variance in 24-well plate experiments (see Moreau et al. 2006) [468]. However, no significant positional bias (P = 0.84; F = 0.68) was observed. Any potential loss of media, which in turn would lead to a reduction in the volume in the plate was mitigated by double sealing the plate-lid gap with parafilm. The efficacy of this procedure was measured by using triplicate cultures of BG-11, with no cells. The impact of evaporation was determined to be negligible over the course of the 5-day experiment, with an average (mean) 5 – 66 μL of media lost depending on the well position in the plate (see **Table S2** in **Appendix**). A single-factor ANOVA again showed no significant variation (P = 0.08; F = 1.61) in evaporation across wells after 168 hours. Despite a slightly higher loss of media on one side of the 24-well plate, this did not appear to correlate with any changes in growth rates of the control experiment. Once the strategy had been evaluated, the individual isolates from the chemostat were characterized as shown in **Figure 4.16**.

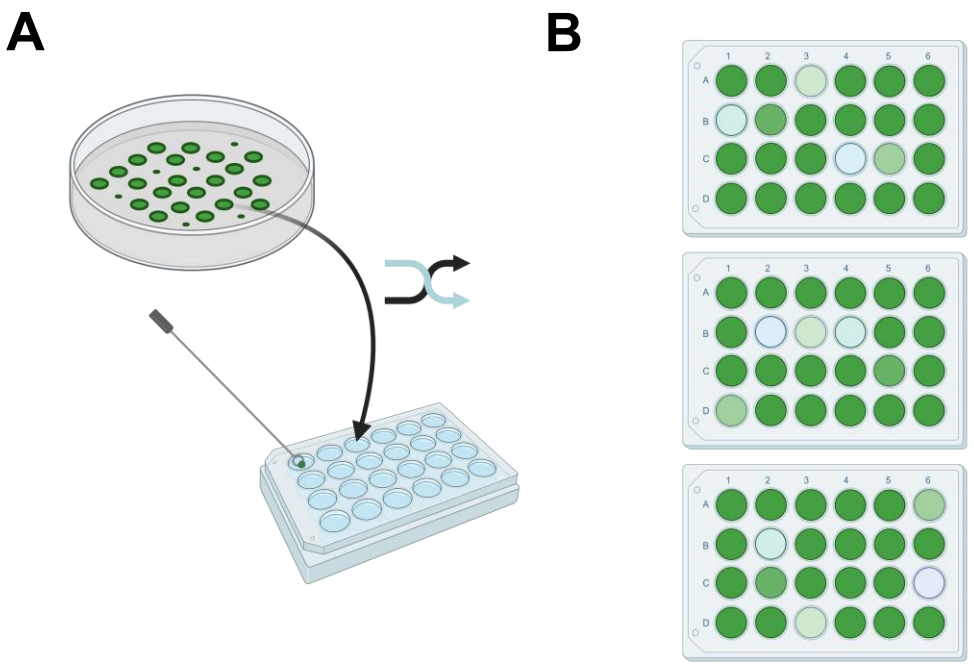


Figure 4.16 | Chemostat isolate screening strategy. **A.** 22 – 23 individual isolates were added directly to the 24 well plates across 3 randomised well positions of 3 separate Corning™ Costar™ 24-well Clear TC-treated Multiple Well Plates (Fisher Scientific™). 1 well of each plate contained media only to monitor for cross contamination of wells. A minimum of 1 triplicate Syn.*Δhox* strain was also included per screening process. **B.** Plates were incubated at 300 µmol photons·m^{-2}·sec^{-1}, 30 °C for 120 hours. (Created with BioRender.com).

4.5.1.1 *Atmospheric CO_2 biomass yields from the Synechocystis Δhox strains isolated from the chemostat*

To avoid potential obfuscation of biomass productivity due to a reduced lag phase in the mutants (see **4.3.2.2**), isolates were instead grown to stationary phase (rather than exponential), to assess maximum biomass yields. Following growth for 120 hours, the biomass from each individual colony was compared to the original progenitor strain Syn.*Δhox* utilising DCW **Figure 4.17**.

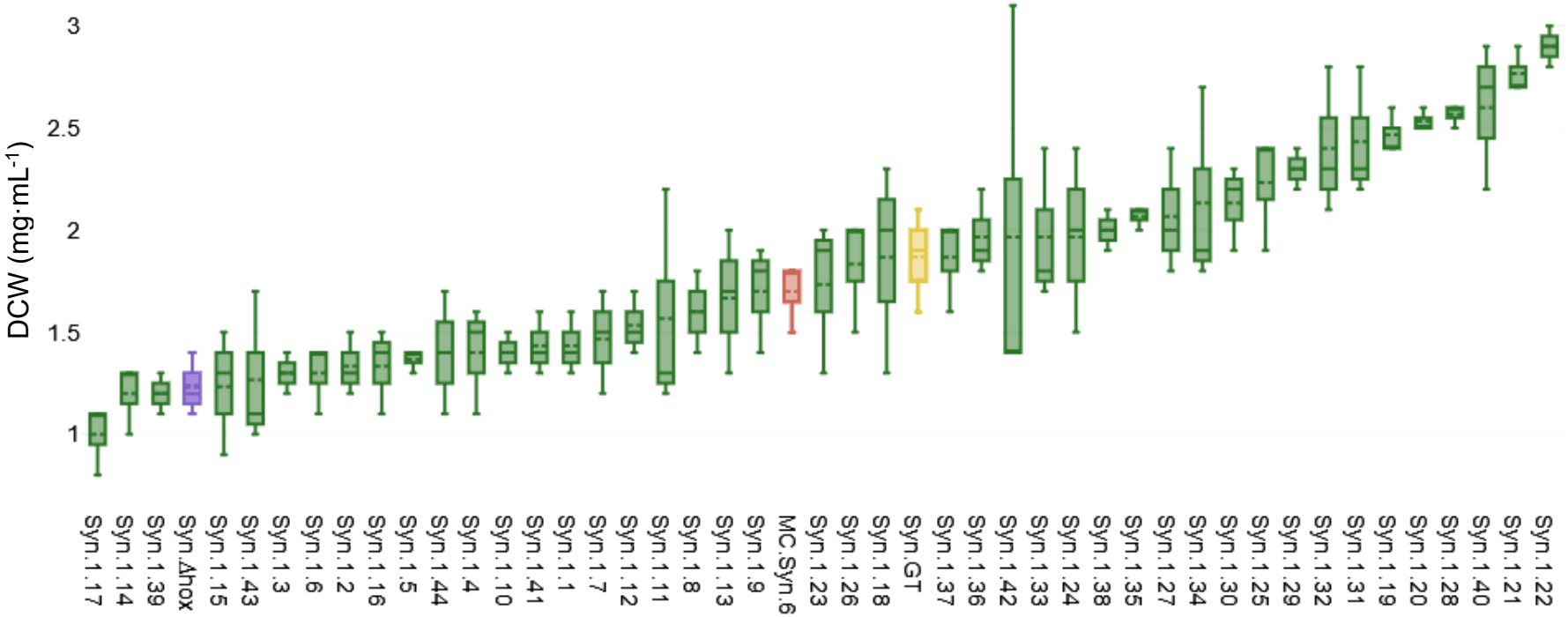


Figure 4.17 | Dry cell weights from 24-well plate screened isolates at 300 µmol photons·m^{-2}·sec^{-1}, 30 °C, 120 hours, in BG-11NH_4 liquid media. Green indicates chemostat isolate samples. Purple indicates Syn.*Δhox* samples. Red indicates MC.Syn.6 samples. Yellow indicates Syn.GT samples. (*n* = 3, error bars show standard deviation).

The strains isolated from the chemostat showed a significant overall improvement in biomass accumulation compared to the respective progenitor strain Syn.*Δhox*. Overall, 93.2% (sum) of the isolated strains showed a nominal improvement in the average biomass accumulation, and this was statistically significant in 18 isolates ($p < 0.05$). When compared to MC.Syn.6, the fastest growing mutant isolated from the multi-cultivator-based approach, just over half of the isolates (54.5%) showed higher average biomass accumulation. Overall, the combined average DCW of all the isolates screened was 1.81 ±0.55 mg·mL^{-1}, compared to 1.23 ±0.12 mg·mL^{-1} in Syn.*Δhox*, 1.87 ±0.2 mg·mL^{-1} in Syn.GT, and 1.21 ±0.14 mg·mL^{-1} in MC.Syn.6. In fact, despite the wide range of DCWs recorded, the triplicate recorded values of the isolates ($N = 132$) were significantly different from Syn.*Δhox* ($p < 0.01$). The total distribution of isolate biomass showed a shift in mean towards higher yields for the conditions investigated (**Figure 4.18**).

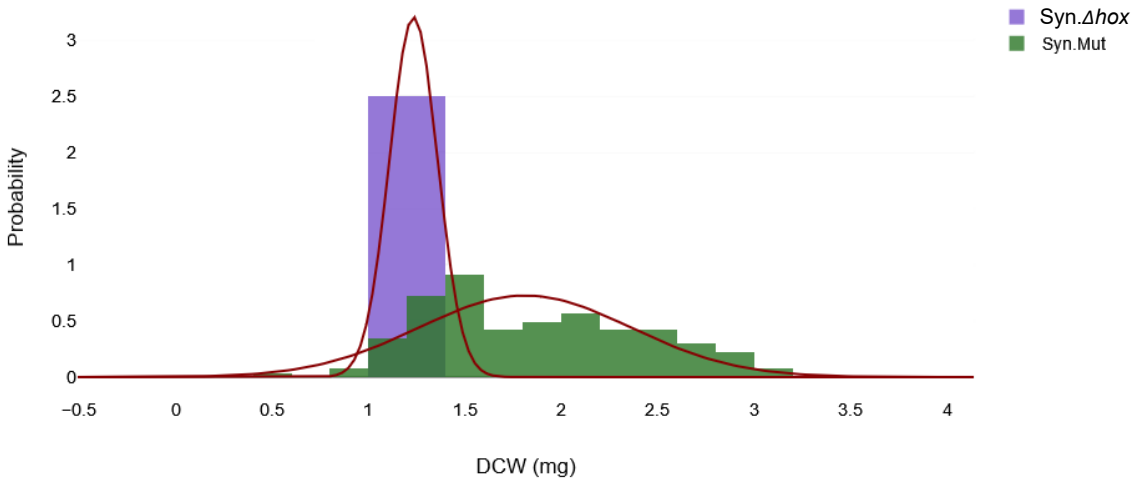


Figure 4.18 | Proportional frequency of *Synechocystis Δhox* chemostat isolates dry cell weight yields from 24-well plate isolates at 300 µmol photons·m^{-2}·sec^{-1}, 30 °C, 120 hours, in BG-11NH$_4$ liquid media. Green indicates chemostat isolate samples ($N = 132$). Purple indicates Syn.*Δhox* ($N = 3$).

Furthermore, despite the shift in mean biomass accumulation towards increased growth, the frequency distribution of biomass yields was relatively broad in comparison to the clonal Syn.*Δhox* population. Given that each mutant isolate is also derived from a single colony prior to

screening, this suggests that population and allele diversity determining biomass accumulation under atmospheric CO_2 was still present within the chemostat, despite a final push towards wash-out. That is, the single colonies isolated at the end of the experiment do not cluster around a single (or even a few) biomass accumulation frequencies. In evolution experiments, with narrow selective environments and where organisms have been genetically "barcoded", (to enable tracking of their relative abundance over time), a consistent dynamic is a trend towards increased abundance of alleles which confer the greatest fitness advantages (see Blundell et al. 2019; Maddamsetti et al. 2015) [469,470]. This suggests that alleles which confer advantage under atmospheric CO_2 concentrations, (or reduced substrate availability), may have faced lower selective pressure than other allelic characteristics.

4.5.1.2 *Saturated CO_2 biomass yields from the Synechocystis ∆hox strains isolated from the chemostat*

Given that cells generally adapt to the conditions under which they are selected, however, it was simultaneously investigated if similar improvements in biomass accumulation would be observed when strains were supplemented with additional CO_2, (as selection was maintained under 5% CO_2 supplementation throughout). Isolates were again screened in 24-well plates using the same strategy as above, however, this was done in a sealable acrylic box, custom built by the University of Nottingham, Department of Engineering workshop team. This sealed box was supplemented with a constant supply of air and CO_2 and calibrated to create a final mix of 1.5% CO_2. Plates were again grown for 120 hours, at 300 µmol photons·m^{-2}·sec^{-1}, 30 °C. Once cultures had grown, DCW measurements were estimated using dried 1.5 mL microcentrifuge tubes, with 1 mL of each culture. Tubes were dried at 80 °C for 48 hours and weighed using an analytical balance. Results are shown in **Figure 4.19**.

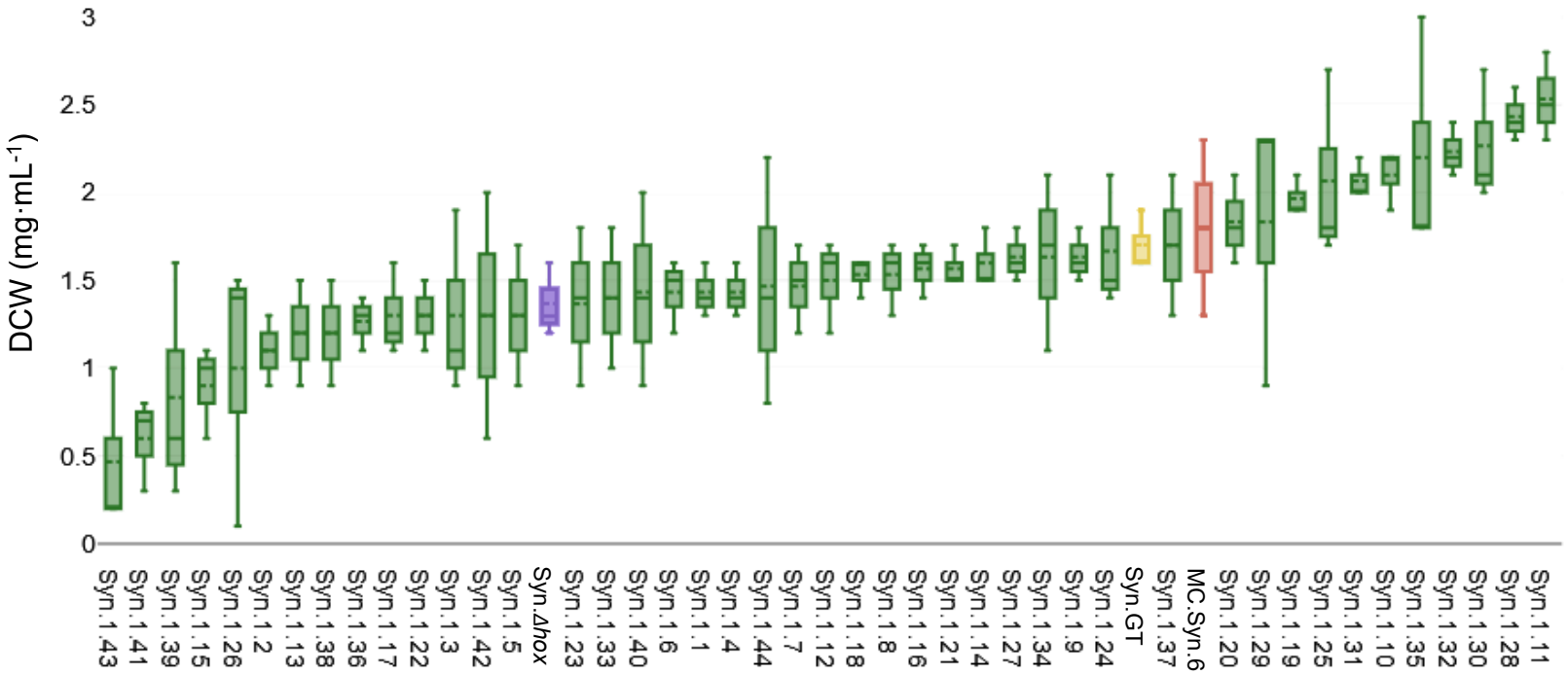


Figure 4.19 | Dry cell weights from 24-well plate screened isolates at 300 µmol photons·m^{-2}·sec^{-1}, 30 °C, 120 hours, 1.5% CO_2, in BG-11NH_4 liquid media. Green indicates chemostat isolate samples. Purple indicates Syn.*Δhox* samples. Red indicates MC.Syn.6 samples. Yellow indicates Syn.GT samples (*n* = 3, error bars show standard deviation).

Despite having been selected with CO_2 supplementation, however, relative improvements in biomass accumulation of the isolates appeared to have diminished compared to equivalent screening without CO_2 (see **Figure 4.17**). The average nominal biomass yields recorded as higher than those recorded for Syn.*Δhox*, were also reduced from 93.2% to 75%. Seven isolates had statistically significant increases in biomass accumulation ($p < 0.05$). In contrast to screening without CO_2 supplementation, where no isolates had significantly lower biomass accumulation than the control, 2 isolates showed significantly lower biomass accumulation ($p < 0.05$). These strains, Syn.1.43 and Syn.1.41, had 66% and 56% lower biomass accumulation than Syn.*Δhox* respectively. The overall distribution of biomass accumulation, and the mean value of isolates screened with CO_2 supplementation, remained higher than the progenitor control (**Figure 4.20**). A concentration of 1.5% CO_2 was selected for screening mutants under increased CO_2 concentration. This concentration was selected to enable the impact of increased CO_2 concentration to be evaluated on the mutants' ability to fix carbon and subsequently form biomass. This concentration was also selected to better avoid selecting mutants adapted to abiotic stresses associated with increased CO_2 concentrations such as increased acidity tolerance, or reduced CO_2 specificity of enzymes under a lower O_2 concentration.

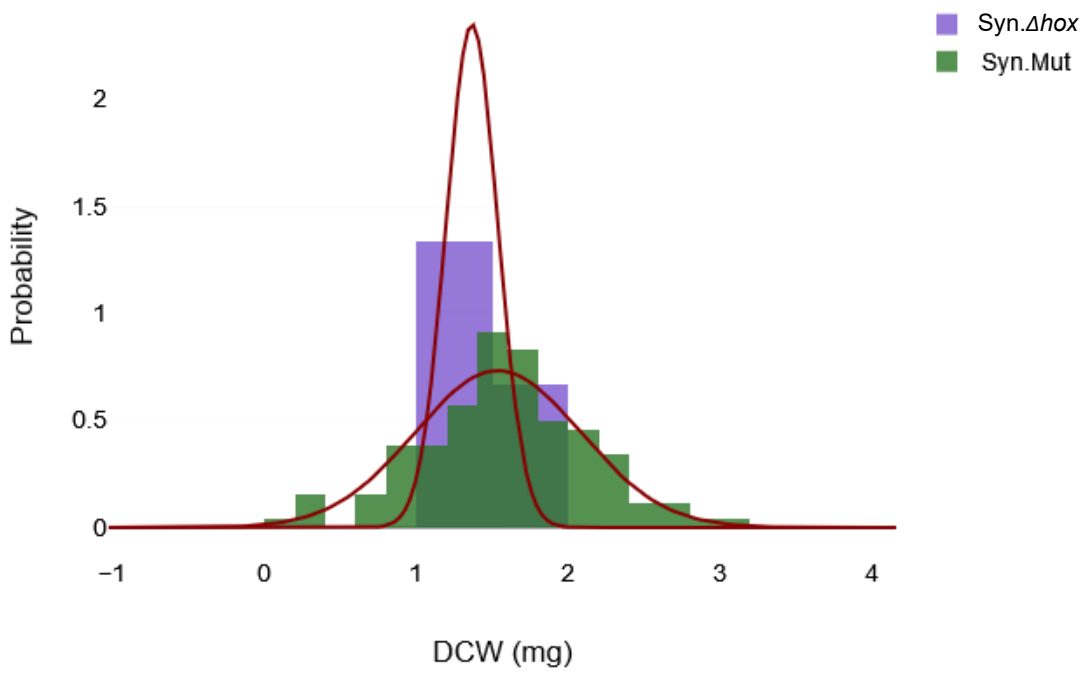


Figure 4.20 | Proportional frequency of dry cell weight yields from 24-well plate *Synechocystis Δhox* chemostat isolate screening at 300 µmol photons·m^{-2}·sec^{-1}, 30 °C, 120 hours, 1.5% CO_2 supplementation, in BG-11NH_4 liquid media. Green indicates chemostat isolate samples (*N* = 132). Purple indicates Syn.*Δhox* (*N* = 3).

The average DCW of all mutants when screened with 1.5% CO_2 supplementation was 1.54 ±0.54 mg·mL^{-1}. These results were surprising and were contrary to what was expected, an increase in growth under similar conditions. However, it is important to note that the second round of screening was performed using 1.5% CO_2, not 5% as per the specific environment of the chemostat. Despite this the overall diversity in the mutant growth phenotypes was broad, with extremes either side of the Syn.*Δhox* progenitor average (**Figure 4.21**).

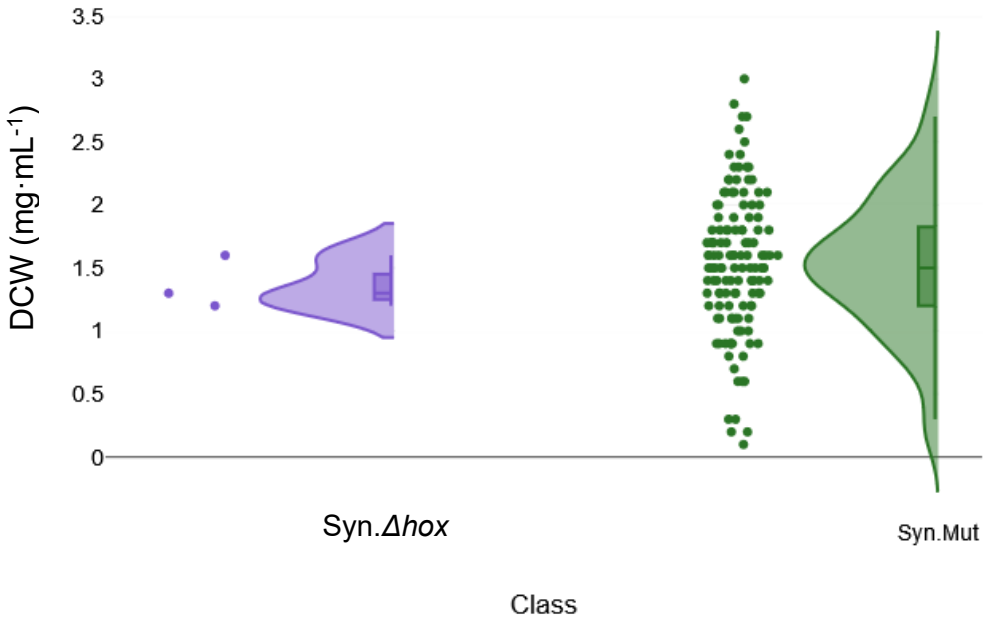


Figure 4.21 | Distribution of all individual dry cell weight yields from 24-well plate isolate screening at 300 µmol photons·m^{-2}·sec^{-1}, 30 °C, 120 hours, 1.5% CO_2 supplementation, in BG-11NH_4 liquid media. Green indicates chemostat isolate samples (*N* = 132). Purple indicates Syn.*Δhox* (*N* = 3).

However, the mean frequency distribution of phenotypes is tighter in **Figures 4.20** and **4.21**, when compared to **Figure 4.18**. This is interesting as it suggests an increase in the CO_2 concentration forces greater allelic convergence within the cells. When this observation is combined with those of the initial screening, this suggests (1) that CO_2 utilisation was influential on the final population diversity, particularly when the concentration was saturated (see **Figure 4.20**), and (2) an advantage was conferred to populations possessing alleles for greater CO_2 uptake at atmospheric concentrations (see **Figure 4.18**). This suggests that the selective environment was effective in directing *Synechocystis* evolution towards phenotypes with both greater substrate uptake and utilisation.

Previous work by Kremer et al. 2018 was described in section **2.7.3.1** [304], and that work highlighted how strains of *Chlamydomonas reinhardtii* adapted to 14°C grew faster at 33°C, than equivalent strains adapted at 33°C. An axiom of evolutionary biology is that organisms will adapt to become 'fitter' for any given environment. What the results in **Figures 4.18** and **4.20** demonstrate, however, is that by controlling

environmental variables it is also possible to indirectly select for desired phenotypic characteristics. As in LaPanse et al. 2021, adapting microalgae in an environment where evolutionary advantage was directly conferred by increased growth selected for faster growing strains. Whereas adapting the same microalgae in an environment where advantage was conferred specifically by 'heat tolerance', selected for heat tolerance. Adapting cyanobacteria, here by minimising the likelihood of non-carbon fixation associated adaptations, may have had a similar outcome. In so far as strains have adapted for the specific selective requirements of this chemostat – by enhancing their carbon fixation mechanisms.

To investigate if there was any significance between the isolates that showed improved growth under ambient CO_2 screening, and the isolates that showed improved growth under 1.5% CO_2 supplementation, 2-tailed T-Tests were performed. The T-tests showed that 10 isolates had significant differences between the DCW results obtained across the two screening regimes. Of these, 2 showed a significant increase ($p < 0.05$) in DCW when supplemented with 1.5% CO_2, and 8 showed a significant ($p < 0.05$) decrease in growth.

4.5.1.3 *Further Synechocystis ∆hox strain growth characteristics*

Two distinct phenotypes were shown to be present amongst the cells isolated from the chemostat (**Figure 4.22**). Pearson correlation demonstrated a moderate negative correlation (< -0.52) between isolates which exhibited strong growth under atmospheric concentrations of CO_2, and isolates with a reduced growth under CO_2. In total, this reduced growth under CO_2 supplementation was present amongst 31 of the 44 colonies (> 70%) characterised. The Pearson correlation of the 'increase in CO_2 supplementation = increases biomass', instead showed a moderate positive correlation (> 0.56). Previous work has already demonstrated that *Synechocystis* sp. PCC 6803 can grow with concentrations of up to 20% CO_2 supplementation without experiencing diminished growth [471].

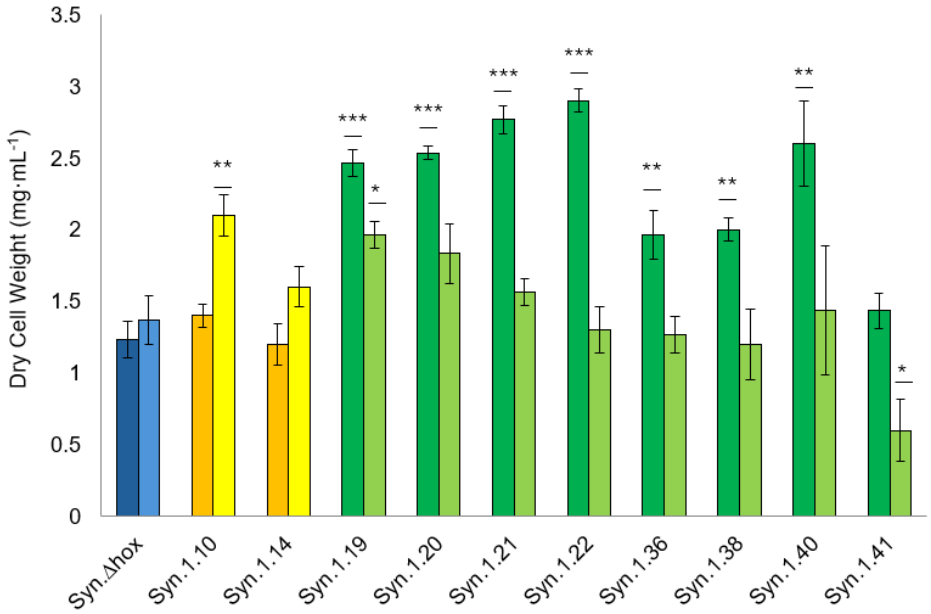


Figure 4.22 | Dry cell weights from 24-well plate screened isolates that showed significant ($p < 0.05$) intraspecific differences in growth at 300 µmol photons·m^{-2}·sec^{-1}, 30 °C, 120 hours, in BG-11NH$_4$ liquid media. Left bars show screening under ambient CO_2, right bars show screening with 1.5% CO_2 supplementation. Green indicates chemostat isolates with significant decreases in growth with 1.5% CO_2. Yellow indicates isolates with significant increases in growth with 1.5% CO_2. Blue indicates Syn.*Δhox* samples. (Asterisks indicate significant differences between isolates and the Syn.*Δhox* samples in the equivalent 24-well plate screen, * $p < 0.05$, ** $p < 0.01$, *** $p < 0.001$, error bars show standard deviation).

There are two possible reasons for this difference. Either, the use of the sealed acrylic box disproportionately affected the growth of the isolates compared to the Syn.*Δhox* controls, or the elevated CO_2 concentration is reducing the growth of the isolates under the conditions screened. Regarding growth in the sealed chamber, however, no inherent observations could be found to suggest why this would diminish growth. Firstly, the light intensities of both conditions were calibrated to 300 µmol photons·m^{-2}·sec^{-1} using a Quantitherm PAR/Temp sensor (Hansatech Instruments™), and both used the same light source in the Reach-in Growth Chamber (Weiss Technik™). The temperature range of the sealed chamber and the specific temperature on the growth chamber shelf was measured using a mercury thermometer over triplicate ~30-minute intervals. It was found to be 30.1 – 30.2 °C, and 27.5 – 30.2 °C respectively. This 2.7 °C fluctuation in temperature seen for the growth chamber shelf

was likely due to the chamber's frequent opening and closing. The optimum temperature range of *Synechocystis* has previously been shown to range from 25 – 40 °C, and so it seems unlikely that this temperature variation was responsible for the differences seen. Given the relative consistency between the two screening conditions, it seems likely that the changes in phenotype were due to the relative CO_2 concentrations.

During the screening process, another observation was made regarding the physiology of the cells, a small number of the inoculated wells, 4 out of 138, had signs of flocculation. This occurred when the cells were screened at 300 µmol photons·m^{-2}·sec^{-1}, 30 °C, for 120 hours. However, during the second round of screening when the CO_2 was elevated to 1.5%, this increased to 30 out of 138 inoculated wells. Flocculation has previously been seen in *Synechocystis,* during ALE to improve tolerance to alcohols [472]. Flocculation in *Synechocystis* has been linked to the secretion of EPS [473]. Increased EPS secretion has also been linked to the resilience of *Synechocystis* cells to high light stress [474]. However, EPS has also been linked to cultures settling in the bottom of the flask, as this was observed in EPS synthesis deletion strains of *Synechocystis* [473]. This latter phenotype was also documented in strains initially selected for further characterisation, Syn.1.11, Syn.1.19, Syn.1.21, Syn.1.27, and Syn.1.36. Following an initial attempt to determine the growth rates of these strains, cultures were left on the bench for 7 days, with no agitation, this was similar to work described by Jittawuttipoka et al. 2013 [473]. All the mutants showed significant settling in the culture flasks, compared to Syn.*Δhox* which remained in a more uniform suspension (**Figure 4.23**).



Figure 4.23 | Culture flasks of *Synechocystis* (Syn.*Δhox*) strains showing settling after 7 days. Cultures are arranged in triplicates, left to right: Syn.*Δhox*, Syn.1.11, Syn.1.19, Syn.1.21, Syn.1.27, and Syn.1.36.

To further characterise the strains, 3 strains were initially selected: Syn.1.11, Syn.1.19, and Syn.1.21. Each of these isolates were selected for different reasons, Syn.1.21 showed the joint highest growth, (with Syn.1.22) during screening with ambient CO_2. Syn.1.11 showed the highest growth during screening with 1.5% CO_2 supplementation, as well as nominally higher growth under ambient CO_2 conditions compared to Syn.*Δhox*. Syn.1.19 was selected as it was the only strain to show significantly higher growth under both screening regimes. These strains were separated onto individual BG-11 solid media plates.

Despite initially selecting three strains, only Syn.1.11 and Syn.1.19 were able to be characterised further. After several weeks of subbing the Syn.1.21 cultures died. Original patch plates had been retained to this point, however, further attempts to revive Syn.1.21 were unsuccessful. Although not assessed statistically, other strains that had previously shown a similar phenotype, strains Syn.1.22 and Syn.1.40, appeared to have also died back. The loss of strains shortly after selection is not uncommon and similar observations have been made in other studies. Patel et al. 2016 utilised EMS treatment to generate *Synechocystis* strains with up to 34% more biomass formation than the control [208]. Following initial selection 14 strains were identified, however following repeated subbing only 7 survived.

4.5.2 *Measuring growth rates of Syn.1.11 and Syn.1.19*

The growth rates of Syn.1.11 and Syn.1.19 were evaluated using nitrate and ammonium chloride under autotrophic conditions, under mixotrophic conditions with 10 mM of glucose supplementation, and with additional inorganic carbon (10 mM of HCO_3^-). Isolates were all grown in 15 mL of liquid media, and inoculated from exponentially growing starter cultures, into their respective medias. All cultures were inoculated at 0.05 OD_{750nm} and grown at 300 µmol photons·m^{-2}·sec^{-1}, 30 °C, with 150 RPM orbital shaking. The growth of the individual strains in BG-11NH_4 liquid medium was compared to Syn.*Δhox* (**Figure 4.24**).

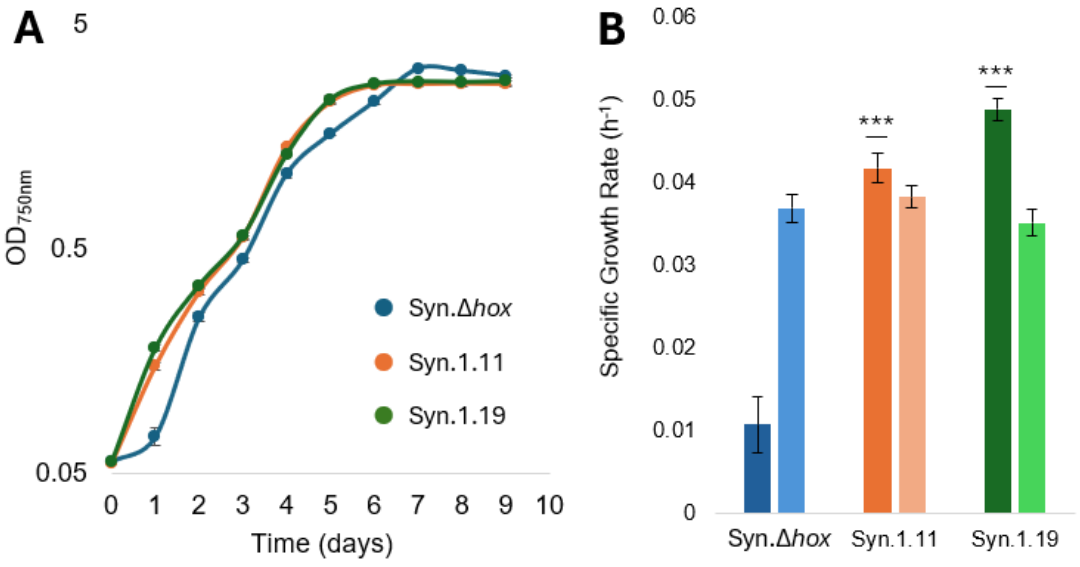


Figure 4.24 | Comparison of the growth of isolates Syn.1.11 (orange) and Syn.1.19 (green), compared to Syn.*Δhox* (blue) in BG-11NH$_4$ liquid media, grown at 300 µmol photons·m^{-2}·sec^{-1}, 30 °C, 150 RPM orbital shaking. **A.** Growth curve of cultures. **B.** Specific growth rates of cultures. Left bars show specific growth rates between 0 and 1 days, right bars show μ_{max} during exponential growth phase. (n = 6, *** p < 0.001, error bars show standard deviation).

In the BG-11NH$_4$ media, the isolates showed a significant increase in their initial specific growth rates compared to Syn.*Δhox*. Syn.1.11 showed a 3.9-fold increase (p < 6E-09), and Syn.1.19 a 4.6-fold increase (p < 5E-10) in growth rate between inoculation and day 1. Although Syn.1.11 showed a 4% increase in specific growth rate during exponential growth, (μ_{max}), this was not statistically significant (P < 0.18). Syn.1.19, also showed a 5% decrease in μ_{max} compared to Syn.*Δhox* over the same period, which was also statistically insignificant (P > 0.13). These results highlight that the mutants once again had an increased growth rate during the lag phase. However, unlike the mutant strains selected during the serial dilution ALE, this appears to have translated into improvements in the overall growth rate, with isolates reaching their final peak OD$_{750nm}$ readings approximately a day before Syn.*Δhox*.

To assess the impact of the fixed nitrogen source on growth, isolates were also grown in BG-11 liquid media containing nitrate (**Figure 4.25**).

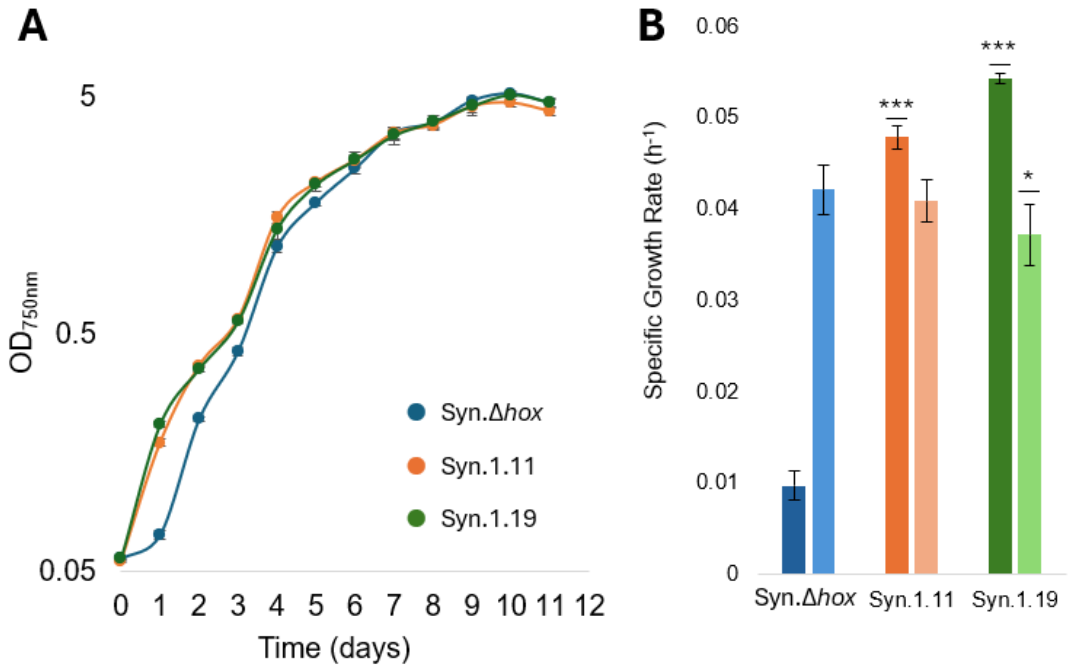


Figure 4.25 | Comparison of the growth of isolates Syn.1.11 (orange) and Syn.1.19 (green), compared to Syn.*Δhox* (blue) in nitrate BG-11 liquid media, grown at 300 µmol photons·m^{-2}·sec^{-1}, 30 °C, 150 RPM orbital shaking. **A.** Growth curve of cultures. **B.** Specific growth rates of cultures. Left bars show specific growth rates between 0 and 1 days, right bars show μ_{max} during exponential growth phase. (n = 6, *** p < 0.001, error bars show standard deviation).

Isolates grown in BG-11 liquid medium with nitrate as the nitrogen source, showed a significant increase in their specific growth rates between inoculation and day 1 when compared to the control. Syn.1.11 showed a slightly lower than 5-fold increase (p < 1.5E-12), and Syn.1.19 a greater than 5.6-fold increase (p < 5.1E-14). However, the use of nitrate resulted in a slight decrease in the specific growth rate of the isolates compared to the control during exponential growth. The Syn.1.11 μ_{max} decreased by 3%, though this was insignificant (p > 0.44). However, peak exponential growth of Syn.1.19 decreased by 12% (p < 0.03).

The growth rate increases confirm that the strains grow better when grown with the original nitrogen source used for the ALE. This is unsurprising, given how ALE applies select fitness pressure based on the chosen selective environment (see Sandberg *et al*. 2019) [202]. Furthermore, they also potentially show that the strains isolated from the chemostat have a shorter lag phase, this was not measured due to the 24-hour sampling window. The shorter lag phase was similar to the phenotype seen

in MC.Syn.6, which was isolated during the serial dilution ALE. It is also possible that these higher initial growth rates indicate that the cultures did not undergo a lag phase, when initially transferred from the exponentially growing starter cultures. These phenotypes have been noted when cells are selected from a period of prolonged exponential growth. Bromig and Weuster-Botz, 2023 [311], utilised ALE to select *E. coli* using an auto diluting series of parallel bioreactors. Cells were repeatedly grown, and they noted the near elimination of the lag phase during selection.

To investigate the impact of an organic carbon source on the growth of isolates, the strains were grown in BG-11NH_4 liquid media supplemented with 10 mM glucose (**Figure 4.26**). Previous work by Gutekunst *et al*. 2014 showed that the bidirectional NiFe-hydrogenase is essential for *Synechocystis* under mixotrophic growth conditions where nitrate is limited [475]. These results showed that Hox functions as an electron sink for reduced ferredoxin/flavodoxin, converting protons to photohydrogen [475]. As these strains are all *Δhox*, organic carbon supplementation could potentially identify if the strains have adapted to alleviate electron stress, and if this is driven by the absence of the Hox enzyme. Furthermore, glucose is catabolised for energy via multiple pathways, including glycolysis, the oxidative pentose phosphate pathway, and the Entner–Doudoroff pathway [476]. Each of these pathways contain numerous enzymes, which if mutated, could result in a phenotype that utilises photosynthesised carbohydrates more efficiently for growth and biomass.

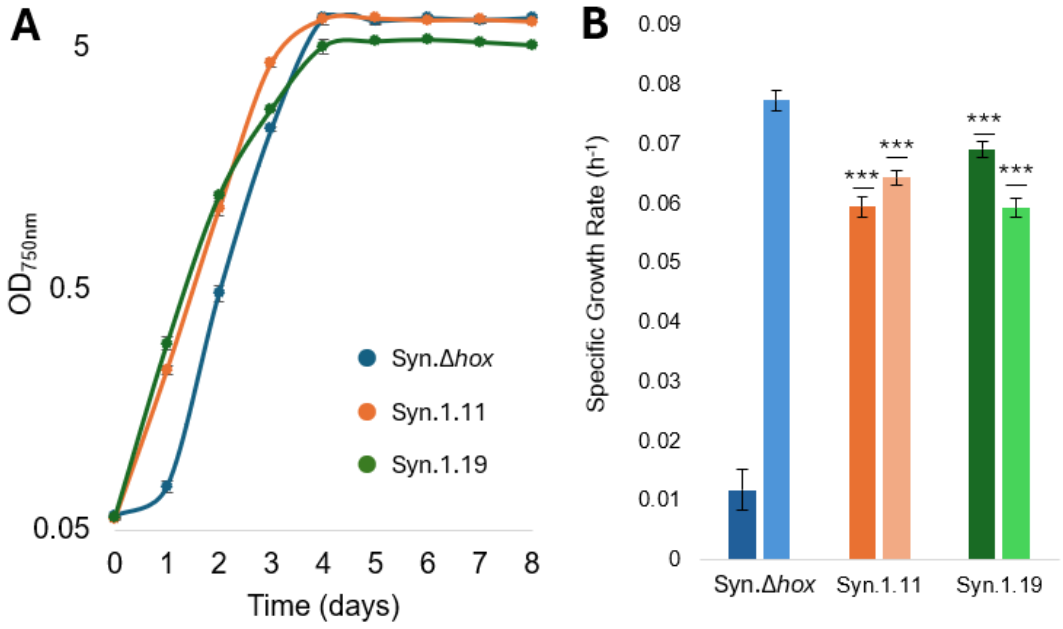


Figure 4.26 | Comparison of the growth of isolates Syn.1.11 (orange) and Syn.1.19 (green), compared to Syn.*Δhox* (blue) in BG-11NH_4 liquid media

supplemented with 10 mM glucose, grown at 300 µmol photons·m^{-2}·sec^{-1}, 30 °C, 150 RPM orbital shaking. **A.** Growth curve of cultures. **B.** Specific growth rates of cultures. Left bars show specific growth rates between 0 and 1 days, right bars show μ_{max} during exponential growth phase. (n = 6, *** p < 0.001, error bars show standard deviation).

The strains maintained a significant increase in biomass formation compared to the control, following inoculation. A 5-fold (p < 8.0E-12) and 5.9-fold (p < 5.4E-12) increase in initial growth rates were seen compared to Syn.*Δhox* between day 0 and day 1. In the isolates the higher growth rates were sustained over the following day but were statistically lower than those of Syn.*Δhox*. Here, there was a difference between growth rates of the isolates compared to Syn.*Δhox*, however, compared to growth in media with and without an organic carbon source (BG-11 and BG-11NH_4). The peak growth rate of Syn.*Δhox* was greater than the peak growth rate of the isolates. When the isolates were grown in BG-11NH_4, there was no significant difference between the growth rates measured during exponential growth phase (μ_{max}). The initial peak specific growth rates of Syn.1.11 and Syn.1.19 were higher than any period of growth for the Syn.*Δhox* cultures. Following glucose supplementation, however, the peak specific growth rate of Syn.1.11 was 13% lower than Syn.*Δhox*, and Syn.1.19 was 11% lower. Furthermore, μ_{max} of Syn.1.11 was 8% higher than growth following inoculation, again unlike in media with no organic carbon supplementation.

These results potentially indicate that the peak growth rate of the isolates was slower than Syn.*Δhox* with glucose supplementation, (even accounting for a reduction in the lag please). Possibly indicating that the isolates are indeed using carbon fixation as a strategy to remediate excess electron stress. If indeed the case, then this is the first successful demonstration of ALE in a photosynthetic prokaryote, using metabolic engineering coupled with optimisation of the selective environment to select for enhanced CO_2 fixation (see section **2.6.2**; **Table 2.4**).

Another possible explanation could be that the isolates are more efficient at assimilating carbon by other concentrating mechanisms in the cell. A common carbon source assimilated via this mechanism is bicarbonate (HCO_3^-), used as a substrate by the enzyme phosphoenolpyruvate carboxylase in the TCA cycle, which is responsible for replenishing the anapleurotic reactions [477]. The HCO_3^- transporters include the enzymes SbtA, BCT1, and BicA [84]. The carbonic anhydrase enzyme converts HCO_3^- to CO_2 in the carboxysome to generate a high CO_2

microenvironment [478]. Therefore, to assess whether the cell had improved its carbon concentrating mechanism as part of the ALE process, cultures were grown in BG-11 supplemented with 10 mM of HCO_3^-, (**Figure 4.27**).

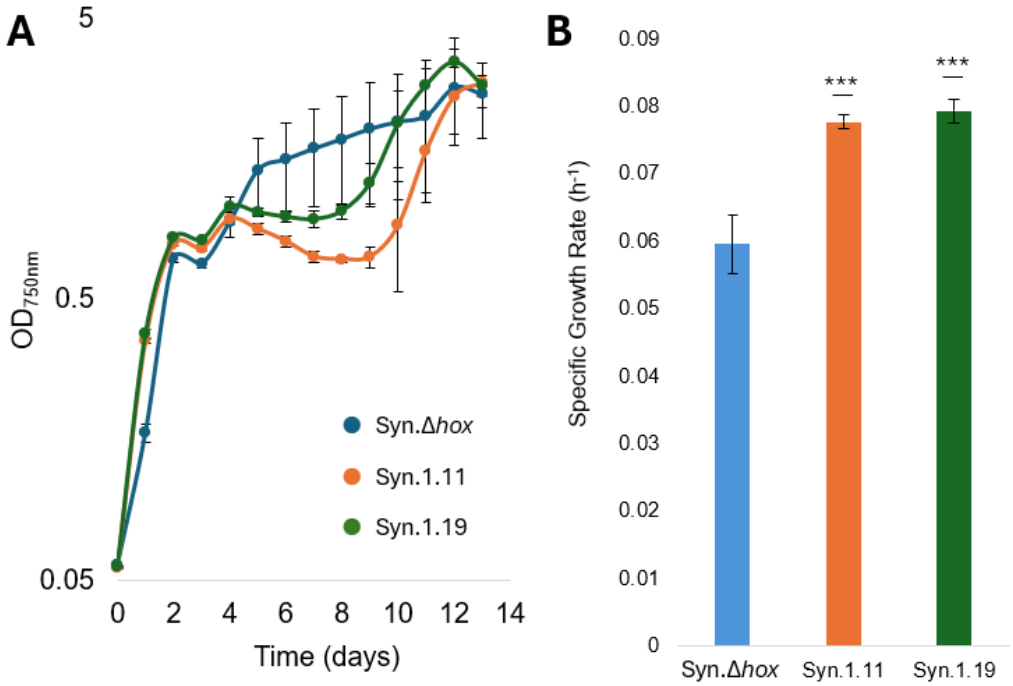


Figure 4.27 | Comparison of the growth of isolates Syn.1.11 (orange) and Syn.1.19 (green), compared to Syn.*Δhox* (blue) in BG-11NH_4 liquid media supplemented with 10 mM HCO_3^-, grown at 300 µmol photons·m^{-2}·sec^{-1}, 30 °C, 150 RPM orbital shaking. **A.** Growth curve of cultures. **B.** Specific growth rates of cultures. Bars show specific growth rates between 1 and 2 days (Syn.*Δhox*), and 0 and 1 days (Syn.1.11 and Syn.1.19) (n = 6, *** p < 0.001, error bars show standard deviation).

Growth curves of isolates supplemented with 10 mM HCO_3^- (**Figure 4.27 A**) showed an unusual, yet consistent growth pattern, in which the culture OD_{750nm} values plateaued on day four at an OD_{750nm} of around ~1. The growth then began to increase slowly. Two of the replicates of the Syn.*Δhox* control also exhibited this phenotype, however, the other 4 replicates did not. This may suggest that this unusual growth pattern is linked to the *Δhox* phenotype specifically, but the ALE has exaggerated this phenotype in the isolates. Perhaps a consequence of the species' polyploidy revealing a recessive allele linked to one of the phenotypes (see Griffin et al. 2023) [388]. The original work done by Eckert et al. 2012 supplemented BG-11 liquid medium with 100 mM of HCO_3^- [409], and the

Δhox strain was grown under either 50 or 700 µmol photons·m^{-2}·sec^{-1}, however, no impact was seen on the growth of the mutant strain. Previous work by Appel *et al*. 2000 did demonstrate an impact on growth for the Δ*hoxH* mutant strain, with a decrease in the growth rate, however this was under 2% CO_2 supplementation, and not HCO_3^- supplementation [479]. The phenotype may further indicate that there has been disruption to EPS synthesis within the mutants (as previously indicated by **Figure 4.23**). Previous work by Gupta et al. 2020 showed that complementation of additional HCO_3^- transporters to cyanobacterium *Picosynechococcus* sp. PCC 7002 resulted in a ~3-fold increase in EPS per mL of medium [186]. If the cell is unable to direct this additional carbon source towards EPS synthesis, and if central metabolism is therefore overwhelmed by a combination of enhanced CO_2 fixation and HCO_3^- assimilation, this could explain the observed mutant growth perturbations despite the additional carbon source.

Given the short period of rapid growth (~1-2 days between days 1-3) seen in the strains during this experiment, the growth rates shown in **Figure 4.27 B.** are not calculated from the same day, but they are still calculated in the same growth period. The two isolates each show only a 1.3-fold increase in the specific growth rate compared to the control, $p < 1.0E-09$ and $p < 1.5E-09$ for Syn.1.11 and Syn.1.19 respectively.

The growth rates of the strains Syn.1.11, Syn.1.19, Syn.*Δhox*, and Syn.GT were evaluated in BG-11NH_4 liquid medium, supplemented with 1.5% CO_2. During the experiment, additional samples were taken to estimate the chlorophyll concentration (see **3.3.3**) (**Figure 4.28**). Samples were also taken to characterise the potential differences in metabolites, DCWs, and pigmentation in the strains during early exponential, late exponential, and stationary phases of growth (days 2, 4, and 6). Therefore, investigating how the pigmentation, biomass, and metabolomes of the strains change compared to the control over all stages of growth.

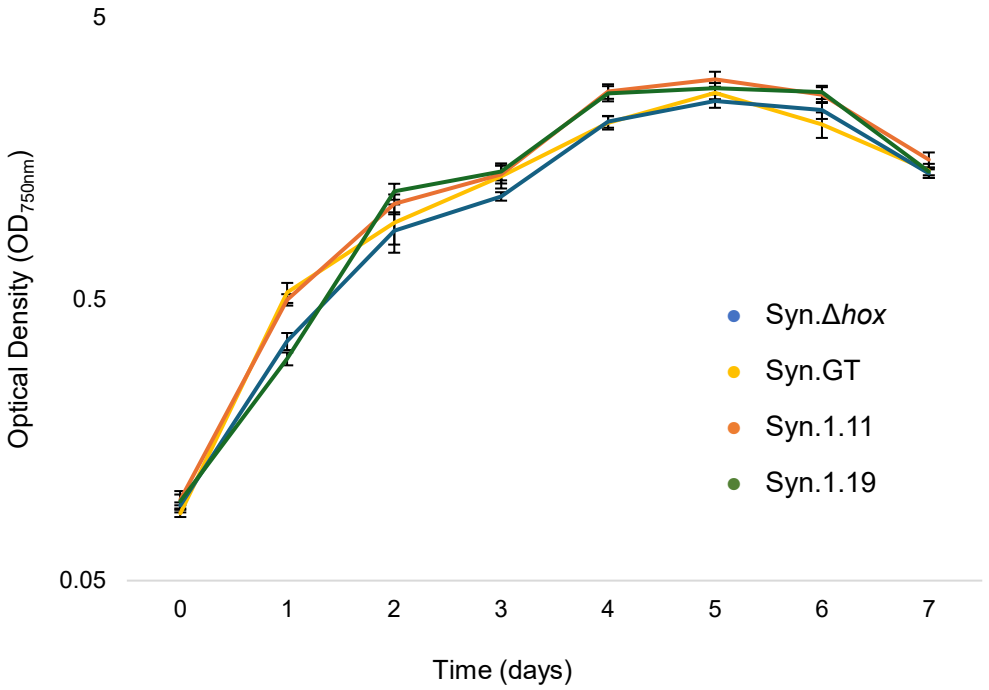


Figure 4.28 | Comparison of the growth of isolates Syn.1.11 (orange) and Syn.1.19 (green), compared to Syn.*Δhox* (blue) and Syn.GT (yellow) in BG-11NH_4 liquid media supplemented with 1.5% CO_2, grown at 300 µmol photons·m^{-2}·sec^{-1}, 30 °C, 150 RPM orbital shaking (*n* = 6, error bars show standard deviation).

Syn.1.11 showed a significantly faster initial growth rate, 22% ±3% higher than Syn.*Δhox* (p < 6.5E-06). The implication of which is that in photobioreactor cultivation, the strain Syn.1.11 could therefore shorten batch cultivation time or increase productivity. This is interesting as even small increases in photosynthetic growth rates can substantially increase productivity at scale (see Kubis & Bar-Even, 2019) [480]. However here, Syn.1.19 showed a significantly slower initial specific growth rate, 13% ±8% compared to Syn.*Δhox* (p < 0.05). During exponential growth (between days 3 and 4), the specific growth rate of Syn.1.19 was not significantly different to that of Syn.*Δhox*, however, Syn.1.11 grew significantly faster than both Syn.*Δhox* and Syn.GT over this period (p < 0.05 and p < 0.0005 respectively) (**Figure 4.29**). With an 11.3% ±8% faster specific growth rate than Syn.*Δhox*. These results are consistent with earlier observations made during the initial isolate screening, in which Syn.1.11 showed an 85% ±12% (standard error, p = 0.0035) improvement in biomass accumulation compared to Syn.*Δhox* with 1.5% CO_2 supplementation. However, Syn.1.19 previously appeared to have been deleteriously affected by 1.5% CO_2 supplementation. In this experiment, however, the negative effects on the

growth of Syn.1.19 were less pronounced. It is not immediately clear why this would occur, however, given the death of previous strains with similar phenotypes post-isolation, it is possible the mutations responsible for this phenotype were unstable, or incurred fitness penalties if retained. Given that this phenotype was weaker in Syn.1.19 relative to other isolates (see **Figure 4.22**) and given that it appears to be absent in **Figure 4.28**, survival of Syn.1.19 post-isolation may have been predicated on the loss of this phenotype.

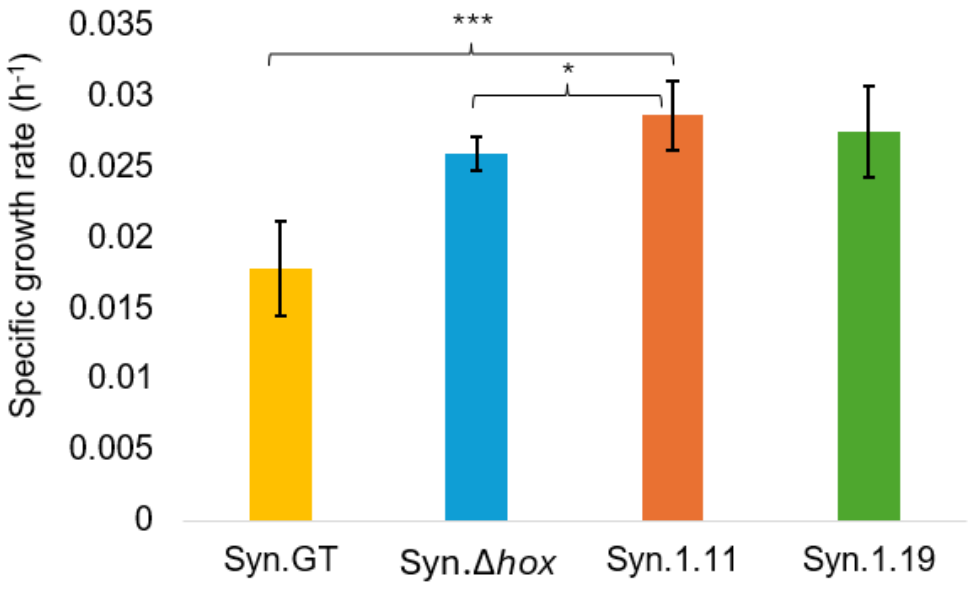


Figure 4.29 | Comparison of μ_{max} of isolates Syn.1.11 (orange) and Syn.1.19 (green), compared to Syn.*Δhox* (blue) and Syn.GT (yellow) in BG-11NH$_4$ liquid media supplemented with 1.5% CO_2, grown at 300 µmol photons·m^{-2}·sec^{-1}, 30 °C, 150 RPM orbital shaking (n = 6, *p < 0.05, ***p < 0.001, error bars show standard deviation).

4.5.3 *Measuring photosynthetic efficiency in the ALE strains*

Samples of Syn.GT, Syn.*Δhox*, Syn.1.11, and Syn1.19 were taken to quantify the relative pigment concentrations on days 2, 4, and 6 following growth in 300 µmol photons·m^{-2}·sec^{-1}, 30 °C, and 1.5% CO_2. Following extraction in *N*,*N*-Dimethylformamide, absorbance between 400 and 800 nm was measured (n = 6), and normalised to OD_{750nm}, and standardised to DCW (see 2.3.3). These spectra are shown in **Figure 4.30**.

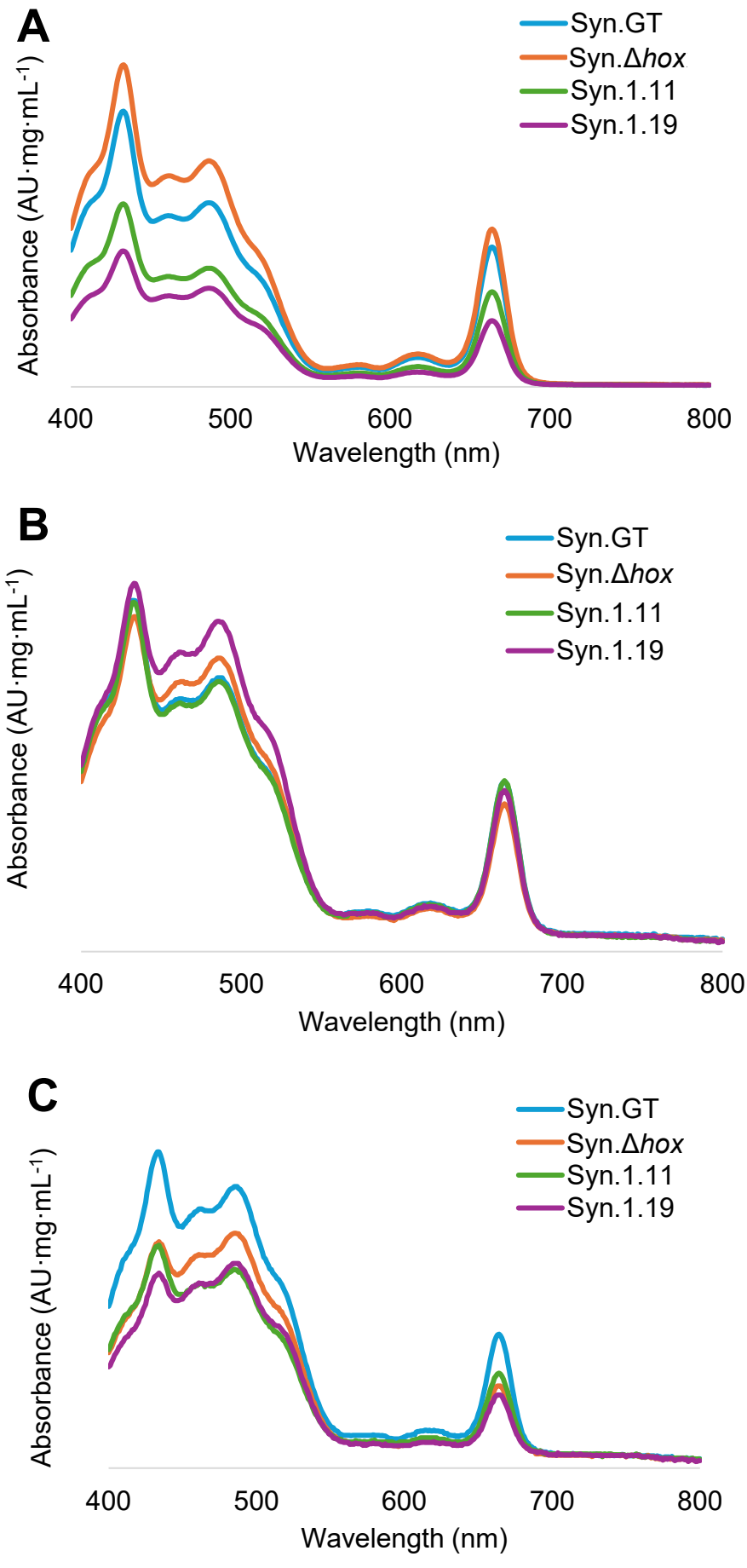

A
Syn.GT
Syn.Δhox
Syn.1.11
Syn.1.19
Absorbance (AU·mg·mL-1)
400
500
600
700
800
Wavelength (nm)
B
Syn.GT
Syn.Δhox
Syn.1.11
Syn.1.19
Absorbance (AU·mg·mL-1)
400
500
600
700
800
Wavelength (nm)
C
Syn.GT
Syn.Δhox
Syn.1.11
Syn.1.19
Absorbance (AU·mg·mL-1)
400
500
600
700
800
Wavelength (nm)

Figure 4.30 | *N*,*N*-Dimethylformamide pigment extraction absorbance spectra, normalized to OD_{750nm}, and standardised to dry cell weights of Syn.GT (blue), Syn.*Δhox* (orange), Syn.1.11 (green), and Syn.1.19 (purple), extracted on days **A.** 2, **B.** 4, **C.** 6 of growth at 300 µmol photons·m^{-2}·sec^{-1}, 30 °C, 1.5% CO_2. (*n* = 6).

During early exponential growth on day 2, the relative abundance of photosynthetic pigmentation appears to be lower in the isolates compared to Syn.*Δhox*. The Syn.GT was included in the analysis to evaluate the impact of the hydrogenase deletion on the phenotype of the cell. The pigments were more abundant in Syn.*Δhox* compared to the Syn.GT strain. Suggesting that the lower concentration of pigments in the ALE strains was not specifically linked to the *Δhox* phenotype. By day 4 there was little difference in the pigmentation between the strains, however as the cultures entered stationary phase, (see **Figure 4.30 C**), the relative abundance decreased across all the *Δhox* strains and the Syn.GT strain. Daily sampling to estimate the chlorophyll concentration of the strains per mL^{-1} of culture during the same experiment showed significant variation between the strains after day 3 (**Figure 4.31**).

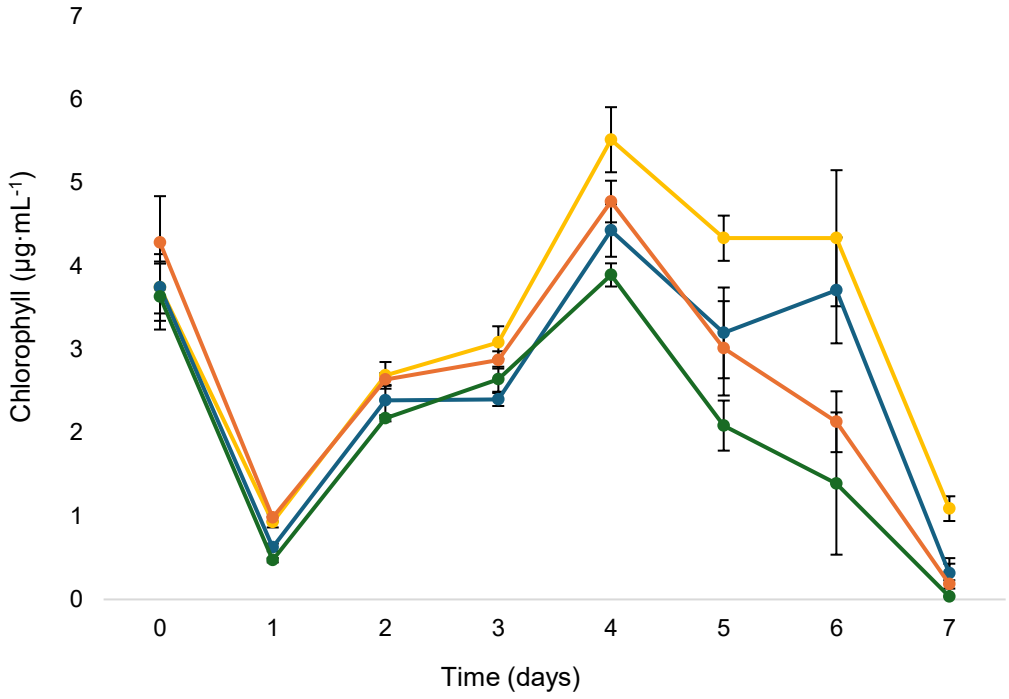


Figure 4.31 | Comparison of chlorophyll concentrations (µg·mL^{-1}) of Syn.1.11 (orange) and Syn.1.19 (green), compared to Syn.*Δhox* (blue) and Syn.GT (yellow) in BG-11NH$_4$ liquid media supplemented with 1.5% CO_2, grown at 300 µmol photons·m^{-2}·sec^{-1}, 30 °C, 150 RPM orbital shaking. (*n* = 6, error bars show standard deviation).

Although no significant differences were observed between the isolates and the Syn.*Δhox* strain immediately following inoculation, Syn.1.11 showed a significantly higher concentration of chlorophyll on days 1, 2, 3 ($p < 0.05$), and a significantly lower concentration on day 6 ($p < 0.05$). Syn.1.19 also exhibited a significantly lower concentration of chlorophyll compared to Syn.*Δhox* on every day following inoculation, except day 3, where it had a significantly higher chlorophyll concentration ($p < 0.05$). Interestingly, this may suggest that Syn.1.11 despite growing significantly ($p < 6.5E-06$) faster than Syn.*Δhox* between days 3 and 4, may have rapidly reduced its photosynthetic apparatus. Measurements were also taken to quantify the chlorophyll concentration based on DCW (**Figure 4.32**). On day 2 of growth, the concentration of chlorophyll was lower as a proportion of mass in Syn.1.19 and decreased by 52% ($p < 0.001$) compared to Syn.*Δhox*. No significant difference was observed during late exponential growth on day 4, however, on day 6 the Syn.1.19 had a slight reduction in chlorophyll content by 13% ±11% ($p < 0.05$).

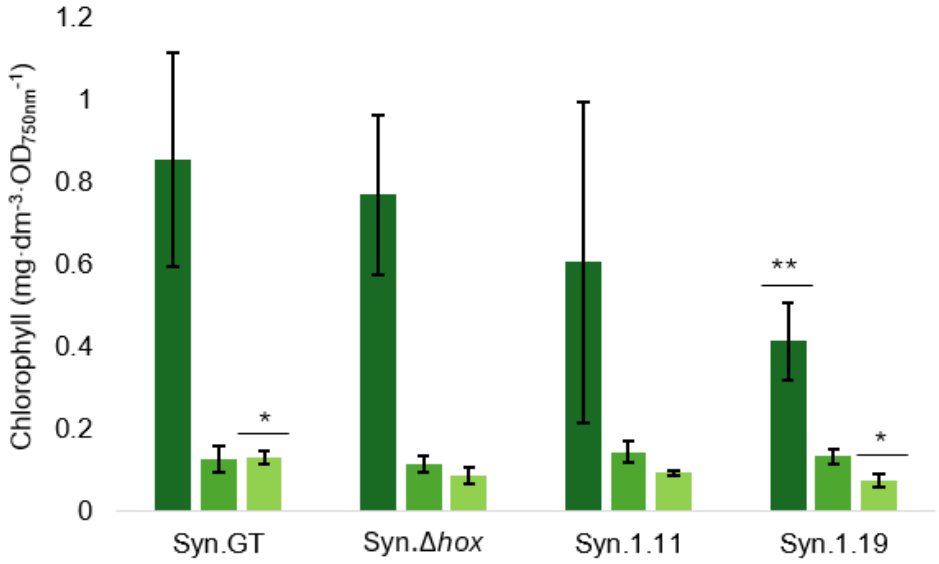


Figure 4.32 | Chlorophyll concentrations in *Synechocystis* strains Syn.GT, Syn.*Δhox*, Syn.1.11, and Syn.1.19 grown at 300 µmol photons·m^{-2}·sec^{-1}, 30 °C, 1.5% CO_2. Left bars shown concentration on day 2, middle bars on day 4, and right bars day 6. Significance is in between the marked value and Syn.*Δhox* strain. (n = 6, *p < 0.05, **p < 0.01, error bars show standard deviation)

The reduction in the concentration of carotenoids per mg of DCW in the isolates mirrored the reductions seen in the chlorophyll (**Figure 4.33**). Syn.1.19 had a 46% ±12% (p < 0.01) reduction in carotenoid pigments compared to Syn.*Δhox* on day 2, and 25% ±19% (p < 0.05) lower on day 6.

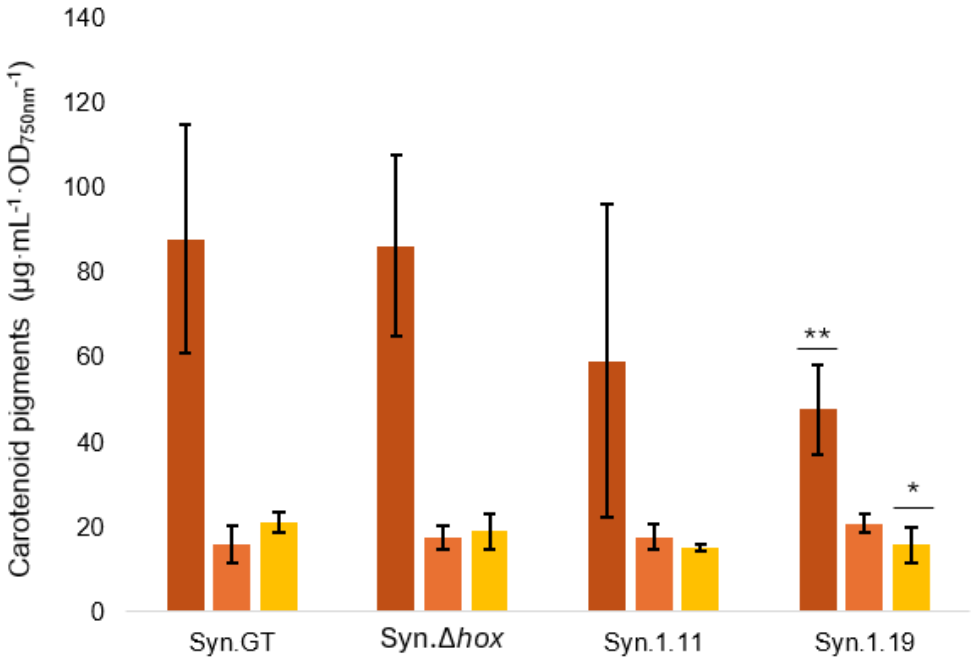


Figure 4.33 | Carotenoid concentrations of *Synechocystis* strains Syn.GT, Syn.*Δhox*, Syn.1.11, and Syn.1.19 grown at 300 µmol photons·m^{-2}·sec^{-1}, 30 °C, 1.5% CO_2. Left bars shown concentration on day 2, middle bars on day 4, and right bars day 6. (n = 6, *p < 0.05, ***p < 0.001, error bars show standard deviation).

The reduction in pigmentation could be advantageous in increasing the growth rate. Hihara *et al*. 2001 demonstrated that during growth on high light genes associated with carbon fixation were upregulated in the cell and the genes associated with the photosynthetic machinery were downregulated [481]. The phenotype in the strains could also be down to alterations in the cell's transcriptomic machinery.

To assess photosynthetic productivity a Clark electrode was utilised. Oxygen evolution rates of the isolates Syn.1.11 and Syn.1.19 were compared to Syn.*Δhox*. Strains were grown to OD_{750nm} ~1, at 300 µmol photons·m^{-2}·sec^{-1}, 30 °C, and standardised to 5 µg·mL^{-1} of chlorophyll. Oxygen evolution of the isolates was measured over 2-minute intervals, from 0 to 932 µmol photons·m^{-2}·sec^{-1}. Syn.1.11 showed a significant increase in oxygen evolution over 127 µmol photons·m^{-2}·sec^{-1} (p < 0.05), and a higher average evolution between intensities of 59 and 331 µmol photons·m^{-2}·sec^{-1} (**Figure 4.34**). Syn.1.11, (although not significant) also showed a 68% decrease in oxygen consumption following no light exposure, potentially indicating that the strain has a lower rate of respiration, or increased concentrations of chlorophyll per cell.

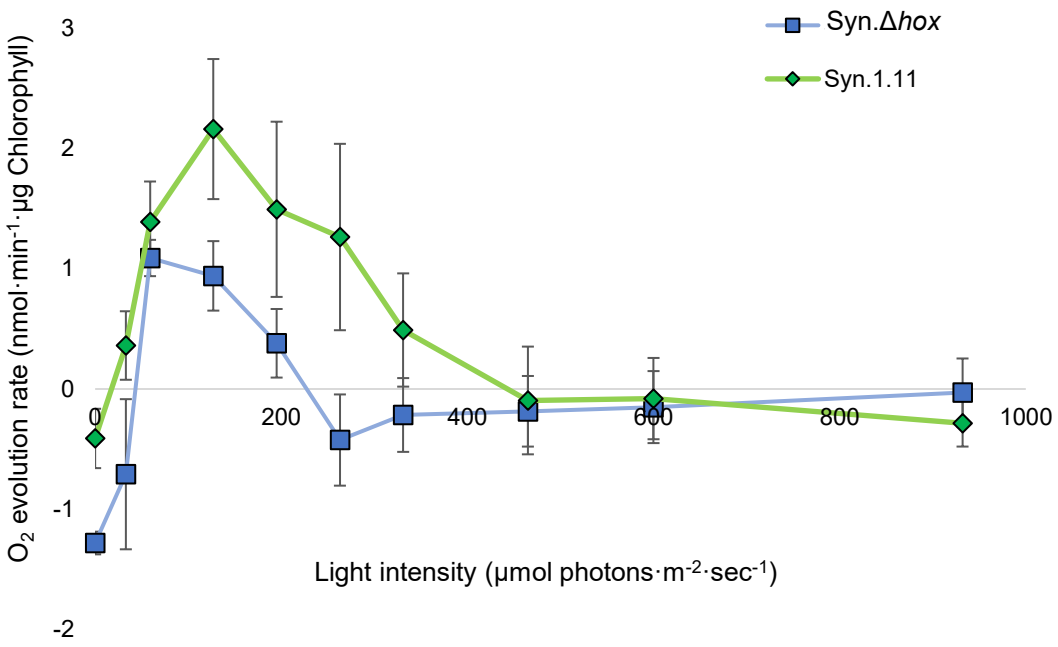


Figure 4.34 | Rates of oxygen evolution in *Synechocystis* sp. PCC 6803 *Δhox* (Syn.*Δhox*), and Syn.1.11 over increasing light intensities at 30 °C measured using a Clark electrode. Cultures were grown in BG-11 and harvested during exponential growth phase (OD_{750nm} = ~1). Data is shown from the mean ± standard error of triplicate independently grown replicates. (*n* = 3).

This reduced rate of respiration was also observed in Syn.1.19, with a 65% lower rate of oxygen consumption during the no light period ($p < 0.01$) (**Figure 4.35**). Syn.1.19 did show a significantly higher rate of oxygen evolution at 59 µmol photons·m^{-2}·sec^{-1} of light, 64% higher than Syn.*Δhox* ($p < 0.05$), however, oxygen evolution was not significantly higher at the other light intensities.

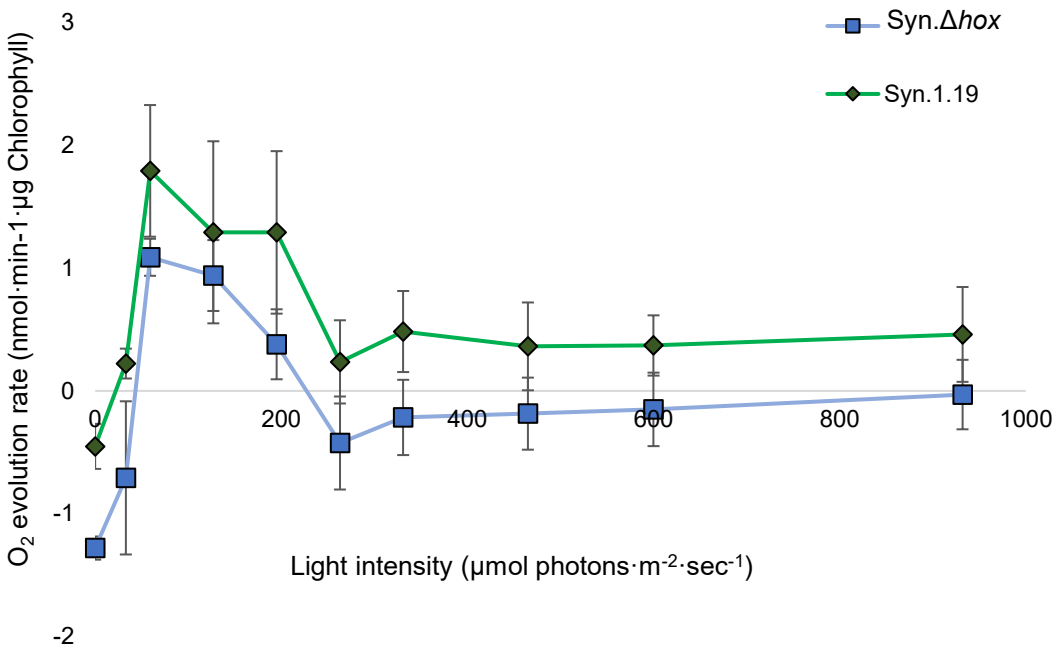


Figure 4.35 | Rates of oxygen evolution in *Synechocystis* sp. PCC 6803 *Δhox* (Syn.*Δhox*), and Syn.1.19 over increasing light intensities at 30 °C measured using a Clark electrode. Cultures were grown in BG-11 and harvested during exponential growth phase (OD_{A750nm} = ~1). Data is shown from the mean ± standard error of triplicate independently grown replicates. (*n* = 3).

These results therefore appear to suggest that both Syn.1.11 and Syn.1.19 are growing as fast as, and at times faster than *Syn.Δhox*, with a reduction in photosynthetic pigmentation per unit of OD_{750nm}. However, the results of the oxygen electrode experiments with standardised chlorophyll concentrations suggest that the photosynthetic apparatus or ratios of photosynthetic proteins is relatively more efficient at evolving oxygen compared to *Syn.Δhox*. Previous work by Lea-Smith et al. 2014 has shown that phycocyanin deletion in *Synechocystis* resulted in a decreased PSI:PSII ratio, and a phenotype with an increased O_2 evolution rate; 41% more O_2 per nmol of chlorophyll under saturating light [482]. A phycocyanin deficient strain (*ΔcpcC1C2*) of *Synechocystis* evolved 21% more O_2 per nmol of chlorophyll in the same study. Although neither Syn.1.11 or Syn.1.19 show variation in the relative abundance of phycocyanin to chlorophyll, a similar decrease in their PSI:PSII ratios may explain how these strains are able to

achieve comparable growth with reduced pigmentation per mg of biomass.

4.6 Genomic and Metabolomic analysis of the best performing *Synechocystis* (Syn.∆*hox*) isolates

4.6.1 *Genotypic characterisation of strain Syn.1.11*

Because of the improved growth rates, and the interesting photosynthetic properties of the isolate Syn.1.11, it was selected for whole genome sequencing. DNA was prepared as previously described in 2.5.1. Sequencing of the progenitor strain, (Syn.*Δhox*) was also carried out to as a reference strain for identifying any genomic variation. Sequencing was performed using a FLO-MIN114 Flow Cell (R10.4.1) and MinION next generation sequencing device (Oxford Nanopore Technologies, United Kingdom). Genome assembly of Syn.*Δhox* was carried out using Geneious™ Prime (v 2024.0), and RefSeq NC_000911 *Synechocystis* sp. PCC 6803 (NCBI) as a genomic scaffold. Sequences of Syn.1.11 were then assembled to the Syn.*Δhox* consensus sequence. Post trimming sequence quality was assessed as 100.0% high quality by the Geneious™ Prime proprietary algorithm.

Regions of low coverage were identified as regions with fewer sequencing reads than ≥ 2 standard deviations from the mean. Variants and polymorphisms were called using the proprietary software's algorithm against the Syn.*Δhox* consensus sequence. In total 2920 variants with non-synonymous predicted changes were detected. Of these, 17 were deletions resulting in frame shifts, 3 were insertions resulting in frame shifts, 2444 were single nucleotide polymorphisms (SNPs) resulting in amino acid substitutions, truncations, or extensions, and 227 were multiple base pair substitutions. Also present were 229 tandem repeat deletions which typically resulted in frame shifts. Of the top 100 SNP, variants with the lowest P-value, 7 resulted in non-synonymous amino acid changes with high confidence. Together with deletions and insertions, these are shown in **Table 4.1**.

Table 4.1 | Top non-synonymous genomic variations between Syn.1.11 and Syn.*Δhox* by combined sequences read confidence (P-value). Annotations transferred from RefSeq NC_000911 *Synechocystis* sp. PCC 6803 (NCBI). (*n* = "Coverage").

SNPs						
Gene	**Coverage**	**Polymorphism Type**	**Protein Effect**	**Variant Frequency**	**Variant P-Value (approximate)**	**Amino Acid / bp Change**
sll1895	243	SNP (transition)	Substitution	95.50%	> 0	P 393 S
glpD	247	SNP (transition)	Substitution	93.10%	> 0	G 253 S
slr0146	222	SNP (transition)	Substitution	93.20%	> 0	L 89 F
lexA	229	SNP (transversion)	Substitution	94.30%	> 0	K 9 I
napA	240	SNP (transversion)	Substitution	95.80%	> 0	A 122 G
acs	252	SNP (transversion)	Substitution	94.40%	> 0	L 56 F
DELETIONS						
sll1905	268	Deletion	Frame Shift	97.40%	6.10E-145	- S 1491
hisB	279	Deletion	Frame Shift	79.20%	7.20E-80	- CCGG 10
gyrA	246	Deletion	Frame Shift	95.10%	4.60E-77	- S 1753
carB	265	Deletion	Frame Shift	91.70%	2.30E-48	- H 1771
sll1643	231	Deletion	Frame Shift	86.10%	4.30E-48	- Y 57
slr0798	240	Deletion	Frame Shift	91.70%	7.30E-44	- C 115
sll0505	223	Deletion	Frame Shift	68.60%	3.10E-42	- K 778
epsB	205	Deletion	Frame Shift	93.70%	3.90E-42	- G 36
clpX	277	Deletion	Frame Shift	86.60%	1.10E-37	- Y 1146
atpG	238	Deletion	Frame Shift	87.80%	6.40E-35	- C 333
amiA	264	Deletion	Frame Shift	85.60%	7.70E-34	- Y 741
menD	236	Deletion	Frame Shift	86.40%	5.80E-32	- Y 1728
fecB	245	Deletion	Frame Shift	63.70%	4.10E-28	YS -> C 358
rpl21	232	Deletion	Frame Shift	84.10%	3.00E-27	- R 334
slr1895	246	Deletion	Frame Shift	82.90%	7.40E-27	- R 430
sll0267	245	Deletion	Frame Shift	82.00%	7.30E-11	- S 1562
sll0550	201	Deletion	Frame Shift	83.60%	1.40E-10	- K 708
INSERTIONS						
sll0069	239	Insertion	Frame Shift	74.90%	4.10E-195	+ G 117
pheA	274	Insertion (tandem repeat)	Frame Shift	65.00%	2.30E-281	+ A 658
sll0142	258	Insertion (tandem repeat)	Frame Shift	62.00%	1.10E-184	+ G 3010

As previously stated in section 2.9.3.1 the error rate of Oxford Nanopore next generation sequencing devices can be as high as ~7-8% of bases called, (though many of these erroneously annotated bases will have been algorithmically excluded during data trimming). The frequency of variants (alleles) outside of this error rate could therefore be an indication of variation within a polyploid genome (see Meirmans et al. 2018) [483].

However, to assess this, the quantification of genome copy number prior to genomic analysis is required [483], which was not carried out here.

The variant with the lowest P-value, gene *sll1895* codes for an uncharacterised protein. Many of the proteins coded for by these genes have been characterised previously and may result in identifiable phenotypes. It is challenging to describe all the mutations given the sheer volume. Those shown above represent mutations identified as different between Syn.1.11 and Syn.*Δhox* with high confidence (lowest P-values of sequenced regions with > 200 sequence coverage), significantly altered protein translations (frame shifts and / or truncations), and where known function correlates to the phenotypes observed.

The *glpD* gene for example, had a SNP changing glycine to serine. This gene codes for the enzyme glycerol-3-phosphate dehydrogenase, a protein responsible for triacylglycerol, and fatty acid synthesis. A *Synechocystis* strain previously engineered to heterologously express the glycerol-3-phosphate dehydrogenase gene was shown to increase the relative lipid concentration by 36% [484].

The *lexA* gene had a SNP converting lysine 9 to isoleucine (K9I). The gene is a global regulator linked to DNA damage repair and the SOS response, but it is also associated with the regulation of genes controlled by inorganic carbon, and it has been shown to be essential for cells under carbon starvation [485]. LexA has also been shown to regulate fatty acid metabolism and the hydrogenase enzyme [485,486]. Furthermore, analysis by Gutekunst *et al*. 2005 previously identified a putative binding side for the global nitrogen metabolism regulator NctA [475]. However, no interaction was seen between the two.

The *slr0798* gene also encodes a significant transcriptional regulator, here RppB [487]. RppB is part of a two-component regulatory system responsible for the synthesis of the PSII and PSI subunits, and photopigment genes [487], acting, therefore, as a global redox regulator within photosynthesis. The *slr0798* gene was shown to be truncated at residue 49 of a predicted 722 sequence, following the deletion of cytosine 115 and a subsequent frameshift mutation. Following deletion of the *rppA* gene, in *Synechocystis*, there was a marked increase in the O_2 evolution rate at 1000 µmol photons·m^{-2}·sec^{-1}, and a faster turnover of degraded D1 proteins. This observation was more pronounced under glucose supplementation [487]. Furthermore, despite a higher abundance of PSII reaction centres, the chlorophyll concentrations were relatively lower in *Synechocystis ΔrppA*, with a higher O_2 evolution rate per mg of chlorophyll

than the WT. Very similar to the phenotype of Syn.1.11 described above in section **4.5.3**.

The *hisB* gene had a deletion of 4 bases at position 10 of the CDS, which led to a frameshift mutation. The *hisB* gene is involved in histidine metabolism and Behle *et al*. 2022 demonstrated that downregulation of this gene led to inhibition of cell division in *Synechocytis* [488].

To help identify possible connections between the mutations identified, putative interactions were visualised using STRING (open access software) protein interaction mapping [419] (**Figure 4.36**). The interaction map suggests that *sll1905* identified as a two-component hybrid regulator and sensor, possibly interacts with 5 other genes *gyrA*, *epsB*, *sll1895*, *sll0267* and *napA*. Suzuki *et al*. 2000 showed that this gene encodes for a histidine kinase, which has been shown to be responsible for initiating low-temperature cellular responses [489].

GyrA is a type II topoisomerase that negatively supercoils closed circular double-stranded DNA, the gene contains a deletion of a C or G at position 1753 of the annotated coding sequence. The *epsB* gene is involved in the synthesis and transportation of EPS [490], cells which are impaired in EPS biosynthesis undergo both transcriptomic and proteomic changes and EPS has been shown to act as a major carbon sink [491]. The gene *sll1895* is an uncharacterised protein, which had a SNP leading to an amino acid substitution of a proline to a serine. Sll0267 is a protein involved in interactions between the cell and the environment and has previously been reported to be differentially expressed under environmental changes, including high light acclimation [492]. The *sll0267* gene codes for a protein containing a GGDEF and EAl domain, which are typical of molecules involved in cyclic diguanylate metabolism. C-di-GMP plays a crucial role in modulating bacterial responses to environmental stimuli. A previous $sll0267_{L1189P}$ mutation was shown to enhance growth under high light conditions [492]. Finally, the *napA* gene has a SNP resulting in a substitution leading to an alanine to glycine switch, the *napA* gene codes for a NapA-type Na^+/H^+ antiporter [493].

A highly significant gene with regards to carbon fixation, which was highlighted as a high confidence mutant, was the *atpG* gene, which has a deletion at cysteine residue 333. The gene codes for the ATP synthase gamma chain and has been shown to be downregulated following inorganic carbon limitation [494]. CarB (carbamoyl-phosphate synthase subunit B) synthesises carbamoyl-phosphate, a necessary precursor for the biosynthesis of nucleotides and arginine [495].

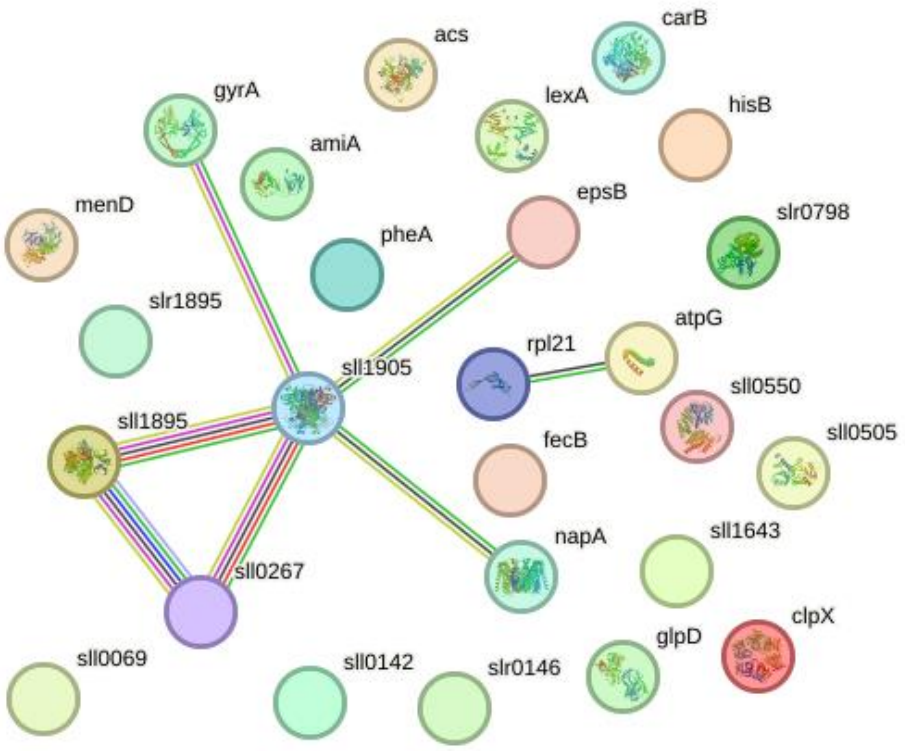


Figure 4.36 | Putative interactions of identified genes with significant variation, (created using STRING v.12)

4.6.2 *Metabolomic characterisation of Syn.1.11 and Syn.1.19*

Samples from Syn.*Δhox*, Syn.GT, Syn.1.11, and Syn.1.19 were taken on days 2, 4, and 6 for metabolomic analysis from cultures grown at 300 µmol photons·m^{-2}·sec^{-1}, 30 °C, 1.5% CO_2 (see **Figure 4.28**). These time points were selected to enable the characterisation of early exponential growth, late exponential growth, and stationary phase growth respectively. Sample optical density readings (OD_{750nm}), (taken separately to assess growth) were used to calculate the volume necessary to remove 2 OD_{750nm} equivalent per mL^{-1}. Metabolomic extractions were then carried out as previously described in **3.6.2**. Following metabolomic extractions, samples were then characterised following the protocol outlined in **3.6.3**. Untargeted metabolomic analysis was performed using CD 3.3 (ThermoFisher Scientific™). Following processing, CD 3.3 results were further analysed using Simca™ P (Sartorius™). A PCA scores plot of the variation between the *Synechocystis* samples was extracted on day 2 as shown in **Figure 4.37**.

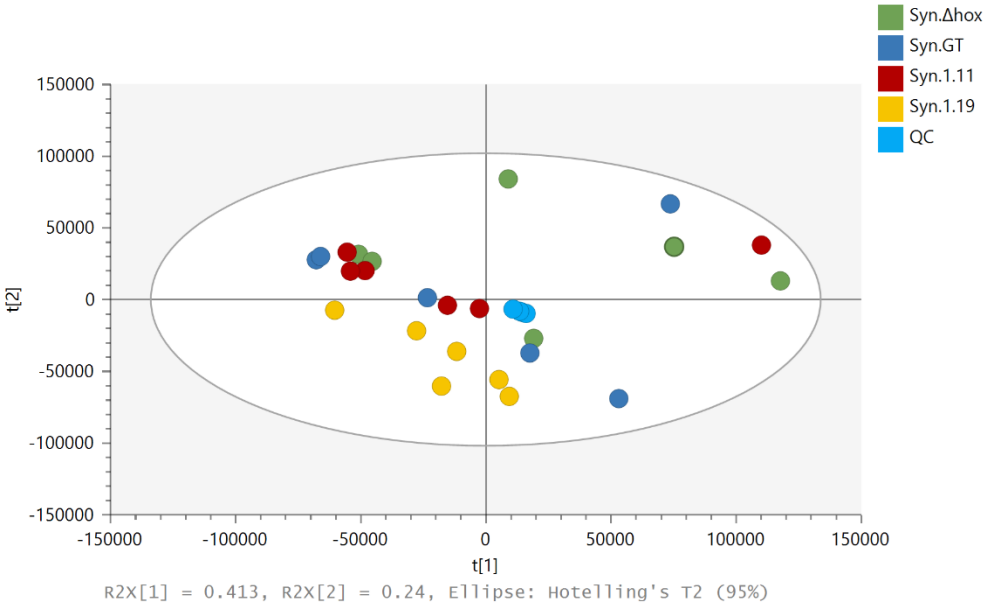


Figure 4.37 | PCA scores plot comparing untargeted metabolomic analyses of Syn.*Δhox* (green), Syn.GT (blue), Syn.1.11 (red), and Syn.1.19 (yellow) grown at 300 µmol photons·m^{-2}·sec^{-1}, 30 °C, 1.5% CO_2 after 2 days of growth. (Four QC samples (light blue); cyanobacteria samples *n* = 6).

The RSD of QC samples was < 30% in > 70% of all peaks, and the **Figure 4.37** PCA QC injections showed tight, consistent clustering. Indicating high instrument stability over repeated injections, and a validated analytical performance for untargeted metabolomics (see Abdelrazig et al. 2020) [420]. Model R^2X (cumulative) = 0.653, indicating that 65.3% of variance within data is captured within principal components shown [496]. The samples from each of the different strains showed both intra- and inter-class separation of metabolite profiles when compared to one another at this time. The relative difference of the selected isolates Syn.1.11 and Syn.1.19 was therefore shown by the first principal component to be limited. Greater variation was shown between Syn.1.19 and other strains during early exponential phase in the second principal component, however, with $R^2X[1]$ intra-class variation. This appears to be largely the result of 1 compound, putatively identified with level 4 confidence. It was hypothesised that this ion (*m/z* = 273.0914, RT = 6.784) could be HEPES, however, the fragmentation pattern neither aligned with *m/z* cloud records, nor did the Fragment Ion Search (FISh) score (39.58) meet the threshold for level 3 identification (see section **3.6.4**), and identification therefore remained inconclusive.

To further assess the differences between the different strains, an OPLS-DA model was generated. The differences between Syn.*Δhox* and Syn.1.11 on day 2 are shown in **Figure 4.38**. Variables with VIP scores > 1 were considered significant within this model (see section **3.6.4**), and a total of 11 variables with a VIP score > 1 were identified from the model. Of these, 5 ions were putatively identified with level 2 confidence (see section **3.6.4**), these were citrulline (VIP = 3.95), glutathione (VIP = 2.17), N-acetyl-lysine (VIP = 1.44), lysine (VIP = 1.23), and trimethyllysine (VIP = 1.18). One ion was identified with level 3 confidence, glutamate (VIP = 1.01), and 5 ions could not be identified (VIP = 3.83, 2.31, 1.88, 1.57, and 1.42).

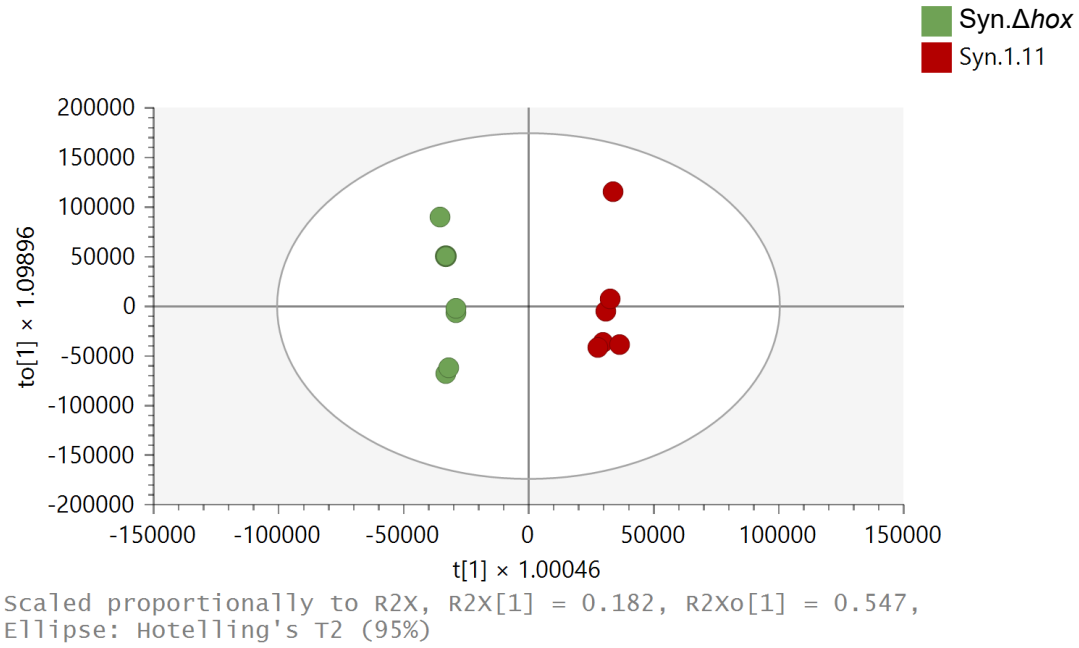


Figure 4.38 | OPLS-DA model comparing the untargeted metabolomic analyses of Syn.*Δhox* (green) and Syn.1.11 (red), grown at 300 µmol photons·m^{-2}·sec^{-1}, 30 °C, 1.5% CO_2 after 2 days of growth. R^2Y = 0.993, Q^2 = 0.96 (*n* = 6).

The model demonstrated robust capture of variation (R^2Y = 0.993) and predictive capability (Q^2 = 0.96) (see section **3.6.4**; Abdelrazig et al. 2020) [420]. To validate this OPLS-DA model, Syn.*Δhox* Q^2 was determined using a permutation test (100 permutations), (**Figure 4.39**). The Q^2 showed a lower regression than R^2Y, with a y intercept of -1.22. Therefore, the model was validated (see section **3.6.4**; Kim et al. 2011) [422]. Permutation analysis of variable Syn.1.11 was also carried out, (**Figure 4.40**), and validated (Q^2 y = -1.37). This was repeated and validated for other OPLS-DA models

generated for days 2 and 4 between each of the different strains (data not shown).

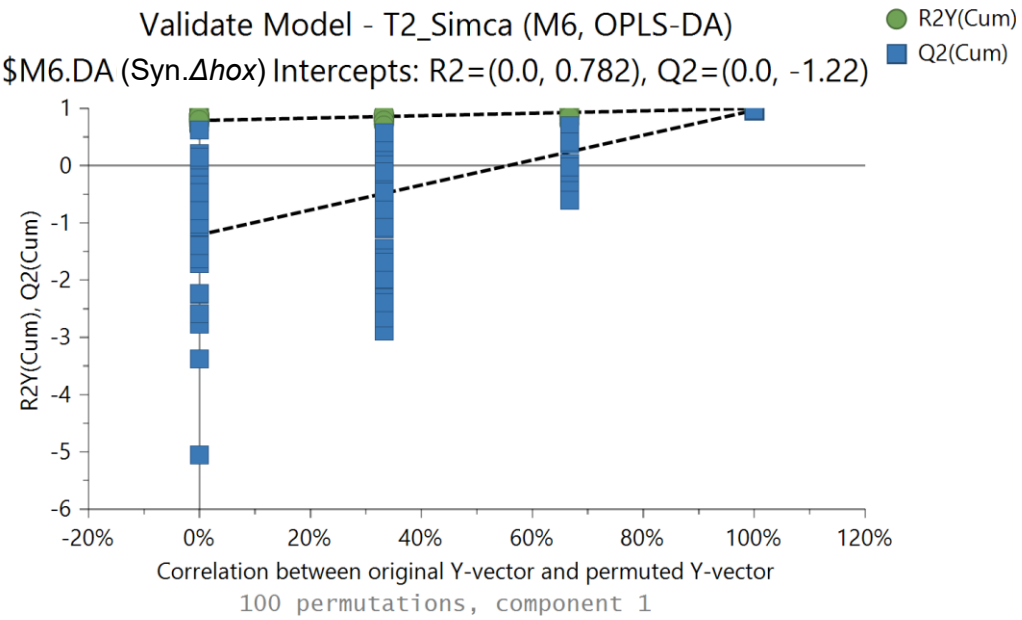


Figure 4.39 | Permutation test of OPLS-DA model Syn.*Δhox* variables comparing the untargeted metabolomic analyses of Syn.*Δhox* and Syn.1.11 grown at 300 µmol photons·m^{-2}·sec^{-1}, 30 °C, 1.5% CO_2 after 2 days of growth. (*n* = 6).

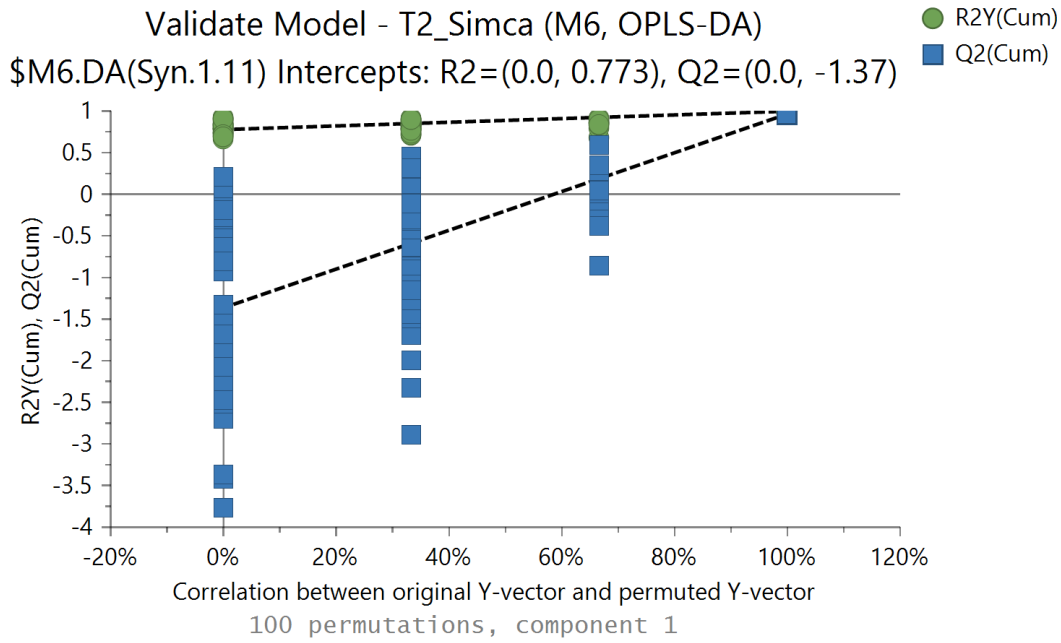


Figure 4.40 | Permutation test of OPLS-DA model Syn.1.11 variables comparing the untargeted metabolomic analyses of Syn.*Δhox* and Syn.1.11 grown at 300 µmol photons·m^{-2}·sec^{-1}, 30 °C, 1.5% CO_2 after 2 days of growth. (*n* = 6).

The differences between the strains on day 4 were also estimated using a PCA model in Simca™ P, shown in **Figure 4.41**. Here, QC samples again indicated high instrument stability, with tight, consistent clustering. The isolate Syn.1.19 again showed the most difference in its metabolic profile compared to the other strains. Syn.GT, Syn.*Δhox* and Syn.1.11 were more similar to one another in their metabolomic profiles, however, there was relatively high variation within the Syn.GT and Syn.1.11 strains. Again, this appears to be due to the influence of the same ion as day 2, shown in **Figure 4.37** (*m/z* = 273.0914, RT = 6.772). Attempts to identify this ion unfortunately remained inconclusive. Separation of the Syn.1.19 samples, however, was due to different variable, putatively identified (level 2) as N-acetyl-ornithine (*m/z* = 175.1070, RT = 8.058). This ion was 7.55 log2-fold higher in Syn.1.19 than the Syn.*Δhox* control.

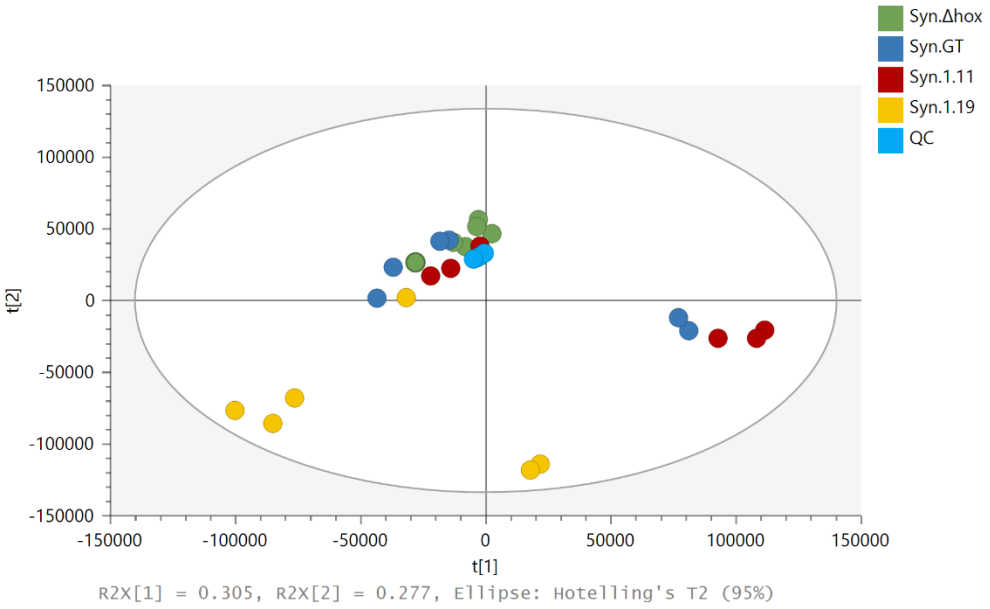


Figure 4.41 | PCA scores comparing untargeted metabolomic analyses of Syn.*Δhox* (green), Syn.GT (blue), Syn.1.11 (red), and Syn.1.19 (yellow) grown at 300 µmol photons·m^{-2}·sec^{-1}, 30 °C, 1.5% CO_2 after 4 days of growth. (Four QC samples (light blue); cyanobacteria samples *n* = 6).

The differences between the strains on day 6 during stationary phase were also estimated using a PCA model in Simca™ P, shown in **Figure 4.42**. Although instrumental consistency was high (indicated by tightly clustered QC sample injections), the relative difference between the strains was shown to be lower than at previous time points. OPLS-DA models between Syn.*Δhox* and the other strains confirmed relatively low variation between the strains at this time point.

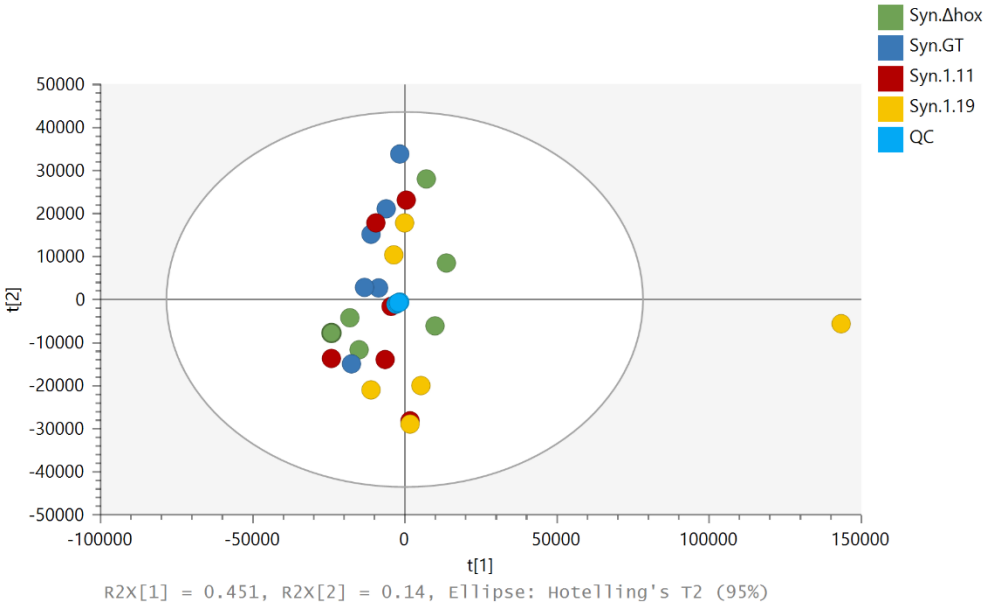


Figure 4.42 | PCA scores comparing untargeted metabolomic analyses of Syn.*Δhox* (green), Syn.GT (blue), Syn.1.11 (red), and Syn.1.19 (yellow) grown at 300 µmol photons·m^{-2}·sec^{-1}, 30 °C, 1.5% CO_2 after 6 days of growth. (Four QC samples (light blue); cyanobacteria samples *n* = 6).

To ensure that samples included are representative, outliers which can disproportionately influence the variation of principal components are typically removed; outliers are identified when their orthogonal coordinates are located outside of the PCA T^2 confidence ellipse (see Cuevas-Delgado et al. 2020) [497]. One outlier sample of isolate Syn.1.19 (indicated by PCA co-ordinates outside the T^2 95% distribution confidence window) was excluded, and a revised PCA model is shown in **Figure 4.43**. Despite removal of the outlier, however, there still appears to be much overlap between the individual classes.

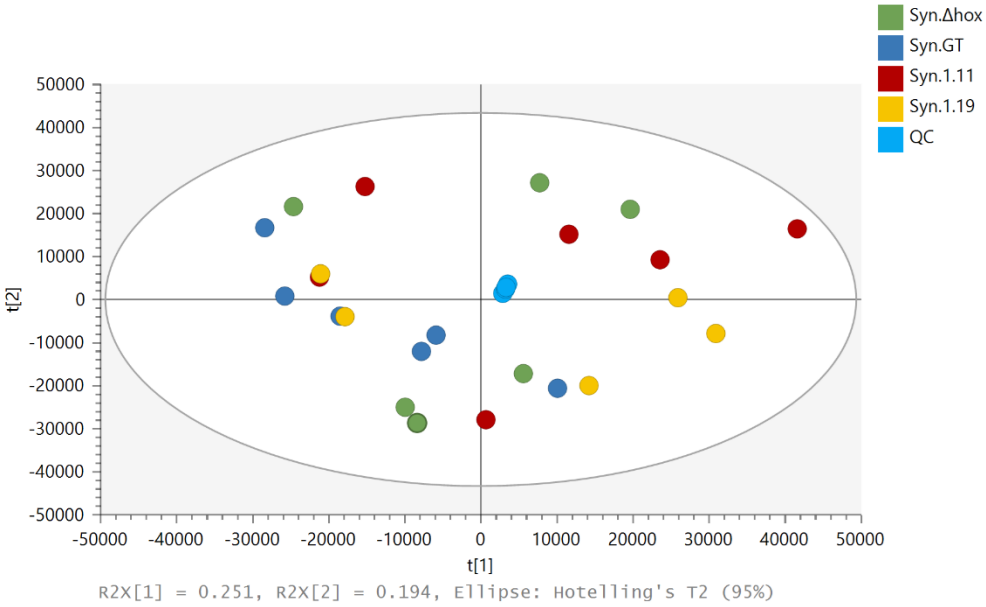


Figure 4.43 | PCA scores comparing untargeted metabolomic analyses of Syn.*Δhox* (green), Syn.GT (blue), Syn.1.11 (red), and Syn.1.19 (yellow) with outlier Syn.1.19 removed, grown at 300 µmol photons·m^{-2}·sec^{-1}, 30 °C, 1.5% CO_2 after 6 days of growth. (Four QC samples (light blue); Syn.*Δhox*, Syn.GT, Syn.1.11 *n* = 6, Syn.1.19 *n* = 5).

Following analysis of the relative differences between the strains, a Simca™ P VIP analysis was carried out using generated OPLS-DA models between Syn.*Δhox*, and the respective isolate classes, and validated using permutation analysis (see **Appendix Figures S3 – S11**). OPLS-DA models generated for stationary phase showed no significant difference between Syn.*Δhox* and the mutant isolates (data not shown). Using a VIP score of ≥ 1, the metabolites identified by the model were referenced to the results from the Compound Discoverer analysis. Metabolites of significant variation from the control were then identified as having a P-value of < 0.05, and a VIP score of ≥ 1. Metabolites identified with level 3 confidence and above from analysis of Syn.1.11 over the 3 time points are shown in **Table 4.2**. Identities are listed based on their putative assignment following analysis with CD 3.3.

Table 4.2 | Significantly different metabolites of Syn.1.11 compared to Syn.*Δhox* from samples grown at 300 µmol photons·m^{-2}·sec^{-1}, 30 °C, 1.5% CO_2, during early exponential, late exponential, and stationary phase. Compounds with mzCloud scores ≥75% and alignment with internal

standards are shown in green. Results with level 3 identification confidence are shown in amber (see **3.6.4**) (*n* = 6).

Putative Identity	Formula	m/z	CD (3.3) P-value	Simca VIP Score	Log2 Fold Change
Early exponential (day 2)					
Citrulline	$C_6H_{13}N_3O_3$	174.0883	2.3E-02	3.95	-1.9
Late exponential (day 4)					
N-Acetyl-aspartate	$C_6H_9NO_5$	174.0407	1.99E-12	1.08	3.93
N-Acetyl-ornithine	$C_7H_{14}N_2O_3$	175.1074	6.43E-05	1.74	4.96
Stationary phase (day 6)					
Unknown	$C_7H_{14}N_2O_3$	132.0369	5.9E-03	1.74	1.16

On day 2, a -1.9 Log2 Fold decrease was seen in citrulline (p < 2.3E-02), a key intermediate of arginine metabolism via ammonium assimilation [498]. In most bacteria, ammonium is assimilated via the glutamine and glutamate cycles [499], however this can also occur via biosynthesis of arginine using glutamate as a precursor. In which two glutamates, an aspartate, and carbamoyl phosphate provide the three nitrogen atoms. Carbamoyl phosphate is synthesized from glutamine, bicarbonate, and ATP [500]. This pathway is regulated by the enzyme N-acetylglutamate kinase (NAGK), itself inhibited by arginine [501]. However, in the presence of a sufficient nitrogen balance, cyanobacteria have been shown to synthesise arginine via the ornithine-ammonia cycle [502,503]. N-acetyl-ornithine is a product of this pathway, showing a 4.96 Log2 Fold increase on day 4 (p < 6.43E-05). This compound is synthesised by *argD* during cyclic ornithine synthesis [500]. N-acetyl-aspartate has previously been shown to be synthesized from TCA cycle derived acetyl-CoA and aspartate in neural mitochondria [504], however, no examples could be found regarding its synthesis in cyanobacteria. N-acetyl-aspartate is deacylated by the aspartoacylase enzyme into aspartate and acetate [505]. Aspartoacylase has putatively been annotated within the *Synechocystis*

genome as *slr1705*, as per a search on KEGG. Previous work has shown that expression of *slr1705* decreased with *nctA* overexpression [506].

A 1.07 Log2-Fold increase in Acetyl-lysine (p < 5.1E-03) was also observed in Syn.1.19 during early exponential growth (**Table 4.3**). Acetylated lysine has previously been shown to be highly enriched within photosynthesis related proteins, including the photosystem II manganese-stabilizing protein [507].

Table 4.3 | Significantly different metabolites of Syn.1.19 compared to Syn.*Δhox* from samples grown at 300 µmol photons·m^{-2}·sec^{-1}, 30 °C, 1.5% CO_2, during early exponential, late exponential, and stationary phase. Compounds with level 2 identity confidence are shown in green. Results with level 3 identification confidence are shown in amber (see **3.6.4**) (n = 6).

Putative Identity	Formula	m/z	CD (3.3) P-value	Simca VIP Score	Log2 Fold Change
Early exponential (day 2)					
Acetyl-lysine	$C_8H_{16}N_2O_3$	187.1088	5.1E-03	2.59	1.07
Late exponential (day 4)					
N-Acetyl-ornithine	$C_7H_{14}N_2O_3$	175.1074	8.9E-08	1.68	7.55
Stationary phase (day 6)					
Unknown	$C_7H_{14}N_2O_3$	132.0369	3.0E-2	1.14	1.16

Relative Log2 Fold changes identified in N-acetyl metabolites, and metabolites within the arginine biosynthesis pathway from day 4 are shown in **Figure 4.43**. Syn.1.19 shows a clear accumulation of acetylated amino acids, as well as a lower abundance of arginine, and acetylated amino acid precursor molecules. The strains vary in how they respond to ammonium uptake, however, the Syn.1.19 metabolite profile seen here, aligns with previous observations by Zhang *et al*. 2018, in which they observed an increased abundance of citrulline, arginine, aspartate, N-acetyl-ornithine, and N-acetyl-glutamate in *Synechocystis* cells after

transition from a low nitrate (2 mM) medium, to a higher nitrate (18 mM) medium [508].

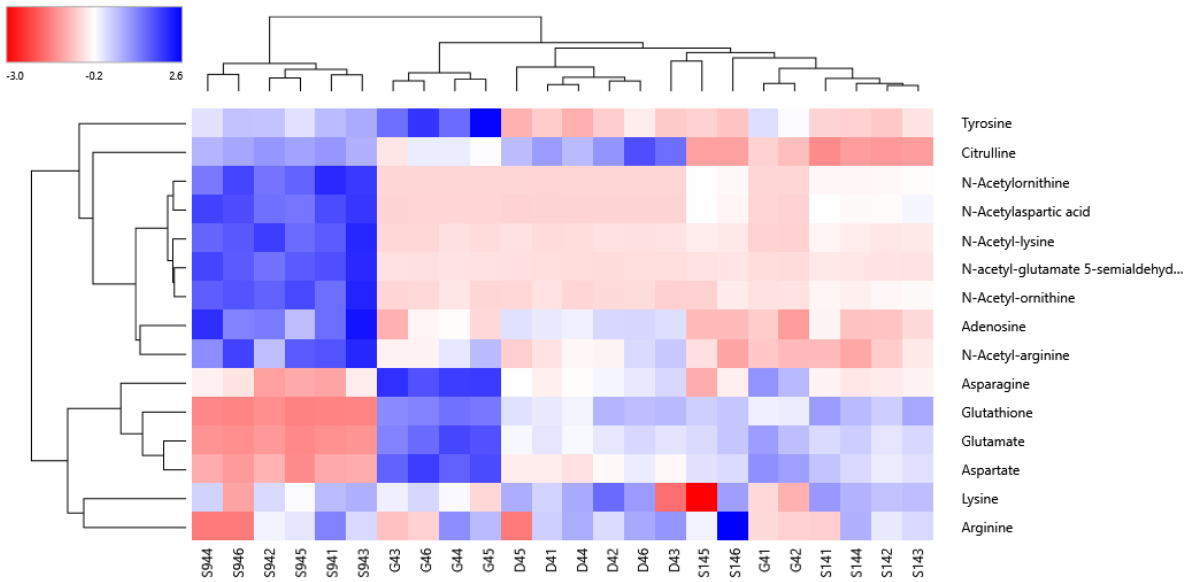


Figure 4.43 | Heatmap showing changes in relative (Log2 Fold) abundance of selected metabolites after 4 days of growth at 300 µmol photons·m^{-2}·sec^{-1}, 30 °C, 1.5% CO_2. Strain files as Syn.GT (G), Syn.*Δhox* (D), Syn.1.11 (S1), and Syn.1.19 (S9).

4.7 Reintegration of *hox* operon into Syn.1.11 and Syn.1.19

To evaluate if the enhanced carbon flux in the strains could be utilised to increase productivity a heterologous construct was designed to re-introduce the *hox* operon back into the chromosome. Cyanobacteria are capable of hydrogen synthesis during photosynthesis via both the nitrogenase and bidirectional hydrogenase enzymes [479,509]. [528529]As the chemostat ALE strains have been selected without a functioning *hox* operon, (and have theoretically become less reliant on the enzyme to manage electron stress), it is unknown if the re-introduction of the operon would result in an increase in hydrogen production. However, complementation of the isolates with a functional hydrogenase would provide useful insight into how related their newly acquired phenotypes are to the specific use of a *Δhox* strain, and how stable adaptations remain with its functionality restored. Therefore, it was selected as a target for heterologous expression.

4.7.1 *pGEM-hox reintegration construct*

A suicide vector was constructed to re-introduce the *hox* operon into the chromosome of both Syn.1.11 and Syn.1.19. The pGEM-T (2996 bp, Promega) vector was selected as the base for the construct design since it cannot replicate in *Synechocystis* and has been utilised extensively in the laboratory to generate knockouts. A knockout cassette was then constructed in the pGEM-T vector, consisting of regions of homology, an antibiotic marker and the *hox* operon. Regions of homology were selected 1926 bp upstream and 1266 bp downstream of the native *hox* operon, enabling the directed integration of the operon into the *hox* region of the chromosome. A 774 bp chloramphenicol acetyltransferase resistance cassette (*cmpR*) was added to allow for selection of the integrated cassette, and finally the *hoxEFUYH* operon (6495 bp) was added (**Figure 4.44**).

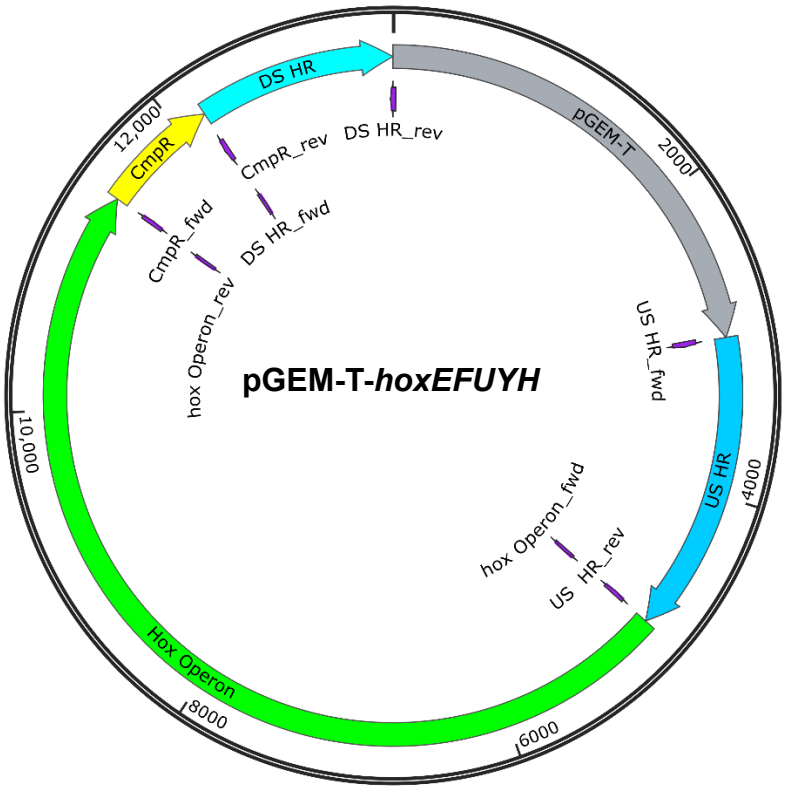


Figure 4.44 | The pGEM-T *hoxEFUYH* integration construct (assembled in SnapGene™).

4.7.2 *pGEM-T hox construct assembly*

The homologous regions were amplified utilising gDNA previously extracted from *Synechocystis* sp. PCC 6803 GT. To amplify the upstream homology region the primers US_HR_fwd (5'-gccatggccgcgggatatcacggggactgttccccagt-3') and US_HR_rev (5'-caacggtcatcaacgagacttgacgtccg-3') were used. To amplify the downstream homology region the primers DS_HR_fwd (5'-aaatagttaaggagtggaaggtaattgag-3') and DS_HR_rev (5'-tcgacctgcaggcggccgcaaatttaatcggagcaggag-3') were used. These were amplified using Q5 DNA polymerase (New England Biolabs) (**Figure 4.45 A**).

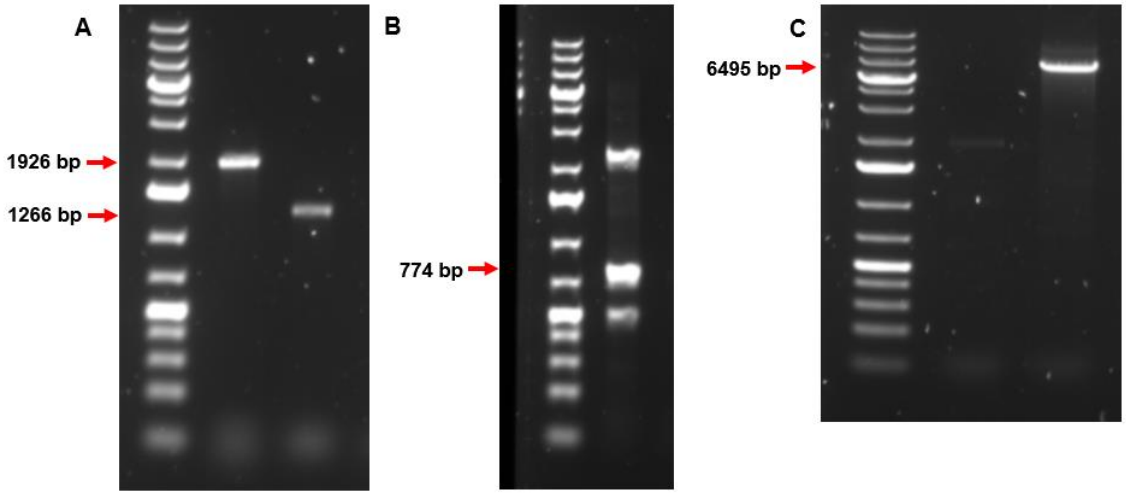


Figure 4.45 | Assembly of pGEM-T *hox*. DNA marker Gene Ruler 1 kb plus (Fisher Scientific™) **A.** Amplification of upstream and downstream regions. **B.** Amplification of *cmpR*. **C.** Amplification of *hoxEFUYH* operon.

Following amplification of the *cmpR* gene cassette using primers CmpR_fwd (5'- gcgggattaagctagcataaaaataagaagc-3') and CmpR_rev (5'- cttccactccttaactatttatcaattcctgcaattc-3') (**Figure 4.45 B**), the *hoxEFUYH* operon was amplified with the primers *hox*_Operon_fwd (5'-agtctcgttgatgaccgttgccaccgatc-3') and *hox*_Operon_rev (5'-ttatgctagcttaatcccgctggatggac-3') (**Figure 4.45 C**). The *hox* operon was amplified from Syn.GT gDNA. Bands were excised from the gel and the DNA was extracted utilising the QIAquick Gel Extraction Kit (Qiagen) according to the manufacturer's instructions. The pGEM-T vector was digested with

the BcuI fast digest enzyme to linearise the vector, the band was excised from the gel and extracted as above. The five bands were then assembled into a 5 fragment HiFi reaction for 90 minutes. Following assembly, the construct was transformed into *E. coli* by heat shock transformation.

Following selection, 8 colonies were obtained and screened via cPCR utilising the primers Hox Operon_fwd, and Hox Operon_rev. One single transformant was identified, which had all the fragments present, and was correctly assembled. The plasmid was purified via DNA miniprep (New England Biolabs). The plasmid was then sent for full plasmid sequencing by Source Bioscience (Nottingham, United Kingdom) as per the organisation's instructions. Full sequence results were received and aligned with the expected sequence (see **Figure S12** in **Appendix**), and the individual *hox* genes were aligned using BLASTn (NCBI) (see **Figures S13 – 17** in **Appendix**). Following confirmation that the construct had been correctly assembled, several attempts were made to transform the construct into Syn.*Δhox*, Syn.1.11, and Syn.1.19 using natural and electroporation transformation strategies. However, this was not successful, and due to time constrains could not be completed.

4.8 Discussion

In **Chapter 4**, an effective ALE pipeline was developed using a chemostat based approach to select for cells with an increased flux towards carbon fixation.

The initial strategy utilised was based on serial dilution, which has been previously utilised to select for faster growing microalgae and cyanobacterial strains with improved productivity. For example, 8400 h of culturing and 100 serial passages was used to evolve a *S. elongatus* sp. PCC 11801 to tolerate 5 $g \cdot L^{-1}$ *n*-butanol and 30 $g \cdot L^{-1}$ 2,3-butanediol [467]. In *Trichomonas variabilis* increases in cell size of more than 30-fold were seen after 45 cycles of selection [364]. Serial transfer relies on the transfer of an aliquot of the culture to fresh medium at regular intervals, to promote additional rounds of growth [201]. The LTEE of *E. coli* being the most famous and most well characterised, this approach has also been utilised to evolve communities. For example, the ALE of communities composed of *Lactobacillus plantarum* and an engineered auxotrophic strain of *Saccharomyces cerevisiae*, the *L. plantaris* strain secreted vitamins required by the *S. cerevisiae* strain and the yeast strain secreted amino acids essential for *L. planetarium* [510]. While serial transfer is easy to

automate and can be conducted in a high throughput manner, it is not applicable to cells which are prone to aggregating. The bigger disadvantage though being the selection pressure, given the need to passage the cells, growth is inherently discontinuous and therefore the ability to control the selective pressure is limited [200].

Continuous culturing is often favoured as the best approach to drive selection in the ALE process, the advantages are clear, selection pressure is constant, without the need to remove cells and passage into new media [200]. The growth rate, population density, nutrient supply, pH, and gas concentration can also be controlled and kept constant. However, there are disadvantages, including the ability to perform replicates in parallel due to the costs of the reactors, cells can also adapt and often avoid being washed out by forming biofilms [200]. In this case the serial transfer was less effective than the continuous strategy over the same time (84 days).

The utilisation of 0.02% CO_2 for the serial dilution ALE was not an effective strategy to select for cyanobacteria with increased biomass formation and furthermore, did not appear to select for strains with improved carbon fixation efficiency either. The initial assumption was that limiting CO_2 may drive the cells to work harder to fix the carbon, given its limited availability. However, it seemed to have had the opposite effect with the cells simply adapting to low CO_2 levels rather than evolving to fix more carbon. The chemostat selection of *Synechocystis* with 5% CO_2 generated cell populations with multiple phenotypes, including increased biomass formation. This phenotype was also probably linked to the utilisation of the *hox* strain, selected to try and engineer a background in which the cell needs to use carbon fixation to sink excess electrons.

ALE selection with the *Synechocystis Δhox* mutant generated strains with both significantly enhanced biomass formation, and increased growth rates. 93.2% of the isolates recovered from the ALE experiment showed a higher average biomass accumulation under atmospheric CO_2 concentrations. The lower concentrations of CO_2 were initially selected to evaluate the efficiency of carbon fixation, the expectation being that cells would be able to grow efficiently at ambient, 1.5% and 5% CO_2. Here, ALE was shown to be a highly effective strategy to select for increased carbon fixation within *Synechocystis* sp. PCC 6803 (**Objective 1**). Specifically, however, when coupled with chemostat selection, and strategies to direct electron stress towards carbon fixation.

The best performing strains had a reduction in their pigmentation per g of DCW during early exponential growth. This was significantly lower in Syn.1.19, with a 52% reduction in chlorophyll and a 46% reduction in

carotenoids. However, the OD_{750nm} of the Syn.1.19 strain was 38% ±28% higher at this point ($p < 0.005$), demonstrating that despite the reduction in pigmentation, the cells were still able to maintain a higher growth rate. Reduced pigmentation would suggest there are fewer reaction centres in the cell, however while not undetermined if this is specifically due to a reduction in PSI or PSII, given higher concentration of chlorophyll in PSI and lower concentration of chlorophyll per unit of OD_{750nm}, this could indicate a higher ratio of PSII to PSI within the mutants. Alternatively, it could also result from a reduction in the number of thylakoid membranes.

Furthermore, following standardisation of the chlorophyll concentration, both strains showed slightly higher rates of oxygen evolution when compared to the progenitor strain at this phase of growth. The rate was 2.3-fold higher in Syn.1.11 at 331 µmol photons·m^{-2}·sec^{-1} ($p < 0.05$). This would suggest that the strains have more efficient photosynthetic apparatus for light intensities which they were selected under (~300 µmol photons·m^{-2}·sec^{-1}). Particularly in structure or relative abundance of PSII, given the increase in rate of oxygen evolution. However, there is no difference between the mutant and the parent strain at higher light intensities (> ~400 µmol photons·m^{-2}·sec^{-1}).

Comparison of the genomic differences between the two strains Syn.1.11 and Syn.*Δhox* showed 2920 variants within the annotated coding regions, including in the *acs* gene, which codes for the acetyl-CoA synthetase, and which has previously been altered in faster growing ALE strains [511]. At this stage it is not clear if the deletions, insertions, and SNPs render the genes inactive; transcriptomic analysis is necessary to assess the impacts of mutations of gene expression. Mutations were also found in the both the ATP synthase and chorismate mutase proteins which have previously been identified in *Synechococcus elongatus* UTEX 2973 [192], a strain that also shows rapid growth immediately following inoculation.

Mutations were also identified in the *rppB* gene, which codes for one half of a two-component master regulator system, which regulates the stoichiometries of PSII, PSI, and photopigment gene expression [487]. The RppB regulator plays a significant role in the control of PQ redox poise in *Synechocystis* [487], and therefore plays a key role in enabling the cells to regulate light induced electron stress. Previous work has shown that both RppB and LexA bind to the regulatory domains of Fd under reducing conditions [512], indicating that these proteins may have possible roles in regulating the redox state of the thylakoid, using reduced / oxidised Fd as the signal [512]. The RppA-RppB two component system has also been shown

to be involved in nickel sensing, and the expression of nickel, cobalt, and zinc resistance genes [513].

Metabolomic analysis of the strains showed that although the overall differences between the populations was not large, there was a significant variation within the abundance of acetylated amino acids, and metabolites involved in arginine biosynthesis. Particularly between Syn.1.19 and the other strains. Previous work has shown that these metabolites are synthesised during ammonia uptake, and arginine biosynthesis [498,500,508]. Given the abundance of these metabolites within Syn.1.19, this may suggest that the ornithine–ammonia cycle plays a role in this adaptation. Acetylation is also one of the mechanisms utilised for post transcriptional modification (PTMs), along with phosphorylation and acetylation, which together comprise more than 90% (~827,000 sites out of ~908,000) of all the reported PTMs. N-lysine acetylation is a reversible yet highly dynamic post-translational modification, previous studies have shown that it plays a key role in carbon metabolism and photosynthesis in *Synehcocystis* [514]. It has also been shown to play a role in the negative regulation of oxygen evolution in *Synechococcus* sp. PCC 7002 [507]. Given the increase in acetylated amino acids in the cell it would be interesting to analyse the acetyl proteome. Recently Jia *et al*. 2023 identified a Gcn5-related N-acetyltransferase (cGNAT2) in *Synechococcus* sp. PCC 7002 [515]. A knockout in this gene resulted in a reduction in both growth capacity and photosynthetic activity, demonstrating that cGNAT2 mediates both growth and photosynthesis through the acetylation of more than 500 lysines, which also includes the K89 of the NdhJ, part of the NDH-1 complex [516].

The data presented both identifies and helps to understand how the differences between the evolved strains and the progenitor strain have enabled the *Synechocystis* isolates to grow faster (**Objective 3**).

Unfortunately, due to time constrains, I was not able to assess if this increased carbon flux could be diverted towards producing more product in the cell. Although a construct was assembled to re-introduce the *hox* operon back into the cell, it couldn't be transformed into the strains (**Objective 4**). Therefore, this could form part of the future work, and it would be interesting to see if hydrogen productivity could be increased in these cells.

Chapter 5.

Adaptive laboratory evolution to enhance nitrogen fixation

5.1 Experimental design

To evaluate the ALE process developed in Chapter 4 and its efficacy in generating evolved strains with improved phenotypes, the chemostat selection process was evaluated using the filamentous and nitrogen fixing bacteria, *Trichormus variabilis*. The goal being to try and improve nitrogen fixation in this strain.

5.1.1 *Identifying strategies to select for enhanced nitrogen fixation*

The flux of electrons towards nitrogen fixation within filamentous cyanobacteria, is primarily derived from the same photolysis reaction of PSII that drives carbon fixation [145]. This source of electrons for nitrogen fixation is from carbohydrates originating from photosynthetic carbon fixation, transported from the filament's vegetative cells, into the heterocysts. These carbohydrates are then used to generate NADPH via the pentose phosphate pathway, an important electron donor that is a source of electrons for the nitrogenase enzyme [144,517] (see **Figure 5.1**). These electrons are transferred from NADPH to the nitrogenase via a heterocyst specific ferredoxin (FdxH) [518], catalysed in a reaction with another heterocyst specific enzyme isomer – here, a truncated non-membrane bound FNR [145,519].

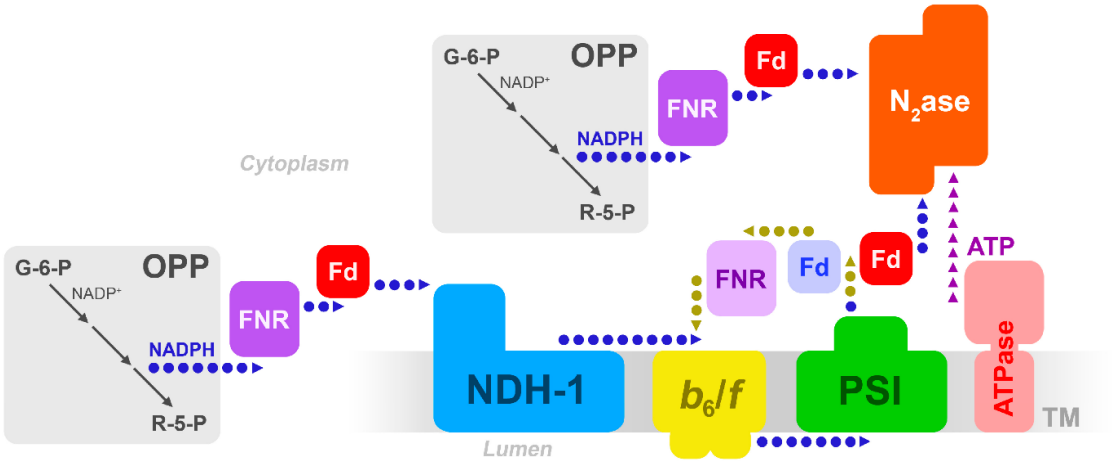


Figure 5.1 | Simplified schematic of possible electron flow to the nitrogenase within a cyanobacteria heterocyst (taken from Magnuson 2019, originally adapted from Magnuson and Cardona 2016) [145,520].

Furthermore, the demanding ATP synthesis for the nitrogenase reaction is provided by abundant PSI complexes, which drive light-induced cyclic electron transport via NADH dehydrogenase (NDH-1) and the cyt b_6f complex [145]. Generation of ATP occurs within the heterocyst thylakoids from electrons transferred via the pentose phosphate pathway [520]. Although primarily through light mediated ETC reactions and not via respiration (see Magnuson 2019) [145]. A proton gradient, generated by this cyclic electron, flow is then used to provide proton motive force for ATP synthesis [145]. Therefore, one approach to encourage more nitrogen fixation in the cells could involve the utilisation of an organic carbon source in the selection media. The addition of an organic carbon source such as fructose would ensure that access to chemical energy for nitrogenase reactions was not limiting, could encourage the cells to use this route as a solution to light induced electron stress.

As discussed previously, there are several electron sinks which cells can use to mitigate excess electrons (see **Figure 4.14**). Electron sinks such as GlsF and Hox could be useful here. When ammonia is generated through nitrogen fixation, it is converted into glutamine [144], the cell could also potentially use this as an electron sink to support the fixation of nitrogen. Furthermore, the generation of protons is also essential for the conversion of dinitrogen gas to ammonia.

5.1.2 *Strategy overview*

The chemostat system in **4.4**, was evaluated in the selection of *Trichormus variabilis* strains. As filamentous cyanobacteria use carbon fixation as a source of energy to supply the fixing of nitrogen, a fixed organic carbon source was added to the BG-11_0 selection media, (20mM of fructose). Fructose was selected as this feeds directly into the pentose phosphate pathway for NADPH synthesis [521], *Trichormus varabilis* can grow on this sugar, and mixotrophic growth with fructose has previously shown an increase in both PSI and nitrogenase activity [522]. Both potentially useful characteristics for increasing nitrogen fixation efficiency within the cells. When coupled with high light stress, BG-11_0A, should encourage the cells to seek an alternative route to sink excess electrons. One potential concern had been that strains placed into the chemostat environment could be uniform in their initial phenotypes.

Previous chemical mutagenesis of *Trichormus variabilis* demonstrated that outgrowth medium can impact the range of mutants generated [523]. Selecting for 5′-fluorocytosine resistance in *Trichormus variabilis*, Chapman and Meeks, 1987 observed that 6 days of growth in a medium with a pH of 6 generated 8.7-fold more resistant mutants than cells cultured at pH 5, and 4.1-fold more resistant mutants than outgrowth in a pH 7 medium [523]. This highlights the importance of both outgrowth medium choice in an ALE experiment, however, also suggests that by using a range of outgrowth media, this could affect the variation within populations prior to selection. With changes to medium components creating initial asymmetric selective pressures, which could result in diversification of the combined population's preferred adaptation strategies. To further increase the phenotypic diversity in the chemostat, and as an alternative strategy to multiple mutagenesis reactions, multiple seed libraries were utilised. Six media compositions were rationally selected as follows:

1. BG-11_0 media: nitrogen-limited media, with minimal selection pressure.

2. BG-11_0A media: supplementation with 20 mM fructose to provide a fixed carbon source to direct electrons towards nitrogen fixation.

3. BG-11_0A + 1.955 mg·L^{-1} $NaMoO_4 \cdot 2H_2O$: added to provide additional co-factor for the nitrogenase enzyme.

4. BG-11_0A + 1mM $NiO_4S \cdot 6H_2O$: added to provide additional co-factor for the hydrogenase, to potentially encourage changes in relative hydrogenase and H_2 abundance within the heterocyst.

5. BG-11_0A made with tap water (NG7 5RD): to provide small additional quantities of nutrients, and potentially vanadium (*Trichormus variabilis* possesses a less used vanadium co-factor nitrogenase). [132]

6. All iterations of BG-11_0A combined.

5.2 Mutagenesis of *Trichormus variabilis*

Prior to mutagenesis, a single colony of *Trichormus variabilis* was selected and used as the progenitor strain for future mutagenesis, ("Ava.WT"). Due to the formation of aggregated clusters of cells by Ava.WT, UV mutagenesis was not performed to mitigate the abundance of non-mutagenised cells within the population library. Mutagenesis was carried out using only chemical mutagens, in this case EMS. (see **Figure 5.2**).

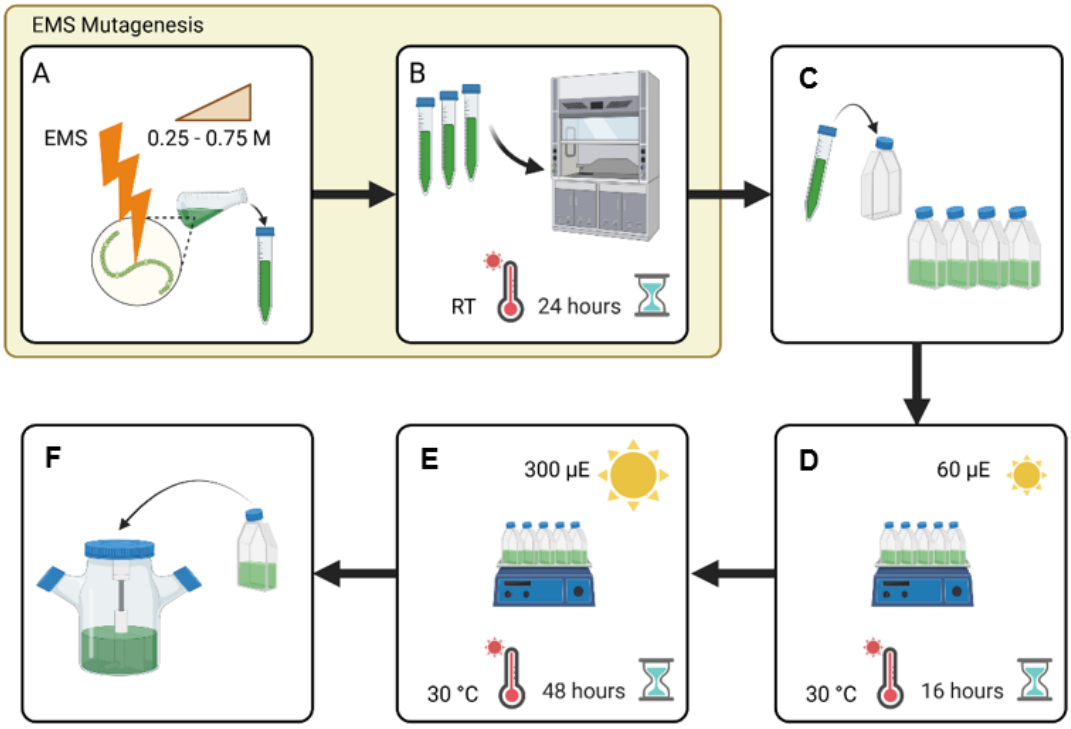


Figure 5.2 | Workflow for the combined physical and chemical mutagenesis strategy to generate a diverse population library. **A – B.** *Trichormus variabilis* (Ava.WT) progenitor strain subjected to chemical mutagenesis. **C.** Mutant libraries seed cultures prepared. **D.** Outgrowth of mutant libraries at 60 µmol photons·m^{-2}·sec^{-1}, 30 °C for ~16 hours. **E.** Acclimatization of mutant libraries 300 µmol photons·m^{-2}·sec^{-1}, 30 °C for 48 hours. **F.** Inoculation of mutant libraries into chemostat selective environment for selection. (Created with BioRender.com).

5.2.1 *EMS mutagenesis in Trichormus variabilis*

To evaluate the impact of EMS upon cell viability a kill curve was generated, where the CFUs of cells processed, (but not mutagenized) were used as a benchmark, from which relative cell viability was calculated. Cultures were treated with 3 concentrations of EMS (0.25 M, 0.5 M, and 0.75 M) previously optimised for *Synechocystis* (**Figure 5.3**).

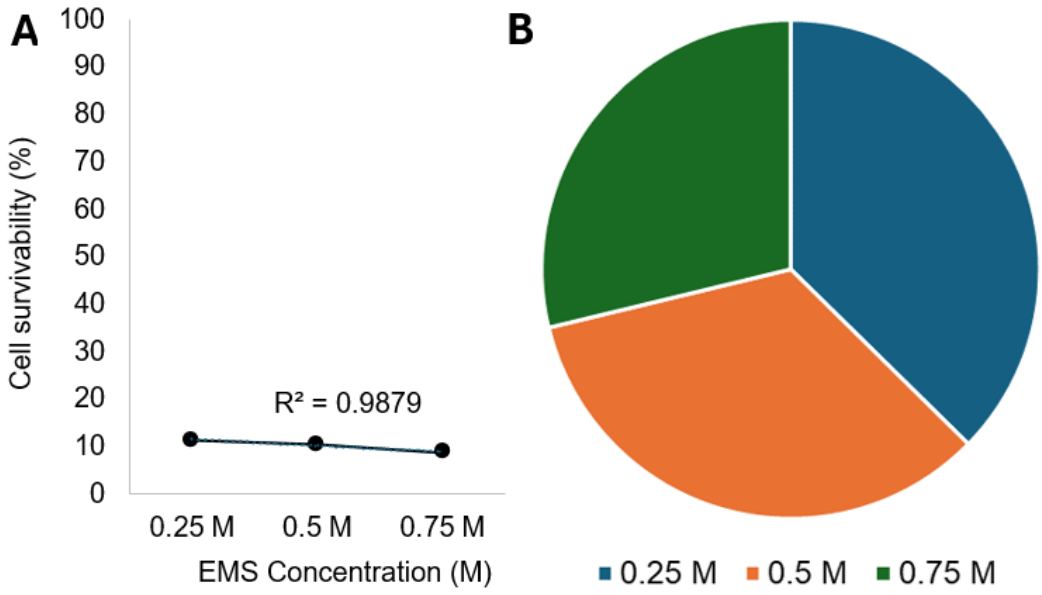


Figure 5.3 | **A.** Kill curve assessing *Trichormus variabilis* cell viability (%) following ethyl methanesulphonate (EMS) treatment. Populations were compared to cells processed without EMS, with linear best fit line y = -1.3126x + 12.802 (R^2 = 0.9879). (*n* = 3, error bars show standard deviation). **B.** Proportion of combined viable populations from each EMS treatment.

Compared to the control plates, the viable cell count decreased by 88.3 – 91.1% from the lowest concentration of EMS to the highest. This decrease in cell viability showed a strong correlation with a linear fit (R^2 = 0.9879) across the concentration range investigated (**Figure 5.3 A**). Compared to the EMS treatment of the *Synechocystis* cells, the remaining total viable cell count from *Trichormus variabilis* was significantly lower, suggesting greater sensitivity of *Trichormus variabilis* to EMS mutagenesis. However, due to the lengthy nature of ALE experiments and limited time available, it was deemed necessary to proceed without first optimising

chemical mutagen dosage. Furthermore, precedent exists for successful ALE selections using highly mutagenized populations. Using a 99% kill rate with chemical alkylating agent MNNG, Bennett et al. 2021 selected for strains of engineered *E. coli* with enhanced methanol substrate utilisation, isolating mutants with > 50% increases in μ_{max} and biomass yield [268]. Selection of photoautotrophic *Chlamydomonas reinhardtii* ALE mutants, with 31% ±20.2% faster growth rates, was performed following a 90% kill rate [279], (the same kill rate used in this experiment).

Therefore, previously optimised EMS concentrations were used for consistency, and the potential impact of a smaller (but more mutagenized) population was noted. Of the total surviving population from all the EMS treatments, 38%, 34%, and 29% of the viable cells were from the 0.25M, 0.5M, and 0.75M treatments respectively (**Figure 5.3 B**). By combining the cells from each of the EMS treatments, the genetic diversity in the overall mutagenised population can be relatively evenly distributed across all 3 treatments. Following mutagenesis of the Ava.WT strain, strains derived from this EMS treatment process were labelled as "Ava.A.[isolate number]".

5.3 Chemostat ALE of *Trichormus variabilis*

5.3.1 *Trichormus variabilis strain selection*

Following EMS mutagenesis, seed culture libraries were added to the Chemostat, and the dilution rate was originally set to 0.04 mL·min^{-1}. Growth was monitored by measuring OD_{750nm}. This was measured ca. every 24 – 48 hours. This strategy was developed to select organisms with the fastest growth rates; the dilution rate was calibrated to constantly maintain a sustained pressure upon the population. This means that cells which are unable to maintain a faster growth rate are washed out of the chemostat as the dilution rate increases. The dilution rate was steadily increased until the cells reached a point where the μ_{max} had been achieved, as determined by OD_{750nm} values. Reaching a maximum dilution rate of 0.28 mL·min^{-1} (therefore $\mu < 0.28$ h^{-1}), and a turnover of 403.2 mL of media every 24 hours. This dilution rate was maintained, and culture density slowly decreased. Once the OD_{750nm} 0.01 was reached, the selection was considered completed and subjected to screening to evaluate the individual strains.

5.3.2 *Isolation of individual Trichormus variabilis strains*

Obtaining single colonies of *Trichormus variabilis* from the chemostat was initially challenging, as when the culture was plated it tended to form either indistinct colonies or biomass mats. This was not an issue that had previously arisen during initial growth utilising the wildtype progenitor strain *Trichormus variabilis* ATCC 29413 (dubbed "Ava.WT"), or during the mutagenesis optimisation work. Therefore, a new strategy (**Figure 5.4**) was developed based on previous work using "bath cavitation" to fragment filaments (see Levine and Thiel 1987) [359,524].

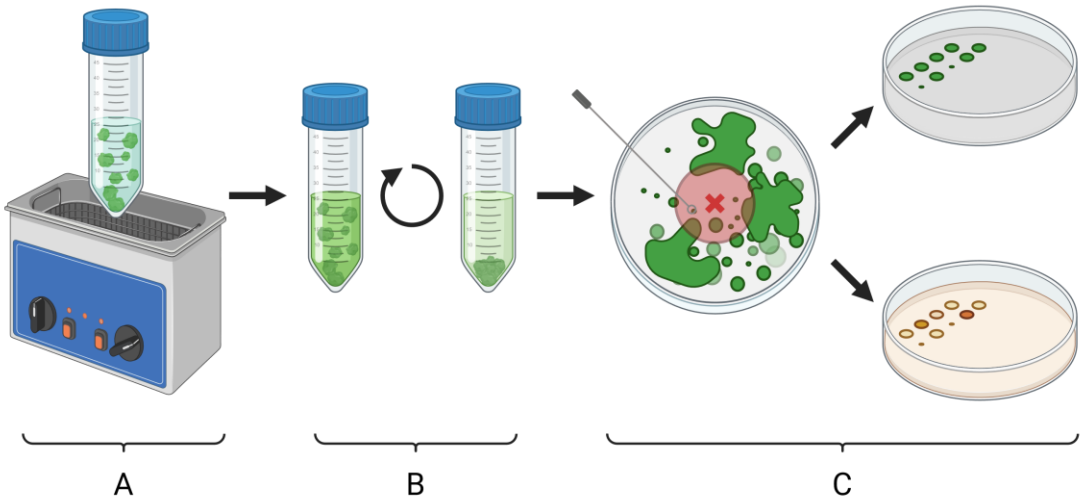


Figure 5.4 | Single colony plating strategy used to isolate individual *Trichormus variabilis* (Ava.WT) chemostat mutants. **A**) aliquots of chemostat cells in 50 mL centrifuge tubes were sonicated at 40 kHz for ≤ 10 seconds 3 – 5 times using a D-Series Ultrasonic Cleaner (GT Sonic). **B**) sonicated spent media aliquots were centrifuged at 1000 g for ≤ 5 seconds until remaining filaments contained ≤ 7 cells. **C**) 100 µL of the top of centrifuged spent media samples were plated onto BG-11_0 solid media via serial dilution. BG-11_0 plates were incubated at 300 µmol photons·m^{-2}·sec^{-1}, 30 °C for ~7-10 days. Once individual colonies appeared these were

isolated onto separate plates of BG-11_0 solid media, with companion plating on LB solid media. (Created with BioRender.com).

The cell sample from the chemostat was initially sonicated 3 – 5 times for $\leq$ 10 seconds to break up the long filaments and reduce culture clumping (**Figure 5.4 A**). Care was taken to ensure the cells were not excessively treated, as ultrasonic treatment can inhibit growth of cyanobacterial cells by damaging the photosynthetic antenna complexes [525]. Cultures were then centrifuged briefly, to separate the longer (heavier) filaments from the shorter ones (**Figure 5.4 B**). This was repeated until no filaments longer than 7 cells were observed under a microscope. 100 µL of the cell culture was then plated via serial dilution onto BG-11_0 solid media, to obtain individual colonies. Once the colonies appeared, these were picked and isolated onto separate BG-11_0 solid media and at the same time plated onto LB solid media (**Figure 5.4 C**).

After 24 hours of incubation at 30 °C, the LB plates showed that some colonies had other bacteria present which were not *Trichormus variabilis*.

5.4 *Trichormus variabilis* strain isolation & consortia identification

Following the successful implementation of a 24-well plate screening strategy in 3.5.1 to identify strains with increased carbon fixation, the strategy was adapted to screen strains with enhanced nitrogen fixation. BG-$11NH_4$ was replaced with BG-11_0 or BG-11_0A where stated.

5.4.1 *Measuring biomass yields*

Following growth for 120 hours, 300 µmol photons·m^{-2}·sec^{-1}, 30 °C, 1 mL of culture was removed from each well, and DCWs measured as previously described (**Figure 5.5**).

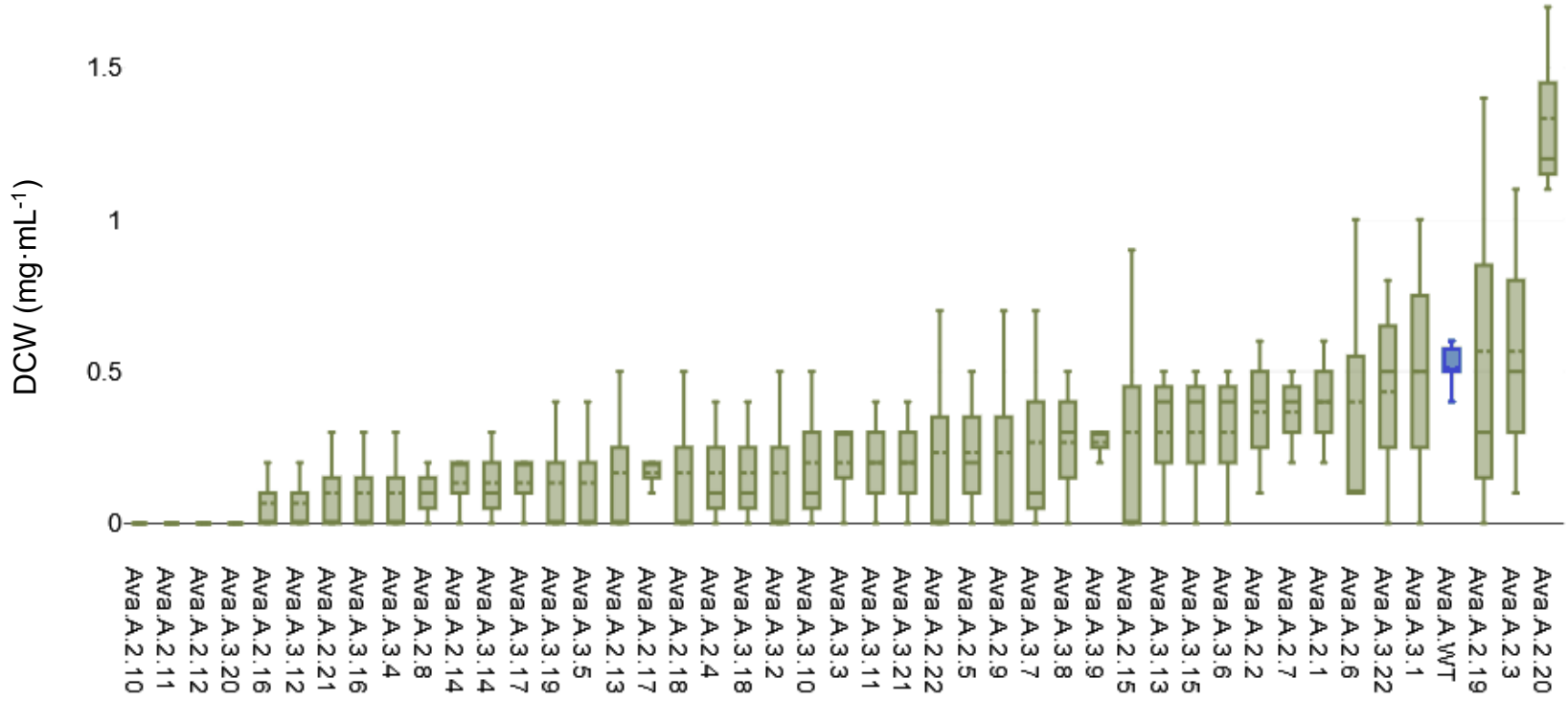


Figure 5.5 | Dry cell weights from 24-well plate screened isolates at 300 µmol photons·m^{-2}·sec^{-1}, 30 °C, 120 hours, in BG-11_0 liquid media. Olive indicates chemostat isolate samples. Blue indicates Ava.WT samples. (*n* = 3, error bars show standard deviation).

In contrast to the previous observations made during chemostat selection of the *Synechocystis Δhox* mutants, only 1 isolate, Ava.A.2.20, had a significant increase in biomass ($p < 0.015$). Furthermore, many replicates did not grow, and 4 strains (Ava.A.2.10, Ava.A.2.11, Ava.2.12, and Ava.A.3.20) showed no growth at all. Ava.A.2.20 showed a 2.9-fold increase in biomass compared to Ava.WT, however, this was the exception. Overall, the distribution of Ava.A.mutant DCWs (n = 132) weighted heavily to the left of the Ava.WT distribution (n = 6) (**Figure 5.6**). The value recorded with the highest overall frequency was 0 mg·mL^{-1}.

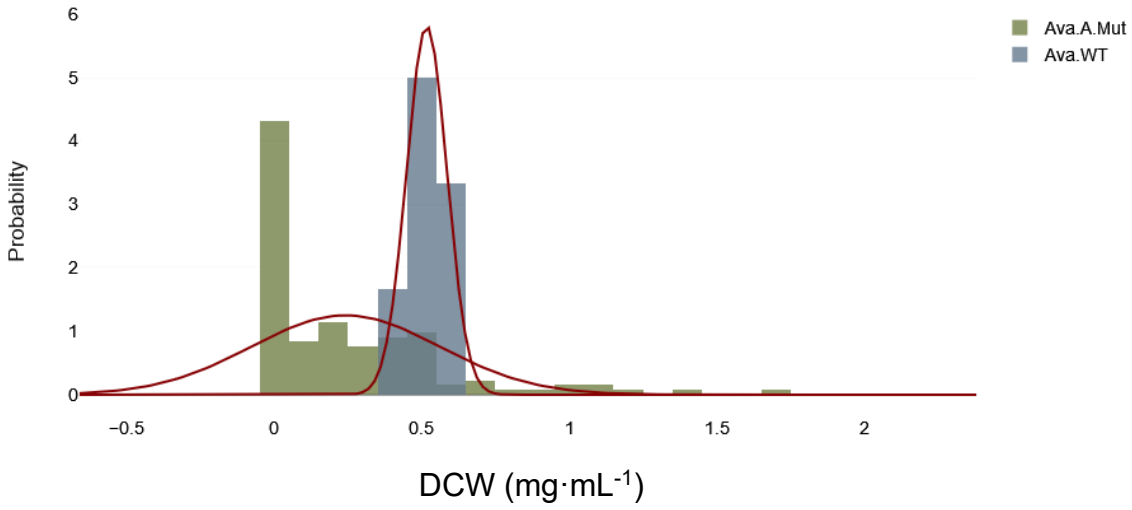


Figure 5.6 | Proportional frequency of dry cell weight yields from 24-well plate isolates at 300 µmol photons·m^{-2}·sec^{-1}, 30 °C, 120 hours, in BG-11$_0$ liquid media. Olive indicates chemostat isolate samples (N = 132). Blue grey indicates Ava.WT (N = 6).

The low frequency of values recorded higher than Ava.WT is more clearly shown in **Figure 5.7**.

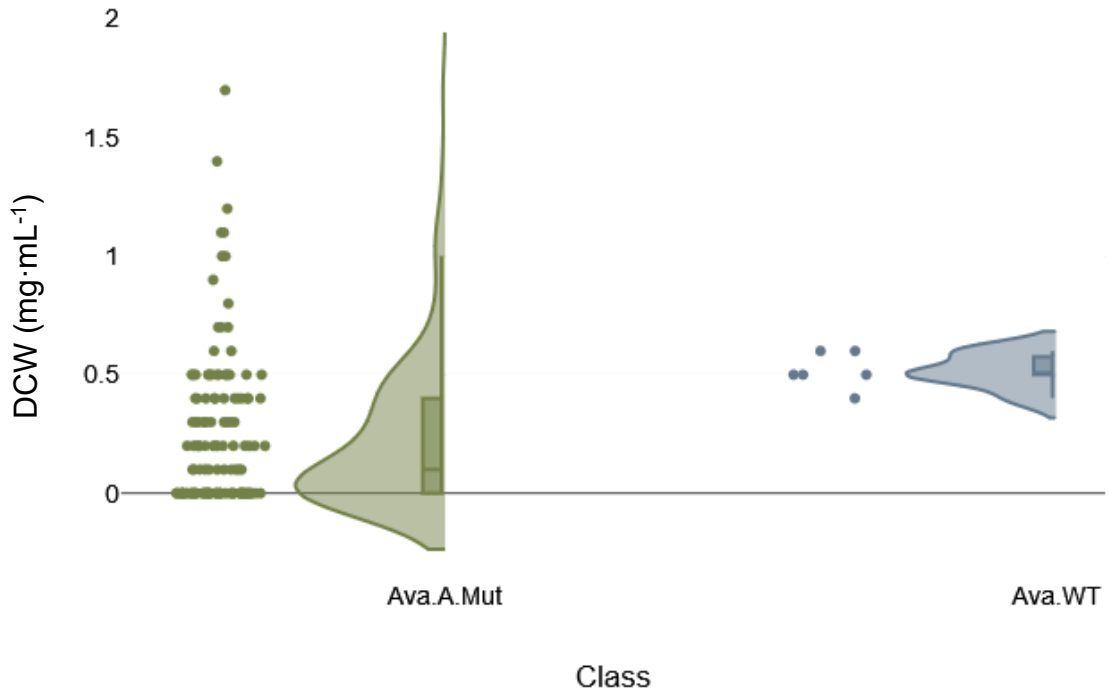


Figure 5.7 | Distribution of all individual dry cell weight yields from 24-well plate isolates at 300 µmol photons·m^{-2}·sec^{-1}, 30 °C, 120 hours, in BG-11_0 liquid media. Olive indicates chemostat isolate samples (*N* = 132). Blue grey indicates Ava.WT (*N* = 6).

To investigate the role of the fructose in the selection process on the phenotypes isolated, the screening was repeated, this time replacing BG-11_0 liquid media, with BG-11_0A liquid media, which was initially used in the selection process. The second screening in contrast, to the first, showed an increase in the biomass accumulation of the strains (**Figure 5.8**). A total of 42 out of the 44 isolates screened showed higher average biomass yields compared to the control. Of these, 15 were statistically significant ($p < 0.05$).

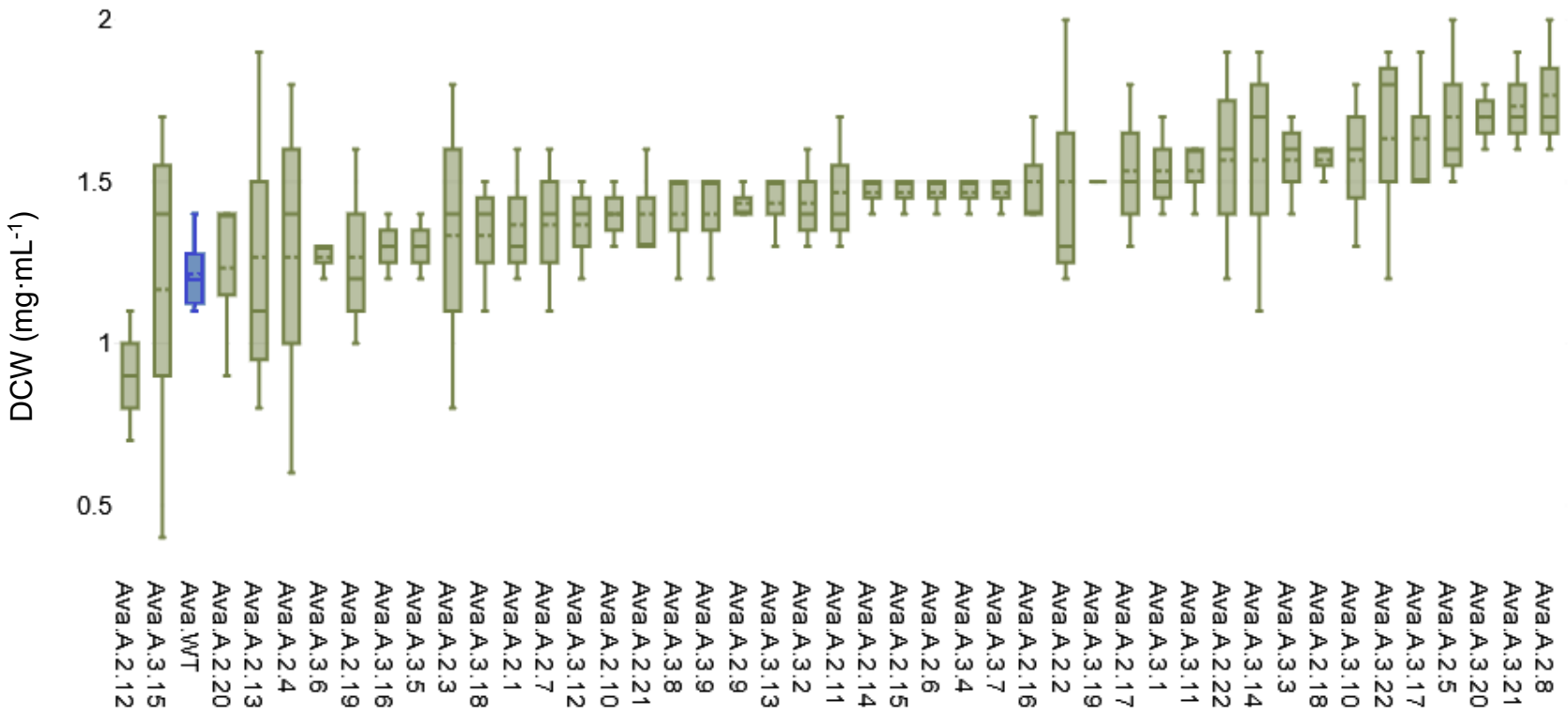


Figure 5.8 | Dry cell weights from 24-well plate screened isolates at 300 µmol photons·m^{-2}·sec^{-1}, 30 °C, 120 hours, in BG-11_0A liquid media. Olive indicates chemostat isolate samples. Blue indicates Ava.WT samples. (*n* = 3, error bars show standard deviation).

This increase in the growth of the isolates was also clear when observing the distribution of the Ava.A.Mutant recorded values compared to the Ava.WT control (**Figure 5.9**). Here, the distribution showed a clear shift to the right of the control.

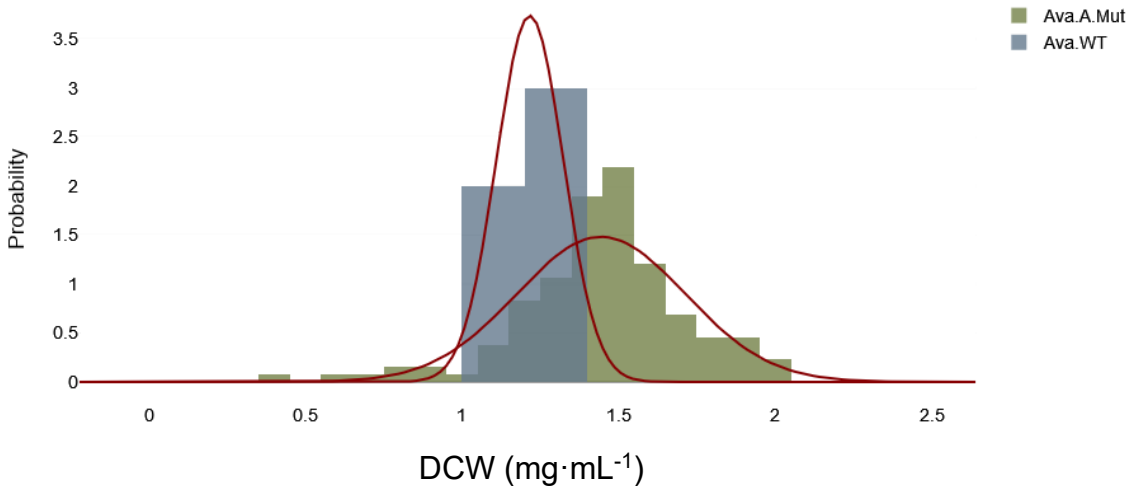


Figure 5.9 | Proportional frequency of dry cell weight yields from 24-well plate isolates at 300 µmol photons·m^{-2}·sec^{-1}, 30 °C, 120 hours, in BG-11_0A liquid media. Olive indicates chemostat isolate samples (*N* = 132). Blue grey indicates Ava.WT (*N* = 6).

The average DCW of all the mutants screened with fructose supplementation was 1.44 ±0.27 mg·mL^{-1}, and 0.24 ±0.32 mg·mL^{-1} with no additional fructose. This was 18% higher ($p < 0.05$), and 54% lower than Ava.WT ($p < 0.05$) under the same conditions (**Figure 5.10**). The cell DCW averaged 1.22 ±0.12 mg·mL^{-1} and 0.52 ±0.08 mg·mL^{-1} with and without fructose supplementation respectively. Indicating a selection for fructose dependence within the isolates. The significant changes in mean biomass accumulation (increased with fructose, and decreased without supplementation), clearly demonstrate that the selective advantage for increased nitrogen fixation has not been conferred by this experimental design, rather, fructose utilisation appears to determine mutant fitness here. Despite this, however, given the insignificant ($P \leq 1$) impact of fructose on Ava.2.20 biomass accumulation compared to Ava.WT, and the significant ($p < 0.015$) increase in biomass accumulation without fructose and diazotrophic growth, I considered that this strain warranted further characterisation.

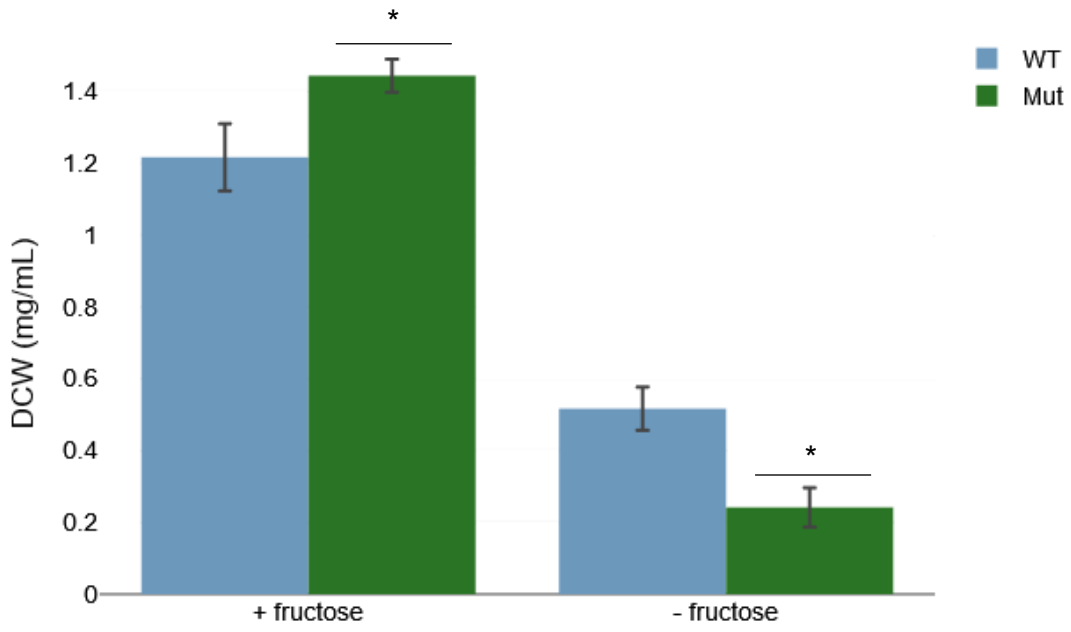


Figure 5.10 | Dry cell weights from 24-well plate screened Ava.A.Mutant isolates compared to Ava.WT grown at 300 µmol photons·m^{-2}·sec^{-1}, 30 °C, 120 hours, in BG-11_0 liquid media – with, and without 10 mM fructose supplementation. (*p < 0.05, error bars show standard deviation).

5.4.2 *Trichormus variabilis Ava.A.2.20 consortia isolation*

Following the isolation of the strains in section **5.3** and subsequent mutant screening, the best performing *Trichormus variabilis* ALE strains were transferred to individual plates of BG-11_0 solid media, and a non-selective companion LB solid media plate (see **3.3.5**). The LB plate was used to identify any potential contaminants. Analysis of the colony morphologies on the LB plates indicated the presence of many non-cyanobacterial cells, which had been co-isolated alongside the *Trichormus variabilis* mutant. Therefore, attempts were made to isolate the individual colonies by streaking individual colonies from the BG-11_0 plates onto new BG-11_0 plates. The *Trichormus variabilis* mutant strain, Ava.A.2.20, which was shown to have the highest rate of biomass accumulation, had an abundance of non-cyanobacterial colonies on its plates. These other

bacterial cells could also be seen under the microscope (x40 magnification).

During the chemostat run, routine contamination monitoring is carried out by plating the cell and supernatant wash out onto non-selective LB solid media. This had previously demonstrated the presence of contamination, however, given the time limit it was decided to only monitor contamination levels, rather than restart the experiment, or attempt to remove the contaminants and risk affecting the outcome of the selection process. The monitoring demonstrated that there was little variation amongst the contaminant phenotypes, and no filamentous fungi were detected (data not shown). Potential causes of contamination could include poor sterility particularly whist continuously introducing new media, however sampling of the media from the "in" line showed that no contamination was present. It was therefore possible that the contaminating organisms may have been introduced via structural degradation of chemostat fittings.

Without these 3D printed fittings, the chemostat based strategy would not have been possible. However, the fittings were made from 3D printer resin which rendered them unsuitable for autoclaving, therefore sterilising them in between ALE runs was challenging. Use of bleach or hydrogen peroxide strategies risked damaging metal components of the fittings (see Kimura et al. 2020) [526], and a UV sterilisation strategy would likely not have sterilised the fittings, due to the challenge of illuminating all bacterial cells / spores simultaneously (see Stewart et al. 2023) [527].

Sterilisation was therefore carried out by submerging the fittings in 70% ethanol solution for 14 days. The fittings were then removed using flame treated forceps, and thoroughly dried inside a class II biological safety cabinet, before being immediately re-assembled back into the chemostat. Following repeated sterilisation of the fittings, they began to disintegrate. The interior metal tubes then became mobile, and so were secured in position using tightly fitted parafilm (**Figure 5.11**). Care was taken to ensure repairs were carried out thoroughly, and repair was attempted in lieu of suitable replacement fittings which were unavailable.



Figure 5.11 | Diminished structural integrity of chemostat components requiring improvised repairs.

Cyanobacterial cultures are prone to contamination, with some references even describing contamination of larger cultivation volumes as “inevitable” [152]. Cyanobacteria have been shown to release an excess abundance of central metabolites such as 2-oxoglutarate and pyruvate during periods of high photosynthetic activity, possibly to reduce the risk of overwhelming photosynthetic metabolism [528,529]. Symbiotic consortia which form mutualistic relationships with cyanobacteria have been shown to have a positive impact in several processes including wastewater treatment [530], long-term cyanobacteria culture stability [531], and even growth [532]. However, the presence of these organisms in the chemostat did make efforts to characterise the Ava.A.2.20 strain more challenging. To identify these potential contaminants the Ava.A.2.20 strain was re-plated onto LB solid media, to try and isolate the strains.

Attempts were made to isolate the Ava.A.2.20 strain from the other contaminating strains via serial dilution plating and then re-streaking to individual colonies on BG-11_0 solid media. BG-11_0 was utilised as it was hypothesised that the contaminating organisms would not be able to fix nitrogen. However, this proved to be unsuccessful, with the individual contaminants exhibiting strong growth on the BG-11_0 solid media. This occurred when the strains were plated with both the Ava.A.2.20 strain following serial dilution, and when the cells were directly transferred from

LB contamination plates by streaking (data not shown). Given that the BG-11_0 media contained only a trace nitrogen source (~318 µg of nitrogen per L^{-1} excluding HEPES), growth of the contaminants on this media was surprising. However, the contaminants did not grow when they were inoculated into BG-11_0 liquid media, with the liquid media variant containing no fixed carbon, and again only a limited nitrogen source. Therefore, it is likely that the strains were utilising the agar in the media as a carbon source in the BG-11_0 solid media, which contains BD Bacto™ Agar (Fisher Scientific™), which is composed of galactose polysaccharide chains. Despite the manufacturer's efforts to "remove extraneous matter", it is possible that sufficient nitrogen contamination remains to support cell growth. Alternatively, the BG-11_0 medium contains 10 mM (2.383 $g \cdot L^{-1}$) HEPES, to buffer pH (see **3.1.2**), which is approximately ~12% nitrogen in elemental composition. This said, no previous evidence of aerobic microorganisms using HEPES as a nutritional source could be found, and previous work by Cook et al. 1977 showed no nutritional uptake of HEPES by *Pseudomonas putida* [533], a "paradigm" of diverse substrate utilisation (see Martins Dos Santos et al. 2004) [534].

However, previous work has shown that growth of cyanobacteria with other species in consortium has significantly enhanced their efficacy as biofertilisers [535–537]. Given the possibility the organisms isolated in Ava.2.20 could be advantageous both for enhancing cyanobacterial and subsequent plant growth (if applied as a soil supplement), an effort was made to identity the organism(s) in consortia.

5.4.2.1 *Identification of the Ava.A.2.20 microbial consortia*

No visible differences were detectable in the colony morphologies of the individual colonies plated onto both the LB and BG-11_0 solid medias. Round beige colonies were observed on the LB solid media (**Figure 5.12**), and small white colonies were observed on the BG-11_0 solid media (data not shown). Based on the morphology it was assumed that only 1 non-cyanobacteria species was present with the Ava.A.2.20 strain. An individual colony was selected for 16S rRNA analysis by cPCR (see **3.4.5.1**), and sequencing was carried out by Source BioScience (Nottingham, United Kingdom). Submission of the sequencing results to Blastn (NCBI) indicated this isolate was a member of the family *Rhizobiaceae*, possibly either the genus *Agrobacterium* or *Rhizobium* (data not shown). This was particularly interesting as members of the *Rhizobium* genus are capable of nitrogen fixation [538].

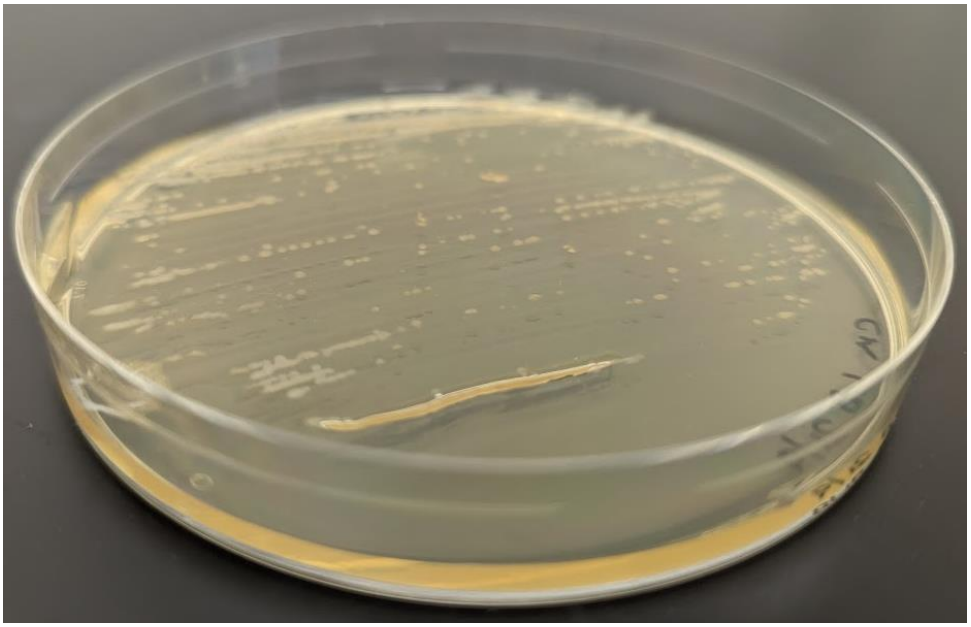


Figure 5.12 | Colony morphology of Ava.A.2.20 streaked for single colonies on LB solid media.

New single colonies were prepared by streaking the original colony onto an LB plate, and 1 colony was selected and grown overnight in LB liquid media at 30 °C. The gDNA was extracted utilising the Quick-DNA Fungal/Bacterial Kit (Zymo™), following the manufacturer's instructions, and prepared for genomic analysis following post-processing and cleaning as detailed in **3.2.3**. However, following several attempts at genomic analysis (see **3.5**), this strain was not a member of the family *Rhizobiaceae*. Using the BV-BRC web resource PATRIC algorithm [539,540], fastq pass files were assembled to reference Genome ID 2067451.3 *Rhizobium* sp. TH135. The assembly, however, demonstrated that there was significant genetic contamination from non-*Rhizobium* DNA, and that an unusually large genome of ~25 Mb had been assembled. The assembly was annotated using the RAST algorithm [541–543], and a possible 16S rRNA sequence isolated. This sequence, and randomly selected regions of the assembled genome were submitted to Blastn (NCBI) to search for sequence similarity. Initial results indicated that this assembled genome was a member of genus *Achromobacter*, a genus that has previously been shown to contaminate laboratory cell cultures [544]. Further submissions from the assembly also identified sequences with high similarity to the genus *Rhizobium*.

Despite the uniform appearance of the colonies present on the solid media plates, it was now clear that more than one species was present

within the Ava.A.2.20 consortia. Given that 2 different organisms had been identified, work was undertaken to try and identify a strategy to selectively isolate these organisms. Samples of Ava.A.2.20 culture was streaked onto solid media variants of LB, BG-11, BG-11_0, GYM, and M9. However, there was still no phenotypic variation observed between the colonies. Previous work by Lamovšek et al. 2014 [417] had shown that phenotypic changes to *Agrobacterium* isolates typically occur following incubation at 12 °C for 1 week. Therefore, a strategy was devised based on this work (**Figure 5.13**). The strategy involved initially growing the cultures at 30^{0}C before being transferred to 4^{0}C for seven days and then a final incubation at room temperature.

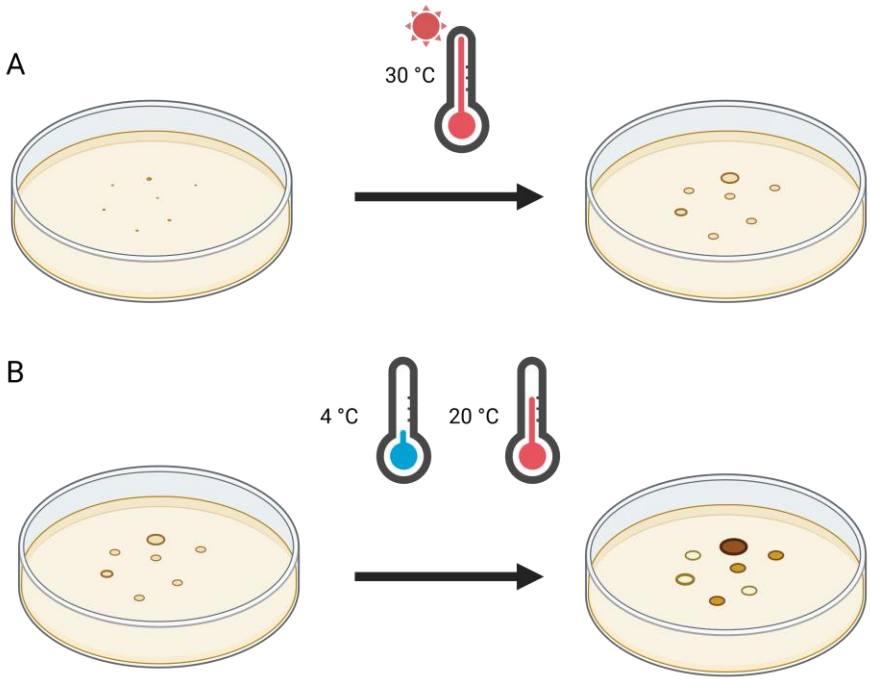


Figure 5.13 | Strategy to elicit distinct consortia phenotypes. **A.** Ava.A.2.20 liquid culture was streaked for single colonies onto LB solid media. Plates were grown at 30 °C for ~16 hours. **B.** Plates were then transferred to 4 °C for 7 days, before being allowed to continue growing at room temperature (18 - 20 °C) for 5 days. (Created with BioRender.com).

Following this strategy, altered phenotypes emerged on the treated plates (**Figure 5.14**). Three distinct phenotypes were identified and selected for further analysis using 16S rRNA cPCR reactions. Following putative identification, axenic strain collections were generated for each isolate.

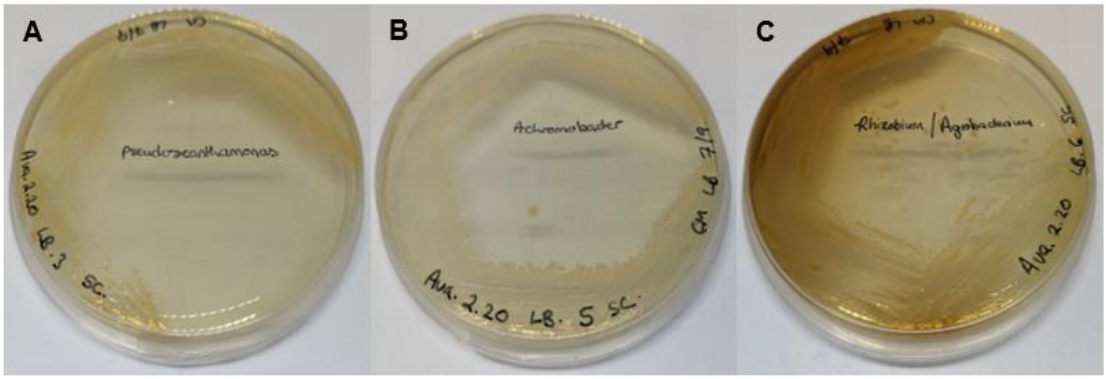


Figure 5.14 | Phenotypic variation of the axenic isolates on LB solid media following repeated 4 °C incubation treatment. **A.** Consortia isolate LB3, putative genus *Pseudoxanthnomonas*. **B.** Consortia isolate LB5, putative genus *Achromobacter*. **C.** Consortia isolate LB6, putative genera *Rhizobium / Agrobacterium*.

Consortia isolates were assigned identification values based on their location on the plate that was originally used for the single colony patches. The three distinct strains were labelled LB3, LB5, and LB6 respectively. The 16S rRNA gene was used to construct phylogenetic trees as shown in **Figure 5.15**. Unlike LB5 and LB6, the isolate LB3 was only identified after growth at 4 °C. Phylogenetic analysis suggested that LB3 is a member of genus *Pseudoxanthomonas*. However, it is also closely related to unidentified or uncultured bacteria. The genus *Pseudoxanthomonas* have previously been shown to coexist in the same ecosystem [545], or even in direct consortia with cyanobacteria [546]. Furthermore, *Pseudoxanthomonas mexicana* has also been shown to synthesise auxin [547], a well characterised plant growth hormone that has a diverse impact on the physiology of cyanobacteria [548]. There is also evidence that *Pseudoxanthomonas* can enhance photosynthetic growth, as soil supplementation of *Vigna radiata* with *Pseudoxanthomonas mexicana* increased plant growth, as well as the average length of roots and shoots [547].

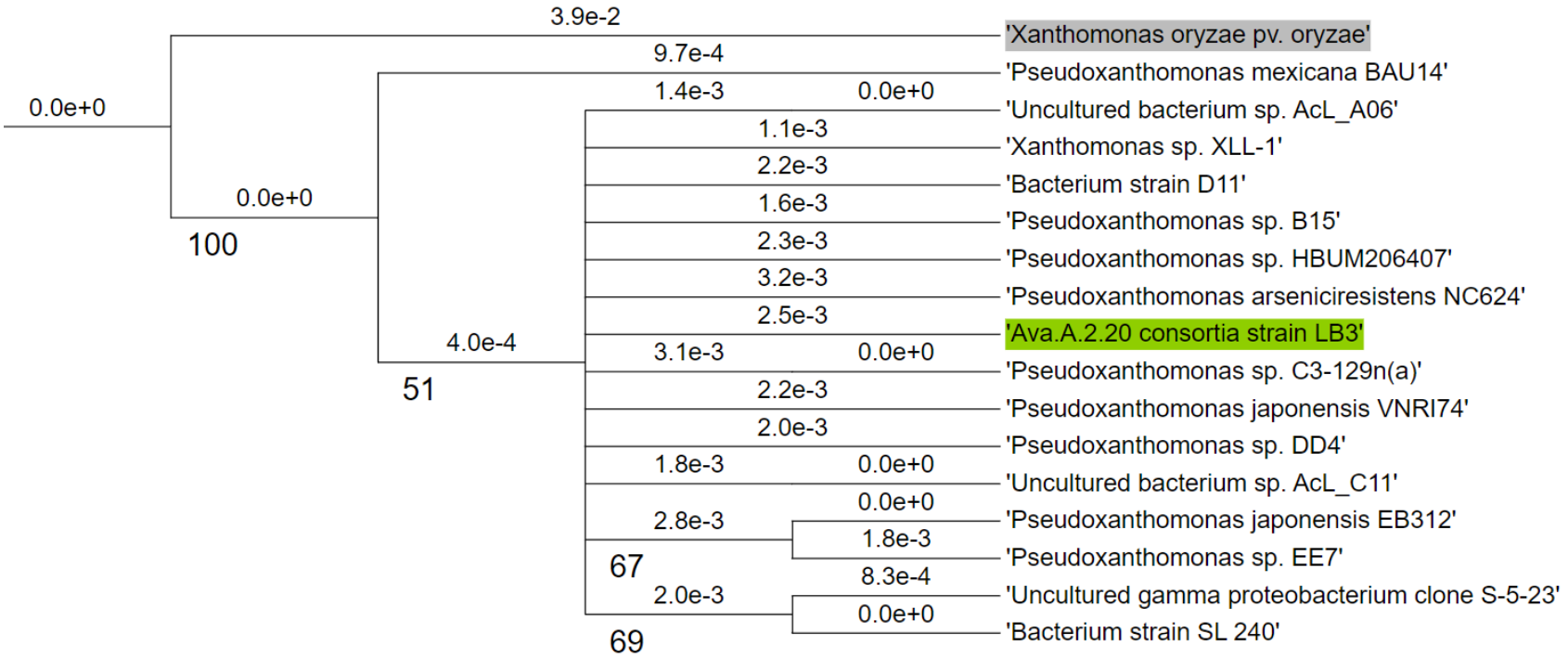


Figure 5.15 | Phylogenetic tree of Ava.A.2.20 LB3 consortia isolate based on the 16S rRNA gene sequence. BLAST (NCBI) was used to identify sequences with a high similarity (megablast). The tree was assembled using Geneious Prime™ (v. 2024.0), rooted to *Xanthomonas oryzae* pv. Oryzae. Bootstrap values are displayed under branches, and branch length is displayed above. (Created with iTOL.embl.de)

A 16S rRNA phylogenetic analysis was also carried out on isolate LB5 (**Figure 5.16**). Comparison of the alignments of the 16S rRNA gene sequence correlated strongly with the previous alignments, generated from the low-quality sequence assembly. The blast results having previously identified *Achromobacter spanius* and *Achromobacter deleyi* as having the highest sequence similarity (data not shown). *Achromobacter species* have also been shown to catabolise plant hormones such as auxins and salicylic acid [549], and frequently exist in the rhizosphere, associating with higher plants [550].

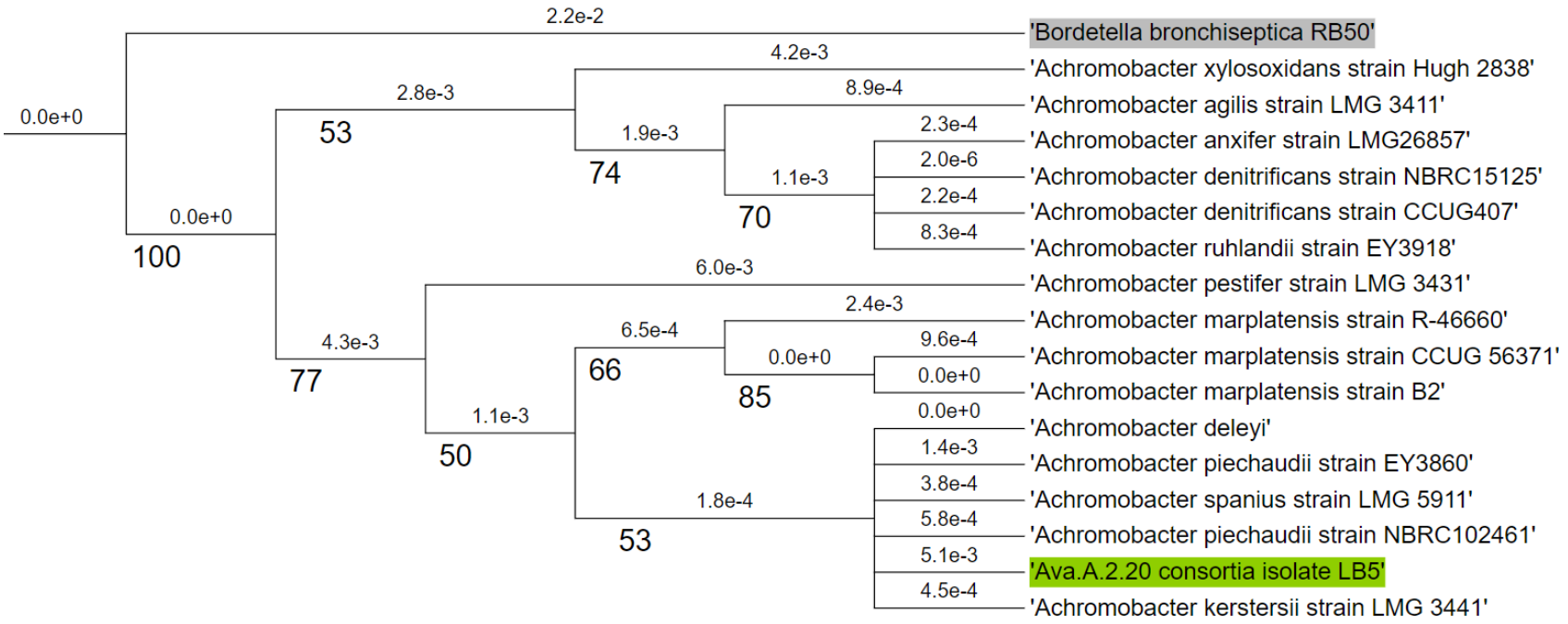


Figure 5.16 | Phylogenetic tree of the Ava.A.2.20 LB5 consortia isolate based on the 16S rRNA gene sequence. BLAST (NCBI) was used to identify highly similar sequences (megablast). The phylogenetic tree was assembled using Geneious Prime™ (v. 2024.0), rooted to *Bordetella bronchiseptica* RB50. Bootstrap values are displayed under branches, and branch length is displayed above. (Created with iTOL.embl.de)

Perhaps most surprisingly, the phylogenetic analysis of the of LB6 16S rRNA gene sequence (**Figure 5.17**) confirmed the identity of a member of family *Rhizobiaceae*. The distinction between members of the *Agrobacterium* and *Rhizobium* genera, however, is still unclear, with some even calling for the reclassification of these two as one genus [551,552], others arguing to the contrary [553], and arguments against arguments to the contrary [554]. Identification of this species within these genus/genera is therefore challenging. This is because significant proportions of these organisms' hereditary material are maintained in extrachromosomal replicons [555], and not the chromosome. This has resulted in several classifications and identifications being based on both phenotypic characteristics, and hereditary information [555,556]. A possibly flawed strategy given the mobility of this hereditary material [557]. Due to these challenges, and the limited time available, concerted efforts to better identify LB6 were not undertaken. This organism thus sits putatively as a possible *Agrobacterium* / *Rhizobium* species.

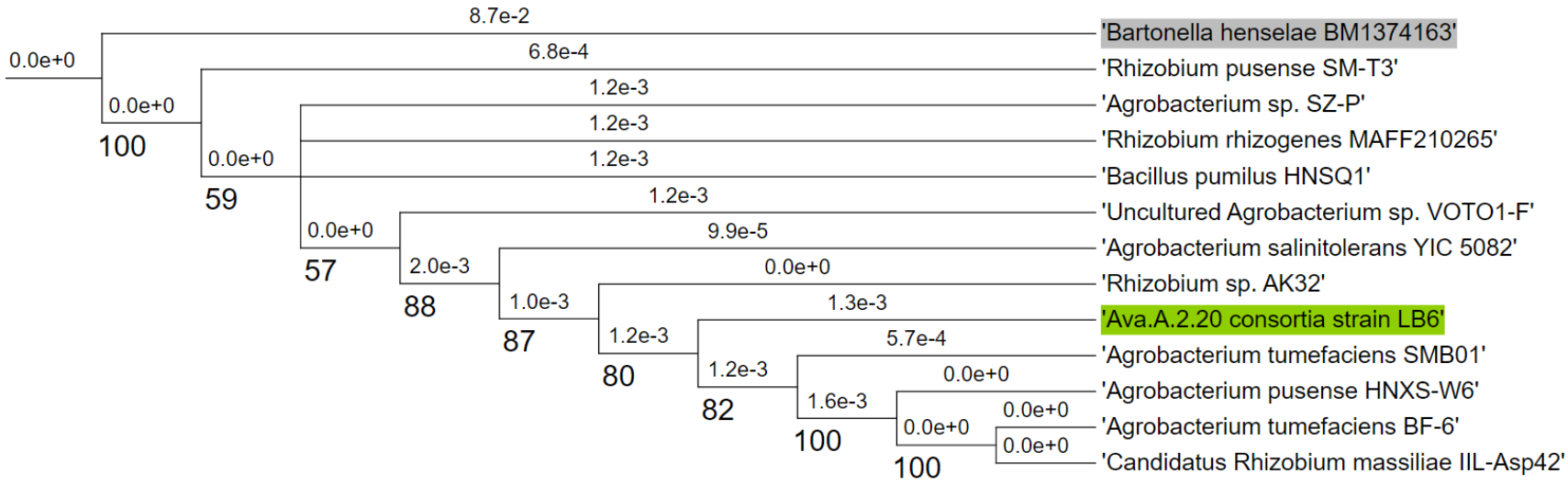


Figure 5.17 | Phylogenetic tree of Ava.A.2.20 LB6 consortia isolate based on the 16S rRNA gene sequence. BLAST (NCBI) was used to identify highly similar sequences (megablast). The phylogenetic tree was assembled using Geneious Prime™ (v. 2024.0) and rooted to *Bartonella henselae* BM1374163. Bootstrap values are displayed under branches, and branch length is displayed above. (Created with iTOL.embl.de)

Both *Agrobacterium* and *Rhizobium* species are known to form close associations with higher plants, especially in their rhizospheres [555–559], where these organisms will likely interact with cyanobacteria. These organisms are also recruited by plants to form rhizosphere associations [560]. Cyanobacteria have been shown to positively influence rhizosphere communities to enhance plant growth by enabling these communities to upregulate nitrogen fixation [561,562], and many species of *Rhizobium* are well known to independently fix nitrogen [563]. As the goal of this work was to generate cyanobacteria strains with enhanced nitrogen fixation capacity, and members of each of the genera isolated in the consortia with Ava.A.2.20 have been shown to improve plant growth yields [547,564–566], the decision was made to include these isolates in future characterisation. To assess if any other species were present within the consortia associated with the Ava.A.2.20 strain, further streaking was performed to obtain single colonies on LB solid media with additional heat treatments > 30 °C. However, no further species were identified.

5.4.2.2 *Isolation of Trichormus variabilis A.2.20 from consortia*

Despite the potential value the isolated organisms provided for the A.2.20 strain, the presence of the different strains made it difficult to independently characterise the cyanobacteria strain. Therefore, it needed to be isolated from the other strains. Following putative identification in 4.5.2.1, isolates were plated from LB solid media, onto BG-11_0 solid media containing a range of antibiotics (**Table 5.1**). Previous work by Heidorn et al. 2011 was used to identify suitable antibiotics and working concentrations for cyanobacteria, however, only streptomycin and spectinomycin were listed for *Trichormus variabilis* specifically [408]. Ampicillin, chloramphenicol, gentamicin, hygromycin, and kanamycin were also selected as they have previously demonstrated inhibition of other cyanobacteria [408,409]. The Ava.WT strain was also plated onto BG-11_0 solid media containing the same concentrations of antibiotics as the control.

Table 5.1 | Antibiotic concentrations of BG-11_0 plates used to screen for antimicrobial sensitivity of the Ava.A.20 strain and the consortia. Ava WT samples were inoculated using 10 µL loops from BG-11_0 liquid culture, and Ava.A.2.20 consortia from LB solid media. Plates were grown at 250 µmol photons·m^{-2}·sec^{-1}, 30 °C for 72 hours. Samples were compared to solid media inoculations without antibiotics to assess growth.

		Effects on growth	
Antibiotic	**Concentration(s) (µg·mL-1)**	**Ava.WT**	**Consortia**
Ampicillin	100	Unaffected	Unaffected
Apramycin	50	Reduced growth	Unaffected
Chloramphenicol	25	Reduced growth	Unaffected
Gentamicin	25	Unaffected	Unaffected
Gentamicin	50	Unaffected	Unaffected
Gentamicin	100	Reduced growth	Reduced growth [a]
Gentamicin	200	Reduced growth [a]	Reduced growth [a]
Hygromycin	50	No growth	No growth
Kanamycin	50	Reduced growth	Unaffected

[a] significant reduction in growth observed under this condition.

None of the antibiotic concentrations tested removed all the individual organisms from the consortia, whilst still maintaining the Ava.A.2.20 cyanobacterial cells. However, 200 µg·mL^{-1} of gentamicin did have an impact on the growth of all the strains. It was therefore selected to try and remove the consortia from the Ava.A.2.20 culture by combining the effects of reduced growth, with the inability of the consortia to grow in BG-11_0 liquid media.

The Ava.A.2.20 liquid culture was re-streaked for single colonies onto BG-11_0 solid media containing 200 µg·mL^{-1} gentamicin. A small portion of the surviving biomass was inoculated in 2 mL of BG-11_0 liquid media containing 100 µg·mL^{-1} gentamicin, and incubated at 60 µmol photons·m^{-2}·sec^{-1}, 30 °C. After ~16 hours, the media volume was increased to 4 mL, and the gentamicin concentration was adjusted to 200 µg·mL^{-1} gentamicin. Following an additional ~16 hours of growth, 10 µL of the liquid culture was plated onto non-selective BG-11_0 solid media, (incubated at 250 µmol photons·m^{-2}·sec^{-1}, 30 °C). A further 50 µL was also plated onto LB solid media and grown for 2 days at 30 °C. There was a

significant decrease in the abundance of the consortia organisms relative to the untreated Ava.A.2.20 culture, (from a bacterial lawn to ~20 - 30 colonies). Small portions of the cell biomass were then patched interchangeably between $BG\text{-}11_0$ solid media supplemented with 200 $\mu g \cdot mL^{-1}$ gentamicin and non-selective media. This occurred until no growth could be detected for the individual consortia on the non-selective LB plates. Following this repeated plating, an axenic culture of *Trichormus variabilis* Ava.A.2.20 was isolated and renamed as "Ava.A.2.20.P".

5.4.3 *Evaluation of the impact of the microbial consortia upon growth of wildtype Trichormus variabilis*

To investigate the impact of each individual consortia species on the growth characteristics of *Trichormus variabilis*, the growth of Ava WT and Ava WT with each of the individual consortia members, LB3, LB5, and LB6 was evaluated and compared directly to the growth rate of the Ava.A.2.20 consortia strain. Cultures were inoculated at 0.1 $\mu g \cdot mL^{-1}$ chlorophyll and grown at 300 µmol photons$\cdot m^{-2} \cdot sec^{-1}$, 30 °C for 18 days. 1 mL of sample culture was removed on day 16 to measure DCWs. Optical density (OD_{750nm}) and chlorophyll (estimated by methanol extraction, described in 2.3.3) were measured every 24 hours. Growth of Ava.WT was compared to the Ava.WT strain inoculated individually with the consortia members LB3, LB5, and LB6, growth data is shown below (**Figure 5.18**). No significant difference was observed in the peak growth rates.

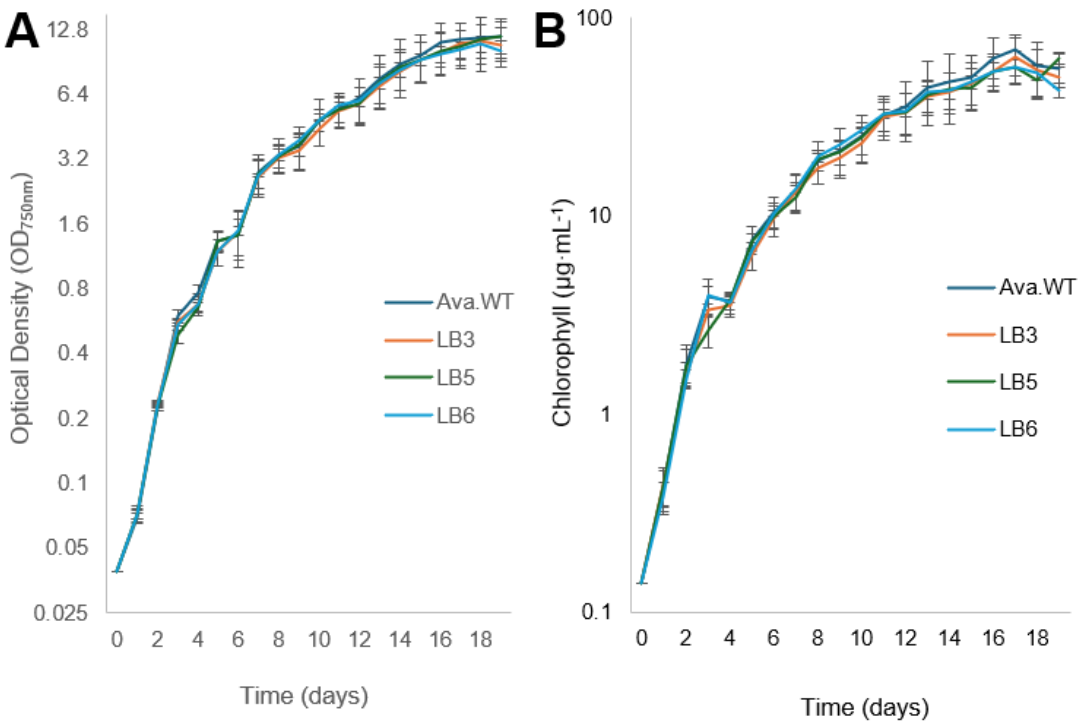


Figure 5.18 | Growth profiles of Ava.WT, and Ava.WT inoculated with LB3, LB5, and LB6, grown at 300 µmol photons·m^{-2}·sec^{-1}, 30 °C for 18 days. **A.** Optical density measurements (OD_{750nm}). **B.** Chlorophyll concentrations (µg·mL^{-1}). (*n* = 3, error bars show standard deviation).

Individually, the consortia strains did not appear to significantly alter the growth rate of the Ava.WT strain. The results of the combinations of 2 different consortia inoculated with Ava.WT are shown in **Figure 5.19**. Although growth was slightly lower in Ava.WT inoculated with LB3 and LB5, this was not significant ($P = 0.56$).

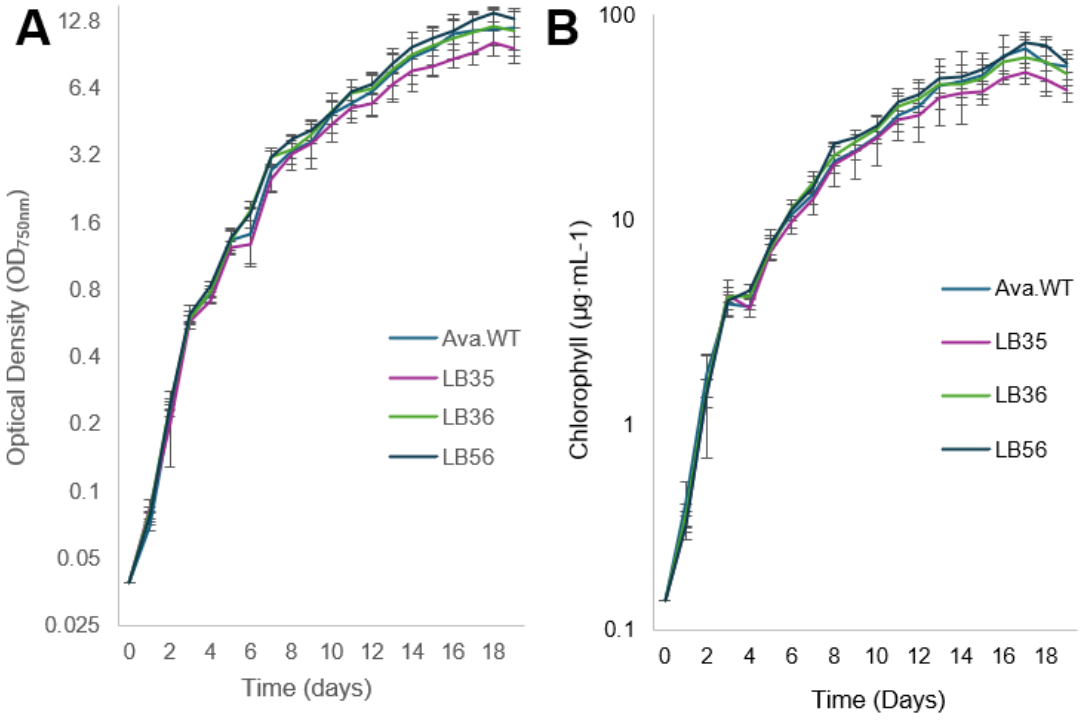


Figure 5.19 | Growth profiles of Ava.WT, and Ava.WT inoculated with LB3,5, LB3,6, and LB5,6, grown at 300 µmol photons·m^{-2}·sec^{-1}, 30 °C for 18 days. **A.** Optical density measurements (OD_{750nm}). **B.** Chlorophyll concentrations (µg·mL^{-1}). (*n* = 3, error bars show standard deviation).

To assess the growth of the complete consortia, both the Ava.WT, and the Ava.WT strain inoculated with all 3 consortium strains were grown alongside the Ava.A.2.20 strain (**Figure 5.20**). The Ava.WT strain inoculated with all 3 members of the consortia grew the fastest, however, this was not statistically significant.

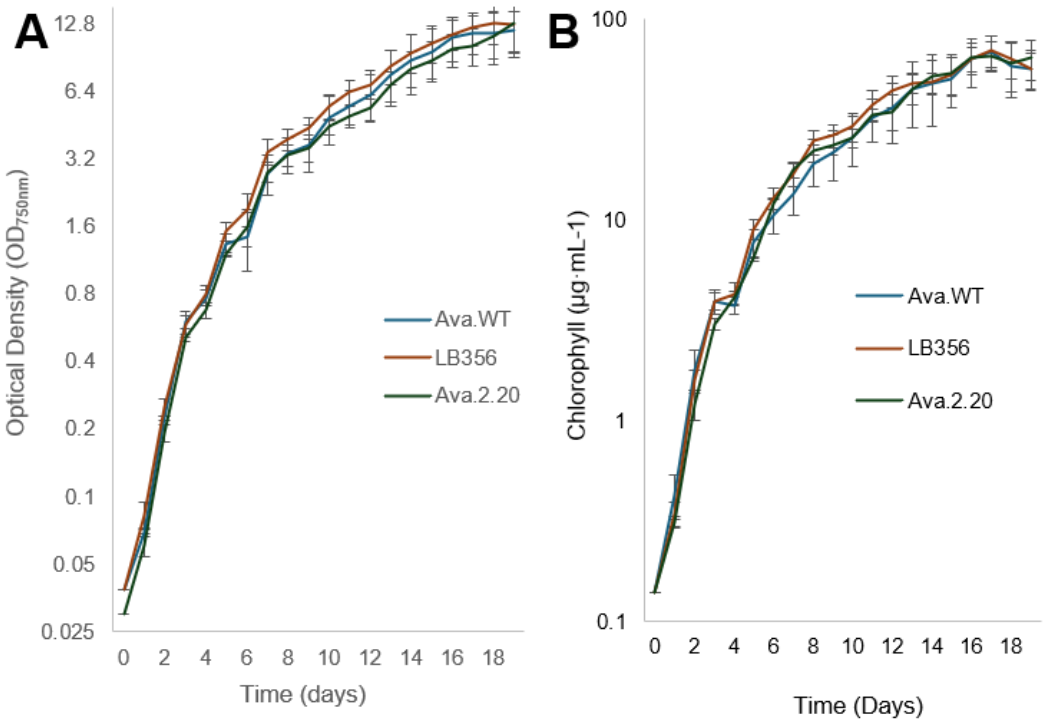


Figure 5.20 | Growth profiles of Ava.WT, Ava.WT inoculated with LB3, 5, and 6, and Ava.A.2.20, grown at 300 µmol photons·m^{-2}·sec^{-1}, 30 °C for 18 days. **A.** Optical density measurements (OD_{750nm}). **B.** Chlorophyll concentrations (µg·mL^{-1}). (*n* = 3, error bars show standard deviation).

Given that the consortia microorganisms typically consume metabolites secreted by cyanobacteria, dry weights of both the supernatants and the cell pellets were measured, to assess overall biomass compared to EPS. One mL samples of each culture were removed at day 16 and placed in prepared 1 mL microcentrifuge tubes. Samples were centrifuged at 8000 g for 15 minutes, and supernatants transferred into separate 1 mL microcentrifuge tubes. Both sets of tubes were dried at 80 °C for 48 hours, before being re-weighed. Combined dry weights of the samples are shown in **Figure 5.21**. Curiously, despite initial screening indicating that the Ava.2.20 consortia showed an increase in biomass accumulation, it showed an overall decrease in DCW. However, this was primarily due to a 60% decrease in the supernatant dry weight ($p < 0.05$). There were no significant differences in either the cell pellet or combined pellet and the supernatant dry weights compared to the control. The highest overall combined dry weight was for Ava.WT inoculated with all 3 consortia isolates, at 6.9 mg·mL^{-1}, compared to 6.7 mg·mL^{-1} for Ava.WT. Showing that all conditions yielded lower final biomass yields than the

control, and indicating improved Ava.2.20 biomass productivity was not sustained post-exponential growth.

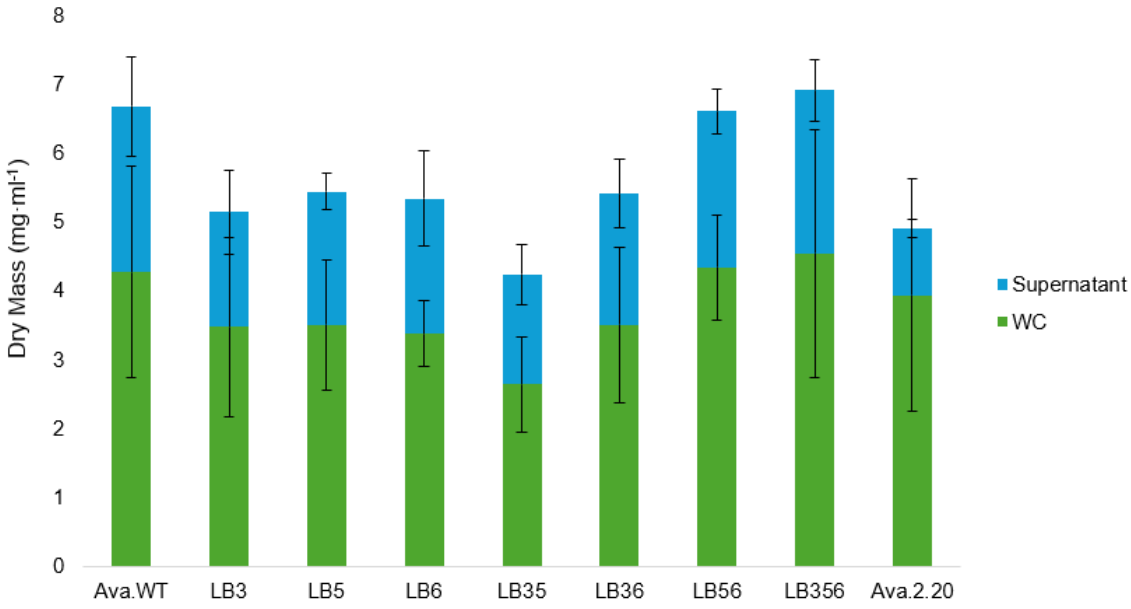


Figure 5.21 | Dry weights of cultures of Ava.WT, Ava.WT inoculated with different combinations of the consortia isolates, and Ava.2.20 grown for 16 days at 300 µmol photons·m^{-2}·sec^{-1}, 30 °C. Dry weight is shown by its source, supernatant (blue) or whole cell pellet (green). Error bars show standard deviation (n = 3, error bars show standard deviation).

One interesting observation made during the analysis was that the ratio of chlorophyll·OD_{750nm}^{-1} measurements from Ava.A.2.20 were higher than the Ava.WT strain 84% (sum) of all days measured (**Figure 5.22**). Analysis showed that this ratio was also significantly ($p < 0.05$) higher on days 0, 4, 7, 8, 14, 15, 16, and 17, while not significantly ($P > 0.05$) lower on any days measured. The same was not true for the different Ava.WT inoculations with individual and combined members of the consortia. Acknowledging the practical challenges of using OD to measure population density of filamentous cyanobacteria, if OD is a consistent estimate of the population density, this may suggest that relative concentrations of chlorophyll to cell density are higher in the Ava.A.2.20 strain. Therefore, this supports the earlier observation that higher biomass accumulation during screening was not only through the presence of the consortia. The *Trichormus variabilis* strain within the Ava.A.2.20 consortia may, in fact, be responsible.

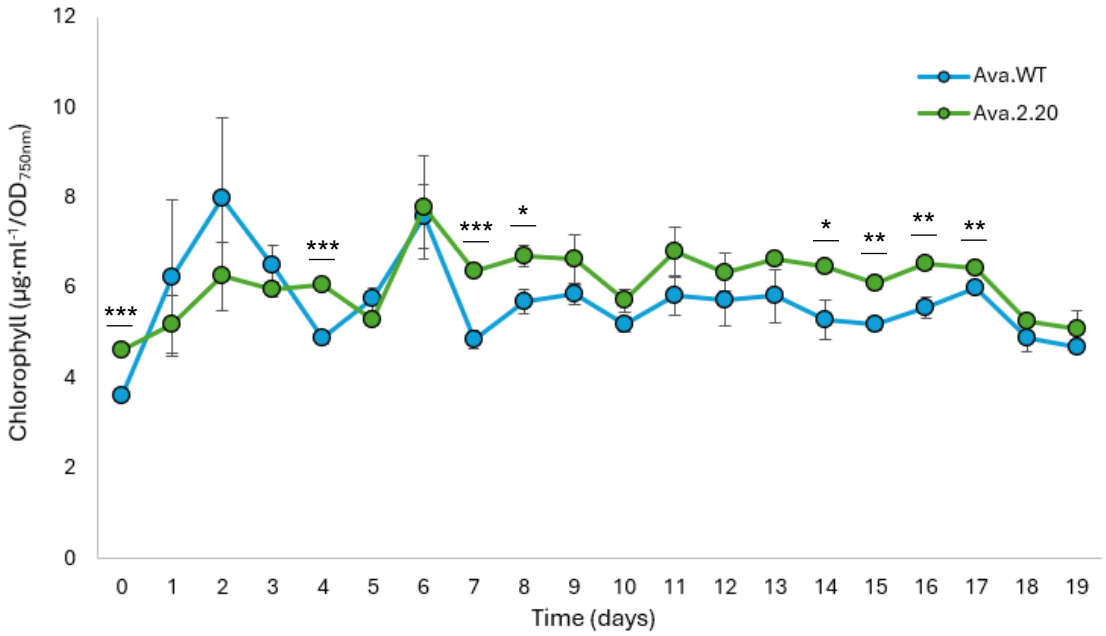


Figure 5.22 | Ratio of recorded estimated chlorophyll concentrations (µg·mL^{-1}) of Ava.WT and Ava.A.2.20 to equivalent recorded OD_{750nm} measurements (n = 3, *p < 0.05, **p < 0.01, ***p < 0.001, error bars show standard deviation).

Peak growth (μ_{max}) of each culture grown in BG-11$_0$, at 300 µmol photons·m^{-2}·sec^{-1}, 30 °C, (using chlorophyll to measure of growth), are shown in **Table 5.2**. Chlorophyll is used here instead, as it is specific to the cyanobacteria and avoids potential bias from non-cyanobacterial cells which may impact on the OD_{750nm} readings, and obscure estimates of cyanobacteria specific growth. Here, only Ava.A.2.20 showed a significantly higher μ_{max} than Ava.WT (p < 0.05), with a 36% ±20% (SD) increase in specific growth rate. This said, Ava.WT + LB3, Ava.WT + LB6, and Ava.WT + LB3,6 showed higher μ_{max} growth rates of 17% ±25% (SD), 18% ±13% (SD), and 35% ±9% (SD) respectively. However, these were statistically insignificant.

Table 5.2 | μ_{max} of Ava.WT, Ava.WT with different combinations of consortia inoculated, and Ava.A.2.20 in BG-11_0, at 300 µmol photons·m^{-2}·sec^{-1}, 30 °C. (Measured using chlorophyll concentrations). (n = 3, *p < 0.05). Colours indicate highest (green) to lowest (brown).

Strain	μ_{max} (h^{-1})	Standard Deviation	T Test to Ava.WT (P value)
Ava.WT	0.0130	0.0025	N/A
Ava.WT + LB3	0.0152	0.0038	0.22
Ava.WT + LB5	0.0118	0.0018	0.64
Ava.WT + LB6	0.0154	0.0020	0.12
Ava.WT + LB3,5	0.0128	0.0023	0.56
Ava.WT + LB3,6	0.0175	0.0016	0.06
Ava.WT + LB5,6	0.0132	0.0020	0.12
Ava.WT + LB3,5,6	0.0136	0.0012	0.34
Ava.A.2.20	0.0177	0.0036	0.01 *

Although co-inoculation with LB3, LB6, and LB3,6 did increase Ava.WT biomass accumulation, the individual consortia did not appear to have a statistically significant impact on the overall growth of Ava.WT. The Ava.WT + LB3,5,6 showed a nominally higher growth rate of 5% ±8% (SD), and given no individual isolate inoculum combinations had shown statistically significant improvements in growth, retention of the intact consortium was preferred to account for this uncertainty. It was also noted that both Ava.WT inoculated with consortia and Ava.2.20 also showed visibly more biofilm formation during these growth experiments (see **Figure 5.23**).

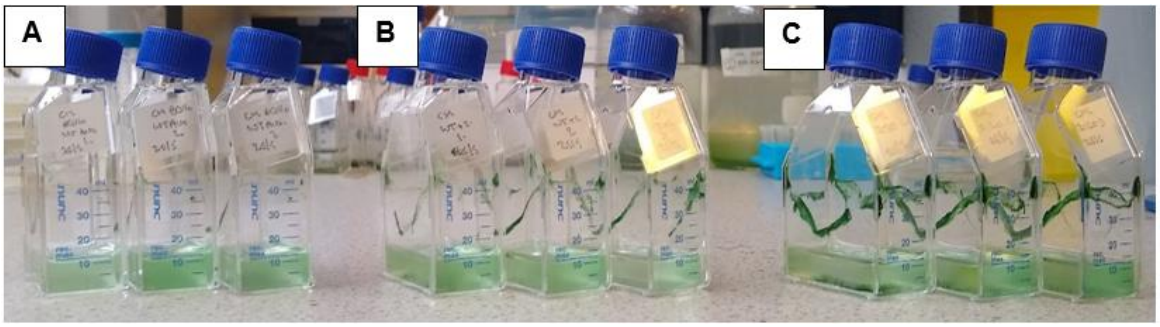


Figure 5.23 | Biofilm formation on triplicates of *Trichormus variabilis* cultures grown in BG-11_0 for 96-hours, at 300 µmol photons·m^{-2}·sec^{-1}, 30 °C. **A.** Ava.WT. **B.** Ava.WT with consortia. **C.** Ava.2.20.

Given an axenic Ava.A.2.20.P strain had been isolated without the consortia, this strain was also included in further analysis. Ava.WT, Ava.WT inoculated with LB3, LB5, and LB6, Ava.A.2.20.P, and Ava.A.2.20 were all grown under 1.5% CO_2 supplementation and 300 µmol photons·m^{-2}·sec^{-1}, at 30 °C. Specific growth rates (h^{-1}) were measured between days 1 and 2, and estimated using both optical density (OD_{750nm}) and chlorophyll concentration (µg·mL^{-1}) (**Figure 5.24**). Although the aim of this specific work was to investigate the use of a chemostat ALE strategy to enhance nitrogen fixation, given the link between carbon fixation and nitrogen fixation (see 4.2.1), it is possible that the limiting factor on the growth of these strains was not the availability of nitrogen. Specific growth rates of Ava.WT with LB3, LB5, and LB6, Ava.A.2.20, and Ava.A.2.20.P were all ~1.3-fold higher than the Ava.WT strain, when using optical density as a measure. However, only the wild-type with the consortia showed a significant increase in growth rate when chlorophyll was used as a measure ($p < 0.001$), increasing by 14%.

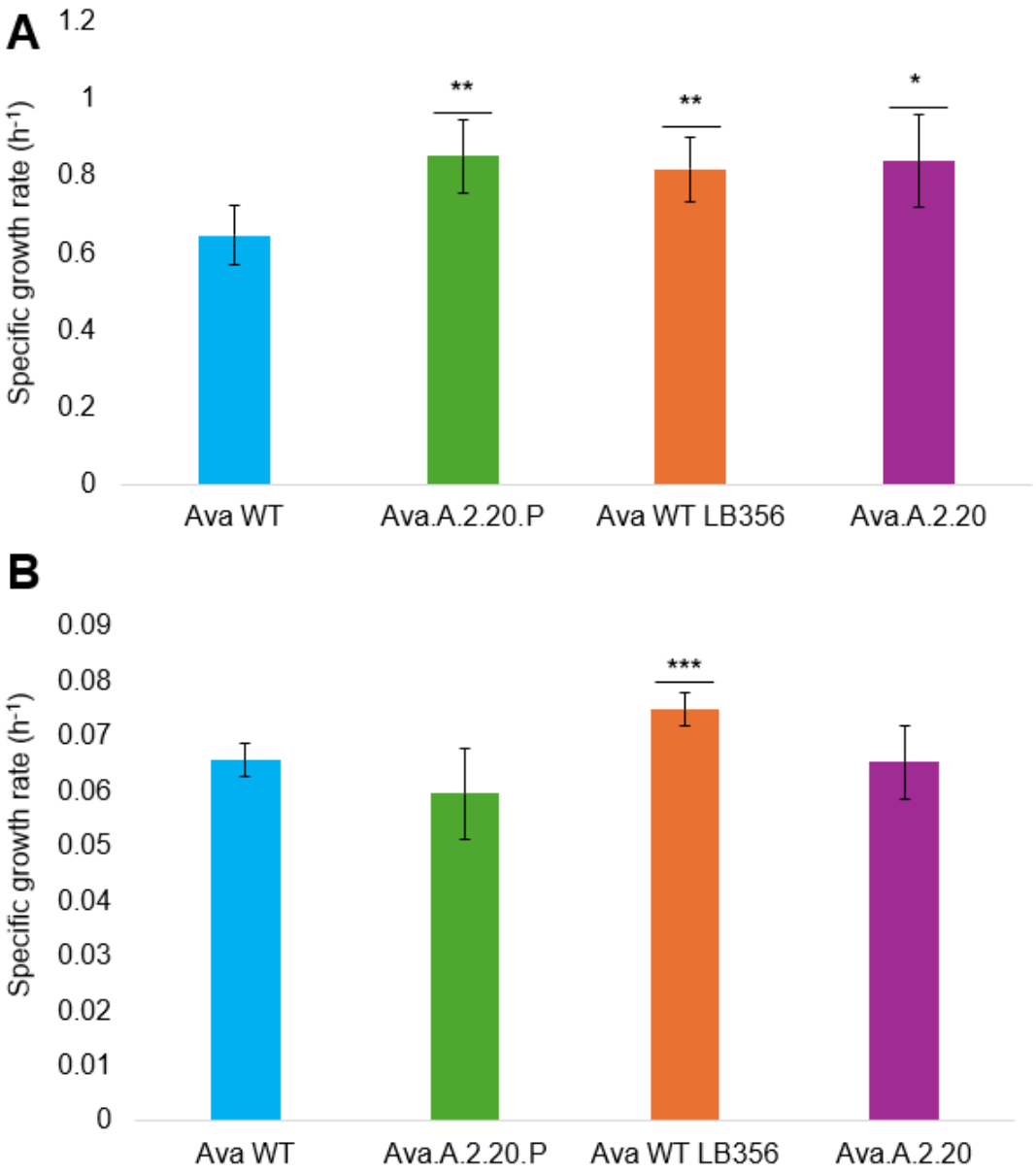


Figure 5.24 | Specific growth rates (h^{-1}) of Ava.WT, Ava.A.2.20.P, Ava.WT with consortia, and Ava.A.2.20 from samples taken between days 1 and 2 of growth at 300 µmol photons·m^{-2}·sec^{-1}, 30 °C, 1.5% CO_2. **A.** Specific growth rates estimated using optical density. **B.** Specific growth rates estimated using chlorophyll concentration. (n = 6, *p < 0.05, **p < 0.01, ***p < 0.001, error bars show standard deviation).

Samples were taken during the growth series on days 2, 4, and 6 for further metabolomic, pigmentation, and DCW analyses (see **Figure 5.25**). These days were chosen as a representation of early exponential, exponential and stationary phase to evaluate any changes in the phenotypic profile during growth.

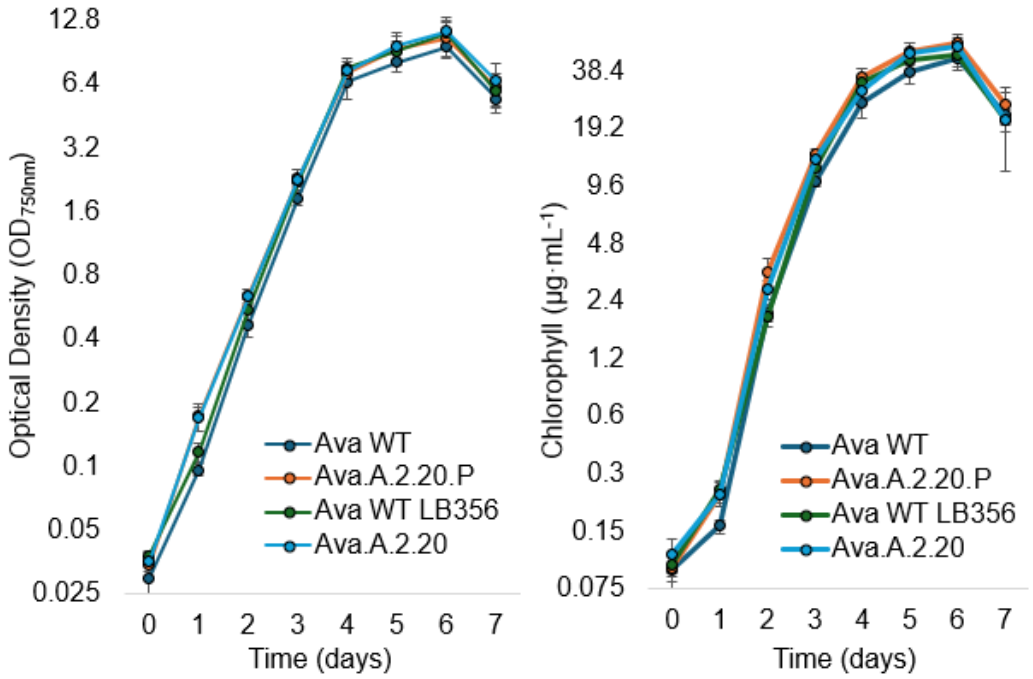
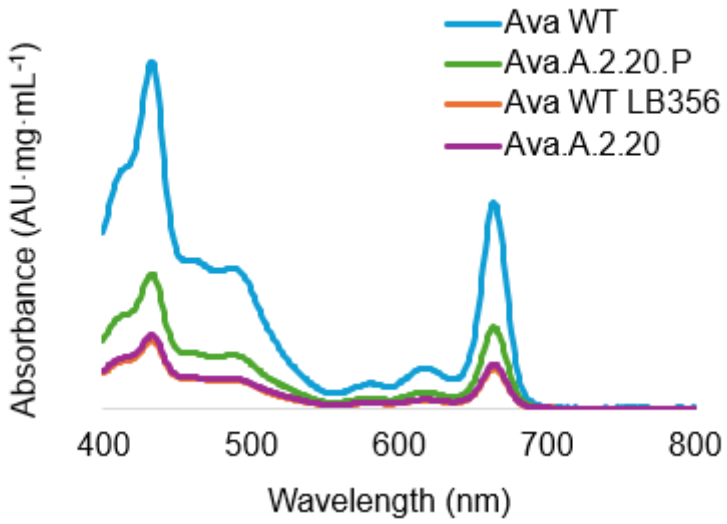


Figure 5.25 | Growth profiles of Ava.WT, Ava.A.2.20.P, Ava.WT inoculated with LB3,5,6, and Ava.A.2.20 grown at 300 µmol photons·m^{-2}·sec^{-1}, 30 °C, 1.5% CO_2. **A.** Optical density measurements (OD_{750nm}). **B.** Chlorophyll concentrations (µg·mL^{-1}). (*n* = 6, error bars show standard deviation).

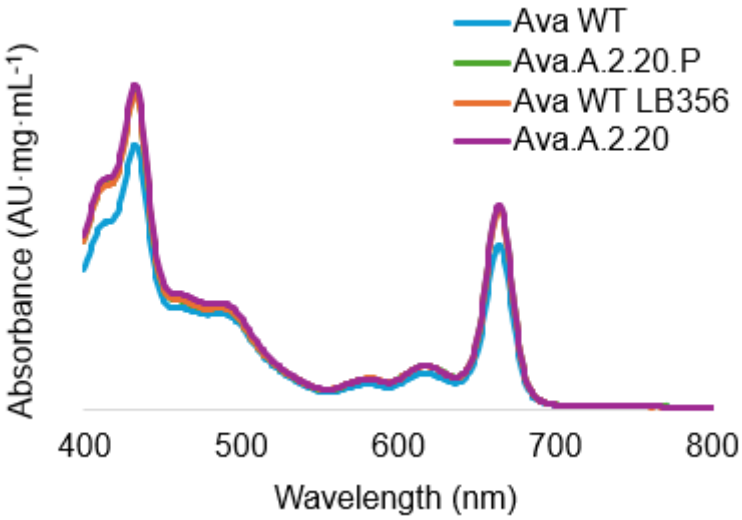
5.4.4 *Measuring the photosynthetic efficiency of Ava.A.2.20 and Ava.A.2.20.P*

Samples of Ava.WT, Ava.A.2.20.P, Ava.WT inoculated with LB3, LB5, and LB6, and Ava.A.2.20 were taken to quantify the relative pigment concentration on days 2, 4, and 6 of growth at 300 µmol photons·m^{-2}·sec^{-1}, at 30 °C, and 1.5% CO_2. Following extraction in *N*,*N*-Dimethylformamide, the absorbance between 400 and 800 nm was measured (*n* = 6) and normalised to OD_{750nm}. These spectra are shown in **Figure 5.26**.

A


Ava WT
Ava.A.2.20.P
Ava WT LB356
Ava.A.2.20
Absorbance (AU·mg·mL⁻¹)
400
500
600
700
800
Wavelength (nm)

B


Ava WT
Ava.A.2.20.P
Ava WT LB356
Ava.A.2.20
Absorbance (AU·mg·mL⁻¹)
400
500
600
700
800
Wavelength (nm)

C

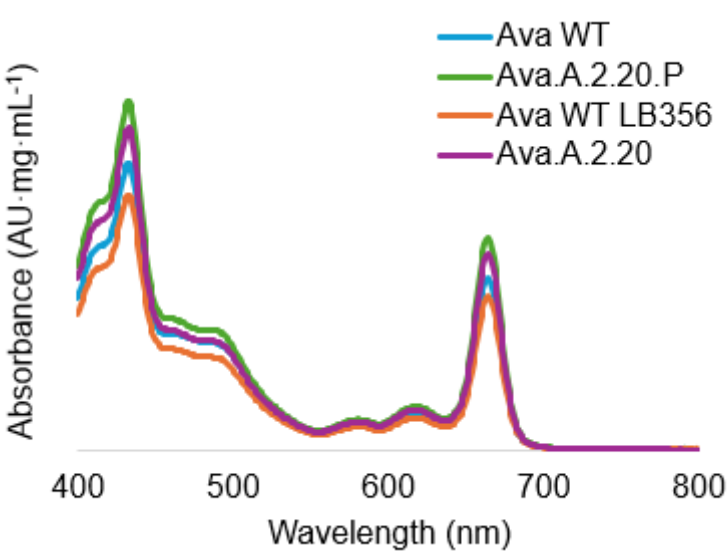

Ava WT
Ava.A.2.20.P
Ava WT LB356
Ava.A.2.20
Absorbance (AU·mg·mL⁻¹)
400
500
600
700
800
Wavelength (nm)

Figure 5.26 | *N*,*N*-Dimethylformamide pigment extraction absorbance spectra (normalized to OD_{750nm}) of Ava.WT (blue), Ava.A.2.20.P (green), Ava.WT with LB3, 5, and 6 (orange), and Ava.A.2.20 (purple), extracted on days **A.** 2, **B.** 4, **C.** 6 of growth at 300 µmol photons·m^{-2}·sec^{-1}, 30 °C, 1.5% CO_2. (*n* = 6).

Most variation between the different strains can be seen during day 2. From these spectra, both chlorophyll and carotenoid concentrations were estimated, and standardised to the DCWs. Relative chlorophyll concentrations are show in **Figure 5.27**. Chlorophyll concentration was significantly lower across all the strains compared to the control Ava.WT on day 2, with Ava.A.2.20.P, Ava.WT with LB3, LB5, and LB6, and Ava.A.2.20 showing 53%, 79%, and 77% reductions respectively. On day 6, however, the relative concentrations of chlorophyll in Ava.A.2.20.P and Ava.A.2.20 were significantly higher than in the Ava.WT strain, with an increase of 29% for Ava.A.2.20.P and 18% for Ava.A.2.20.

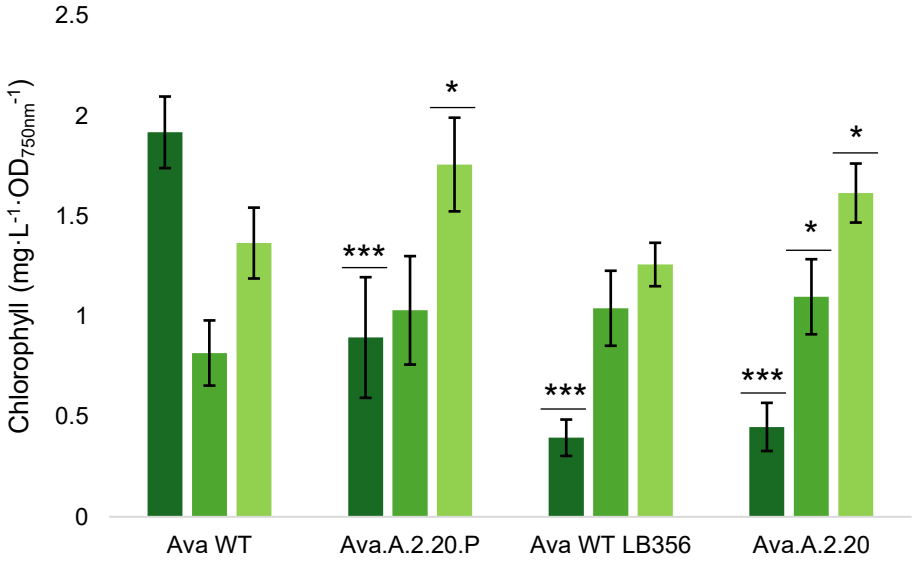


Figure 5.27 | Chlorophyll concentrations of *Trichormus variabilis* strains Ava.WT, Ava.A.2.20.P, and *Trichormus variabilis* strains with consortia Ava.WT LB3,5,6, and Ava.A.2.20, grown at 300 µmol photons·m^{-2}·sec^{-1}, 30 °C, 1.5% CO_2. Left bars shown concentration on day 2, middle bars on day 4, and right bars day 6. (*n* = 6, **p* < 0.05, ****p* < 0.001, error bars show standard deviation)

Similarly, the initial carotenoid concentration from each of the strains was also lower on day 2 compared to the Ava.WT strain (**Figure**

5.28). With reductions of 56%, 78%, and 77% observed in Ava.A.2.20.P, Ava.WT LB3, LB5, LB6, and Ava.A.2.20. Relative concentrations of carotenoids increased slightly in Ava.2.20 on day 6, by 6%.

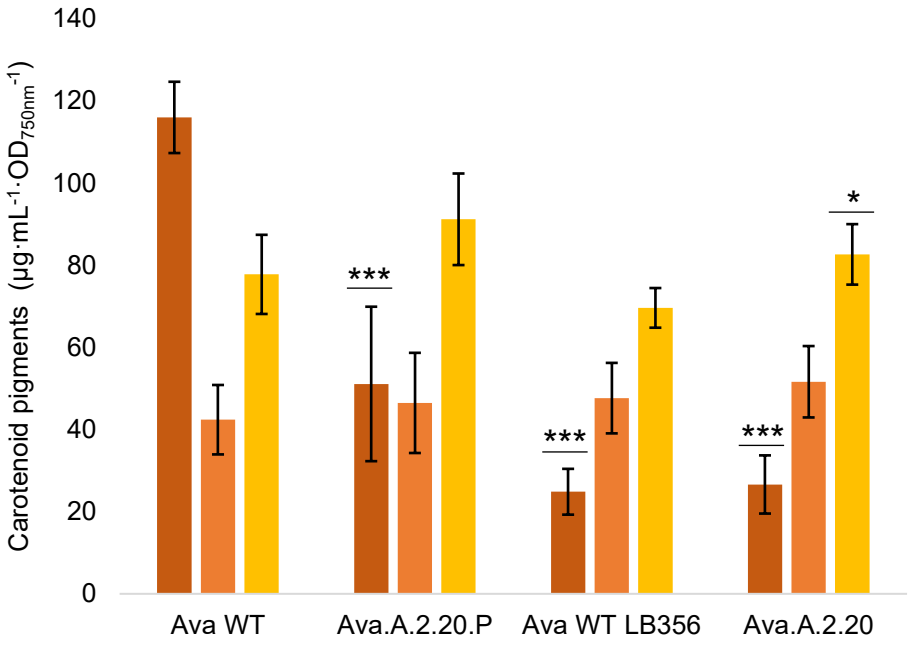


Figure 5.28 | Carotenoid concentrations of *Trichormus variabilis* strains Ava.WT, Ava.A.2.20.P, and *Trichormus variabilis* strains with consortia Ava.WT LB3,5,6, and Ava.A.2.20, grown at 300 µmol photons·m^{-2}·sec^{-1}, 30 °C, 1.5% CO_2. Left bars shown concentration on day 2, middle bars on day 4, and right bars day 6. (n = 6, *p < 0.05, ***p < 0.001, error bars show standard deviation)

To assess the relative photosynthetic productivity in the axenic Ava.A.2.20.P strain compared to the WT Ava.WT strain, oxygen evolution rates were measured using a Clark electrode (**Figure 5.29**). *Trichormus variabilis* Ava.A.2.20.P already appeared to have a distinct phenotype, which was independent from the consortia. The isolate Ava.A.2.20.P showed an overall lower peak in oxygen evolution across the light range investigated (33 to 932 µmol photons·m^{-2}·sec^{-1}). From an intensity of 127 µmol photons·m^{-2}·sec^{-1} to 600 µmol photons·m^{-2}·sec^{-1}, oxygen evolution was significantly lower (p < 0.05). However, unlike Ava.WT, Ava.A.2.20.P did not exhibit photoinhibition and continued evolving oxygen between 734 and 932 µmol photons·m^{-2}·sec^{-1}. Furthermore, the rate of respiration of

Ava.A.2.20.P was significantly lower than Ava.WT during no light treatment ($p < 0.005$), a reduction of 54%.

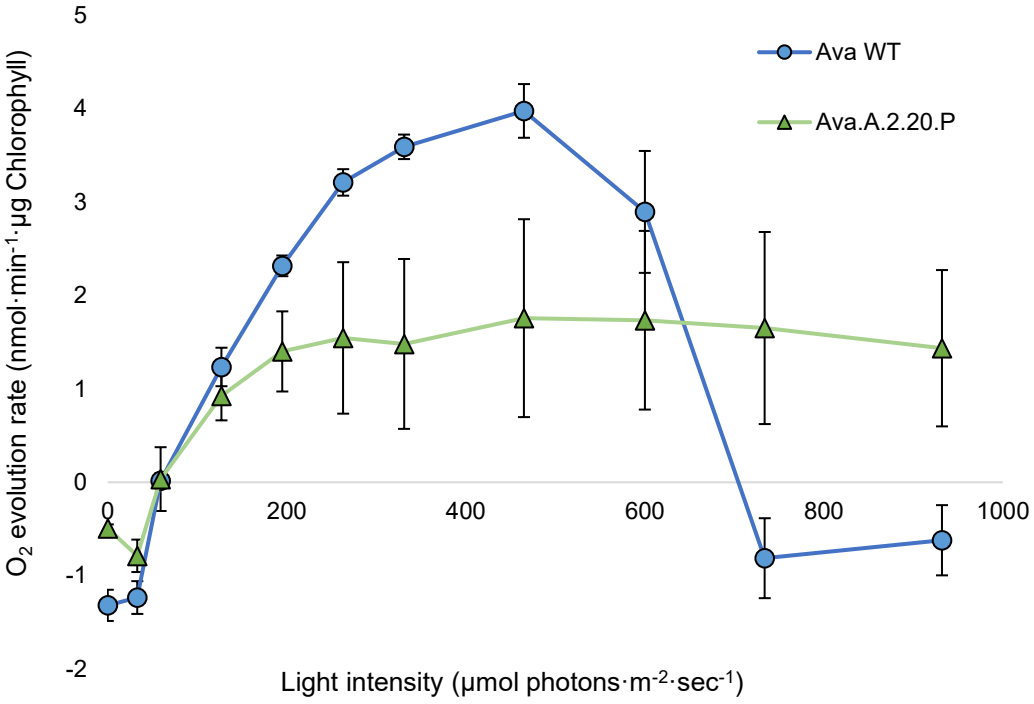


Figure 5.29 | Photoinhibition curve of *Trichormus variabilis* strains Ava.WT and Ava.A.2.20.P. Cultures were grown in 3 independent triplicates, for 3 days, and sampled during early exponential phase (1.5 – 2 OD_{750nm}). Oxygen evolution rates calculated over 2-minute intervals of increasing light intensities. Error bars represent the standard error of the mean (n = 3).

The differences seen in the pigmentation concentration and the rate of oxygen evolution of the axenic *Trichormus variabilis* isolate Ava.A.2.20.P, (without consortia), appear to suggest that the strain had significantly changed compared to the original Ava.WT progenitor strain, and that this was independent of the consortia. Overall, the Ava.A.2.20.P mutant showed a lower rate of oxygen evolution than the control. While this phenotype was highly interesting, without further information on the abundance and architecture of specific photosynthetic apparatus, it is difficult to predict how this phenotype has arisen. This should therefore inform future work.[587587]

5.5 Genomic and metabolomic characterisation of the *Trichormus variabilis* isolate Ava.A.2.20.P

Genomic characterisation of the axenic isolate Ava.A.2.20.P was performed by comparing variation between the sequenced mutant genome and the sequenced genome of the progenitor strain (Ava WT). Metabolomic characterisation was also undertaken to identify potential changes caused by the ALE and the selective pressure on the cell and potential changes caused by the consortia LB3, 5, and 6.

5.5.1 *Genome analysis of the axenic Trichormus variabilis Ava.A.2.20.P*

Following extraction and preparation of the gDNA from both Ava.A.2.20.P, and Ava WT the quality and quantity of the DNA were assessed. Ava WT and Ava.A.2.20.P were prepared for Nanopore sequencing following the ligation sequencing protocol SQK-LSK109. Prepared libraries were sequenced using an FLO-MIN114 Flow Cell (R10.4.1) MinION® (Oxford Nanopore Technologies). Genome assembly of Ava.WT was carried out using Geneious™ Prime (v 2024.0), and RefSeq NC_007413 *Trichormus variabilis* ATCC 29413 (NCBI) as a genomic scaffold. Sequences of Ava.A.2.20.P were then assembled to the Ava.WT consensus sequence. Post trimming sequence quality was assessed as 100.0% high quality by the Geneious™ Prime proprietary algorithm. Regions of low coverage were identified as regions with fewer sequencing reads than ≥ 2 standard deviations from the mean. Variants and polymorphisms were called using the proprietary software's algorithm against the *Trichormus variabilis* ATCC 29413 Ava.WT consensus sequence. In total 1791 variants with non-synonymous predicted changes were detected. Of these, 9 were deletions which resulted in a frame shift, 1 was an insertion resulting in a frame shift, 1555 were single nucleotide polymorphisms (SNPs) which resulted in either amino acid substitutions, truncations, or extensions, and 201 were multiple base pair substitutions. Also present were 227 tandem repeat deletions, which typically result in frame shifts. Evaluating the top 100 SNP variants with the lowest P-value, 7 resulted in amino acid changes with high confidence. Together with deletions and insertions, these are shown in **Table 5.3**.

Table 5.3 | Top non-synonymous genomic variations between Ava.WT and Ava.A.2.20.P by combined sequences read confidence (P-value). Annotations transferred from RefSeq NC_007413 *Trichormus variabilis* ATCC 29413 (NCBI). (*n* = "coverage").

SNPs						
Gene	**Coverage**	**Polymorphism Type**	**Protein Effect**	**Variant Frequency**	**Variant P-Value (approximate)**	**Change**
hetI	136	SNP (transition)	Substitution	91.90%	1.50E-272	Asp 64 Gly
ava_3215	137	SNP (transversion)	Substitution	95.60%	7.70E-253	Thr 4 Pro
ava_4262	132	SNP (transition)	Substitution	93.20%	2.30E-233	Ser 110 Pro
ndk	107	SNP (transition)	Substitution	93.50%	2.50E-200	Ile 91 Thr
ava_4855	109	SNP (transition)	Substitution	89.90%	3.40E-182	Ile 562 Val
ava_4645	133	SNP (transition)	Substitution	88.70%	4.50E-182	Asp 351 Gly
ava_2585	106	SNP (transition)	Substitution	84.90%	2.70E-135	Ser 183 Pro
DELETIONS						
ava_2041	141	Deletion	Frame Shift	79.40%	8.40E-22	- C or T 656
ava_0871	159	Deletion	Frame Shift	85.50%	6.70E-21	- C or G 428
ava_0152	125	Deletion	Frame Shift	80.80%	7.70E-21	- C 20
ava_0365	125	Deletion	Frame Shift	88.00%	3.10E-19	- C or T 998
ava_4980	112	Deletion	Frame Shift	86.60%	4.30E-16	- C or T 285
ava_1337	43	Deletion	Frame Shift	83.70%	1.10E-15	- A or C 162
ava_3146	108	Deletion	Frame Shift	80.60%	5.80E-11	- C or G 175
ava_4268	106	Deletion	Frame Shift	74.50%	2.50E-07	- A or G 114
INSERTIONS						
nifH	112	Insertion (tandem repeat)	Frame Shift	79.50%	4.60E-102	+ C 134

Of the highlighted mutations with the lowest P-values, the insertion of a single nucleotide into the sequence of *nifH* at base pair 134 resulted in a frame shift within the sequence. Leucine 45 being converted into proline, and a stop codon introduced at residue 52. This is very interesting as *nifH* encodes a subunit of the nitrogenase enzyme. The subsequent frameshift resulting in a truncation, and loss of ~70% of the amino acids. However, the genome sequence had several copies of the *nifH* gene, with

a total of 5 copies in the genome (KEGG annotations). *Trichormus variabilis* possess multiple nitrogenase gene operons, and a total of 3 different nitrogenase enzymes [567]. It is unclear from analysis of the flanking regions which copy of the *nifH* gene has been mutated here, however, the sequence aligns with *ava_4478* (see **Figure S9** in **Appendix**). Despite the annotation of this sequence, however, no examples of specific literature discussing the sequence could be found. Annotation homology putatively assigns limited similarity in amino acid sequence to an NifH/CfbC nitrogenase-like enzyme; similar enzymes have previously been shown to be involved in coenzyme F_{430} biosynthesis [568]. Coenzyme F_{430} has been shown to be involved in anaerobic methane formation, and potentially in the oxidation of short chain alkanes (see Thauer 2019) [569]. NifH/CfbC nitrogenase-like enzymes maintain a high degree of sequence conservation with nitrogenase reductase subunits and may also be involved in redox reactions [568].

The *ndk* gene had a SNP resulting in an amino acid change from serine to threonine, Ndk has previously been shown to act as a DNA repair protein in *Anabaena*/*Nostoc* sp. strain PCC 7120 [570], responsible for fixing double strand breaks. It not obvious why such a mutation would be selected for under these conditions, however, the gene has been shown to be upregulated following salt stress and UV stress, so could be response to the EMS treatment [571]. This said, Ndk has previously been shown to play a role in plant photosynthesis (see Dorian & Rivoal, 2014) [572]. With two isoforms, both concentrated in the chloroplasts, and involved in oxidative stress management and energy metabolism respectively. They have a key role in balancing intracellular nucleotide triphosphate and diphosphate abundance [572].

The *hetI* gene had a SNP changing Asp 64 to Gly, this gene encodes the protein HetI which is similar to the SfP protein from *Bacillus subtilis* and the EntD protein from *E. coli*, these proteins are required for the export of cyclic peptides [362]. HetI has been shown to relieve suppression of heterocyst formation by HetN, which has also been shown to play a role in fatty acid metabolism [573]. Though not specifically measured, heterocyst abundance was noted to be lower, and the size of the cells appeared larger in Ava.A.2.20.P compared to the Ava.WT strain when compared under a light microscope. Although this would be surprising, given that heterocyst cells depend on carbon supplied from neighbouring vegetative cells and this would be reduced by fructose supplementation (see section **2.7.2.2**), heterocyst abundance would first need to be accurately assessed before further analysis could be performed here.

Ava_4855 shares homology with the WD-40 repeat-containing serine/threonine kinase proteins. WD40 enzymes are well characterised in eukaryotes and are enriched in cyanobacteria [574]. However, their role in cyanobacteria is relatively less well known. Within eukaryotes these proteins are involved in many functions, including cell signalling, transcriptional regulation, and controlling aspects of cell division [575]. The gene *ava_2585* has been putatively annotated as an NAD dependent epimerase/dehydratase. In *Pectobacterium carotovorum* these proteins have been shown to play a role in cell surface properties [576].

However, many hypothetical proteins were not annotated. Of these within **Table 5.3**, two are thought to be involved in NADPH dependent reactions, which could also play a role in increasing NADPH availability, depending on the specific role of the proteins. However, this analysis would benefit from higher confidence in available annotations.

5.5.2 *Metabolomic characterisation of the isolate Trichormus variabilis*

To assess the metabolic profile of the *Trichormus variabilis* isolates, both with and without the consortia, samples were taken from Ava.WT, Ava.A.2.20.P, Ava.WT inoculated with LB3, LB5, and LB6, and Ava.A.2.20.P grown at 300 μmol photons·m^{-2}·sec^{-1}, at 30 °C, and 1.5% CO_2, (see **Figure 5.25**). Metabolomic extractions were carried out as previously described in 2.6.2 on 6 replicates harvested from days 2, 4, and 6, however, due to unforeseen and repeated hardware issues, only 3 samples of each class from day 2 were able to be processed fully. These samples nonetheless provide some insight into the metabolomes of these classes during the early exponential phase of growth.

Following sample processing using the mass spectrometer, untargeted metabolomic data was processed using CD 3.3 (ThermoFisher Scientific™), and this processed data was analysed using Simca™ P (Sartorius™). A PCA model was generated to assess overall differences between the samples. A relative plot of this model is shown in **Figure 5.30**. This shows that the Ava.WT samples were the most divergent from all the other strains, and that there was relatively little difference between the Ava.A.2.20.P, Ava.WT LB3, LB5, and LB6, and Ava.2.20 strains. Tight clustering of the QC samples indicates high instrument stability.

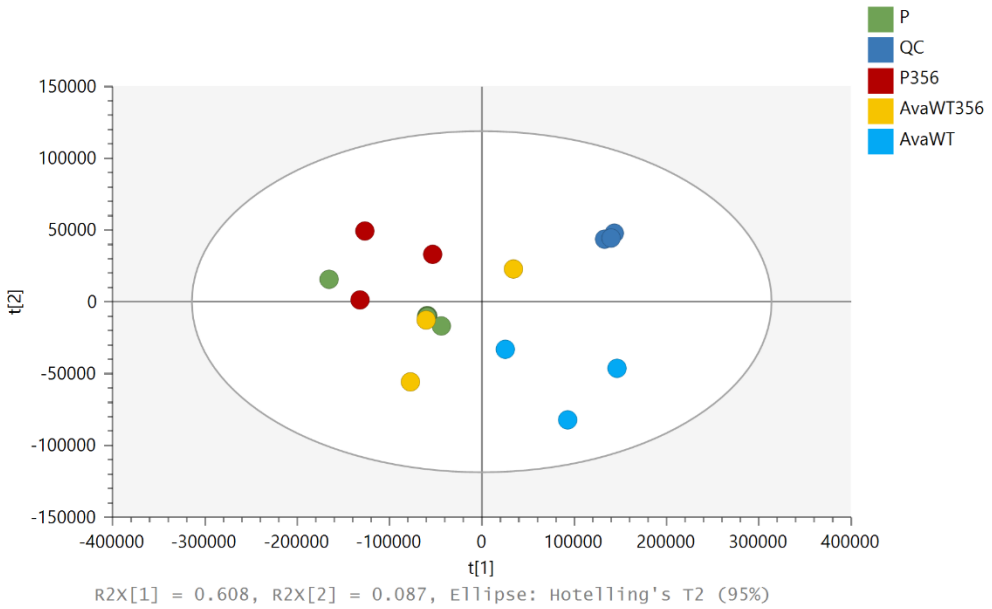


Figure 5.30 | PCA model comparing untargeted metabolomic analyses of Ava.WT (light blue), Ava.A.2.20.P (green), Ava.WT inoculated with LB3, LB5, LB6 (yellow), and Ava.A.2.20 (red) grown at 300 µmol photons·m^{-2}·sec^{-1}, 30 °C, 1.5% CO_2 after 2 days of growth. (Three QC samples (blue); *n* = 3).

To compare the specific differences between the Ava.WT strain and the other strains, OPLS-DA models were generated between Ava.WT and each of the other strains, and between Ava.2.20.P and Ava.A.2.20. However, these models were not validated to show significant difference between any of the classes when permutation analysis was carried out.

Putatively identified metabolites were, however, further assessed using the VIP Score analysis of Simca™ P to identify significant differences. VIP scores were compared to the results of the Compound Discoverer analysis, and metabolites with both a VIP score ≥ 1, and an adjusted P value of < 0.05 were selected. No significantly different metabolites were identified using this criterion between the Ava.WT and any of the other strains, or between the Ava.A.2.20.P strain and the Ava.A.2.20 strain. However, many metabolites did show relatively large changes between the strains with and without the consortia.

The amino acids proline (VIP > 7.7), leucine (VIP > 6.7), and alanine (VIP > 3.7) were all >1 Log2-fold higher in samples with the consortia present compared to the strains with no consortia. Previous work by Perera *et al*. 2021 showed that in the microalgal species *Coelastrella* sp. IS3, grown in consortia with *Variovorax paradoxus* IS1, there was a significant increase in both proline and alanine concentrations, as well as other amino

acids [577]. These compounds likely support strains in consortia with an accessible source of nitrogen. This work also showed a significant increase in lipid production in the consortia cultures, potentially as a result of the heterotrophic consortia being able to dedicate fewer resources to nitrogen metabolism, and more to carbohydrate synthesis [577]. Demonstrating the advantage of microbial consortium in allowing strains to specialise their metabolisms.

5.6 Evaluating the impact of fructose supplementation on the selection process

The *Trichormus variabilis* strains isolated using the chemostat driven selection in **5**.4 appear to have, on average, become more reliant on the fructose supplementation to sustain enhanced growth (see **Figures 5.5**, **5.8**). This outcome was not the original aim of the experiment, as we sought to identify strategies which enhanced the growth and nitrogen fixation without making them dependent on macronutrient supplementation. When these strains were supplemented with fructose however, the relative improvement in biomass accumulation suggested that this strategy could be successfully used to improve nitrogen fixation within filamentous cyanobacteria. To both investigate the impact fructose supplementation had on the phenotypes isolated from chemostat selection, and to refine this approach for selecting strains with enhanced biomass formation, the chemostat selection of *Trichormus variabilis* was repeated without fructose.

A culture of the same Ava WT progenitor strain used in **5**.4 was mutagenized following the same workflow outlined in **Figure 5.2** (see **3.4.1.2** for further details). However, previously were all the steps utilised BG-11_0A and its derived variants, these were replaced with BG-11_0 and BG-11_0 derived media variants. Following mutagenesis of Ava.WT, the strains derived from this selection were labelled as “Ava.B.[isolate number]”.

5.6.1 *Trichormus variabilis autotrophic strain selection*

Harvesting of 5 mL samples of the population were taken from spent media at semi-regular intervals (every ~2-3 days). These libraries were labelled from 1 to 24, with the library number referring to its relative position after inoculation. Library 1 was harvested 6 days after EMS

treatment, and library 2 was harvested 8 days after, and so on. Cyrostocks were created from these libraries following an established method already utilised in the laboratory. These 5 mL samples were centrifuged at 5000 g for 10 – 15 minutes, at 4 °C, until a stable pellet was obtained. Supernatants were discarded, and the pellets were resuspended in 1 mL of a cryoprotective solution, (0.5 x BG-11_0 liquid medium, 5% methanol, 8% dimethylsulfoxide). Samples were transferred to 1.5 mL cryovials and stored at -80 °C until all population samples were collected.

Once the chemostat selection was complete, cryostock samples were revived. The cells were pelleted by centrifugation at 5000 g for 10 minutes, and the pellets were resuspended in 1 mL of fresh BG-11_0 medium. Cultures were transferred to individual T25 cell culture flasks containing 4 mL of BG-11_0 liquid media, and flasks were covered using 1 layer of white tissue roll to prevent death of cultures due to excess light exposure following culture revival. These libraries were grown at 60 µmol photons·m^{-2}·sec^{-1}, at 30 °C, for 48 hours, before the paper coverings were removed. Growth was then maintained for an additional 48 hours at 300 µmol photons·m^{-2}·sec^{-1}, 30 °C, at which point all cultures showed strong visible growth.

To evaluate the biomass formation of these libraries, 0.5 mL of the culture was first adjusted to 0.1 OD_{750nm} in 15 mL centrifuge tubes using fresh BG-11_0 liquid medium. Aliquots of 1.1 mL of these cell culture mixes was then aliquoted at random into triplicate Corning™ Costar™ 24-well Clear TC-treated Multiple Well Plates (Fisher Scientific™). This was done across 3 plates in total. These 24-well plate libraries were grown at 300 µmol photons·m^{-2}·sec^{-1}, at 30 °C, for 5 days. DCWs were measured by transferring 1 mL of culture from each well into pre-dried 1.5 mL microcentrifuge tubes, drying the tubes for 48 hours at 80 °C, and re-weighing each tube using an analytical balance. The DCW was measured as the difference in weights of the tubes from before and after drying the culture solutions. The results of this library screen are shown in **Figure 5.31**.

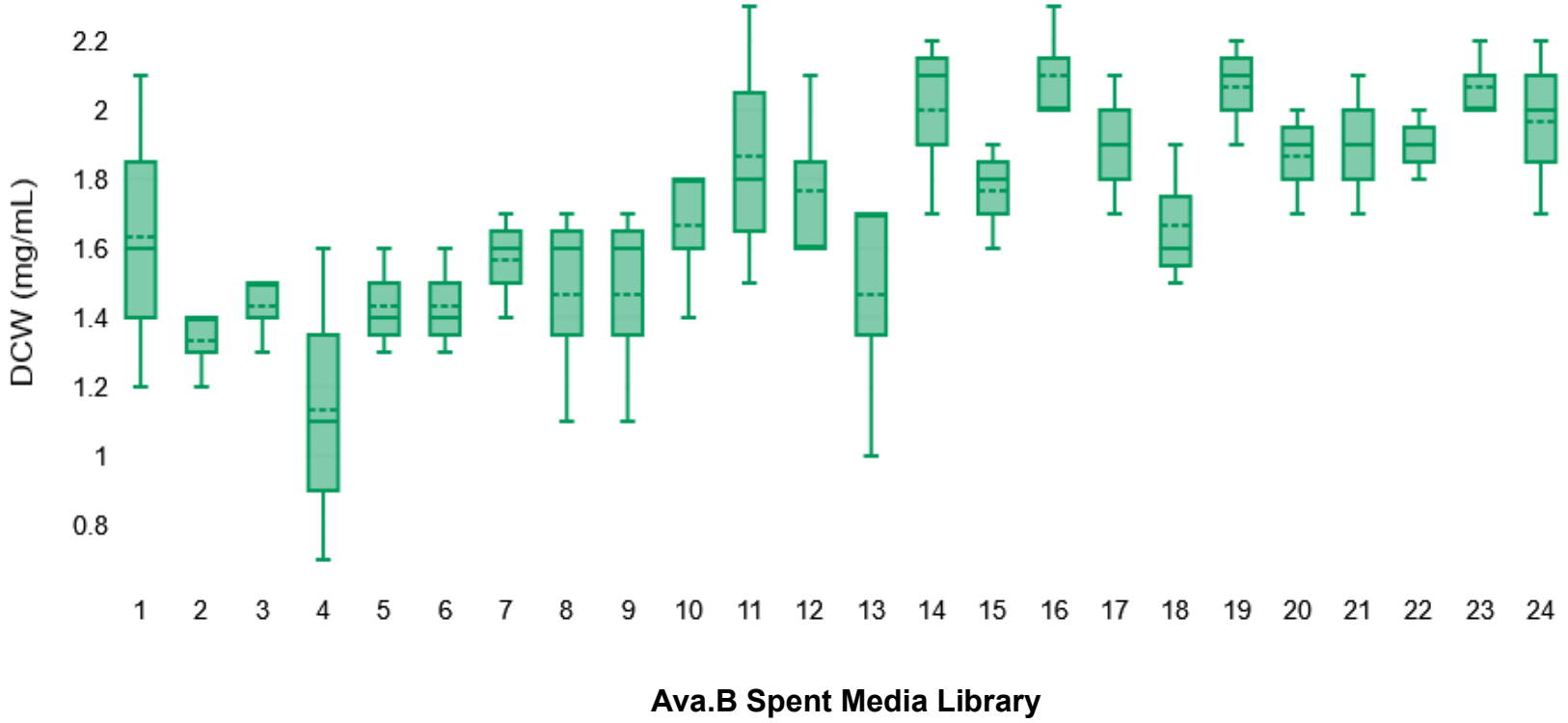


Figure 5.31 | Dry cell weights (mg·mL^{-1}) from 24-well plate screened Ava.B population libraries, sampled from chemostat spent media every 2-3 days, at 300 µmol photons·m^{-2}·sec^{-1}, 30 °C, 144 hours, in BG-11$_0$ liquid media (n = 3, error bars show standard deviation).

No significant difference was observed ($P > 0.32$) between population 1, isolated from the beginning of the chemostat selection, and population 24, isolated at the end. However, observing the overall trend of these results, libraries appeared to show a steady increase in the average biomass formation. To assess this, the 24 library populations were separated into 4 quartiles based on their overall sampling position. Quartile "a" contained Ava.B library cultures 1 – 6, quartile "b" contained Ava.B library cultures 7 – 12 etc. The mean DCW of each quartile increased in line with the sampling stage of the experiment and time in the chemostat, with average DCWs across populations a – d being 1.4 ±0.27, 1.63 ±0.28, 1.81 ±0.29, and 1.96 ±0.16 mg·mL^{-1}. Using a one-way analysis of variance test, mean sampling quartile was shown to have a significant impact on biomass accumulation ($F_{3,71} = 14.89$, $p < 0.001$). The distribution of measured DCWs from each quartile are shown in **Figure 5.32**.

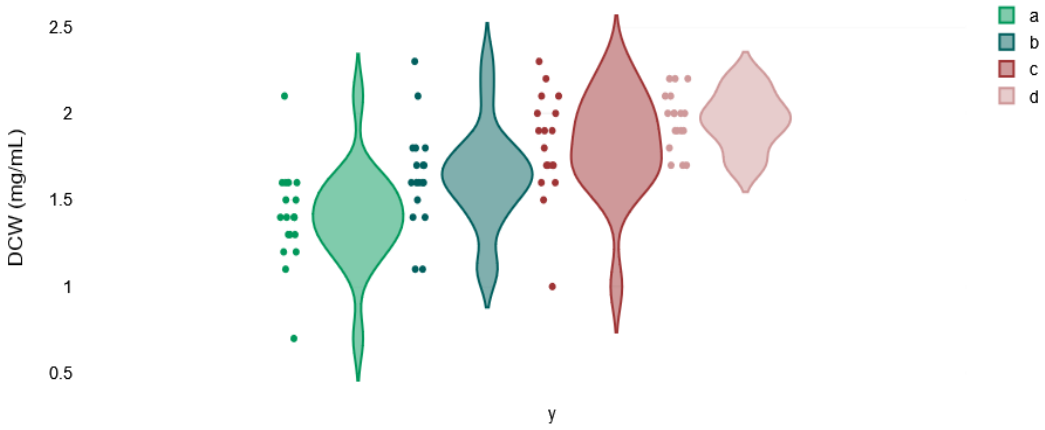


Figure 5.32 | Distribution of dry cell weight measurements (mg·mL^{-1}) across Ava.B chemostat time sampling quartiles, grown at 300 µmol photons·m^{-2}·sec^{-1}, 30 °C, 144 hours, in BG-11$_0$ liquid media. "**a**" – Ava.B sampling libraries 1 – 6. "**b**" Ava.B sampling libraries 7 – 12. "**c**" Ava.B sampling libraries 13 – 18. "**d**" Ava.B sampling libraries 19 – 24 ($N = 18$).

5.6.2 *Trichormus variabilis strain isolation following autotrophic selection*

Following completion of the selection process individual strains were again isolated following the same strategy as described in **5.3.2** (see

Figure 5.4). A total of 66 single colonies were isolated onto BG-11_0 solid media, coupled with LB solid media plating. Unlike the previous selection, which included fructose, the overall abundance of contaminants that appeared on the companion LB solid media plating was lower. No data is available for a direct comparison with the Ava.A strain isolation, however, 8 strains showed associated contamination during the Ava.B strain isolation. To avoid adding any bias into the selection process and subsequently the results, and because previous selection had not removed strains with contamination, the first 44 strains were selected for characterisation. Of the 44 selected strains Ava.B.3, Ava.B.13, Ava.B.40, Ava.B.41, and Ava.B.43 contained cells other than *Trichormus variabilis*.

5.6.3 *Measuring biomass yields*

Isolates were screened using the same strategy as described in 4.5.1, with isolated colonies plated in triplicate into Corning™ Costar™ 24-well Clear TC-treated Multiple Well Plates (Fisher Scientific™) using 1 µL sterile loops. Plates were grown at 300 µmol photons·m^{-2}·sec^{-1}, at 30 °C, for 120 hours, and 1 mL of each well was transferred to a pre-dried, pre-weighed 1.5 mL microcentrifuge tube. Samples were dried at 80 °C for 48 hours and weighed using an analytical balance. DCWs were estimated by calculating the difference between the tube weights before and after drying the samples (**Figure 5.33**).

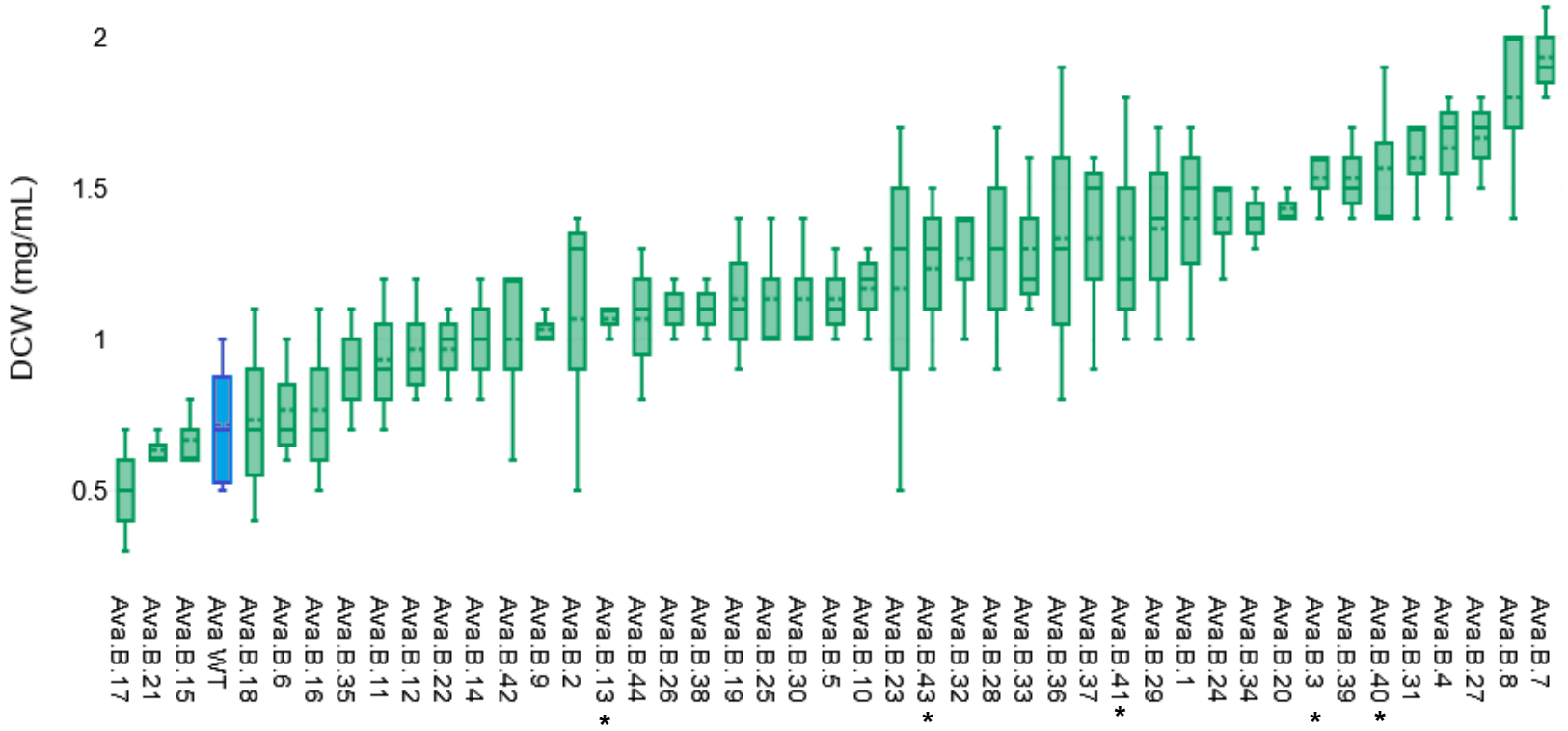


Figure 5.33 | Dry cell weights (mg·mL^{-1}) from *Trichormus variabilis* (Ava.B) mutant isolate screening. Plates grown at 300 µmol photons·m^{-2}·sec^{-1}, 30 °C, 120 hours, in BG-11$_0$ liquid media. Green shows Ava.B chemostat isolates. Blue shows Ava WT progenitor strain. (*n* = 3; ***** = non-axenic, error bars show standard deviation)

The Ava.B isolate screening showed an increase in the average biomass of the screened isolates compared to the Ava WT strain, 1.19 ±0.38 compared to 0.72 ±0.2 $mg \cdot mL^{-1}$ respectively. Furthermore, this was shown to be statistically significant ($p < 0.002$). No significant difference was observed between the means of the cultures with contamination (1.35 ±0.3 $mg \cdot mL^{-1}$) and the cultures without the contamination (1.15 ±0.39 $mg \cdot mL^{-1}$). The highest performing strain (Ava.B.7) showed a significant 2.7-fold increase in biomass accumulation compared to the WT strain ($p < 0.00005$). Here, the presence of contamination did not significantly affect the growth of isolates ($P > 0.095$).

5.6.4 *Specific impact of fructose supplementation*

Compared to the Ava.A isolates obtained in **5**.4, Ava.B isolates selected in a chemostat without fructose showed a significantly higher biomass accumulation of > 4.9-fold when screened in 24-well plates using $BG\text{-}11_0$ liquid media ($p < 0.4E\text{-}60$) (**Figure 5.34**). No significant differences were seen in the Ava.WT biomass accumulation between these two 120-hour 24-well plate screens at 300 µmol $photons \cdot m^{-2} \cdot sec^{-1}$, 30 °C ($P > 0.05$). These results suggest that the addition of fructose significantly diminished the biomass accumulation of *Trichormus variabilis* strains in autotrophic conditions, and perhaps suggests that using fixed carbon to direct electron stress towards nitrogen fixation was not an effective strategy. Whilst there are several examples of cyanobacteria being cultured in mixotrophic (see Wan *et al*. 2015) [578], or even heterotrophic conditions [299], in the literature there are no examples of autotrophs becoming dependent on the addition of sugar following adaptative evolution.

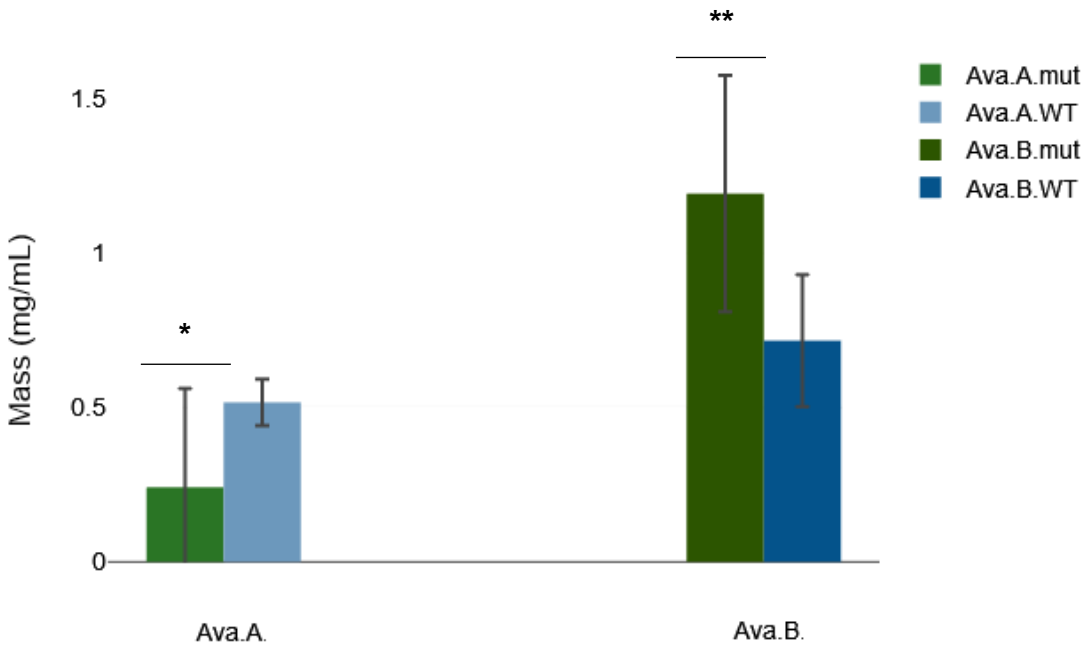


Figure 5.34 | Combined dry cell weights of all Ava. WT and mutant samples screened in BG-11_0 liquid media in 24-well plates, grown at 300 µmol photons·m^{-2}·sec^{-1}, 30 °C, 120 hours – in both chemostat experiments. Green indicates mutant populations of Ava.A and Ava.B strains. Blue indicates Ava.WT, screened either with Ava.A or Ava.B mutants. (*p < 0.05, **p < 0.01, error bars show standard deviation).

5.7 Discussion

In this chapter, the use of a chemostat selection was validated with the model filamentous cyanobacteria *Trichormus variabilis* ATCC 29413.

Initial attempts were made to select for cells with increased biomass and subsequently a higher rate of nitrogen fixation utilising an organic carbon source, fructose. However, this approach was inefficient, resulting in a large proportion of the cells having less biomass and generating strains which were highly dependent on mixotrophic growth conditions. Despite this, one strain was isolated, the Ava.A.2.20 strain, which had a significantly higher growth rate than the original Ava.WT strain. The increase in biomass formation was shown to be 2.9-fold higher after 120 hours of growth.

This strain was originally isolated as part of a heterotrophic consortium, the individual members of this consortium were successfully isolated, and putatively identified. The individual strains were then added to the WT strain, Ava.WT, either as individual strains or as combined

strains. The individual strains had little impact on the growth of the *Trichormus variabilis* WT strain, however, when all three members of the consortia were added, the growth rate of *Trichormus variabilis* increased by ~1.3-fold following the addition of 1.5% CO_2 ($p < 0.01$). No changes in growth of Ava.A.2.20.P was observed with consortia and 1.5% CO_2 supplementation, however.

Several studies have shown that both cyanobacteria and algae can exist in mutualistic relationships, these relationships can consist of other microorganisms, invertebrates such as molluscs, sponges and coral as well as plants [327]. Heterotrophic bacteria have been shown to form highly productive relationships with cyanobacteria, these relationships are often based on nutrient recycling [531], and often prolong the viability of both cells [536]. Phototrophic organisms such as cyanobacteria often produce significant amounts of dissolved organic matter (DOM), this is often the main source of carbon and energy for mutualistic heterotrophic bacteria [579]. It is likely that the consortia strains are benefiting from this DOM release from the *Trichormus variabilis* cells. Heterotrophs have been shown to benefit autotrophs in several ways, these include remineralising DOM, which mostly consists of biopolymers, these large molecules are often inaccessible to cyanobacteria [529]. Heterotrophs can also protect cyanobacteria against opportunistic predators including grazers by producing a range of antimicrobial, antifungal or antilarval inhibitors [580–582]. Some heterotrophs have been shown to facilitate iron uptake [583], enhance vitamin availability [584], promote cell division [585], and reduce oxidative stress through the production of catalase enzymes, superoxide dismutases and glutathione reductase enzymes [586]. These relationships often develop and thrive in ecological niches, driven by the selective pressure from the environment. This is similar to the evolutionary pressure applied during ALE, which is a process designed to mimic natural selection, obtaining ameliorated organisms, which have accumulated beneficial mutations during the ALE process [587].

The presence of the heterotrophic strains led to the Ava strain significantly altering its photosynthetic pigments, with significant reductions seen in both the chlorophyll and carotenoid content during early exponential growth. Interestingly the axenic Ava.A.2.20.P strain also had a significant reduction in its pigmentation profile and a ~1.3-fold increase in the exponential growth rate ($p < 0.01$). Suggesting that the Ava.A.2.20.P strain had also evolved independently of the consortia, although it is not clear what impact the presence of the consortia had on the strain's evolution. The oxygen evolution rate was evaluated in both the Ava.WT strain and the axenic Ava.A.2.20.P strain, demonstrating that the evolved

strain had a 54% lower rate of respiration ($p < 0.01$), a ~44% lower peak rate of oxygen evolution ($p < 0.05$), it was also less susceptible to photoinhibition. Potentially suggesting that the reaction centres are more resistant to photoinhibition, but this may have come at a performance cost as evidenced by the lower rate of oxygen evolution.[609]

Omic characterisation of the different strains proved challenging. Evaluating the metabolic profile of each individual strain in a consortium is difficult and previous studies have initially deduced metabolic pathways from the genomic data of organisms to understand community interactions [588]. Whilst higher concentrations of amino acids were seen in these strains, it is not 100% certain which strain was responsible for these increases. Ideally the metabolomics of each individual strain would be analysed alongside the consortia strains and compared to metaproteomics and metatranscriptomics. To help elucidate the function of each strain in the consortia and the role it plays in the mutualistic relationship. However, due to time constraints this was not possible. Another interesting approach, which could be combined with the omics is to measure specific elemental fluxes, which can provide insights into the fate of specific compounds in the microbial network [589]. The approach often involves utilising labelled ^{13}C, ^{15}N or ^{18}O. This approach was successfully utilised to demonstrate the coupling of anaerobic methane oxidation to nitrate reduction in archaea, and the subsequent utilisation of the nitrite by an annamox population [589].

Furthermore, genomic analysis revealed that many of the mutations which had accumulated in the genome of the Ava.A.2.20.P strain had occurred in genes which have yet to be fully annotated. Making evaluating the impact of these mutations on the strain difficult to assess. Several interesting candidates were identified with mutations including the putatively annotated *nifH* and *hetI* genes, both could play a role in the improved growth rate and assumed nitrogen fixation rate seen in the axenic Ava.A.2.20.P strain. Given the potential for *nifH* to use ATP in reactions not directly linked to nitrogen fixation, a truncation (and potential deletion) in this protein could increase the availability of ATP for nitrogen fixation reactions. It would be interesting to recreate these mutations in the Ava.WT strain and evaluate the impact on both the growth rate and nitrogen fixation. However, it is likely that the combined genomic mutations in Ava.A.2.20.P are responsible for the improved phenotype.

Collectively, however, these characterisation investigations have assisted in identifying possible indications of how the *Trichormus variabilis* isolate Ava.A.2.20.P has evolved (**Objective 3**).

Repeating the selection process without the addition of the fructose proved to be a more efficient ALE process, selecting strains with improved biomass accumulation, (and assumed nitrogen fixation). These chemostat ALE experiments both generated strains with significantly improved growth, and showed the strategy is effective to select for enhanced strains of *Trichormus variabilis* sp. ATCC 29413 (**Objective 2**). The strains selected under autotrophic conditions require further omic characterisation however, to see of the changes in these strains are similar to the ones in the Ava.A.2.20.P strain.

Chapter 6.

General discussion and future work

6.1 General discussion

Cyanobacteria are capable of utilising CO_2 as their sole carbon source, making them attractive biotech chassis in the fight to reduce GHG emissions. Furthermore, as many of these organisms are also capable of fixing nitrogen, they could also be useful in reducing the ecological impact of the highly polluting agricultural sector. Cyanobacteria have many potential biotech applications, ranging from agriculture (including aquaculture), food, environmental remediation, bioenergy in the form of bioethanol and hydrogen, and pharmaceutical biotechnology. As cyanobacteria produce a range of compounds which can be used as antimicrobials, anti-inflammatories, immunosuppressants, anticoagulants and antitumor agents [590]. Despite their huge potential they are still hampered by several factors including poor growth rates, when compared to other heterotrophic and autotrophic bacteria. The cost of the photobioreactors needed to scale them, and robustness within strains. Strains that often work well in a small-scale laboratory setting often crash in larger scale reactors, particularly within non-sterile race way ponds [591].

Work to improve their productivity has to date mainly focused on how to re-direct metabolic flux down specific product pathways, and less on how to optimise these organisms for large scale industrial application. Work carried out in the field thus far has evaluated ways to improve the efficiency of specific carbon fixation enzymes, including RuBisCO [158]. With billions of years of prior experience, the best strain engineers are often the cells themselves. The aim of this project was therefore to use adaptive laboratory evolution, coupled with an optimised selection strategy, to generate strains with enhanced growth and biomass formation.

6.1.1 *ALE to increase carbon fixation*

In **Chapter 4**, an ALE pipeline was developed to enable the selection of strains with improved carbon fixation. Building on established knowledge from the literature, chemical and UV mutagenesis were used to increase variation within the chosen strains. The selection of exponentially growing cells with a limited carbon source has previously been shown to be very effective in heterotrophic bacteria. LaCroix *et al*. 2014 showed that the serial transfer of *E. coli* on a minimal glucose medium increased the growth rates of the *E. coli* strains by 1.6-fold [239]. The use of serial transfer strategies has previously been shown to be very effective in improving high

light tolerance in *Synechocystis* by both Dann *et al*. 2021, and Yoshikawa *et al*. 2021 [284,289]., and the strategy has also been used effectively by Perrineau *et al*. 2014 to select for strains of the green alga *Chlamydomonas reinhardtii* with a 35% increase in growth rate [288]. However, that selection process lasted for 17 months. Improved growth rates of 18.6% were seen in *Synechocystis* after 84 days of selection with 0.02% CO_2. However, despite the improved growth rates, this did not equate to improvements in the biomass. Indicating that in this selective environment, 'fitter' *Synechocystis* cells may equate to a more streamlined metabolism, rather than increased substrate uptake or utilisation.

6.1.1.1 *Culturing strategy for increased carbon fixation*

The manual chemostat selection in this work was shown to be effective in selecting for strains with increased biomass formation. However, chemostat selection to improve growth remains less utilised elsewhere than more straightforward batch selection methods (See **Table 2.5**). Work by Wong *et al*. 2018 provided a "a scalable do-it-yourself (DIY) framework" chemostat strategy used to improve the growth of populations of *Saccharomyces cerevisiae* [592]. As part of this work, an operational chemostat was assembled from available materials. Following an initial literature search early in the project, no examples could be found in the literature of ALE linked to continuous chemostat selection being used to improve the growth of cyanobacteria. Therefore, this may be one of the first such utilisations of this approach in cyanobacteria.

6.1.1.2 *Coupling selective environment pressures with engineered strains*

Previous work has demonstrated the value of ALE selection upon strains engineered to direct metabolic flux (see **2.6.2**). In this work, a strategy was devised to directly couple biomass formation with growth during selection. Existing knowledge of light induced electron transport was used to aid the selection of a suitable strain, in this case *Synechocystis* sp. PCC 6803 *Δhox*, and a selective media that could be used to direct electron flux towards carbon fixation. To encourage the cyanobacteria to use carbon fixation to sink excess electrons in the cell, 5% CO_2 was also used. Following selection for 84 days, 93.2% of the isolates showed improved biomass accumulation during the screening process, higher than

the previous serial dilution strategy (54.5%). Two phenotypes were identified, each showed a different sensitivity to growth with 1.5% CO_2. Strains from both phenotypes showed improved biomass formation, 1.85-fold in Syn.1.11 with 1.5% CO_2, and 2-fold in Syn.1.19 with atmospheric CO_2. These results are comparable to those seen with the green algae, *Haematococcus pluvialis*, which was grown with 15% CO_2 (Cheng *et al*. 2016). Strains were isolated which had 1.3-fold more biomass than the wildtype strain following repeated selections with increasing concentrations of CO_2 [593].

6.1.1.3 *Characterising mutant Synechocystis phenotypes*

As previously stated in section **2.6.3**, once strains with the desired phenotype have been isolated, characterising these mutants to understand the basis for any changes remains a challenge. The isolated mutant strains showed multiple phenotypic differences from the *Synechocystis Δhox* strain. Strains showed a settling phenotype, with the cells settling to the bottom of the flask. This was similar to observations made by Jittawuttipoka *et al*. 2013, following the deletion of multiple genes responsible for EPS production [473]. One of the genes involved in EPS production, sll*0923* (*epsB*) was also identified as having been heavily truncated in Syn.1.11 due to a frame shift mutation. Pererira *et al*. 2019 showed through experimental knockouts that deletion of *sll0923* did not reduce the total carbohydrate content of the cells [594], and the homologue *wzc* in *E. coli* has previously been identified as a membrane porin protein [595]. This possibly shows that by reducing the export of carbon as EPS, the cells may use this additional carbon for growth.

Pigmentation was also significantly altered within the isolates, with strains showing lower concentrations of both chlorophyll and carotenoids during early exponential phase per mgDCW. Despite these reductions, when standardised to the same chlorophyll concentration, Syn.1.11 showed a 2.3 times higher rate of O_2 evolution at 331 µmol photons·m^{-2}·sec^{-1} compared to the Syn.*Δhox* strain, (however there was significant variation within replicates). The *lexA* gene codes for a transcriptional regulatory repressor protein [596]. Work by Srivastava *et al*. 2023, showed that the overexpression of the *lexA* gene in *Anabaena* sp. PCC 7120 heavily impacted the expression of proteins involved in photosynthesis [597]. Reducing expression of the phycobilisome rod-core linker protein, CpcG2, the PSI subunit II protein PsaD, the plastocyanin protein PetE, and several other proteins involved in electron transport, and carbon metabolism. A

later study also showed that overexpression of the *lexA* gene also resulted in reduced photodamage to PSII, whilst increasing the photoinhibition of PSI [598]. This may potentially explain why the Syn.1.11 strain continued to evolve oxygen under greater light stress compared to the control.

A truncation was also identified in the *rppB* gene in Syn.1.11, which could potentially lead to a deletion. An *ΔrppA* deletion strain of *Synechocystis* had a similar phenotype to the Syn.1.11 strain, showing higher oxygen evolution rates and a reduced photopigment concentration. The phenotype was also exaggerated when supplemented with 5 mM of glucose under 40 μmol photons·m^{-2}·sec^{-1} illumination [487]. Syn.1.11 only showed a higher growth rate during exponential phase following supplementation with 10 mM of glucose at 300 μmol photons·m^{-2}·sec^{-1}. Given that a significant proportion of nickel within the cells is used during the assembly of the hydrogenase enzyme (see Ermler *et al*. 1998) [599], (deleted within Syn.1.11), and nickel ions have been shown to induce deleterious effects in the cell such as DNA damage (see López-Maury *et al*. 2002), it may be advantageous to the cells to reduce nickel import / increase export. The *nrsBACD* operon, contains at least three proteins involved in nickel efflux [513], and has previously been shown to be regulated by the RppA-RppB system [513].

Furthermore, mutations present within this strain align closely with many of those previously identified in *Synechococcus elongatus* UTEX 2973. *Synechococcus elongatus* UTEX 2973, was previously thought to be the fastest growing strain of cyanobacteria, with a doubling time of 1.9 hrs in BG-11 media at 41°C under continuous 500 μmol photons·m^{-2}·s^{-1} white light with 3% CO_2 [190]. It is closely related to *Synechococcus elongatus* sp. PCC 7942, with only 55 SNPs and insertion deletion indels separating the two genomes [192]. Similar mutations were found in Syn.1.11 as those present in UTEX 2973, for example mutations were found in the sequences encoding the ATP synthase (here *atpG* rather than *atpA*), and the chorismite mutase. The contribution of those mutations in improving the growth of *Synechococcus elongatus* UTEX 2973 was confirmed by Ungerer et al. 2018, as when *Synechococcus elongatus* sp. PCC 7942 alleles were introduced, this reduced UTEX 2973 growth by 49% and 16% respectively [192].

The ATP synthase is a key protein within the electron transport chain, and previous work by Sunamura et al. 2010 showed the insertion of a kanamycin resistance cassette into the *atpG* gene, resulting in a Leu198–Val222 substitution which resulted in a strain with a 2.3-fold increase in ATP hydrolysis, although no significant impact on growth [600]. However, this investigation only presented the growth of these mutants at 30 μmol

photons·m^{-2}·s^{-1}, whereas selection here was under 300 µmol photons·m^{-2}·s^{-1}. As the Syn.1.11 strain also has a deletion within this range, this mutation may provide a beneficial phenotype for the cell. However previous work has also shown that ATP has a high binding affinity for Mg^{2+} ions [601], and high ATP levels can deplete cellular concentrations of Mg^{2+} [602]. In protein synthesis, Mg^{2+} ions are used to chelate rRNA molecules during ribosome assembly [603], and they are utilised in photosynthesis as part of the central core of the chlorophyll molecule [604]. Therefore, it is possible that this mutation may allow the cells to improve its growth rate by reducing the effects of ATP depletion on Mg^{2+}. Given that previous work has not shown any impacts on growth, due to a mutation in this gene, it is also possible that this mutation is simply a result of the specific selection pressures of the ALE process. Further investigation would be necessary to confirm this.

Metabolomic characterisation of the strains showed variation between the isolates and the control during both early exponential and late exponential growth. Analysis of highly significant variation between the classes highlighted a relative abundance of acetylated amino acids. In the evolutionary process and as part of the adaptation to the selective environment in the chemostat, the cells may have adapted by utilising arginine biosynthesis as an electron sink. L-arginine is converted to cyanophycin, utilising aspartic acid, at a cost of 1 ATP molecule per amino acid [605]. Poly hydroxybutyrates (PHB) are biopolymers similar to cyanophycin; both are utilised as storage molecules, with cyanophycin acting as a nitrogen storage molecule [606]. Batista *et al*. 2018 suggested that PHB synthesis may act as an electron sink in the cell [607], it is therefore plausible that arginine biosynthesis may be being utilised by the cells as an excess electron sink. However, further work would be necessary to confirm this.

6.1.2 *ALE to increase nitrogen fixation*

In **Chapter 5**, the use of a chemostat ALE strategy was successfully validated with filamentous cyanobacteria.

The utilisation of a chemostat based selection strategy was shown to be very effective in isolating fast-growing phenotypes under the diazotrophic selection conditions selected. With highest performing strains yielded a 2.7-fold accumulation in biomass, compared to the progenitor strain. *Trichormus variabilis* strains selected under the mixotrophic growth

conditions showed an average decrease in biomass across the population when grown photoautotrophically. This was compensated for via organic carbon supplementation, with fructose. Furthermore, these experiments also showed how the population of the chemostat can be progressively enhanced over time. The DCW of the diazotrophically selected populations increased on average by 0.19 $mg \cdot mL^{-1}$ every 2 – 3 days. The ALE also demonstrated the importance of the selection process and the parameters utilised to select the best performing strains. The strains selected following growth on a fixed carbon source were highly dependent on fructose, with over 90% of the isolates showing this phenotype. This does not necessarily mean that electrons are not being directed towards nitrogen fixation; however, this would require further investigation.

6.1.2.1 *Potential additive effects of a consortium*

One potential solution which has been suggested to increase both the stability and robustness of cyanobacterial strains for biotechnology is the use of designed or naturally occurring cyanobacterial consortium. The ALE experiments here were not initially designed to select for a consortium; however, this was the outcome. The best performing strain Ava.A.2.20 being part of a consortia. The prolonged culturing of both the photoautotrophic strain and the heterotrophic strains led to the development of a mutualistic relationship between the strains. Previous work by Zhang *et al*. 2014 demonstrated how two auxotrophic populations of *E. coli*, one a leucine and one a lysine auxotroph, could adapt together in a consortium, which resulted in a 3-fold increase in the growth rates of both strains [608]. Here we were able to demonstrate that the consortia isolated from ALE with the Ava.A.2.20 strain was able to alter the phenotype of the Ava.WT strain, and selectively improve its growth.

Regarding the specific mechanisms by which this may be possible, however, further work is needed to understand how the strains interact together and what benefits they gain from the mutualistic relationship. *Trichormus variabilis* is a model filamentous cyanobacteria, however, the annotation of its genome is less well developed than other cyanobacteria such as *Synechocystis.* This hampered attempts to identify gene candidates in the axenic Ava.A.2.20.P strain, as most of the genes with mutations were classified as hypothetical proteins which have yet to be annotated. Herrernan *et al*. 2024 previously isolated strains of *Clostridium autoethanogenum* using a chemostat based selection, however, despite improvements in the growth rates, they observed no significant differences

in the productivity of either ethanol or acetate [609]. It will be interesting to see if there is an improvement in nitrogen fixation in this strain and if this can be utilised to improve crop biomass.

6.2 Conclusions

In summary, this work has demonstrated the use of ALE coupled with continuous selection has been a useful strategy for selecting improved strains of both *Synechocystis* and *Trichormus variabilis* with enhanced growth and biomass formation. *Synechocystis* strains were isolated with a 2-fold higher biomass accumulation, and a 28% increase in the maximum growth rate (μ_{max}) under atmospheric CO_2 concentrations (section **4.5.1.1**). This was coupled with a 1.5-fold increase in biomass accumulation under saturating CO_2 conditions (section **4.5.1.2**). Demonstrating that ALE can be used to select for photosynthetic prokaryotes with increased autotrophic growth, and substrate utilisation. This work has demonstrated that ALE selection in a continuous reactor can be more effective for selecting for increased photoautotrophic growth and biomass formation than serial transfer methods (sections **4.3** and **4.4**). This work has also demonstrated that ALE is an effective method for selecting strains of nitrogen-fixing cyanobacteria, with up to 2.7-fold increase in biomass accumulation (section **5.6.3**) and a 36% higher μ_{max} (section **5.4.3**) under photoautotrophic diazotrophic conditions. To my knowledge, this is the first example of ALE being used to select for enhanced diazotrophic growth. It has also highlighted the importance of the selection process and the need to carefully consider what that basis should be. For example, ALE selection with fixed carbon supplementation superseded the selective pressures for increased diazotrophic growth, and selected for strains highly dependent on that carbon source (section **5.4.1**). This work has also demonstrated that cross-talk between the regulatory mechanisms governing carbon fixation and nitrogen assimilation could be a valuable future target for strain engineering to increase growth and biomass accumulation (section **4.6**).

This work has, therefore, contributed to the growing body of literature demonstrating the potential of Adaptive Laboratory Evolution as an effective tool for strain engineering.

6.3 Future work

6.3.1 *Continued Characterisation*

Further work would prioritise continued characterisation of the isolates by expanding on previous metabolomic work and including both transcriptomic and proteomic analysis. This would assist in identifying which specific mutations were most likely to be responsible for the phenotypes seen in the strains. This is necessary due to the thousands of identified non-synonymous mutations within each isolate, which makes it challenging to identify which mutations are the most valuable for future targeted engineering strategies. Metabolomic characterisation of the strains grown in a growth medium with an alternative pH buffer could resolve if the ion responsible for variation in **Figures 4.37** and **4.41** was indeed the buffer, HEPES. This could also provide insight into the impact of this buffer on cell metabolism, and identify if it is nutritionally available to the cells. Transcriptomic analysis could also assist in identifying potentially relevant changes in non-coding sequences responsible for regulating gene expression. It could also help identify other adaptations not directly linked to increased carbon fixation, by assessing relative expression of other electron sinks. Additionally, control for genome copy number prior to genome sequencing would allow for an assessment of polyploid allele variation. Which, if assessed with sequencing of Syn.1.19, could offer insight into why some isolate populations were non-viable post-isolation (see section **4.5.1**).

If mutations linked to the phenotype showing increased growth at atmospheric CO_2 concentrations, but diminished growth with 1.5% CO_2 (**Figure 4.22**), were present in only a portion of the Syn.1.19 genome. Further omic characterisation should also include analysis of the isolates under conditions which replicate the ALE selective environment (continuous dilution and 5% CO_2), to assist in understanding the adaptation process. Growth under diurnal conditions should be addressed to more specifically assess isolate recovery times. Future work would also include a second round of chemostat selection on the best performing strains to identify if these cyanobacteria ALE strategies are effective multiple times. Given the potentially interesting adaptations seen in the *Synechocystis* strains, which could be linked to nitrogen assimilation, the strains could be supplemented with metabolic intermediates from the L-Arginine biosynthesis pathway, such as glutamate, aspartate, and asparagine.

Furthermore, many of the identified mutations remain putatively linked to phenotypic observations. To assist in elucidating this, identified genes could either be knocked out or mutated in the wildtype strain, or heterologously expressed in the wildtype strain. Further omic characterisation would also be useful, combining metabolomics with transcriptomics and proteomics. Given the significant roles of the transcriptional regulators, *lexA* and *rppB* would be a good initial target for characterisation (see Srivastava *et al*. 2022; see Li and Sherman 2000) [487,598]. Future work should also seek to complete and characterise the effects of the *hox* operon reintegration on strain productivity. In *Trichormus variabilis*, deletion of the *ava_4478* gene could also be a good target; it would be valuable to determine if this gene is indeed involved in coenzyme F_{430} biosynthesis, and if removal of this gene is responsible for the fast growth phenotype observed in Ava.A.2.20.P. Furthermore, to better understand the basis for oxygen evolution phenotypes in both *Synechocystis* and *Trichormus variabilis* mutants, characterisation of photosynthetic apparatus, such as PSI:PSII ratios and determining chlorophyll concentration per cell, would be performed.

6.3.2 *Strategy Optimisation*

Further protocol optimisation would also be valuable. Previous work has shown that many unwanted phenotypes can emerge during ALE selection, depending on the selection pressure applied, such as organisms adapted to stationary phase growth [610]. Biofilming strains which can also be carried over but may not have the necessary desired phenotypes [311] . Utilising the successful selective criteria from the diazotrophic and *Δhox* mediated ALE experiments, future work should seek to refine the selective approach by identifying if and / how the strains successfully circumvented the applied selective pressure.

Additionally, there are many engineering strategies that when coupled with ALE, could increase the selective pressure on the cell. Genome replication engineering assisted continuous evolution (GREACE) [611], is a strategy in which mutants are introduced into the DnaQ protein, the proofreading element of the DNA polymerase complex. These facilitate mutations through error prone genome replication [611]. This strategy allows for real time mutagenesis of strains as they adapt to environmental stress. Potentially allowing for the rapid tailoring of strains via a selective pipeline.

Another interesting avenue would be utilising ALE to adapt multiple strains simultaneously, although we did evolve a consortium of strains this was not the intended outcome, and it would be interesting to pre-select strains based on their phenotypes. The metabolic burden of different pathways can then be shared across a population (see Konstantinidis *et al*. 2021) [510]. Many cyanobacteria exist in a symbiotic partnership [612], and such a strategy could generate enhanced phenotypes which may address the current challenges with utilising cyanobacteria at scale [510].

6.3.3 *Optimising Expression*

Akin to optimising cellular 'software' rather than 'hardware', global transcriptional machinery engineering (gTME) allows for the screening of different transcriptomic profiles to identify strains with an improved growth rate. Without the need to alter any other proteins within the cells, this strategy has the added benefit of not introducing deleterious mutations within the isolate's genome [613]. A gTME was attempted as part of this thesis, error prone PCR was carried out on the *sigA* and *sigC* genes, SigA is the equivalent of the σ^{70} housekeeping gene and is essential in the cell, while SigC is a group 2 sigma factor and part of the RNA polymerase (RNAP). The mutated gene libraires were cloned into the pSEVA plasmid, however, repeated attempts to transform the library into *Synechocystis* sp. PCC 6803 were unsuccessful resulting in a very small number of colonies. Therefore, given the limited library size the strategy was abandoned to focus on the ALE work. Future work should focus on designing a more efficient expression construct for *Synechocystis* to enable the transformation efficiency of the library to be increased.

6.4 Plans for Dissemination

Following acceptance of my thesis I currently aim to disseminate my work through publication, focusing on the optimisation of ALE strategies for the selection of cyanobacteria with increased growth and biomass formation.

References

1. Calvin, K. *et al.* IPCC, 2023: Climate Change 2023: Synthesis Report. Contribution of Working Groups I, II and III to the Sixth Assessment Report of the Intergovernmental Panel on Climate Change [Core Writing Team, H. Lee and J. Romero (eds.)]. IPCC, Geneva, Switzerland. (2023) doi:10.59327/IPCC/AR6-9789291691647.001.

2. Ritchie, H., Rosado, P. & Roser, M. Greenhouse gas emissions. *OurWorldInData.org* https://ourworldindata.org/greenhouse-gas-emissions (2020).

3. The Paris Agreement - Publication | UNFCCC. https://unfccc.int/documents/184656.

4. Mac Dowell, N., Fennell, P. S., Shah, N. & Maitland, G. C. The role of CO2 capture and utilization in mitigating climate change. *Nature Climate Change 2017 7:4* **7**, 243–249 (2017).

5. Technology Roadmap - Carbon Capture and Storage 2013 – Analysis - IEA. https://www.iea.org/reports/technology-roadmap-carbon-capture-and-storage-2013.

6. Abu-Ghosh, S., Dubinsky, Z., Verdelho, V. & Iluz, D. Unconventional high-value products from microalgae: A review. *Bioresour Technol* **329**, 124895 (2021).

7. Burnap, R. L. Systems and photosystems: Cellular limits of autotrophic productivity in cyanobacteria. *Front Bioeng Biotechnol* **3**, 117998 (2015).

8. Bernstein, H. C. *et al.* Unlocking the constraints of cyanobacterial productivity: Acclimations enabling ultrafast growth. *mBio* **7**, 949–965 (2016).

9. (IPCC), I. P. on C. C. Annex VII: Glossary. *Climate Change 2021 – The Physical Science Basis* 2215–2256 (2023) doi:10.1017/9781009157896.022.

10. (IPCC). Chapter 5: Global Carbon and other Biogeochemical Cycles and Feedbacks | Climate Change 2021: The Physical Science Basis. https://www.ipcc.ch/report/ar6/wg1/chapter/chapter-5/ (2021).

11. (IPCC). Chapter 7: The Earth's Energy Budget, Climate Feedbacks, and Climate Sensitivity | Climate Change 2021:

The Physical Science Basis. https://www.ipcc.ch/report/ar6/wg1/chapter/chapter-7/ (2021).

12. Ko, M. K. W., Sze, N. D., Molnar, G. & Prather, M. J. Global warming from chlorofluorocarbons and their alternatives: Time scales of chemistry and climate. *Atmospheric Environment. Part A. General Topics* **27**, 581–587 (1993).

13. Montzka, S. A. *et al.* A decline in global CFC-11 emissions during 2018−2019. *Nature 2021 590:7846* **590**, 428–432 (2021).

14. Newman, P. A. *et al.* What would have happened to the ozone layer if chlorofluorocarbons (CFCs) had not been regulated? *Atmos Chem Phys* **9**, 2113–2128 (2009).

15. Kammerer, S., Borho, I., Jung, J. & Schmidt, M. S. Review: CO2 capturing methods of the last two decades. *International Journal of Environmental Science and Technology* **20**, 8087–8104 (2023).

16. Nazir, S. M., Cloete, J. H., Cloete, S. & Amini, S. Efficient hydrogen production with CO2 capture using gas switching reforming. *Energy* **185**, 372–385 (2019).

17. Pfaff, I. & Kather, A. Comparative thermodynamic analysis and integration issues of CCS steam power plants based on oxy-combustion with cryogenic or membrane based air separation. *Energy Procedia* **1**, 495–502 (2009).

18. Chen, K. *et al.* Integrated technology for dust removal and denitration of high-temperature flue gas in coal-fired power plants. *Fuel* **342**, 127687 (2023).

19. Madejski, P., Chmiel, K., Subramanian, N. & Kuś, T. Methods and Techniques for CO2 Capture: Review of Potential Solutions and Applications in Modern Energy Technologies. *Energies 2022, Vol. 15, Page 887* **15**, 887 (2022).

20. Pires, J. C. M., Martins, F. G., Alvim-Ferraz, M. C. M. & Simões, M. Recent developments on carbon capture and storage: An overview. *Chemical Engineering Research and Design* **89**, 1446–1460 (2011).

21. Osman, A. I., Hefny, M., Abdel Maksoud, M. I. A., Elgarahy, A. M. & Rooney, D. W. Recent advances in carbon capture storage and utilisation technologies: a review. *Environmental Chemistry Letters 2020 19:2* **19**, 797–849 (2020).

22. Campo, M. C. *et al.* Carbon dioxide removal for methane upgrade by a VSA process using an improved 13X zeolite. *Fuel Processing Technology* **143**, 185–194 (2016).

23. Xu, D. *et al.* Effects of water vapour on CO2 capture with vacuum swing adsorption using activated carbon. *Chemical Engineering Journal* **230**, 64–72 (2013).

24. Varghese, A. M. & Karanikolos, G. N. CO2 capture adsorbents functionalized by amine – bearing polymers: A review. *International Journal of Greenhouse Gas Control* **96**, 103005 (2020).

25. Li, J. R. *et al.* Carbon dioxide capture-related gas adsorption and separation in metal-organic frameworks. *Coord Chem Rev* **255**, 1791–1823 (2011).

26. Han, Y. & Ho, W. S. W. Polymeric membranes for CO2 separation and capture. *J Memb Sci* **628**, 119244 (2021).

27. Ahmadi, M., Janakiram, S., Dai, Z., Ansaloni, L. & Deng, L. Performance of Mixed Matrix Membranes Containing Porous Two-Dimensional (2D) and Three-Dimensional (3D) Fillers for CO2 Separation: A Review. *Membranes 2018, Vol. 8, Page 50* **8**, 50 (2018).

28. Nayak, N., Mehrotra, R. & Mehrotra, S. Carbon biosequestration strategies: a review. *Carbon Capture Science & Technology* **4**, 100065 (2022).

29. Bui, M. *et al.* Carbon capture and storage (CCS): the way forward. *Energy Environ Sci* **11**, 1062–1176 (2018).

30. Lackey, G., Vasylkivska, V. S., Huerta, N. J., King, S. & Dilmore, R. M. Managing well leakage risks at a geologic carbon storage site with many wells. *International Journal of Greenhouse Gas Control* **88**, 182–194 (2019).

31. IPCC. *Carbon Dioxide Capture and Storage*. (2005).

32. Wilberforce, T., Olabi, A. G., Sayed, E. T., Elsaid, K. & Abdelkareem, M. A. Progress in carbon capture technologies. *Science of The Total Environment* **761**, 143203 (2021).

33. Doelman, J. C. *et al.* Afforestation for climate change mitigation: Potentials, risks and trade-offs. *Glob Chang Biol* **26**, 1576–1591 (2020).

34. Zomer, R. J. *et al.* Global Tree Cover and Biomass Carbon on Agricultural Land: The contribution of agroforestry to

global and national carbon budgets. *Scientific Reports 2016 6:1* **6**, 1–12 (2016).

35. Doelman, J. C. *et al.* Afforestation for climate change mitigation: Potentials, risks and trade-offs. *Glob Chang Biol* **26**, 1576–1591 (2020).

36. Mertens, J. *et al.* Carbon capture and utilization: More than hiding CO2 for some time. *Joule* **7**, 442–449 (2023).

37. Rafiee, A., Rajab Khalilpour, K., Milani, D. & Panahi, M. Trends in CO2 conversion and utilization: A review from process systems perspective. *J Environ Chem Eng* **6**, 5771–5794 (2018).

38. Jadhav, S. G., Vaidya, P. D., Bhanage, B. M. & Joshi, J. B. Catalytic carbon dioxide hydrogenation to methanol: A review of recent studies. *Chemical Engineering Research and Design* **92**, 2557–2567 (2014).

39. Zhang, J., Singh, R. & Webley, P. A. Alkali and alkaline-earth cation exchanged chabazite zeolites for adsorption based CO2 capture. *Microporous and Mesoporous Materials* **111**, 478–487 (2008).

40. Bi, F., Ehsan, M. F., Liu, W. & He, T. Visible-Light Photocatalytic Conversion of Carbon Dioxide into Methane Using Cu2O/TiO2 Hollow Nanospheres. *Chin J Chem* **33**, 112–118 (2015).

41. Graça, I. *et al.* CO2 hydrogenation into CH4 on NiHNaUSY zeolites. *Appl Catal B* **147**, 101–110 (2014).

42. Mohd Yasin, N. H., Maeda, T., Hu, A., Yu, C. P. & Wood, T. K. CO2 sequestration by methanogens in activated sludge for methane production. *Appl Energy* **142**, 426–434 (2015).

43. Phillips, A. J. *et al.* Engineered applications of ureolytic biomineralization: a review. *Biofouling* **29**, 715–733 (2013).

44. Heveran, C. M. *et al.* Biomineralization and Successive Regeneration of Engineered Living Building Materials. *Matter* **2**, 481–494 (2020).

45. Ng, I. S., Keskin, B. B. & Tan, S. I. A Critical Review of Genome Editing and Synthetic Biology Applications in Metabolic Engineering of Microalgae and Cyanobacteria. *Biotechnol J* **15**, 1900228 (2020).

46. Berg, I. A. Ecological Aspects of the Distribution of Different Autotrophic CO2 Fixation Pathways. *Appl Environ Microbiol* **77**, 1925 (2011).

47. Huber, H. *et al.* A dicarboxylate/4-hydroxybutyrate autotrophic carbon assimilation cycle in the hyperthermophilic Archaeum Ignicoccus hospitalis. *Proc Natl Acad Sci U S A* **105**, 7851–7856 (2008).

48. Evans, M. C., Buchanan, B. B. & Arnon, D. I. A new ferredoxin-dependent carbon reduction cycle in a photosynthetic bacterium. *Proc Natl Acad Sci U S A* **55**, 928–934 (1966).

49. Ljungdhal, L. G. The Autotrophic Pathway of Acetate Synthesis in Acetogenic Bacteria. *Annu Rev Microbiol* **40**, 415–450 (1986).

50. Gong, F., Cai, Z. & Li, Y. Synthetic biology for CO2 fixation. *Sci China Life Sci* **59**, 1106–1114 (2016).

51. Bassham, J. A., Benson, A. A. & Calvin, M. The Path of Carbon in Photosynthesis VIII. The Role of Malic Acid. (1950) doi:10.2172/910351.

52. Pavan, M. *et al.* Advances in systems metabolic engineering of autotrophic carbon oxide-fixing biocatalysts towards a circular economy. *Metab Eng* **71**, 117–141 (2022).

53. Schuchmann, K. & Müller, V. Energetics and Application of Heterotrophy in Acetogenic Bacteria. *Appl Environ Microbiol* **82**, 4056 (2016).

54. Whitham, J. M., Tirado-Acevedo, O., Chinn, M. S., Pawlak, J. J. & Grunden, A. M. Metabolic response of Clostridium ljungdahlii to oxygen exposure. *Appl Environ Microbiol* **81**, 8379–8391 (2015).

55. Emerson, D. F. & Stephanopoulos, G. Limitations in converting waste gases to fuels and chemicals. *Curr Opin Biotechnol* **59**, 39–45 (2019).

56. Liu, W. *et al.* Trends and future challenges in hydrogen production and storage research. *Environmental Science and Pollution Research* **27**, 31092–31104 (2020).

57. Li, S., Tabatabaei, M., Li, F. & Ho, S. H. A review of green biohydrogen production using anoxygenic photosynthetic bacteria for hydrogen economy: Challenges and opportunities. *Int J Hydrogen Energy* **54**, 218–238 (2024).

58. Kruger, N. J. & Von Schaewen, A. The oxidative pentose phosphate pathway: structure and organisation. *Curr Opin Plant Biol* **6**, 236–246 (2003).

59. Stirbet, A., Lazár, D., Guo, Y. & Govindjee, G. Photosynthesis: basics, history and modelling. *Ann Bot* **126**, 511–537 (2020).

60. Phillips, R. & Milo, R. A feeling for the numbers in biology. *Proc Natl Acad Sci U S A* **106**, 21465–21471 (2009).

61. Tcherkez, G. The mechanism of Rubisco-catalysed oxygenation. *Plant Cell Environ* **39**, 983–997 (2016).

62. Prywes, N., Phillips, N. R., Tuck, O. T., Valentin-Alvarado, L. E. & Savage, D. F. Rubisco Function, Evolution, and Engineering. *Annu Rev Biochem* **92**, 385–410 (2023).

63. Leegood, R. C. A welcome diversion from photorespiration. *Nature Biotechnology 2007 25:5* **25**, 539–540 (2007).

64. Erb, T. J. & Zarzycki, J. A short history of RubisCO: The rise and fall (?) of Nature's predominant CO2 fixing enzyme. *Curr Opin Biotechnol* **49**, 100 (2018).

65. Wilson, R. H. & Whitney, S. M. Improving CO2 Fixation by Enhancing Rubisco Performance. *Directed Enzyme Evolution: Advances and Applications* 101–126 (2017) doi:10.1007/978-3-319-50413-1_4.

66. Studer, R. A., Christin, P. A., Williams, M. A. & Orengo, C. A. Stability-activity tradeoffs constrain the adaptive evolution of RubisCO. *Proc Natl Acad Sci U S A* **111**, 2223–2228 (2014).

67. Bainbridge, G. *et al.* Engineering Rubisco to change its catalytic properties. *J Exp Bot* **46**, 1269–1276 (1995).

68. Kannappan, B. & Gready, J. E. Redefinition of rubisco carboxylase reaction reveals origin of water for hydration and new roles for active-site residues. *J Am Chem Soc* **130**, 15063–15080 (2008).

69. Tcherkez, G. G. B., Farquhar, G. D. & Andrews, T. J. Despite slow catalysis and confused substrate specificity, all ribulose bisphosphate carboxylases may be nearly perfectly optimized. *Proc Natl Acad Sci U S A* **103**, 7246–7251 (2006).

70. Sato, N. Are cyanobacteria an ancestor of chloroplasts or just one of the gene donors for plants and algae? *Genes (Basel)* **12**, 823 (2021).

71. Rosgaard, L., de Porcellinis, A. J., Jacobsen, J. H., Frigaard, N. U. & Sakuragi, Y. Bioengineering of carbon

fixation, biofuels, and biochemicals in cyanobacteria and plants. *J Biotechnol* **162**, 134–147 (2012).

72. Parmar, A., Singh, N. K., Pandey, A., Gnansounou, E. & Madamwar, D. Cyanobacteria and microalgae: A positive prospect for biofuels. *Bioresour Technol* **102**, 10163–10172 (2011).

73. Bothe, H., Schmitz, O., Yates, M. G. & Newton, W. E. Nitrogen Fixation and Hydrogen Metabolism in Cyanobacteria. *Microbiology and Molecular Biology Reviews* **74**, 529–551 (2010).

74. Smith, C., Hill, A. K. & Torrente-Murciano, L. Current and future role of Haber–Bosch ammonia in a carbon-free energy landscape. *Energy Environ Sci* **13**, 331–344 (2020).

75. Vavitsas, K. *et al.* Doing synthetic biology with photosynthetic microorganisms. *Physiol Plant* **173**, 624–638 (2021).

76. Yokota, A., Sawada, K. & Wada, M. Boosting Anaplerotic Reactions by Pyruvate Kinase Gene Deletion and Phosphoenolpyruvate Carboxylase Desensitization for Glutamic Acid and Lysine Production in Corynebacterium glutamicum. *Adv Biochem Eng Biotechnol* **159**, 181–198 (2016).

77. Durall, C., Rukminasari, N. & Lindblad, P. Enhanced growth at low light intensity in the cyanobacterium Synechocystis PCC 6803 by overexpressing phosphoenolpyruvate carboxylase. *Algal Res* **16**, 275–281 (2016).

78. Price, G. D., Badger, M. R., Woodger, F. J. & Long, B. M. Advances in understanding the cyanobacterial CO2-concentrating- mechanism (CCM): Functional components, Ci transporters, diversity, genetic regulation and prospects for engineering into plants. *J Exp Bot* **59**, 1441–1461 (2008).

79. Price, G. D. & Howitt, S. M. Topology mapping to characterize cyanobacterial bicarbonate transporters: BicA (SulP/SLC26 family) and SbtA. *Mol Membr Biol* **31**, 177–182 (2014).

80. Omata, T., Takahashi, Y., Yamaguchi, O. & Nishimura, T. Structure, function and regulation of the cyanobacterial high-affinity bicarbonate transporter, BCT1. *Functional Plant Biology* **29**, 151–159 (2002).

81. Long, B. M. *et al.* Carboxysome encapsulation of the CO2-fixing enzyme Rubisco in tobacco chloroplasts. *Nature Communications 2018 9:1* **9**, 1–14 (2018).

82. Andrews, T. J. & Abel, K. M. Kinetics and subunit interactions of ribulose bisphosphate carboxylase-oxygenase from the cyanobacterium, Synechococcus sp. *Journal of Biological Chemistry* **256**, 8445–8451 (1981).

83. Lechno-Yossef, S. *et al.* Cyanobacterial carboxysomes contain an unique rubisco-activase-like protein. *New Phytologist* **225**, 793–806 (2020).

84. Price, G. D. Inorganic carbon transporters of the cyanobacterial CO2 concentrating mechanism. *Photosynth Res* **109**, 47–57 (2011).

85. Schirrmeister, B. E., De Vos, J. M., Antonelli, A. & Bagheri, H. C. Evolution of multicellularity coincided with increased diversification of cyanobacteria and the Great Oxidation Event. *Proc Natl Acad Sci U S A* **110**, 1791–1796 (2013).

86. Pisciotta, J. M., Zou, Y. & Baskakov, I. V. Light-Dependent Electrogenic Activity of Cyanobacteria. *PLoS One* **5**, e10821 (2010).

87. Herrero, A., Stavans, J. & Flores, E. The multicellular nature of filamentous heterocyst-forming cyanobacteria. *FEMS Microbiol Rev* **40**, 831–854 (2016).

88. Badger, M. R. & Price, G. D. CO2 concentrating mechanisms in cyanobacteria: molecular components, their diversity and evolution. *J Exp Bot* **54**, 609–622 (2003).

89. Shevela, D., Kern, J. F., Govindjee, G. & Messinger, J. Solar energy conversion by photosystem II: principles and structures. *Photosynthesis Research 2023 156:3* **156**, 279–307 (2023).

90. Messinger, J. & Shevela, D. Principles of photosynthesis. *Fundamentals of Materials for Energy and Environmental Sustainability* 302–314 (2011) doi:10.1017/CBO9780511718786.028.

91. Govindjee & Shevela, D. Adventures with cyanobacteria: A personal perspective. *Front Plant Sci* **2**, 11696 (2011).

92. Stadnichuk, I. N., Krasilnikov, P. M. & Zlenko, D. V. Cyanobacterial phycobilisomes and phycobiliproteins. *Microbiology (Russian Federation)* **84**, 101–111 (2015).

93. Arteni, A. A., Ajlani, G. & Boekema, E. J. Structural organisation of phycobilisomes from Synechocystis sp. strain PCC6803 and their interaction with the membrane. *Biochimica et Biophysica Acta (BBA) - Bioenergetics* **1787**, 272–279 (2009).

94. Kirilovsky, D., Kaňa, R. & Prášil, O. Mechanisms Modulating Energy Arriving at Reaction Centers in Cyanobacteria. 471–501 (2014) doi:10.1007/978-94-017-9032-1_22.

95. Wang, F. & Chen, M. Chromatic Acclimation Processes and Their Relationships with Phycobiliprotein Complexes. *Microorganisms* **10**, (2022).

96. Şener, M. *et al.* Förster Energy Transfer Theory as Reflected in the Structures of Photosynthetic Light-Harvesting Systems. *ChemPhysChem* **12**, 518–531 (2011).

97. De Lichtenberg, C., Kim, C. J., Chernev, P., Debus, R. J. & Messinger, J. The exchange of the fast substrate water in the S 2 state of photosystem II is limited by diffusion of bulk water through channels – implications for the water oxidation mechanism. *Chem Sci* **12**, 12763–12775 (2021).

98. Luciński, R. & Jackowski, G. The structure, functions and degradation of pigment-binding proteins of photosystem II. *Acta Biochim Pol* **53**, 693–708 (2006).

99. Zhang, B. & Sun, L. Why nature chose the Mn4CaO5 cluster as water-splitting catalyst in photosystem II: a new hypothesis for the mechanism of O–O bond formation. *Dalton Transactions* **47**, 14381–14387 (2018).

100. Joliot, P., Barbieri, G. & Chabaud, R. UN NOUVEAU MODELE DES CENTRES PHOTOCHIMIQUES DU SYSTEME II*. *Photochem Photobiol* **10**, 309–329 (1969).

101. KOK, B., FORBUSH, B. & McGLOIN, M. COOPERATION OF CHARGES IN PHOTOSYNTHETIC O2 EVOLUTION–I. A LINEAR FOUR STEP MECHANISM. *Photochem Photobiol* **11**, 457–475 (1970).

102. Joliot, P. & Kok, B. *Oxygen Evolution in Photosynthesis*. *Energetics of Photosynthesis* (Academic Press, 1975). doi:10.1016/B978-0-12-294350-8.50013-1.

103. Nixon, P. J., Michoux, F., Yu, J., Boehm, M. & Komenda, J. Recent advances in understanding the assembly and repair of photosystem II. *Ann Bot* **106**, 1–16 (2010).

104. Romero, E., Novoderezhkin, V. I. & Van Grondelle, R. Quantum design of photosynthesis for bio-inspired solar-energy conversion. *Nature 2017 543:7645* **543**, 355–365 (2017).

105. Khorobrykh, S., Tsurumaki, T., Tanaka, K., Tyystjärvi, T. & Tyystjärvi, E. Measurement of the redox state of the plastoquinone pool in cyanobacteria. *FEBS Lett* **594**, 367–375 (2020).

106. Lea-Smith, D. J., Bombelli, P., Vasudevan, R. & Howe, C. J. Photosynthetic, respiratory and extracellular electron transport pathways in cyanobacteria. *Biochimica et Biophysica Acta (BBA) - Bioenergetics* **1857**, 247–255 (2016).

107. Kurisu, G., Zhang, H., Smith, J. L. & Cramer, W. A. Structure of the Cytochrome b6f Complex of Oxygenic Photosynthesis: Tuning the Cavity. *Science (1979)* **302**, 1009–1014 (2003).

108. Kuchmina, E., Wallner, T., Kryazhov, S., Zinchenko, V. V. & Wilde, A. An expression system for regulated protein production in Synechocystis sp. PCC 6803 and its application for construction of a conditional knockout of the ferrochelatase enzyme. *J Biotechnol* **162**, 75–80 (2012).

109. Durán, R. V., Hervás, M., De La Rosa, M. A. & Navarro, J. A. The Efficient Functioning of Photosynthesis and Respiration in Synechocystis sp. PCC 6803 Strictly Requires the Presence of either Cytochrome c6 or Plastocyanin. *Journal of Biological Chemistry* **279**, 7229–7233 (2004).

110. Fromme, P., Jordan, P. & Krauß, N. Structure of photosystem I. *Biochimica et Biophysica Acta (BBA) - Bioenergetics* **1507**, 5–31 (2001).

111. Jordan, P. *et al.* Three-dimensional structure of cyanobacterial photosystem I at 2.5 Å resolution. *Nature 2001 411:6840* **411**, 909–917 (2001).

112. Medipally, H. *et al.* Light-Driven NADPH Cofactor Recycling by Photosystem I for Biocatalytic Reactions. *ChemCatChem* **15**, e202300821 (2023).

113. Hart, S. E., Schlarb-Ridley, B. G., Bendall, D. S. & Howe, C. J. Terminal oxidases of cyanobacteria. *Biochem Soc Trans* **33**, 832–835 (2005).

114. Sun, X. & Wen, T. Physiological roles of plastid terminal oxidase in plant stress responses. *J Biosci* **36**, 951–956 (2011).

115. Berry, S., Schneider, D., Vermaas, W. F. J. & Rögner, M. Electron transport routes in whole cells of Synechocystis sp. Strain PCC 6803: The role of the cytochrome bd-type oxidase. *Biochemistry* **41**, 3422–3429 (2002).

116. McDonald, A. E. *et al.* Flexibility in photosynthetic electron transport: The physiological role of plastoquinol terminal oxidase (PTOX). *Biochimica et Biophysica Acta (BBA) - Bioenergetics* **1807**, 954–967 (2011).

117. Howitt, C. A. & Vermaas, W. F. J. Quinol and cytochrome oxidases in the cyanobacterium Synechocystis sp. PCC 6803. *Biochemistry* **37**, 17944–17951 (1998).

118. Weber, J. & Senior, A. E. ATP synthesis driven by proton transport in F1F0-ATP synthase. *FEBS Lett* **545**, 61–70 (2003).

119. Neupane, P., Bhuju, S., Thapa, N. & Bhattarai, H. K. ATP Synthase: Structure, Function and Inhibition. *Biomol Concepts* **10**, 1–10 (2019).

120. Boyer, P. D. The binding change mechanism for ATP synthase — Some probabilities and possibilities. *Biochimica et Biophysica Acta (BBA) - Bioenergetics* **1140**, 215–250 (1993).

121. Itoh, H. *et al.* Mechanically driven ATP synthesis by F1-ATPase. *Nature 2004 427:6973* **427**, 465–468 (2004).

122. Nishi, T. & Forgac, M. The vacuolar (H+)-ATPases — nature's most versatile proton pumps. *Nature Reviews Molecular Cell Biology 2002 3:2* **3**, 94–103 (2002).

123. Postgate, J. *Nitrogen Fixation*. (University Press, Cambridge, 1998).

124. Soumare, A. *et al.* Exploiting Biological Nitrogen Fixation: A Route Towards a Sustainable Agriculture. *Plants 2020, Vol. 9, Page 1011* **9**, 1011 (2020).

125. Daramola, D. A. & Hatzell, M. C. Energy Demand of Nitrogen and Phosphorus Based Fertilizers and Approaches to Circularity. *ACS Energy Lett* **8**, 1493–1501 (2023).

126. Do Nascimento, M. *et al.* Prospects of using biomass of N2-fixing cyanobacteria as an organic fertilizer and soil conditioner. *Algal Res* **43**, 101652 (2019).

127. Dashora, K. Nitrogen Yielding Plants: The Pioneers of Agriculture with a Multipurpose. *American-Eurasian Journal of Agronomy* **4**, 34–37 (2011).

128. Berman-Frank, I., Lundgren, P. & Falkowski, P. Nitrogen fixation and photosynthetic oxygen evolution in cyanobacteria. *Res Microbiol* **154**, 157–164 (2003).

129. Latysheva, N., Junker, V. L., Palmer, W. J., Codd, G. A. & Barker, D. The evolution of nitrogen fixation in cyanobacteria. *Bioinformatics* **28**, 603–606 (2012).

130. Lery, L. M. S., Bitar, M., Costa, M. G. S., Rössle, S. C. S. & Bisch, P. M. Unraveling the molecular mechanisms of nitrogenase conformational protection against oxygen in diazotrophic bacteria. *BMC Genomics* **11**, S7 (2010).

131. Mus, F., Colman, D. R., Peters, J. W. & Boyd, E. S. Geobiological feedbacks, oxygen, and the evolution of nitrogenase. *Free Radic Biol Med* **140**, 250–259 (2019).

132. Kentemich, T., Danneberg, G., Hundeshagen, B. & Bothe, H. Evidence for the occurrence of the alternative, vanadium-containing nitrogenase in the cyanobacterium Anabaena variabilis. *FEMS Microbiol Lett* **51**, 19–24 (1988).

133. Jimenez-Vicente, E. *et al.* Sequential and differential interaction of assembly factors during nitrogenase MoFe protein maturation. *Journal of Biological Chemistry* **293**, 9812–9823 (2018).

134. Natzke, J., Noar, J. & Bruno-Bárcena, J. M. Azotobacter vinelandii Nitrogenase Activity, Hydrogen Production, and Response to Oxygen Exposure. *Appl Environ Microbiol* **84**, 1208–1226 (2018).

135. Rutledge, H. L. & Tezcan, F. A. Electron transfer in nitrogenase. *Chem Rev* **120**, 5158 (2020).

136. Winter, H. C. & Burris, R. H. Stoichiometry of the adenosine triphosphate requirement for N2 fixation and H2 evolution by a partially purified preparation of Clostridium pasteurianum. *Journal of Biological Chemistry* **243**, 940–944 (1968).

137. Osburn, F. S., Wagner, N. D. & Scott, J. T. Biological stoichiometry and growth dynamics of a diazotrophic

cyanobacteria in nitrogen sufficient and deficient conditions. *Harmful Algae* **103**, 102011 (2021).

138. Hu, Y. & Ribbe, M. W. Biosynthesis of the Iron-Molybdenum Cofactor of Nitrogenase. *J Biol Chem* **288**, 13173 (2013).

139. Fay, P. Oxygen relations of nitrogen fixation in cyanobacteria. *Microbiol Rev* **56**, 340 (1992).

140. Herrero, A., Muro-Pastor, A. M. & Flores, E. Nitrogen Control in Cyanobacteria. *J Bacteriol* **183**, 411 (2001).

141. Cai, Y. & Wolk, C. P. Anabaena sp. strain PCC 7120 responds to nitrogen deprivation with a cascade-like sequence of transcriptional activations. *J Bacteriol* **179**, 267–271 (1997).

142. Khudyakov, I. Y. & Golden, J. W. Different functions of HetR, a master regulator of heterocyst differentiation in Anabaena sp. PCC 7120, can be separated by mutation. *Proc Natl Acad Sci U S A* **101**, 16040–16045 (2004).

143. Thomas, J. *et al.* Formation of glutamine from [13n]ammonia, [13n]dinitrogen, and [14C]glutamate by heterocysts isolated from Anabaena cylindrica. *J Bacteriol* **129**, 1545 (1977).

144. Böhme, H. Regulation of nitrogen fixation in heterocyst-forming cyanobacteria. *Trends Plant Sci* **3**, 346–351 (1998).

145. Magnuson, A. Heterocyst Thylakoid Bioenergetics. *Life 2019, Vol. 9, Page 13* **9**, 13 (2019).

146. Giddings, T. H. & Staehelin, L. A. Observation of microplasmodesmata in both heterocyst-forming and non-heterocyst forming filamentous cyanobacteria by freeze-fracture electron microscopy. *Arch Microbiol* **129**, 295–298 (1981).

147. Hania, A., López-Adams, R., Prášil, O. & Eichner, M. Protection of nitrogenase from photosynthetic O2 evolution in Trichodesmium: methodological pitfalls and advances over 30 years of research. *http://ps.ueb.cas.cz/doi/10.32615/ps.2023.007.html* **61**, 58–72 (2023).

148. Toepel, J., Karande, R., Klähn, S. & Bühler, B. Cyanobacteria as whole-cell factories: current status and future prospectives. *Curr Opin Biotechnol* **80**, 102892 (2023).

149. Kim, D. S., Moreno-Cabezuelo, J. Á., Schulz, E. N., Lea-Smith, D. J. & Sagaram, U. S. Recent advances in engineering fast-growing cyanobacterial species for enhanced CO2 fixation. *Frontiers in Climate* **6**, 1412232 (2024).

150. Jones, P. R. Genetic instability in cyanobacteria - An elephant in the room? *Front Bioeng Biotechnol* **2**, 89300 (2014).

151. Molina, D. *et al.* Biological contamination and its chemical control in microalgal mass cultures. *Applied Microbiology and Biotechnology 2019 103:23* **103**, 9345–9358 (2019).

152. Zhu, Z. *et al.* Overcoming the Biological Contamination in Microalgae and Cyanobacteria Mass Cultivations for Photosynthetic Biofuel Production. *Molecules 2020, Vol. 25, Page 5220* **25**, 5220 (2020).

153. Guillaume, M. C. & Branco dos Santos, F. Assessing and reducing phenotypic instability in cyanobacteria. *Curr Opin Biotechnol* **80**, 102899 (2023).

154. Ohta, K., Beall, D. S., Mejia, J. P., Shanmugam, K. T. & Ingram, L. O. Metabolic engineering of Klebsiella oxytoca M5A1 for ethanol production from xylose and glucose. *Appl Environ Microbiol* **57**, 2810–2815 (1991).

155. Gao, Z., Zhao, H., Li, Z., Tan, X. & Lu, X. Photosynthetic production of ethanol from carbon dioxide in genetically engineered cyanobacteria. *Energy Environ Sci* **5**, 9857–9865 (2012).

156. Włodarczyk, A., Selão, T. T., Norling, B. & Nixon, P. J. Newly discovered Synechococcus sp. PCC 11901 is a robust cyanobacterial strain for high biomass production. *Commun Biol* **3**, (2020).

157. Gibson, B., Wilson, D. J., Feil, E. & Eyre-Walker, A. The distribution of bacterial doubling times in the wild. *Proceedings of the Royal Society B: Biological Sciences* **285**, (2018).

158. Zhou, J., Zhu, T., Cai, Z. & Li, Y. From cyanochemicals to cyanofactories: A review and perspective. *Microb Cell Fact* **15**, 1–9 (2016).

159. Noreña-Caro, D. & Benton, M. G. Cyanobacteria as photoautotrophic biofactories of high-value chemicals. *Journal of CO2 Utilization* **28**, 335–366 (2018).

160. Zhang, Y., Nielsen, J. & Liu, Z. Engineering yeast metabolism for production of terpenoids for use as perfume ingredients, pharmaceuticals and biofuels. *FEMS Yeast Res* **17**, (2017).

161. Lapczynski, A., Bhatia, S. P., Letizia, C. S. & Api, A. M. Fragrance material review on geranyl linalool. *Food and Chemical Toxicology* **46**, S176–S178 (2008).

162. De Castro, K. A., Byun, E. Y. & Rhee, H. Diketene and acetylated meldrum's acid: Agents for a facile teprenone synthesis via carroll rearrangement. *Bull Korean Chem Soc* **30**, 2155–2157 (2009).

163. Formighieri, C. & Melis, A. Heterologous synthesis of geranyllinalool, a diterpenol plant product, in the cyanobacterium Synechocystis. *Appl Microbiol Biotechnol* **101**, 2791–2800 (2017).

164. Ray, S., Abraham, J., Jordan, N., Lindsay, M. & Chauhan, N. Synthetic, Photosynthetic, and Chemical Strategies to Enhance Carbon Dioxide Fixation. *C 2022, Vol. 8, Page 18* **8**, 18 (2022).

165. Politaeva, N., Ilin, I., Velmozhina, K. & Shinkevich, P. Carbon Dioxide Utilization Using Chlorella Microalgae. *Environments 2023, Vol. 10, Page 109* **10**, 109 (2023).

166. Sales, C. R. G., Da Silva, A. B. & Carmo-Silva, E. Measuring Rubisco activity: challenges and opportunities of NADH-linked microtiter plate-based and 14C-based assays. *J Exp Bot* **71**, 5302–5312 (2020).

167. Barta, C., Carmo-Silva, A. E. & Salvucci, M. E. Rubisco Activase Activity Assays. *Methods in Molecular Biology* **684**, 375–382 (2011).

168. Davidi, D. *et al.* Highly active rubiscos discovered by systematic interrogation of natural sequence diversity. *EMBO J* **39**, e104081 (2020).

169. Lin, M. T., Occhialini, A., Andralojc, P. J., Parry, M. A. J. & Hanson, M. R. A faster Rubisco with potential to increase photosynthesis in crops. *Nature 2014 513:7519* **513**, 547–550 (2014).

170. Wang, W., Liu, X. & Lu, X. Engineering cyanobacteria to improve photosynthetic production of alka(e)nes. *Biotechnol Biofuels* **6**, 1–9 (2013).

171. Zhou, J., Zhang, H., Meng, H., Zhang, Y. & Li, Y. Production of optically pure d-lactate from CO2 by blocking the PHB

and acetate pathways and expressing d-lactate dehydrogenase in cyanobacterium Synechocystis sp. PCC 6803. *Process Biochemistry* **49**, 2071–2077 (2014).

172. Davies, F. K., Work, V. H., Beliaev, A. S. & Posewitz, M. C. Engineering limonene and bisabolene production in wild type and a glycogen-deficient mutant of Synechococcus sp. PCC 7002. *Front Bioeng Biotechnol* **2**, 96024 (2014).

173. Adebiyi, A. O., Jazmin, L. J. & Young, J. D. 13C flux analysis of cyanobacterial metabolism. *Photosynth Res* **126**, 19–32 (2015).

174. Nieves-Morión, M., Flores, E., Whitehouse, M. J., Thomen, A. & Foster, R. A. Single-cell measurements of fixation and intercellular exchange of c and n in the filaments of the heterocyst- forming cyanobacterium anabaena sp. Strain pcc 7120. *mBio* **12**, (2021).

175. Winter, G. & Krömer, J. O. Fluxomics - connecting 'omics analysis and phenotypes. *Environ Microbiol* **15**, 1901–1916 (2013).

176. Lopez, J. S., Garcia, N. S., Talmy, D. & Martiny, A. C. Diel variability in the elemental composition of the marine cyanobacterium Synechococcus. *J Plankton Res* **38**, 1052–1061 (2016).

177. Clark, R. L. *et al.* Light-Optimized Growth of Cyanobacterial Cultures: Growth Phases and Productivity of Biomass and Secreted Molecules in Light-Limited Batch Growth. *Metab Eng* **47**, 230 (2018).

178. Zhu, X. G., De Sturler, E. & Long, S. P. Optimizing the Distribution of Resources between Enzymes of Carbon Metabolism Can Dramatically Increase Photosynthetic Rate: A Numerical Simulation Using an Evolutionary Algorithm. *Plant Physiol* **145**, 513–526 (2007).

179. Zavřel, T. *et al.* Monitoring fitness and productivity in cyanobacteria batch cultures. *Algal Res* **56**, 102328 (2021).

180. Liu, X., Sheng, J. & Curtiss, R. Fatty acid production in genetically modified cyanobacteria. *Proc Natl Acad Sci U S A* **108**, 6899–6904 (2011).

181. Lindberg, P., Park, S. & Melis, A. Engineering a platform for photosynthetic isoprene production in cyanobacteria, using Synechocystis as the model organism. *Metab Eng* **12**, 70–79 (2010).

182. Yao, L., Qi, F., Tan, X. & Lu, X. Improved production of fatty alcohols in cyanobacteria by metabolic engineering. *Biotechnol Biofuels* **7**, 1–9 (2014).

183. Ungerer, J. *et al.* Sustained photosynthetic conversion of CO 2 to ethylene in recombinant cyanobacterium Synechocystis 6803. *Energy Environ Sci* **5**, 8998–9006 (2012).

184. Durall, C., Lindberg, P., Yu, J. & Lindblad, P. Increased ethylene production by overexpressing phosphoenolpyruvate carboxylase in the cyanobacterium Synechocystis PCC 6803. *Biotechnol Biofuels* **13**, 1–13 (2020).

185. Aikawa, S. *et al.* Glycogen production for biofuels by the euryhaline cyanobacteria Synechococcus sp. strain PCC 7002 from an oceanic environment. *Biotechnol Biofuels* **7**, 1–8 (2014).

186. Ruffing, A. M. Improved free fatty acid production in cyanobacteria with Synechococcus sp. PCC 7002 as host. *Front Bioeng Biotechnol* **2**, 91413 (2014).

187. Atsumi, S., Higashide, W. & Liao, J. C. Direct photosynthetic recycling of carbon dioxide to isobutyraldehyde. *Nature Biotechnology 2009 27:12* **27**, 1177–1180 (2009).

188. Kanno, M., Carroll, A. L. & Atsumi, S. Global metabolic rewiring for improved CO2 fixation and chemical production in cyanobacteria. *Nature Communications 2017 8:1* **8**, 1–11 (2017).

189. Shen, C. R. & Liao, J. C. Photosynthetic production of 2-methyl-1-butanol from CO 2 in cyanobacterium Synechococcus elongatus PCC7942 and characterization of the native acetohydroxyacid synthase. *Energy Environ Sci* **5**, 9574–9583 (2012).

190. Hirokawa, Y., Suzuki, I. & Hanai, T. Optimization of isopropanol production by engineered cyanobacteria with a synthetic metabolic pathway. *J Biosci Bioeng* **119**, 585–590 (2015).

191. Taton, A. *et al.* Heterologous Expression of Cryptomaldamide in a Cyanobacterial Host. *ACS Synth Biol* **9**, 3364–3376 (2020).

192. Halfmann, C., Gu, L., Gibbons, W. & Zhou, R. Genetically engineering cyanobacteria to convert CO2, water, and light

into the long-chain hydrocarbon farnesene. *Appl Microbiol Biotechnol* **98**, 9869–9877 (2014).

193. Sengupta, A. *et al.* Photosynthetic Co-production of Succinate and Ethylene in a Fast-Growing Cyanobacterium, Synechococcus elongatus PCC 11801. *Metabolites 2020, Vol. 10, Page 250* **10**, 250 (2020).

194. Polyzois, A., Kirilovsky, D., Dufat, T. H. & Michel, S. Effects of Modification of Light Parameters on the Production of Cryptophycin, Cyanotoxin with Potent Anticancer Activity, in Nostoc sp. *Toxins 2020, Vol. 12, Page 809* **12**, 809 (2020).

195. Santos-Merino, M., Singh, A. K. & Ducat, D. C. New applications of synthetic biology tools for cyanobacterial metabolic engineering. *Front Bioeng Biotechnol* **7**, 440298 (2019).

196. Camsund, D. & Lindblad, P. Engineered transcriptional systems for cyanobacterial biotechnology. *Front Bioeng Biotechnol* **2**, 108406 (2014).

197. Huang, H. H., Camsund, D., Lindblad, P. & Heidorn, T. Design and characterization of molecular tools for a Synthetic Biology approach towards developing cyanobacterial biotechnology. *Nucleic Acids Res* **38**, 2577–2593 (2010).

198. Abe, K. *et al.* Engineering of a green-light inducible gene expression system in Synechocystis sp. PCC6803. *Microb Biotechnol* **7**, 177–183 (2014).

199. Callura, J. M., Dwyer, D. J., Isaacs, F. J., Cantor, C. R. & Collins, J. J. Tracking, tuning, and terminating microbial physiology using synthetic riboregulators. *Proc Natl Acad Sci U S A* **107**, 15898–15903 (2010).

200. Tsinoremas, N. F., Kutach, A. K., Strayer, C. A. & Golden, S. S. Efficient gene transfer in Synechococcus sp. strains PCC 7942 and PCC 6301 by interspecies conjugation and chromosomal recombination. *J Bacteriol* **176**, 6764–6768 (1994).

201. Behler, J., Vijay, D., Hess, W. R. & Akhtar, M. K. CRISPR-Based Technologies for Metabolic Engineering in Cyanobacteria. *Trends Biotechnol* **36**, 996–1010 (2018).

202. Viola, S., Rühle, T. & Leister, D. A single vector-based strategy for marker-less gene replacement in Synechocystis sp. PCC 6803. *Microb Cell Fact* **13**, 1–12 (2014).

203. Liang, F. & Lindblad, P. Effects of overexpressing photosynthetic carbon flux control enzymes in the cyanobacterium Synechocystis PCC 6803. *Metab Eng* **38**, 56–64 (2016).

204. Liang, F. & Lindblad, P. Synechocystis PCC 6803 overexpressing RuBisCO grow faster with increased photosynthesis. *Metab Eng Commun* **4**, 29–36 (2017).

205. Gupta, J. K., Rai, P., Jain, K. K. & Srivastava, S. Overexpression of bicarbonate transporters in the marine cyanobacterium Synechococcus sp. PCC 7002 increases growth rate and glycogen accumulation. *Biotechnol Biofuels* **13**, 17 (2020).

206. Velmurugan, R. & Incharoensakdi, A. Overexpression of glucose-6-phosphate isomerase in Synechocystis sp. PCC 6803 with disrupted glycogen synthesis pathway improves exopolysaccharides synthesis. *Algal Res* **57**, 102357 (2021).

207. Roussou, S., Albergati, A., Liang, F. & Lindblad, P. Engineered cyanobacteria with additional overexpression of selected Calvin-Benson-Bassham enzymes show further increased ethanol production. *Metab Eng Commun* **12**, e00161 (2021).

208. Whitney, S. M., Houtz, R. L. & Alonso, H. Advancing Our Understanding and Capacity to Engineer Nature's CO2-Sequestering Enzyme, Rubisco. *Plant Physiol* **155**, 27–35 (2011).

209. Cai, Z., Liu, G., Zhang, J. & Li, Y. Development of an activity-directed selection system enabled significant improvement of the carboxylation efficiency of Rubisco. *Protein Cell* **5**, 552–562 (2014).

210. Iñiguez, C. *et al.* Evolutionary trends in RuBisCO kinetics and their co-evolution with CO2 concentrating mechanisms. *The Plant Journal* **101**, 897–918 (2020).

211. Yu, J. *et al.* Synechococcus elongatus UTEX 2973, a fast growing cyanobacterial chassis for biosynthesis using light and CO2. *Scientific Reports 2015 5:1* **5**, 1–10 (2015).

212. Zhou, J. & Li, Y. SNPs deciding the rapid growth of cyanobacteria are alterable. *Proc Natl Acad Sci U S A* **116**, 3945 (2019).

213. Ungerer, J., Wendt, K. E., Hendry, J. I., Maranas, C. D. & Pakrasi, H. B. Comparative genomics reveals the molecular

determinants of rapid growth of the cyanobacterium Synechococcus elongatus UTEX 2973. *Proc Natl Acad Sci U S A* **115**, E11761–E11770 (2018).

214. Oliver, J. W. K., Machado, I. M. P., Yoneda, H. & Atsumi, S. Cyanobacterial conversion of carbon dioxide to 2,3-butanediol. *Proc Natl Acad Sci U S A* **110**, 1249–1254 (2013).

215. Lips, D. Fuelling the future of sustainable sugar fermentation across generations. *Engineering Biology* **6**, 3–16 (2022).

216. Mavrommati, M., Daskalaki, A., Papanikolaou, S. & Aggelis, G. Adaptive laboratory evolution principles and applications in industrial biotechnology. *Biotechnol Adv* **54**, 107795 (2022).

217. Hirasawa, T. & Maeda, T. Adaptive Laboratory Evolution of Microorganisms: Methodology and Application for Bioproduction. *Microorganisms* **11**, (2023).

218. Dragosits, M. & Mattanovich, D. Adaptive laboratory evolution - principles and applications for biotechnology. *Microbial Cell Factories* vol. 12 64 Preprint at https://doi.org/10.1186/1475-2859-12-64 (2013).

219. Sandberg, T. E., Salazar, M. J., Weng, L. L., Palsson, B. O. & Feist, A. M. The emergence of adaptive laboratory evolution as an efficient tool for biological discovery and industrial biotechnology. *Metabolic Engineering* vol. 56 1–16 Preprint at https://doi.org/10.1016/j.ymben.2019.08.004 (2019).

220. LaCroix, R. A., Palsson, B. O. & Feist, A. M. A model for designing adaptive laboratory evolution experiments. *Appl Environ Microbiol* **83**, 3115–3131 (2017).

221. Shepelin, D., Hansen, A. S. L., Lennen, R., Luo, H. & Herrgård, M. J. Selecting the Best: Evolutionary Engineering of Chemical Production in Microbes. *Genes 2018, Vol. 9, Page 249* **9**, 249 (2018).

222. Gerrish, P. J. & Lenski, R. E. The fate of competing beneficial mutations in an asexual population. *Genetica 1998 102:0* **102**, 127–144 (1998).

223. Uecker, H. & Hermisson, J. On the Fixation Process of a Beneficial Mutation in a Variable Environment. *Genetics* **188**, 915–930 (2011).

224. Conrad, T. M., Lewis, N. E. & Palsson, B. O. Microbial laboratory evolution in the era of genome-scale science. *Mol Syst Biol* **7**, 509 (2011).

225. Patel, V. K. *et al.* Rapid budding EMS mutants of Synechocystis PCC 6803 producing carbohydrate or lipid enriched biomass. *Algal Res* **16**, 36–45 (2016).

226. Leon, D., D'Alton, S., Quandt, E. M. & Barrick, J. E. Innovation in an E. coli evolution experiment is contingent on maintaining adaptive potential until competition subsides. *PLoS Genet* **14**, e1007348 (2018).

227. Lalejini, A., Ferguson, A. J., Grant, N. A. & Ofria, C. Adaptive Phenotypic Plasticity Stabilizes Evolution in Fluctuating Environments. *Front Ecol Evol* **9**, 715381 (2021).

228. Lenski, R. E., Rose, M. R., Simpson, S. C. & Tadler, S. C. Long-term experimental evolution in Escherichia coli. I. Adaptation and divergence during 2000 generations. *American Naturalist* **138**, 1315–1341 (1991).

229. Lenski, R. E. & Travisano, M. Dynamics of adaptation and diversification: A 10,000-generation experiment with bacterial populations. *Proc Natl Acad Sci U S A* **91**, 6808–6814 (1994).

230. Weikert, C., Sauer, U. & Bailey, J. E. Use of a glycerol-limited, long-term chemostat for isolation of Escherichia coli mutants with improved physiological properties. *Microbiology (N Y)* **143**, 1567–1574 (1997).

231. Ferea, T. L., Botstein, D., Brown, P. O. & Rosenzweig, R. F. Systematic changes in gene expression patterns following adaptive evolution in yeast. *Proc Natl Acad Sci U S A* **96**, 9721–9726 (1999).

232. Sonderegger, M. & Sauer, U. Evolutionary engineering of Saccharomyces cerevisiae for anaerobic growth on xylose. *Appl Environ Microbiol* **69**, 1990–1998 (2003).

233. Kuyper, M., Winkler, A. A., Van Dijken, J. P. & Pronk, J. T. Minimal metabolic engineering of Saccharomyces cerevisiae for efficient anaerobic xylose fermentation: A proof of principle. *FEMS Yeast Res* **4**, 655–664 (2004).

234. Jansen, M. L. A., Daran-Lapujade, P., De Winde, J. H., Piper, M. D. W. & Pronk, J. T. Prolonged Maltose-Limited Cultivation of Saccharomyces cerevisiae Selects for Cells

with Improved Maltose Affinity and Hypersensitivity. *Appl Environ Microbiol* **70**, 1956–1963 (2004).

235. Kuyper, M. *et al.* Evolutionary engineering of mixed-sugar utilization by a xylose-fermenting Saccharomyces cerevisiae strain. *FEMS Yeast Res* **5**, 925–934 (2005).

236. Guimarães, P. M. R., François, J., Parrou, J. L., Teixeira, J. A. & Domingues, L. Adaptive evolution of a lactose-consuming Saccharomyces cerevisiae recombinant. *Appl Environ Microbiol* **74**, 1748–1756 (2008).

237. Lee, D. H. & Palsson, B. O. Adaptive evolution of escherichia coli K-12 MG1655 during growth on a nonnative carbon source, L-l,2-propanediol. *Appl Environ Microbiol* **76**, 4158–4168 (2010).

238. Garcia Sanchez, R. *et al.* Research improved xylose and arabinose utilization by an industrial recombinant Saccharomyces cerevisiae strain using evolutionary engineering. *Biotechnol Biofuels* **3**, (2010).

239. Hong, K. K., Vongsangnak, W., Vemuri, G. N. & Nielsen, J. Unravelling evolutionary strategies of yeast for improving galactose utilization through integrated systems level analysis. *Proc Natl Acad Sci U S A* **108**, 12179–12184 (2011).

240. Zelle, R. M., Harrison, J. C., Pronk, J. T. & Van Maris, A. J. A. Anaplerotic role for cytosolic malic enzyme in engineered saccharomyces cerevisiae strains. *Appl Environ Microbiol* **77**, 732–738 (2011).

241. Ochoa-Estopier, A., Lesage, J., Gorret, N. & Guillouet, S. E. Kinetic analysis of a Saccharomyces cerevisiae strain adapted for improved growth on glycerol: Implications for the development of yeast bioprocesses on glycerol. *Bioresour Technol* **102**, 1521–1527 (2011).

242. Merico, A., Ragni, E., Galafassi, S., Popolo, L. & Compagno, C. Generation of an evolved Saccharomyces cerevisiae strain with a high freeze tolerance and an improved ability to grow on glycerol. *J Ind Microbiol Biotechnol* **38**, 1037–1044 (2011).

243. Cadière, A., Ortiz-Julien, A., Camarasa, C. & Dequin, S. Evolutionary engineered Saccharomyces cerevisiae wine yeast strains with increased in vivo flux through the pentose phosphate pathway. *Metab Eng* **13**, 263–271 (2011).

244. Utrilla, J. *et al.* Engineering and adaptive evolution of Escherichia coli for d-lactate fermentation reveals GatC as a xylose transporter. *Metab Eng* **14**, 469–476 (2012).

245. Kim, S. R. *et al.* Rational and Evolutionary Engineering Approaches Uncover a Small Set of Genetic Changes Efficient for Rapid Xylose Fermentation in Saccharomyces cerevisiae. *PLoS One* **8**, (2013).

246. Zhou, H., Cheng, J. sheng, Wang, B. L., Fink, G. R. & Stephanopoulos, G. Xylose isomerase overexpression along with engineering of the pentose phosphate pathway and evolutionary engineering enable rapid xylose utilization and ethanol production by Saccharomyces cerevisiae. *Metab Eng* **14**, 611–622 (2012).

247. Scalcinati, G. *et al.* Evolutionary engineering of Saccharomyces cerevisiae for efficient aerobic xylose consumption. *FEMS Yeast Res* **12**, 582–597 (2012).

248. Kok, S. *et al.* Laboratory evolution of new lactate transporter genes in a jen1Δ mutant of Saccharomyces cerevisiae and their identification as ADY2 alleles by whole-genome resequencing and transcriptome analysis. *FEMS Yeast Res* **12**, n/a-n/a (2012).

249. Yu, S., Zhao, Q., Miao, X. & Shi, J. Enhancement of lipid production in low-starch mutants Chlamydomonas reinhardtii by adaptive laboratory evolution. *Bioresour Technol* **147**, 499–507 (2013).

250. Carroll, S. M. & Marx, C. J. Evolution after Introduction of a Novel Metabolic Pathway Consistently Leads to Restoration of Wild-Type Physiology. *PLoS Genet* **9**, (2013).

251. Klimacek, M. *et al.* Stepwise metabolic adaption from pure metabolization to balanced anaerobic growth on xylose explored for recombinant Saccharomyces cerevisiae. *Microb Cell Fact* **13**, 1–12 (2014).

252. Novy, V. *et al.* Process intensification through microbial strain evolution: Mixed glucose-xylose fermentation in wheat straw hydrolyzates by three generations of recombinant Saccharomyces cerevisiae. *Biotechnol Biofuels* **7**, (2014).

253. Smith, J., van Rensburg, E. & Görgens, J. F. Simultaneously improving xylose fermentation and tolerance to lignocellulosic inhibitors through evolutionary engineering of recombinant Saccharomyces cerevisiae harbouring xylose isomerase. *BMC Biotechnol* **14**, (2014).

254. Zha, J., Shen, M., Hu, M., Song, H. & Yuan, Y. Enhanced expression of genes involved in initial xylose metabolism and the oxidative pentose phosphate pathway in the improved xylose-utilizing Saccharomyces cerevisiae through evolutionary engineering. *J Ind Microbiol Biotechnol* **41**, 27–39 (2014).

255. Lenski, R. E. *et al.* Sustained fitness gains and variability in fitness trajectories in the long-term evolution experiment with Escherichia coli. *Proceedings of the Royal Society B: Biological Sciences* **282**, (2015).

256. LaCroix, R. A. *et al.* Use of adaptive laboratory evolution to discover key mutations enabling rapid growth of Escherichia coli K-12 MG1655 on glucose minimal medium. *Appl Environ Microbiol* **81**, 17–30 (2015).

257. Latif, H. *et al.* Adaptive evolution of Thermotoga maritima reveals plasticity of the ABC transporter network. *Appl Environ Microbiol* **81**, 5477–5485 (2015).

258. Sandberg, T. E. *et al.* Evolution of E. coli on [U-13C]glucose reveals a negligible isotopic influence on metabolism and physiology. *PLoS One* **11**, (2016).

259. Szappanos, B. *et al.* Adaptive evolution of complex innovations through stepwise metabolic niche expansion. *Nat Commun* **7**, (2016).

260. Rajaraman, E. *et al.* Transcriptional analysis and adaptive evolution of Escherichia coli strains growing on acetate. *Appl Microbiol Biotechnol* **100**, 7777–7785 (2016).

261. van Rossum, H. M. *et al.* Requirements for carnitine shuttle-mediated translocation of mitochondrial acetyl moieties to the yeast cytosol. *mBio* **7**, (2016).

262. Cordova, L. T. *et al.* Co-utilization of glucose and xylose by evolved Thermus thermophilus LC113 strain elucidated by 13C metabolic flux analysis and whole genome sequencing. *Metab Eng* **37**, 63–71 (2016).

263. Radek, A. *et al.* Miniaturized and automated adaptive laboratory evolution: Evolving Corynebacterium glutamicum towards an improved D-xylose utilization. *Bioresour Technol* **245**, 1377–1385 (2017).

264. Pfeifer, E., Gätgens, C., Polen, T. & Frunzke, J. Adaptive laboratory evolution of Corynebacterium glutamicum towards higher growth rates on glucose minimal medium. *Sci Rep* **7**, (2017).

265. Ho, P. W., Swinnen, S., Duitama, J. & Nevoigt, E. The sole introduction of two single-point mutations establishes glycerol utilization in Saccharomyces cerevisiae CEN.PK derivatives. *Biotechnol Biofuels* **10**, (2017).

266. Sandberg, T. E., Lloyd, C. J., Palsson, B. O. & Feist, A. M. Laboratory evolution to alternating substrate environments yields distinct phenotypic and genetic adaptive strategies. *Appl Environ Microbiol* **83**, (2017).

267. Moser, J. W. *et al.* Implications of evolutionary engineering for growth and recombinant protein production in methanol-based growth media in the yeast Pichia pastoris. *Microb Cell Fact* **16**, (2017).

268. Marques, W. L. *et al.* Elimination of sucrose transport and hydrolysis in Saccharomyces cerevisiae: A platform strain for engineering sucrose metabolism. *FEMS Yeast Res* **17**, (2017).

269. Thyer, R. *et al.* Custom selenoprotein production enabled by laboratory evolution of recoded bacterial strains. *Nat Biotechnol* **36**, 624–631 (2018).

270. Wannier, T. M. *et al.* Adaptive evolution of genomically recoded Escherichia coli. *Proc Natl Acad Sci U S A* **115**, 3090–3095 (2018).

271. Strucko, T. *et al.* Laboratory evolution reveals regulatory and metabolic trade-offs of glycerol utilization in Saccharomyces cerevisiae. *Metab Eng* **47**, 73–82 (2018).

272. Papapetridis, I. *et al.* Laboratory evolution for forced glucose-xylose co-consumption enables identification of mutations that improve mixed-sugar fermentation by xylose-fermenting Saccharomyces cerevisiae. *FEMS Yeast Res* **18**, (2018).

273. Zhang, W. *et al.* Adaptive Evolution Relieves Nitrogen Catabolite Repression and Decreases Urea Accumulation in Cultures of the Chinese Rice Wine Yeast Strain Saccharomyces cerevisiae XZ-11. *J Agric Food Chem* **66**, 9061–9069 (2018).

274. Mohamed, E. T. *et al.* Generation of an E. coli platform strain for improved sucrose utilization using adaptive laboratory evolution. *Microb Cell Fact* **18**, 1–14 (2019).

275. Igeño, M. I., Macias, D. & Blasco, R. A Case of Adaptive Laboratory Evolution (ALE): Biodegradation of Furfural by

Pseudomonas pseudoalcaligenes CECT 5344. *Genes 2019, Vol. 10, Page 499* **10**, 499 (2019).

276. Tsiamis, G. *et al.* Continuous Adaptive Evolution of a Fast-Growing Corynebacterium glutamicum Strain Independent of Protocatechuate. *Front Microbiol* **10**, 460509 (2019).

277. Diao, J. *et al.* Rewiring metabolic network by chemical modulator based laboratory evolution doubles lipid production in Crypthecodinium cohnii. *Metab Eng* **51**, 88–98 (2019).

278. Espinosa, M. I. *et al.* Adaptive laboratory evolution of native methanol assimilation in Saccharomyces cerevisiae. *Nature Communications 2020 11:1* **11**, 1–12 (2020).

279. Millán, C. *et al.* Improving glucose and xylose assimilation in Azotobacter vinelandii by adaptive laboratory evolution. *World J Microbiol Biotechnol* **36**, 1–11 (2020).

280. Wang, Y. *et al.* Adaptive laboratory evolution enhances methanol tolerance and conversion in engineered Corynebacterium glutamicum. *Communications Biology 2020 3:1* **3**, 1–15 (2020).

281. Promdonkoy, P., Mhuantong, W., Champreda, V., Tanapongpipat, S. & Runguphan, W. Improvement in d-xylose utilization and isobutanol production in S. cerevisiae by adaptive laboratory evolution and rational engineering. *J Ind Microbiol Biotechnol* **47**, 497–510 (2020).

282. Liu, Y. *et al.* Developing rapid growing Bacillus subtilis for improved biochemical and recombinant protein production. *Metab Eng Commun* **11**, e00141 (2020).

283. Lakhssassi, N. *et al.* EMS-Induced Mutagenesis of Clostridium carboxidivorans for Increased Atmospheric CO2 Reduction Efficiency and Solvent Production. *Microorganisms 2020, Vol. 8, Page 1239* **8**, 1239 (2020).

284. Lim, H. G. *et al.* Generation of Pseudomonas putida KT2440 Strains with Efficient Utilization of Xylose and Galactose via Adaptive Laboratory Evolution. *ACS Sustain Chem Eng* **9**, 11512–11523 (2021).

285. Bennett, R. K. *et al.* Improving the Methanol Tolerance of an Escherichia coli Methylotroph via Adaptive Laboratory Evolution Enhances Synthetic Methanol Utilization. *Front Microbiol* **12**, 638426 (2021).

286. Ali, N. Adaptive Laboratory Evolution of Scenedesmus obliquus for Increased Carbohydrate Content and Biomass

Productivity. *Master's Theses* (2021) doi:10.15368/theses.2021.29.

287. Gassler, T., Baumschabl, M., Sallaberger, J., Egermeier, M. & Mattanovich, D. Adaptive laboratory evolution and reverse engineering enhances autotrophic growth in Pichia pastoris. *Metab Eng* **69**, 112–121 (2022).

288. Zhang, J., Jin, B., Fu, J., Wang, Z. & Chen, T. Adaptive Laboratory Evolution of Halomonas bluephagenesis Enhances Acetate Tolerance and Utilization to Produce Poly(3-hydroxybutyrate). *Molecules* **27**, 3022 (2022).

289. Du, C. *et al.* Co-utilization of multiple lignocellulose-derived sugars and inhibitors by the robust mutant Kluyveromyces marxianus through adaptive laboratory evolution. *Fuel* **315**, 122816 (2022).

290. Gjetø, D. O. A High-Throughput Chemostat Array for Adaptive Laboratory Evolution of Microalgae. *80 s.* (2022).

291. Arora, N., Lo, E. & Philippidis, G. P. A two-prong mutagenesis and adaptive evolution strategy to enhance the temperature tolerance and productivity of Nannochloropsis oculata. *Bioresour Technol* **364**, 128101 (2022).

292. Mueller, J., Willett, H., Feist, A. M. & Niu, W. Engineering Pseudomonas putida for improved utilization of syringyl aromatics. *Biotechnol Bioeng* **119**, 2541–2550 (2022).

293. Ling, C. *et al.* Muconic acid production from glucose and xylose in Pseudomonas putida via evolution and metabolic engineering. *Nat Commun* **13**, 1–14 (2022).

294. Barten, R. *et al.* Genetic mechanisms underlying increased microalgal thermotolerance, maximal growth rate, and yield on light following adaptive laboratory evolution. *BMC Biol* **20**, 1–14 (2022).

295. Varunraj, R., Priyadharshini, U., Vijay, K. & Balamurugan, S. Adaptive laboratory evolution empowers lipids and biomass overproduction in Chlorella vulgaris for environmental applications. *Environ Res* **238**, 117125 (2023).

296. Fae Neto, W. A., Tomkins, J. L. & Kennington, W. J. Improved biomass production of a microalga through adaptative laboratory evolution to a high light environment. *J Appl Phycol* **35**, 1009–1021 (2023).

297. Wickham-Smith, C., Malys, N. & Winzer, K. Improving carbon monoxide tolerance of Cupriavidus necator H16 through adaptive laboratory evolution. *Front Bioeng Biotechnol* **11**, 1178536 (2023).

298. Antonicelli, G. *et al.* Expanding the product portfolio of carbon dioxide and hydrogen-based gas fermentation with an evolved strain of Clostridium carboxidivorans. *Bioresour Technol* **387**, 129689 (2023).

299. Li, D. & Zhao, Q. Study of carbon fixation and carbon partitioning of evolved Chlorella sp.'s strain under different carbon dioxide conditions. *Biocatal Agric Biotechnol* **48**, 102655 (2023).

300. Wefelmeier, K. *et al.* Engineering the methylotrophic yeast Ogataea polymorpha for lactate production from methanol. *Front Bioeng Biotechnol* **11**, 1223726 (2023).

301. Dann, M. *et al.* Enhancing photosynthesis at high light levels by adaptive laboratory evolution. *Nat Plants* **7**, 681–695 (2021).

302. Lenski, R. E. Revisiting the Design of the Long-Term Evolution Experiment with Escherichia coli. *J Mol Evol* **91**, 241–253 (2023).

303. Blount, Z. D., Borland, C. Z. & Lenski, R. E. INAUGURAL ARTICLE by a Recently Elected Academy Member:Historical contingency and the evolution of a key innovation in an experimental population of Escherichia coli. *Proc Natl Acad Sci U S A* **105**, 7899 (2008).

304. Blount, Z. D., Borland, C. Z. & Lenski, R. E. Historical contingency and the evolution of a key innovation in an experimental population of Escherichia coli. *Proc Natl Acad Sci U S A* **105**, 7899 (2008).

305. Perrineau, M. M. *et al.* Using Natural Selection to Explore the Adaptive Potential of Chlamydomonas reinhardtii. *PLoS One* **9**, e92533 (2014).

306. Yoshikawa, K. *et al.* Mutations in hik26 and slr1916 lead to high-light stress tolerance in Synechocystis sp. PCC6803. *Commun Biol* **4**, 1–10 (2021).

307. Hu, L. *et al.* Divergent metabolic and transcriptomic responses of Synechocystis sp. PCC 6803 to salt stress after adaptive laboratory evolution. *Algal Res* **47**, 101856 (2020).

308. Tillich, U. M., Lehmann, S., Schulze, K., Dühring, U. & Frohme, M. The Optimal Mutagen Dosage to Induce Point-Mutations in Synechocystis sp. PCC6803 and Its Application to Promote Temperature Tolerance. *PLoS One* **7**, e49467 (2012).

309. Mills, L. A., McCormick, A. J. & Lea-Smith, D. J. Current knowledge and recent advances in understanding metabolism of the model cyanobacterium Synechocystis sp. PCC 6803. *Biosci Rep* **40**, 20193325 (2020).

310. Stanier, R. Y., Kunisawa, R., Mandel, M. & Cohen-Bazire, G. Purification and properties of unicellular blue-green algae (order Chroococcales). *Bacteriol Rev* **35**, 171 (1971).

311. Ikeuchi, M. & Tabata, S. Synechocystis sp. PCC 6803 - A useful tool in the study of the genetics of cyanobacteria. *Photosynth Res* **70**, 73–83 (2001).

312. Koskinen, S., Kurkela, J., Linhartová, M. & Tyystjärvi, T. The genome sequence of Synechocystis sp. PCC 6803 substrain GT-T and its implications for the evolution of PCC 6803 substrains. *FEBS Open Bio* **13**, 701 (2023).

313. Kaneko, T. *et al.* Sequence Analysis of the Genome of the Unicellular Cyanobacterium Synechocystis sp. Strain PCC6803. II. Sequence Determination of the Entire Genome and Assignment of Potential Protein-coding Regions. *DNA Research* **3**, 109–136 (1996).

314. Nakamura, Y., Kaneko, T., Hirosawa, M., Miyajima, N. & Tabata, S. CyanoBase, a www database containing the complete nucleotide sequence of the genome of Synechocystis sp. strain PCC6803. *Nucleic Acids Res* **26**, 63–67 (1998).

315. Thiel, T. *et al.* Complete genome sequence of Anabaena variabilis ATCC 29413. *Stand Genomic Sci* **9**, 562–573 (2013).

316. Mannan, R. M. & Pakrasi, H. B. Dark heterotrophic growth conditions result in an increase in the content of photosystem II units in the filamentous cyanobacterium Anabaena variabilis ATCC 29413. *Plant Physiol* **103**, 971 (1993).

317. Higo, A., Isu, A., Fukaya, Y., Ehira, S. & Hisabori, T. Application of CRISPR Interference for Metabolic Engineering of the Heterocyst-Forming Multicellular Cyanobacterium Anabaena sp. PCC 7120. *Plant Cell Physiol* **59**, 119–127 (2018).

318. Meeks, J. C. *et al.* An overview of the Genome of Nostoc punctiforme, a multicellular, symbiotic Cyanobacterium. *Photosynth Res* **70**, 85–106 (2001).

319. Cordara, A. *et al.* Analysis of the light intensity dependence of the growth of Synechocystis and of the light distribution in a photobioreactor energized by 635 nm light. *PeerJ* **2018**, e5256 (2018).

320. Martínez, L., Redondas, V., García, A. I. & Morán, A. Optimization of growth operational conditions for CO2 biofixation by native Synechocystis sp. *Journal of Chemical Technology and Biotechnology* **86**, 681–690 (2011).

321. Elena, S. F. & Lenski, R. E. Evolution experiments with microorganisms: the dynamics and genetic bases of adaptation. *Nature Reviews Genetics 2003 4:6* **4**, 457–469 (2003).

322. LaPanse, A. J., Krishnan, A. & Posewitz, M. C. Adaptive Laboratory Evolution for algal strain improvement: methodologies and applications. *Algal Res* **53**, 102122 (2021).

323. Kremer, C. T., Fey, S. B., Arellano, A. A. & Vasseur, D. A. Gradual plasticity alters population dynamics in variable environments: Thermal acclimation in the green alga chlamydomonas reinhartdii. *Proceedings of the Royal Society B: Biological Sciences* **285**, (2018).

324. Gresham, D. & Hong, J. The functional basis of adaptive evolution in chemostats. *FEMS Microbiol Rev* **39**, 2–16 (2015).

325. LaCroix, R. A., Palsson, B. O. & Feist, A. M. A model for designing adaptive laboratory evolution experiments. *Appl Environ Microbiol* **83**, (2017).

326. Trovão, M. *et al.* Random Mutagenesis as a Promising Tool for Microalgal Strain Improvement towards Industrial Production. *Mar Drugs* **20**, 440 (2022).

327. Rozen, D. E., Philippe, N., Arjan De Visser, J., Lenski, R. E. & Schneider, D. Death and cannibalism in a seasonal environment facilitate bacterial coexistence. *Ecol Lett* **12**, 34–44 (2009).

328. Carmona, S. B. *et al.* Evolution of an Escherichia coli PTS− strain: a study of reproducibility and dynamics of an adaptive evolutive process. *Appl Microbiol Biotechnol* **104**, 9309–9325 (2020).

329. Basso, T. P. *et al.* Engineering xylose fermentation in an industrial yeast: continuous cultivation as a tool for selecting improved strains. *Lett Appl Microbiol* **76**, 1–10 (2023).

330. Bromig, L. & Weuster-Botz, D. Accelerated Adaptive Laboratory Evolution by Automated Repeated Batch Processes in Parallelized Bioreactors. *Microorganisms* **11**, 275 (2023).

331. Lee, D. H., Feist, A. M., Barrett, C. L. & Palsson, B. Cumulative Number of Cell Divisions as a Meaningful Timescale for Adaptive Laboratory Evolution of Escherichia coli. *PLoS One* **6**, e26172 (2011).

332. Cabanelas, I. T. D., Kleinegris, D. M. M., Wijffels, R. H. & Barbosa, M. J. Repeated nitrogen starvation doesn't affect lipid productivity of Chlorococcum littorale. *Bioresour Technol* **219**, 576–582 (2016).

333. Gresham, D. & Dunham, M. J. The enduring utility of continuous culturing in experimental evolution. *Genomics* **104**, 399–405 (2014).

334. Hu, X., Tang, X., Bi, Z., Zhao, Q. & Ren, L. Adaptive evolution of microalgae Schizochytrium sp. under high temperature for efficient production of docosahexaeonic acid. *Algal Res* **54**, 102212 (2021).

335. Beaulieu, M., Cabana, H. & Huot, Y. Adverse effects of atrazine, DCMU and metolachlor on phytoplankton cultures and communities at environmentally relevant concentrations using Fast Repetition Rate Fluorescence. *Science of The Total Environment* **712**, 136239 (2020).

336. Fuerst, E. P. & Norman, M. A. Interactions of Herbicides with Photosynthetic Electron Transport. *Weed Sci* **39**, 458–464 (1991).

337. Alifano, P., Palumbo, C., Pasanisi, D. & Talà, A. Rifampicin-resistance, rpoB polymorphism and RNA polymerase genetic engineering. *J Biotechnol* **202**, 60–77 (2015).

338. Barrick, J. E. *et al.* Genome evolution and adaptation in a long-term experiment with Escherichia coli. *Nature 2009 461:7268* **461**, 1243–1247 (2009).

339. Foster, J. S., Singh, A. K., Rothschild, L. J. & Sherman, L. A. Growth-phase dependent differential gene expression in Synechocystis sp. strain PCC 6803 and regulation by a group 2 sigma factor. *Arch Microbiol* **187**, 265–279 (2007).

340. Lopo, M. *et al.* Experimental and Modeling Analysis of Synechocystis sp. PCC 6803 Growth. *J Mol Microbiol Biotechnol* **22**, 71–82 (2012).

341. El Shafay, S. M., Gaber, A., Alsanie, W. F. & Elshobary, M. E. Influence of Nutrient Manipulation on Growth and Biochemical Constituent in Anabaena variabilis and Nostoc muscorum to Enhance Biodiesel Production. *Sustainability 2021, Vol. 13, Page 9081* **13**, 9081 (2021).

342. Khan, M. I., Shin, J. H. & Kim, J. D. The promising future of microalgae: current status, challenges, and optimization of a sustainable and renewable industry for biofuels, feed, and other products. *Microbial Cell Factories 2018 17:1* **17**, 1–21 (2018).

343. Cohen, S. E. & Golden, S. S. Circadian Rhythms in Cyanobacteria. *Microbiology and Molecular Biology Reviews* **79**, 373–385 (2015).

344. Mutalipassi, M. *et al.* Symbioses of Cyanobacteria in Marine Environments: Ecological Insights and Biotechnological Perspectives. *Mar Drugs* **19**, (2021).

345. Aranda, Y. N., Bhatt, P., Ates, N., Engel, B. A. & Simsek, H. Cyanophage-cyanobacterial interactions for sustainable aquatic environment. *Environ Res* **229**, 115728 (2023).

346. Rossi, F. & De Philippis, R. Role of Cyanobacterial Exopolysaccharides in Phototrophic Biofilms and in Complex Microbial Mats. *Life 2015, Vol. 5, Pages 1218-1238* **5**, 1218–1238 (2015).

347. Allaf, M. M. & Peerhossaini, H. Cyanobacteria: Model Microorganisms and Beyond. *Microorganisms* **10**, 696 (2022).

348. Zheng, Y. *et al.* Genetic Diversity for Accelerating Microbial Adaptive Laboratory Evolution. *ACS Synth Biol* **10**, 1574–1586 (2021).

349. Chen, J., Miller, B. F. & Furano, A. V. Repair of naturally occurring mismatches can induce mutations in flanking DNA. *Elife* **3**, (2014).

350. Cotner, S. & Wassenburg, D. 5.10 Point Mutations Affect Gene Expression – The Evolution and Biology of Sex. https://open.lib.umn.edu/evolutionbiology/chapter/5-10-point-mutations-affect-gene-expression-2/.

351. Ho, E. K. H. *et al.* High and Highly Variable Spontaneous Mutation Rates in Daphnia. *Mol Biol Evol* **37**, 3258–3266 (2020).

352. Snyman, M., Huynh, T. V., Smith, M. T. & Xu, S. The genome-wide rate and spectrum of EMS-induced heritable mutations in the microcrustacean Daphnia: on the prospect of forward genetics. *Heredity (Edinb)* **127**, 535–545 (2021).

353. Shibai, A. *et al.* Mutation accumulation under UV radiation in Escherichia coli. *Sci Rep* **7**, (2017).

354. Izutsu, M. & Lenski, R. E. Experimental test of the contributions of initial variation and new mutations to adaptive evolution in a novel environment. *Front Ecol Evol* **10**, 958406 (2022).

355. Koksharova, O. & Wolk, C. Genetic tools for cyanobacteria. *Appl Microbiol Biotechnol* **58**, 123–137 (2002).

356. Bonilla, B. *et al.* The Shu complex prevents mutagenesis and cytotoxicity of single-strand specific alkylation lesions. *Elife* **10**, (2021).

357. Foster, P. L. In Vivo Mutagenesis. *Methods Enzymol* **204**, 114 (1991).

358. Liu, C. *et al.* Sodium azide mutagenesis induces a unique pattern of mutations. *PLoS Genet* **21**, e1011634 (2025).

359. Brown, T. A. Mutation, Repair and Recombination. (2002).

360. Tripathi, A. K. & Kumar, H. D. Mutagenesis by ethidium bromide, proflavine and mitomycin C in the cyanobacterium Nostoc sp. *Mutation Research Letters* **174**, 175–178 (1986).

361. Ikehata, H. & Ono, T. The Mechanisms of UV Mutagenesis. *J Radiat Res* **52**, 115–125 (2011).

362. Ichida, H., Morita, R., Shirakawa, Y., Hayashi, Y. & Abe, T. Targeted exome sequencing of unselected heavy-ion beam-irradiated populations reveals less-biased mutation characteristics in the rice genome. *Plant Journal* **98**, 301–314 (2019).

363. V), N. R. C. (US) C. on the B. E. of I. R. (BEIR. Genetic Effects of Radiation. (1990).

364. Youk, J. *et al.* Quantitative and qualitative mutational impact of ionizing radiation on normal cells. *Cell Genomics* **4**, 100499 (2024).

365. Wells, J. A., Vasser, M. & Powers, D. B. Cassette mutagenesis: an efficient method for generation of multiple mutations at defined sites. *Gene* **34**, 315–323 (1985).

366. Watabe, K., Mimuro, M. & Tsuchiya, T. Development of a high-frequency in vivo transposon mutagenesis system for Synechocystis sp. PCC 6803 and Synechococcus elongatus PCC 7942. *Plant Cell Physiol* **55**, 2017–2026 (2014).

367. Sega, G. A. A review of the genetic effects of ethyl methanesulfonate. *Mutation Research/Reviews in Genetic Toxicology* **134**, 113–142 (1984).

368. Kondo, N., Takahashi, A., Ono, K. & Ohnishi, T. DNA Damage Induced by Alkylating Agents and Repair Pathways. *J Nucleic Acids* **2010**, (2010).

369. Sinha, R. P. & Häder, D. P. UV-induced DNA damage and repair: a review. *Photochemical & Photobiological Sciences* **1**, 225–236 (2002).

370. Richardson, C. & Jasin, M. Frequent chromosomal translocations induced by DNA double-strand breaks. *Nature* **405**, 697–700 (2000).

371. Masuma, R., Kashima, S., Kurasaki, M. & Okuno, T. Effects of UV wavelength on cell damages caused by UV irradiation in PC12 cells. *J Photochem Photobiol B* **125**, 202–208 (2013).

372. Mullenders, L. H. F. Solar UV damage to cellular DNA: from mechanisms to biological effects. *Photochem Photobiol Sci* **17**, 1842–1852 (2018).

373. Currin, A. *et al.* The evolving art of creating genetic diversity: From directed evolution to synthetic biology. *Biotechnol Adv* **50**, (2021).

374. Ehling-Schulz, M. & Scherer, S. UV protection in cyanobacteria. *Eur J Phycol* **34**, 329–338 (1999).

375. Hitomi, K. *et al.* Bacterial cryptochrome and photolyase: characterization of two photolyase-like genes of Synechocystis sp. PCC6803. *Nucleic Acids Res* **28**, 2353–2362 (2000).

376. Levine, E. & Thiel, T. UV-inducible DNA repair in the cyanobacteria Anabaena spp. *J Bacteriol* **169**, 3988–3993 (1987).

377. Pang, Q. & Hays, J. B. UV-B-Inducible and Temperature-Sensitive Photoreactivation of Cyclobutane Pyrimidine Dimers in Arabidopsis thaliana. *Plant Physiol* **95**, 536–543 (1991).

378. Wolk, C. P., Cai, Y. & Panoff, J. M. Use of a transposon with luciferase as a reporter to identify environmentally responsive genes in a cyanobacterium. *Proceedings of the National Academy of Sciences* **88**, 5355–5359 (1991).

379. Black, T. A. & Wolk, C. P. Analysis of a Het- mutation in Anabaena sp. strain PCC 7120 implicates a secondary metabolite in the regulation of heterocyst spacing. *J Bacteriol* **176**, 2282–2292 (1994).

380. Koksharova, O. A., Popova, A. A., Plyuta, V. A. & Khmel, I. A. Four New Genes of Cyanobacterium Synechococcus elongatus PCC 7942 Are Responsible for Sensitivity to 2-Nonanone. *Microorganisms 2020, Vol. 8, Page 1234* **8**, 1234 (2020).

381. Baselga-Cervera, B., Jacobsen, K. A., Ford Denison, R. & Travisano, M. Experimental evolution in the cyanobacterium Trichormus variabilis: increases in size and morphological diversity. *Evolution (N Y)* **77**, 1216–1225 (2023).

382. Shastri, A. A. & Morgan, J. A. Flux Balance Analysis of Photoautotrophic Metabolism. *Biotechnol Prog* **21**, 1617–1626 (2005).

383. Shahkouhi, A. M. & Motamedian, E. Reconstruction of a regulated two-cell metabolic model to study biohydrogen production in a diazotrophic cyanobacterium Anabaena variabilis ATCC 29413. *PLoS One* **15**, e0227977 (2020).

384. Liang, F., Englund, E., Lindberg, P. & Lindblad, P. Engineered cyanobacteria with enhanced growth show increased ethanol production and higher biofuel to biomass ratio. *Metab Eng* **46**, 51–59 (2018).

385. Wojtasiewicz, B. & Stoń-Egiert, J. Bio-optical characterization of selected cyanobacteria strains present in marine and freshwater ecosystems. *J Appl Phycol* **28**, 2299 (2016).

386. Tao, Y., Wolinska, J., Hölker, F. & Agha, R. Light intensity and spectral distribution affect chytrid infection of cyanobacteria via modulation of host fitness. *Parasitology* **147**, 1206–1215 (2020).

387. Beal, J. *et al.* Robust estimation of bacterial cell count from optical density. *Commun Biol* **3**, (2020).

388. Osborne, J. & Killeen, P. R. Replication Statistics. *Best Practices in Quantitative Methods* 102–124 (2008) doi:10.4135/9781412995627.

389. Andrade, C. Understanding the Difference Between Standard Deviation and Standard Error of the Mean, and Knowing When to Use Which. *Indian J Psychol Med* **42**, 409–410 (2020).

390. Student. The Probable Error of a Mean. *Biometrika* **6**, 1 (1908).

391. Chamovitz, D., Sandmann, G. & Hirschberg, J. Molecular and biochemical characterization of herbicide-resistant mutants of cyanobacteria reveals that phytoene desaturation is a rate-limiting step in carotenoid biosynthesis. *Journal of Biological Chemistry* **268**, 17348–17353 (1993).

392. Zavřel, T., Sinetova, M. A. & Červený, J. Measurement of Chlorophyll a and Carotenoids Concentration in Cyanobacteria. *Iss* **5**, (2015).

393. Stamatakis, K., Tsimilli-Michael, M. & Papageorgiou, G. C. On the question of the light-harvesting role of β-carotene in photosystem II and photosystem I core complexes. *Plant Physiology and Biochemistry* **81**, 121–127 (2014).

394. Zakar, T., Laczko-Dobos, H., Toth, T. N. & Gombos, Z. Carotenoids assist in cyanobacterial photosystem II assembly and function. *Front Plant Sci* **7**, 173308 (2016).

395. Brindley, C., Acién, F. G. & Fernández-Sevilla, J. M. The oxygen evolution methodology affects photosynthetic rate measurements of microalgae in well-defined light regimes. *Biotechnol Bioeng* **106**, 228–237 (2010).

396. Li, Y., Lin, Y., Loughlin, P. C. & Chen, M. Optimization and effects of different culture conditions on growth of Halomicronema hongdechloris - A filamentous cyanobacterium containing chlorophyll f. *Front Plant Sci* **5**, 79927 (2014).

397. CLARK, L. C., WOLF, R., GRANGER, D. & TAYLOR, Z. Continuous recording of blood oxygen tensions by polarography. *J Appl Physiol* **6**, 189–193 (1953).

398. Sanger, F., Nicklen, S. & Coulson, A. R. DNA sequencing with chain-terminating inhibitors. *Proceedings of the National Academy of Sciences* **74**, 5463–5467 (1977).

399. Chait, E., Page, G. & Hunkapiller, M. Battle of the DNA sequencers. *Nature* **333**, 477–478 (1988).

400. Hu, T., Chitnis, N., Monos, D. & Dinh, A. Next-generation sequencing technologies: An overview. *Hum Immunol* **82**, 801–811 (2021).

401. Baudhuin, L. M. *et al.* Confirming Variants in Next-Generation Sequencing Panel Testing by Sanger Sequencing. *The Journal of Molecular Diagnostics* **17**, 456–461 (2015).

402. Al-Shuhaib, M. B. S. & Hashim, H. O. Mastering DNA chromatogram analysis in Sanger sequencing for reliable clinical analysis. *Journal of Genetic Engineering and Biotechnology* **21**, 1–12 (2023).

403. Pereira, R., Oliveira, J. & Sousa, M. Bioinformatics and Computational Tools for Next-Generation Sequencing Analysis in Clinical Genetics. *Journal of Clinical Medicine 2020, Vol. 9, Page 132* **9**, 132 (2020).

404. Griese, M., Lange, C. & Soppa, J. Ploidy in cyanobacteria. *FEMS Microbiol Lett* **323**, 124–131 (2011).

405. Griffin, P. C., Robin, C. & Hoffmann, A. A. A next-generation sequencing method for overcoming the multiple gene copy problem in polyploid phylogenetics, applied to Poa grasses. *BMC Biol* **9**, 1–18 (2011).

406. Ejigu, G. F. & Jung, J. Review on the Computational Genome Annotation of Sequences Obtained by Next-Generation Sequencing. *Biology 2020, Vol. 9, Page 295* **9**, 295 (2020).

407. Chevez-Guardado, R. & Peña-Castillo, L. Promotech: a general tool for bacterial promoter recognition. *Genome Biol* **22**, 1–16 (2021).

408. Schymanski, E. L. *et al.* Identifying small molecules via high resolution mass spectrometry: Communicating confidence. *Environ Sci Technol* **48**, 2097–2098 (2014).

409. Gertsman, I. & Barshop, B. A. Promises and pitfalls of untargeted metabolomics. *J Inherit Metab Dis* **41**, 355–366 (2018).

410. Viant, M. R. *et al.* Use cases, best practice and reporting standards for metabolomics in regulatory toxicology. *Nature Communications 2019 10:1* **10**, 1–10 (2019).

411. Sumner, L. W. *et al.* Proposed minimum reporting standards for chemical analysis Chemical Analysis Working Group (CAWG) Metabolomics Standards Initiative (MSI). *Metabolomics* **3**, 211 (2007).

412. Sake, C. L., Newman, D. M. & Boyle, N. R. Evaluation of quenching methods for metabolite recovery in photoautotrophic Synechococcus sp. PCC 7002. *Biotechnol Prog* **36**, e3015 (2020).

413. Prasannan, C. B., Jaiswal, D., Davis, R. & Wangikar, P. P. An improved method for extraction of polar and charged metabolites from cyanobacteria. *PLoS One* **13**, e0204273 (2018).

414. Dunn, W. B. *et al.* Procedures for large-scale metabolic profiling of serum and plasma using gas chromatography and liquid chromatography coupled to mass spectrometry. *Nat Protoc* **6**, 1060–1083 (2011).

415. Milman, B. L. General principles of identification by mass spectrometry. *TrAC Trends in Analytical Chemistry* **69**, 24–33 (2015).

416. Guo, J. & Huan, T. Comparison of Full-Scan, Data-Dependent, and Data-Independent Acquisition Modes in Liquid Chromatography-Mass Spectrometry Based Untargeted Metabolomics. *Anal Chem* **92**, 8072–8080 (2020).

417. Fu, X. *et al.* Longitudinal Fragment Profiles Based on Multi-Collision Energy Tandem Mass Spectra Improve the Accuracy of Metabolite Identification in Untargeted Metabolomics. *Anal Chem* **57**, 41 (2025).

418. Worley, B. & Powers, R. Multivariate Analysis in Metabolomics. *Curr Metabolomics* **1**, 92–107 (2013).

419. Parsons, H. M., Ekman, D. R., Collette, T. W. & Viant, M. R. Spectral relative standard deviation: a practical benchmark in metabolomics. *Analyst* **134**, 478–485 (2009).

420. Yamamoto, S. *et al.* Analysis of the correlation between dipeptides and taste differences among soy sauces by using metabolomics-based component profiling. *J Biosci Bioeng* **118**, 56–63 (2014).

421. Bertani, G. Lysogeny at Mid-Twentieth Century: P1, P2, and Other Experimental Systems. *J Bacteriol* **186**, 595 (2004).

422. Allen, M. M. & Stanier, R. Y. Growth and division of some unicellular blue-green algae. *J Gen Microbiol* **51**, 199–202 (1968).

423. Zwietering, M. H., Jongenburger, I., Rombouts, F. M. & Van't Riet, K. Modeling of the Bacterial Growth Curve. *Appl Environ Microbiol* **56**, 1875–1881 (1990).

424. Koch, A. L. Growth Measurement. *Methods for General and Molecular Microbiology, 3rd Edition* 172–199 (2014) doi:10.1128/9781555817497.CH9.

425. Heidorn, T. *et al.* Synthetic Biology in Cyanobacteria: Engineering and Analyzing Novel Functions. *Methods Enzymol* **497**, 539–579 (2011).

426. Eckert, C. *et al.* Genetic Analysis of the Hox Hydrogenase in the Cyanobacterium Synechocystis sp. PCC 6803 Reveals Subunit Roles in Association, Assembly, Maturation, and Function. *J Biol Chem* **287**, 43502 (2012).

427. Wolf, L., Suarez, G., Barrick, J., Li, V. & Rodriguez, A. Barrick Lab :: ProtocolsEthanolPrecipitation. https://barricklab.org/twiki/bin/view/Lab/ProtocolsEthanolPrecipitation (2021).

428. Akligoh, H. & Molloy, J. Chemically Competent Cell Preparation [Calcium Chloride Method]. https://www.protocols.io/view/chemically-competent-cell-preparation-calcium-chlo-261ge4k8dv47/v1/references (2022).

429. Green, M. R. & Sambrook, J. Cloning and Transformation with Plasmid Vectors. *Cold Spring Harb Protoc* **2021**, pdb.top101170 (2021).

430. Grigorieva, G. & Shestakov, S. Transformation in the cyanobacterium Synechocystis sp. 6803. *FEMS Microbiol Lett* **13**, 367–370 (1982).

431. Englund, E., Andersen-Ranberg, J., Miao, R., Hamberger, B. & Lindberg, P. Metabolic Engineering of Synechocystis sp. PCC 6803 for Production of the Plant Diterpenoid Manoyl Oxide. *ACS Synth Biol* **4**, 1270–1278 (2015).

432. Schmelling, N. Chlorophyll Extraction in Cyanobacteria V.2. https://www.protocols.io/view/chlorophyll-extraction-in-cyanobacteria-14egn3wzl5dy/v2 (2016).

433. Edwards, U., Rogall, T., Blöcker, H., Emde, M. & Böttger, E. C. Isolation and direct complete nucleotide determination of entire genes. Characterization of a gene coding for 16S ribosomal RNA. *Nucleic Acids Res* **17**, 7843–7853 (1989).

434. Lamovšek, J., Geric Stare, B. & Urek, G. Isolation of non-pathogenic Agrobacterium spp. biovar 1 from agricultural soils in Slovenia. *Phytopathol Mediterr* **53**, 130–139 (2014).

435. Darling, A. C. E., Mau, B., Blattner, F. R. & Perna, N. T. Mauve: Multiple Alignment of Conserved Genomic Sequence With Rearrangements. *Genome Res* **14**, 1394 (2004).

436. Szklarczyk, D. *et al.* The STRING database in 2023: protein–protein association networks and functional enrichment analyses for any sequenced genome of interest. *Nucleic Acids Res* **51**, D638–D646 (2023).

437. Abdelrazig, S. *et al.* Metabolic characterisation of Magnetospirillum gryphiswaldense MSR-1 using LC-MS-based metabolite profiling. *RSC Adv* **10**, 32548–32560 (2020).

438. Hong, Y. S. *et al.* 1H NMR-based metabonomic assessment of probiotic effects in a colitis mouse model. *Arch Pharm Res* **33**, 1091–1101 (2010).

439. Kim, E. J. *et al.* Metabolite profiling of angelica gigas from different geographical origins using 1H NMR and UPLC-MS analyses. *J Agric Food Chem* **59**, 8806–8815 (2011).

440. Notley-McRobb, L. & Ferenci, T. The generation of multiple co-existing mal-regulatory mutations through polygenic evolution in glucose-limited populations of Escherichia coli. *Environ Microbiol* **1**, 45–52 (1999).

441. Carbon dioxide now more than 50% higher than pre-industrial levels | National Oceanic and Atmospheric Administration. https://www.noaa.gov/news-release/carbon-dioxide-now-more-than-50-higher-than-pre-industrial-levels.

442. Kodym, A. & Afza, R. Physical and chemical mutagenesis. *Methods Mol Biol* **236**, 189–204 (2003).

443. Wang, Z. *et al.* Effect of sodium thiosulfate on the depletion of photosynthetic apparatus in cyanobacterium Synechocystis sp. PCC 6803 cells grown in the presence of glucose. *Photosynthetica* **40**, 383–387 (2002).

444. Shevell, D. E., Friedman, B. M. & Walker, G. C. Resistance to alkylation damage in Escherichia coli: Role of the Ada

protein in induction of the adaptive response. *Mutation Research/Fundamental and Molecular Mechanisms of Mutagenesis* **233**, 53–72 (1990).

445. Bolton, J. R., Linden, K. G. & Asce, M. Standardization of Methods for Fluence (UV Dose) Determination in Bench-Scale UV Experiments. *Journal of Environmental Engineering* **129**, 209–215 (2003).

446. Hood, R. D., Higgins, S. A., Flamholz, A., Nichols, R. J. & Savage, D. F. The stringent response regulates adaptation to darkness in the cyanobacterium Synechococcus elongatus. *Proc Natl Acad Sci U S A* **113**, E4867–E4876 (2016).

447. Muramatsu, M. & Hihara, Y. Acclimation to high-light conditions in cyanobacteria: from gene expression to physiological responses. *Journal of Plant Research 2011 125:1* **125**, 11–39 (2011).

448. Matson, M. M. *et al.* Adaptive laboratory evolution for improved tolerance of isobutyl acetate in Escherichia coli. *Metab Eng* **69**, 50–58 (2022).

449. Gao, S. *et al.* Isolation of axenic cyanobacterium and the promoting effect of associated bacterium on axenic cyanobacterium. *BMC Biotechnol* **20**, 1–11 (2020).

450. Riaz, S. *et al.* Generation of miniploid cells and improved natural transformation procedure for a model cyanobacterium Synechococcus elongatus PCC 7942. *Front Microbiol* **13**, 959043 (2022).

451. Mahlmann, D. M., Jahnke, J. & Loosen, P. Rapid determination of the dry weight of single, living cyanobacterial cells using the Mach-Zehnder double-beam interference microscope. *Eur J Phycol* **43**, 355–364 (2008).

452. Robertson, B. R., Button, D. K. & Koch, A. L. Determination of the biomasses of small bacteria at low concentrations in a mixture of species with forward light scatter measurements by flow cytometry. *Appl Environ Microbiol* **64**, 3900–3909 (1998).

453. Loferer-Krößbacher, M., Klima, J. & Psenner, R. Determination of bacterial cell dry mass by transmission electron microscopy and densitometric image analysis. *Appl Environ Microbiol* **64**, 688–694 (1998).

454. Wang, G. *et al.* Recent progress in adaptive laboratory evolution of industrial microorganisms. *J Ind Microbiol Biotechnol* **50**, 23 (2023).

455. Kirk, J. T. Light and Photosynthesis in Aquatic Ecosystems - . (1994).

456. Qiang, H., Richmond, A. & Zarmi, Y. Combined effects of light intensity, light-path and culture density on output rate of Spirulina platensis (Cyanobacteria). *Eur J Phycol* **33**, 165–171 (1998).

457. Wang, Q. J. *et al.* Net light-induced oxygen evolution in photosystem I deletion mutants of the cyanobacterium Synechocystis sp. PCC 6803. *Biochimica et Biophysica Acta (BBA) - Bioenergetics* **1817**, 792–801 (2012).

458. Vermeersch, L. *et al.* On the duration of the microbial lag phase. *Curr Genet* **65**, 721–727 (2019).

459. Bertranda, R. L. Lag Phase Is a Dynamic, Organized, Adaptive, and Evolvable Period That Prepares Bacteria for Cell Division. *J Bacteriol* **201**, (2019).

460. Watanabe, S. *et al.* Intensive DNA Replication and Metabolism during the Lag Phase in Cyanobacteria. *PLoS One* **10**, e0136800 (2015).

461. Werner, A., Broeckling, C. D., Prasad, A. & Peebles, C. A. M. A comprehensive time-course metabolite profiling of the model cyanobacterium Synechocystis sp. PCC 6803 under diurnal light:dark cycles. *The Plant Journal* **99**, 379–388 (2019).

462. Roach, T. & Krieger-Liszkay, A. Regulation of Photosynthetic Electron Transport and Photoinhibition.

463. Latifi, A., Ruiz, M. & Zhang, C. C. Oxidative stress in cyanobacteria. *FEMS Microbiol Rev* **33**, 258–278 (2009).

464. Grund, M., Jakob, T., Wilhelm, C., Bühler, B. & Schmid, A. Electron balancing under different sink conditions reveals positive effects on photon efficiency and metabolic activity of Synechocystis sp. PCC 6803. *Biotechnol Biofuels* **12**, 1–14 (2019).

465. Frías, J. E. & Flores, E. Induction of the nitrate assimilation nirA operon and protein-protein interactions in the maturation of nitrate and nitrite reductases in the cyanobacterium Anabaena sp. strain PCC 7120. *J Bacteriol* **197**, 2442–2452 (2015).

466. Navarro, F., Martín-Figueroa, E., Candau, P. & Florencio, F. J. Ferredoxin-Dependent Iron–Sulfur Flavoprotein Glutamate Synthase (GlsF) from the Cyanobacterium Synechocystis sp. PCC 6803: Expression and Assembly in Escherichia coli. *Arch Biochem Biophys* **379**, 267–276 (2000).

467. Downing, S. & Downing, T. G. The metabolism of the non-proteinogenic amino acid β-N-methylamino-L-alanine (BMAA) in the cyanobacterium Synechocystis PCC6803. *Toxicon* **115**, 41–48 (2016).

468. Allahverdiyeva, Y. *et al.* Flavodiiron proteins Flv1 and Flv3 enable cyanobacterial growth and photosynthesis under fluctuating light. *Proc Natl Acad Sci U S A* **110**, 4111–4116 (2013).

469. Allahverdiyeva, Y. *et al.* Flavodiiron proteins Flv1 and Flv3 enable cyanobacterial growth and photosynthesis under fluctuating light. *Proc Natl Acad Sci U S A* **110**, 4111–4116 (2013).

470. Allahverdiyeva, Y., Isojärvi, J., Zhang, P. & Aro, E. M. Cyanobacterial Oxygenic Photosynthesis is Protected by Flavodiiron Proteins. *Life* **5**, 716 (2015).

471. Zhang, P. *et al.* Operon flv4-flv2 Provides Cyanobacterial Photosystem II with Flexibility of Electron Transfer. *Plant Cell* **24**, 1952–1971 (2012).

472. Chukhutsina, V., Bersanini, L., Aro, E. M. & Van Amerongen, H. Cyanobacterial flv4-2 Operon-Encoded Proteins Optimize Light Harvesting and Charge Separation in Photosystem II. *Mol Plant* **8**, 747–761 (2015).

473. Balsera, M. *et al.* Ferredoxin:thioredoxin reductase (FTR) links the regulation of oxygenic photosynthesis to deeply rooted bacteria. *Planta 2012 237:2* **237**, 619–635 (2012).

474. Mustila, H., Allahverdiyeva, Y., Isojärvi, J., Aro, E. M. & Eisenhut, M. The bacterial-type [4Fe–4S] ferredoxin 7 has a regulatory function under photooxidative stress conditions in the cyanobacterium Synechocystis sp. PCC 6803. *Biochimica et Biophysica Acta (BBA) - Bioenergetics* **1837**, 1293–1304 (2014).

475. Frankenberg, N. & Lagarias, J. C. Phycocyanobilin:Ferredoxin Oxidoreductase ofAnabaena sp. PCC 7120: BIOCHEMICAL AND SPECTROSCOPIC CHARACTERIZATION. *Journal of Biological Chemistry* **278**, 9219–9226 (2003).

476. Siegel, L. M. & Davis, P. S. Reduced Nicotinamide Adenine Dinucleotide Phosphate-Sulfite Reductase of Enterobacteria: IV. THE ESCHERICHIA COLI HEMOFLAVOPROTEIN: SUBUNIT STRUCTURE AND DISSOCIATION INTO HEMOPROTEIN AND FLAVOPROTEIN COMPONENTS. *Journal of Biological Chemistry* **249**, 1587–1598 (1974).

477. De Rosa, E. *et al.* [NiFe]-hydrogenase is essential for cyanobacterium Synechocystis sp. PCC 6803 aerobic growth in the dark. *Scientific Reports 2015 5:1* **5**, 1–12 (2015).

478. McIntosh, C. L., Germer, F., Schulz, R., Appel, J. & Jones, A. K. The [NiFe]-hydrogenase of the cyanobacterium synechocystis sp. PCC 6803 works bidirectionally with a bias to H2 production. *J Am Chem Soc* **133**, 11308–11319 (2011).

479. Burgstaller, H. *et al.* Synechocystis sp. PCC 6803 Requires the Bidirectional Hydrogenase to Metabolize Glucose and Arginine Under Oxic Conditions. *Front Microbiol* **13**, 896190 (2022).

480. Reyes, L. H., Gomez, J. M. & Kao, K. C. Improving carotenoids production in yeast via adaptive laboratory evolution. *Metab Eng* **21**, 26–33 (2014).

481. Pereira, R. *et al.* Adaptive laboratory evolution of tolerance to dicarboxylic acids in Saccharomyces cerevisiae. *Metab Eng* **56**, 130–141 (2019).

482. Papadopoulou, E., Rodriguez de Evgrafov, M. C., Kalea, A., Tsapekos, P. & Angelidaki, I. Adaptive laboratory evolution to hypersaline conditions of lactic acid bacteria isolated from seaweed. *N Biotechnol* **75**, 21–30 (2023).

483. Yu, X., Shi, F., Liu, H., Tan, S. & Li, Y. Programming adaptive laboratory evolution of 4-hydroxyisoleucine production driven by a lysine biosensor in Corynebacterium glutamicum. *AMB Express* **11**, 66 (2021).

484. Srivastava, V. *et al.* Adaptive laboratory evolution of the fast-growing cyanobacterium Synechococcus elongatus PCC 11801 for improved solvent tolerance. *J Biosci Bioeng* **131**, 491–500 (2021).

485. Moreau, J. E. *et al.* Growth factor induced fibroblast differentiation from human bone marrow stromal cells in vitro. *Journal of Orthopaedic Research* **23**, 164–174 (2005).

486. Blundell, J. R. *et al.* The dynamics of adaptive genetic diversity during the early stages of clonal evolution. *Nat Ecol Evol* **3**, 293–301 (2019).

487. Maddamsetti, R., Lenski, R. E. & Barrick, J. E. Adaptation, clonal interference, and frequency-dependent interactions in a long-term evolution experiment with escherichia coli. *Genetics* **200**, 619–631 (2015).

488. Kanervo, E., Lehto, K., Ståhle, K., Lehto, H. & Mäenpää, P. Characterization of growth and photosynthesis of Synechocystis sp. PCC 6803 cultures under reduced atmospheric pressures and enhanced CO2 levels. *Int J Astrobiol* **4**, 97–100 (2005).

489. Matsusako, T., Toya, Y., Yoshikawa, K. & Shimizu, H. Identification of alcohol stress tolerance genes of Synechocystis sp. PCC 6803 using adaptive laboratory evolution. *Biotechnol Biofuels* **10**, 307 (2017).

490. Jittawuttipoka, T. *et al.* Multidisciplinary Evidences that Synechocystis PCC6803 Exopolysaccharides Operate in Cell Sedimentation and Protection against Salt and Metal Stresses. *PLoS One* **8**, e55564 (2013).

491. Foster, J. S., Havemann, S. A., Singh, A. K. & Sherman, L. A. Role of mrgA in peroxide and light stress in the cyanobacterium Synechocystis sp. PCC 6803. *FEMS Microbiol Lett* **293**, 298–304 (2009).

492. Gutekunst, K. *et al.* The Bidirectional NiFe-hydrogenase in Synechocystis sp. PCC 6803 Is Reduced by Flavodoxin and Ferredoxin and Is Essential under Mixotrophic, Nitrate-limiting Conditions. *Journal of Biological Chemistry* **289**, 1930–1937 (2014).

493. Chen, X. *et al.* The Entner-Doudoroff pathway is an overlooked glycolytic route in cyanobacteria and plants. *Proc Natl Acad Sci U S A* **113**, 5441–5446 (2016).

494. Kai, Y., Matsumura, H. & Izui, K. Phosphoenolpyruvate carboxylase: three-dimensional structure and molecular mechanisms. *Arch Biochem Biophys* **414**, 170–179 (2003).

495. Badger, M. The roles of carbonic anhydrases in photosynthetic CO2 concentrating mechanisms. *Photosynth Res* **77**, 83–94 (2003).

496. Appel, J., Phunpruch, S., Steinmüller, K. & Schulz, R. The bidirectional hydrogenase of Synechocystis sp. PCC 6803

works as an electron valve during photosynthesis. *Arch Microbiol* **173**, 333–338 (2000).

497. Kubis, A. & Bar-Even, A. Synthetic biology approaches for improving photosynthesis. *J Exp Bot* **70**, 1425–1433 (2019).

498. Elanskaya, I. V. *et al.* Phycobilisomes from the mutant cyanobacterium Synechocystis sp. PCC 6803 missing chromophore domain of ApcE. *Biochimica et Biophysica Acta (BBA) - Bioenergetics* **1859**, 280–291 (2018).

499. Lea-Smith, D. J. *et al.* Phycobilisome-Deficient Strains of Synechocystis sp. PCC 6803 Have Reduced Size and Require Carbon-Limiting Conditions to Exhibit Enhanced Productivity. *Plant Physiol* **165**, 705–714 (2014).

500. Hihara, Y., Kamei, A., Kanehisa, M., Kaplan, A. & Ikeuchi, M. DNA Microarray Analysis of Cyanobacterial Gene Expression during Acclimation to High Light. *Plant Cell* **13**, 793–806 (2001).

501. Meirmans, P. G., Liu, S. & Van Tienderen, P. H. The Analysis of Polyploid Genetic Data. *Journal of Heredity* **109**, 283–296 (2018).

502. Wang, X., Xiong, X., Sa, N., Roje, S. & Chen, S. Metabolic engineering of enhanced glycerol-3-phosphate synthesis to increase lipid production in Synechocystis sp. PCC 6803. *Appl Microbiol Biotechnol* **100**, 6091–6101 (2016).

503. Oliveira, P. & Lindblad, P. LexA, a transcription regulator binding in the promoter region of the bidirectional hydrogenase in the cyanobacterium Synechocystis sp. PCC 6803. *FEMS Microbiol Lett* **251**, 59–66 (2005).

504. Kizawa, A. *et al.* The LexA transcription factor regulates fatty acid biosynthetic genes in the cyanobacterium Synechocystis sp. PCC 6803. *Plant J* **92**, 189–198 (2017).

505. Li, H. & Sherman, L. A. A Redox-Responsive Regulator of Photosynthesis Gene Expression in the Cyanobacterium Synechocystis sp. Strain PCC 6803. *J Bacteriol* **182**, 4268 (2000).

506. Behle, A. *et al.* Manipulation of topoisomerase expression inhibits cell division but not growth and reveals a distinctive promoter structure in Synechocystis. *Nucleic Acids Res* **50**, 12790–12808 (2022).

507. Suzuki, I., Dmitry A, L., Kanesaki, Y., Mikami, K. & Murata, N. The pathway for perception and transduction of low-

temperature signals in Synechocystis. *EMBO J* **19**, 1327 (2000).

508. Martinussen, J. & Hammer, K. The carB gene encoding the large subunit of carbamoylphosphate synthetase from Lactococcus lactis is transcribed monocistronically. *J Bacteriol* **180**, 4380–4386 (1998).

509. Zhang, Y., Hu, C. & Chen, M. Induced Exopolysaccharide Synthesis and the Molecular Mechanism in Synechocystis sp. PCC 6803 Under Clinorotation. *Microgravity Sci Technol* **30**, 857–864 (2018).

510. Santos, M. *et al.* Absence of KpsM (Slr0977) Impairs the Secretion of Extracellular Polymeric Substances (EPS) and Impacts Carbon Fluxes in Synechocystis sp. PCC 6803 . *mSphere* **6**, (2021).

511. Abdel-Salam, E. M., Figueroa-Gonzalez, T. & Leister, D. Transcriptomic meta-analysis and functional validation identify genes linked to adaptation and involved in high-light acclimation in Synechocystis sp. PCC 6803. *Frontiers in Photobiology* **1**, 1290382 (2023).

512. Inaba, M., Sakamoto, A. & Murata, N. Functional expression in Escherichia coli of low-affinity and high-affinity Na+(Li+)/H+ antiporters of Synechocystis. *J Bacteriol* **183**, 1376–1384 (2001).

513. Wang, H. L., Postier, B. L. & Burnap, R. L. Alterations in Global Patterns of Gene Expression in Synechocystis sp. PCC 6803 in Response to Inorganic Carbon Limitation and the Inactivation of ndhR, a LysR Family Regulator. *Journal of Biological Chemistry* **279**, 5739–5751 (2004).

514. Lever, J., Krzywinski, M. & Altman, N. Points of Significance: Principal component analysis. *Nat Methods* **14**, 641–642 (2017).

515. Cuevas-Delgado, P., Dudzik, D., Miguel, V., Lamas, S. & Barbas, C. Data-dependent normalization strategies for untargeted metabolomics—a case study. *Anal Bioanal Chem* **412**, 6391–6405 (2020).

516. Flores, E. Studies on the Regulation of Arginine Metabolism in Cyanobacteria Should Include Mixotrophic Conditions. *mBio* **12**, (2021).

517. Herrero, A., Flores, E. & Imperial, J. Nitrogen Assimilation in Bacteria. doi:10.1016/B978-0-12-.

518. Flores, E., Arévalo, S. & Burnat, M. Cyanophycin and arginine metabolism in cyanobacteria. *Algal Res* **42**, 101577 (2019).

519. Forchhammer, K. & Selim, K. A. Carbon/nitrogen homeostasis control in cyanobacteria. *FEMS Microbiol Rev* **44**, 33–53 (2020).

520. Bolay, P. *et al.* The Novel PII-Interacting Protein PirA Controls Flux into the Cyanobacterial Ornithine-Ammonia Cycle. *mBio* **12**, (2021).

521. Bolay, P. *et al.* The novel pii-interacting protein pira controls flux into the cyanobacterial ornithine-ammonia cycle. *mBio* **12**, (2021).

522. Zyśk, M. *et al.* The Impact of Acetyl-CoA and Aspartate Shortages on the N-Acetylaspartate Level in Different Models of Cholinergic Neurons. *Antioxidants 2020, Vol. 9, Page 522* **9**, 522 (2020).

523. Le Coq, J., An, H. J., Lebrilla, C. & Viola, R. E. Characterization of Human Aspartoacylase: the brain enzyme responsible for Canavan disease. *Biochemistry* **45**, 5878 (2006).

524. Osanai, T. *et al.* Metabolomic analysis reveals rewiring of Synechocystissp. PCC 6803 primary metabolism by ntcA overexpression. *Environ Microbiol* **16**, 3304–3317 (2014).

525. Chen, Z. *et al.* Lysine Acetylome Analysis Reveals Photosystem II Manganese-stabilizing Protein Acetylation is Involved in Negative Regulation of Oxygen Evolution in Model Cyanobacterium Synechococcus sp. PCC 7002. *Mol Cell Proteomics* **16**, 1297 (2017).

526. Zhang, H. *et al.* The cyanobacterial ornithine–ammonia cycle involves an arginine dihydrolase. *Nature Chemical Biology 2018 14:6* **14**, 575–581 (2018).

527. Mishra, A. K., Kaushik, M. S. & Tiwari, D. N. Nitrogenase and Hydrogenase: Enzymes for Nitrogen Fixation and Hydrogen Production in Cyanobacteria. *Cyanobacteria: From Basic Science to Applications* 173–191 (2019) doi:10.1016/B978-0-12-814667-5.00008-8.

528. Jain, I. P. Hydrogen the fuel for 21st century. *Int J Hydrogen Energy* **34**, 7368–7378 (2009).

529. Lebrouhi, B. E., Djoupo, J. J., Lamrani, B., Benabdelaziz, K. & Kousksou, T. Global hydrogen development - A

technological and geopolitical overview. *Int J Hydrogen Energy* **47**, 7016–7048 (2022).

530. Konstantinidis, D. *et al.* Adaptive laboratory evolution of microbial co-cultures for improved metabolite secretion. *Mol Syst Biol* **17**, 10189 (2021).

531. Kang, S. *et al.* Adaptive Laboratory Evolution of Eubacterium limosum ATCC 8486 on Carbon Monoxide. *Front Microbiol* **11**, 501413 (2020).

532. Hanke, G. T., Satomi, Y., Shinmura, K., Takao, T. & Hase, T. A screen for potential ferredoxin electron transfer partners uncovers new, redox dependent interactions. *Biochimica et Biophysica Acta (BBA) - Proteins and Proteomics* **1814**, 366–374 (2011).

533. López-Maury, L., García-Domínguez, M., Florencio, F. J. & Reyes, J. C. A two-component signal transduction system involved in nickel sensing in the cyanobacterium Synechocystis sp. PCC 6803. *Mol Microbiol* **43**, 247–256 (2002).

534. Mo, R. *et al.* Acetylome analysis reveals the involvement of lysine acetylation in photosynthesis and carbon metabolism in the model cyanobacterium synechocystis sp. PCC 6803. *J Proteome Res* **14**, 1275–1286 (2015).

535. Jia, K. *et al.* Deciphering the structure, function, and mechanism of lysine acetyltransferase cGNAT2 in cyanobacteria. *Plant Physiol* **194**, 634–661 (2024).

536. Yokoyama, R. Sense or nonsense? The role of protein acetylation in cyanobacterial photosynthesis and growth. *Plant Physiol* **194**, 595–597 (2024).

537. Nürnberg, D. J. *et al.* Intercellular diffusion of a fluorescent sucrose analog via the septal junctions in a filamentous cyanobacterium. *mBio* **6**, (2015).

538. Hurley, J. K. *et al.* Structure-function relationships in Anabaena ferredoxin: Correlations between X-ray crystal structures, reduction potentials, and rate constants of electron transfer to ferredoxin:NADP+ reductase for site-specific ferredoxin mutants. *Biochemistry* **36**, 11100–11117 (1997).

539. Alcántara-Sánchez, F., Leyva-Castillo, L. E., Chagolla-López, A., González de la Vara, L. & Gómez-Lojero, C. Distribution of isoforms of ferredoxin-NADP+ reductase

(FNR) in cyanobacteria in two growth conditions. *Int J Biochem Cell Biol* **85**, 123–134 (2017).

540. Magnuson, A. & Cardona, T. Thylakoid membrane function in heterocysts. *Biochimica et Biophysica Acta (BBA) - Bioenergetics* **1857**, 309–319 (2016).

541. Alfarouk, K. O. *et al.* The Pentose Phosphate Pathway Dynamics in Cancer and Its Dependency on Intracellular pH. *Metabolites* **10**, 1–16 (2020).

542. Valiente, E. F., Nieva, M., Avendaño, M. C. & Maeso, E. S. Uptake and Utilization of Fructose by Anabaena variabilis ATCC 29413. Effect on Respiration and Photosynthesis. *Plant Cell Physiol* **33**, 307–313 (1992).

543. Chapman, J. S. & Meeks, J. C. Conditions for mutagenesis of the nitrogen-fixing cyanobacterium Anabaena variabilis. *J Gen Microbiol* **133**, 111–118 (1987).

544. Wolk, C. P. & Wojciuch, E. Simple methods for plating single vegetative cells of, and for replica-plating, filamentous blue-green algae. *Arch Mikrobiol* **91**, 91–95 (1973).

545. Zhang, G., Zhang, P., Liu, H. & Wang, B. Ultrasonic damages on cyanobacterial photosynthesis. *Ultrason Sonochem* **13**, 501–505 (2006).

546. Kimura, T., Yahata, H. & Uchiyama, Y. Examination of Material Compatibilities with Ionized and Vaporized Hydrogen Peroxide Decontamination. *Journal of the American Association for Laboratory Animal Science* **59**, 703–711 (2020).

547. Stewart, S. A., Domínguez-Robles, J., Donnelly, R. F. & Larrañeta, E. Evaluation of sterilisation techniques for 3D-printed implantable devices. *RPS Pharmacy and Pharmacology Reports* **2**, 1–12 (2023).

548. Cano, M. *et al.* Glycogen synthesis and metabolite overflow contribute to energy balancing in cyanobacteria. *cell.comM Cano, SC Holland, J Artier, RL Burnap, M Ghirardi, JA Morgan, J YuCell reports, 2018•cell.com* **23**, 667–672 (2018).

549. Ataeian, M., Liu, Y., Kouris, A., Hawley, A. K. & Strous, M. Ecological Interactions of Cyanobacteria and Heterotrophs Enhances the Robustness of Cyanobacterial Consortium for Carbon Sequestration. *Front Microbiol* **13**, 780346 (2022).

550. Muñoz, R. & Guieysse, B. Algal–bacterial processes for the treatment of hazardous contaminants: A review. *Water Res* **40**, 2799–2815 (2006).

551. Christie-Oleza, J. A., Sousoni, D., Lloyd, M., Armengaud, J. & Scanlan, D. J. Nutrient recycling facilitates long-term stability of marine microbial phototroph–heterotroph interactions. *Nature Microbiology 2017 2:9* **2**, 1–10 (2017).

552. Zhang, L. *et al.* Construction and analysis of an artificial consortium based on the fast-growing cyanobacterium Synechococcus elongatus UTEX 2973 to produce the platform chemical 3-hydroxypropionic acid from CO2. *Biotechnol Biofuels* **13**, 1–14 (2020).

553. Cook, A. M., Daughton, C. G. & Alexander, M. Phosphonate utilization by bacteria. *J Bacteriol* **133**, 85–90 (1978).

554. Martins Dos Santos, V. A. P., Heim, S., Moore, E. R. B., Strätz, M. & Timmis, K. N. Insights into the genomic basis of niche specificity of Pseudomonas putida KT2440. *Environ Microbiol* **6**, 1264–1286 (2004).

555. Peng, X. & Bruns, M. A. Development of a nitrogen-fixing cyanobacterial consortium for surface stabilization of agricultural soils. *J Appl Phycol* **31**, 1047–1056 (2019).

556. Toribio, A. J. *et al.* Design and validation of cyanobacteria-rhizobacteria consortia for tomato seedlings growth promotion. *Scientific Reports 2022 12:1* **12**, 1–15 (2022).

557. Kholssi, R. *et al.* A consortium of cyanobacteria and plant growth promoting rhizobacteria for wheat growth improvement in a hydroponic system. *South African Journal of Botany* **142**, 247–258 (2021).

558. Sawada, H., Kuykendall, L. D. & Young, J. M. Changing concepts in the systematics of bacterial nitrogen-fixing legume symbionts. *J Gen Appl Microbiol* **49**, 155–179 (2003).

559. Olson, R. D. *et al.* Introducing the Bacterial and Viral Bioinformatics Resource Center (BV-BRC): a resource combining PATRIC, IRD and ViPR. *Nucleic Acids Res* **51**, D678 (2023).

560. Wattam, A. R. *et al.* Improvements to PATRIC, the all-bacterial Bioinformatics Database and Analysis Resource Center. *Nucleic Acids Res* **45**, D535 (2017).

561. Aziz, R. K. *et al.* The RAST Server: Rapid Annotations using Subsystems Technology. *BMC Genomics* **9**, 75 (2008).

562. Overbeek, R. *et al.* The SEED and the Rapid Annotation of microbial genomes using Subsystems Technology (RAST). *Nucleic Acids Res* **42**, D206 (2014).

563. Brettin, T. *et al.* RASTtk: A modular and extensible implementation of the RAST algorithm for building custom annotation pipelines and annotating batches of genomes. *Sci Rep* **5**, (2015).

564. Gray, J. S., Birmingham, J. M. & Fenton, J. I. Got black swimming dots in your cell culture? Identification of Achromobacter as a novel cell culture contaminant. *Biologicals* **38**, 273 (2010).

565. Koo, H. *et al.* Comparison of two bioinformatics tools used to characterize the microbial diversity and predictive functional attributes of microbial mats from Lake Obersee, Antarctica. *J Microbiol Methods* **140**, 15–22 (2017).

566. Sánchez, O., Diestra, E., Esteve, I. & Mas, J. Molecular characterization of an oil-degrading cyanobacterial consortium. *Microb Ecol* **50**, 580–588 (2005).

567. Huda, N. ul, Tanvir, R., Badar, J., Ali, I. & Rehman, Y. Arsenic-Resistant Plant Growth Promoting Pseudoxanthomonas mexicana S254 and Stenotrophomonas maltophilia S255 Isolated from Agriculture Soil Contaminated by Industrial Effluent. *Sustainability (Switzerland)* **14**, 10697 (2022).

568. Žižková, E. *et al.* Control of cytokinin and auxin homeostasis in cyanobacteria and algae. *Ann Bot* **119**, 151–166 (2017).

569. Nascimento, F. X., Glick, B. R. & Rossi, M. J. Multiple plant hormone catabolism activities: an adaptation to a plant-associated lifestyle by Achromobacter spp. *Environ Microbiol Rep* **13**, 533–539 (2021).

570. Abod, É., Laslo, É., Szentes, S., Lányi, S. & Mara, G. Plant Growth-Promoting Bacteria: Strategies to Improve Wheat Growth and Development Under Sustainable Agriculture. *Plant Growth Promoting Rhizobacteria for Agricultural Sustainability* 1–17 (2019) doi:10.1007/978-981-13-7553-8_1.

571. Young, J. M., Kuykendall, L. D., Martínez-Romero, E., Kerr, A. & Sawada, H. A revision of Rhizobium Frank 1889, with an emended description of the genus, and the inclusion of all species of Agrobacterium Conn 1942 and Allorhizobium undicola de Lajudie et al. 1998 as new combinations: Rhizobium radiobacter, R. rhizogenes, R. rubi, R. undicola and R. vitis. *Int J Syst Evol Microbiol* **51**, 89–103 (2001).

572. Velázquez, E. *et al.* Analysis of core genes supports the reclassification of strains Agrobacterium radiobacter K84 and Agrobacterium tumefaciens AKE10 into the species Rhizobium rhizogenes. *Syst Appl Microbiol* **33**, 247–251 (2010).

573. Farrand, S. K., van Berkum, P. B. & Oger, P. Agrobacterium is a definable genus of the family Rhizobiaceae. *Int J Syst Evol Microbiol* **53**, 1681–1687 (2003).

574. Young, J. M., Kuykendall, L. D., Martínez-Romero, E., Kerr, A. & Sawada, H. Classification and nomenclature of Agrobacterium and Rhizobium. *Int J Syst Evol Microbiol* **53**, 1689–1695 (2003).

575. Ormeño-Orrillo, E. *et al.* Taxonomy of rhizobia and agrobacteria from the Rhizobiaceae family in light of genomics. *Syst Appl Microbiol* **38**, 287–291 (2015).

576. Graham, P. H. *et al.* Proposed minimal standards for the description of new genera and species of root- and stem-nodulating bacteria. *Int J Syst Bacteriol* **41**, 582–587 (1991).

577. Ormeño-Orrillo, E. & Martínez-Romero, E. Phenotypic tests in Rhizobium species description: An opinion and (a sympatric speciation) hypothesis. *Syst Appl Microbiol* **36**, 145–147 (2013).

578. Zhu, L. *et al.* Insights into the mechanism of the effects of rhizosphere microorganisms on the quality of authentic Angelica sinensis under different soil microenvironments. *BMC Plant Biol* **21**, 1–15 (2021).

579. Jiménez-Vázquez, K. R. *et al.* The plant beneficial rhizobacterium Achromobacter sp. 5B1 influences root development through auxin signaling and redistribution. *The Plant Journal* **103**, 1639–1654 (2020).

580. Liu, Y. *et al.* Unraveling Mechanisms and Impact of Microbial Recruitment on Oilseed Rape (Brassica napus L.) and the Rhizosphere Mediated by Plant Growth-Promoting

Rhizobacteria. *Microorganisms 2021, Vol. 9, Page 161* **9**, 161 (2021).

581. Mao, Q. *et al.* Leptolyngbya sp. XZMQ and Bacillus XZM co-inoculation reduced sunflower arsenic toxicity by regulating rhizosphere microbial structure and enzyme activity. *Environmental Pollution* **341**, 123001 (2024).

582. Prasanna, R. *et al.* Cyanobacteria-based bioinoculants influence growth and yields by modulating the microbial communities favourably in the rhizospheres of maize hybrids. *Eur J Soil Biol* **75**, 15–23 (2016).

583. Lindström, K. & Mousavi, S. A. Effectiveness of nitrogen fixation in rhizobia. *Microb Biotechnol* **13**, 1314–1335 (2020).

584. Matse, D. T., Huang, C. H., Huang, Y. M. & Yen, M. Y. Effects of coinoculation of Rhizobium with plant growth promoting rhizobacteria on the nitrogen fixation and nutrient uptake of Trifolium repens in low phosphorus soil. *J Plant Nutr* **43**, 739–752 (2020).

585. Leite, R. de A. *et al.* Co-inoculation of Rhizobium and Bradyrhizobium promotes growth and yield of common beans. *Applied Soil Ecology* **172**, 104356 (2022).

586. Wang, K. T. *et al.* Improved grain yield and lowered arsenic accumulation in rice plants by inoculation with arsenite-oxidizing Achromobacter xylosoxidans GD03. *Ecotoxicol Environ Saf* **206**, 111229 (2020).

587. Inoue-Kashino, N., Kashino, Y., Satoh, K., Terashima, I. & Pakrasi, H. B. PsbU provides a stable architecture for the oxygen-evolving system in cyanobacterial photosystem II. *Biochemistry* **44**, 12214–12228 (2005).

588. Thiel, T. & Pratte, B. S. Regulation of Three Nitrogenase Gene Clusters in the Cyanobacterium Anabaena variabilis ATCC 29413. *Life 2014, Vol. 4, Pages 944-967* **4**, 944–967 (2014).

589. Jasper, J. *et al.* Chimeric Interaction of Nitrogenase-Like Reductases with the MoFe Protein of Nitrogenase. *Chembiochem* **21**, 1733 (2020).

590. Thauer, R. K. Methyl (Alkyl)-Coenzyme M Reductases: Nickel F-430-Containing Enzymes Involved in Anaerobic Methane Formation and in Anaerobic Oxidation of Methane or of Short Chain Alkanes. *Biochemistry* **58**, 5198 (2019).

591. Rajaram, H., Kumar, A., Kirti, A. & Pandey, S. Double strand break (DSB) repair in Cyanobacteria: Understanding the process in an ancient organism. *DNA Repair (Amst)* **95**, 102942 (2020).

592. Rai, S., Singh, S., Shrivastava, A. K. & Rai, L. C. Salt and UV-B induced changes in Anabaena PCC 7120: physiological, proteomic and bioinformatic perspectives. *Photosynth Res* **118**, 105–114 (2013).

593. Dorion, S. & Rivoal, J. Clues to the functions of plant NDPK isoforms. *Naunyn Schmiedebergs Arch Pharmacol* **388**, 119–132 (2014).

594. Bauer, C. C. *et al.* Suppression of heterocyst differentiation in Anabaena PCC 7120 by a cosmid carrying wild-type genes encoding enzymes for fatty acid synthesis. *FEMS Microbiol Lett* **151**, 23–30 (1997).

595. Hu, X. J. *et al.* Prokaryotic and Highly-Repetitive WD40 Proteins: A Systematic Study. *Sci Rep* **7**, (2017).

596. Smith, T. F., Gaitatzes, C., Saxena, K. & Neer, E. J. The WD repeat: a common architecture for diverse functions. *Trends Biochem Sci* **24**, 181–185 (1999).

597. Islam, R., Brown, S., Taheri, A. & Dumenyo, C. K. The Gene Encoding NAD-Dependent Epimerase/Dehydratase, wcaG, Affects Cell Surface Properties, Virulence, and Extracellular Enzyme Production in the Soft Rot Phytopathogen, Pectobacterium carotovorum. *Microorganisms 2019, Vol. 7, Page 172* **7**, 172 (2019).

598. Perera, I. A. *et al.* Impact of Nitrate and Ammonium Concentrations on Co-Culturing of Tetradesmus obliquus IS2 with Variovorax paradoxus IS1 as Revealed by Phenotypic Responses. *Microb Ecol* **83**, 951–959 (2022).

599. Wan, N., Abernathy, M., Tang, J. K. H., Tang, Y. J. & You, L. Cyanobacterial photo-driven mixotrophic metabolism and its advantages for biosynthesis. *Front Chem Sci Eng* **9**, 308–316 (2015).

600. McCarren, J. *et al.* Microbial community transcriptomes reveal microbes and metabolic pathways associated with dissolved organic matter turnover in the sea. *Proc Natl Acad Sci U S A* **107**, 16420–16427 (2010).

601. Franks, A. *et al.* Inhibition of fungal colonization by Pseudoalteromonas tunicata provides a competitive

advantage during surface colonization. *Appl Environ Microbiol* **72**, 6079–6087 (2006).

602. Holmstrom, C., Rittschof, D. & Kjelleberg, S. Inhibition of Settlement by Larvae of Balanus amphitrite and Ciona intestinalis by a Surface-Colonizing Marine Bacterium. *Appl Environ Microbiol* **58**, 2111–2115 (1992).

603. James, S. G., Holmström, C. & Kjelleberg, S. Purification and characterization of a novel antibacterial protein from the marine bacterium D2. *Appl Environ Microbiol* **62**, 2783–2788 (1996).

604. Amin, S. A. *et al.* Photolysis of iron-siderophore chelates promotes bacterial-algal mutualism. *Proc Natl Acad Sci U S A* **106**, 17071–17076 (2009).

605. Croft, M. T., Lawrence, A. D., Raux-Deery, E., Warren, M. J. & Smith, A. G. Algae acquire vitamin B12 through a symbiotic relationship with bacteria. *Nature 2005 438:7064* **438**, 90–93 (2005).

606. Amin, S. A. *et al.* Interaction and signalling between a cosmopolitan phytoplankton and associated bacteria. *Nature 2015 522:7554* **522**, 98–101 (2015).

607. Hünken, M., Harder, J. & Kirst, G. O. Epiphytic bacteria on the Antarctic ice diatom Amphiprora kufferathii Manguin cleave hydrogen peroxide produced during algal photosynthesis. *Plant Biol (Stuttg)* **10**, 519–526 (2008).

608. Lee, S. R. & Kim, P. Current Status and Applications of Adaptive Laboratory Evolution in Industrial Microorganisms. *J Microbiol Biotechnol* **30**, 793 (2020).

609. Gómez-Consarnau, L. *et al.* Light stimulates growth of proteorhodopsin-containing marine Flavobacteria. *Nature 2006 445:7124* **445**, 210–213 (2007).

610. Tang, J. Microbial Metabolomics. *Curr Genomics* **12**, 391 (2011).

611. Abram, F. Systems-based approaches to unravel multi-species microbial community functioning. *Comput Struct Biotechnol J* **13**, 24–32 (2015).

612. Żymańczyk-Duda, E., Samson, S. O., Brzezińska-Rodak, M. & Klimek-Ochab, M. Versatile Applications of Cyanobacteria in Biotechnology. *Microorganisms* **10**, (2022).

613. Quinn, J. C. *et al.* Nannochloropsis production metrics in a scalable outdoor photobioreactor for commercial applications. *Bioresour Technol* **117**, 164–171 (2012).

614. Wong, B. G., Mancuso, C. P., Kiriakov, S., Bashor, C. J. & Khalil, A. S. Precise, automated control of conditions for high-throughput growth of yeast and bacteria with eVOLVER. *Nature Biotechnology 2018 36:7* **36**, 614–623 (2018).

615. Cheng, J. *et al.* Gradient domestication of Haematococcus pluvialis mutant with 15% CO2 to promote biomass growth and astaxanthin yield. *Bioresour Technol* **216**, 340–344 (2016).

616. Pereira, S. B. *et al.* The role of the tyrosine kinase Wzc (Sll0923) and the phosphatase Wzb (Slr0328) in the production of extracellular polymeric substances (EPS) by Synechocystis PCC 6803. *Microbiologyopen* **8**, e00753 (2019).

617. Temel, D. B. *et al.* Regulatory interactions between a bacterial tyrosine kinase and its cognate phosphatase. *Journal of Biological Chemistry* **288**, 15212–15228 (2013).

618. Butala, M., Žgur-Bertok, D. & Busby, S. J. W. The bacterial LexA transcriptional repressor. *Cellular and Molecular Life Sciences* **66**, 82–93 (2009).

619. Srivastava, A. *et al.* Cd-induced cytosolic proteome changes in the cyanobacterium Anabaena sp. PCC7120 are mediated by LexA as one of the regulatory proteins. *Biochimica et Biophysica Acta (BBA) - Proteins and Proteomics* **1871**, 140902 (2023).

620. Srivastava, A. *et al.* Regulatory role of LexA in modulating photosynthetic redox poise and cadmium stress tolerance in the cyanobacterium, Anabaena sp. PCC7120. *Environ Exp Bot* **195**, 104790 (2022).

621. Ermler, U., Grabarse, W., Shima, S., Goubeaud, M. & Thauer, R. K. Active sites of transition-metal enzymes with a focus on nickel. *Curr Opin Struct Biol* **8**, 749–758 (1998).

622. Sunamura, E. I., Konno, H., Imashimizu-Kobayashi, M., Sugano, Y. & Hisabori, T. Physiological Impact of Intrinsic ADP Inhibition of Cyanobacterial FoF1 Conferred by the Inherent Sequence Inserted into the γ Subunit. *Plant Cell Physiol* **51**, 855–865 (2010).

623. Pecoraro, V. L., Hermes, J. D. & Cleland, W. W. Stability constants of Mg2+ and Cd2+ complexes of adenine nucleotides and thionucleotides and rate constants for formation and dissociation of MgATP and MgADP. *Biochemistry* **23**, 5262–5271 (1984).

624. Wolf, F. I. & Cittadini, A. Chemistry and biochemistry of magnesium. *Mol Aspects Med* **24**, 3–9 (2003).

625. Laursen, B. S., Sørensen, H. P., Mortensen, K. K. & Sperling-Petersen, H. U. Initiation of Protein Synthesis in Bacteria. *Microbiology and Molecular Biology Reviews* **69**, 101–123 (2005).

626. Structure of chlorophyll A. *Nature* **133**, 321 (1934).

627. Forchhammer, K. & Selim, K. A. Carbon/nitrogen homeostasis control in cyanobacteria. *FEMS Microbiol Rev* **44**, 33–53 (2020).

628. Bolay, P. *et al.* The novel pii-interacting protein pira controls flux into the cyanobacterial ornithine-ammonia cycle. *mBio* **12**, (2021).

629. Batista, M. B. *et al.* PHB biosynthesis counteracts redox stress in Herbaspirillum seropedicae. *Front Microbiol* **9**, 330624 (2018).

630. Zhang, X. & Reed, J. L. Adaptive Evolution of Synthetic Cooperating Communities Improves Growth Performance. *PLoS One* **9**, e108297 (2014).

631. Heffernan, J. *et al.* Adaptive laboratory evolution of Clostridium autoethanogenum to metabolize CO2 and H2 enhances growth rates in chemostat and unravels proteome and metabolome alterations. *Microb Biotechnol* **17**, e14452 (2024).

632. Zambrano, M. M., Siegele, D. A., Almirón, M., Tormo, A. & Kolter, R. Microbial Competition: Escherichia coli Mutants That Take Over Stationary Phase Cultures. *Science (1979)* **259**, 1757–1760 (1993).

633. Wang, X. *et al.* GREACE-assisted adaptive laboratory evolution in endpoint fermentation broth enhances lysine production by Escherichia coli. *Microb Cell Fact* **18**, 1–13 (2019).

634. Papaefthimiou, D. *et al.* Differential patterns of evolution and distribution of the symbiotic behaviour in nostocacean cyanobacteria. *Int J Syst Evol Microbiol* **58**, 553–564 (2008).

635. Alper, H. & Stephanopoulos, G. Global transcription machinery engineering: A new approach for improving cellular phenotype. *Metab Eng* **9**, 258–267 (2007).

636. McGuffie, M. J. & Barrick, J. E. pLannotate: engineered plasmid annotation. *Nucleic Acids Res* **49**, W516 (2021).

Appendices

Table S1 | Mean μ_{max} (h^{-1}) 24-well plates bias screening using Syn.*Δhox*. Cells were inoculated into 1.1 mL of BG-11 media, and μ_{max} determined for each well utilising OD_{750nm}. Plates incubated for 168 hours at 300 µmol photons·m^{-2}·sec^{-1}, 30 °C. Green indicates a higher well μ_{max}, red indicates a lower. (*n* = 3; ± indicates standard deviation).

	1	2	3	4	5	6
A	0.014964 ±0.001	0.016924 ±0.002	0.016994 ±0.002	0.016911 ±0.0007	0.015688 ±0.003	0.016816 ±0.004
B	0.01662 ±0.001	0.016358 ±0.0008	0.016548 ±0.0005	0.016309 ±0.001	0.016827 ±0.002	0.016698 ±0.004
C	0.0169 ±0.0009	0.014879 ±0.004	0.015629 ±0.003	0.017085 ±0.0007	0.015849 ±0.003	0.015994 ±0.004
D	0.016855 ±0.002	0.016973 ±0.003	0.015706 ±0.002	0.014826 ±0.004	0.016332 ±0.001	0.015799 ±0.004

Table S2 | Mean volume loss (mL) 24-well plates bias screening using 1.1 mL of BG-11 liquid media only. Plates incubated for 168 hours at 300 µmol photons·m^{-2}·sec^{-1}, 30 °C. Blue indicates relatively lower media loss per well, red indicates higher. (*n* = 3; ± indicates standard deviation).

	1	2	3	4	5	6
A	0.014 ±0.01	0.037 ±0.01	0.045 ±0.02	0.036 ±0.01	0.059 ±0.02	0.066 ±0.02
B	0.016 ±0.01	0.016 ±0.02	0.014 ±0.01	0.015 ±0.01	0.027 ±0.02	0.048 ±0.02
C	0.016 ±0.01	0.014 ±0.01	0.005 ±0.01	0.017 ±0.01	0.036 ±0.02	0.05 ±0.03
D	0.016 ±0.01	0.032 ±0.02	0.023 ±0.01	0.014 ±0.01	0.049 ±0.02	0.049 ±0.02

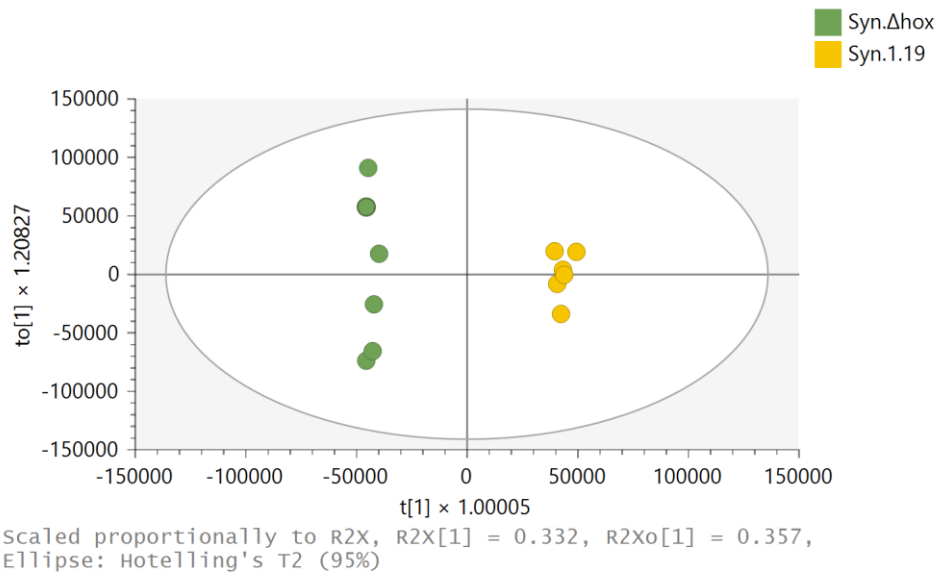


Figure S3 | OPLS-DA model comparing the untargeted metabolomic analyses of Syn.*Δhox* (green) and Syn.1.19 (amber) during early exponential growth phase. Grown at 300 µmol photons·m^{-2}·sec^{-1}, 30 °C, 1.5% CO_2 after 2 days of growth. R^2Y = 0.996, Q^2 = 0.968 (n = 6).

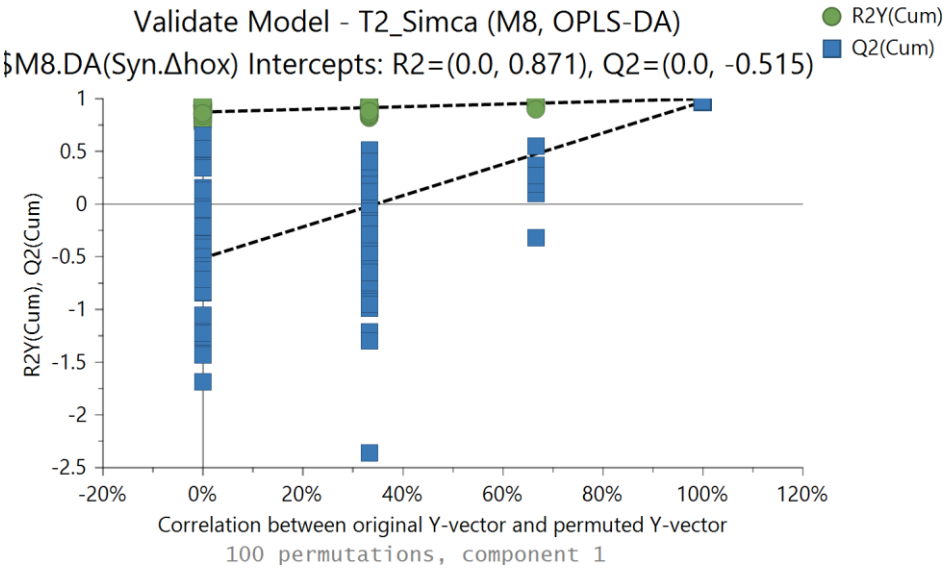


Figure S4 | Permutation test of OPLS-DA model Syn.*Δhox* variable comparing the untargeted metabolomic analyses of Syn.*Δhox* and Syn.1.19 during early exponential growth phase at 300 µmol photons·m^{-2}·sec^{-1}, 30 °C, 1.5% CO_2 after 2 days of growth. (n = 6).

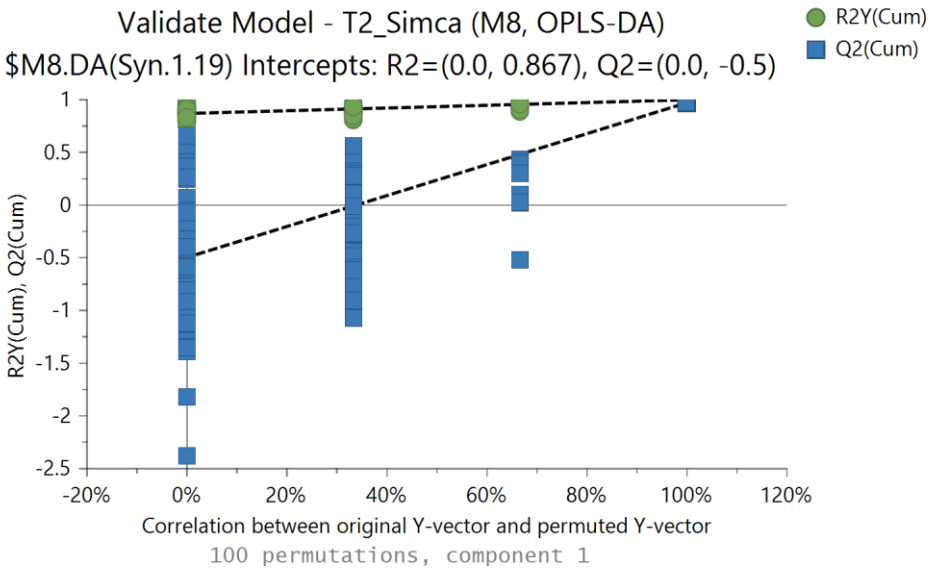


Figure S5 | Permutation test of OPLS-DA model Syn.1.19 variable comparing the untargeted metabolomic analyses of Syn.*Δhox* and Syn.1.19 during early exponential growth phase at 300 µmol photons·m^{-2}·sec^{-1}, 30 °C, 1.5% CO_2 after 2 days of growth. (n = 6).

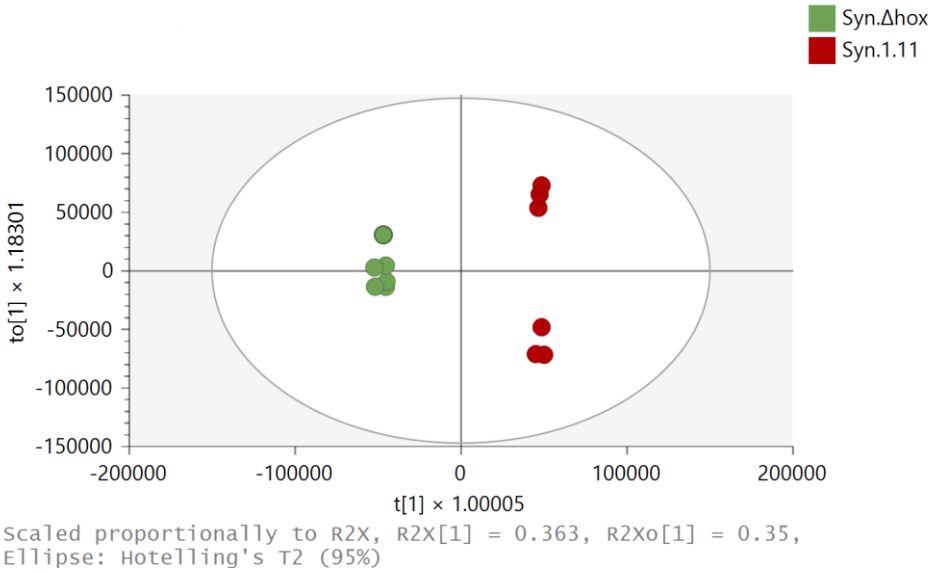


Figure S6 | OPLS-DA model comparing the untargeted metabolomic analyses of Syn.*Δhox* (green) and Syn.1.11 (red) during late exponential growth phase. Grown at 300 µmol photons·m^{-2}·sec^{-1}, 30 °C, 1.5% CO_2 after 4 days of growth. R^2Y = 0.997, Q^2 = 0.95 (n = 6).

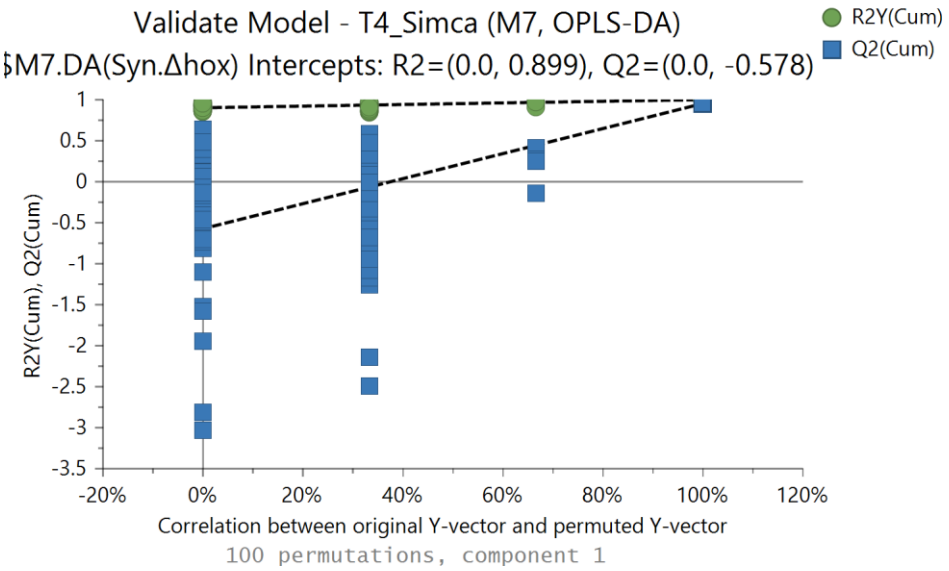


Figure S7 | Permutation test of OPLS-DA model Syn.*Δhox* variable comparing the untargeted metabolomic analyses of Syn.*Δhox* and Syn.1.11 during late exponential growth phase at 300 µmol photons·m^{-2}·sec^{-1}, 30 °C, 1.5% CO_2 after 4 days of growth. (n = 6).

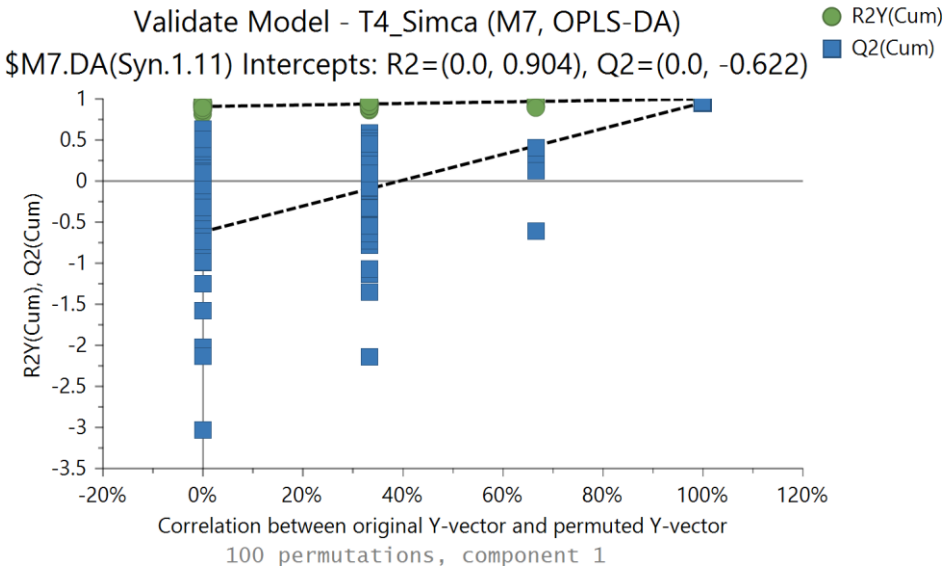


Figure S8 | Permutation test of OPLS-DA model Syn.1.11 variable comparing the untargeted metabolomic analyses of Syn.*Δhox* and Syn.1.11 during late exponential growth phase at 300 µmol photons·m^{-2}·sec^{-1}, 30 °C, 1.5% CO_2 after 4 days of growth. (n = 6).

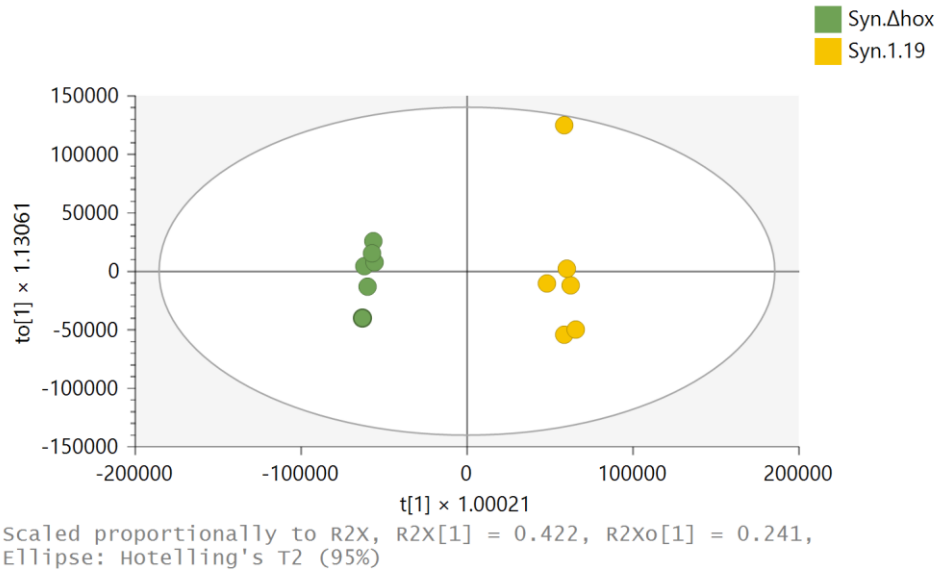


Figure S9 | OPLS-DA model comparing the untargeted metabolomic analyses of Syn.*Δhox* (green) and Syn.1.19 (amber) during late exponential growth phase. Grown at 300 µmol photons·m^{-2}·sec^{-1}, 30 °C, 1.5% CO_2 after 4 days of growth. R^2Y = 0.995, Q^2 = 0.962 (n = 6).

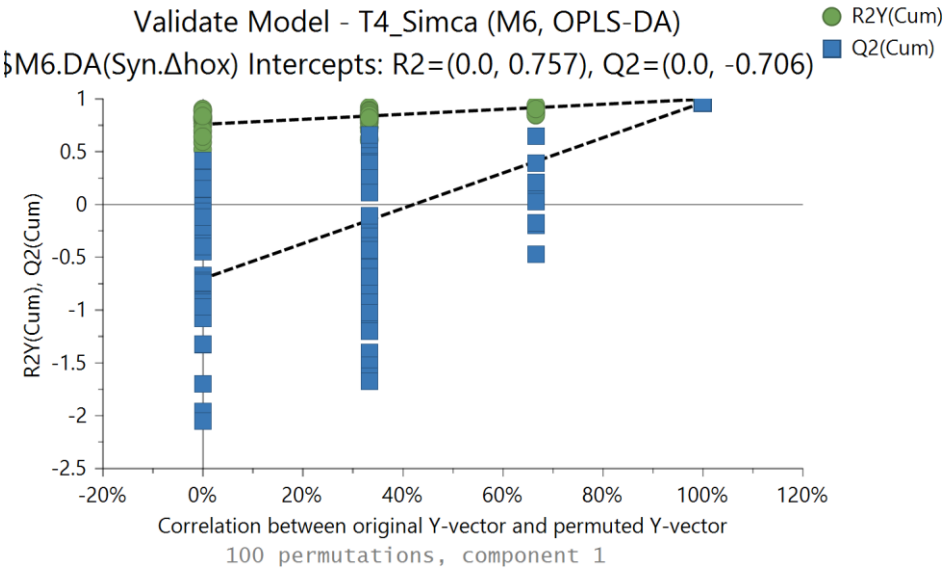


Figure S10 | Permutation test of OPLS-DA model Syn.*Δhox* variable comparing the untargeted metabolomic analyses of Syn.*Δhox* and Syn.1.19 during late exponential growth phase at 300 µmol photons·m^{-2}·sec^{-1}, 30 °C, 1.5% CO_2 after 4 days of growth. (n = 6).

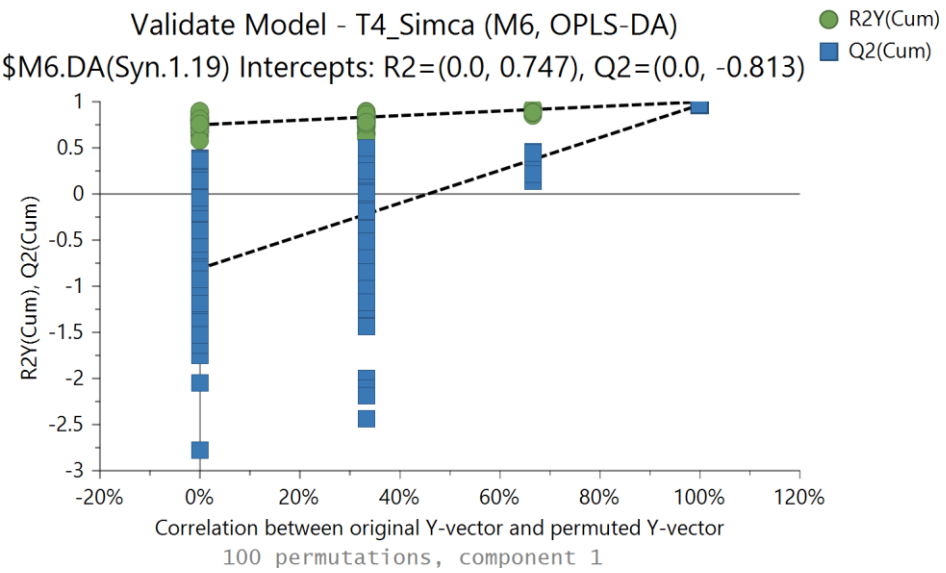


Figure S11 | Permutation test of OPLS-DA model Syn.1.19 variable comparing the untargeted metabolomic analyses of Syn.*Δhox* and Syn.1.19 during late exponential growth phase at 300 µmol photons·m^{-2}·sec^{-1}, 30 °C, 1.5% CO_2 after 4 days of growth. (n = 6).

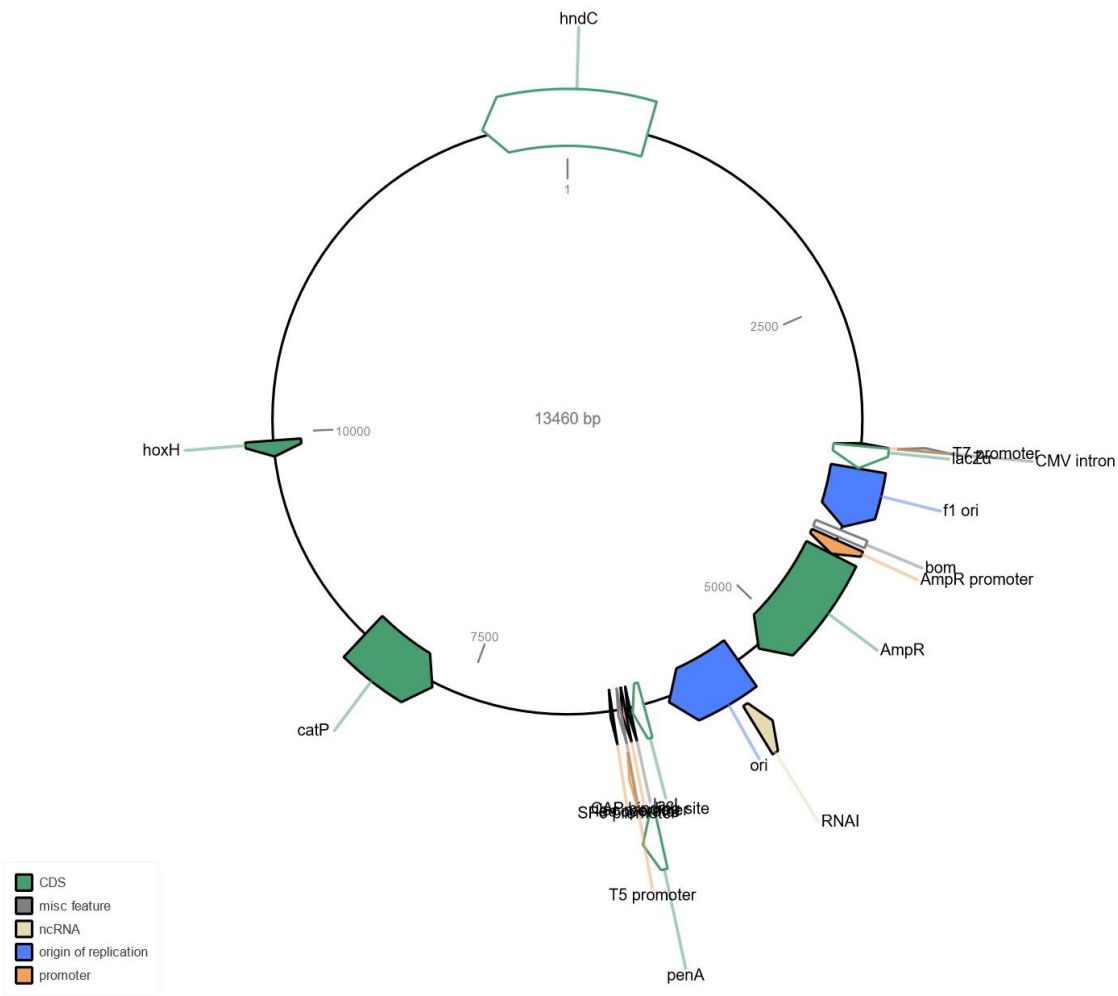


Figure S12 | Schematic of sequencing results from pGEM-*hox*, automatically annotated using pLannotate [614] by Source Bioscience (Nottingham, United Kingdom).

```
>HoxE
Sequence ID: Query_8364903 Length: 522
Range 1: 1 to 522

Score:965 bits(522), Expect:0.0,
Identities:522/522(100%),  Gaps:0/522(0%), Strand: Plus/Minus

Query  1034  TTAACTGTTACTTAACCAAGGTTGTATCGCCGCCAATACCGCTTCGTCATTCTGCTTGCC  1093
              ||||||||||||||||||||||||||||||||||||||||||||||||||||||||||||
Sbjct  522   TTAACTGTTACTTAACCAAGGTTGTATCGCCGCCAATACCGCTTCGTCATTCTGCTTGCC  463

Query  1094  CAACACTTTGCCGTCATAGACCACGGCTGGGGCAATGCCACAGGCTCCAATGCAACGGGC  1153
              ||||||||||||||||||||||||||||||||||||||||||||||||||||||||||||
Sbjct  462   CAACACTTTGCCGTCATAGACCACGGCTGGGGCAATGCCACAGGCTCCAATGCAACGGGC  403

Query  1154  CGTCACCAAGGACATTTGTCCATCCTCTGTCGTTTCCCCCGGTTTCAGATGGACTTCCTG  1213
              ||||||||||||||||||||||||||||||||||||||||||||||||||||||||||||
Sbjct  402   CGTCACCAAGGACATTTGTCCATCCTCTGTCGTTTCCCCCGGTTTCAGATGGACTTCCTG  343

Query  1214  ATCTAGGGTTTTCAGCAAATCCCCCGCCCCTTTAACGTAGCAAGCCGTTCCCAAGCAGAC  1273
              ||||||||||||||||||||||||||||||||||||||||||||||||||||||||||||
Sbjct  342   ATCTAGGGTTTTCAGCAAATCCCCCGCCCCTTTAACGTAGCAAGCCGTTCCCAAGCAGAC  283

Query  1274  CACACAGGTATGTTTCCCACTGGGTTTAAGGGAAAAAAGATGGTAAAAAGTCGCCACTCC  1333
              ||||||||||||||||||||||||||||||||||||||||||||||||||||||||||||
Sbjct  282   CACACAGGTATGTTTCCCACTGGGTTTAAGGGAAAAAAGATGGTAAAAAGTCGCCACTCC  223

Query  1334  AAACACCCGGCTGAGGGGTAATTTAAGCCCCCGGGCTACGTAGAGCAGAACATCCTCTTC  1393
              ||||||||||||||||||||||||||||||||||||||||||||||||||||||||||||
Sbjct  222   AAACACCCGGCTGAGGGGTAATTTAAGCCCCCGGGCTACGTAGAGCAGAACATCCTCTTC  163

Query  1394  CAGGTAGCCAAAAATTTCCTGGGCTTTATGCAGGATTTCAATGAGGGCATCCTGATTAAA  1453
              ||||||||||||||||||||||||||||||||||||||||||||||||||||||||||||
Sbjct  162   CAGGTAGCCAAAAATTTCCTGGGCTTTATGCAGGATTTCAATGAGGGCATCCTGATTAAA  103

Query  1454  TTGGTTGCGCTTCATGGTGGCGTCTAACACCTTAAAACGCTTGTCTCCACTAGGATGGGC  1513
              ||||||||||||||||||||||||||||||||||||||||||||||||||||||||||||
Sbjct  102   TTGGTTGCGCTTCATGGTGGCGTCTAACACCTTAAAACGCTTGTCTCCACTAGGATGGGC  43

Query  1514  CGCAGATGGGGGCACAGTTTGGCGATCGGTGGCAACGGTCAT  1555
              |||||||||||||||||||||||||||||||||||||||||
Sbjct  42    CGCAGATGGGGGCACAGTTTGGCGATCGGTGGCAACGGTCAT  1
```

Figure S13 | Alignment of sequencing results from pGEM-*hox* (Query) with *sll1220* (*hoxE*) by BLASTn (NCBI).

```
>HoxF
Sequence ID: Query_8364904 Length: 1602
Range 1: 1 to 957

Score:1768 bits(957), Expect:0.0,
Identities:957/957(100%),  Gaps:0/957(0%), Strand: Plus/Minus

Query  1    CCACAAACCCGATTGGGCTGGATAGGGTGGTCTTGGTCGGGGCGTTCCCCGTTTTCCTTC  60
            ||||||||||||||||||||||||||||||||||||||||||||||||||||||||||||
Sbjct  957  CCACAAACCCGATTGGGCTGGATAGGGTGGTCTTGGTCGGGGCGTTCCCCGTTTTCCTTC  898

Query  61   CACTGAGGCAATTAATGCTGTTTCTTCACCGCAGACAAAGGCACCGGCTCCTACTCGTAT  120
            ||||||||||||||||||||||||||||||||||||||||||||||||||||||||||||
Sbjct  897  CACTGAGGCAATTAATGCTGTTTCTTCACCGCAGACAAAGGCACCGGCTCCTACTCGTAT  838

Query  121  ATCAATCTTGAAATCAATGGGAGAGTCAAAAATTTGGGTGCCCATCAGGCCATAACGTTT  180
            ||||||||||||||||||||||||||||||||||||||||||||||||||||||||||||
Sbjct  837  ATCAATCTTGAAATCAATGGGAGAGTCAAAAATTTGGGTGCCCATCAGGCCATAACGTTT  778

Query  181  AGCCTGTTGGATCGCTTTTTGCAGTCGTTGGATAGCTAGGGGGTATTCCGCCCGCACATA  240
            ||||||||||||||||||||||||||||||||||||||||||||||||||||||||||||
Sbjct  777  AGCCTGTTGGATCGCTTTTTGCAGTCGTTGGATAGCTAGGGGGTATTCCGCCCGCACATA  718

Query  241  AATGTAACCATGGTTAGCCCCCACTGCATAGGCGGCGATCGCCATACCTTCGAGGATGCG  300
            ||||||||||||||||||||||||||||||||||||||||||||||||||||||||||||
Sbjct  717  AATGTAACCATGGTTAGCCCCCACTGCATAGGCGGCGATCGCCATACCTTCGAGGATGCG  658

Query  301  ATGGGGATCACTTTCCAACACACTGCGGTCCATGAAAGCACCGGGATCGCCTTCGTCAGC  360
            ||||||||||||||||||||||||||||||||||||||||||||||||||||||||||||
Sbjct  657  ATGGGGATCACTTTCCAACACACTGCGGTCCATGAAAGCACCGGGATCGCCTTCGTCAGC  598

Query  361  ATTGCAGATGACATATTTTTGCTGGCCGGGCATTTTGGCCACTGTGGCCCATTTCAAGCC  420
            ||||||||||||||||||||||||||||||||||||||||||||||||||||||||||||
Sbjct  597  ATTGCAGATGACATATTTTTGCTGGCCGGGCATTTTGGCCACTGTGGCCCATTTCAAGCC  538

Query  421  GGTGGGATAACCGCCCCCACCCCGACCCCGCAGACCACTTTTGTTCATTTCCACGATCAC  480
            ||||||||||||||||||||||||||||||||||||||||||||||||||||||||||||
Sbjct  537  GGTGGGATAACCGCCCCCACCCCGACCCCGCAGACCACTTTTGTTCATTTCCACGATCAC  478

Query  481  TTCCTCTGGGGTCATTTCATAGACAACCTTATGAAGCTGTTCGTAGCCCCCTAGGGCGAT  540
            ||||||||||||||||||||||||||||||||||||||||||||||||||||||||||||
Sbjct  477  TTCCTCTGGGGTCATTTCATAGACAACCTTATGAAGCTGTTCGTAGCCCCCTAGGGCGAT  418

Query  541  GTATTCATCAATGGATTCGGGATCAATCCGGCCTGAATTTTCCAAAGCAATATTCCTTTG  600
            ||||||||||||||||||||||||||||||||||||||||||||||||||||||||||||
Sbjct  417  GTATTCATCAATGGATTCGGGATCAATCCGGCCTGAATTTTCCAAAGCAATATTCCTTTG  358

Query  601  CAGGGCGTAGAAGGGATGGTGGGGATCACCACTGATTAAGCCTGTTTCTGCAACTGCATC  660
            ||||||||||||||||||||||||||||||||||||||||||||||||||||||||||||
Sbjct  357  CAGGGCGTAGAAGGGATGGTGGGGATCACCACTGATTAAGCCTGTTTCTGCAACTGCATC  298

Query  661  GGGTTTCTGCAATTTTTTGACAATATCCCCCACCTGGTCTGGGGTAACAAATTCGTAGAG  720
            ||||||||||||||||||||||||||||||||||||||||||||||||||||||||||||
Sbjct  297  GGGTTTCTGCAATTTTTTGACAATATCCCCCACCTGGTCTGGGGTAACAAATTCGTAGAG  238

Query  721  TTGATTCCGGTCATCCACCGCCACTAGGGGGCCCCGGCCACAAAACTTCATACAGCCTAC  780
            ||||||||||||||||||||||||||||||||||||||||||||||||||||||||||||
Sbjct  237  TTGATTCCGGTCATCCACCGCCACTAGGGGGCCCCGGCCACAAAACTTCATACAGCCTAC  178

Query  781  CCCACAGACTTCCACTTTTTCTTCCAATCCTGCTGCGGCGATCGCCGTGGTGAGAttttt  840
            ||||||||||||||||||||||||||||||||||||||||||||||||||||||||||||
Sbjct  177  CCCACAGACTTCCACTTTTTCTTCCAATCCTGCTGCGGCGATCGCCGTGGTGAGATTTTT  118

Query  841  tttCACCGTCTCCCCTTCAGAAGAAAGACAACCGGCAGCACTACAACAACGAATGCGAAT  900
            ||||||||||||||||||||||||||||||||||||||||||||||||||||||||||||
Sbjct  117  TTTCACCGTCTCCCCTTCAGAAGAAAGACAACCGGCAGCACTACAACAACGAATGCGAAT  58

Query  901  TTTTGTTTGTTTCTCACGGCTTTTGGTGGCAATTTCCTTTAATTCTTTAATGTCCAT  957
            |||||||||||||||||||||||||||||||||||||||||||||||||||||||||
Sbjct  57   TTTTGTTTGTTTCTCACGGCTTTTGGTGGCAATTTCCTTTAATTCTTTAATGTCCAT  1
```

Figure S14 | Alignment of sequencing results from pGEM-*hox* (Query) with *sll1221* (*hoxF*) by BLASTn (NCBI).

```
>HoxU
Sequence ID: Query_8364905 Length: 717
Range 1: 1 to 717

Score:1303 bits(705), Expect:0.0,
Identities:713/717(99%),  Gaps:0/717(0%), Strand: Plus/Minus

Query  11394  CTACCTGACCCATTCCTTTTCTTTACGGGCAGTGGCTAAAAACTCCACCTTACGGCGATC  11453
              ||||||||||||||||||||||||||||||||||||||||||||||||||||||||||||
Sbjct  717    CTACCTGACCCATTCCTTTTCTTTACGGGCAGTGGCTAAAAACTCCACCTTACGGCGATC  658

Query  11454  GCCAATTTTTTCAGCAGTAGTTTCTCCTTTATGGAAGATAGAACCCGTGGGACAGGCATC  11513
              ||||||||||||||||||||||||||||||||||||||||||||||||||||||||||||
Sbjct  657    GCCAATTTTTTCAGCAGTAGTTTCTCCTTTATGGAAGATAGAACCCGTGGGACAGGCATC  598

Query  11514  CACACATTTGCCACAGGAAGTACAGGCATCAACGGTTCCCCAGGGCTGATTTAAACCAGA  11573
              ||||||||||||||||||||||||||||||||||||||||||||||||||||||||||||
Sbjct  597    CACACATTTGCCACAGGAAGTACAGGCATCAACGGTTCCCCAGGGCTGATTTAAACCAGA  538

Query  11574  AACAATTTTGCATTCTGCGCCCCGGTAAGCCACATCCCAAACGTGGGCTCCCTCAATTTC  11633
              ||||||||||||||||||||||||||||||||||||||||||||||||||||||||||||
Sbjct  537    AACAATTTTGCATTCTGCGCCCCGGTAAGCCACATCCCAAACGTGGGCTCCCTCAATTTC  478

Query  11634  ATCGCAAACTCGCACACAACGGGTACAGAGAGTACAACGGTTATGATCAATGCCAAACAT  11693
              |||||||||||||||||||||||||||||||| ||||||||||||||||||||||||||||
Sbjct  477    ATCGCAAACTCGCACACAACGGGTACAGAGAATACAACGGTTATGATCAATGCCAAACAT  418

Query  11694  GGGATGGGATAAATCCACTTCTCGCTTGGGAAATTGATATTTAAATCGGCTGTGACCCAT  11753
              |||||||||||||||||||||||||||||||||||||||||||||||||||||||||| ||||
Sbjct  417    GGGATGGGATAAATCCACTTCTCGCTTGGGAAATTGATATTTAAATCGGCTGTGATCCAT  358

Query  11754  ACCCACCGTAATGGCCATATCTTGCAATTCACAGTTGCCGTTAGCCACACAAATGGCACA  11813
              ||||||||||||||||||||||||||||||||||||||||||||||||||||||||||||
Sbjct  357    ACCCACCGTAATGGCCATATCTTGCAATTCACAGTTGCCGTTAGCCACACAAATGGCACA  298

Query  11814  GACATGATTGCCTTCGGAAAAAAGTAATTCCACTGTCATACGTCGGTAATTTTACAATTT  11873
              |||||||||||||||||||||||||||||||||||||||||||||||||||||||| ||||||
Sbjct  297    GACATGATTGCCTTCGGAAAAAAGTAATTCCACTGTCATACGTCGGTAATTTTGCAATTT  238

Query  11874  TTCTGTGTTGGTGTGGACTACCATTTCTTCGCTCACAGCGGTAACGCAGGCGGGCATCAA  11933
              ||||||||||||||||||||||||||||||||||||||||||||||||||||||||||||
Sbjct  237    TTCTGTGTTGGTGTGGACTACCATTTCTTCGCTCACAGCGGTAACGCAGGCGGGCATCAA  178

Query  11934  TTTATTCGTGCCTTCCACTTCCACCATGCACAAACGACAGGCTGCCGCTTCTGAAATCCC  11993
              ||||||||||||||||||||||||||||||||||||||||||||||||||||||||||||
Sbjct  177    TTTATTCGTGCCTTCCACTTCCACCATGCACAAACGACAGGCTGCCGCTTCTGAAATCCC  118

Query  11994  TTCTAAATGACAAAGGGTGGGAATGGGAACCCCTGCTTCTTTAGCCGCTTGCAAAATACT  12053
              ||||||||| ||||||||||||||||||||||||||||||||||||||||||||||||||||
Sbjct  117    TTCTAAATGGCAAAGGGTGGGAATGGGAACCCCTGCTTCTTTAGCCGCTTGCAAAATACT  58

Query  12054  TGCGCCTTCTTCAATGGCGATCGCCTTATCATCAATGGTTAAAGTAACAACAGACAT  12110
              ||||||||||||||||||||||||||||||||||||||||||||||||||||||||
Sbjct  57     TGCGCCTTCTTCAATGGCGATCGCCTTATCATCAATGGTTAAAGTAACAACAGACAT  1
```

Figure S15 | Alignment of sequencing results from pGEM-*hox* (Query) with *sll1223* (*hoxU*) by BLASTn (NCBI).

```
>HoxY
Sequence ID: Query_8364906 Length: 549
Range 1: 1 to 549

Score:1009 bits(546), Expect:0.0,
Identities:548/549(99%),  Gaps:0/549(0%), Strand: Plus/Minus

Query  10800  TTAACCAAATTTGATCATTGCTCGCCCTTCCATGAGGGGATGTTCCCCATTTAATAATGG  10859
              ||||||||||||||||||||||||||||||||||||||||||||||||||||||||||||
Sbjct  549    TTAACCAAATTTGATCATTGCTCGCCCTTCCATGAGGGGATGTTCCCCATTTAATAATGG  490

Query  10860  TTCTAGCGTTGCTCGAATACGGTGGGCATCGGGAGGACAACCGGGCATAAAAATATCCAC  10919
              ||||||||||||||||||||||||||||||||||||||||||||||||||||||||||||
Sbjct  489    TTCTAGCGTTGCTCGAATACGGTGGGCATCGGGAGGACAACCGGGCATAAAAATATCCAC  430

Query  10920  CGGAATAACCTCATGTAGGGGAATAACCTTGTCTAATAGAGGCGGCACAATACCAGGTTC  10979
              ||||||||||||||||||||||||||||||||||||||||||||||||||||||||||||
Sbjct  429    CGGAATAACCTCATGTAGGGGAATAACCTTGTCTAATAGAGGCGGCACAATACCAGGTTC  370

Query  10980  ATCGGGCAGTTGAGGCGTCCCATCTCCCAGTTCAATATAGGCTCGGCGCAGAACCGGATC  11039
              ||||||||||||||||||||||||||||||||||||||||||||||||||||||||||||
Sbjct  369    ATCGGGCAGTTGAGGCGTCCCATCTCCCAGTTCAATATAGGCTCGGCGCAGAACCGGATC  310

Query  11040  GCTACCTTTGAGCATATTACGCATACCGGGGACATTGGCGGTTACAGCACAGTCCCCAAA  11099
              ||||||||||||||||||||||||||||||||||||||||||||||||||||||||||||
Sbjct  309    GCTACCTTTGAGCATATTACGCATACCGGGGACATTGGCGGTTACAGCACAGTCCCCAAA  250

Query  11100  GGAAATTACTACCTTCGTTTTCTGTCTCAACCCCAAAGCTAACTCTAAATTTTCTTCGTT  11159
              |||||||||||||||||||||||||||||| ||||||||||||||||||||||||||||
Sbjct  249    GGAAATTACTACCTTCGTTTTCTGTCTCAACTCCAAAGCTAACTCTAAATTTTCTTCGTT  190

Query  11160  GGCGATCGCCCCTTCCACTAGGCAAACATCCACATTGTCCGGGTATTCCTTGAGATCAGA  11219
              ||||||||||||||||||||||||||||||||||||||||||||||||||||||||||||
Sbjct  189    GGCGATCGCCCCTTCCACTAGGCAAACATCCACATTGTCCGGGTATTCCTTGAGATCAGA  130

Query  11220  ACCAACGGGACTGAAAACCACATCAACTTTTTGAGCGAGATCAATGAGCCATTCGTCCAT  11279
              ||||||||||||||||||||||||||||||||||||||||||||||||||||||||||||
Sbjct  129    ACCAACGGGACTGAAAACCACATCAACTTTTTGAGCGAGATCAATGAGCCATTCGTCCAT  70

Query  11280  ATCAAGGAAGGACATATGACAGCCGGAACAACCAGCGAGCCAAACGGTAGCAAAACGAAT  11339
              ||||||||||||||||||||||||||||||||||||||||||||||||||||||||||||
Sbjct  69     ATCAAGGAAGGACATATGACAGCCGGAACAACCAGCGAGCCAAACGGTAGCAAAACGAAT  10

Query  11340  TTTAGCCAT  11348
              |||||||||
Sbjct  9      TTTAGCCAT  1
```

Figure S16 | Alignment of sequencing results from pGEM-*hox* (Query) with *sll1224* (*hoxY*) by BLASTn (NCBI).

```
>HoxH
Sequence ID: Query_8364907 Length: 1425
Range 1: 1 to 1425

Score:2610 bits(1413), Expect:0.0,
Identities:1421/1425(99%),  Gaps:0/1425(0%), Strand: Plus/Minus

Query  8521  TTAATCCCGCTGGATGGACTTAATTAGTTCCCCCTGAGGGTTAACTAAATCGATCATCAA  8580
              ||||||||||||||||||||||||||||||||||||||||||||||||||||||||||||
Sbjct  1425  TTAATCCCGCTGGATGGACTTAATTAGTTCCCCCTGAGGGTTAACTAAATCGATCATCAA  1366

Query  8581  TGGCATTTGTCCCGCTGCATGGGTAGAACAACTAAGGCAGGGATCATAACAACGAATACC  8640
              ||||||||||||||||||||||||||||||||||||||||||||||||||||||||||||
Sbjct  1365  TGGCATTTGTCCCGCTGCATGGGTAGAACAACTAAGGCAGGGATCATAACAACGAATACC  1306

Query  8641  CGCTTCCACCCGGTTTAAAAACCCTTCTTGCACATCATGATTGCGAATGTAGTGTTTGGC  8700
              ||||||||||||||||||||||||||||||||||||||||||||||||||||||||||||
Sbjct  1305  CGCTTCCACCCGGTTTAAAAACCCTTCTTGCACATCATGATTGCGAATGTAGTGTTTGGC  1246

Query  8701  AATTTGGGCCACGGTTTTATTCATGGCTAAGTTATTGTTGCCCGTGGCAATGATCAAATT  8760
              ||||||||||||||||||||||||||||||||||||||||||||||||||||||||||||
Sbjct  1245  AATTTGGGCCACGGTTTTATTCATGGCTAAGTTATTGTTGCCCGTGGCAATGATCAAATT  1186

Query  8761  CGCTTTCTTAATTAGACCATCTTCATCTATCTTGTAATGGTGGAATAAAGTACCCCGGGG  8820
              | ||||||||||||||||||||||||||||||||||||||||||||||||||||||||||
Sbjct  1185  CACTTTCTTAATTAGACCATCTTCATCTATCTTGTAATGGTGGAATAAAGTACCCCGGGG  1126

Query  8821  TGCTTCGCCCACTCCCACCGCTTCGGTACAATTAATTTCTGCCTTAGCTCGACAATTTTT  8880
              |||||||| ||||||||||||||||||||||||||||||||||||||||||||||||||||
Sbjct  1125  TGCTTCGCTCACTCCCACCGCTTCGGTACAATTAATTTCTGCCTTAGCTCGACAATTTTT  1066

Query  8881  GGACAAAATATCAGGGTCAGCCATTAACAATTCGATGGCTTCTAAACAGGCAAGAATTTC  8940
              ||||||||||||||||||||||||||||||||||||||||||||||||||||||||||||
Sbjct  1065  GGACAAAATATCAGGGTCAGCCATTAACAATTCGATGGCTTCTAAACAGGCAAGAATTTC  1006

Query  8941  CACCAAGCGGGCGTAATGATAAAAGAAAGAGGACGTGGCCACACCTCCAGCCCGTTGCCG  9000
              ||||||||||||||||||||||||||||||||||||||||||||||||||||||||||||
Sbjct  1005  CACCAAGCGGGCGTAATGATAAAAGAAAGAGGACGTGGCCACACCTCCAGCCCGTTGCCG  946

Query  9001  ATATTCTTCTAATTCTTGGTCTGCTTCCGGGGTGCCAATGTGATGACAAACATTAAGGCG  9060
              ||||||||||||||||||||||||||||||||||||||||||||||||||||||||||||
Sbjct  945   ATATTCTTCTAATTCTTGGTCTGCTTCCGGGGTGCCAATGTGATGACAAACATTAAGGCG  886

Query  9061  GGCAAGGGGACCAACCCGATAAATGCCATCGGGATAACCCAGAGATTTGTAGTAGGGAGA  9120
              |||||||||||||||||||||||||||||||||||||||||||||||||||||||||| |
Sbjct  885   GGCAAGGGGACCAACCCGATAAATGCCATCGGGATAACCCAGAGATTTGTAGTAGGGAAA  826

Query  9121  TTTTAAATAGGACCATTTTTCCACCGATTCACCAATAAAATCAGCGTAATTATCTTCACT  9180
              ||||||||||||||||||||||||||||||||||||||||||||||||||||||||||||
Sbjct  825   TTTTAAATAGGACCATTTTTCCACCGATTCACCAATAAAATCAGCGTAATTATCTTCACT  766

Query  9181  GAGATTGTCCGCGACAATATTGCCTTCACTGTCGGTAAACCGCAGGGAGCCGCCATAATG  9240
              ||||||||||||||||||||||||||||||||||||||||||||||||||||||||||||
Sbjct  765   GAGATTGTCCGCGACAATATTGCCTTCACTGTCGGTAAACCGCAGGGAGCCGCCATAATG  706

Query  9241  TTCCCATTCATTATTTTTCCCAACTAAGCCCATAAATAGGGAGGGAAATTTGCCAAATTC  9300
              ||||||||||||||||||||||||||||||||||||||||||||||||||||||||||||
Sbjct  705   TTCCCATTCATTATTTTTCCCAACTAAGCCCATAAATAGGGAGGGAAATTTGCCAAATTC  646

Query  9301  TGCCACTTCTGTTTGGAAGCGGTCCAACATATTTTTAAACAAATTTAAGGCTAAATAAAC  9360
              ||||||||||||||||||||||||||||||||||||||||||||||||||||||||||||
Sbjct  645   TGCCACTTCTGTTTGGAAGCGGTCCAACATATTTTTAAACAAATTTAAGGCTAAATAAAC  586

Query  9361  GGTTTCTTTTGCTTCTGGTAAACGGTCCACAATCCATTGTCTGCCTTCTTCCGACAACGG  9420
              ||||||||||||||||||||||||||||||||||||||||||||||||||||||||||||
Sbjct  585   GGTTTCTTTTGCTTCTGGTAAACGGTCCACAATCCATTGTCTGCCTTCTTCCGACAACGG  526

Query  9421  CGATCGGACTCCACCGGGCACTGACCAAGCAGAGTGGAttttttttAGCTCCCAAAAGTTC  9480
              ||||||||||||||||||||||||||||||||||||||||||||||||||||||||||||
Sbjct  525   CGATCGGACTCCACCGGGCACTGACCAAGCAGAGTGGATTTTTTTAGCTCCCAAAAGTTC  466

Query  9481  AATTACCGTTTGGCCAAATTGCCGTAACCGAATACCTGCCCTAGCTAAATCGGGGTCAGC  9540
              ||||||||||||||||||||||||||||||||||||||||||||||||||||||||||||
Sbjct  465   AATTACCGTTTGGCCAAATTGCCGTAACCGAATACCTGCCCTAGCTAAATCGGGGTCAGC  406

Query  9541  AGCAATTAAACCAAACACATTGCGAGTAGCGGGATCACTGTCCCAACCAAGCAGAAAATC  9600
              ||||||||||||||||||||||||||||||||||||||||||||||||||||||||||||
Sbjct  405   AGCAATTAAACCAAACACATTGCGAGTAGCGGGATCACTGTCCCAACCAAGCAGAAAATC  346

Query  9601  AGGACTGCTGAGATGGAAAAAACTTAGGGCGTGGGATTGGGTAATTTGCCCTAAATTCAT  9660
              ||||||||||||||||||||||||||||||||||||||||||||||||||||||||||||
Sbjct  345   AGGACTGCTGAGATGGAAAAAACTTAGGGCGTGGGATTGGGTAATTTGCCCTAAATTCAT  286

Query  9661  TAAACGGCGCAGTTTTTCCCCGGCTGGAGGGATTTGCACCGCCAGTAACTTATCCCCGGT  9720
              ||||||||||||||||||||||||||||||||||||||||||||||||||||||||||||
Sbjct  285   TAAACGGCGCAGTTTTTCCCCGGCTGGAGGGATTTGCACCGCCAGTAACTTATCCCCGGT  226

Query  9721  TTTAGCCGCACAGAGCAGATGGCTAACCGGACAAATGCCGCAAATACGGGCGGTAATACC  9780
              ||||||||||||||||||||||||||||||||||||||||||||||||||||||||||||
Sbjct  225   TTTAGCCGCACAGAGCAGATGGCTAACCGGACAAATGCCGCAAATACGGGCGGTAATACC  166

Query  9781  AGCCATTTCCCACATGGGACGACCTTCGCAAAATTTTTCAAAACCCCGATACTCCACCAC  9840
              ||||||||||||||||||||||||||||||||||||||||||||||||||||||||||||
Sbjct  165   AGCCATTTCCCACATGGGACGACCTTCGCAAAATTTTTCAAAACCCCGATACTCCACCAC  106

Query  9841  ATGGAAACGAACATCATCTACGTTGCCCTGGTCGTTGAGGAAAATGGAGATTTTGGCATG  9900
              ||||||||||||||||||||||||||||||||||||||||||||||||||||||||||||
Sbjct  105   ATGGAAACGAACATCATCTACGTTGCCCTGGTCGTTGAGGAAAATGGAGATTTTGGCATG  46

Query  9901  GCCTTCAATCCGGGTAACGGGATCGATAACAATGGTCTTAGACAT  9945
              |||||||||||||||||||||||||||||||||||| ||||||||
Sbjct  45    GCCTTCAATCCGGGTAACGGGATCGATAACAATGGTTTTAGACAT  1
```

Figure S16 | Alignment of sequencing results from pGEM-*hox* with *sll1226* (*hoxH*) by BLASTn (NCBI).

```
Score:1644 bits(890), Expect:0.0,
Identities:892/894(99%),  Gaps:0/894(0%), Strand: Plus/Plus

Query  1    ATGAGTATCGACAAGAAAATTAGACAAATTGCTTTCTACGGTAAAGGCGGTATTGGTAAG  60
            ||||||||||||||||||||||||||||||||||||||||||||||||||||||||||||
Sbjct  1    ATGAGTATCGACAAGAAAATTAGACAAATTGCTTTCTACGGTAAAGGCGGTATTGGTAAG  60

Query  61   TCTACCACTTCTCAAAACACCTTGGCAGCTATGGCAGAAATGGGTCAACGCATCCTCATC  120
            ||||||||||||||||||||||||||||||||||||||||||||||||||||||||||||
Sbjct  61   TCTACCACTTCTCAAAACACCTTGGCAGCTATGGCAGAAATGGGTCAACGCATCCTCATC  120

Query  121  GTAGGTTGCGACCCTAAAGCTGACTCCACCCGTTTGATGCTCCATTCCAAAGCTCAAACC  180
            ||||||||||||||||||||||||||||||||||||||||||||||||||||||||||||
Sbjct  121  GTAGGTTGCGACCCTAAAGCTGACTCCACCCGTTTGATGCTCCATTCCAAAGCTCAAACC  180

Query  181  ACCGTACTTCACTTGGCGGCTGAACGTGGTGCAGTAGAAGACCTCGAACTCGACGAAGTA  240
            |||||||||||||||||||||||||||||||||||| | ||||||||||||||||||||
Sbjct  181  ACCGTACTTCACTTGGCGGCTGAACGTGGTGCAGTAGAAGAYCYCGAACTCGACGAAGTA  240

Query  241  ATGCTGACTGGTTTCCGTGGCGTTAAGTGCGTAGAATCTGGTGGTCCAGAACCCGGTGTA  300
            ||||||||||||||||||||||||||||||||||||||||||||||||||||||||||||
Sbjct  241  ATGCTGACTGGTTTCCGTGGCGTTAAGTGCGTAGAATCTGGTGGTCCAGAACCCGGTGTA  300

Query  301  GGTTGCGCTGGTCGTGGTATCATCACCGCCATTAACTTCTTAGAAGAAAACGGCGCTTAC  360
            ||||||||||||||||||||||||||||||||||||||||||||||||||||||||||||
Sbjct  301  GGTTGCGCTGGTCGTGGTATCATCACCGCCATTAACTTCTTAGAAGAAAACGGCGCTTAC  360

Query  361  CAAGACGTTGACTTCGTATCTTATGACGTATTAGGCGACGTTGTATGCGGTGGTTTCGCA  420
            ||||||||||||||||||||||||||||||||||||||||||||||||||||||||||||
Sbjct  361  CAAGACGTTGACTTCGTATCTTATGACGTATTAGGCGACGTTGTATGCGGTGGTTTCGCA  420

Query  421  ATGCCTATCCGCGAAAATAAAGCGCAAGAAATCTACATCGTTACCTCTGGTGAAATGATG  480
            ||||||||||||||||||||||||||||||||||||||||||||||||||||||||||||
Sbjct  421  ATGCCTATCCGCGAAAATAAAGCGCAAGAAATCTACATCGTTACCTCTGGTGAAATGATG  480

Query  481  GCGATGTATGCTGCTAACAACATCGCTCGTGGTATTTTGAAATATGCACACACTGGTGGT  540
            ||||||||||||||||||||||||||||||||||||||||||||||||||||||||||||
Sbjct  481  GCGATGTATGCTGCTAACAACATCGCTCGTGGTATTTTGAAATATGCACACACTGGTGGT  540

Query  541  GTACGTTTAGGCGGCTTGATTTGTAATAGCCGTAACGTTGACAGAGAAATCGAACTCATC  600
            ||||||||||||||||||||||||||||||||||||||||||||||||||||||||||||
Sbjct  541  GTACGTTTAGGCGGCTTGATTTGTAATAGCCGTAACGTTGACAGAGAAATCGAACTCATC  600

Query  601  GAAACTCTGGCAAAACGTTTGAACACCCAAATGATTCACTACGTACCCCGCGACAACATT  660
            ||||||||||||||||||||||||||||||||||||||||||||||||||||||||||||
Sbjct  601  GAAACTCTGGCAAAACGTTTGAACACCCAAATGATTCACTACGTACCCCGCGACAACATT  660

Query  661  GTTCAACACGCTGAGTTGCGCCGGATGACAGTTAACGAATACGCACCCGACAGCAACCAA  720
            ||||||||||||||||||||||||||||||||||||||||||||||||||||||||||||
Sbjct  661  GTTCAACACGCTGAGTTGCGCCGGATGACAGTTAACGAATACGCACCCGACAGCAACCAA  720

Query  721  GGTAACGAATACCGGATTTTGGCTAACAAAATCATCAACAACGAAAACCTAAAGATTCCT  780
            ||||||||||||||||||||||||||||||||||||||||||||||||||||||||||||
Sbjct  721  GGTAACGAATACCGGATTTTGGCTAACAAAATCATCAACAACGAAAACCTAAAGATTCCT  780

Query  781  ACCCCAATTGAGATGGAAGAATTAGAAGAGTTGCTGATTGAGTTCGGTATTCTCGAAAGC  840
            ||||||||||||||||||||||||||||||||||||||||||||||||||||||||||||
Sbjct  781  ACCCCAATTGAGATGGAAGAATTAGAAGAGTTGCTGATTGAGTTCGGTATTCTCGAAAGC  840

Query  841  GAAGAAAATGCTGCAAAAATGATTGCTACAACTTCAGAAAGCAAATCTAAGTAA  894
            ||||||||||||||||||||||||||||||||||||||||||||||||||||||
Sbjct  841  GAAGAAAATGCTGCAAAAATGATTGCTACAACTTCAGAAAGCAAATCTAAGTAA  894
```

Figure S17 | Alignment of sequencing results from putative *nifH* (Query) with *ava_4478* by BLASTn (NCBI).